HUNGARIAN

Journal of

INDUSTRIAL CHEMISTRY

Edited by

the Hungarian Oil & Gas Research Institute (MÁFKI),
the Research Institute for Heavy Chemical Industries (NEVIKI),
the Research Institute for Technical Chemistry of the
Hungarian Academy of Sciences (MÜKKI),
the Veszprém University of Chemical Engineering (VVE).
Veszprém (Hungary)

Volume 3 1975 ~~Suppl.~~ No. 1.

CODEN: HJICAI

The "Hungarian Journal of Industrial Chemistry (Veszprém)" is a joint publication of the Veszprém scientific institutions of the chemical industry that deals with the results of applied and fundamental research in the field of chemical processes, unit operations and chemical engineering. The papers are published in three or four numbers at irregular intervals in one annual volume, in the English, Russian, French and German languages.

Editorial Office:
Veszprémi Vegyipari Egyetem,
"Hungarian Journal of Industrial Chemistry" Editorial Board:
H – 8201 Veszprém, Schönherz Z. u. 10. Hungary.

HUNGARIAN

Journal of

INDUSTRIAL CHEMISTRY

Edited by

the Hungarian Oil & Gas Research Institute (MÁFKI),
the Research Institute for Heavy Chemical Industries (NEVIKI),
the Research Institute for Technical Chemistry of the
Hungarian Academy of Sciences (MÜKKI),
the Veszprém University of Chemical Engineering (VVE).
Veszprém (Hungary)

Volume 3. 1975 Number 1.—4.

CODEN: HJICAI

The "Hungarian Journal of Industrial Chemistry (Veszprém)" is a joint publication of the Veszprém scientific institutions of the chemical industry that deals with the results of applied and fundamental research in the field of chemical processes, unit operations and chemical engineering. The papers are published in three or four numbers at irregular intervals in one annual volume, in the English, Russian, French and German languages.

Editorial Office:
Veszprémi Vegyipari Egyetem,
"Hungarian Journal of Industrial Chemistry" Editorial Board:
H — 8201 Veszprém, Schönherz Z. u. 10. Hungary.

CONTENTS

BAKHVALOVA, V.P.: see GARTSMAN, A.N.

BÁTHORY, J.: see Mrs. MARKÓ-MONOSTORY, B.

BENKŐ, B. and MARTON Gy.: Examination of a Baffle Plate--Type Tubular Reactor II. 157

BENKŐ, B.: see LÁSZLÓ, A.

BERKES, R., UJHIDY, A. und KOVÁCS, S.: Verlängerung der Verweilzeit in Rotationsdünnschichtapparaten. (The Extension of Residence Time in Rotary Thin Film Reactors) ... 171

BHAT, G.N.: see SINGH, B. and OLBRICH, W.O.

BLICKLE, T.: see GYENIS, J. and KISS, Z.

BOSCHÁN, P., FÜLÖP, J., SEITZ, K. und VAJDA, T.: Untersuchungen über die Zusammenhänge des Durchschnittswertes von den die chemischen Transportprozesse beschreibenden Potentialfunktionen. (The Examination of the Relations Existing Among the Mean Values of Potential Functions which Describe the Chemical Transport Processes) 537

Mrs. CSÁSZÁR, E.: see DÉVAY, J. and GÁRDOS, Gy.

CSIKÓS, Cs.: see Mrs. MARKÓ-MONOSTORY, B.

CSUKÁS, B.: see Mrs. FILKA, J. and ORMÓS, Z.

DÉVAY, J., RATKOVICS, F., SZEILER, B., Mrs. CSÁSZÁR, E. and DOMONKOS, L.: Problems Related to the Long-Term Operation of Copper-Lye Carbon Monoxide Removal Units in Ammonia Plants 51

DÉVAY, J., KOVÁCS, L., HORKAY, F. und MÉSZÁROS, L.: Untersuchungen der Alterung von Lacken auf Polyurethan-Basis auf Grund dielektrischer Relaxationserscheinungen. (The Examination of the Ageing of Polyurethane Varnish based on the Dielectric Relaxation Phenomena) 71

DÉVAY, J.: see GARAI, T.

DOMONKOS, L.: see DÉVAY, J.

Mrs. FILKA, J., ORMÓS, Z. and CSUKÁS, B.: Studies on the Flow Dynamic Characteristics of the Flotation Technique 617

FRATZSCHER, W., HEBECKER, D. und HONSCHA, J.: Energetische Eigenschaften plasmabildender Gase der Tieftemperatur--Plasmatechnik. (The Energetic Properties of Plasma Forming Gases in the Low Temperature Plasme Technique) . 115

FÜLÖP, J., MONOSTORI, E., NÉMETH, G. und VAJDA, T.: Theoretische Untersuchung des Auswaschungsmechanismus von salzhaltigen Filterschlammschichten. (Theoretical Examination of the Washing Mechanism of Filter Cakes) 527

FÜLÖP, J.: see BOSCHÁN, P.

GARAI, T., RÓNAY, D. and DÉVAY, J.: The Possibility of Applying Aluminium Alloys as Sacrifical Anodes in Cathodic Protection 603

GÁRDOS, Gy., KUN SZABÓ, T., PÉCHY, L. and RÉDEY, Á.: Catalytic Dehydrogenation of Tetrahydrothiophene II. 309

GÁRDOS, Gy., PÉCHY, L., RÉDEY, Á. and Mrs. CSÁSZÁR, E.: Investigations on the Decarbonylation of Furfural over Metal-Oxide Catalysts in the Presence of Steam 577

GÁRDOS, Gy., PÉCHY, L., Mrs. CSÁSZÁR, E. and Mrs. SZIGETI, B.: Investigation of Furan Production from Furfural over Noble Metal Catalysts 589

GARTSMAN, A.N., IERMAKOVA, A., BAKHVALOVA, V.P., RASSADNIKOVA, N.I.: The Mass Transfer Accompanied by Chemical Reaction in a Gas-Liquid-Solid Catalyst Three Phase System (Russian) 37

GREGA, J.: see MÉSZÁROS, L.

GYENIS, J. and BLICKLE, T.: Determination of the Axial Dispersion Coefficient in System of Inhomogeneous Mixing ... 251

GYENIS, J. and BLICKLE, T.: Diaphragm Crystallizer, Simultaneously Transmitting Heat and Momentum 265

GYENIS, J. and BLICKLE, T.: The Application of Pulsating Diaphragm-Type Crystallizer in Solvent Dewaxing 289

HEBECKER, D.: see FRATZSCHER, W.

HONSCHA, J.: see FRATZSCHER, W.

HORKAY, F.: see DÉVAY, J.

HORVÁTH, A.: see ILLÉS, V.

HORVÁTH, G.: An Experiment for the Determination of the Degree of Mixing of a Suspension 467

HORVÁTH, G.: see SZOLCSÁNYI, P.

IERMAKOVA, A.: see GARTSMAN, A.N.

ILLÉS, V. und HORVÁTH, A.: Kinetisch-mathematisches Modell der Benzinpyrolyse I. Zersetzungsgeschwindigkeitsgleichung kinetisches Modell. (The Kinetic Model of Naphtha Steam Cracking I. The Rate Equation of Decomposition, the Kinetic Model) 369

ILLÉS, V. und HORVÁTH, A.: Kinetisch-mathematisches Modell der Benzinpyrolyse II. Produktverteilung, Ausbeutekurven, kinetisch-mathematisches Modell. (The Kinetic Model of Naphtha Steam Cracking II. Production Distribution, Yield Curves, the Mathematics of the Kinetic Model) ... 391

IMJANITOW, N.S.: Azidität von Matellcarbonyllösungen. Beziehung zwischen der Azidität und katalytischen Aktivität. (The Acidity of Metal Carbonyl Solutions. The Relation between the Acidity and Catalytic Activity) 331

de JONGE, J.: The Reaction between Sodium Amalgam and Ethyl Alcohol 497

KARDOS, J.: see VONDRAN, J.

KASAMANYAN, M.A.: see KIRILLOV, V.A.

KIRILLOV, V.A., KASAMANYAN, M.A.: The Investigation of Mass Transfer Taking Place between the Packing and Liquid in a Three Phase Static Bed Reactor (Russian) 21

KISS, Z., BLICKLE, T. and UJHIDY, A.: Data Concerning the Calculation of Kinetic Constants Characteristic of Reaction Rates in Heterogeneous Catalytic Hydrogenation Dehalogenation 429

KOVÁCS, L.: see DÉVAY, J.

KOVÁCS, S.: see BERKES, R.

KREIDL, J.: see LÁSZLÓ, A.

KUMAR, R.N.: see SINGH, B.

KUN SZABÓ, T.: see GÁRDOS, Gy.

LÁSZLÓ, A., BENKŐ, B., STEFKÓ, B. and KREIDL, J.: Examination of a Baffle Plate Type Tubular Reactor I. 141

LÁSZLÓ, A.: Generalization and Classification of the Coefficients of Transport Processes 647

MAGYAR, M.: see TUREK, F.

Mrs. MARKÓ-MONOSTORY, B., CSIKÓS, Cs. and BÁTHORY, J.: Dehydrogenation of Normal Hexane on a Modified Platinum Catalyst 357

MARTON, Gy.: Studies on the Optimum Operation Mode of a Two-Phase Extraction-Coupled Reactor Cascade 663

MARTON, Gy.: Determination of the Quasi-Optimum Operation Mode of a Two-Phase, Extraction-Coupled Reactor 677

MARTON, Gy.: see BENKŐ, B.

MÉSZÁROS, I.: The Role of Natural Inhibitors in Thermal Degradation of Polymethacrylate Additives 549

MÉSZÁROS, L.: Prüfung von Fragen der Sicherheits-, Zuverlässigkeit- und Risiko-Optimierung bei Gross-Systemen der Chemischen Industrie. (The Problems of Security, Reliability and Risk Optimization of Large-Sized Systems in the Chemical Industry) 79

MÉSZÁROS, L.: see DÉVAY, J.

MÉSZÁROS, L., Mrs. SZABÓ, M., GREGA, J. and TASI, L.: Agitators Built Up of New Elements and the Application Thereof .. 689

MOHILLA, R.: A Rapid Method for Checking the Validity and for Determining the Parameters of a Piston-Flow-Dispersed Tubular Model 459

MONOSTORI, E.: see FÜLÖP, J.

NÉMETH, G.: see FÜLÖP, J.

OLBRICH, W.O. and BHAT, G.N.: Evaluation of Temperatur Profile in a Gas-Solid Reacting Fixed Bed at Constant Wall Temperature 519

ORMÓS, Z., CSUKÁS, B. and PATAKI, K.: Studies on Granulation in Fluidized Bed V. Study on the Particle Size Distribution of Granulates 193

ORMÓS, Z., CSUKÁS, B. and PATAKI, K.: Studies on Granulation in Fluidized Bed VI. Granulation in Mechanically Agitated Fluidized Bed 631

ORMÓS, Z.: see Mrs. FILKA, J.

PALÁNCZ, B.: Controllability Tests on a Flowthrough Drying Process with Linearization of the Distributive Model .. 127

PATAKI, K.: see ORMÓS, Z.

PÉCHY, L.: see GÁRDOS, Gy.

Mrs. RAŅOGAJEC-KOMOR, M.: see VÉRTES, A.

RASSADNIKOVA, N.I.: see GARTSMAN, A.N.

RATKOVICS, F.: see DÉVAY, J.

RÉDEY, Á.: see GÁRDOS, Gy.

RÓNAY, D.: see GARAI, T.

SEITZ, K.: see BOSCHÁN, P.

SINGH, B., KUMAR, R.N. and BHAT, G.N.: Kinetics of Vapour Phase Synthesis of Vinylacetate 411

SMIRNOV, N.N.: The Mathematical Models of Ion Exchange Processes (Russian) 1

SPEIER, G.: Kinetics and Mechanism of the Dimerization of Ethylene Using $[Co(C_2H_4)(PPh_3)_3]_2$ as Catalyst 449

STEFKÓ, B.: see LÁSZLÓ, A.

Mrs. SZABÓ, M.: see MÉSZÁROS, L.

SZEILER, B.: see DÉVAY, J.

Mrs. SZIGETI, B.: see GÁRDOS, Gy.

SZOLCSÁNYI, P. and HORVÁTH, G.: Power Requirement of the Intensification of Stirring 489

TAMÁS, F. and VÁRADI, T.: Role of Poly-Reactions in the Hydration of Cement 347

TAMÁS, F.: see VÉRTES, A.

TASI, L.: see MÉSZÁROS, L.

TŐRÖS, R.: Generalization of the Entropy of Mixing II. 227

TUREK, F. und MAGYAR, M.: Eine vereinfachte Methode zur Ermittlung des Stoffüberganges in Blasensäulen. (A Simple Method to Ascertain the Mass Transfer in Bubble Cap Plate Columns) 557

UJHIDY, A.: see BERKES, R. and KISS, Z.

VAJDA, T.: Berechnung der Verweilzeitverteilung in Fliessbettapparaten auf Grund eines Rezirkulationsmodells. (The Calculation of Residence Time Distribution in Fluidized Bed Reactors Based on a Recycling Model) 91

VAJDA, T. and VIRÁG, T.: Theoretical Examination of the Operation of Spray Driers 217

VAJDA, T.: see BOSCHÁN, P. and FÜLÖP, J.

VÁRADI, T.: see TAMÁS, F.

VÉRTES, A., Mrs. RANOGAJEC-KOMOR, M. and TAMÁS, F.: Brownmillerite Hydration by Mössbauer Spectrometry 339

VIRÁG, T.: see VAJDA, T.

VONDRAN, J. and KARDOS, J.: Bestimmung der Verfügbarkeit einer kapazitätsgeteilten Parallelschaltung mit interner Kapazitätsreserve. (Determination of Applicability of a Parallel Connection Consisting of More Capacity Units and Having Inner Capacity Reserves) 565

СОДЕРЖАНИЕ

БАТ, Г.Н.: см. СИНГ, Б. и ОЛБРИХ, В.О.

БАТОРИ, Й.: см. МАРКО-МОНОШТОРИ, Б.

БАХВАЛОВА, В.П.: см. ГАРЦМАН, А.Н.

БЕНКО, Б. и МАРТОН, Дь.: Изучение реактора-трубы с направляющими пластинками 157

БЕНКО, Б.: см. ЛАСЛО, А.

БЕРКЕШ, Р., УЙХИДЫ, А. и КОВАЧ, Ш.: Повышение среднего времени пребывания в ротационных пленочных аппаратах 171

БЛИКЛЕ, Т.: см. ДЕНИШ, Я. и КИШШ, З.

БОШАН, П., ФЮЛЕП, Я., СЕЙЦ, К. и ВАЙДА, Т.: Испытания соотношений связанных со средним значением потенциальной функции, описывающей транспортные процессы химической промышленности . 537

ВАЙДА, Т.: Расчет распределения времени нахождения в гейзеровом аппарате на основе рециркуляционной модели 91

ВАЙДА, Т. и ВИРАГ, Т.: Теоретическое исследование процессов работы распылительных сушильных установок 217

ВАЙДА, Т.: см. ФЮЛЕП, Я. и БОШАН, П.

ВАРАДЫ, Т.: см. ТАМАШ, Ф.

ВЕРТЕШ, А., РАНОГАЕЦ-КОМОР, М. и ТАМАШ, Ф.: Изучение гидратации браунмиллерита при помощи Месбауеровской спектроскопии . . 339

ВИРАГ, Т.: см. ВАЙДА, Т.

ВОНДРАН, Й. и КАРДОШ, И.: Определение применяемости параллельного соединения с деленной емкостью и внутренним запасом емкости 565

ГАРАИ, Т., РОНАИ, Д. и ДЕВАИ, Й.: Возможности применения алюминиевых сплавов в протекторной защите от коррозии 603

ГАРДОШ, Дь., КУН САБО, Т., ПЕЧИ, Л. и РЕДЕИ, А.: Каталитическая дегидрогенизация тетрагидротиофена в тиофен II. 309

ГАРДОШ, Дь., ПЕЧИ, Л., РЕДЕИ, А. и ЧАСАР, Э.: Изучение декарбонилирования фурфурола в присутствии водяного пара на окисле металла, применимом в качестве катализатора 577

ГАРДОШ, Дь., ПЕЧИ, Л., ЧАСАР, Э. и СИГЕТИ, Б.: Изучение получения фурана из фурфурола на катализаторе из благородного металла 589

ГАРЦМАН, А.Н., ЕРМАКОВА, А., БАХВАЛОВА, В.А. и РАССАДНИКОВА, Н.И.: Массоперенос с химической реакцией в трехфазной системе газ-жидкость-твердый катализатор 37

ГРЕГА, Й.: см. МЕСАРОШ, Л.

ДЕВАИ, Й., РАТКОВИЧ, Ф., СЕЙЛЕР, Б., ЧАСАР, Э. и ДОМОНКОШ, Л.: Проблемы постоянной работы башни для очистки окиси углерода медно-аммиачным раствором, на заводе синтеза аммиака . . 51

ДЕВАИ, Й., КОВАЧ, Л., ХОРКАИ, Ф. и МЕСАРОШ, Л.: Изучение старения полиуретановых лаков на основе явлений диэлектрической релаксации 71

ДЕВАИ, Й.: см. ГАРАИ, Т.

ДЕНИШ, Я. и БЛИКЛЕ, Т.: Определение коэффициента осевого перемешивания в системах неоднородного смешивания 251

ДЕНИШ, Я. и БЛИКЛЕ, Т.: Установка для кристаллизации с перегородкой пропускающей и импульс и теплоту 265

ДЕНИШ, Я. и БЛИКЛЕ, Т.: Применение пульсационной установки кристаллизации с перегородкой для удаления парафинов с помощью растворителя 289

ДОМОНКОШ, Л.: см. ДЕВАИ; Й.

ДЭ ЙОНГЕ, Я.: Реакция между амальгамой натрия и этиловым спиртом 497

ЕРМАКОВА, А.: см. ГАРЦМАН, А. Н.

ИЛЛЕШ, В. и ХОРВАТ, А.: Кинетическая математическая модель пиролиза бензина I. Уравнение скорости разложения, кинетическая модель 369

ИЛЛЕШ, В. и ХОРВАТ, А.: Кинетическая математическая модель пиролиза бензина II. Распределение продуктов, кривые выхода, кинетическая математическая модель 391

ИМЯНИТОВ, Н. С.: Определение кислотности растворов карбонилов металлов при повышенных температурах и давлениях. Соотношение между кислотностью и каталитической активностью . . 331

КАРДОШ, И.: см. ВОНДРАН, Й.

КАСАМАНЯН, М. А.: см. КИРИЛЛОВ, В. А.

КИРИЛЛОВ, В. А. и КАСАМАНЯН, М. А.: Исследование процессов массообмена между жидкостью и насадкой в трехфазном неподвижном слое 21

КИШШ, З., БЛИКЛЕ, Т. и УЙХИДЫ, А.: Данные к вычислению кинетических констант, характерных для скорости реакции при гетерогенной каталитической дегидрогенизации с дегалогенизацией 429

КОВАЧ, Л.: см. ДЕВАИ, Й.

КОВАЧ, Ш.: см. БЕРКЕШ, Р.

КРЕИДЛ, Й.: см. ЛАСЛО, А.

КУМАР, Р. Н.: см. СИНГ, Б.

КУН САБО, Т.: см. ГАРДОШ, Дь.

ЛАСЛО, А., БЕНКО, Б., ШТЕФКО, Б. и КРЕИДЛ, Й.: Изучение реактора-трубы с направляющими пластинками I. 141

ЛАСЛО, А.: Обобщение и систематизация коэффициентов транспортных процессов 647

МАДЯР, М.: см. ТУРЕК, Ф.

МАРКО-МОНОШТОРИ, Б., ЧИКОШ, Ч. и БАТОРИ, Й.: Дегидрогенизация н-гексана с применением модифицированного платинового катализатора 357

МАРТОН, Дь.: Изучение оптимального режима двухфазного реактора-каскада, комбинированного с экстракцией 663

МАРТОН, Дь.: Изучение квазиоптимального режима двухфазного реактора-каскада, комбинированного с экстракцией 677

МАРТОН, Дь.: см. БЕНКО, Б.

МЕСАРОШ, И.: Роль природных ингибиторов в термической деградации добавок полиметакрилатного типа 549

МЕСАРОШ, Л.: Изучение вопросов оптимальной безопасности, надежности и риска в химических системах 79

МЕСАРОШ, Л., САБО, М., ГРЕГА, Й. и ТАШИ, Л.: Мешалки, построенные из новых элементов, и их применение 689

МЕСАРОШ, Л.: см. ДЕВАИ, Й.

МОНОШТОРИ, Э.: см. ФЮЛЕП, Я.

МОХИЛЛА, Р.: Быстрый метод для проверки правильности дисперсионной трубчатой модели идеального вытеснения и для определения ее параметров 459

НЕМЕТ, Г.: см. ФЮЛЕП, Я.

ОЛБРИХ, В. О. и БАТ, Г. Н.: Определение распределения температуры в реакторе с неподвижным слоем псевдоожиженного материала и с постоянной температурой стены 519

ОРМОШ, З., ЧУКАШ, Б. и ПАТАКИ, К.: Изучение грануляции в псевдоожиженном слое V. Исследование распределения расмеров зерен в продуктах грануляции 193

ОРМОШ, З., ЧУКАШ, Б. и ПАТАКИ, К.: Изучение грануляции в псевдоожиженном слое VI. Грануляция в механически смешанном псевдоожиженном слое 631

ОРМОШ, З.: см. ФИЛКА, Й.

ПАЛАНЦ, Б.: Исследование управляемости процесса проточной сушки с помощью приведения дистрибутивной модели к линейному виду 127

ПАТАКИ, К.: см. ОРМОШ, З.

ПЕЧИ, Л.: см. ГАРДОШ, Дь.

РАНОГАЕЦ-КОМОР, М.: см. ВЕРТЕШ, А.

РАССАДНИКОВА, Н. И.: см. ГАРЦМАН, А. Н.

РАТКОВИЧ, Ф.: см. ДЕВАИ, Й.

РЕДЕИ, А.: см. ГАРДОШ, Дь.

РОНАИ, Д.: см. ГАРАИ, Т.

САБО, М.: см. МЕСАРОШ, Л.

СЕЙЛЕР, Б.: см. ДЕВАИ, Й.

СЕЙЦ, К.: см. БОШАН, П.

СИГЕТИ, Б.: см. ГАРДОШ, Дь.

СИНГ, Б., КУМАР, Р. Н. и БАТ, Г. Н.: Кинетика синтеза винилацетата в паровой фазе 411

СМИРНОВ, Н. Н.: Математические модели процесса ионного обмена 1

СОЛЧАНИ, П. и ХОРВАТ, Г.: Потребляемая мощность интенсификации перемешивания 489

ТАМАШ, Ф. и ВАРАДЫ, Т.: Роль полимеризационных реакций в гидратации цемента 347

ТАМАШ, Ф.: см. ВЕРТЕШ, А.

ТАШИ, Л.: см. МЕСАРОШ, Л.

ТЭРЭШ, Р.: Обобщение понятия энтропии смешивания II. 227

ТУРЕК, Ф. и МАДЯР, М.: Упрощенный метод оценки массопередачи в реакторе продувного типа 557

УЙХИДЫ, А.: см. БЕРКЕШ, Р. и КИШШ, З.

ФИЛКА, Ю., ОРМОШ, З. и ЧУКАШ, Б.: Изучение аэродинамических условий способа взвешивания 617

ФРАТЧЕР, В., ХЕБЕКЕР, Д. и ХОНША, Й.: Энергетические свойства плазмообразующих газов низкотемпературной плазмотехники . 115

ФЮЛЕП, Я., МОНОШТОРИ, Э., НЕМЕТ, Г. и ВАЙДА, Т.: Теоретическое испытание механизма промывания слоя фильтрующегося отжатого осадка, содержащего соль 527

ФЮЛЕП, Я.: см. БОШАН, П.

ХЕБЕКЕР, Д.: см. ФРАТЧЕР, В.

ХОНША, Й.: см. ФРАТЧЕР, В.

ХОРВАТ, А.: см. ИЛЛЕШ, В.

ХОРВАТ, Г.: Испытание на определение смешанности суспензии . . . 467

ХОРВАТ, Г.: см. СОЛЧАНИ, П.

ХОРКАИ, Ф.: см. ДЕВАИ, Й.

ЧАСАР, Э.: см. ДЕВАИ, Й. и ГАРДОШ, Дь.

ЧИКОШ, Ч.: см. МАРКО-МОНОШТОРИ, Б.

ЧУКАШ, Б.: см. ОРМОШ, З. и ФИЛКА, Ю.

ШПЕЙЕР, Г.: Кинетика и механизм димеризации этилена с применением $[Co(C_2H_4)(PPh_3)_3]_2$ в качестве катализатора 449

ШТЕФКО, Б.: см. ЛАСЛО, А.

Hungarian Journal
of Industrial Chemistry
Veszprém
Vol. 3. pp. 1-20 (1975)

МАТЕМАТИЧЕСКИЕ МОДЕЛИ ПРОЦЕССА ИОННОГО ОБМЕНА

Н.Н.Смирнов

(Ленинградский технологический институт им.Ленсовета,
Кафедра процессов и аппаратов химической технологии)

Поступила в редакцию 7 января 1974 г.

Процессы, основанные на ионном обмене, играют все более важную роль в современных технологиях. Математическое моделирование единиц таких процессов, решение модели и выведение важных для практики результатов (оптимизация) являются важными инженерными задачами. Автор излагает и систематизирует известные типы моделей. Изученные модели относятся к следующим типам аппаратов:

- непрерывный ионный обмен в колонне с неподвижным слоем
- непрерывный ионный обмен в смешанном реакторе котельного типа в случае смоляной суспенсии
- полунепрерывный ионный обмен в смешанном реакторе котельного типа в случае смоляной суспенсии.

Одной из основных задач современного развития химической науки и техники является разработка и внедрение в практику новых методов анализа и расчета типовых процессов и аппаратов химической технологии с широким использованием средств вычислительной техники.

В настоящее время к числу таких процессов могут быть отнесены и процессы ионного обмена, которые получают все более широкое распространение и приобретают важное значение во многих отраслях производства, например, химическая, атомная, пищевая, медицинская, гидрометаллургическая промышленности, опреснение и очистка воды, удаление из организма токсических веществ, консервирование крови и т.д.

Сложность физико-химических превращений, протекающих в гетерогенной системе жидкость - твердое тело (ионообменная смола), требует совместного рассмотрения факторов, определяющих гидродинамический режим и массообмен в системе, а также собственно химическую кинетику.

В общем виде задача математического описания процесса ионного обмена, протекающего в изотермических условиях, может быть сформулирована в виде следующей системы дифференциальных уравнений [1,2,3,4].

Уравнение материального баланса процесса для жидкой фазы

$$\frac{\partial c}{\partial \tau} = - \operatorname{div} \Phi_{диф.} - \operatorname{div}(c,V) + \Phi_{хим.}$$

Уравнение статики процесса

$$\bar{c} = \varphi(c_1,\ldots c_n)$$

Уравнение кинетики процесса

$$\frac{\partial c}{\partial \tau} = f(c_1,\ldots c_n,\bar{c}_1,\ldots \bar{c}_n,d_3,w,\ldots)$$

Уравнение движения жидкой фазы

$$\rho\frac{Dw}{\partial \tau} = -\nabla p + \bar{F} + \mu\nabla\bar{w} + (\xi+\frac{\mu}{3})\nabla \operatorname{div} \bar{w}$$

Уравнение неразрывности потока

$$\frac{\partial \rho}{\partial \tau} + \operatorname{div}(\rho,\bar{w}) = 0$$

Эта система уравнений должна быть дополнена начальными и граничными условиями, которые определяют распределение равновесных и текущих концентраций во времени и в пространстве, а также их значения

на границе раздела взаимодействующих фаз. Однако даже при полном задании граничных и начальных условий решение задачи в обшем виде требует еще конкретизации функций φ и f, которые очень часто не удается представить в явном виде.

Таким образом, полная система математических уравнений, описывающих процесс ионного обмена, является очень сложной и в обшем случае не имеет аналитического решения. Даже при рассмотрении отдельных, частных задач ионного обмена в большинстве случаев необходимо применение теории подобия или электронно-вычислительных машин. Вследствие этого до настоящего времени почти отсутствуют обобщенные методы инженерного расчета и моделирования ионообмен - ных процессов, в частности, с использованием средств вычислительном техники. При этом глубокое знание кинетических закономерностей процесса ионного обмена должно являться основой его расчета и моделирования.

Настоящая работа посвящена разработке инженерных методов расчета и моделирования процесса ионного обмена преимущественно на основе математического описания кинетики процесса в условиях внешней и смешанной диффузии с использованием электронных вычислительных машин.

Непрерывный процесс в колонном аппарате вытеснения с неподвижным слоем ионообменной смоль [5,6,7,8]

Для составления математической модели, описывающей процесс физико-химического превращения вещества в неподвижном слое ионообменной смолы, предварительно аналитически исследуется математическое описание ионного обмена на одном зерне. В основу этого описания была положена физическая модель, которая предполагает

наличие тонкой диффузионной пленки на границе раздела фаз: зерно ионообменной смолы - раствор. В случае, когда скорость процесса лимитируется диффузией ионов в пленке, диффузионный поток вытесняющих ионов через жидкую пленку, окружающую зерно, равен:

$$dI = 4\pi r_o^2 D' \frac{c(n_o - n_e)}{\delta} d\tau \qquad (1)$$

Количество вытесняющих ионов в частицу ионита за время $d\tau$ соответствует изменению их содержания в самой частице, т.е.

$$dI = \frac{4\pi r_o^3}{3} a dN \qquad (2)$$

Приравнивая диффузионные потоки на основании электронейтральности раствора, получим исходное дифференциальное уравнение, описывающее кинетику процесса на одном зерне

$$\frac{dN}{d\tau} = \frac{3D'c}{\delta r_o a}(n_o - n_e) \qquad (3)$$

Для рещения уравнения (3) необходимо выразить n через мольную долю поглощаемого иона в зерне ионита. Если для изотопного обмена, для которого константа равновесия равна I, а также для случая обмена равновалентных ионов, когда $n = \frac{N}{K_c - (K_c - 1)N}$ при ряде допущений найдены решения уравнения (3), то для случая обмена разновалентных ионов аналитического решения (3) в общем виде не получено.

Используя основные характеристики равновесного состояния: кажущуюся константу равновесия обмена и коэффициент разделения, определяющий селективность поглощения одних ионов по сравнению с другими и зависящий от эквивалентной доли поглощаемого компонента в ионите и в растворе, можно аналитически получить зависимость $R = f(N)$, которая для обмена $Me^{2+} - H^+$ будет иметь следующий вид

$$R = \sqrt{AN + \left[\frac{A(1-N)}{2}\right]^2} + \frac{A(1-N)}{2} \qquad (4)$$

При концентрации раствора менее 0,05 $\frac{\text{мг-экв}}{\text{мл}}$, что является одним из условий внешней диффузии и $N \leq 0,9$, функциональная зависимость $R = f(N)$ может быть записана в виде:

$$R = A(1-N) \tag{5}$$

На основании определения коэффициента разделения и уравнения (5) величина мольной доли поглощаемого компонента на границе пленка-зерно может быть выражена следующим уравнением:

$$n_e = \frac{N}{A(1-N)-A(1-N)N+N} \tag{6}$$

Интегрируя уравнение (3) при найденном значении мольной доли компонента на границе пленка - зерно ($N = 0$ при $\tau = 0$), получаем кинетическое уравнение, описывающее процесс на одном зерне в условиях пленочной диффузии:

$$K\tau = A_1\left(\frac{1}{1-N}\right) + A_2\left[\frac{1}{1-N} + \ln(1-N)\right] +$$

$$+ A_3\left[\frac{1}{1-N} + 2\ln(1-N) - (1-N)\right] + C \tag{7}$$

где $A_1 = \frac{1}{n_o}$; $A_2 = \frac{1-2A}{n_o A}$; $A_3 = \frac{1}{n_o}$; $C = \frac{A-1}{n_o A}$

Коэффициент $K = \frac{3D'c}{\delta r_o a}$ является сложной кинетической характеристикой процесса и зависит от гидродинамических, концентрационных, физико-химических свойств системы, поскольку $\delta = f(w,c)$; $D' = f(c,n_o)$, а величина a характеризует свойства ионообменной смолы. По своему физическому смыслу коэффициент K может быть назван удельной производительностью реактора (ионообменника), а само произведение $K\tau$ является мерой выражения эффективности его работы.

Предложенная кинетическая модель может быть развита с учетом влияния внутренней диффузии на общую скорость процесса при введении в уравнение (7) вместо δ=const величины эквивалентной толщины пленки δ_e. В этом случае, принимая послойный характер физико-химического превращения в зерне, кинетическое уравнение примет вид:

$$K d\tau = \frac{[A+(1-2A)N+AN^2](1+\alpha-\alpha\sqrt[3]{1-N})}{n_o A-2n_o AN+n_o AN^2}dN \qquad (8)$$

При изменении концентрации раствора в пределах $0 \le C \le 1.10^{-2}$ $\frac{\text{мг-экв}}{\text{мл}}$ численное значение коэффициента $A \ge 100$ и, следовательно, уравнение (8) можно записать в форме:

$$K n_o d\tau = (1+\alpha-\alpha\sqrt[3]{1-N})dN \qquad (9)$$

Величина коэффициента α зависит от приведенных коэффициентов диффузии в жидкой пленке и в зерне смолы. Таким образом, оказалось возможным количественно выразить влияние внутридиффузионной составляющей для случая, когда лимитирующей стадией процесса является внешнедиффузионная кинетика.

Однако для инженерного расчета необходимо знать функциональную зависимость $K=f(w,c,r_o)$, которая имеет следующий вид:

$$K_{n_o=1} = bc\sqrt{w} \qquad (10)$$

Величина коэффициента b зависит от радиуса зерна ионита и природы обменивающихся ионов.

Так как весь слой ионообменной смолы состоит из элементарных неравновесных слоев, то математическое описание процесса следует дополнить функцией $K=f(n_o)$, которую можно выразить в следующей форме:

$$K = K_{n_o=1} \cdot n_o^d \qquad (11)$$

Тогда окончательно K будет равно:

$$K = bc\sqrt{w} \cdot n_{o_{m_i}}^d \qquad (12)$$

Величину мольной доли в растворе ($n_{o_{m_i}}$), поступающего на m_i слой, можно найти из уравнения материального баланса для m_{i-1} слоя, которое имеет вид:

$$n_{o_{m_i}} = n_{o_{m_{i-1}}} - \frac{\Delta N}{\Delta \tau}\beta, \text{ где } \beta = \frac{4av}{\pi D_a wc} \qquad (13)$$

Таким образом, описание математической модели процесса физико - химического превращения вещества в неподвижном слое ионообменной смолы в условиях гидродинамического режима вытеснения, пленочной, диффузионной и частично смешанной кинетики можно выразить системой [7], [8], [12] и [13].

Предложенная система уравнений при заданных исходных технологических условиях проведения прочесса $c, w, D_a, n_{o_{m_i}}, H_{сл}$ и т. д. позволяет рассчитать удельную производительность реактора (K) и кинетическую кривую $n_o = f(\tau)$, которая является основой для расчета реактора (ионообменника).

Непрерывный процесс в аппарате смешения с суспендированным слоем ионообменной смолы [9,10,11]

Ионный обмен между движущейся сферической частицей смолы и турбулентным потоком жидкости, содержащей поглощаемый компонент,

должен подчиняться общим закономерностям кинетики гетерогенных процессов, причем собственно химическая реакция протекает только в одной фазе - ионите. В этих условиях особое значение приобретают процессы переноса вещества между твердой частицей ионита и турбулентным потоком жидкости. Следовательно, при рассмотрении кинетики ионного обмена, в общем случае, должны быть учтены как процесс переноса поглощаемого вещества через пограничный слой от ядра потока к поверхности частицы, так и перенос вещества внутри частицы. Внутри твердой частицы ($0 \le r \le r_o$) процесс переноса вещества с учетом химической реакции может быть описан дифференциальным уравнением вида:

$$\frac{\partial \bar{c}}{\partial \tau} = \bar{D}'\left(\frac{\partial^2 \bar{c}}{\partial r^2} + \frac{2}{r}\frac{\partial \bar{c}}{\partial r}\right) - k\bar{c} \qquad (14)$$

В нем величина k учитывает химическую активность ионообменной смолы по отношению к поглощаемому компоненту, указывая на химическую связы между ними, что, очевидно, будет эквивалентно изменению количества вещества, равному $k\bar{c}$. Рассматривая зерно ионита, как молекулярную модель, можно считать, что коэффициент k по своему физическому смыслу должен характеризовать также физико-химические свойства обменивающихся ионов, учитывать конфигурацию матрицы, количество активных групп, участвующих в образовании ионных пар, и т.д.

Перенос вещества через пленку жидкости, окружающую частицу , носит сложный характер, так как эта пленка состоит из нескольких слоев с различным характером течения. Если ввести коэффициент турбулентной диффузии, то перенос вещества через пленку может быть описан дифференциальным уравнением вида:

$$\frac{\partial c_e}{\partial \tau} = D_e'\left(\frac{\partial^2 c_e}{\partial r^2} + \frac{2}{r}\frac{\partial c_e}{\partial r}\right) \qquad (15)$$

Таким образом, кинетика процесса на одиночной частице ионита

радиуса r_o, окруженной приведенной пленкой жидкости толщиной δ, может быть описана следующим обобщенным дифференциальным уравнением с разрывными физико-химическими коэффициентами:

$$\frac{\partial c}{\partial \tau} = D'_{(r)} \left(\frac{\partial^2 c}{\partial r^2} + \frac{2}{r}\frac{\partial c}{\partial r}\right) - k_{(r)}c \qquad (16)$$

$$D'_{(r)} = \begin{cases} \bar{D}' & \text{при} \quad 0 \le r \le r_o \\ D'_e & \text{при} \quad r_o < r \le r_o+\delta \end{cases}$$

$$k_{(r)} = \begin{cases} k & \text{при} \quad 0 \le r \le r_o \\ 0 & \text{при} \quad r_o < r \le r_o+\delta \end{cases}$$

При составлении математического описания кинетику процесса было принято, что на внешней поверхности приведенной пленки концентрация поглощаемого вещества должна быть равна концентрации поглощаемого вещества в потоке

$$c_e(r_o+\delta,\tau) = c_o \qquad (17)$$

а на границе раздела фаз (поверхность частицы) должны выполняться условия

$$\bar{c}(r_o,\tau) = k_c c_e(r_o,\tau) \qquad (18)$$

$$\frac{k_D,\partial \bar{c}(r_o,\tau)}{\partial z} = \frac{\partial c_e(r_o,\tau)}{\partial r} \qquad (19)$$

Первое условие (18) отражает скачок концентраций, который в общем случае наблюдается на границе раздела фаз при равновесии. Условие (19) представляет равенство потоков вещества из приведенной пленки и потока вещества в глубь частицы: коэффициент k_D, при этом имеет вид:

$$k_{D'} = \frac{\bar{D}'}{D'_e}$$

Условия (18) и (19) должны быть дополнены начальным условием

$$\begin{aligned} \bar{c}(r,0) &= 0 \\ c_e(r,0) &= 0 \end{aligned} \qquad (20)$$

и условием симметрии в центре сферической частицы

$$\frac{\partial \bar{c}(0,\tau)}{\partial z} = 0 \qquad (21)$$

Уравнения (14) - (16) с краевыми условиями (17) - (21) были решены операционным методом, который успешно используется при решении задач по тепло- и массопереносу. При этом переход от изображений к соответствующим оригиналам распределений концентраций был осуществлен с помощью теоремы разложения. Изменение общего количества целевого компонента, поглощенного частицей ионита, во времени определяется выражением вида:

$$m_{(\tau)} = -\int_0^\tau j_D(\xi)d\xi = 4\pi r_o^2 \bar{D}' \int_0^\tau -\text{grad}\ \bar{c}(r_o,\tau)d\xi \qquad (22)$$

Произведя соответствующую подстановку в уравнение (22) выражения $\bar{c}(r_o,\tau)$ и выражения распределения концентраций и проведя соответствующие вычисления, получим следующую кинетическую зависимость, описывающую процесс ионного обмена между одиночной сферической частицей и потоком жидкости.

$$m_{(\tau)} = 8\pi c_o \bar{D}' k_c \sum_{n=1}^{\infty} \left(\frac{r_o + \delta}{\varphi_n \sin[k_D^{0,5}(k_r-1)\mu_n]} - \right.$$

$$\left. - \frac{k_n(r_o+\delta)}{\varphi_n} \cdot \frac{\cos \eta_n}{\sin \eta_n \sin[k_D^{0,5}(k_r-1)\mu_r]} \cdot \frac{\exp(S_{n,\tau})-1}{S_n} \right) \qquad (23)$$

Зависимость (23) является общей, так как из нее могут быть получены частные зависимости, описывающие смешанную и внутридиффузионную кинетику процесса ионного обмена, а также уравнение, соответствующее степени физико-химического превращения вещества в ионообменной смоле. В области внутридиффузионной кинетики уравнение (14) совпадает с уравнением (16) при краевых условиях

$$\bar{c}(r,0) = 0; \quad \bar{c}(r_o,\tau) = k_c c_o; \quad \frac{\partial \bar{c}(0,\tau)}{\partial r} = 0 \qquad (24)$$

Решение уравнения (14) совместно с краевыми условиями (24) операционным методом позволяет получить выражение для распределения концентрации (профиль концентрации) в сферической частице ионита, которое имеет вид

$$\bar{c}(r,\tau) = c_o k_c [1 + \sum_{n=1}^{\infty} 2(-1)^n \frac{r_o \sin(\frac{n\pi r}{r_o})}{r(1+\frac{kr_o^2}{\bar{D}'\pi^2 n^2})\pi n}] \cdot$$

$$\exp(-\frac{n^2\pi^2\bar{D}'}{r_o^2}\tau - k\tau) \qquad (25)$$

Далее из кинетической зависимости можно получить уравнение, по которому на основе анализа экспериментальных данных возможно рассчитать теоретически численное значение коэффициента диффузии поглощаемого компонента в зерне ионообменной смолы $\bar{D}'$ и определить его зависимость от степени физико-химического превращения вещества в ионите

$$\bar{D}' = f(\frac{m(\tau)}{m(\tau)_\infty})$$

В задачах расчета промышленных реакторов с перемешивающими устройствами для проведения процесса ионного обмена наибольший интерес представляет нахождение средних по обьему значений концентрации (в этом числе и в ионообменной смоле). Переход к интегральным характеристикам может быть осуществлен при помощи интегрирования по времени и по поверхности частицы потока поглощаемого вещества

$$\bar{c}_{(\tau)} = \int_0^{\tau} \int_{(F)} -\bar{D}' \frac{\partial \bar{c}(r_o,\tau)}{\partial r} dF d\tau \qquad (26)$$

где $\bar{c}(r_o,\tau)$ - решение уравнения (16) с граничными и начальными условиями, записанными ранее.

На основе полученных выше математических моделей кинетики процесса можно рассчитать ионный обмен в аппарате смешения непрерывного действия. Для этого необходимо дополнительно учесть случайное время пребывания каждой отдельной частицы ионита в реакционном обьеме. Осреднением значения концентрации в уравнении (26) с учетом распределения частиц ионообменной смолы по временам пребывания можно получить выражение для нахождения средней концентрации поглощаемого компонента в одиночной частице ионообменной смолы

$$\bar{c}_{cp} = \int_0^{\infty} \frac{1}{\tau_{cp}} \exp\left(-\frac{\tau}{\tau_{cp}}\right) d\tau \int_0^{\tau} \int_{(F)} -\bar{D}' \frac{\partial \bar{c}(r_o,\tau)}{\partial r} dF d\tau \qquad (27)$$

С учетом сказанного выше количество вещества, поглощенное всем суспендированным слоем ионообменной смолы, будет определяться соотношением

$$M = N_o \int_0^{\infty} m_{(\tau)} f(\tau) d\tau \qquad (28)$$

где $f(\tau)d\tau$ - плотность вероятности времени пребывания частиц ионообменной смолы в аппарате.

Средняя концентрация поглощаемого компонента в реакционном

объеме будет

$$c_{cp} = \frac{Vc_o - \bar{M}}{V}$$

При обработке экспериментальных данных по предлагаемой модели проводится сравнение между теоретической зависимостью

$$c_{cp} = \frac{Vc_o - N_o \int_0^{\infty} m_{(\tau)} f(\tau) d\tau}{V} \qquad (30)$$

и экспериментальным значением c_{cp} с использованием метода последовательных приближений.

Периодический процесс в аппарате смешения с суспендированным слоем ионообменной смолы [9,12]

Приведенные выше кинетические модели могут быть использованы и для расчета процесса ионного обмена в аппаратах (с турбулизаторами) периодического действия.

Действительно, интегральный материальный баланс по поглощаемому компоненту для аппарата периодического действия за промежуток времени от 0 до τ может быть записан в виде

$$Vc_o\tau - N_o \int_0^{\tau} \int_{(F)} -\bar{D}, \frac{\partial \bar{c}(r_o,\tau)}{\partial r} dF d\tau = Vc_{cp} \qquad (31)$$

Отсюда для c_{cp} получим

$$c_{cp} = c_o - \frac{N_o}{V} \int_0^{\tau} \int_{(F)} -\bar{D}, \frac{\partial \bar{c}(r_o,\tau)}{\partial r} dF d\tau \qquad (32)$$

Далее требуется провести сопоставление теоретических решений с результатами экспериментальных исследований. Поскольку в соотношение (32) входит кинетическая зависимость вида $m(\tau)$, которая является функцией величины c_{cp}, то для нахождения c_{cp} необходимо использовать метод последовательных приближений.

В заключение рассмотрения математических моделей процесса ионного обмена в аппаратах смешения периодического и непрерывного действия следует отметить, что для определения констант неизвестных функций математического описания процесса целесообразно использовать данные экспериментальных исследований. При этом эксперименты выявляют влияние гидродинамических (D_e',δ) и концентрационных параметров (c,N_o), а также природы вещества ($\bar{D}$;k) на общую скорость физико-химического превращения вещества на ионообменной смоле. Так, для процессов ионного обмена, проводимых в аппаратах с перемешивающими устройствами, параметры внешнедиффузионного сопротивления D_e' и δ могут быть представлены в форме зависимостей от числа Рейнольдса, как основной характеристики интенсивности турбулентных пульсаций, размеров аппарата и перемешивающего устройства, а также геометрических величин, влияющих на масштаб турбулентных, пульсаций

$$D_e' = f_1(Re,\Gamma)$$
$$\delta = f_2(Re,\Gamma) \qquad (33)$$

Полупериодический процесс в аппарате смешения с суспендированным слоем ионообменной смолы [13]

Анализ и расчет полупериодического процесса, протекающего в неустановившемся режиме, сложен и требует, прежде всего, определения массового потока взаимодействующих веществ, как функции времени. Поэтому для математического описания такого процесса целесообразно использовать вероятностные методы и построенные с их по-

мощью статистические модели.

На основе физической модели и кинетического механизма изучаемого явления, а следовательно, и характера связи величин, используемых для описания явления, была составлена общая зависимость, описывающая физико-химическую кинетику процесса.

$$y = \gamma x \exp(-zx) \tag{34}$$

где $$\gamma = \frac{z^2}{\int_0^\infty x \exp(-x)dx}$$

$$y = \frac{c_\tau}{c_{max}} = \frac{c_\tau V_a}{aV_{cm}} \quad \text{и} \quad x = \frac{\tau_{процесса}}{\tau_{контакта}}$$

В этом случае при достижении максимальной концентрации ионов водорода в потоке на выходе из реактора, что соответствует условию

$$\frac{dy}{dx} = 0; \quad x_{max} = \frac{1}{z}; \quad \tau_{max} = \frac{V_a}{zv}$$

Если $\frac{d^2y}{dx^2} = 0$, что характеризует окончание процесса ионного обмена, то $x = 2/z$ и время завершения процесса ионного обмена будет равно

$$\tau_{кон} = \frac{2V_a}{zv}$$

Зная кинетическую кривую процесса, описываемую уравнением (34), можно найти период вымывания ионов водорода из реакционного обьема, как продолжение всей кривой отклика системы.

При полном перемешивании в реакционном обьеме период вымывания соответствует уравнению

$$\frac{dy}{dx} = -\psi y$$

или $y(\tau)=y_o \exp(-\phi y)$ где $\phi=v/V_a$ и следовательно $y(x)=y_o \exp(-x)$. Значение y определяется по уравнению (34) при значении $x=2/z$. Таким образом, после приведения к одному и тому же аргументу уравнение для процесса полного вымывания ионов водорода потоком из реакционного объема принимает следующий вид:

$$y(x) = \frac{2\gamma}{z} \exp(-2-\frac{2}{z}+x) \qquad (35)$$

Полное математическое описание всей кривой физико-химической кинетики ионного обмена и вымывания в полупериодическом процессе в условиях полного перемешивания будет иметь следующий вид:

$$\begin{aligned} y(x) &= \gamma x \exp(-zx) \quad \text{при} \quad x \le \frac{2}{z} \\ y(x) &= \frac{2\gamma}{z} \exp(-2-\frac{2}{z}+x) \quad \text{при} \quad x \ge \frac{2}{z} \end{aligned} \qquad (36)$$

Коэффициенты γ и z являются зависимыми величинами от гидродинамических концентрационных и геометрических условий. Поэтому полученные расчетным путем на электронной цифровой вычислительной машине численные значения этих коэффициентов могут быть скоррелированы в зависимости от условий экспериментов.

На основе предлагаемой статистической модели можно рассчитать кинетические кривые процесса, как в одном реакторе, так и в нескольких соединенных последовательно аппаратах.

Адекватность предлагаемых математических моделей проверена на многочисленных экспериментах по ионному обмену K^+,Na^+,Mg^{2+},Ca^{2+}, Sr^{2+},Ba^{2+},Cu^{2+},Zn^{2+},Ni^{2+},Co^{2+},Cd^{2+},Fe^{3+} на катионите марки КУ-2, проведенных в широком диапазоне изменений гидродинамических, геометрических и концентрационных параметров.

На основе разработанных математических моделей физико-химической кинетики ионного обмена были предложены методы анализа и

моделирования процесса с помощью электронных вычислительных машин и составлены алгоритмы для расчета коэффициента удельной производительности ионообменных реакторов и выходных кинетических кривых.

В заключение автор выражает благадарность профессору, доктору наук Анталу Ласло, профессору доктору наук Палу Солчани, сотрудникам кафедры процессов и аппаратов химической технологии Веспремского химико-технологического института за обсуждение работы.

ОСНОВНЫЕ ОБОЗНАЧЕНИЯ

ρ плотность жидкой фазы

μ вязкость жидкой фазы

p гидростатическое давление

a динамическая емкость ионообменной смолы

c текущая концентрация компонента в жидкой фазе

c_o начальная концентрация компонента в жидкой фазе

c_e концентрация компонента в пограничном слое жидкой фазы, окружающей зерно ионообменной смолы

$\bar{c}$ концентрация компонента в ионообменной смоле

D' коэффициент диффузии компонента в жидкой фазе

D'_e эффективный коэффициент диффузии компонента в жидкой фазе

$\bar{D}'$ окружающей зерно ионообменной смолы

D_a коэффициент диффузии компонента в ионообменной смоле

r диаметр аппарата

R радиус зерна ионообменной смолы

K_c коэффициент разделения

k_c константа равновесия

k

k_c константа распределения

k константа скорости химической реакции

δ толщина жидкой пленки, окружающей зерно ионообменной смолы

N мольная доля компонента в зерне ионообменной смолы

N_o количество твердой фазы

n_o мольная доля компонента в жидкой фазе

n_e мольная доля компонента в жидкой пленке, окружающей зерно ионообменной смолы

V_a обьем аппарата

V обьем жидкой фазы

V_{cm} обьем ионообменной смолы

F внешняя поверхность зерна ионообменной смолы

τ время

w линейная скорость движения жидкой фазы

v обьемная скорость подачи жидкой фазы

m количество компонента, поглощенного зерном ионообменной смолы

M общее количество компонента, поглощенного ионообменной смолой

Re число Рейнольдса

$b, d, \alpha, \beta, \gamma, z$ коэффициенты

ЛИТЕРАТУРА

1. В.В.РАЧИНСКИЙ, Введение в общую теорию динамики сорбции и хроматографии. Наука, 1964.
2. Г.В.САМСОНОВ, Е.Б.ТРОСТЯНСКАЯ, Г.Э.ЕЛЬКИН, Ионный обмен.Наука, 1969
3. Ю.А.КОКОТОВ, В.А.ПАСЕЧНИК, Равновесие и кинетика ионного обмена. Химия, 1970.
4. А.М.КОРОЛЬКОВ, Теоретические основы ионообменной технологии. Лиесма, 1968.
5. А.И.ВОЛЖИНСКИЙ, Н.Н.СМИРНОВ, П.Г.РОМАНКОВ, ТОХТ, 3. №3, 472 1969., 6, №1, 118 (1970)
6. А.И.ВОЛЖИНСКИЙ, Н.Н.СМИРНОВ, П.Г.РОМАНКОВ, В.К.ВИКТОРОВ. ТОХТ, 4, №1, 118 (1970)
7. Н.К.ГАЛКИНА, В.Б.АРЕФЬЕВ, М.М.СЕНЯВИН, Сборник „Теория ионного обмена и хроматографии". Наука, 1968, стр. 159.
8. D.TOUDERR, Chimica e l'Industria 100, №7, 1058,(1968)
9. Б.А.КРАСИЛЬНИКОВ, И.Н.ТАГАНОВ, Н.Н.СМИРНОВ, П.Г.РОМАНКОВ, ТОХТ, 5, №2, 219 (1971)
10. В.С.ГОЛУБЕВ, Г.М.ПАНЧЕНКОВ, Сборник кинетика каталитических процессов, Химия, 1969, стр. 74.
11. K.STAMBERG, J.PROCHAZKA, Chem. listy 59, 1295 (1965).
12. Н.Н.СМИРНОВ, А.И.ВОЛЖИНСКИЙ, И.С.ПАВЛУШЕНКО, П.Г.РОМАНКОВ, ЖПХ, 43, №11 2457 (1970)
13. А.И.ВОЛЖИНСКИЙ, О.А.ГАЛКИН, Н.Н.СМИРНОВ, П.Г.РОМАНКОВ, ЖПХ, 46, №5, 982 (1973)

SUMMARY

The processes based on ion play more and more important role in up to date technologies. The mathematical modelling of such operational units, the solution of the models and the conclusion (optimalization) being important for the praxis is a significant task of an engineer. - The author summarizes and methodizes the known types of the models. The models taken into account are related to the following ion exchangers:

Continuously operated, packed column ion exchanger; continuous ion exchange in a mixed tank reactor filled with resin slurry; semi-continuous ion exchange in a mixed tank reactor filled with resin slurry.

Hungarian Journal
of Industrial Chemistry
Veszprém
Vol. 3. pp. 21-35 (1975)

ИССЛЕДОВАНИЕ ПРОЦЕССОВ МАССООБМЕНА МЕЖДУ ЖИДКОСТЬЮ И НАСАДКОЙ В ТРЕХФАЗНОМ НЕПОДВИЖНОМ СЛОЕ

Кириллов В.А., Касаманян М.А.

Институт Катализа СО АН СССР

Поступила в редакцию 23. февр. 1974.

Проведено исследование гидродинамической обстановки в трехфазном неподвижном слое с помощью электроконтактной методики.

Показано, что жидкую фазу можно рассматривать в виде непрерывной пульсирующий пленки на поверхности твердых частиц. Получено приближенное решение для расчета коэффициентов массообмена между жидкостью и насадкой. Проведено экспериментальное исследование.

Реактора с трехфазным неподвижным слоем катализатора, работающие при прямоточном восходящем движении газа и жидкости занимают важное место в химической промышленности. При их проектировании необходимо знание процессов массопереноса между твердым катализатором и газожидкостной смесью, находящейся в свободном объеме слоя. До настоящего времени этим вопросам уделялось крайне мало внимания и в настоящей работе будет предпринята попытка в какой-то степени заполнить этот пробел.

I. Гидродинамическая обстановка в свободном объеме слоя.

При экспериментальном исследовании гидродинамической обстановки в свободном объеме слоя была использована электроконтактная методика, основанная на измерении изменения электрического сопротивления между электродами при прохождении газовых пузырей. Эксперименталь-

ная установка представляла собой колонну Д = 100 мм, в которую насыпались стеклянные шары диаметром d = 18 мм. Непосредственно в слое устанавливался сферический датчик, представляющий собой полый шар (d = 18 мм) из токонепроводящего материала. В пяти точках его поверхности были установлены никелированные цилиндры заподлицо к последней. Внутри цилиндров изолировано вкладывались иглы. Цилиндры служили одним электродом, а иглы - вторым. К датчику подводился переменный ток высокой частоты, а выводы от него подсоединялись последовательно к электронно-вычислительной машине IRA-5. В процессе исследования варьировались скорости газа и жидкости в пределах $\bar{U}_1$ = 3-205 см/сек, $\bar{U}_2$ = 0,26-2,5 см/сек соответственно.

Градуировка датчика и ЭВМ проводилась в статических условиях, при этом находилась зависимость между толщиной пленки жидкости на поверхности сферы и показаниями ЭВМ в цифровом коде. По методике, приведенной в [1] определялись времена опроса датчиков и шаг дискретизации.

Обработка результатов проводилась на основании методов теории вероятности. При этом находились математическое ожидание, дисперсия, среднеквадратичная частота прохождения пузырей [1].

Было получено, что при широком варьировании скоростей газа и жидкости ни одна из ординат случайного процесса не обращались в нуль. Это означало, что газовая фаза не имела непосредственного контакта с твердым телом. Скорость жидкости слабо влияет на среднее расстояние прохождения пузырей от поверхности зерна. Жидкая фаза представляет собой пульсирующую с частотой прохождения пузырей пленку, средняя толщина которой может быть рассчитана по найденной эмпирической зависимости:

$$\frac{m}{d} = 0{,}15\ \bar{F}_{2_1}^{-0{,}1} \qquad (1)$$

Таким образом, для анализа процессов массопереноса между жидкостью и твердым телом можно принять жидкую фазу в виде пленки постоянной тощины, но с переменной скоростью течения, зависящей от

соотношения объемных расходов и частот прохождения пузырей.

2. Анализ процессов массопереноса

Анализ процессов массопереноса между жидкостью и твердым телом по сути дела сводится к анализу решения уравнений конвективной диффузии и неустановившегося пограничного слоя. Рассмотрим предварительно процессы массообмена для стационарного распределения концентраций в диффузионном пограничном слое. Математическое описание в этом случае имеет вид:

$$\frac{\partial u}{\partial x} + \frac{\partial v}{\partial y} = 0 \qquad (2)$$

$$\frac{\partial u}{\partial t} + u\frac{\partial u}{\partial x} + v\frac{\partial u}{\partial y} = -\frac{1}{\rho}\frac{\partial P}{\partial x} + \nu\frac{\partial^2 u}{\partial y^2} \qquad (3)$$

$$-\frac{1}{\rho}\frac{\partial P}{\partial x} = \frac{\partial U_e(x,t)}{\partial t} + U_e\frac{\partial U_e(x,t)}{\partial x} \qquad (4)$$

$$U\frac{\partial c}{\partial x} + V\frac{\partial c}{\partial y} = D\frac{\partial^2 c}{\partial y^2} \qquad (5)$$

Для решения дифференциальных уравнений необходимы следующие граничные условия:

$$y=0; \quad u=0; \quad v=0; \quad c=c^* \qquad (6)$$

$$y=m; \quad u=u_e(x,t); \quad c=0; \qquad (7)$$

$$x=0; \quad c=0; \quad t=0; \quad u=u_2 \qquad (8)$$

u_e - скорость на внешней границе пограничного слоя, т.е. можно принять, что

$$U_e = [\frac{U_1+U_2}{2} + \frac{U_2-U_1}{2} \cdot \cos\omega t]\sin\frac{x}{R} \qquad (9)$$

Поскольку процессы переноса вещества не оказывают влияние на поле скоростей вокруг частицы, то систему (2-8) можно разбить на две части, из которых первая (2-4) описывает поле скоростей, а вторая (5) - диффузию вещества в жидкой пленке.

Интегрирование (2-4) выполняется, как правило, методом последовательных приближений, основанном согласно [2] на следующем рассуждении. В начальный момент времени при движении из состояния покой пограничный слой очень тонок, но важен вклад вязкого члена $\nu\frac{\partial^2 u}{\partial y^2}$ по сравнению с конвективными членами, сохраняющими обычные значения. Вязкие силы уравновешиваются ускорением $\frac{\partial u}{\partial t}$ и величиной давления, в которой для начальных моментов времени преобладает $\frac{\partial U_e}{\partial t}$,

Поскольку рассматривается периодическое движение, то указанные предположения будут, очевидно, выполняться для всех моментов времени. С учетом указанных допущений из системы (2-4) можно получить

$$\frac{\partial u}{\partial t} - \nu\frac{\partial^2 u}{\partial y^2} = \frac{\partial U_e}{\partial t} \qquad (10)$$

Это уравнение с учетом (6-7) соответствует уравнению типа теплопроводности с внутренними периодически действующими источниками тепла:

$$\frac{\partial u}{\partial t} - \nu\frac{\partial^2 u}{\partial y^2} = -\beta\omega\sin\omega t \qquad (11)$$

где $$\beta = \frac{U_2-U_1}{2}\sin\frac{x}{R}$$

Приближенное решение (11) можно получить на основании разработанного П. Цоем способа, заключающегося в совместном использова-

нии интегрального преобразования Лапласа и вариационного метода Ритца [3]. Опустив из-за громоздкости все промежуточные преобразования, приведем окончательное выражение:

$$U(x,y,t) = \frac{y}{m}[A+B\cos\omega t] + \frac{2}{\pi}\sin\frac{\pi y}{m}\cdot B\cdot$$

$$\cdot\left\{\frac{\lambda\sin\omega t - \cos\omega t}{1+\lambda^2} + \frac{\exp\left[-\frac{\nu\pi^2}{m^2}t\right]}{1+\lambda^2}\right\} \qquad (12)$$

где $A = \frac{U_1+U_2}{2}\sin\frac{x}{R}$; $\lambda = \frac{\nu\pi^2}{m^2\omega}$;

Обратная величина λ имеет смысл формпараметра для нестационарного пограничного слоя и характеризует профиль скорости в нем в зависимости от частоты внешних возмущений. $M_{гид}=\frac{m^2}{\nu}$ является масштабом времени установления гидродинамического пограничного слоя и характеризует его инерционные свойства.

Из теории пограничного слоя известно [4], что при обтекании осесимметричных тел возможен отрыв потока от боковой поверхности зерна. Условием отрыва является равенство

$$\left.\frac{\partial u}{\partial y}\right|_{y=0} = 0 \qquad (13)$$

Кроме того отрыв возможен только там,где $\frac{\partial U_e}{\partial x}<0$. Наиболее вероятной точкой отрыва является та, в которой абсолютная величина $\frac{\partial U_e}{\partial x}$ имеет максимальное значение, т.е.

$$\frac{dU_e}{dx} = -\frac{A}{R} - \frac{B}{R}\cos\omega t \qquad (14)$$

Правая часть в (14) может быть величиной положительной или

отрицательной в зависимости от знака $\cos\omega t$. Это означает, что при обтекании частицы точка отрыва будет перемещаться по боковой поверхности зерна, при этом в окрестных слоях жидкости будет создаваться хорошее перемешивание. Отсюда следует, что величина коэффициентов массообмена в трехфазном неподвижном слое всегда больше, чем при обтекании частиц только одной жидкостью.

Для расчета поля концентраций в пленке жидкости решение (12) и уравнение конвективной диффузии (5) можно упростить, рассматривая установившееся движение пузырей, процессы переноса на малых расстояниях от поверхности зерна, т.е. при $\frac{y}{m} \ll 1$ и предполагая малой кривизну пограничного слоя. В этом случае (12) запишется как

$$U(x,y,t) = \frac{y}{m} A + B\cos\omega t + \frac{2B}{1+\lambda^2}(\lambda\sin\omega t - \cos\omega t) \qquad (15)$$

Уравнение (5) упростится до вида

$$\sin\frac{x}{R} A_1 y U_2 \frac{\partial c}{\partial x} = D\frac{\partial^2 c}{\partial y^2} \qquad (16)$$

$$A_1 = \frac{1}{m}\left[\frac{U_1+U_2}{2U_2} - \frac{U_2-U_1}{2U_2}\cos\omega t + \frac{U_2-U_1}{U_2(1+\lambda^2)}(\lambda\sin\omega t - \cos\omega t)\right]$$

при $y=0 \quad c=c^*$

$y=\infty \quad c=0$

$x=0 \quad c=0 \qquad (17)$

Последние граничное условие согласно [5] означает, что в лобовой точке концентрация растворенного вещества близка в объемной на удалении от поверхности.

Уравнение (16) подстановкой

$$z = R \ln \operatorname{tg}\frac{x}{2R} \qquad (18)$$

сводится к виду

$$A_1 y U_2 \frac{\partial c}{\partial z} = D \frac{\partial^2 c}{\partial y^2} \qquad (19)$$

введением новой переменной, предложенной в [5]

$$\eta = \left(\frac{A_1 U_2}{D}\right)^{\frac{1}{3}} \frac{y}{z^{1/3}} \qquad (20)$$

Уравнение (19) преобразуется до:

$$\frac{\partial^2 c}{\partial \eta^2} + \frac{2}{3}\eta^2 \frac{\partial c}{\partial \eta} = 0 \qquad (21)$$

при $\eta=0 \quad c=c^*$

$\eta\to\infty \quad c=0 \qquad (22)$

Решение (19) с учетом (22) выглядит следующим образом:

$$C = K_1 \int_0^{\eta} \exp\left(-\frac{2}{9} H^3\right) dH + K_2 \qquad (23)$$

K_1, K_2 - константы, определяемые из граничных условий. Окончательно имеет

$$C = C^*\left[1 - \frac{\int_0^{\eta} \exp\left(-\frac{2}{9} H^3\right) dH}{\int_0^{\infty} \exp\left(-\frac{2}{9} H^3\right) dH}\right] \qquad (24)$$

Для перехода от (24) к исходным переменным (x,y,t) проделаем с полученным решением следующие преобразования. Поскольку уравнение (19) инвариантно относительно замены z на $z+z_0$, где z_0 - константа, то верхний интеграл в (24) преобразуется следующим образом:

$$\int_0^{\eta} \exp\left(-\frac{2}{9}H^3\right)dH = \int_0^{\left(\frac{A_1U_2}{D}\right)^{\frac{1}{3}} \frac{y}{(z+z_0)^{\frac{1}{3}}}} \exp\left(-\frac{2}{9}H^3\right)dH \qquad (25)$$

Выбирал $z_0 = R \ln \operatorname{tg} \frac{x_0}{2R}$, где x_0 - длина дуги лобовой части зерна, вокруг которой концентрация растворенного вещества равна нулю кончательное решение имеет вид:

$$C(x,y,t) \begin{cases} 0 & \text{при } x \le x_0 \qquad (26) \\ C^*\left(1 - \dfrac{\int_0^{\left(\frac{A_1U_2}{D}\right)^{\frac{1}{3}} \frac{y}{[R \ln(\operatorname{tg}\frac{x}{2R} \operatorname{tg}\frac{x_0}{2R})]^{\frac{1}{3}}}} \exp\left(-\frac{2}{9}H^3\right) dH}{\int_0^{\infty} \exp\left(-\frac{2}{9}H^3\right) dH}\right) & \text{при } x > x_0 \qquad (27) \end{cases}$$

На основании (27) можно рассчитать толщину диффузионного пограничного слоя (δ), а по ней определить коэффициент массообмена.

$$j = -D \left.\frac{\partial c}{\partial y}\right|_{y=0} = D \frac{c^*}{\delta} \qquad (28)$$

Знаменатель этого выражения в соответствии с [5] выражается через интеграл Эйлера второго рода и равен 0,67.

$$\delta = \frac{1}{0,67} \left(\frac{D}{A_1U_2}\right)^{\frac{1}{3}} \left[R \ln \frac{\operatorname{tg}\frac{x}{2R}}{\operatorname{tg}\frac{x_0}{2R}}\right]^{\frac{1}{3}} \qquad (29)$$

$$Sh = \frac{R}{\delta} = 0,67 \left(\frac{A_1U_2}{D} R^2\right)^{\frac{1}{3}} \left[\ln \frac{\operatorname{tg}\frac{x}{2R}}{\operatorname{tg}\frac{x_0}{2R}}\right]^{-\frac{1}{3}} \qquad (30)$$

или

$$\frac{Sh}{Sc^{0,33}} = 0{,}67\left(\ln\frac{tg\frac{x}{2R}}{tg\frac{x_0}{2R}}\right)^{-\frac{1}{3}} \cdot Re_2^{\frac{1}{3}} \cdot \left(\frac{R}{m}\right)^{\frac{1}{3}} \cdot$$

$$\cdot\left[\frac{U_1+U_2}{2U_2} - \frac{U_2-U_1}{2U_2}\cos\omega t + \frac{U_2-U_1}{U_2(1+\lambda^2)}(\lambda\sin\omega t-\cos\omega t)\right]^{\frac{1}{3}} \qquad (31)$$

Выражение (31) определяет распределение коэффициентов массообмена по боковой поверхности зерна в зависимости от скоростей газа и жидкости, а также частот прохождения пузырей для стационарных условий.

Для расчета химических реакторов обычно требуются коэффициенты массообмена усредненные по боковой поверхности зерна и за период пульсаций. Такое выражение можно получить из (31) проведя интегрирование по x и t.

В этом случае

$$\frac{Sh}{Sc^{0,33}} = 0{,}67\, Re_2^{\frac{1}{3}}\left(\frac{R}{m}\right)^{\frac{1}{3}} \cdot \frac{2}{\pi R}\int_0^{\pi R}\left(\ln\frac{tg\frac{x}{2R}}{tg\frac{x_0}{2R}}\right)^{-\frac{1}{3}} dx \cdot$$

$$\cdot\frac{1}{2\pi}\int_0^{2\pi}\left[\frac{U_1+U_2}{2U_2} - \frac{U_2-U_1}{2U_2}\cos y + \frac{U_2-U_1}{U_2(1+\lambda^2)}(\lambda\sin y - \cos y)\right]^{\frac{1}{3}} dy \qquad (32)$$

Анализ 32 был проведен численно. Полученные результаты для разных значений λ приведены на рис.1. Как следует из этого рисунка, величина λ при изменении ее в пределах 0,001-5 (что соответствует практической области изменения) оказывает довольно слабое влияние на значения, отложенные по оси ординат. Это обстоятельство дает возможность не учитывать зависимость λ от U_1 и U_2, аппроксимировать представленные по (32) расчеты следующим выражением:

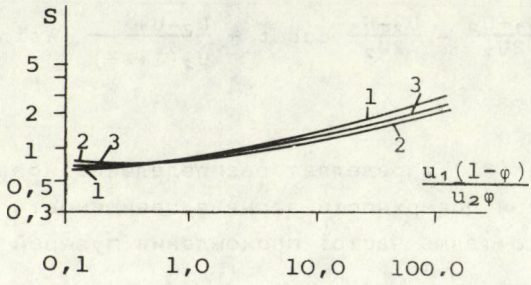

Рис.1. Влияние параметра на условия обмена между жидкостью и твердым телом в ТНС. 1-λ=0,001; 2-λ=1,0 ; 3-λ=5,0 ;

$$\frac{\overline{Sh}}{Sc^{0,33}} = 3,78\{0,7+0,12[\frac{\bar{U}_1(1-\varphi)}{\bar{U}_{2\varphi}}]^{0,62}\}\overline{Re_2}^{0,33}(\frac{R}{m})^{0,33} \qquad (33)$$

Для расчета массообмена в нестационарных условиях, т.е. когда не успевает сформироваться диффузионный пограничный слой можно воспользоваться результатами следующего приближенного анализа: математическое описание переноса вещества через жидкую пленку в нестационарных условиях имеет вид

$$D\frac{\partial^2 c}{\partial y^2} = \frac{\partial c}{\partial t} \qquad (34)$$

при
$$y=0 \quad c=c_o$$
$$y=\delta \quad c=c_1 \qquad (35)$$
$$t=0 \quad c=c_o$$

Приближенное решение (34) с учетом (35) было получено с использованием уже упоминавшейся методики [3] в виде:

$$c(y,t) = c_o + \frac{y}{\delta}(c_1-c_o) + 2(c_1-c_o)\sin\frac{\pi y}{\delta}\exp\left[-\frac{D\pi^2}{\delta^2}t\right] \qquad (36)$$

Откуда

$$j = -D(c_1-c_o)\left\{\frac{1}{\delta} + \frac{2\pi}{\delta}\exp\left[-\frac{D\pi^2}{\delta^2}t\right]\right\} \qquad (37)$$

Если диффузионный пограничный слой устанавливается за время равное τ, то

$$J = \frac{1}{\tau}\int_o^\tau j d\tau = -D(c_1-c_o)\left\{\frac{1}{\delta} + \frac{\delta}{\pi D\tau}\left(1-\exp\left[-\frac{D\pi^2}{\delta^2}\tau\right]\right)\right\} \qquad (38)$$

Переходя к коэффициентам обмена получим

$$\frac{Sh(\tau)}{Sh} = 1 + \frac{\delta^2}{\pi D\tau}\left(1-\exp\left[-\frac{D\pi^2}{\delta^2}\tau\right]\right) \qquad (39)$$

$Sh(\tau)$ - критерий Шервуда, определенный для неустановившегося процесса массообмена. Величина $M_{диф}=\delta^2/D\pi^2$ характеризует инерционные свойства диффузионного пограничного слоя и является масштабом времени переходных режимов в нем. Поскольку $\delta\approx\delta_o Sc^{-0,33}$, где δ_o толщина гидродинамического пограничного слоя, то

$$\frac{M_{диф}}{M_{гид}} = Sc^{0,33} \qquad (40)$$

Для жидкостей $Sc=500-2000$, следовательно, более инерционными являются процессы массопереноса, чем импульса.

3. Экспериментальное исследование массообмена между жидкостью и твердым телом

Экспериментальное исследование массообмена между жидкостью и твердым телом проводилось с помощью известной стационарной методики, основанной на измерении убыли веса контрольных растворимых тел, помещенных в слой ими подобных частиц.

Экспериментальная установка представляла собой колонну квадратного сечения 100×100 мм и высотой - 500 мм. Газ и жидкость двигались восходящим прямотоком. Их скорость варьировалась в пределах U_1=0-50см/сек, U_2=0,01-2см/сек, температура 5-40 °С. Исследования проводились на шариках 30 и 8 мм, кольцах Рашига 12.12.2. Для последних в качестве определяющего размера выбиралась величина $R_{экв}=\frac{1+d}{4}$. Контрольные элементы изготовлялись отливкой в графито - вые матрицы.

Коэффициенты молекулярной диффузии указанных веществ в воде выбирались по [6], а равновесные концентрации определялись экспериментально и сравнивались с данными, приведенными в [7] .

Как и следовало из теоретического анализа, коэффициенты массообмена даже при небольших газасодержаниях значительно отличаются от системы жидкость - твердое /рис.2./. Характер зависимости Sh от U_1 и U_2 сильно зависит от их абсолютных величин и соотношения объемных расходов.

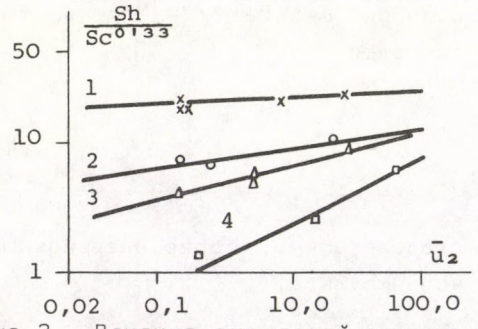

Рис.2. Влияние скоростей газа и жидкости на коэффициенты обмена. Шарики d=8 мм, бензойная кислота. 1-$\bar{U}_1$=6,2см/с 2-$\bar{U}_1$=0,25см/с, 3-$\bar{U}_1$=0,125см/с, 4-$\bar{U}^1$=0.

Для получения единой зависимости была использована формула (33). Результаты обработки приведены на рис. 3. По оси ординат отложено отношение $Sh_{эк}/Sh$ Оказалось, что (33) дает

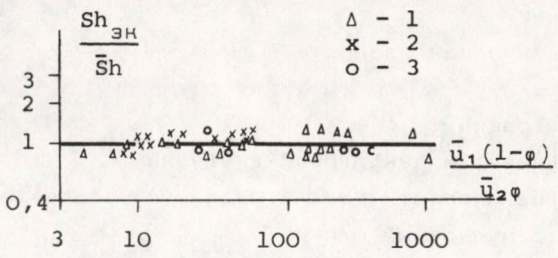

Рис.3. Сравнение расчетных и экспериментальных значений Sh. 1-шарики d=8мм бензойная кислота, 2-шарики d=30 мм, гидрокинон, 3-кольца Рашига 12.12.2, бензойная кислота.

наилучшее согласование с экспериментом, если вместо коэффициента 3,78 положить величину в 1,25 раза меньшую. Таким образом, для расчета коэффициентов массообмена между жидкостью и насадкой в ТНС можно рекомендовать зависимость:

$$\frac{\bar{Sh}}{Sc^{0,33}} = 3,02\ \{0,7+0,12\ [\frac{\bar{U}_1(1-\varphi)}{\bar{U}_{2\varphi}}]^{0,62}\}\ (\frac{R}{m})^{0,33}\ Re_2^{0,33} \qquad (42)$$

УСЛОВНЫЕ ОБОЗНАЧЕНИЯ

$\bar{U}_1, \bar{U}_2$ скорость газа и жидкости, отнесенные к свободному сечению слоя, соответственно

m толщина пленки жидкости на поверхности зерна

d размер частиц слоя

x,y координаты в направлении течения и перпендикулярном к нему, соответственно

u, v	скорости по координатам x и y, соответственно
ρ	плотность жидкости
P	давление
ν	кинематическая вязкость
t	время
c	концентрация
D	коэффициент молекулярной диффузии
U_1, U_2	истинные скорости газа и жидкости, соответственно
ω	частота пульсаций пленки
R	радиус зерна
φ	доля газовой фазы в свободном объеме слоя газосодержание определяемая по [8]

$$Sh=\frac{\beta R}{D}\ ;\quad Sc=\frac{\nu}{D}\ ;\quad Re_2=\frac{\bar{U}_2 R}{\nu(1-\varphi)}\ ;\quad Fr_1=\frac{\bar{U}_1^2}{gd}\ ;$$

$$S=\frac{Sh}{Pe^{0,33}\,0,67\left(\frac{R}{m}\right)^{0,33}\frac{2}{\pi R}\int_{x_0}^{\pi R}\left[\ln\frac{tg\frac{\Delta}{2R}}{tg\frac{x_0}{2R}}\right]^{-\frac{1}{3}}dx}\ ;$$

ЛИТЕРАТУРА

1. Е.Г.ДУДНИКОВ. Построение математических моделей химико-технологических объектов. Л., Химия, 1970.

2. П.ЧЖЕН. Отрывные течения. М. Мир, 1. 1972.

3. П.В.ЦОЙ. Методы расчета отдельных задач тепломассопереноса. М., Энергия, 1971.

4. Г.ШЛИХТИНГ. Теория пограничного слоя. М., Ил., 1956.

5. В.Г.ЛЕВИЧ. Физико-химическая гидродинамика. М., 1959.

6. Р.РИД, Т.ШЕРВУД, Свойства газов и жидкостей. Л.,Химия, 1971.

7. Справочник по растворимости. 1.1. 1331, 1969.

8. Г.К.ЗИГАНШИН, А.ЕРМАКОВА. ТОХТ, 4.4, 494, 1970.

SUMMARY

Using the electrocontact methodics the hydrodynamic characteristics of a three phase static bed reactor was investigated.

It was shown that the liquid phase can be regarded as a continuous, pulsating layer covering the surface of the solid particles. An approximate formula was derived for the description of the coefficient of mass transfer taking place between the packing and the liquid.

Hungarian Journal
of Industrial Chemistry
Veszprém
Vol. 3.pp. 37-50 (1975)

МАССОПЕРЕНОС С ХИМИЧЕСКОЙ РЕФКЦИЕЙ В ТРЕХФАЗНОЙ СИСТЕМЕ ГАЗ-ЖИДКОСТЬ-ТВЕРДЫЙ КАТАЛИЗАТОР

Гарцман А.Н., Ермакова А., Бахвалова В.П., Рассадникова Н.И.

Институт Катализа СО АН СССР

Поступила в редакцию 23. февр. 1974.

Изучен массоперенос в трехфазной системе газ-жидкость-твердый катализатор методом модельной реакции гидрирования н-гептена-1. Опыты проводились в неподвижном и псевдосжиженном слое катализатора, в режиме неоднородного и однородного псевдоожижения.

Показано, что лимитирующей стадией массопереноса в неподвижном слое катализатора является перенос реагентов к внешней поверхности катализатора, а в псевдоожиженном слое - массоперенос на границе раздела фаз газ-жидкость. В режиме однородного псевдоожижения наблюдается резкий рост коэффициента массопереноса по сравнению с режимом неоднородного псевдоожижения. Недостатком режима однородного псевдоожижения является сильное расширение слоя.

В работах [1],[2] показано, что в случае простой реакции $A_г \xrightarrow{\text{абсорбция}} A_ж \xrightarrow{\text{реакция}} B_ж$, скорость которой описывается уравнением первого порядка, наблюдаемая константа скорости связана с коэффициентами массопереноса уравнением:

$$\frac{1}{H_н C_{кат}} = \frac{1}{\beta_{2-ж}} + \frac{1}{\beta_{ж-т}} + \frac{1}{H^* C_{кат}} \qquad (1)$$

где $$\beta_{2-ж} = K_{2-ж} \cdot a_{2-ж} \quad (2a)$$

$$\beta_{ж-т} = K_{ж-т} \cdot a_{ж-т} \quad (2b)$$

$$a_{ж-т} = \frac{6}{d} C_{кат} \quad (2c)$$

$$C_{кат} = 1-\varepsilon \quad (2d)$$

$$K = \frac{6}{d} \sqrt{KD_э} \left[\frac{1}{th\varphi} - \frac{1}{\varphi}\right] \quad (2e)$$

$$\varphi = \frac{d}{2} \sqrt{K/D_э} \quad (2f)$$

Члены суммы (1) представляют собой сопротивление переносу реагента А соответственно на границе раздела фаз газ-жидкость, жидкость-твердый катализатор и внутри пор катализатора. Их соотношение определяет область протекания химической реакции. Наблюдаемая константа скорости в общем случае находится в сложной зависимости от истинной константы скорости (К), диаметра частиц катализатора и гидродинамических условий, определяющих характер протекания процессов внешнего массопереноса. При достаточно быстром протекании последних максимальное значение $K_н$ будет равным К*. В этом случае скорость процесса определяется скоростью диффузии реагентов внутри зерна катализатора и не зависит от гидродинамических условий. Чем меньше диаметр зерна, тем больше К*. Следовательно, при переходе от неподвижного слоя катализатора к псевдоожиженному, в результате дробления зерна мы повышаем тот предел, к которому можем стремиться $K_н$, т.е. расширяем область интенсификации внешних процессов массопереноса.

В литературе опубликован ряд работ [3-9], посвященных изучению газо-жидкостных каталитических реакций в неподвижном и псевдоожиженном слое катализатора. Приведенные вышеуказанными авторами предположения о природе лимитирующей стадии процесса носят в основном качественный характер. В то же время, для управления химическим процессом с целью повышения его эффективности необходимо знать природу лимитирующей стадии и возможные пределы интенсификации.

В настоящей работе поставлена задача проанализировать какого влияние каждого из членов суммы представленной уравнением (1), на наблюдаемую константу скорости, при проведении газо-жидкостной реакции в неподвижном и псевдоожиженном слое катализатора.

В работе (10) было показано существование в ТПС двух режимов псевдоожижения: неоднородного и однородного. Последний характеризуется высокой внешней „организованностью": равномерным распределением твердых частиц и мелких газовых пузырей по всему объему жидкости. Режим однородного псевдоожижения характеризуется также резким ростом газосодержания.(11). Эти качества дают основание предполагать, что режим однородного псевдоожижения обеспечивает более интенсивное протекание процессов массопереноса, чем режим неоднородного псевдоожижения, следовательно, он будет оптимальным для проведения газо-жидкостных каталитических реакций. В данной работе сделана попытка проверить это предположение.

Для решения поставленной задачи проводилось экспериментальное изучение реакции гидрирования н-гептена-1 на опытной установке производительностью 300 л/ч по жидкости. Описание экспериментальной установки и методики эксперимента приведено в (2).

Кинетика реакции гидрирования н-гептена-1 на Ni-скелетном катализаторе была изучена ранее, она опубликована в работе[13]. Установлено, что реакция в кинетической области описывается уравнением первого порядка по водороду. Порядок реакции по непредельному соединению в изучаемой нами области концентраций-нулевой.

Проведено три серии опытов:одна - в неподвижном слое катализатора, вторая- в режиме неоднородного псевдоожижения, третья- в режиме однородного псевдоожижения. Линейную скорость жидкости, определяющую переход из области неоднородного в область однородного псевдоожижения, при заданном диаметре зерна катализатора и скорости газа рассчитали при помощи уравнения (10)

$$W_{од}^{(3)} = W_{кр}^{(2)}\left(1 + 13{,}4\,\frac{W_г^{0{,}5}}{d}\right) \qquad (3)$$

Скорость протекания процесса гидрирования на опытной установке характеризовали при помощи наблюдаемой константы, рассчитанной из соотношения:

$$K_н = \frac{Q_ж(y_н - y_к)}{X^* q_{кат}} \text{ , сек}^{-1} \qquad (4)$$

Результаты экспериментов (см. табл. 1,2) показали, что наблюдаемая константа скорости существенно зависит от гидродинамической обстановки в реакторе: от линейной скорости газа и жидкости, от диаметра частиц катализатора, от состояния катализатора (неподвижный, псевдоожиженный слой), от режима псевдоожижения (однородный, неоднородный).

С целью выяснения природы лимитирующей стадии процесса в тех или иных условиях, ниже сделана попытка проанализировать каков вклад каждого их членов суммы (1) в наблюдаемую константу скорости.

Неподвижный слой

Условия и результаты опытов представлены в табл. 1. Существенное влияние линейной скорости жидкости и слабое влияние скорости газа на наблюдаемую константу позволяет сделать предположение, что лимитирующим этапом в неподвижном слое катализатора является массоперенос на границе раздела фаз жидкость-твердый катализатор. Чтобы проверить это предположение, приведена приближенная оценка коэффициентов массопереноса. $\beta_{г-ж}$ и $\beta_{ж-т}$. Согласно модели „проникновения" Хигби (12) для расчета коэффициента $K_{г-ж}$ можно использовать выражение:

$$K_{ж-т} = 2\sqrt{\frac{D_м}{\pi t^*}} \qquad (5)$$

где t^* - среднее время контакта поверхностных элементов газа и жидкости. Если газ барботирует через жидкость, то $t^* \simeq \frac{d_п}{w_п}$. Приняв диаметры пузырьков равными 0,2-0,6 см, скорость их движения 15-35

см/сек, интервал величины $K_{г-ж}$ (для $D_м=10^{-5}$ см²/сек) будет равным $0,015 < K_{г-ж} < 0,04$ см/сек.

Значение $a_{г-ж}$ очень трудно оценить, но для приближенных оценок можно принять, что $a_{г-ж}=10$ см$^{-1}$. Тогда $\beta_{г-ж}=0,15 \div 0,4$сек$^{-1}$. Для расчета коэффициента $K_{ж-т}$ использовали критериальное уравнение, предложенное В.А. Кирилловым для области

$$0,1<Re_{ж},Re_{г}<2.10^{2}$$

$$\frac{Nu}{P_2^{0,33}} = 3,02\{0,7 + 0,12[\frac{W_г(1-\varphi)}{W_ж\varphi}]^{0,62}\}(\frac{d}{2m})^{0,33}Re_ж^{0,33} \qquad (6)$$

Удельную межфазную поверхность $a_{ж-т}$ рассчитали при помощи уравнения (2с). Результаты расчета приведены в таблице 1. Данные таблицы показывают, что в большинстве опытов при низких скоростях жидкости (0,12-0,45 см/сек) коэффициенты $K_н C_{кат}$ и $\beta_{ж-т}$ величины одного порядка, примерно в 5-10 раз меньше, чем $K^* C_{кат}$ и $\beta_{г-ж}$. Следовательно, основным лимитирующим этапом внешнего массопереноса в неподвижном слое катализатора является перенос на границе раздела фаз жидкость - твердое тело. Однако, это утверждение теряет справедливость при более высоких скоростях жидкости (0,8-2,0 см/сек). В этих условиях наблюдаемая константа скорости возрасла настолько, что $У_н$ и K^* стали величинами одного порядка, следовательно, скорости процессов внешнего и внутреннего массообмена стали соизмеримыми. Предел, к которому может стремиться $K_н$ - это K^* - в неподвижном слое относительно низок: $K^*=0,4$ при $d=3,4$ и $K^*=0,75$ при $d=1,6$ мм. Это свидетельствует о том, что возможность интенсификации процесса в неподвижном слое ограничена.

Псевдоожиженный слой

Результаты расчета приведены в таблице 2. При переходе к трехфазному псевдоожиженному слою пропорционально уменьшению размера зерна увеличится коэффициент K^*, следовательно, повысится тот уровень, к которому можно стремиться при интенсификации процессов внешнего массопереноса. Возрасло также значение $\beta_{ж-т}$, в основном

за счет увеличения $a_{ж-т}$. Коэффициенты $K^*C_{кат}$ и $\beta_{ж-т}$ в режиме ТПС - величины одного порядка.

Концентрацию катализатора рассчитали из уравнения (2d), порозность псевдоожиженного слоя определили по данным работы [2].

Результаты экспериментов представлены в табл. 2. Приближенная оценка коэффициентов $\beta_{ж-т}$ и $\beta_{г-ж}$ проводилась вышеописанным способом. Произведение наблюдаемой константы скорости $K_н C_{кат}$ в области неоднородного псевдоожижения примерно на порядок меньше чем $K^*C_{кат}$ и $\beta_{ж-т}$ и соизмеримо со значением $\beta_{г-ж}$. Этот факт свидетельствует о том, что в области неоднородного псевдоожижения лимитирующей стадией процесса является массоперенос на границе раздела фаз газ-жидкость.

При переходе в область однородного псевдоожижения при низких скоростях газа сохраняется соотношение $K_н C_{кат} \approx 0,1 \beta_{ж-т}$ и $K_н C_{кат} \approx 0,1\, K^*C_{кат}$. Однако, при $W_г \geq 5$ см/сек и $W_ж \geq 2$ см/сек происходит резкий рост наблюдаемой константы, $K_н$ и K^* становятся величинами одного порядка. На рис. 1. представлена зависимость $K_н$ от линейной скорости газа. Резкий рост наблюдаемой константы $K_н$ с увеличением скорости газа характеризует область однородного псевдоожижения, и незначительный рост - область неоднородного псевдоожижения. В последнем случае увеличение расхода газа не приводит к существенному изменению гидродинамики слоя, к увеличению межфазной поверхности, так как газ проскакивает в виде больших пузырей, соизмеримых с диаметром реактора, или по каналам. Этим объясняются сравительно низкие значения $K_н$ и слабая зависимость от скорости газа.

В области однородного псевдоожижения газ проходит слой в виде мелких пузырей, создавая при этом достаточно большую поверхность контакта фаз. Увеличение расхода газа приводит по видимому не только к росту газосодержания и удельной поверхности контакта , но увеличивает скорость обновления межфазной поверхности. Следовательно, в области однородного псевдоожижения резко улучшаются условия массопереноса на границе раздела фаз газ-жидкость по сравнению с неоднородным псевдоожиженным слоем.

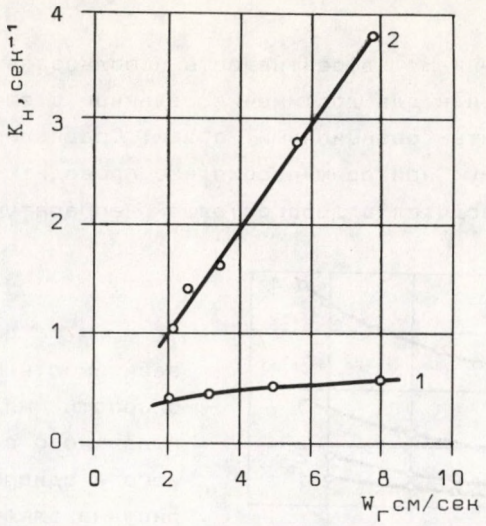

Рис. 1. Зависимость наблюдаемой константы скорости от линейной скорости газа.
1-Режим неоднородного псевдоожижения.
2-Режим однородного псевдоожижения.

Сравнение эффективности работы реактора гидрирования в неподвижном и псевдоожиженном слое

Сравнение может быть проведено по двум критериям: первый критерий- это значение наблюдаемой константы $K_н$ - выражающее отношение числа молей прогидрированного вещества к количеству (объему или весу) взятого катализатора в единицу времени. Очевидно, что при прочих равных условиях с ростом $K_н$ пропорционально уменьшается количество катализатора необходимое для достижения заданной степени превращения. Оценка эффективности по первому критерию особенно важна в тех случаях,в которых используется дорогостоящий катализатор (Pt,Pd).

Вторым критерием является произведение $K_н C_{кат}$, выражающее количество прореагировавшего продукта в единице объема реакционной смеси. Объем реактора при прочих равных условиях обратно пропорционален произведению $K_н C_{кат}$. Второй критерий указывает, что с расширением ТПС, приводящим к уменьшению концентрации катализатора,

при том же значении $K_н$ эффективность использования реакционного объема падает, так как для достижения заданной степени превращения необходимо увеличить реакционный объем. Сравнение эффективности процессов по второму критерию необходимо проводить в тех случаях, когда процесс проводится в дорогостоящей аппаратуре, под высоким давлением.

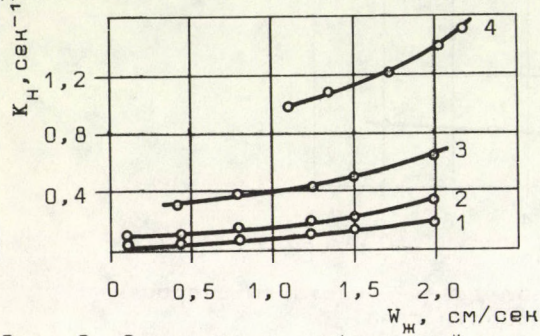

Рис. 2. Зависимость наблюдаемой константы скорости от линейной скорости жидкости. 1-неподвижный слой, d=3,4мм 2-неподв.слой, d=1,6мм, 3-режим неод - нородного псевдоожижения, d=0,2мм, 4-режим однородного псевдоожижения, d= =0,1 мм.

На рис. 2. показана зависимость $K_н$ от линейной скорости жидкости для неподвижного слоя, неоднородного и однородного ТПС. Из рисунка следует, что переход от неподвижного слоя катализатора к неоднородному ТПС увеличивает $K_н$ всего в 2-4 раза, переход к режиму однородного псевдоожижения приводит к росту $K_н$, следовательно к сокращению количества катализатора в 10-15 раз. Однако, как отмечалось выше, рост $K_н$ в ТПС не означает пропорционального уменьшения реакционного объема. Чтобы убедиться в этом, необходимо обратиться к рисунку 3., где показана зависимость $K_н$, $C_{кат}$ и их произведения - $K_н C_{кат}$ от скорости жидкости. Падение $C_{кат}$ с ростом $W_ж$ сглаживает рост $K_н C_{кат}$. Поскольку режим однородного псевдоожижения достигается при больших расширениях слоя, чем режим неоднородного псевдоожижения, несмотря на более высокие значения $K_н$ в режиме однородного псевдоожижения, значения $K_н C_{кат}$ для обеих режимов отличаются несущественно. Следовательно, при переходе к режиму однородного ТПС выигрыш в реакционном объеме невелик. Сильное расширение слоя является недостатком режима однородного псевдоожижения.

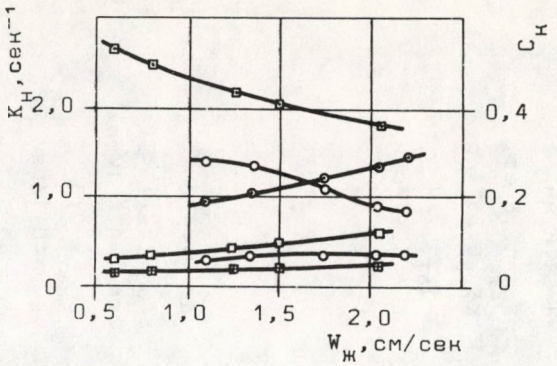

Рис. 3. Зависимость $K_н$, $C_{кат}$, и $K_н C_{кат}$ от линейной скорости жидкости.
□ - режим неоднородного псевдоожижения
○ - режим однородного псевдоожижения
+ - $K_н C_{кат}$
. - $K_н$
– $-C_{кат}$

Таблица 1. Гидрирование н-гептена-1 в неподвижном слое катализатора

Условия опытов и результаты.

№ п/п	$W_ж$ см/сек	$W_г$ см/сек	$K_н$ сек$^{-1}$	$K_н C_{кат}$ сек$^{-1}$	$\beta_{ж-т}$ сек$^{-1}$	Примечание
1.	0,12	5,7	0,053	0,032	0,065	d= 1,6 мм
2.	0,45	5,7	0,520	0,031	0,080	P_{H_2} = 2,3 ат
3.	0,82	5,7	0,180	0,110	0,260	K* =0,75 1/сек
4.	1,24	5,7	0,160	0,096	0,300	$C_{кат}$ = 0,6
5.	2,00	5,7	0,310	0,190	0,350	K = 40 1/сек
6.	0,45	2,2	0,057	0,034	0,080	t = 23 ^{o}C
7.	0,45	3,6	0,059	0,035	0,080	
8.	0,45	10,0	0,074	0,044	0,090	
9.	0,12	6,2	0,007	0,004	0,009	
10.	0,45	6,2	0,040	0,024	0,060	d= 0,34 см
11.	0,82	6,2	0,080	0,048	0,070	P_{H_2} = 2,1 ат
12.	1,24	6,2	0,110	0,066	0,080	K* =0,4 1/сек
13.	2,03	6,2	0,140	0,087	0,098	$C_{кат}$ = 0,6
14.	0,45	2,3	0,053	0,032	0,051	K = 40 1/сек
15.	0,45	3,6	0,054	0,032	0,051	t = 23 ^{o}C
16.	0,45	5,1	0,056	0,034	0,060	
17.	0,45	12,1	0,074	0,044	0,060	

Таблица 2. Гидрирование н-гептена-1 в псевдоожиженном слое катализатора
Условия опытов и результаты.

№ п/п	$W_ж$ см/сек	$W_г$ см/сек	$K_н$ сек$^{-1}$	$C_{кат}$ 1/1	$K_н C_{кат}$ сек$^{-1}$	$\beta_{ж-Т}$ сек$^{-1}$	$K^* C_{кат}$ сек$^{-1}$	$\beta_{2-ж}$ сек$^{-1}$	Примечание
1.	0,28	1,70	0,37	0,49	0,18	1,70	2,94	0,22	неоднородный
2.	1,24	2,10	0,41	0,44	0,18	1,82	2,64	0,22	псевдоожижен.
3.	0,61	2,10	0,28	0,52	0,15	1,47	3,12	0,18	слой
4.	1,50	2,10	0,47	0,41	0,19	1,86	2,46	0,23	d=0,19 мм
5.	2,00	2,10	0,60	0,37	0,22	1,98	2,22	0,28	K*=6,0 1/сек
6.	1,50	2,00	0,39	0,41	0,16	1,86	2,46	0,19	K=40 1/сек
7.	1,50	3,40	0,44	0,41	0,18	1,86	2,46	0,22	P_{H_2}=2,1 ат
8.	1,50	4,80	0,46	0,41	0,19	1,86	2,46	0,23	t= 23 ^{o}C
9.	1,50	8,00	0,53	0,41	0,22	1,86	2,46	0,28	
10.	1,10	2,50	0,95	0,28	0,27	2,86	3,02	0,33	однородный
11.	1,34	2,50	1,04	0,27	0,28	3,08	2,92	0,35	псевдоожижен.
12.	1,76	2,50	1,20	0,22	0,26	2,86	2,38	0,33	слой
13.	2,03	2,50	1,35	0,18	0,24	2,52	1,95	0,31	d=0,1 мм
14.	2,20	2,50	1,45	0,17	0,25	2,46	1,84	0,33	K*=10,8 1/сек
15.	2,00	2,10	1,04	0,18	0,19	2,52	1,95	0,23	K=40 1/сек
16.	2,00	3,30	1,70	0,18	0,31	2,52	1,95	0,44	P_{H_2}=2,3 ат
17.	2,00	5,40	2,90	0,18	0,53	2,52	1,95	0,95	t= 23 ^{o}C
18.	2,00	7,50	3,90	0,18	0,70	2,52	1,95	1,92	

ОБОЗНАЧЕНИЯ

a - удельная межфазная поверхность, $см^{-1}$.
$C_{кат}$ - концентрация катализатора в жидкости, л/л.
$d_{кат}$ - диаметр частицы катализатора, см.
$d_{п}$ - диаметр газового пузыря, см.
$D_{э}$ - коэфф. эффект. диффузии внутри пористого зерна, $см^2$/сек.
$D_{м}$ - коэффициент молекулярной диффузии, $см^2$/сек.
$K_{н}$ - суммарная наблюдаемая константа скорости реакции первого порядка, учитывающая влияние процессов, внешнего и внутреннего массопереноса, 1/сек.
K^* - наблюдаемая константа скорости реакции первого порядка, учитывающая диффузионное торможение внутри пористого зерна, 1/с
K - истинная константа скорости реакции первого порядка, 1/сек.
q - навеска катализатора, л.
$Q_{ж}$ - расход жидкого сырья, л/сек.
t^* - среднее время контакта поверхностных элементов газа и жидкости, сек.
$V_{ж}$ - объем жидкой фазы в реакторе, л.
$w_{ж}$ - линейная скорость жидкости, отнесенная к полному сечению реактора, см/сек.
$W_{г}$ - то же для газа,
$W_{п}$ - скорость свободного всплывания пузыря, см/сек.
$W_{кр}$ - скорость начала псевдоожижения в двухфазной системе жидкость-твердое тело, см/сек.
W_{og} - скорость жидкости, при которой наступает режим однородного псевдоожижения, см/сек.
X^* - равновесная концентрация растворенного водорода в гептане, моль/л.
$У_{н}, У_{к}$ начальная и конечная концентрации н-гептана-1 в растворе, моль/л.
β - коэффициент массопереноса, отнесенный к единице объема жидкости, 1/сек.
$\gamma_{т}$ - удельный вес катализатора, кг/м³.
$\gamma_{ж}$ - удельный вес жидкости, кг/м³.
ε - порозность слоя катализатора [-] .
$V_{ж}$ - вязкость жидкости, $см^2$/сек.
$V_{г}$ - вязкость газа, $см^2$/сек.
$ф_{г}$ - параметр Тиле [-] .

$Nu = \frac{K_{ж-т} d}{D_{м}}$ критерий Нуссельта; $Re_{ж} = \frac{W_{ж} d}{V_{ж}}$; $Re_{г} = \frac{W_{г} d}{V_{г}}$ критерий Рейнольдца; $Pr = \frac{V_{ж}}{D_{м}}$ критерий Прандтля; $Ar = d^3 \gamma_{ж} (\gamma_{т} - \gamma_{ж}) / u_{ж}^2$ критерий Архимеда.

СПИСОК ЛИТЕРАТУРЫ

1. СЛИНЬКО,М.Г.,ЕРМАКОВА,А.,ЗИГАНШИН,Г.К.,СТЕФОГЛО,Е.Ф., ТОХ Т.7,1, 35(1973).

2. ЗИГАНШИН,Г.Х.,канд.дисс.,Институт катализа СО АН СССР,1971г.
3. SHERWOOD,T.K., FARKAS,E.I., Chem.Eng.Sci.,21, 573,(1966).
4. KÖLBEL,H.,MANNING,B.Z.,Elektrochem. 66,774,(1962).
5. SATTERFIELD,C.M.,PELLOSSOT,A.A.,SHERWOOD,T.K., Am.Inst.Chem. Engrs.Journ., 15, №2, 226, 1969г.
6. KÖLBEL,H.,HAMMER,H.,De Chema Monograph.,49, 277,(1964).
7. SLESSER,C.G.,HIGHET,I.,Brit.Chem.Eng.11, 247,(1966).
8. ROSS,L.D.,Chem.Eng.Progr., 61, №10, 77,(1965).
9. МАШКИНА,А.В.,ЕРМАКОВА,А.,САВОСТИН,Д.А.,Нефтехимия,5,№4,583, (1965).
10. ЕРМАКОВА,А.,ЗИГАНШИН,Г.Х.,СЛИНЬКО,М.Г.,ТОХТ,4,№1,95,(1970).
11. ЕРМАКОВА,А.,ЗИГАНШИН,Г.Х., ТОХТ,4, №2, 286,(1970).
12. АСТАРИТА,Дж. Массопередача с химической реакцией,„Химия", 1971г.
13. ЗИГАНШИН,Г.Х.,СТЕФОГЛО,Е.Ф.,ЕРМАКОВА,А.,Кинетика и катализ, 14, №2, 530,(1973).

SUMMARY

The mass transfer was investigated in a gas - liquid - solid catalyst three phase system, as a model reaction the hydrogenation of n-heptene-1 was studied. Experiments were carried out using a static and a fluidized bed reactor, the fluidized system was inhomogeneous or homogeneous.

It was proved that the rate determining step of the mass transfer in a static catalyst layer is the reagent transfer to the surface of the catalyst; but in the case of fluidized bed this rate determining process is the mass transfer through the gas - liquid boundary layer. Using a homogeneous fluidized bed, as compared to the inhomogeneous system, a sharp increase of the mass transfer coefficient can be observed. The disadvantage of a homogeneous fluidized system is the significant extension of the layer.

Hungarian Journal
of Industrial Chemistry
Veszprém
Vol.3. pp. 51-70 (1975)

PROBLEMS RELATED TO THE LONG-TERM OPERATION OF COPPER-LYE CARBON MONOXIDE REMOVAL UNITS IN AMMONIA PLANTS

J. DÉVAY, F. RATKOVICS, B. SZEILER*, Mrs. E. CSÁSZÁR*
and L. DOMONKOS

(Veszprém University of Chemical Engineering, Department of Physical Chemistry and Pét Nitrogen Works*)

Received: May 8, 1974.

The oxidation and reduction equilibria established in carbon monoxide removal with a copper ammonium formate solution, the so-called copper-lye, was examined. It was concluded that under industrial conditions the oxidation of copper ions occurs at a practically constant rate, whereas their reduction rate is dependent of the concentration of cuprous ions present. On the basis of these conclusions, the conditions for stable operation and the preferable manner for eliminating disturbances in the operation of the plant were determined.

INTRODUCTION

The technique for the removal of the carbon monoxide content from industrial gases based on absorption with a copper ammonium formate solution, the so-called copper-lye, has been known for a long time. In spite of the fact that this technique is widely used, especially in ammonia plants, there are very few publications that deal in detail with the theoretical fundamentals of the procedure, to be found in literature. The reason for this is probably that

the procedure is simple and if the necessary amount of copper, formic acid and ammonia are added to make up for the losses and the operation is appropriately controlled, the solution once prepared may be in operation for years, theoretically for an infinite time. However, it was experienced in the Péti Nitrogénmüvek (Pét Nitrogen Works) that from time to time, in an unpredictable manner, the steady-state operational conditions of the copper-lye-type carbon monoxide removal plant showed an abrupt change, the ratio of monovalent to divalent copper ions in the solution was shifted in the direction of an increase in the concentration of the divalent ion, and it was not possible to restore normal operating conditions through the application of the usual changes in the working parameters. The length of the undisturbed periods is generally several years, but nevertheless it seemed important to elucidate the cause of the disturbance, because experience shows that the elimination of such disturbances takes several days and involves considerable expense.

In order to find the cause of the disturbance and the possibility of its elimination or preferable termination, experiments were carried out with the co-operation of the Research Laboratory of the Pét Nitrogen Works and the Department of Physical Chemistry of the Veszprém University of Chemical Engineering. The aim of the present paper is to summarize the results of these experiments. However, prior to describing the experiments, it seems to be necessary to present a brief summary of the technological process used, its most important characteristics and the experiences in connection with the disturbance.

Characteristics of the Copper-Lye Type Carbon Monoxide Removal Unit

The flow diagram of the plant in question is shown in Figure 1. The gas to be purified (1) passes the scrubber (2), the sodium hydroxide washing unit (3) and the spray trap (4). The copper-lye, having left the scrubber (2) passes on through the residual

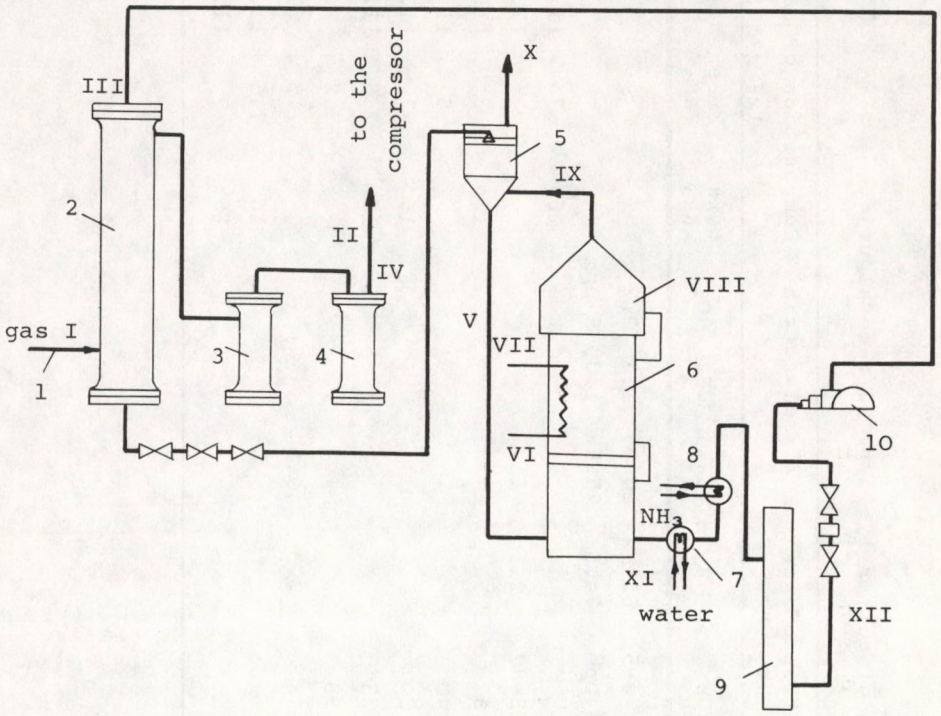

Fig. 1. Flow diagram of the plant

gas scrubber (5) to the decomposition column (6) and through the water (7) and ammonia-operated cooler (8) into the storage unit (9), from there to the copper-lye pumps and back again to the scrubber. The sampling and measuring points are marked by Roman characters in the Figure. The parameters characteristic of steady--state operating conditions are summarized in Table 1.

The composition of the copper-lye operating satisfactorily may fluctuate but within narrow limits, the characteristic figures being presented in Table 2.

Table 1. Operating characteristics of copper-lye type CO removal unit

Desig-nation	Pressure, atm.	Tempera-ture, °C	Composition of gas (or dissolved gas) vol.%						Composition of copper--lye g/100 ml			
			CO_2	CO	H_2	N_2	CH_4	O_2	total NH_3	Free NH_3	Cu^I	Cu^{II}
I	121	18-20	0.5	4-5	65-72	20-25	1.3	0.2				
II	119	15	20 ppm	5 ppm	74.5	25.5	1.3	5 ppm				
III	125	8-10							16	7	11.5	2.5
IV	800 mm w.g.	15	11-11	85-87	2.5	1					11.0	3.0
V		45-50	7.5	62					12	3	11.0	3.0
VI		65	11.5	40						5	11.2	2.8
VII		75	10	30					16	7	11.2	2.8
VIII		82	15.5	23					16	7.5	11.3	2.7
IX		75	12.5	55						3.2		
X	280 mm w.g.	40	16.5	78	2.5	0.8				2.5		
XI		45							16	7.5	11.5	2.5
XII		8-10							16	7	11.3	2.7

Table 2. Characteristic data of copper-lye in steady-state operation

Component	Concentration g/100 ml
cuprous	10.5 - 11.5
cupric	2.5 - 3.5
total copper	13 - 14
carbonate-CO_2	4
formic-acid-CO_2	8 - 11
total CO_2	15
total NH_3	16
oil content	0.01

The experience acquired in connection with the unexpected and seemingly unreasonable disturbances, mentioned in the introduction, can be summarized as follows:

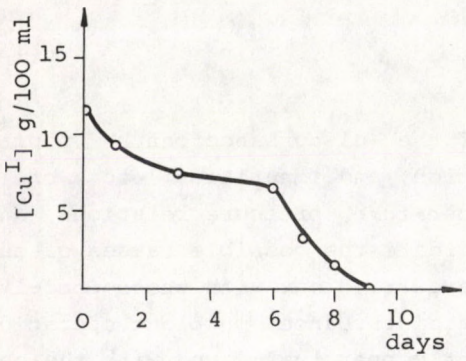

Fig.2. Changes in the cuprous ion content of the copper-lye during disturbance

The usual monovalent copper content of 10-11 g/100 ml of the copper-lye shows a gradual decrease. In such a case the plant management reacts by carrying out the usual measures (controlling the temperature and the level in the regenerator) and in general the process can be reserved in this manner. However, in some cases, these usual measures prove to be ineffective. It also may occur that due to some failure in the apparatus it is impossible to carry out temperature or level control. In such cases, the concentration of cuprous copper in the copper-lye undergoes an abrupt decrease and a disturbance in plant

Table 3. Variations in the cuprous ion content of copper-lye in a typical disturbance

Time	Copper, g/100 ml cuprous	cupric	Remark
Starting	11.5	2.5	normal operation
1 day	9.2	3.9	commencing disturbance
3 days	7.27	4.7	
6 days	6.61	5.86	
7 days	3.1	7.9	
8 days	1.7	10.1	
9 days	0.1	10.2	

operation results. Changes in the cuprous ion content of the copper-lye during such a period are shown in Table 3 and Fig. 2.

Laboratory Experiments

Fundamentally, the cause of the disturbance can be sought either in the copper-lye (composition, and impurities, etc.) or in the technological parameters (temperature, pressure relations, and residence times). In order to elucidate the possible causes of the phenomenon, comparative tests were carried out with the copper-lye that had to be exchanged due to a disturbance in plant operation (in the following termed "spent copper lye") and with the one newly prepared and working appropriately (in the following termed "fresh copper lye"). The results of these examinations are summarized in Table 4.

It is apparent from Table 4 that the most important difference between the spent and the fresh sample is the following: all of the copper content of the spent copper-lye is present in the form of cupric copper, whereas the fresh sample contains a considerable amount of cuprous copper. The further analytical data reveal no

Table 4. Characteristics of fresh and spent copper-lye

Analysis results	Spent copper-lye	Fresh copper-lye
Total copper content, g/100 ml	10.60	14.40
Cuprous copper content	0.10	11.05
Carbonate carbon dioxide	4.48	2.68
Total carbon dioxide	10.76	13.94
Total ammonia	22.35	17.03
Evaporation residue	33.73	29.14

significant difference. (The tests were carried out with the usual testing methods) [1].

An attempt was made to find the answer to the question: what non-volatile components are enriched during the long-term operation of the copper-lye. For this purpose, the ignition residue of the copper-lyes was examined by spectroscopy. The analysis was made to obtain a comparison and consequently it was considered satisfactory to obtain semi-quantitative data. The orders of magnitude of the different contaminants are presented in Table 5.

It is apparent from the data shown in Table 5 that some elements are enriched in the spent copper-lye. The solution contains considerable amounts of iron (in the form of iron oxide and hydroxide) and aluminium. The enrichment is about tenfold in the case of Fe, Si, Mg, Mn, Cr, Ni and Ca, about a hundredfold in the case of Al and Pb, and no enrichment occurs with Na, Zn and W. The amount of elements not mentioned in the table was below the limit of detection.

The most important property of copper-lye for the present purpose is that it can be reduced by carbon monoxide (the rate of reduction) and the rate of oxidation by oxygen, since the ratio of mono and divalent copper ions is determined by these quantities.

Table 5. Order of magnitude of non-volatile impurities of fresh and spent copper-lye

Component	% by wt. in ignition residue	
	spent copper-lye	fresh copper-lye
Fe	X - O,X	O,X - O,OX
Al	O,X	O,OOX
Si	O,OX - O,X	O,OX
Mg	O,X	O,OX
Mn	O,OX	O,OOX
Pb	O,OX - O,X	O,OOX
Sn	O,OOX	O,OOX
Ni	O,OOX - O,OX	O,OOX
Cr	O,OOX - O,OX	traces
Ca	O,OX - O,X	O,OOX - O,OX
Na	O,X	O,X
Zn	less than O,OX	less than O,OX
W	less than O,OX	less than O,OX

At first, examinations concerning the rate of oxidation were carried out.

Examination on the Oxidation of Copper-Lye

Under plant conditions, the copper-lye is necessarily in contact with oxygen and consequently there is a possibility for its oxidation. It is not probable that considerable oxidation may occur, except by air oxygen in the storage container and by the oxygen content of the gas to be purified ($P_{O2} \approx$ 0.2 atm). Accordingly, oxidation - whether it occurs in the storage container or in the absorption column - is brought about by oxygen of a partial pressure of 0.2 atm. Accordingly, the examination was carried out in such a way that basically this procedure was realized.

It should be mentioned that the spent copper-lye contained no cuprous ions and consequently part of the copper content had to be reduced before oxidation. This was carried out by the addition of hydrazine, whereby care had to be exercised not to allow any excess hydrazine to remain.

Oxidation was followed by titration in such a manner that the copper-lye was agitated in contact with air and a sample was taken from time to time. (An attempt was also made to follow the oxidation process by the measurement of the oxygen consumption, but gases escaping from the copper-lye falsified the results of these measurements). The results are shown in Table 6. (The requirement of titrant solution, which is proportional to the concentration of cuprous ions, is plotted against time.)

The data contained in the Table are illustrated by Figures 3 and 4.

Table 6. Oxidation of copper-lye

Oxidation of copper-lye in air					
Time of oxidation (min.)	ml titrant required (proportional to cuprous content)				
	spent copper-lye		fresh copper-lye		
	20°C	40°C	20°C	30°C	40°C
0	9.6	9.6	18.8	18.8	18.8
20	8.5	8.1	16.0	14.6	13.1
40	7.4	6.3	12.3	11.15	10.0
60	6.3	4.2	10.7	9.1	7.0
80	5.0	3.2	8.5	6.7	4.5
100	3.65	1.6	6.5	4.4	2.8
120	2.1	0.85	5.1	2.7	1.5
140		0.3	3.5	1.5	0.6
170			1.6	0	0
200			0		

It was strikingly apparent that whereas the spent copper lye is oxidized at a constant rate (zero-order reaction), the oxidation rate of the fresh copper-lye is dependent on the progress of the reaction. In general, in the case of spent copper-lye

$$-\frac{dx}{dt} = k = -\frac{\Delta x}{\Delta t}$$

and in the case of a fresh copper-lye

$$-\frac{dx}{dt} = k\, x^n$$

(where dx is the amount transformed, t is time, k is the rate constant and n is the order of the reaction) are the equations describing the reaction rate.

The kinetic order was determined graphically and was found to be n = 0.43. This can approximately be taken as 0.5 and accordingly the equation describing the rate of oxidation is the following:

$$-\frac{dx}{dt} = k \cdot x^{1/2}$$

The activation energy, calculated on the basis of the temperature-dependence of the rate con-

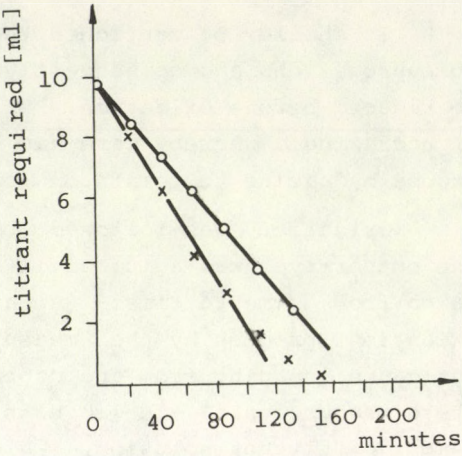

Fig. 3. Oxidation of boiled spent copper-lye. o - 20°C; x - 40°C

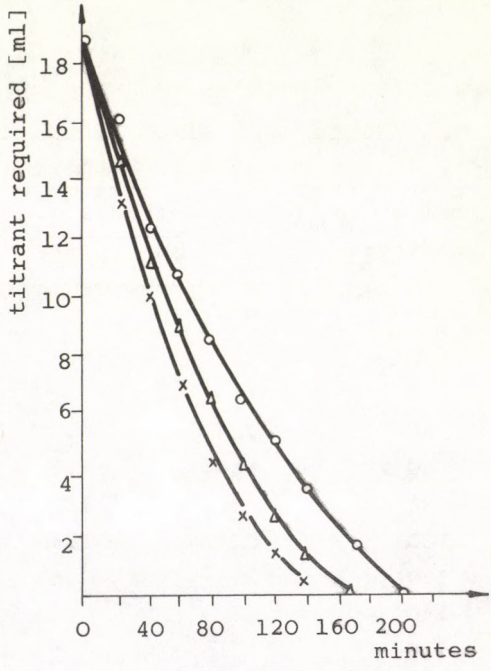

Fig. 4. Oxidation of boiled fresh copper-lye. o - 200°C, Δ - 300°C, x - 400°C

stants, is for the spent copper-lye E_{spent} = 3,600 cal/moles and for the fresh copper-lye E_{fresh} = 5,100 cal/moles.

The following conclusions were drawn from the data presented in the foregoing and from the qualitative picture:

Any oil content present in the copper-lye forms a film on the surface which hinders the passage of oxygen into the solution. In spent copper-lye, having a relatively significant oil-content, the rate of oxidation is determined by the diffusion rate of O_2 across the oil film. The chemical reaction is faster than diffusion through the film. This picture seems to be supported by the fact that the activation energy of the process is considerably lower in spent copper-lye than in the fresh one. The fresh copper-lye is oxidized more quickly than the spent one and this is possible only if in this case the diffusion process in the boundary layer is faster than in the spent copper-lye. Due to the faster diffusion, the chemical process becomes rate-determining in this solution, and hence the rate of oxidation is dependent, not only on the rate of diffusion, but also on the cuprous ion concentration of the solution.

It seems to be self-evident that the difference between the properties of the two solutions may be connected with the oil contamination of the spent copper-lye.

The higher activation value calculated from the data of the fresh copper-lye are in agreement with the fact that in this case the chemical process is the rate-determining one.

Examination of the Reduction of Copper-Lye

One of the processes of regeneration is the reduction of part of the copper content, depending on the cuprous:cupric ratio in the solution.

The reduction experiments were carried out with carbon monoxide in such a manner that the solution to be tested was saturated with carbon monoxide of 1 atm. pressure and a sample was with-

drawn from the solution from time to time, in order to determine the cuprous:cupric ratio. The reaction of the reduction with carbon monoxide is composed of a number of partial processes. Carbon monoxide is absorber by the ammonia-containing copper formate complex and the CO exerts its action in the compound thus formed.

In the first stage of the examinations it was concluded that the reduction proceeds at the highest rate at a temperature of about 40°C if the partial pressure of CO is atmospheric. The other aim of the experiments was the elucidation of the kinetics of the reduction process. It was expected that this will furnish an answer to the question why the spent copper-lye became unreducible.

The results of the reduction experiments are contained in Table 7. These results were illustrated in such a manner that the rate of reduction, plotted against the cuprous ion concentration, was drawn into a single diagram (Fig. 5).

Table 7/1. Reduction of 10 ml spent + 90 ml fresh copper-lye with CO

time/hours	cuprous, g/100 ml	time/hours	cuprous, g/100 ml
0	8.7	5	11.95
1	8.96	6	12.46
2	10.04	19	12.59
3	10.68	20	13.10

Table 7/2. Reduction of 20 ml spent + 80 ml fresh copper-lye with CO

0	8.1	5	9.98
1	8.17	6	10.23
2	8.26	7	10.62
3	9.15	23	13.35
4	9.66		

Table 7/3. Reduction of 30 ml spent + 60 ml fresh copper-lye with CO

time/hours	cuprous, g/100 ml	time/hours	cuprous, g/100 ml
0	6.42	6	8.90
1	6.67	7	8.96
2	6.80	23	10.68
3	7.63	24	10.87
4	8.07	25	11.25
5	8.71		

Table 7/4. Reduction of 40 ml spent + 60 ml fresh copper-lye with CO

0	4.96	6	6.99
1	5.09	22	10.17
2	5.47	23	10.93
3	6.10	24	11.57
4	6.55	25	12.94
5	6.93	46	13.41

Table 7/5. Reduction of 60 ml spent + 40 ml fresh copper-lye with CO

0	2.89	26	7.62
1	2.94	42	8.96
2	3.50	43	9.47
3	4.00	44	10.17
4	4.32	45	10.98
5	5.59	46	10.36
20	5.78	66	12.60
21	6.17	67	12.39
22	6.42	68	13.34
23	6.42		
24	6.80		
25	7.37		

It can be concluded that in the case of copper-lyes of 19 g/100 ml total copper concentration, the reaction occurs at the highest rate in the lye containing 8.5 g/100 ml cuprous copper. At cuprous ion concentrations either higher or lower than that, the reaction rate shows a very rapid decrease. The auto-catalytic character of the reaction suggests that the presence of cuprous ions accelerates the absorption of CO.

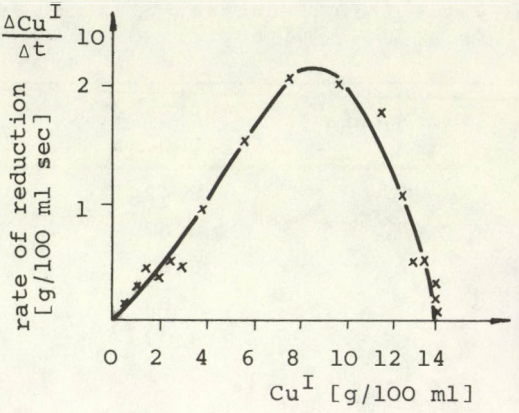

Fig.5. Rate of reduction, plotted against cuprous ion concentration

It is assumed that the reaction is an auto-catalytic one, which can formally be described by a rate equation of the following form:

$$\frac{d[Cu^I]}{dt} = K\,[Cu^I][Cu^{II}]$$

The experiments confirmed that the reaction rate is not influenced to an appreaciable degree by the following factors: oil content, metal ion impurities, and ammonia and ammonium carbonate in the concentration range present in the fresh and spent copper lye.

The rate of reduction as a function of the cuprous copper content was determined by mixing spent and properly working fresh lyes to various ratios.

If fresh, properly working lye was totally oxidized with air and thereupon reduced with CO, the reduction was found to start very slowly, after a period of 72 hours (Table 8).

Accordingly, it can be concluded that the reduction of copper-lye with CO and in the case of a constant excess of CO, depends both on the cuprous ion content and the cupric ion concent-

Table 8. 100 ml boiled copper-lye (fresh) oxidized with air followed by reduction with CO

time/hours	cuprous, g/100 ml	time/hours	cuprous, g/100 ml
1	0	102	2.54
2	0	103	2.67
3	0	104	3.81
4	0	120	4.20
72	0.95	125	4.83
73	0.95	127	6.36
74	1.02	149	7.31
75	1.21	157	7.82
76	1.27	168	8.96
96	1.91	216	12.27
100	2.29		

ration. It appears that the concentration of cuprous ions influences the amount of CO bound by absorption and thereby influences the rate of reduction. The influence of cupric ion concentration is readily understood, since this component is one of the materials taking part in the reaction. The rate of the reduction process also depends on the temperature. Its optimum value is determined by the relative ratio of two processes of opposed effects. At low temperatures, the reaction rate becomes low, whereas at higher temperatures the absorption is supressed. The results of the examinations carried out with respect to these are shown in Figure 6.

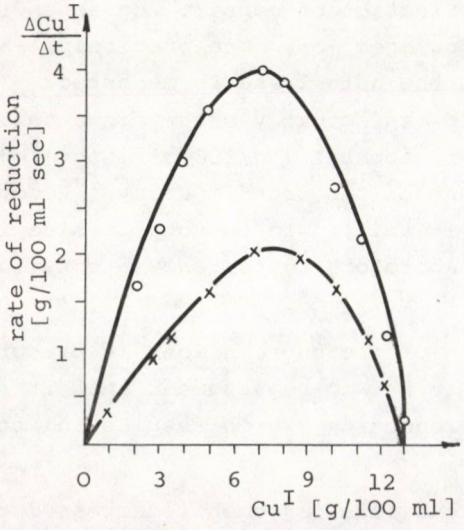

Fig.6. Rate of reduction, plotted against cuprous ion concentration. o - 80°C; x - 50°C

DISCUSSION

In the opinion of the authors, a change in the cuprous:cupric ratio in a copper-lye, having worked properly for years on end, is brought about by the simultaneous action of a number of factors. In the authors' opinion, the probable process of the development of the disturbance is the following:

1. In the course of operation, iron salts accumulate in the copper-lye. These are mainly corrosion products, present in the copper-lye either in a dissolved form or as a floating precipitate. This fact remains unnoticed by the plant management, because the analytical prescription for the determination of cuprous copper contains titration with permanganate. In this titration, an amount of ferrous salts equivalent to the amount of cuprous copper is titrated, because the ferric salt added to the solution oxidizes the cuprous copper. It follows that any iron present as impurity, together with cuprous copper, can be only in the form of the divalent form. However, this means that ferrous ions present as impurity are in the course of the titration determined together with the ferrous ions produced in the oxidation of copper. Consequently, the result obtained is an erroneous one, or, more precisely, an amount of cuprous ions higher than the actual one is measured. In the case of 10 % iron content (this can actually occur) in a solution containing 10 g/100 ml copper, about 1.4 g/100 ml monovalent copper can be found only on account of the iron impurity. Accordingly, the cuprous:cupric ratio is shifted to the cupric side in the course of use, whereas the laboratory tests show a constant value.

2. The rate of the oxidation of the cuprous ions is practically constant and consequently it has to be assumed that it is the decrease in the rate of the reduction which results in the change of the cuprous:cupric ratio.

If the concentration of cuprous ions is somehow decreased to a value below 7.5 g/100 ml, an abrupt decrease in the rate of the

reduction reaction is to be expected. In such a manner, a situation may be brought about in which the rate of reduction is lower than that of oxidation. Should this be the case, the rate of reduction is decreased even faster and the disturbance in plant operation is brought about.

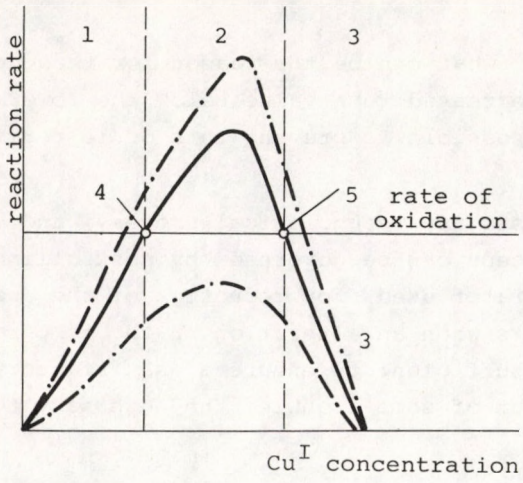

Fig. 7. Equilibrium of oxidation and reduction of copper-lye. 1 - ratio of cuprous ion decreases; disturbance; 2 - ratio of cuprous ion increases; 3 - ratio of cuprous ion decreases; 4 - unstable working point; 5 - steady state working point

These conditions are schematically illustrated in Figure 7. It is self-evident that the rate of oxidation is dependent on the surface area of the containers, the shape of the latter, and the O_2 content of the gas to be purified, etc. - all parameters that are not likely to show abrupt changes, but are, to a good approximation, constant. This is illustrated by the horizontal straight line in Figure 7. The rate of reduction, when plotted against the cuprous ion concentration, os described by a bell-shaped curve.

The rates of reduction and oxidation are equal at two concentrations. The higher concentration is the stable working point whereas the lower one is unstable. These points define three areas (broken lines). In the range of the lowest cuprous ion concentrations, reduction is slower than oxidation, and accordingly disturbance is caused in the operation. In the middle area, reduction is faster and consequently the cuprous ion concentration in the solution is increasing. In the third area, oxidation is faster and the

concentration of cuprous ions is decreased as long as the value corresponding to the working point is reached.

It should also be noted that the position of the working point can be shifted by altering the temperature or duration of the reduction. A reduction corresponding to a higher temperature and another to a lower one, respectively, are shown in the Figure drawn with a dotted line.

The question is now, what can be the reason for the cuprous ion concentration to be decreased to a value below the lower working point, and how is it possible to prevent this or to terminate the disturbance.

According to the customary technological process, and under normal conditions the process can be governed by controlling the temperature of the regenerator used for reduction of the copper lye. The disturbance occurs when an alteration in the temperature of the regenerator is insufficient to ensure a satisfactory reduction rate (or, on account of some trouble, the necessary temperature cannot be ensured).

It seems very probable that the oily emulsion collected in the regenerator column may take up a considerable fraction of the volume of the upper conical part of the regenerator, whereby its useful volume is decreased to an appreciable degree. It is very likely that disturbances that cannot be compensated by increasing the temperature, are brought about first of all by a decrease in residence time caused by the above-mentioned procedure. If follows from the foregoing that there are two possibilities for the elimination of disturbances of this kind:

1. Changing the copper-lye for a fresh one of high cuprous ion content of faultless operation, with simultaneous emptying and de-oiling of the regenerator column.

2. Intensive reduction of the copper-lye; however, this can be successful only with simultaneous emptying of the regenerator.

Reduction can be carried out in such a manner that the working solution of adequate cuprous copper content is prepared in

the regenerator (or in a separate apparatus) by increasing the residence time, by making use of the CO content of the solution, or by the addition of metallic copper. The experiments have shown that working and oxidized copper-lyes can be mixed with each other, as long as it is observed that the cuprous ion content of the solution is not decreased below the critical value (about 6 g/100 ml).

REFERENCES

1. KERESZTES, M., Nitrogénipar (Nitrogen Industries), Budapest, Müszaki Könyvkiadó, 1955.

РЕЗЮМЕ

Авторами исследовано равновесие окисления и восстановления окиси углерода с помощью медно-аммиачного раствора.

Установлено, что скорость окисления ионов меди практически постоянна, а скорость восстановления зависит от концентрации ионов закиси меди в заводских условиях. На основании этого установлены условия стабильной работы башни и целесообразные методы устранения перебоев в эксплуатации.

Hungarian Journal
of Industrial Chemistry
Veszprém
Vol. 3. pp. 71-78 (1975)

UNTERSUCHUNGEN DER ALTERUNG VON LACKEN AUF POLYURETHAN-BASIS AUF GRUND DIELEKTRISCHER RELAXATIONSERSCHEINUNGEN

J. DÉVAY, L. KOVÁCS*, F. HORKAY*, L. MÉSZÁROS

(Universität für Chemische Industrie Veszprém, Lehrstuhl für Physikalische Chemie, BUDALAKK Farben- und Kunstharzfabrik, Budapest*)

Eingegangen am 8. Juli 1974.

Es wurde mit Hilfe dielektrischer Meßmethoden die bei atmosphärischer Beanspruchung auftretende Alterung von Polyurethanlacken geprüft, die durch aromatischen, bzw. aliphatischen Isozyanat verhärtet wurden.

Den Strukturänderungen im Laufe des Alterungsprozesses wurden durch die Messung der Veränderungen der Aktivierungsenergiewerte und Dispersionsbereiche gefolgt, die auf Grund der Temperaturabhängigkeit des bei verschiedenen Frequenzwerten gemessenen dielektrischen Faktors bestimmt wurden.

Der dielektrische Faktor der Stoffe, die polare Gruppen enthalten, hängt in bedeutendem Maße von der beim Messen gebrauchten Frequenz und von der Temperatur der Probe ab. Die Erscheinung ist damit zu erklären, daß diese Gruppen - infolge ihrer thermischen Energie - eine ungeordnete statistische Bewegung vollführen, die das äußere elektrische Feld mit Hilfe des auf die Dipole verübten Drehmoments zu orientieren versucht. Die Orientation der polaren Gruppen erhöht die Polarisation in bedeutendem Maße und dadurch auch den dielektrischen Faktor. Bei festgelegter Frequenz nimmt

die Orientationswirkung durch die Erhöhung der Temperatur anfangs zu, später jedoch, beim weiteren Steigen der thermischen Bewegung tritt eine Desorientation auf. Bei ständiger Temperatur wird durch die Erhöhung der Frequenz die Orientation immer schwerer, was mit der Trägheit der polaren Gruppen zu erklären ist, so nimmt also die Polarisation, d.h. der dielektrische Faktor mit der steigenden Frequenz ab. Die Erhöhung des dielektrischen Faktors bei steigender Temperatur, bzw. dessen Sinken bei steigender Frequenz spielen sich im Bereich der Temperatur-, bzw. Frequenzwerte ab, die charakteristisch auf die Beweglichkeit der polaren Gruppen, auf die Beschränkung ihres Bewegens sind. Dieser Temperatur-, bzw. Frequenzbereich wird als Dispersionsbereich bezeichnet, die Temperatur, bzw. die Frequenz, die zum Inflexionspunkt der die Temperatur-, bzw. die Frequenzabhängigkeit des dielektrischen Faktors darstellenden Kurve gehört, ist die Relaxationstemperatur (t_r), bzw. die Relaxationsfrequenz (ω_r) [1, 2, 3].

Die bei der Alterung auftretenden strukturellen Veränderungen der Lackanstriche sind mit dem Entstehen oder Zerlegen der polaren Gruppen, bzw. mit der Veränderung deren Umgebung verbunden, deswegen zeigen sie sich sehr merklich bei der Verschiebung der Relaxationsbereiche.

Die Temperaturabhängigkeit der Relaxationsfrequenz kann mit guter Annäherung durch die Arrhenius-Gleichung

$$\omega_r = A\, e^{-\frac{E_a}{RT}}$$

dargestellt werden, wo E_a die Aktivierungsenergie der Dipolorientation bedeutet. Die Veränderung der Aktivierungsenergie beim Altern weist auf die Veränderung der Beschränktheit der Dipolorientation hin, was als Folge der Vernetzung, der Degradation, sowohl der Verdampfung des Lösungs- und Erweichungsmittels sein kann.

Sowohl die Verschiebung des Relaxationsbereiches, als auch die Veränderung der Aktivationsenergie ist für die Veränderung der Struktur der Anstriche bezeichnend, deshalb wurde bei den Untersuchungen die Veränderung beider Werte in Betracht genommen.

Im Laufe unserer Untersuchungen wurde mit besonderer Rücksicht auf die Wechselwirkung der Pigmente-Bindemittel die unter atmosphärischen Umständen stattgefundene Alterung der farblosen und der mit Anatas, bzw. Rutil pigmentierten Modifikationen der mit aliphatischem und aromatischem Isozyanat verhärteten Polyurethanlacke geprüft.

Die zu den Untersuchungen gebrauchten Anstriche wurden mittels einer Sprühpistole auf säurebeständige Stahlplatten mit Durchmesser von 30 mm in zwei Schichten 40-60 µm dick aufgebracht. Die vorbereiteten Probeplatten wurden bis zum Beginn der Beanspruchung, bzw. den Untersuchungen bei Zimmertemperatur, vor Licht geschützt und bei einem relativen Feuchtigkeitsgehalt von etwa 60 % aufbewahrt.

Ein Teil der auf diese Weise vorbereiteten Platten wurde nach zweiwöchigem Trocknen einer atmosphärischen Beanspruchung ausgesetzt, der andere Teil wurde in Laboratoriumsumständen zur Feststellung der Veränderungen bei Lagerung ohne Beanspruchung aufbewahrt.

Die in den Proben auftretenden Strukturänderungen wurden mit Hilfe der thermodielektrischen Analyse festgestellt; der dielektrische Faktor ist bei Frequenzwerten 200, 500, 700 und 1000 Hz gemessen worden, wobei die Temperatur der Proben zwischen 20 - 150^{o} mit einer Geschwindigkeit von ungefähr 2 ^{o}C/Minute geändert wurde [4].

Zur Veranschaulichung der so erhaltenen dielektrischen Spektren werden auf Abb. 1 die bei 1000 Hz gemessenen dielektrischen Spektren der mit Rutil und Anatas pigmentierten Modifikationen des mit aliphatischem Isozyanat gehärteten Polyurethananstrichen gezeigt, und zwar, im Zustand ohne Beanspruchung und nach einem sechsmonatigen atmosphärischen Alterungsprozeß.Auf der Abbildung 1 ist die Verschiebung des Dispersionsbereiches in Richtung der höheren Temperatur gut zu sehen.

Die Bewertung der dielektrischen Spektren geschah auf Grund der Verschiebung der Relaxationstemperatur und der Veränderung der Aktivierungsenergie; zum Vergleich dienten die Proben ohne Beanspruchung.

Die Abb. 2 zeigt die Veränderung der Relaxationstemperatur der farblosen, bzw. mit Rutil und mit Anatas pigmentierten Modifikationen des mit aliphatischem Isozyanat gehärteten Polyurethananstriches nach Lagerung ohne Beanspruchung und im Falle atmosphärischer Beanspruchung.

Es konnte festgestellt werden, daß sich die Relaxationstemperatur der Anstriche bei Lagerung ohne Beanspruchung nach etwa 2 Monaten stabilisiert hat und änderte sich während der Untersuchungen nicht weiter. Die Erhöhung der Relaxationstemperatur in den ersten 2 Monaten ist mit der weiteren Verhärtung zu erklären, die mit der weiteren langsamen Vernetzung nach dem Trocknen im Zusammenhang steht.

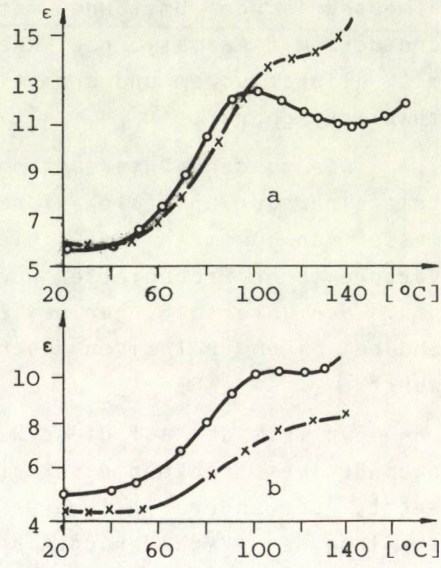

Abb.1.Dielektrisches Spektrum des mit aliphatischem Isozyanat gehärteten Polyurethananstriches; a) pigmentiert mit Rutil; b) pigmentiert mit Anatas; o - ohne Beanspruchung, x - nach einem sechsmonatigen atmosphärischen Alterungsprozeß

Bei atmosphärischer Beanspruchung zeigt sich die Wirkung der Pigmentierung viel prägnanter. Im Falle des farblosen Anstriches beginnt die Relaxationstemperatur nach zweimonatiger Beanspruchung zu steigen, was auf die Änderung der Struktur des Anstriches, wahrscheinlich auf die auftretende Oxydation hinweist.Eine ähnliche Erscheinung kann auch bei der Relaxationstemperaturveränderung des mit Anatas pigmentierten Anstriches festgestellt werden, mit dem Unterschied, daß der Beginn der Oxydation in diesem Fall durch die Pigmente verzögert wird. Dagegen stabilisiert sich die Relaxationstemperatur des mit Rutil pigmentierten Anstriches - ähnlich wie bei denen ohne Beanspruchung - nach einer einmonatigen Verhärtung und ändert sich auch bei weiterer Beanspruchung nicht mehr. Das weist darauf hin, daß das Rutil-

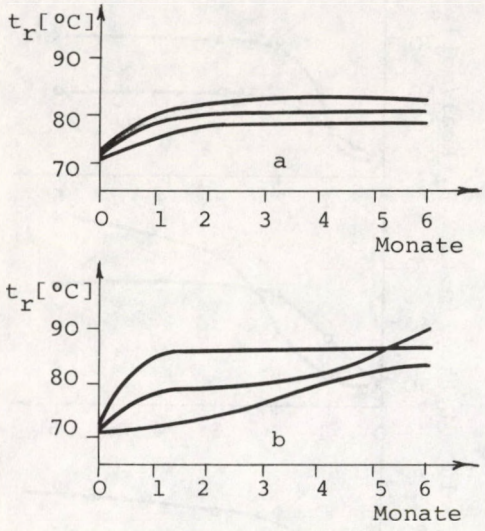

Abb. 2. Veränderung der Relaxationstemperatur des mit aliphatischem Isozyanat gehärteten Polyurethananstriches; a) bei Lagerung ohne Beanspruchung; b) bei atmosphärischer Beanspruchung; 1: farblos, 2: pigmentiert mit Anatas, 3: pigmentiert mit Rutil

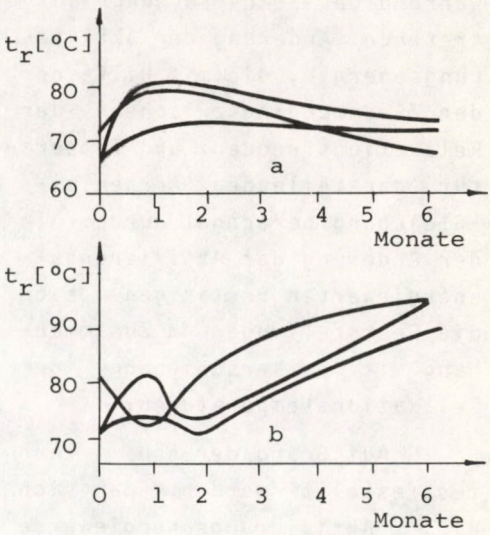

Abb. 3. Veränderung der Relaxationstemperatur des mit aromatischem Isozyanat gehärteten Polyurethananstriches; a) bei Lagerung ohne Beanspruchung, b) bei atmosphärischer Beanspruchung; 1: farblos, 2: pigmentiert mit Anatas, 3: pigmentiert mit Rutil

pigment die Stabilität,die Wetterbeständigkeit des Bindemittels in großem Maße erhöht.

Die Relaxationstemperatur der mit aromatischem Isozyanat gehärteten Polyurethananstriche (Abb. 3) zeigt auch im Falle der Lagerung ohne Beanspruchung eine wesentliche Veränderung, mit Ausnahme der mit Rutil pigmentierten Modifikation, die sich gleich denen auf der Abb. 2 stabilisierte. Bei atmosphärischer Beanspruchung jedoch wirkte die stabilisierende Wirkung des Rutils nur eine kurze Zeit (ungefähr 1 Monat), die Oxydation und Zersetzung des Bindenmittels konnte weder mit Anatas, noch mit Rutil verhindert werden.

Abb. 4 und 5 zeigen die während der Beanspruchung auftretende Änderung der Aktivierungsenergie, die mit Hilfe der den Zusammenhang zwischen der Relaxationsfrequenz und Temperatur darstellenden Arrhenius--Gleichung berechnet wurde. In der Änderung der Aktivierungsenergiewerten bestätigen sich die Feststellungen im Zusammenhang mit der Verschiebung der Relaxationstemperaturen.

Auf Grund der Abb. 4 kann festfestellt werden, daß sich die Aktivierungsenergiewerte bei den Anstrichen, die ohne Beanspruchung gelagert wurden, bei allen drei Modifikationen nach 2 Monaten stabilisiert haben. Nach einer atmosphärischen Beanspruchung bewahrt diese Eigenschaft nur der mit Rutil pigmentierte Anstrich, die Aktivierungsenergie der zwei anderen Modifikationen zeigt eine wesentliche Strukturänderung auf.

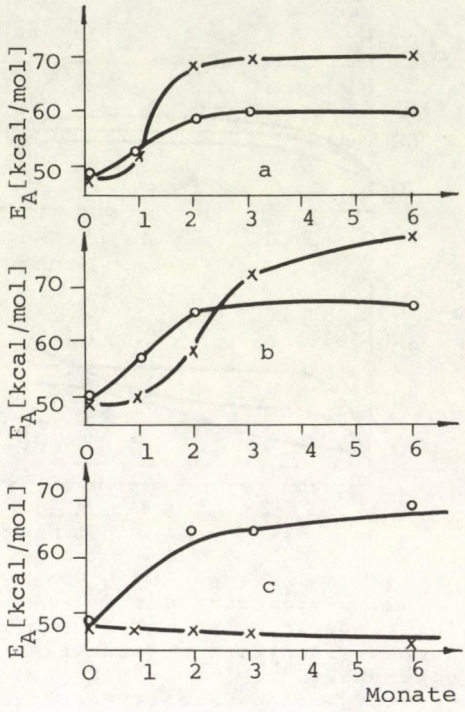

Abb.4. Veränderung der Aktivierungsenergie des mit aliphatischem Isozyanat gehärteten Polyurethanstriches; a) pigmentiert mit Rutil, b) pigmentiert mit Anatas, c) farblos, o - bei Lagerung ohne Beanspruchung, x - bei atmosphärischer Beanspruchung

Die Abb. 5 zeigt die Aktivierungsenergie der Anstriche mit Polyurethan-Bindemittel, die mit aromatischem Isozyanat gehärtet sind. Bei Lagerung ohne Beanspruchung stabilisierte sich die Aktivierungsenergie und damit die Struktur des Anstriches nur im Falle des mit Rutil pigmentierten Anstriches, bei den farblosen, bzw. bei den mit Anatas pigmentierten Modifikationen zeigte die Aktivierungsenergie auch während der Lagerung schon eine wesentliche Veränderung. Bei atmosphärischer Beanspruchung kann man bei allen drei Typen eine Veränderung feststellen, die auf Oxydation, bzw.

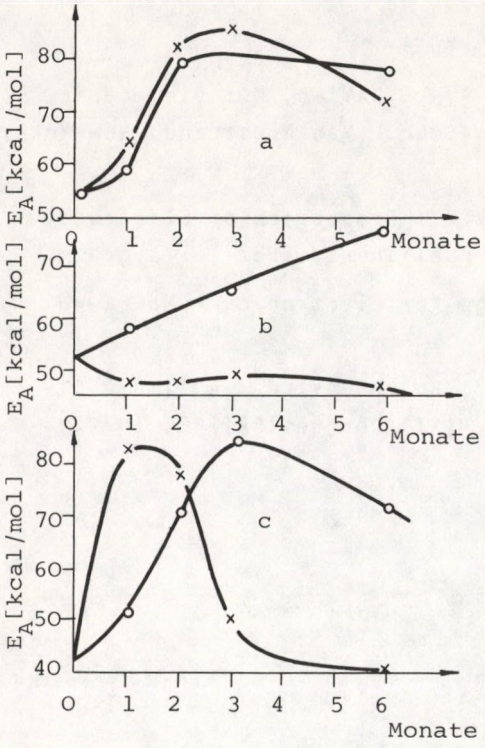

Abb. 5. Veränderung der Aktivierungsenergie des mit aromatischem Isozyanat gehärteten Polyurethananstriches;a) pigmentiert mit Rutil, b) pigmentiert mit Anatas, c) farblos; o - bei Lagerung ohne Beanspruchung, x - bei atmosphärischer Beanspruchung

Degradation zurückzuführen sind. Die Aktivierungsenergie des mit Rutil pigmentierten Anstriches ist nahe deren ohne Beanspruchung, besonders in den ersten 3 Monaten, was auch in diesem Falle beweist, daß Rutil günstig auf die Wetterbeständigkeit wirkt.

Auf Grund der dielektrischen Untersuchungen kann festgestellt werden, daß das mit aliphatischem Isozyanat gehärtete Polyurethan-Bindemittel nur mit Rutil pigmentiert eine sehr gute Wetterbeständigkeit aufweist,die Stabilität des mit aromatischem Isozyanat gehärteten Polyurethans jedoch konnte auch Rutil nicht andauernd verbessern.Diese Erscheinung weist eindeutig darauf hin, daß die Anwendbarkeit, in diesem Falle die Wetterbeständigkeit eines Anstriches nicht ausschließlich durch das Bindemittel bestimmt wird. Eine sehr wichtige Rolle spielt auch die Wechselwirkung zwischen Pigment und Bindemittel. Unsere Ergebnisse stehen im Einklang mit den praktischen Erfahrungen, und das bedeutet zugleich, daß die dielektrische Meßtechnik sehr empfindlich auf die Strukturänderung der Anstriche reagiert, so kann sie also beim Nachweisen der Alterungsprozesse gut gebraucht werden, deshalb wird beabsichtigt, die Untersuchungen später auch auf andere Bindemittel und Pigmente zu erstrecken.

LITERATUR

1. HILL, N., VAUGHAN, W.E., PRICE, A.H., DAVIES, M.: Dielectric Properties and Molecular Behaviour. (Van Nonstrand, New York, 1969)

2. BOGORODITSKII, N.P., PASYNKOV, V.V.: Properties of Electronic Materials. (Boston Technical Publishers, 1967.)

3. JAMES J. LICARI: Plastic Coatings for Electronics. (McGraw-Hill, New York, 1970.)

4. MÉSZÁROS, L., KOVÁCS, L., HORKAY, F., DÉVAY, J.: A Simple Dielectric Measuring Method ... (XI' Congres FATIPEC 1972.)

РЕЗЮМЕ

При помощи диэлектрического метода измерения было исследовано старение полиуретановых лаков с ароматической и алифатической изоцианатовой сетной, происходящее в следствии подвержения атмосферной нагрузке.

Происходящие в процессе старения структурные изменения мы наблюдали с помощью изменения энергий активации и сдвига областей дисперсии, которые определялись на основании зависимости от температуры, измеренной при различных фрекванциях диэлектрического фактора.

Hungarian Journal
of Industrial Chemistry
Veszprém
Vol.3. pp. 79-90 (1975)

PRÜFUNG VON FRAGEN DER SICHERHEITS-, ZUVERLÄSSIGKEITS- UND RISIKO-OPTIMIERUNG BEI GROSS-SYSTEMEN DER CHEMISCHEN INDUSTRIE

L. MÉSZÁROS

(Forschungsinstitut der Chemischen Schwerindustrie, Budapest)

Eingegangen am 24 Mai 1974.

In dieser Arbeit werden die Sicherheit, die Zuverlässigkeit und das Risiko, sowie deren Zusammenhang erörtert, um den Parameterbereich von optimalen Risiko der Inbetriebhaltung aller Funktionen der Großsysteme in der chemischen Industrie, auf der Grundlage eines Modells des Systems, bestimmen zu können.

EINLEITUNG

Entsprechend der konventionellen Interpretierung der Sicherheit, werden die Planung und Herstellung von Einrichtungen ausreichender Sicherheit, gemäß der Betriebspraxis, um Unfälle, Betriebsstörungen und Pannen, oder katastrophale Fehler zu vermeiden, auch bei Systemen in der chemischen Industrie im allgemeinen unter Rücksichtnahme auf den sogenannten Sicherheitsfaktor durchgeführt.Nach dieser deterministischen Betrachtungsweise wird der Sicherheitsfaktor bestenfalls, z.B. in Anbetracht von Einzelgeräten, an Hand irgendwelcher Erfahrungsbemessungen der verschiedenen Maschinenelemente der chemischen Industrie verfolgt. Mit den Sicherheits- und

Ermüdungsfaktoren rücken Erwägungen in den Vorderung, die eher mit statischen, bzw. Festigkeits-Überlegungen, als mit der Lebensdauer oder mit einer einwandfrei betriebssicheren Arbeit in Zusammenhang stehen. Es ist evident, daß keiner der genannten Faktoren vermag, über die dynamischen Eigenschaften bei Verwendung eines gegebenen Systems der chemischen Industrie genügende Information zu erteilen. Hierzu wäre es nötig, an Stelle der konventionellen Sinngebung der Sicherheit, ein neues, viel allgemeineres und eindeutigeres, auch die Gefährlichkeit des Betriebs verratendes Sicherheitsmaß einzuführen.

Wir vermuten, daß das Maß der Sicherheit einerseits den gemeinsamen wichtigeren Eigenschaften und Beschaffenheiten der Großsysteme in der chemischen Industrie zugeordnet werden sollte, und zwar in Abhängigkeit davon, welche Information über die Erfüllung der von uns gegenüber den verschiedenen Teilsystemen, Erzeugnissen, Geräten und Bauelementen gestellten Anforderungen und Aufgaben gewünscht wird, anderseits glauben wir dieses Maß dem einheitlichen Gebrauch der mit den sicherheitstechnischen Maßnahmen in Verbindung stehenden verschiedenen Aufwände, wie z.B. Arbeits- und Kostenaufwände, beiordnen zu müssen.

Von diesen, einander oft wiedersprechenden Anforderungen muß jedenfalls beim Fortbestehen dieser Widersprüche - die optimale Lösung, bzw. das entsprechende Schema für die z.B. Lagerung oder Inbetriebhaltung von Großsystemen der chemischen Industrie erwählt werden. Eine befriedigende Beantwortung der Fragen, die mit in diesem Problemen auftauchenden Aufgaben in Zusammenhang stehen, benötigt aber die Einführung einer neuen, das heutige physikalische Weltbild spiegelnden, indeterministischen (stochastischen) Betrachtungsart, wo dann das Risiko der sicherheitstechnischen Entscheidungen auf das Minimum reduziert werden kann. Unser geschildertes Verfahren ist zunächst der konventionellen Interpretierung der Sicherheit völlig entgegengesetzt, denn es wird nun von der indeterministischen Untersuchung von komplexen Großsystemen der chemischen Industrie, und nicht umgekehrt, von der Prüfung einzelner Einrichtungen, bzw. Reaktoren deterministisch ausgegangen.

Es folgt aus dem oben gesagten, daß Sicherheit und Zuverlässigkeit nicht allein von den objektiven Faktoren eines chemoindustriellen Systems (z.B. von dessen Instrumentenausrüstungsgrad), sondern auch von der Wartungsmethoden und der technologischen Leitung abhängig sind. Die Leitung stellt in System die Personal Erfordernisse - d.h. die subjektiven Bedingungen - dar. Aus dem WEBER—FECHNER-schen [1] psychophysischen Gesetz folgt, daß keine hundertprozentig zuverlässige Betriebsleitung und kein solches Personal gibt, da der Aufwand, z.B. in Gemeinkosten ausgedrückt, bei einer Zuverlässigkeit von 100 % unendlich wäre*. Mit Rücksicht auf die oben gesagten, ist allein eine solche Praxis richtig, wo die technologische Führung und die Systementwicklung unter der persönlichen Lenkung eines solchen Leiters erfolgt, der über die nötigen Kenntnisse und Erfahrungen verfügt, und folglich - manche mögliche Fehlgriffe der Leitung selbtsverständlich in Erwägung gezogen - für die Produktion des Betriebes jederzeit verantwortlich ist. In gewissem Maße muß hier also auch mit einem sogenannten "sozialistischen Risiko" gerechnet werden. Diese Fragen werden viel ausführlicher von MACHÁCS [3] und von seinem Mitverfassern in ihrer Arbeit erörtert.

Im folgenden werden die sicherheitstheoretischen Begriffsbestimmungen, sowie die Beziehungen zwischen Risiko und Zuverlässigkeit, von dem Standpunkt einer Suche nach der optimalen Sicherheit

---

*Da die Eigenschaften der von DOBO u. SZAJCZ [2] definierten Aufwandfunktion (z.B. Arbeit) durch das WEBER-FECHNER-sche psychophysische Gesetz befriedigt werden, läßt sich das Maß R des Aufwandes im Falle, daß wir die Zuverlässigkeit des technologischen Leitens mit einer Wahrscheinlichkeit P und einer Zuverlässigkeit Δp erhöhen wollen, folgendermaßen schreiben:

$$R(p_1,p_2) = P \int_{p_1}^{p_2} \frac{dp}{1-p} = \ln \left(\frac{1 - p_1}{1 - p_2}\right)^P$$

wo $p_2 = p_1+\Delta p$. Ist also p kongruent zu 1, dann geht $R(p_1,p_2)$ ins Unendliche. Folglich ist die Limitierung notwendig. Das ist eins der Probleme, worauf wir die Aufmerksamkeit hinlenken möchten. Der andere Faktor, der der Steigerung der Zuverlässigkeit Grenzen stellt, ist der Stress-Effekt und dessen Größe.

behandelt. Die in diesem Sinn vorgenommenen, geschilderten Untersuchungen gehören zum Problemkreis der nichtlinearen Programmierung.

1. Grundbegriffe der Sicherheitstheorie

Begriff der Sicherheit. Wird bei einer Einrichtung bzw. einem System in Gang die Wahrscheinlichkeit der Wirksankeit bestimmter oder aller Funktionen durch $P(A)$, und deren Risiko durch $\varepsilon(A)$ bezeichnet, so wird das Maß der Aufrechterhaltung des partiell oder völlig störungslosen (fehlerfreien) Zustandes, d.h. die Größe

$$B(A) = \frac{P(A) - \varepsilon(A)}{P(A)} \tag{1}$$

der Sicherheitsgrad, oder kurz die Sicherheit genannt.

Da, nach [3], das Risiko $\varepsilon(A)$ eines Ereignisses A allemal der Wahrscheinlichkeit $P(\bar{A})$ des adversativen Ereignisses $\bar{A}$ gleich ist, d.h.:

$$\varepsilon(A) = P(\bar{A}) \tag{2}$$

woher für die Sicherheit nach (1) gilt:

$$B(A) = \frac{2\,P(A) - 1}{P(A)} \tag{3}$$

wo $0 \leqq B(A) \leqq 1$ ist*. Wird in der Beziehung nach (3) mit einem stochastischen Prozeß $P(A) = P_A(t)$ berechnet, dann kann der erhaltene Ausdruck

$$B(A) = B_A(t) = \frac{2\,P_A(t) - 1}{P_A(t)} \tag{4}$$

*Von einer Sicherheit zu sprechen, ist, laut der Definition (1-3) dann und nur dann rational, wenn $\varepsilon(A) = P(A)$ $P(A)$.

für eine in weiterem Sinn genommene Definition der Sicherheit erachtet werden. Die Funktion $P_A(t)$ in der Gleichung nach (4) wird die Zustandswahrscheinlichkeit-Funktion genannt. Die Art und Weise ihrer Bestimmung, im Falle nicht MARKOV-scher Prozeße, sind in unserer Arbeit [4] erörtert. Das Risiko und die Zuverlässigkeit sind ebenfalls (siehe Bericht [5]) komplementäre Begriffe, d.h.:

$$p(A) + \varepsilon(A) = 1, \tag{5}$$

wo p(A) als die Zuverlässigkeit des Ergebnisses A gilt.

Hieraus folgt, daß es unter Sicherheit, Zuverlässigkeit und Risiko einen eindeutigen Zusammenhang gibt. Bedeutet z.B. das Ereignis A die Lebensdauer des chemo-industriellen Systems $A = \{\xi\}$ wo ξ die Wahrscheinlichkeitsvariable ist, so wird das Risiko

$$\varepsilon(A) = P(\{\xi<t\}) = F(t) \tag{6}$$

nach Gleichung (2), als die Verteilungsfunktion des Systems gelten. Dann, nach (5), erhalten wir für die Zuverlässigkeitsfunktion des Systems:

$$p(\{\xi \geqq t\}) = 1 - F(t) \tag{7}$$

Im Falle eines exponentiellen Risikos, z.B. mit dem Parameter $\lambda = 10^{-6}$/Stunde, erhält die Zuverlässigkeitsfunktion, nach Gleichung (7), die Form:

$$p(\{\xi \geqq t\}) = e^{-\lambda t} \tag{8}$$

und so gilt als die Sicherheit nach (1):

$$B_A(t) = 2 - e^{\lambda t} \tag{9}$$

Ist $B_A(t) = 90\ \%$ die vorgeschriebene Sicherheit, dann, um zu verhindern, daß die Sicherheit unter den erwünschten Wert sinkt, soll die Erneuerung eines Großsystems der Chemischen Industrie binnen einem Zeitraum von

$$t \quad \frac{\ln 1{,}1}{10^{-6}} = 10^5 \text{ Stunde}$$

erfolgen.

Wir wollen hier bemerken, daß die Sicherheit auch mit der "Verblüffheit" ausgedrückt werden kann. Unter "Verblüffheit" wird hier die Wahrnehmung oder die Information von einem unwahrscheinlichen Vorfall eines Ereignisses in Zusammenhang mit einem Großsystemen verstanden. Ist die Verblüffheit*, die z.B. aus der Formation einer explosionsgefährdeten Konzentration entspringen kann, zu groß, dann bezweifeln wir die Wirklichkeit der Information,oder die Richtigkeit unserer Wahrnehmung. Wenn wir dabei nach einem Fehler suchen, werden wir einen auch oft finden. Läßt sich der Vorfall, z.B. eine Panne, auf mehrere Ursachen zurückführen, dann wird deren Entstehung derjenigen Ursache beigemessen, bei deren Wirkung das Auftreten des Fehlers, bzw. der Panne am wenigsten überraschend ist. Je kleiner die Verblüffheit ist, desto größer wird also die Sicherheit, und folglich soll ein durch irgendwelches Schadhaftwerden (oder einen technologischen Fehler) verursachter z.B. Unfall dem Zufall, als einer systematisch wirkenden Ursache zugemutet werden. Nach [4] kann nun die Sicherheit, laut der BRAVAIS-Formulierung durch eine χ^2-Probe bestimmt werden, d.h.:

$$B(A) = e^{-\frac{1}{2}\chi^2} \tag{10}$$

wo:

$$\chi^2 = \sum_{j=1}^{m} \sum_{k=1}^{n} \frac{(\nu_j - Np_j\, q_k)^2}{Np_j\, q_k} \tag{11}$$

während p_j für die Wahrscheinlichkeit der Ereignisse A_j ($j = 1, 2, 3, \ldots, m$) q_k für die der Ereignisse B_k ($k = 1, 2, 3, \ldots, n$) und ν_j als Häufigkeitswert der Ereignisse $A_j \cdot B_k$ gelten. Die Beziehung nach (11) verfolgt offenbar eine χ^2-Verteilung von Freiheitsgrad $(mn - 1)$, d.h.:

$$\lim_{N\to\infty} P(\chi^2\, mn < x) = \frac{1}{2^{\frac{\ell-1}{2}}\, \Gamma(\frac{\ell-1}{2})} \int_0^x u^{\frac{\ell-3}{2}}\, u^{-\frac{u}{2}}\, du = K_{\ell-1}(x), \tag{12}$$

*Als Definition, laut L. MÉSZÁROS [4], gilt für die "Verblüffheit":

$$S(A) = \frac{\varepsilon(A)}{P(A)}$$

wodurch die Sicherheit: $B(A) = 1 - S(A)$.

wo $\ell = mn$, und N die Anzahl der Versuche ist. Im allgemeinen ist die Verwendung einer χ^2-Probe dann zweckmäßig, wenn N so groß ist, daß es für alle Werte von j und k gilt: $Np_B \cdot q_k \geq 10$.

Aus dem gesagten folgt, daß die Begriffe von Sicherheit und Verblüffheit korrelativ sind. Ist also die Beziehung nach (10) nahezu 1 gleich, so kann unsere Hypothese für das eingetroffene Ereignis (z.B. einen Fehler) mit der Sicherheit nach (10) angenommen werden. Es ist klar, daß der Zusammenhang nach (10) vor allem in der Festlegung der Risikoübernahme vom Leiter, und seiner persönlichen Verantwortung eine Bedeutung zu haben vermag.

2. BESTIMMUNG DER SICHERHEIT DURCH STOCHASTISCHE PROZESSE

Die Zuverlässigkeit eines einwandfreien Betriebs wird, bei Aufstellung von Großsystemen in der chemischen Industrie, auf Grund der Prüfung der Systemstruktur besprochen. Auf der Grundlage der nach [6] definierten Strukturenmatrix, und mit Einführung eines strukturellen Maßstabs, kann die resultierende Zuverlässigkeit des von MACHÁCS [7] beschriebenen großen und komplizierten Systems bereits festgestellt werden. Sei der Betriebsstand aller Funktionen des Systems durch Ereignis A, und dessen Risiko (der Ausbesserungszustand), auf Grund von 1. [2] durch $\bar{A}$ bezeichnet. Dann wird der Systemszustand, als Funktion der Zeit, für zunehmende t-Werte abwechselnd entweder Zustand A oder Zustand $\bar{A}$ annehmen. So stellt $X(t,\omega)$ einen stochastischen Prozeß dar, wo ω ein elementares Ereignis ist. Wollen wir nun den stochastischen Prozeß $\{x(t,\omega),\ 0 \leq t < \infty\}$ folgendermassen interpretieren:

$$g\,[x(t,\omega)] = \begin{matrix} 1, \text{ wenn } & \omega \in A \\ 0, \text{ wenn } & \omega \notin A \end{matrix} \qquad (13)$$

Die Erwartung davon ist:

$$P_A(t) = M\{g[x(t,\omega)]\} = \int_{\Omega} g[x(t,\omega)]dP(\omega), \qquad (14)$$

wo Ω den Phasenraum darstellt. Zeigt das umweltbedingte Schadhaft-

werden eine Gleichverteilung im Intervall [O,T], dann sind die Zustandswahrscheinlichkeit-Funktion nach (14) und die in der Arbeit [5] definierte Wirksamkeit des Systems gleich, d.h.:

$$P_A(t) = f_T = \frac{1}{T} \int_o^T M\{g[x(t,\omega)]\}dt \tag{15}$$

Deshalb wird die Sicherheit, auf Grund der Gleichung nach 1. (4), die Form

$$B_A(T) = \frac{2\, f_T - 1}{f_T} \tag{16}$$

annehmen. Hieraus folgt, daß die Sicherheit des Systems unter den gestellten Bedingungen erst dann optimal sein wird, wenn die Wirksamkeit des Systems ebenfalls optimal ist.

Sind der Betriebsstand und der Ausbesserungszustand des Systems von exponentieller Verteilung, mit Parameters λ bzw. γ, so gilt als eine stationäre Sicherheits:

$$B = \lim_{T \to o} B_A(T) = \frac{\gamma - \lambda}{\gamma} \tag{17}$$

wo $\lambda < \gamma$, woraus es nun an der Hand liegt, daß der Erwartungswert des Systems-Betriebsstandes $1/\lambda$ größer als der Erwartungswert $1/\gamma$ des dem Schadhaftwerden entsprechenden Ausbesserungszustandes ist.

3. MODELL ZUR BESTIMMUNG DES OPTIMALEN RISIKOS

Das Risiko kann (nach [4]) für optimal erachtet werden, wenn der Erwartungswert für den Verlust eines - z.B. wegen Explosionsgefahr - gefährderten Objekts nullwertig ist. Auch in solchem Fall gibt es also ein Risiko, das aber im Sinne der Definition nach [4] gefahrlos ist. Nehmen wir an, daß es in einem gegebenen Großsystem der chemischen Industrie für den Fall, daß eine Fehlerbeseitigung mit einer Zeitdauer von $\xi = t$ genau k-mal eintreten wird, die folgende relative Wahrscheinlichkeit gibt:

$$P(\Psi = k|\xi = t) = \frac{(\lambda t)^k e^{-\lambda t}}{k\,!} \tag{18}$$

wo λ ein gegebener Konstant ist,während ξ eine Wahrscheinlichkeits-veränderliche von exponentieller Verteilung, mit einem Parameter μ darstellt.

Dem oben gesagte gemäß, bestehen folgende $P(\Psi = k)$ Wahrscheinlichkeiten:

$$P(\Psi=k) = \int_0^\infty P(\Psi=k|\xi=t)\mu e^{-\mu t}dt = \int_0^\infty \frac{(\lambda t)^k e^{-\lambda t}}{k\,!}\mu e^{-\mu t}dt = \frac{\mu\lambda^k}{(\mu+\lambda)^{k+1}} \tag{19}$$

und so soll der Parameter μ, insofern wir wünschen, daß die Fehlerbeseitigung bei einer beliebigen Beobachtung wenigstens k-mal mit einer Wahrscheinlichkeit von $(1-\varepsilon_1)$ eintrete, den Wert:

$$1 - \varepsilon_1 \leqq \frac{\mu}{\lambda + \mu} \sum_{i=k}^{\infty} \left(\frac{\lambda}{\lambda + \mu}\right)^i = \left(\frac{\lambda}{\lambda + \mu}\right)^k, \tag{20}$$

d.h.

$$\mu \leqq \lambda \left(\frac{1}{\sqrt[k]{1 - \varepsilon_1}} - 1\right) \tag{21}$$

haben. Wollen wir nun, daß eine Fehlerbeseitigung bei mindestens einer Anzahl κ ($\kappa \leqq N$) der Beobachtungen nicht weniger als k-mal und wenigstens mit einer Wahrscheinlichkeit von $1 - \varepsilon_2$ eintreten soll, so muß die Bedingung:

$$1 - \varepsilon_2 \leqq \sum_{\ell=\kappa}^{N} \binom{N}{\kappa} \left(\frac{\lambda}{\lambda + \mu}\right)^{k\ell} \left(\frac{\mu}{\mu + \lambda}\right)^{(N-\kappa)k} \tag{22}$$

erfüllt werden. Daraus kann für den Wert von N schon keine Ungleichung mehr in einer expliciten Form dargestellt werden. Nach (20) und (22) gilt nun für den Parameterbereich eines optimalen Risikos:

$$\Delta\varepsilon = \frac{(1-\varepsilon_2)+(1-\varepsilon_2)}{2} \leqq 1 - \frac{1}{2}\left[\left(\frac{\lambda}{\lambda+\mu}\right)^k + \sum_{\ell=\kappa}^{N}\left(\frac{N}{\kappa}\right)\left(\frac{\lambda}{\mu+\lambda}\right)^{k\ell}\left(\frac{\mu}{\mu+\lambda}\right)\right]^{(N-\kappa)k} \tag{23}$$

wo die Wahl von ε_1 und ε_2 eine solche ist, für die der Erwartungswert des obengenannten Verlustes nullwertig ist. Nach (23) wird die von verantwortlichem Leiter getroffene Entscheidung erst dann optimal, wenn diese Entscheidung das ε Risiko:

$$\varepsilon \in \Delta\varepsilon \tag{24}$$

d.h. des optimalen Parameterbereiches ist. Diesem optimalen Risiko nach (24) entspricht ein Sicherheitswert:

$$B(A) = \frac{1 - 2\varepsilon}{1 - \varepsilon} \tag{25}$$

wo $\varepsilon = \varepsilon(A)$ das Risiko der Fehlerbeseitigung (von Ereignis A) ist. Wenn wir wollen, daß die Zuverlässigkeit der z.B. in Reihen geschalteten Teilsysteme eines Großsystems der chemischen Industrie (siehe [4]) der optimalen Entscheidung entsprechen soll, muß die Zuverlässigkeit des Teilsystems, dessen Zuverlässigkeitwert $p_1 = 0{,}971$ ist, um eine Größe $\delta_1 = 0{,}015$, den Wert $p_2 = 0{,}980$ um eine Größe $\delta_2 = 0{,}06$, und die Werte $p_3 = 0{,}985$, $p_4 = 0{,}990$ und $p_5 = 0{,}993$ um Größe $\delta_3 = \delta_4 = \delta_5 = 0$ erhöht werden, um auf diese Weise sichern zu können, daß die resultierende Zuverlässigkeit $p(A) = 0{,}924$, bei einem Minimal-Arbeitsaufwand, dem optimalen Risiko $\varepsilon(A) = 0{,}086$ entspreche.

Aus der Beschreibung dieses Modells wird es nun klar, daß die Bestimmung des optimalen Risikos, sogar in verhältnismäßig weniger komplexen Fällen, keine leichte Aufgabe ist, und daß die Lösung solcher Aufgaben ins Gebiet der nichtlinearen Programmierung gehört.

LITERATUR

1. MÉSZÁROS, L., Rendszerek megbizhatóságának alakulása hibás alkatrészek kicserélése esetén. Nehézvegyipari Kutató Intézet, Jelentés (Gestaltung der Zuverlässigkeit von Systemen beim Austausch beschädigter Konstruktionselemente. Bericht des Forschungsinstitutes der Chemischen Schwerindustrie) Budapest, 1972. p. 2-42.

2. DOBÓ, A. und SZAJCZ, S., Magyar Tudományos Akadémia, Matematika és Fizikai Tudományok Osztályának Közleményei (Ungarische Akademie der Wissenschaften; Mitteilungen der Abteilung der Wissengebiete Mathematik und Physik) XV, 427 (1965)

3. MACHÁCS, M., BIKFALVI, MÉSZÁROS, L., SZALAY, TAKÁCS, Automatika elemek, készülékek és berendezések megbizhatósága (Elemző Tanulmány OMFB). (Zuverlässigkeit von Elementen, Geräten und Einrichtungen der Automatik; Analytisches Studium, OMFB) Budapest, März 1973, p. 3-86)

4. MÉSZÁROS, L., Az átlagosnál veszélyesebb (különösen veszélyes) vegyipari üzemek optimális biztonságának meghatározása. Nehézvegyipari Kutató Intézet, Jelentés. (Bestimmung der optimalen Sicherheit bei besonders gefährlichen Betrieben der chemischen Industrie. Bericht des Forschungsinstitutes der Chemischen Schwerindustrie) I, 2-31; II, 2-58, Budapest, 1970.

5. MACHÁCS, M. und MÉSZÁROS, L., Über die technische Anwendung von rekurrenten Prozessen, mit besonderer Rücksicht auf das Problem der Automatisierung, I. (12. Internationale Tagung der Elektrotechniker, Sektion 1/2, Berlin, 1967) p. 2-10)

6. MÉSZÁROS, L., Strukturfunktion und Zuverlässigkeit des Gerätes Typ NOR-J1 (Konferenz und Ausstellung Automatisierung in der chemischen und Erdölindustrie, Budapest, 21-24. November 1972 (p. 285-298).

7. MAHÁCS, M. und NEMESKÉRI, S., Vegyipari üzemek automatikai karbantartó szervezetének tervezési kérdései. Nehézvegyipari Kutató Intézet, Jelentés (Fragen der Plannung einer Organisation zur Wartung der Automatik von Betrieben der chemischen Industrie. Bericht des Forschungsinstitutes der Chemischen Schwerindustrie) Budapest, 1966 (p. 3-42).

РЕЗЮМЕ

Данная работа занимается взаимосвязью безопастности, надежности и риска на основе одной из моделей системы с целью определения области оптимального параметра риска для эксплуатации сложных химических систем во всех функциях.

Hungarian Journal
of Industrial Chemistry
Veszprém
Vol. 3. pp. 91-114 (1975)

BERECHNUNG DER VERWEILZEITVERTEILUNG IN FLIESSBETTAPPARATEN AUF GRUND EINES REZIRKULATIONSMODELLS

T. VAJDA

(Forschungsinstitut für Technische Chemie der Ungarischen Akademie der Wissenschaften, Budapest)

Eingegangen am 6. Juni 1974.

Die Arbeit gibt eine mathematische Beschreibung des allgemeinen Mechanismus von Fließbettapparaten und vom Fließbettverfahren im allgemeinen auf Grund eines Rezirkulationsmodells. Wir betrachten das Modell des in einem Fließbett entstehenden Strömungsbildes sowohl unter der Bedingung einer Nullmischung als auch im Falle einer im mittleren, kritischen Bereich zustandekommenden vollständigen Mischung. Es wurden die durch die physikalischen Modelle gelieferten, die Ausgangskonzentration des getriebenen Stoffes betreffenden Gleichungen gelöst und aus den erhaltenen Resultaten, die durch die inneren Zusammenhänge der Modelle definierten Verweilzeitverteilungen bestimmt. Der Vergleich der beiden Modelle und daher auch die Klarlegung der Rolle der Vermischung im mittleren Bereich geschieht durch die Anwendung dieser Modelle für die Berechnung derselben Größe.

I. EINLEITUNG

Die Technik der Fließbettschicht ist im Falle von Gas-Feststoff-Systemen in erster Reihe für grobe - in der Fluidisationsschicht nicht aufbereitbare - Stoffe entwickelt worden. Ein strömungstechnisch völlig ähnlicher Stofftransport kann aber auch im

Falle von Gas-Flüssigkeit-, Flüssigkeit-Flüssigkeit- (heterogen), sowie Flüssigkeit-Feststoff-Systemen verwirklicht werden. In solchen Fällen ist der getriebene Stoff - wie es zum Beispiel beim Gas-Feststoff-Fließbettsystem die Körner sind - stets die dichtere, das treibende Medium hingegen die dünnere Substanz. Allgemein gefasst könnte man sagen, daß das Fließbettverfahren eine für die intensive und kontinuierliche Berührung von gewissen Zweiphasensystemen geeignete Methode darstellt, bei welcher dem Querschnitt entlang gleichzeitig zwei von einander abweichende Strömungsformen auftreten, wobei die dichtere Phase innerhalb des Apparats rezirkuliert.

Es gibt zwar vielerleie Untersuchungsmethoden zur Bestimmung der Charakteristika von Fließbettströmungsformen, bei den in der Literatur mitgeteilten Zusammenhängen handelt es sich jedoch entweder um erfahrungsmäßig gewonnene Daten, die nur unter gewissen speziellen Umständen gelten, oder um komplizierte halbempirische Gleichungen [1-7]. Eine mathematische Beschreibung des Mechanismus des Fließbettverfahrens mit Anspruch auf umfassenden Charakter stellt ein bisher unberührtes Gebiet dar, trotzdem sind Methoden zur Berechnung der Parameter bekannt, die eine allgemeine Behandlungsweise ermöglichen [1-3]. Diese Parameter sind die folgenden:

a) Geschwindigkeit des treibenden Mediums im mittleren Fließbettbereich (beim Gas-Feststoff-System offensichtlich die Geschwindigkeit des Gases im Rohr);

b) Geschwindigkeit des getriebenen Stoffes im mittleren Bereich, sowie im äußeren ringförmigen Raum, in dem die Bewegung des Stoffes von der Gravitationskraft bestimmt wird;

c) Durchmesser des mittleren Bereichs, welcher in gewissen Fällen als Apparatenangabe fungieren kann, in anderen Fällen wieder - wenn obiger Bereich nur durch die gegenseitige Wirkung des treibenden Mediums und des getriebenen Stoffes entsteht - ist dieser als Funktion sonstiger Angaben zu betrachten.In ersterem Fall ist der Durchmesser einfach mit dem Durchmesser des Einsatzrohres identisch.

In der Arbeit wird schließlich - durch die Modellierung des charakteristischen Fließbett-Strömungsbildes nach entsprechenden Gesichtspunkten - die Verweilzeitverteilung des getriebenen Stoffes in kontinuierlich wirkenden Fließbettapparaten als Funktion der Kenndaten der Apparate und sonstiger Parameter angegeben. In Kenntnis der Verweilzeitverteilung können nähmlich mit Hilfe einfacher Berechnungen zahlreiche Fragen aus der Praxis beantwortet werden (beim Trocknen z.B. die Verminderung des durchschnittlichen Feuchtigkeitsgehaltes, bei Fließbett-Adsorber-Desorbern die durchschnittliche Sättigung des Adsorbenten, die durchschnittliche Verweilzeit der Körner, im allgemeinen die Konstruktion von Fließbettapparaten). Die erzielten Resultate können aber auch für Auswertung jedweder Versuche mit dem Fließbettverfahren verwendet werden.

II. DAS PHYSIKALISCH-MATHEMATISCHE MODELL

1. Beschreibung der vereinfachenden Voraussetzungen

Das in Fließbettapparaten entstehende Strömungsbild kann - abgesehen von den unwesentlichen Abweichungen infolge unterschiedlicher technologischer Ausführungen - am besten, und zwar unabhängig von der Art des strömenden Mediums, anhand des folgenden schematischen Schnittbildes (Abb.1) gezeigt werden.Die durch Pfeile dargestellten Massengeschwindigkeiten beschreiben das Strömungsbild offenbar nur in ihren Hauptzügen, aber eine unserer wesentlichen Voraussetzungen ist gerade, daß auf diese Weise der tatsächliche Verlauf durch seine entscheidenden Momente erfasst wird.

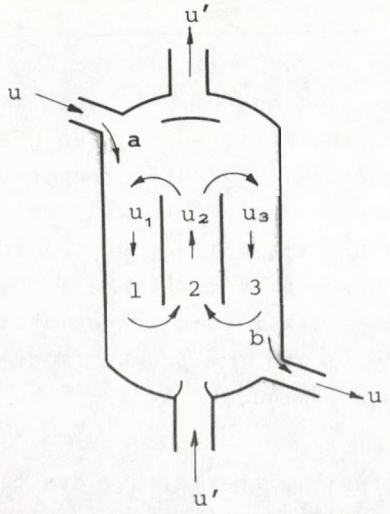

Abb. 1

Es ist leicht einzusehen, daß obige schematische Abbildung durch ein äquivalentes strömungstechnisches Modell ersetzt werden kann, welches in Bezug auf die Massengeschwindigkeit und die Rückkopplung gleich ist, jedoch wird der Prozeß deutlicher veranschaulicht (Abb.2). Die Abschnitte 1 , 2 und 3 in Abbildung 2 sind

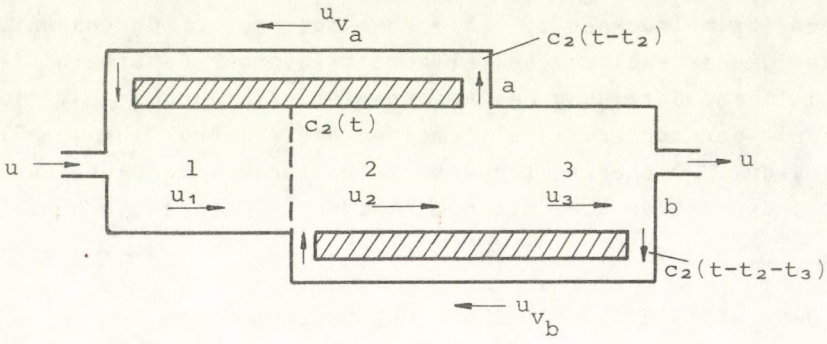

Abb.2.

der Reihe nach die entsprechenden Bereiche von Abbildung 1. Die zwei, die Rückkopplung symbolisierenden Kanäle sind Modelle der Rezirkulation in den Punkten a und b des Apparates. Die zwei Kanäle sind idealisiert, das heißt eine Nullmenge des Stoffes hält sich in ihnen eine Nullzeit lang auf.

Der getriebene Stoff strömt in das Fließbett mit Volumgeschwindigkeit u ein, und im Falle eines stationären Betriebes ist die Strömungsgeschwindigkeit nach außen zu dieselbe. In den drei Bereichen betragen die Werte der Volumgeschwindigkeiten der Strömung bei demselben Stoff u_1, u_2 und u_3. Die Volumgeschwindigkeit des Ein- und Ausströmens des treibenden Mediums beträgt u', dieser Wert ist in Abbildung 2. - die dort nur mehr die Parameter des getriebenen Stoffes enthält - zweckmäßigerweise nicht angeführt. In den Punkten a und b in Abbildung 1 und im Strömungsmodell wird der getriebene Stoff mit den Volumgeschwindigkeiten u_{v_a} bzw. u_{v_b} rückgekoppelt.

Da wir das Ziel verfolgen, die Verweilzeitverteilung des getriebenen Stoffes zu bestimmen, ist die Volumkonzentration dessel-

ben in den drei Bereichen des Fließbettapparates als Funktion der Zeit zu betrachten. Im allgemeinen Fall ist diese Konzentration eine Funktion des Ortes und der Zeit. Nimmt man jedoch in den Bereichen eine vereinfachte "korkartige" Strömung von homogenen Geschwindigkeitsprofil an, so kann die Ortsabhängigkeit in der Funktion der Konzentration zu Differenzen des Zeitarguments transformiert werden. Uns interessieren nur die an den Endpunkten der einzelnen Bereiche erzielten Konzentrationswerte. Zur Durchführung obiger Operation genügt es daher, wenn die Verweilzeiten in den drei Bereichen bekannt sind. Diese können auf die bekannte Weise berechnet werden:

$$t_1 = \frac{V_1}{u_1} = \frac{(R^2-r^2)\pi m}{2\,u_1},\quad t_2 = \frac{V_2}{u_2} = \frac{r^2\pi m}{u_2},\quad t_3 = \frac{V_3}{u_3} = \frac{(R^2-r^2)\pi m}{2\,u_3} \qquad (1)$$

Hier ist $2R$ = Außendurchmesser des Fließbettapparates,
$2r$ = Durchmesser des Futterrohres,
m = Höhe des Apparates.

Die Volumen der Bereiche V_1, V_2, V_3 in obiger Aufteilung sind mit Hilfe dieser Apparatenkenndaten berechnet worden.

Auf Grund von Abb. 2 können für die Bestimmung der sechs Volumgeschwindigkeiten des getriebenen Stoffes Knotenpunktgleichungen aufgestellt werden:

$$\begin{aligned} u + u_{V_a} &= u_1 \\ u_1 + u_{V_b} &= u_2 \\ u_2 &= u_3 + u_{V_a} \\ u_3 &= u + u_{V_b} \end{aligned} \qquad (2)$$

Da der Matrixrang des Koeffizienten gleich 3 ist, sind die Gleichungen (2) von einander nicht unabhängig, und drei von den sechs Volumgeschwindigkeiten sind freie Parameter. Wir führen nun die Rezirkulationsquotienten

$$\varphi_a = \frac{u_{V_a}}{u_2} \quad \text{und} \quad \varphi_b = \frac{u_{V_b}}{u_3}$$

ein, wodurch sich für die Volumgeschwindigkeiten in den drei Bereichen - wenn man u, φ_a und φ_b als unabhängige Veränderlichen betrachtet - folgende Werte ergeben:

$$u_1 = u\,\frac{1-\varphi_a+\varphi_a\varphi_b}{1-\varphi_a-\varphi_b+\varphi_a\varphi_b}\,,\quad u_2 = u\,\frac{1}{1-\varphi_a-\varphi_b+\varphi_a\varphi_b}\,,\quad u_3 = u\,\frac{1}{1-\varphi_b} \tag{3}$$

Anderseits ergibt sich aus Abb. 1 die völlig plausible Annahme, daß in den Randbereichen 1 und 3 - infolge geometrischer und strömungstechnischer Ähnlichkeiten - die Verweilzeiten ungefähr übereinstimmen, $t_1 = t_3$. Demzufolge ist $u_1 = u_3$, und ausgehend hiervon kann mit Hilfe von (3) zwischen den Rezirkulationsquotienten eine Beziehung aufgestellt werden:

$$\varphi_a = \frac{\varphi_b}{1+\varphi_b} \tag{4}$$

Selbstverständlich kann auch der andere Rezirkulationsquotient als Funktion eines anderen interessanten Parameters angegeben werden. Ist dieser z.B. die Volumgeschwindigkeit u' des treibenden Mediums, so erhalten wir unter Voraussetzung eines Funktionszusammenhanges $u_2 = \alpha(u')$, mit sicherlich monoton wachsender Tendenz (das treibende Medium und der getriebene Stoff sind im Bereich 2 in intensivester Wechselwirkung) für $\varphi_b = \frac{\alpha(u') - u}{\alpha(u') + u}$, und daraus unter Verwendung von (4): $\varphi_a = \frac{1}{2}\left(1 - \frac{u}{\alpha(u')}\right)$.

2. Die Untersuchungsmethode

Unsere Berechnungen haben - nach DANCKWERTS [8] - in ihren Hauptzügen folgenden Gang: beim Eintritt in das Fließbett wird, mit Unterbrechung des bis dahin kontinuierlich einströmenden gewöhnlichen Betriebsstoffes, zum Zeitpunkt t = 0, während der Dauer t_b ein entsprechender Indikatorstoff, ebenfalls mit Volumgeschwindigkeit u, eingeführt. Dieser Prozeß wird in der von uns benutzten

Eintrittsfunktion $c_b(t)$ dargestellt:

$$c_b(t) = \begin{cases} 0 & \text{wenn} \quad t \leq 0 \\ 1 & \text{wenn} \quad 0 < t \leq t_b \\ 0 & \text{wenn} \quad t_b < t \end{cases} \tag{5}$$

Eine wichtige Bedingung ist die folgende: $t_b \ll t_1, t_2, t_3$.

Nun werden - ausgehend vom gegebenen Modell - Gleichungen für die Konzentration c des auf obige Weise eingeführten und beim Austritt erscheinenden Indikators aufgestellt, sodann wird das so erhaltene mathematische Problem gelöst und auf die übliche Weise aus der Funktionsform c(t) die Dichtefunktion der gesuchten Verweilzeitverteilung gebildet:

$$\rho(t) = \frac{c(t)}{\int_0^\infty c_b(t)dt} = \frac{c(t)}{t_b} \tag{6}$$

Die Funktion, die ein Partikel betreffend die Dichte der exakten Verweilzeitverteilung - die die Wahrscheinlichkeit angibt, mit welcher ein Partikel, das im Zeitpunkt $t = 0$ in den Apparat eingetreten ist, diesen bis zum Zeitpunkt t verläßt - beschreibt, wird durch den Grenzübergang von (6) erhalten:

$$\rho_e(t) = \lim_{t_b \to 0} \rho(t) \tag{7}$$

Die Dichtefunktion (6) eignet sich also vor allem für die Interprätation von Versuchsresultaten. Funktion $\rho_e(t)$ ist jedoch bereits identisch mit der Gewichtsfunktion, die in der von der Systemübertragungstheorie her bekannten Duhamelschen These vorkommt, und zwar, wenn $c_b(t)$ eine Eintritt-Konzentrationsfunktion beliebiger Form ist, so erhält man beim Austritt folgende Konzentrationsänderung $c_k(t)$:

$$c_k(t) = \int_0^\infty c_b(\tau)\rho_e(t - \tau)\, d\tau, \tag{8}$$

angenommen $\rho_e(\tau) = 0$, wenn $\tau < 0$.

3. Die vom Modell gelieferten Gleichungen

Bei der Aufstellung der Gleichung der Konzentration c(t) auf Grund des Modells in Abb. 2 wurden zwei Extremfälle berücksichtigt: einmal der Fall, wenn in sämtlichen Bereichen des Fließbettapparates korkartige Strömeverlaufen, und zweitens der Fall, wenn im Bereich 2 eine vollständige Mischung erfolgt, aber die Strömung ansonsten völlig der ersteren ähnlich ist. Wir haben diese Methode angewandt, da wir davon überzeugt sind, daß die Realität irgendwo zwischen den beiden Extremfällen liegt. Die Gleichungen selbst können auf Grund des Erhaltungsgesetzes aufgeschrieben werden.

Die zum Zeitpunkt t am Anfang des Bereiches 2 bestehende Konzentration wird mit $c_2(t)$ bezeichnet. Es ist leicht einzusehen, daß mit der bereits erwähnten Methode der Zeitargument-Transformation die gesuchte Ausgangskonzentration c(t) aus c_2 auf folgende Weise bestimmt werden kann:

$$c(t) = c_2 (t - t_2 - t_3) \tag{9}$$

Im Falle einer korkartigen Strömung kann für obigen Punkt unter Anwendung sämtlicher bisheriger Zeichen, sowie obiger Zeitverschiebung für den Indikator eine Erhaltungsgleichung aufgeschrieben werden:

$$uc_b(t - t_1) + u_{V_a} c_2(t - t_2 - t_1) + u_{V_b} c_2(t - t_2 - t_3) = u_2 c_2(t). \tag{10}$$

Mit Hilfe des Zusammenhanges (9) kann (10) sofort in die gesuchte auf c bezogene Gleichung umgebildet werden,und es wird auch berücksichtigt, daß die Verweilzeiten in Bereichen 1 und 3 identisch sind:

$$uc_b(t - t_1) + (u_{V_a} + u_{V_b}) c(t) - u_2 c(t + t_1 + t_2) = 0 \tag{11}$$

Unser Modell führte also im ersteren Fall zu einer linearen, inhomogenen Funktionsgleichung.

Im Bereich 2 beträgt die Konzentration bei vollständiger Mischung gleichzeitig für den ganzen Bereich $c_2(t)$ (so daß in ihrer bisherigen Interprätation auch die Verweilzeit t_2 ihren Sinn verliert). In diesem Fall ist die Stoffbilanz für den Indikator im Bereich 2 (unter Berücksichtigung dessen, daß $t_1 = t_3$) die folgende:

$$V_2 \frac{d\,c_2}{dt} = uc_b(t - t_1) + (u_{V_a} + u_{V_b})\, c_2(t - t_1) - u_2 c_2(t) \qquad (12)$$

Mit Hilfe eines Zusammenhanges ähnlich wie bei (9); $c(t) = c_2(t - t_1)$, könnte auch Gleichung (12) sofort auf die gesuchte Form gebracht werden, die Lösung derselben wäre aber schwieriger als in ihrer jetzigen Form. Daher wird diese Transformation erst nach der Lösung von (12), anhand der Funktionsform $\rho_e(t)$ durchgeführt. Es zeigt sich also, daß das Modell im zweiten Fall eine lineare, inhomogene, sogenannte Hystero-Differentialgleichung erster Ordnung lieferte, die vor allem dadurch gekennzeichnet ist, daß die Größe der Veränderung der Unbekannte zu einem gegebenen Zeitpunkt auch von jenen Werten beeinflußt wird, die die Unbekannte zu anderen Zeitpunkten annimmt.

II. LÖSUNG DER DEN PROZESS BESCHREIBENDEN GLEICHUNGEN

1. Der Fall ohne Mischung

Betrachten wir das folgende mathematische Problem: Auf Grund von (11) ist die Gleichung

$$uc_b(t - t_1) + (u_{V_a} + u_{V_b})\, c(t) - u_2 c(t + t_1 + t_2) = 0$$

zu lösen, wobei gemäß des inhomogenen Gliedes (5)

$$c_b(t) = \begin{cases} 0 & \text{wenn } t \le 0 \\ 1 & \text{wenn } 0 < t \le t_b \\ 0 & \text{wenn } t_b < 0 \end{cases}$$

sowie auf Grund von Abb. 2 aus der physikalischen Überlegung offensichtlich hervorgeht, daß

$$c(t) = 0 \quad \text{wenn} \quad t \leq 2\,t_1 + t_2 \tag{13}$$

Wir führen nun die Laplace-Transformierten der Konzentration und der Eingangsfunktion mit folgender Bezeichnung ein:

$$\mathcal{L}[c(t)] \equiv \int_0^\infty e^{-pt} c(t)dt = f(p); \quad \mathcal{L}[c_b(t)] = f_b(p) \tag{14}$$

Transformiert man diese Gleichung unter Verwendung von (5) und (13), so ergibt sich zwischen den in (14) definierten Größen folgender Zusammenhang:

$$uf_b\, e^{-pt_1} + (u_{V_a} + u_{V_b})f - u\, f\, e^{p(t_1+t_2)} = 0 \tag{15}$$

Aus dieser Gleichung kann die Transformierte f(p) der Unbekannten - die Funktionsform f_b benützend - ausgedrückt werden:

$$f(p) = \frac{u\,(1 - e^{-pt_b})}{p(u_2 e^{p(2t_1+t_2)} - (u_{V_a} + u_{V_b})e^{pt_1})} \left(\equiv \frac{G(p)}{H(p)}\right) \tag{16}$$

Die inverse Transformation kann mit Hilfe des Entwicklungssatzes für Laplace-sche Transformierten durchgeführt werden (die Wurzeln von H(p) sind von einfachen Charakter):

$$c(t) = \sum \frac{G(p_\ell)}{H'(p_\ell)} e^{p_\ell t} = \sum_\ell \frac{u\,(1 - e^{-p_\ell t_b})e^{p_\ell t}}{p_\ell((2t_1+t_2)u_2 e^{p_\ell(2t_1+t_2)} - t_1(u_{V_a}+u_{V_b})e^{p_\ell t_1}} \tag{17}$$

da p = 0 keine Polstelle ist, und die übrigen Pole:

$$p_\ell = \frac{1}{t_1 + t_2}\left(\ln \frac{u_{V_a} + u_{V_b}}{u_2} + 2\,\pi i \ell\right); \tag{18}$$

$$\ell = 0, \pm 1, \pm 2, \ldots$$

Multipliziert man den Zähler und Nenner von (17) mit $e^{-p_\ell(2t_1+t_2)}$, so erhält man unter Benutzung von (18):

$$c(t) = \frac{u}{u_2(t_1+t_2)} \sum_\ell \frac{(1 - e^{-p_\ell t_b}) e^{p_\ell(t-2t_1-t_2)}}{p_\ell} \tag{19}$$

Aus (2) folgt, daß $\mathrm{Re}[p_\ell] < 0$, daher kann (19) in folgender Form weiter entwickelt werden:

$$c(t) = \frac{u}{u_2(t_1+t_2)} \left[\sum_\ell \int_o^\infty e^{p_\ell(t'-t_b-2t_1-t_2)}\,dt' - \sum_\ell \int_o^\infty e^{p_\ell(t'-2t_1-t_2)}\,dt'\right] \tag{20}$$

Vertauscht man die Reihenfolge des Summierens und Integrierens und setzt man die Werte von p_ℓ aus (18) ein, so erhält man nach der Summierung:

$$c(t) = \frac{u}{u_2(t_1+t_2)} \left\{ \int_t^\infty \left[e^{\frac{t'-t_b-2t_1-t_2}{t_1+t_2}} \chi_o \sum_{k=0}^\infty \delta\left(\frac{t'-t_b-2t_1-t_2}{t_1+t_2} - k\right) dt'\right] - \right.$$

$$\left. - \int_t^\infty \left[e^{\frac{t'-2t_1-t_2}{t_1+t_2}} \chi_o \sum_{k=0}^\infty \delta\left(\frac{t'-2t_1-t_2}{t_1+t_2} - k\right)\right] dt'\right\} \tag{21}$$

wobei der Zusammenhang für die bekannte Funktionsreihe verwendet wurde (ξ kontinuierliche Veränderliche, $\xi \geq 0$; δ die Dirac-sche Deltafunktion):

$$\sum_{\ell=-\infty}^{\infty} e^{2\pi i \ell \xi} = \sum_{k=0}^{\infty} \delta(\xi - k) \tag{22}$$

weiters ist folgende Bezeichnung eingeführt worden:

$$\chi_o = \ln \frac{u_{v_a} + u_{v_b}}{u_2} \tag{23}$$

Die Integrationen in (21) können durchgeführt werden, das Resultat kann mit Hilfe der θ Einheitsfunktion aufgeschrieben werden:

$$c(t) = \frac{u}{u_2} \sum_{k=0}^{\infty} e^{\chi_o k} [\Theta(t-2t_1-t_2-k(t_1+t_2)) - \Theta(t-t_b-2t_1-t_2-k(t_1+t_2))] \tag{24}$$

Aus (24) kann nun gemäß (6) die gesuchte Dichtefunktion gebildet werden, indem man (23), sowie die Resultate laut (3) und die Definition der Rezirkulationsquotienten verwendet:

$$\rho(t) = \frac{1-\varphi_a-\varphi_b+\varphi_a\varphi_b}{t_b} \sum_{k=0}^{\infty} (\varphi_a+\varphi_b-\varphi_a\varphi_b)^k [\Theta(t-2t_1-t_2-k(t_1+t_2)) - \Theta(t-t_b-2t_1-t_2-k(t_1+t_2))] \tag{25}$$

Schließlich kann man gemäß (7) die Funktion der exakten Verweilzeit-Verteilungsdichte berechnen, welche - wie leicht einzusehen - auf die Einheitsform normalisiert ist:

$$\rho_e(t) = \lim_{t_b \to o} \rho(t) = (1-\varphi_a-\varphi_b+\varphi_a\varphi_b) \sum_{k=0}^{\infty} (\varphi_a+\varphi_b-\varphi_a\varphi_b)^k \delta(t-2t_1-t_2-k(t_1+t_2)) \tag{26}$$

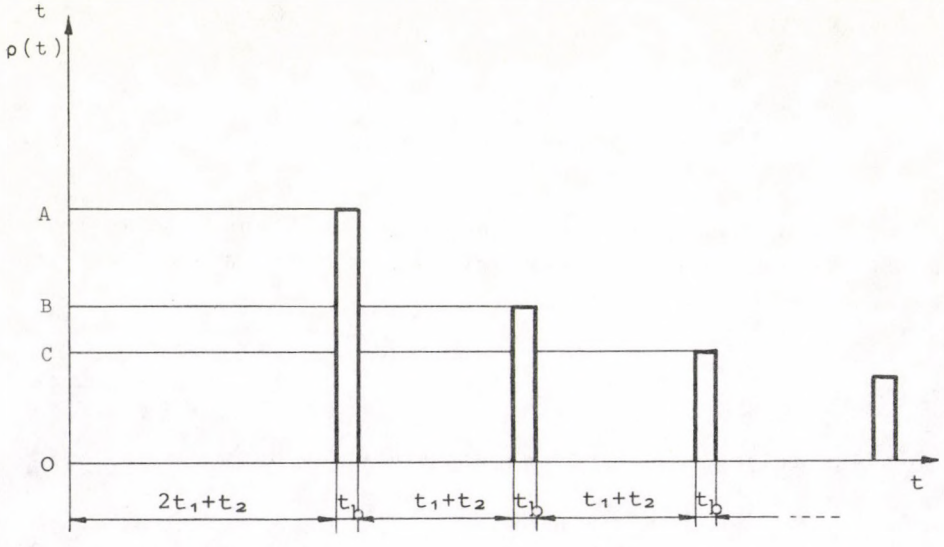

Abb. 3. A-$(1-\varphi_a-\varphi_b+\varphi_a\varphi_b)/t_b$ B- $(1-\varphi_a-\varphi_b+\varphi_a\varphi_b)(\varphi_a+\varphi_b-\varphi_a\varphi_b)/t_b$

C- $(1-\varphi_a-\varphi_b+\varphi_a\varphi_b)(\varphi_a+\varphi_b-\varphi_a\varphi_b)^2/t_b$

Der Verlauf der Dichtefunktion (25) ist auf Abb. 3 zu sehen: die Voraussetzung der idealisierten, korkartigen Strömung ohne Mischung ergibt auch in der Ausgangskonzentration (also auch in der Dichtefunktion) idealisierte Impulse.

2. Der Fall mit vollständiger Mischung

Gemäß (12) ist folgendes mathematische Problem zu lösen:

$$V_2 \frac{d\,c_2}{dt} = uc_b(t-t_1) + (u_{V_a} + u_{V_b})c_2(t-t_1) - u_2c_2(t),$$

wobei das inhomogene Glied aus (5), bzw. aus den Vorangehenden bekannt ist, und die Ausgangsbedingung ist offensichtlich

$$c_2(t) = 0, \quad \text{wenn} \quad t \leq 0 \tag{27}$$

Wir wollen nun den Intervall $0 \leq t < \infty$ auf Strecken von Länge t_1 aufteilen, und unsere Gleichung streckenweise untersuchen. Im Intervall $0 \leq t < t_1$ ist jedes Glied der rechten Seite Null, also ist $c_2^I(t)$ eine Konstante, bzw. wegen (27) gleich Null. (Der obere Index zeigt an, um welchen untersuchten Zeitabschnitt c_2 es sich handelt.)

Im Intervall $t_1 \leq t < 2t_1$ sind zwei Glieder der rechten Seite ungleich Null, so daß die zu lösende Gleichung wie folgt lautet:

$$V_2 \frac{dc_2^{II}}{dt} = uc_b(t - t_1) - u_2c_2^{II} \tag{28}$$

Die Lösung von (28) beträgt unter Berücksichtigung der Form des inhomogenen Gliedes von (5):

$$c_2^{II}(t) = \begin{cases} \frac{u}{u_2}\left(1 - e^{\frac{u_2}{V_2}(t_1-t)}\right) & \text{wenn } t_1 \leq t < t_1 + t_b \\ \frac{u}{u_2}\left(e^{\frac{u_2}{V_2}(t_1+t_b-t)} - e^{\frac{u_2}{V_2}(t_1-t)}\right) & \text{wenn } t_1+t_b \leq t < 2t_1 \end{cases}$$

wo die auftretende Integrationskonstanten so bestimmt wurden, daß $c_2^{II}(t)$ eine kontinuierliche Funktion ergebe.

Im nächsten Intervall $2t_1 \leq t < 3t_1$ (und nachher stets) übernimmt das zweite Glied der rechten Seite praktisch die Rolle des inhomogenen Teiles. Unter Verwendung des Resultats von (29) ist daher in diesem Fall folgende Gleichung zu lösen:

$$V_2 \frac{d\, c_2^{III}}{dt} = (u_{V_a} + u_{V_b}) c_2^{II}(t - t_1) - u_2 c_2^{III} \tag{30}$$

welche - im Hinblick auf die Struktur von (29) - in den Teilintervallen $2t_1 \leq t < 2t_1 + t_b$ und $2t_1 + t_b \leq t < 3t_1$ verschiedene Formen annimt.

Es ist jedoch zu bemerken, daß nur ein Zusatz je Interval mit dem beschriebenen sukzessiven Integrationsverfahren berechnet wird. Die vollständige Lösung baut sich aus der "Superposition von Konzentrationshuben" auf, indem zu dem in einem gegebenen Intervall berechneten Zusatz stets auch die "abklingenden" Teile der in der zweiten Hälfte des betreffenden Intervalls gültigen Zusätze der vorangegangenen Intervalle hinzuzugeben sind. So beträgt in dem letzten untersuchten Fall

$$c_2(t) = c_2^{III} + c_2^{II'}(+ c_2^{I'}) \tag{31}$$

wobei der Strich zeigt, daß aus (29) der abklingende Teil zu wählen ist; das Glied in Klammern ist nur der Form halber aufgeschrieben worden. Obiges ungewöhnliche Verhalten der Lösungsfunktion folgt aus dem linearen Charakter und aus der speziellen Struktur unserer Gleichung.

Wir schreiben nun die allgemeine, im Intervall $nt_1 \leq t < (n+1)t_1$ gültige, durch die beschriebene Methode entwickelte Lösung auf, ohne die bezeichneten Integrationen durchzuführen, damit würde nämlich der Algorythmus der Berechnung verloren gehen. Das untersuchte Intervall muß offensichtlich auch hierbei in zwei Teile geteilt werden, daher:

$$c_2(t) = \begin{cases} B_{n-1}(t) & \text{wenn} \quad nt_1 \le t < nt_1 + t_b \\ B_n(t) & \text{wenn} \quad nt_1 + t_b \le t < (n+1)t_1 \end{cases} \tag{32}$$

Hier ist

$$A_n(t) = \left\{ \frac{u}{V_2} \left[\frac{u_{V_a} + u_{V_b}}{V_2} \right]^{n-1} \int_{nt_1}^{t} \int_{2t_1}^{t'''-t_1} \cdots \int_{t_1}^{t''-t_1} e^{\frac{u_2}{V_2}t'} \, dt' dt'' .. dt^n \right\} e^{-\frac{u_2}{V_2}[t-(n-1)t}$$

$$B_n(t) = \sum_{k=1}^{n} \frac{u}{V_2} \left[\frac{u_{V_a} + u_{V_b}}{V_2} \right]^{k-1} \left\{ \int_{kt_1+t_b}^{t} \left[\cdots \left[\int_{2t_1+t_b}^{t''-t_1} \left[\int_{t_1+t_b}^{t''-t_1} \Theta \cdot e^{\frac{u_2}{V_2}t'} \, dt' + \right. \right. \right. \right.$$

$$\left. \left. \left. \left. + A_1'(t_1+t_b) \right] dt'' + A_2'(2t_1+t_b) \right] \cdots \right] dt^k + A_k'(kt_1+t_b) \right\} e^{-\frac{u_2}{V_2}[t-(k-1)t_1]};$$

$$A_n'(t) = \frac{A_n(t)}{\frac{u}{V_2} \left[\frac{u_{V_a} + u_{V_b}}{V_2} \right]^{m-1} \cdot e^{-\frac{u_2}{V_2}[t-(n-1)t_1]}}$$

Wir bilden nun gemäß (6) unter Benutzung von (32) die Dichtefunktion $\rho_2(t)$, die man erhält, indem man an die Stelle von $c(t)$ vorläufig $c_2(t)$ schreibt. Nach dem Grenzübergang laut (7) stellt man fest, daß die exakte Wahrscheinlichkeitsdichte einen viel einfacheren Ausdruck ergibt, in welchem die mehrmals erwähnte Transformation des Arguments bereits durchführbar ist:

$$\rho_{e_2}(t) = \lim_{t_b \to o} \rho_2(t) = \lim_{t_b \to o} \frac{c_2(t)}{t_b} = \tag{33}$$

$$= \sum_{k=1}^{\infty} \frac{u}{V_2} \left[\frac{u_{V_a} + u_{V_b}}{V_2} \right]^{k-1} \frac{(t-kt_1)^{k-1}}{(k-1)!} \Theta(t-kt_1) \, e^{\frac{u_2}{V_2}(kt_1-t)}$$

nach Transformation $t \to t - t_1$:

$$\rho_e(t) = \sum_{k=2}^{\infty} \frac{u}{V_2} \left[\frac{u v_a + u v_b}{V_2}\right]^{k-2} \frac{(t-kt_1)^{k-2}}{(k-2)!} \theta(t-kt_1) e^{-\frac{u_2}{V_2}(kt_1-t)} \qquad (34)$$

wo θ die Einheitsfunktion darstellt.

Es ist leicht einzusehen, daß diese Funktion $\rho_e(t)$ ebenfalls auf die Einheitsform normalisiert ist:

$$\int_0^{\infty} \rho_e(t)dt = \sum_{k=2}^{\infty} \frac{u}{V_2}\left[\frac{u v_a + u v_b}{V_2}\right]^{k-2} \frac{1}{(k-2)!} \int_{kt_1}^{\infty} (t - kt_1)^{k-2} e^{\frac{u_2}{V_2}(kt_1-t)} dt =$$

$$= \sum_{k=2}^{\infty} \frac{u}{V_2} \left[\frac{u v_a + u v_b}{V_2}\right]^{k-2} \frac{1}{(k-2)!} \int_0^{\infty} x^{k-2} e^{\frac{u_2}{V_2} x} dx =$$

$$= \sum_{k=2}^{\infty} \frac{u}{V_2} \left[\frac{u v_a + u v_b}{V_2}\right]^{k-2} \frac{1}{(k-2)!} \frac{(k-2)!}{\left(\frac{u_2}{V_2}\right)^{k-1}} = \sum_{k=2}^{\infty} \frac{u}{u_2}\left[\frac{u v_a + u v_b}{u_2}\right]^{k-2}$$

auf die Rezirkulationsquotienten übergehend erhalten wir:

$$\sum_{k=0}^{\infty} (1-\varphi_a-\varphi_b+\varphi_a\varphi_b)(\varphi_a+\varphi_b-\varphi_a\varphi_b)^k = (1-\varphi_a-\varphi_b+\varphi_a\varphi_b) \frac{1}{1-(\varphi_a+\varphi_b-\varphi_a\varphi_b)} = 1$$

Abbildung 4 zeigt den Verlauf der Konzentrationsfunktion (32) und auch der entsprechenden Dichtefunktion. Die gezeigten Kurven besitzen sämtliche Merkmale der von den experimentellen Untersuchungen her bekannten Dichtefunktionen der Verweilzeitverteilung.

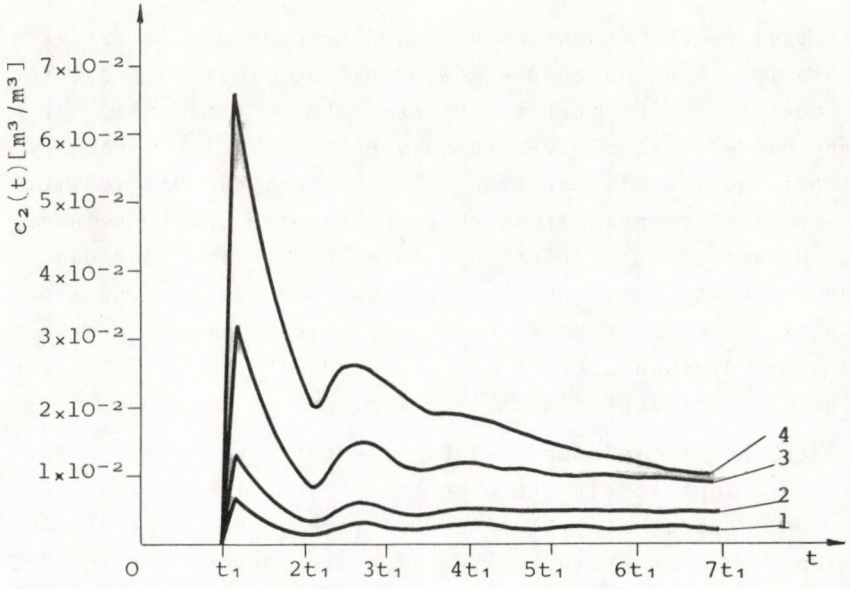

Abb. 4. R = 0,05 m 1 - u = $0{,}6\times10^{-6}$ m^3/sec φ_b = 0,50
r = 0,03 m 2 - u = $1{,}2\times10^{-6}$ m^3/sec φ_b = 0,75
m = 0,15 m 3 - u = $3{,}0\times10^{-6}$ m^3/sec φ_b = 0,90
t_b = 5 sec 4 - u = $6{,}0\times10^{-6}$ m^3/sec φ_b = 0,95

IV. DISKUSSION DES MODELLS

Auf Grund der vorhin beschriebenen Resultate ergibt sich die Frage, inwieweit die Verwendbarkeit unseres Grundmodells von der Annahme einer vollständigen Vermischung im Bereich 2 beeinflußt wird. Die strömenden und getriebenen Medien sind im Bereich 2 in intensiver Berührung, und das Strömungsbild ist hier eher turbulent als laminar oder korkartig. Dadurch tritt eine gewisse Vermischung auf, deren Größe nicht bekannt ist, aber sicherlich zwischen zwei Grenzfällen - nämlich der Nullmischung (korkartige Strömung) und der vollständigen Vermischung - liegt.

Die Frage, welche Bedeutung der Kenntnis des Maßes der Vermischung zukommt, kann durch die Anwendung der zwei untersuchten Fälle des Modells für die Berechnung derselben Größen entschieden werden. Wenn die entsprechenden Größen voneinander nicht sehr verschieden sind, so ist mit Sicherheit anzunehmen, daß die im mittleren Bereich existierende Vermischung unbekannten Grades kein wesentliches Merkmal des Fließbettapparates darstellt, und daß es von keiner Bedeutung ist, welcher Fall bei der Berechnung eines Problems angewandt wird, denn es ergibt sich jedenfalls, innerhalb der Grenzen, die die Genauigkeit des Grundmodells ermöglicht, ein die tatsächliche Lage annäherndes Resultat.

Man betrachte folgenden Prozeß: als getriebener Stoff soll in den Fließbettapparat eine körnige Masse eintreten, deren Stoff mit dem in den Apparat eingeblasenen Gas (treibendes Medium) in eine Reaktion scheinbar ersten Grades eingeht. Nehmen wir an, daß der reagierende Anteil der eintretendern Körner (X) eine Einheit beträgt, so kann die Veränderung des reagierenden Anteils des im Moment $t = 0$ eingetretenen Kornes mit guter Annäherung durch folgenden Zusammenhang beschrieben werden:

$$X = e^{-\mu t} \tag{35}$$

Im Falle von Problemen aus der Praxis ist es notwendig, daß der durchschnittliche reagierende Anteil des austretendes Stoffes $\bar{X}$ bekannt sei, und zwar - falls alle übrigen äußeren Kenndaten unverändert bleiben - in Abhängigkeit von der durchschnittlichen Verweilzeit $\bar{t}$. Obige Größe können unter Verwendung der mit Hilfe des Modells erhaltenen Dichtefunktionen der Verweilzeitverteilungen (26) bzw. (34) einzeln berechnet werden:

$$\bar{X} = \int_0^\infty e^{-\mu t} \rho_e(t)dt, \quad \bar{t} = \int_0^\infty t \rho_e(t)dt \tag{36}$$

Wird eine Gleichung von (36) im Wege irgendeines, in der Dichtefunktion $\rho_e(t)$ figurierenden geeigneten Parameters in die andere eingesetzt, so erhalten wir die gesuchte Funktionsbeziehung $\bar{X} = \bar{X}(\bar{t})$.

Bezeichnen wir die Resultate für den Fall ohne Vermischung mit Index (1), und für den Fall mit vollständiger Mischung mit Index (2). Nach Integration von (36) erhalten wir:

$$\bar{X}_{(1)} = (1-\varphi_a-\varphi_b+\varphi_a\varphi_b)\,\frac{e^{-\mu(2t_1+t_2)}}{1-(\varphi_a+\varphi_b-\varphi_a\varphi_b)e^{-\mu(t_1+t_2)}}$$

$$\bar{t}_{(1)} = \bar{t}_{(2)} = 2t_1 + t_2 + \frac{\varphi_a+\varphi_b-\varphi_a\varphi_b}{1-\varphi_a-\varphi_b+\varphi_a\varphi_b}\,(t_1+t_2) \qquad (37)$$

$$\bar{X}_{(2)} = (1-\varphi_a-\varphi_b+\varphi_a\varphi_b)\,\frac{e^{-2\mu t_1}}{1+\mu t_2-(\varphi_a+\varphi_b-\varphi_a\varphi_b)e^{-\mu t_1}}$$

Hierbei wurde berücksichtigt, daß auch die durchschnittliche Verweilzeit des völlig durchmischten Bereichs 2 den bereits bekannten Wert t_2 besitzt. Unter Verwendung von (1) und (3) können durch Einführung der Volumquotienten σ_1, σ_2 der entsprechenden Bereiche des getriebenen Stoffes, sowie des Stoffrückmischungs-Quotienten $\Psi = \frac{u}{u_{V_b}}$ die Gleichung der durchschnittlichen Verweilzeit von (37) umgeformt werden:

$$\bar{t}_{(1)} = \frac{2\sigma_1 V_1 + \sigma_2 V_2}{u}\,, \qquad \bar{t}_{(2)} = \frac{2\,\sigma_1 V_1 + \sigma_2 V_2}{u} \qquad (38)$$

Auf dieselbe Weise können auch $\bar{X}_{(1)}$ und $\bar{X}_{(2)}$ umgebildet werden, und führt man die erwähnten Substitutionen durch Beseitigung des Parameters u durch, so erhält man die gesuchten Endformeln: $\bar{t} = \bar{t}_{(1)} = \bar{t}_{(2)}$:

$$\bar{X}_{(1)} = \frac{\Psi}{2+\Psi}\,\frac{\exp\left[-\mu\bar{t}\,\frac{2\chi\,\frac{\Psi}{1+\Psi}+\frac{\Psi}{2+\Psi}}{2\chi+1}\right]}{1-\frac{2}{2+\Psi}\exp\left[-\mu\bar{t}\,\frac{\chi\,\frac{\Psi}{1+\Psi}+\frac{\Psi}{2+\Psi}}{2\chi+1}\right]} \qquad (39)$$

$$\bar{X}_{(2)} = \frac{\Psi}{2+\Psi} \frac{\exp\left[-\mu\bar{t}\,\frac{2\,\chi\,\frac{\Psi}{1+\Psi}}{2\,\chi+1}\right]}{1+\mu\bar{t}\,\frac{\frac{\Psi}{2+\Psi}}{2\chi+1}-\frac{2}{2+\Psi}\exp\left[-\mu\bar{t}\,\frac{\chi\,\frac{\Psi}{1+\Psi}}{2\chi+1}\right]}$$

wobei der Quotient $\chi = \frac{\sigma_1 V_1}{\sigma_2 V_2}$ eingeführt worden ist, welcher die Verteilung der gesamten, zu einem gegebenen Zeitpunkt im Apparat anwesenden getriebenen Stoffmenge unter den einzelnen Bereichen angibt.

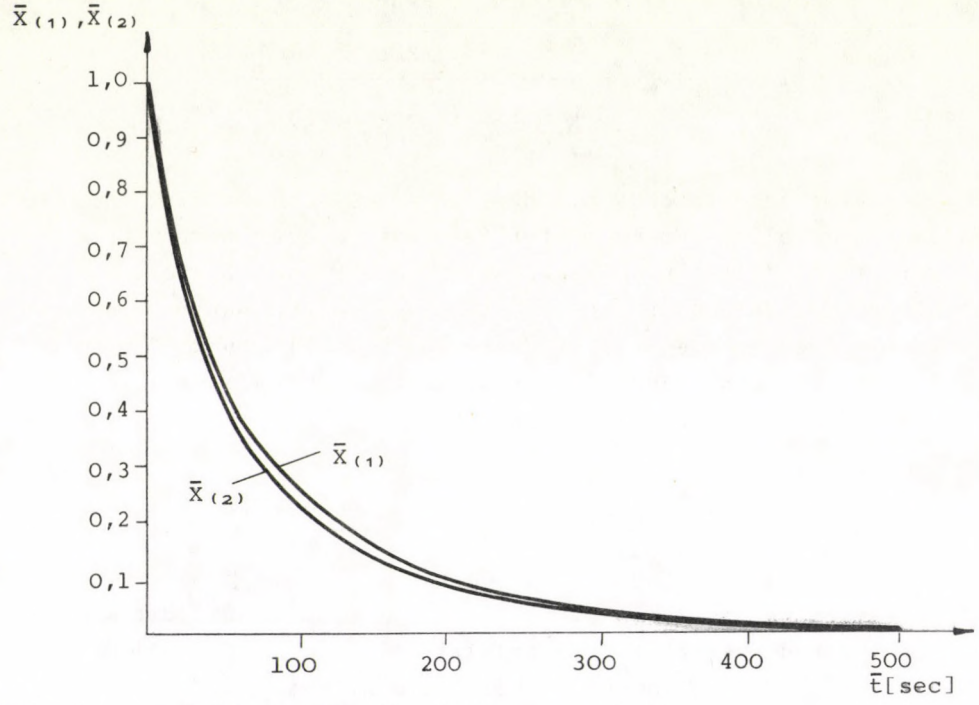

Abb. 5. $\mu = 0{,}02\ \mathrm{sec}^{-1}$; $\Psi = 0{,}50$; $\chi = 5{,}00$

Die Funktionsbeziehungen $\bar{X}_{(1)}(\bar{t})$ und $\bar{X}_{(2)}(\bar{t})$ sind unter Angabe der möglichen Werte der vorkommenden Parameter auch grafisch dargestellt worden. Abb. 5 zeigt die Kurven. Es ist festzustellen, daß die Abweichung der durch zwei untersuchte Fälle erhaltenen Re-

ultate niemals mehr als 10 % ihres Mittelwertes beträgt. Es ist also auf Grund obiger Ausführungen offensichtlich, daß die Annahme der Vermischung im Bereich 2 im Modell keine entscheidende Rolle spielt, zumindest im Falle des gezeigten Beispiels nicht.

Es soll noch erwähnt werden, daß im Falle des Grenzüberganges $\chi \to \infty$ die Gleichung von (39) in einander übergehend: dies ist eine logische Folge dessen, daß obiger Grenzfall gerade die Ausschaltung des Bereichs 2 bedeutet.

V. ZUSAMMENFASSUNG, KONKLUSIONEN

Obige Berechnungen lieferten den Beweis für die Hypothese, daß die Aufteilung des angewandten Modells im Falle überhaupt keiner, oder einer vollständiger Mischung zu nicht beachtenswert unterschiedlichen Zahlenwerten führt. Auf diese Weise konnten wir unser Ziel, nämlich die Bestimmung der Dichtefunktion der Verweilzeitverteilung eines durch einen Fließbettapparat strömenden, getriebenen Stoffes, sowohl mit den Wahrscheinlichkeitsdichten von (26) als auch (34) - trotz deren vollkommen verschiedenen mathematischen Formen - auf gleicherweise zufriedenstellende Art erreichen. Für die Verwendung in der Praxis ist natürlich der einfachere Ausdruck (26) zu bevorzugen.

Die Formeln unter (39) besitzen den praktischen Wert, daß mit ihrer Hilfe im Falle einer sich in einem Gas-Feststoff-Phasen Fließbettreaktor abspielenden Reaktion scheinbar ersten Grades der durchschnittliche reagierende Anteil der Körner in Abhängigkeit von der durchschnittlichen Verweilzeit derselben bestimmt werden kann. Einer der beiden Parameter bestimmt das Maß der inneren Rezirkulation, während der andere mit dem Verhältnis der tatsächlichen Volumen der einzelnen Fließbettbereiche zu einander zusammenhängt.

Wir möchten noch bemerken, daß die angestrebte allgemeine Formulierung der Dichtefunktionen (26) und (34) in dem Fall nützlich ist, wenn die Verweilzeitverteilung eines konkreten Problems im Zusammenhang mit Fließbettapparaten gesucht wird. In solchen Fällen sind die freien Parameter auf die Weise zu verändern, wie es der Zweckmäßigkeit am besten entspricht.

ZEICHENERKLÄRUNG

c Konzentration des Indikatorstoffes beim Austritt ($m^3 \cdot m^{-3}$)

c_b Eintrittskonzentrations-Funktion ($m^3 \cdot m^{-3}$)

c_k Austrittskonzentrations-Funktion im allgemeinen Fall ($m^3 \cdot m^{-3}$)

c_2 Konzentration des Indikatorstoffes am Anfang des Bereiches 2 bzw. im Bereich 2 ($m^3 \cdot m^{-3}$)

f, f_b Laplace-Transformierte der Konzentrationsfunktionen

k, ℓ Laufende Summierungsindices

m Höhe des Fließbettapparates (m)

p Parameter der Laplace-Transformation

p_ℓ Polstellen der Laplace-Transformierten f

$2r$ Durchmesser des Futterrohres (m)

$2R$ Durchmesser des Fließbettapparates (m)

t Zeitkoordinate (sec)

$\bar{t}$ durchschnittliche Verweilzeit (sec)

t_1, t_2, t_3 Verweilzeiten in den drei Bereichen (sec)

t_b Breite des Eingangsimpulses (sec)

u Volumgeschwindigkeit des getriebenen Stoffes ($m^3\ sec^{-1}$)

u' Volumgeschwindigkeit des treibenden Mediums ($m^3\ sec^{-1}$)

u_1, u_2, u_3 Volumgeschwindigkeiten des getriebenen Stoffes in den drei Bereichen ($m^3\ sec^{-1}$)

u_{V_a}, u_{V_b} Volumgeschwindigkeiten des rezirkulierenden getriebenen Stoffes ($m^3\ sec^{-1}$)

V_1, V_2, V_3 Volumen der drei Bereiche (m^3)

X reagierender Anteil (1)

$\bar{X}$ durchschnittlicher reagierender Anteil (1)

α Impulsübertragungsfunktion

μ Reaktionszeitkonstante (sec^{-1})

φ_a, φ_b Rezirkulationsquotienten (1)

ρ Dichtefunktion der Verweilzeitverteilung (sec^{-1})

ρ_e Wahrscheinlichkeitsdichte des Einkorns (sec^{-1})

σ_1, σ_2 Volumquotienten des getriebenen Stoffes im entsprechenden Bereich (1)

Ψ Stoffrückmischungsquotient beim Austritt aus dem Fließbettapparat (1)

χ Effektive Volumenrate der Bereiche (1)

LITERATUR

1. BECKER, H.A., Chem. Eng. Sci. 13, 245 (1961)
2. THORLEY, B. et al., Can. J. Chem. Engs. 184, 10 (1959)
3. MALEK, M.A. et al., Ind. Eng. Chem. 2, 31 (1963)
4. MADONNA, L., LAMA, R.F., Brit. Chem. Eng. 6, 524 (1961)
5. MALEK, M.A. et al., Ind. Eng. Chem. 4, 123 (1965)
6. DUKLER, A.E. et al., Am. I. Chem. Eng. J. 10, 44 (1964)

7. GLOYER, W., Chem. Eng. 75, 93 (1968)

8. DANCKWERTS, P.V., Chem. Eng. Sci. 2, 1 (1953)

DANKSAGUNG

Ich möchte den Herren Professor Dr. T. BLICKLE, Dr. P. ÁRVA und Dr. R. TÖRÖS meinen Dank für ihre wertvollen Ratschläge und ihre Hilfe aussprechen, die sie mir im Laufe meiner Arbeit gewähren ließen.

РЕЗЮМЕ

В статье дается общее математическое описание гейзеровых процессов и аппаратов на основе рециркуляционной модели.

Картину течения, возникающего в гейзеровом слое, моделировали при условиях как нулевого, так и полного смешения в центральной, критической области.

Дается решение уравнений физической модели, относящихся к конечной концентрации пропущенного вещества, и использование результатов для определения распределения времени нахождения.

Сравнение двух моделей и выяснение роли центрально-областного смешения проводилось с использованием моделей в одинаковых расчетах.

Hungarian Journal
of Industrial Chemistry
Veszprém
Vol. 3. pp.115-126 (1975)

ENERGETISCHE EIGENSCHAFTEN PLASMABILDENDER GASE DER TIEFTEMPERATUR-PLASMATECHNIK

W. FRATZSCHER, D. HEBECKER und J. HONSCHA

(Technische Hochschule für Chemie "Carl Schorlemmer"
Leuna-Merseburg)

Eingegangen am 20. September 1974.

In der Arbeit sind ausgehend von den Eigenschaften des Plasmazustandes die Notwendigkeit der Einschätzung der energetischen Eigenschaften plasmabildender Gase aufgezeigt. Hierzu eignen sich kalorische Zustandsgrößen wie Entalpie und Exergie, wenn sie insbesondere als spezifische Energiedichten unter Verwendung des Volumenvergrößerungskoeffizienten der Dissoziation dargestellt werden.

Im folgenden wird ein Verfahren zur Berechnung der Exergie plasmabildender Gase angegeben, das mit hoher Genauigkeit und rechentechnisch vorteilhaft arbeitet. Ausgangswerte sind Angaben aus bekannten Tabellenwerken für die Einzelgase. Einige Berechnungsergebnisse werden in Form von Diagrammen wiedergegeben und diskutiert. Dabei lassen sich die energetischen Vorteile der Verwendung plasmabildender Gase im Dissoziationsbereich verdeutlichen.

1. EIGENSCHAFTEN PLASMABILDENDER GASE

Das Plasma wird im zunehmenden Maße in der Stoffwirtschaft sowie der Energie- und Werkstofftechnik genutzt. Der Schwerpunkt liegt dabei im Temperaturbereich bis 10^4 Kelvin, ein Bereich, der als Tieftemperaturplasma bezeichnet wird. Bekanntlich wird als

Plasma ein Gemisch aus Molekülen, Atomen, Elektronen und Ionen eines Stoffes bezeichnet. Von einem thermischen Plasma spricht man, wenn seine Bestandteile im vollständigen statistischen Gleichgewicht vorliegen und die Partielgeschwindigkeiten einer Maxwellverteilung folgen.

Für die technische Anwendung des Plasmas sind interessant

- die hohe Temperatur
- der hohe spezifische Energieinhalt und
- das Auftreten von elektrisch geladenen Teilchen [1, 2, 3].

Für stoffwirtschaftliche Prozesse sind die ersten beiden Gesichtspunkte von Bedeutung. Sie kommen bei folgenden Reaktionstypen zum Tragen:

1. Reaktionen, bei denen durch die Temperaturerhöhung das Gleichgewicht auf die Seite des gewünschten Produktes verschoben wird.
2. Reaktionen, die aufgrund ihrer Kinetik eine hohe Temperatur für ausreichende Reaktionsgeschwindigkeiten erfordern.
3. Reaktionen, die über Zwischenstufen laufen, die bei niedrigen Temperaturen nicht existieren.
4. Reaktionen, bei denen die Eigenschaften der Endprodukte durch hohe Temperaturen verbessert werden.
5. Endotherm verlaufende Reaktionen mit großen Reaktionsenthalpien, bei denen durch den hohen spezifischen Energieinhalt des Plasmas als Energieträger hohe Reaktionsraumbelastungen erreicht werden können [5, 6, 8].

Im folgenden sollen die plasmabildenden Gase für den zuletzt genannten Verwendungszweck untersucht werden. Deshalb stehen für die Auswahl und Bewertung der plasmabildenden Gase ihre energetischen Eigenschaften zur Verfügung [7]. Als energetische Eigenschaften lassen sich ansehen die je Trägergaseinheit transportierte Energiemenge, die Temperatur bei der diese Energiemenge zur Verfügung gestellt werden kann und die Qualität dieser Energiemenge bei einem entsprechenden Übertragungsprozess. Diese Eigenschaften werden durch den thermodynamischen Zustand des Plasmas bestimmt. Der

Einfluß weiterer physikalischer Parameter wie Wärmeleitfähigkeit, Zähigkeit, elektrische Leitfähigkeit, Diffusionskoeffizient usw. infolge Dissoziation wurde in dieser Arbeit nicht untersucht.

Der spezifische Energieinhalt wird durch die Energiedichte - definiert als die je Volumen oder Moleinheit im Plasma gebundene Energie - erfaßt. Die Angabe von Entalpiewerten für das Plasma ist demgegenüber problematisch, da sie veränderlich und schwer meßbar sind. Außerdem läßt sich für das Plasma nur eine mittlere Massentemperatur errechnen, die nur begrenzt Aussagen zu den tatsächlichen Verhältnissen im Reaktor machen kann.

Die Qualität der Energie läßt sich allgemein durch die Exergie ausdrücken. Da die Exergie der beliebig umwandelbare Teil der Energie ist, stellt die Angabe der Exergie eines plasmabildenden Gases ein Maß für die mindestens aufzuwendende Elektroenergie zur Erzeugung des Plasmas dar. Deshalb eignet sich die Exergie zur Kennzeichnung wesentlicher Seiten der energetischen Eigenschaften.

Für den für plasmabildende Gase interessierenden Temperaturbereich lassen sich die Exergien nur mit großen Fehlern aus vorhandenen Diagrammen entnehmen. Im folgenden wird deshalb ein Verfahren zur Berechnung der Dissoziationsexergie vorgeschlagen, das ausgehend von bekannten Tabellenwerten numerisch zu genauen Werten führt.

2. BERECHNUNG DER EXERGIE VON PLASMEN

Da zur Bewertung der plasmabildenden Gase die Energiedichte herangezogen werden soll, ist es zweckmäßig die Intensität der Dissoziation durch den Volumenvergrößerungskoeffizienten zu kennzeichnen. Es ist

$$\beta = \frac{\sum_{j=1}^{n} \nu_{i,j} \cdot R_j}{\sum_{k=1}^{m} \nu_{i,k} \cdot r_k} \qquad (1)$$

mit

R_j - Molanteil der Verbindung j im Ausgangsgemisch

r_k - Molanteil der Verbindung k im Gleichgewichtsgemisch

$\nu_{i,j}; \nu_{i,k}$ - stöchiometrische Koeffizienten zur Kennzeichnung der Anzahl der Atome des Elements i in den Verbindungen j bzw. k.

Der Volumenvergrößerungskoeffizient ist ein Maß für die Energietransportleistung. Er ist auch für die Kennzeichnung von Mehrkomponentensystemen anwendbar. Für bimolekulare Gase ergibt sich ein einfacher Zusammenhang mit dem Dissoziationsgrad α entsprechend

$$\beta = 1 + \alpha$$

Im Bild 1 ist der Verlauf des Volumenvergrößerungskoeffizienten für einige bimolekulare Gase als Funktion der Temperatur angegeben.

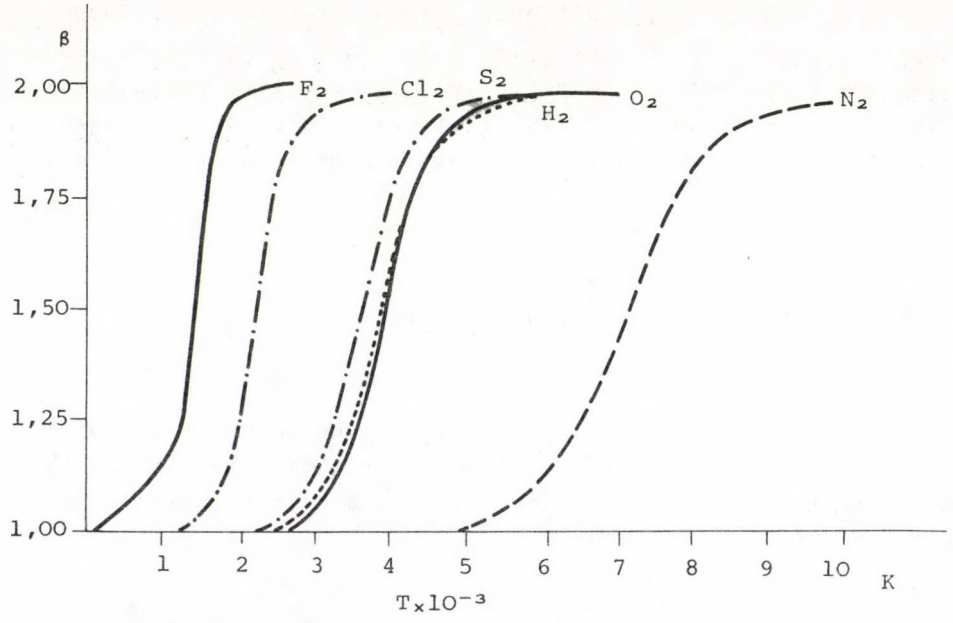

Bild 1. Abhängigkeit des Volumenvergrößerungskoeffizienten von der Temperatur bei der Dissoziation von Gasen

Zur Berechnung der Exergie geht man zweckmäßig von der Definitionsgleichung aus [4, 9, 11]

$$E = (H - H_U) - T_U\ (S - S_U) \tag{2}$$

Als Umgebungszustand wird der Standardzustand (293 K, 1 atm) der jeweils stabilsten Modifikation verwendet. Für die in Bild 1 aufgeführten Gase ist dies stets die zweiatomige Verbindung. Beim Schwefel ist hierbei eine Aggregatszustandsänderung zu berücksichtigen.

Werden die plasmabildenden Gase als ideale Gase angesehen, so läßt sich die Enthalpie H in Gl. (2) nach der Beziehung

$$H = \beta \sum_{k=1}^{m} r_k\ H_k^*(T) \tag{3}$$

bestimmen. Die Enthalpien der Einzelgase $H_k^*(T)$ können entsprechenden Tabellenwerken entnommen werden [10]. Die Multiplikation mit dem Volumenvergrößerungskoeffizient ergibt die Energiedichte. Für die Entropie des plasmabildenden Gases gilt

$$S = S_T + \Delta S_M + \Delta S_p \tag{4}$$

Dabei stellt S_T die Temperaturfunktion der Entropie, ΔS_M den Mischungsanteil und ΔS_p den Druckanteil dar. Die Temperaturfunktion bestimmt sich aus der Beziehung

$$S_T = \beta \sum_{k=1}^{m} r_k\ S_k(T) \tag{5}$$

Durch die Multiplikation mit β erreicht man den gleichen Bezugspunkt wie für die Enthalpie. Die Entropien der Einzelgase können entweder entsprechenden Tabellenwerken [10] unmittelbar entnommen werden oder über die Enthalpie, die reduzierte freie Enthalpie ϕ und die Gleichgewichtskonstante K_p berechnet werden. Für die Auswertung der Beziehungen auf Rechenautomaten ist der letzte Weg vorteilhafter, da hierzu ein kleinerer Speicherplatzbedarf erforderlich ist. Für bimolekulare Gase gestaltet sich die Rechnung besonders einfach. Die Entropien der atomar vorliegenden Anteile bestimmen sich aus der Beziehung

$$S_k^A(T) = \phi^A(T) + \frac{(H^{*A}(T) - H_U^{*A}) + (H_U^A - H_o^A)}{T} \qquad (6)$$

Dabei stellt $(H^{*A}(T) - H_U^{*A})$ die Gesamtenthalpieänderung (infolge Änderung des thermischen und des chemischen Zustandes) zwischen der laufenden Temperatur T und der Standardtemperatur, die gleich der Umgebungstemperatur gesetzt ist, dar. Der Term $(H_U^A - H_o^A)$ entspricht der Enthalpie des Umgebungszustands bezogen auf 0.K.

Aus dem Ansatz

$$\Delta G = \Delta H - T\Delta S = - RT \ln K_p \qquad (7)$$

läßt sich unter Benutzung von Gl. (6) die Entropie der molekular vorliegenden Anteile des Plasmas bestimmen. Für zweiatomige Gase gilt

$$S_k^M(T) = R \ln K_p + \frac{H^{*M}(T) + 2[\phi^A(T)\cdot T - H_U^{*A} + (H_U^A - H_o^A)]}{T} \qquad (8)$$

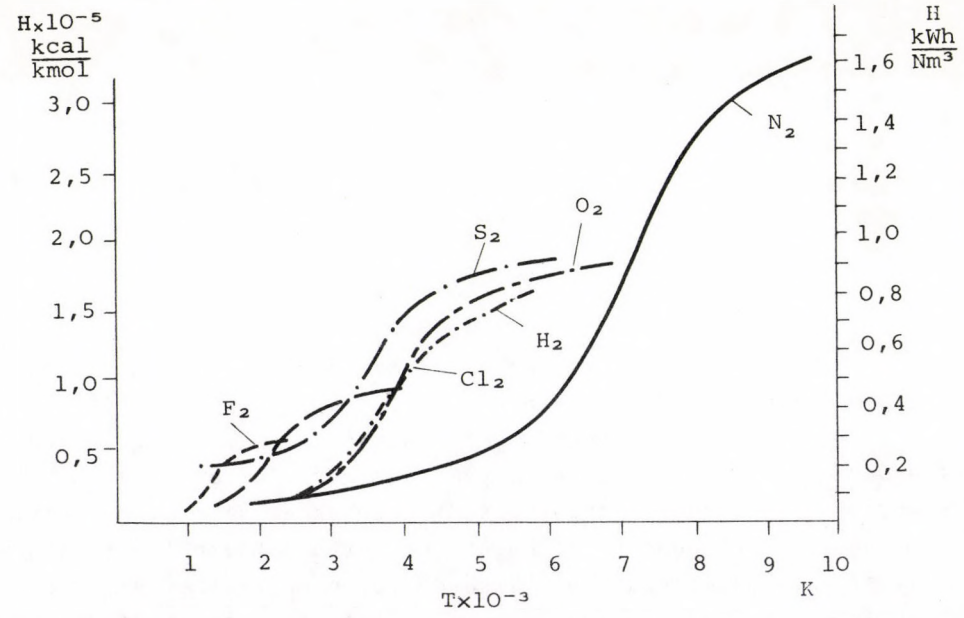

Bild 2. Enthalpie dissoziierender Gase als Funktion der Temperatur

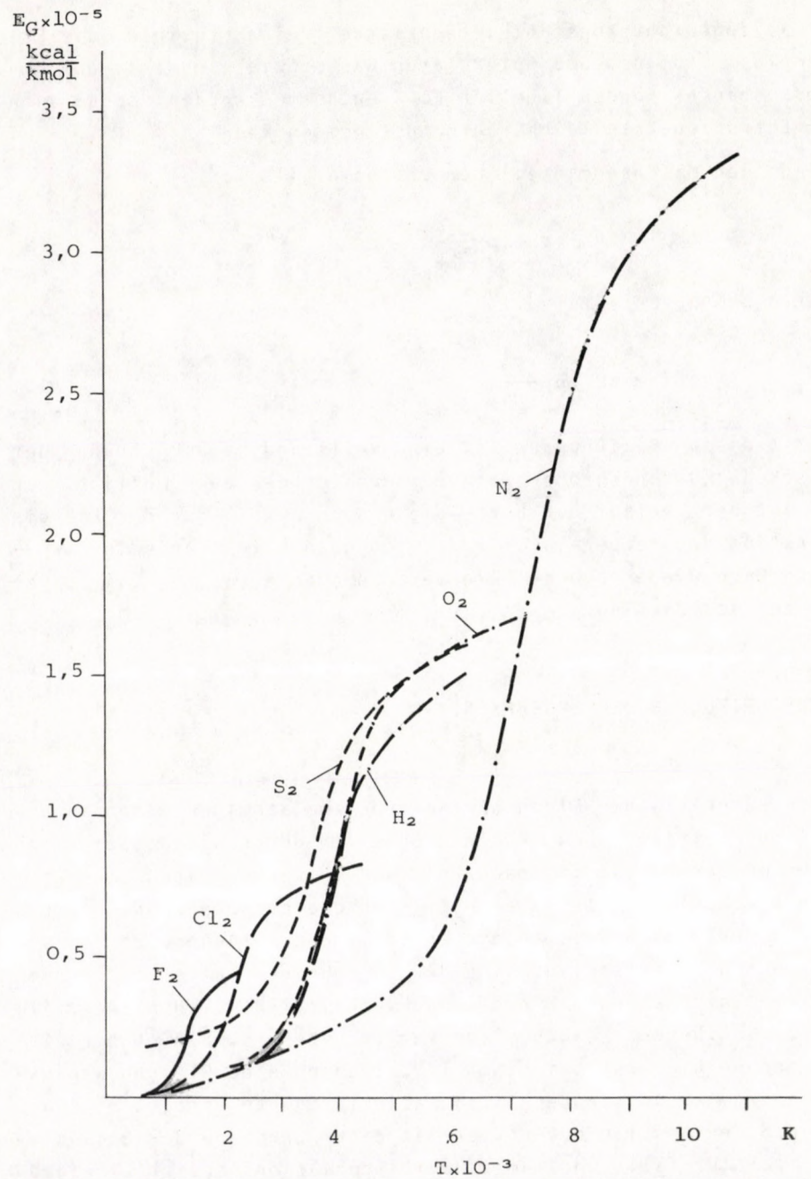

Bild 3. Exergie dissoziierender Gase als Funktion der Temperatur

Gleichgewichtskonstante, reduzierte freie Enthalpie, die Enthalpien der atomaren und molekularen Gase sowie die Werte des Umgebungszustandes können Tabellen [10] entnommen werden, sodaß auch dieser Entropiebetrag leicht berechnet werden kann.

Für den Mischungsanteil der Entropie gilt

$$\Delta S_M = \beta R \sum_{k=1}^{m} r_K \ln \frac{1}{r_K} \tag{9}$$

und für den Druckanteil

$$\Delta S_p = \beta R \ln \frac{p_U}{p} \tag{10}$$

Mit diesen Beziehungen ist eine vollständige Berechnung der kalorischen Zustandsgrößen der plasmabildenden Gase möglich. In Bild 2 ist der Verlauf der Enthalpie und in Bild 3 der der Exergie als Funktion der Temperatur für die schon in Bild 1 erfaßten zweiatomigen Gase wiedergegeben. Die Berechnungen erfolgten bis zu vollständigen Dissoziation.

3. EINSCHÄTZUNGEN DER ERGEBNISSE

Die energetischen Eigenschaften von zweiatomigen Gasen in höheren Temperaturbereichen werden maßgeblich durch die Dissoziation - die Größe der Dissoziationsenergie und der zugehörige Temperaturbereich - bestimmt. In Tabelle 1 sind die entsprechenden Werte für die untersuchten Gase angegeben. Mit einer Zunahme der Dissoziationsenergie verschiebt sich der zugehörige Temperaturbereich zu höheren Temperaturen. Dieser Sachverhalt läßt sich nach Gl.(7) darauf zurückführen, daß bei starker Endothermie, d.h. hoher Dissoziationsenergie erst bei hohen Temperaturen eine Gleichgewichtsverschiebung zugunsten der Dissoziationsprodukte erfolgt. Bild 1 zeigt, daß der Anstieg der Kurven mit einer Erhöhung der Dissoziationstemperatur fällt und damit der Dissoziationsbereich eine größere Temperaturspanne umfaßt. Eine geringfügige Abweichung hiervon ergibt sich beim Vergleich von Wasserstoff und Sauerstoff. Zusam-

Tabelle 1. Dissoziationsenergie und Temperaturbereich für die Dissoziation einiger zweiatomiger Gase bei P = 1 atm

Gas	Dissoziationsenergie bei $T_\alpha = 0{,}5$ $\frac{kcal}{kmol}$	Temperaturbereich K
Fluor	34 151	400 - 1800
Chlor	53 510	1500 - 3200
Schwefel	94 052	2600 - 4900
Wasserstoff	95 988	2800 - 5200
Sauerstoff	112 940	2900 - 5100
Stickstoff	209 575	5400 - 9200

menfassend zu diesem Bild kann festgestellt werden, daß die Breite des Dissoziationsgebietes eine Auswahl des günstigsten Energieträgers entsprechend den Prozesserfordernissen nach energetischen Gesichtspunkten erforderlich macht.

Bild 2 läßt erkennen, daß bei vollständiger Dissoziation von Stickstoff die 5 bis 8 - fache Menge im Vergleich zu Fluor und Chlor und die doppelte Menge im Vergleich zu Wasserstoff, Sauerstoff oder Schwefel eingebracht werden kann. Eine gewisse Sonderstellung nimmt Schwefel ein. Entsprechend dem Einsatz bei hohen Temperaturen werden die unter 1000°C vorhandenen höheren Schwefelverbindungen und alle flüssigen und festen Phasen bei der Gleichgewichtsberechnung vernachlässigt. Aufgrund der Wahl des Umgebungszustandes ist in der Enthalpie des Schwefels die Bildungsenthalpie von S_2 aus festem Schwefel enthalten.

Der Kurvenverlauf in Bild 3 gleicht dem von Bild 2, d.h. die qualitativen Einflüsse auf Enthalpie und Exergie stimmen überein. Aufgrund der Höhe der Temperatur ist eine solche Aussage zu erwarten. Während die Enthalpie die Qualität an Energie kennzeichnet, die je Mengeneinheit plasmabildendes Gas eingesetzt werden muß, gibt die Exergie den Mindestbetrag an, der bei reversibler Führung des Prozesses erforderlich ist. Andererseits kennzeichnet die Exergie die maximal wiedergewinnbare Nutzarbeit bei reversibler Führung des Anwendungsprozesses.

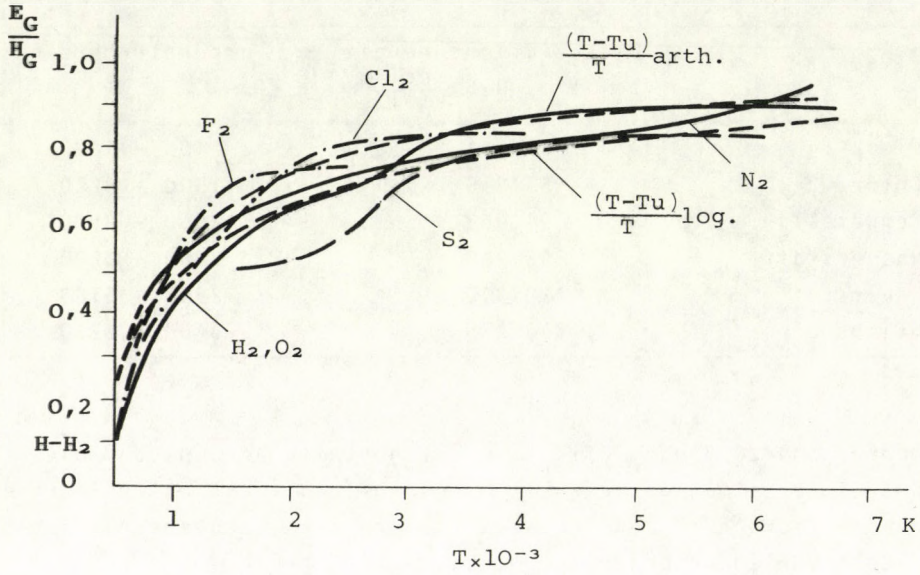

Bild 4. Verhältnis von Exergie zu Enthalpie in Abhängigkeit von der Temperatur für verschiedene Gase

Das Verhältnis $(\frac{E}{H})$ stellt ein Kriterium zur Einschätzung der energetischen Eigenschaften plasmabildender Gase dar. Für die untersuchten Gase ist dieses Verhältnis in Bild 4 dargestellt. Im Vergleich dazu werden die Werte der Carnotfunktion $(T - T_U/T)$ unter Benutzung arithmetischer und logarithmischer Mittelwerte eingezeichnet. Daraus läßt sich ein effektiver Einsatz der Gase im Dissoziationsbereich ablesen. Die Abweichungen von der Carnotfunktion nehmen richtig mit zunehmender Temperatur ab. Die größten Abweichungen ergeben sich bei den einzelnen Gasen bei einem Dissoziationsgrad von α = 0,8 oder β = 1,8. Nach Abschluß der Dissoziation verschlechert sich die energetische Kennzahl und erreicht Werte, die unter denen der nichtdissoziierten Gase liegen.

LITERATURVERZEICHNIS

1. MIERDEL, G., Was ist Plasma. VEB Verlag Technik Berlin 1973, 1 Aufl.

2. Autorenkollektiv, Plasmachemie-wissenschaftliche Grundlagen und technische Anwendungen. Urania Gesellschaft zur Verbreitung wiss. Kenntnisse Bezirksvorstand Gera

3. BOSNJAHOVIC, F., Technische Thermodynamik II. Teil. Verlag Theodor Steinkopf Dresden und Leipzig 1965.

4. WUKALOWITSCH, M. und NOWIKOW, I., Technische Thermodynamik mit einem Anhang von Fratzscher, W.: Einführung des Exergiebegriffes in die technische Thermodynamik VEB Fachbuchverlag 1962.

5. NEUBECK, FELTING, Chem.-Ing. Technik 42, 439 (1970)

6. SCHIRMER, DOST, Chemische Technik 21, 129 (1969)

7. SENNEWALD, SCHALLUS, POHL, Chem.-Ing. Technik 35, 1 (1963)

8. LANDT, U., Chem.-Ing. Technik 42, 617 (1970)

9. BAEHR, H.D. und SCHMIDT, E.F., Die Berechnung der Exergie von Verbrennungsgasen unter Berücksichtigung der Dissoziation BMK 16 (1964) 2, S. 62/66

10. ГЛУГИКО, Термодинамические свойства индивидуальных вегцеств Издательство академии наук СССР, Москва 1962

11. В.В.РЫБАКОВ, М.П.БУРГАСОВ, Термодинамический расчет высокотемпературного газа. Издательство „Машиностроение" Москва 1968

РЕЗЮМЕ

Статья занимается энергетическими свойствами плазмообразующих газов. Рассматривает калорийные определяющие состояния, энтальпию и энергию как удельные энергетические плотности в зависимости от коэффициента увеличения объема при диссоциации.

Автор предлагает способ расчета энергии плазмообразующих газов. Расчет сравнительно прост и точность его большая.

Необходимые при расчетах данные для некоторых газов приводятся в таблицах. Несколько результатов расчета дается в форме диаграмм. Кроме того рассматриваются энергетические преимущества использования плазмообразующих газов.

Hungarian Journal
of Industrial Chemistry
Veszprém
Vol.3. pp. 127-140 (1975)

CONTROLLABILITY TESTS ON A FLOWTHROUGH DRYING PROCESS WITH LINEARIZATION OF THE DISTRIBUTIVE MODEL

B. PALÁNCZ

(Budapest Technical University, Institute of Machinery for Technical Chemistry and Agricultural Industries)

Received: August 7. 1974.

The present paper deals with the controllability of a distributive model describing the process of flowthrough drying by means of linearization of the model. This problem is of especial significance in connection with the thermodynamical optimization of the process in connection with the selection of the allowed modes of control. The described method - which can advantageously be applied in the case of other similar problems as well - is illustrated by a numerical example.

INTRODUCTION

Drying, that is to say, removal of the moisture content of various materials by caloric processes, is one of the most widely used operations in chemical industry.

Drying, in a similar way to any caloric process, is expensive, and consequently the determination of the amount of drying medium, heat requirement and overall dimensions of the apparatus are very important from an economic point of view.

Accordingly, it is necessary that the drying operation be carried out in the most economical and, from a technological point of view, optimal manner. The aforesaid lead to the determination of the optimum conditions of the operation.

The most often used drying technique is flowthrough drying. In the case of the thermodynamical optimization of flowthrough drying, the function giving the changes in the ecergy of the system [1] or its form expressed in terms of expenses have to be minimized:

$$K_p = \int_0^{\tau_v} \frac{L}{G} (b_{gb} - b_{gk})\, d\tau + B_{so} - B_{sv} \tag{1}$$

where the exergy of the solid material is the function of the temperature and moisture content of the phase in question [2], that is

$$\begin{aligned} b_g &= b_g[x_L(\tau),\ t_L(\tau)] \\ B_s &= B_s[X(\tau),\ t_{na}(\tau)] \end{aligned} \tag{2}$$

since the expenses of the process, as referred to dry material, are the following:

$$K_p^e = \int_0^{\tau_v} \frac{L}{G} (c_{gb} - c_{gk})\, d\tau + C_{so} - C_{sv}$$

If it is assumed that there is a linear relationship between the specific exergy of the drying air and the moist substance on the one hand, and the c_g and C_s specific expense factors on the other, further that the proportionality factor is the same for both phases [1], i.e.

$$\begin{aligned} c_g &= \ell b_g \\ C_s &= \ell B_s + C_s^o \end{aligned}$$

where C_s^o is the specific economic value of the solid material in equilibrium with the environment, we can write

$$K_p = K_p^e/\ell = \int_0^{\tau_v} \frac{L}{G} (b_{gb} - b_{gk})\, d\tau + B_{so} - B_{sv}$$

where K_p is the exergy expense of the process.

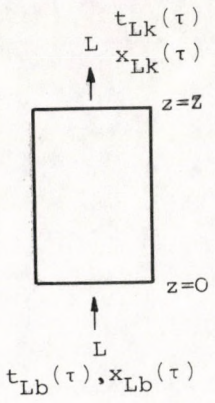

Fig. 1

According to this the driving parameters of the system are the functions $x_{Lb}(\tau)$ and $t_{Lb}(\tau)$; moreover the state of changes of the system are the characteristics of the drying medium, i.e. the functions $x_{Lk}(\tau)$ and $t_{Lk}(\tau)$ (see Fig. 1).

The Mathematical Model

The model describing the changes of the state variables in time are the following [3]:

$$\frac{dX}{d\tau} = - \frac{a_p}{\rho_{szt}} N , \tag{3}$$

$$L \frac{\partial x_L}{\partial z} + \rho_L \varepsilon \frac{\partial x_L}{\partial \tau} = a_p N, \tag{4}$$

$$- Lc_{nL} \frac{dt_L}{dz} = \alpha_{kv} a_p (t_L - t_F) +$$

$$+ L (r_o + c_{pwG} t_L) \frac{\partial x_L}{\partial z} - N a_p (r_o + c_{pwG} t_L) \tag{5}$$

$$c_{na} \frac{\rho_{szt}}{a_p} \frac{dt_F}{d\tau} = \alpha_{kv} (t_L - t_F) - N(r_o + c_{pwG} t_F - c_w t_F) \qquad (6)$$

where

$$N = \sigma (x_F - x_b) f, \qquad (7)$$

in case of $X > X_{kr}$, $f = 1$ $\quad x_F = \varphi(t_F)$,

if $X_e < X \leq X_{kr}$, $0 < f \leq 1$ $\quad x_F = x_{Fkr}$

if $X = X_e$, than $f = 0$

where

$$f = aX + b$$

$$a = \frac{1}{X_{kr} - x_e} \qquad (8)$$

$$b = \frac{X_e}{X_{kr} - X_e}$$

The conditions of unequivocalness are the following:

$$\begin{aligned} X(Z,o) &= X_o \\ x_L(o,\tau) &= x_{Lb}(\tau) \\ t_L(o,\tau) &= t_{Lb}(\tau) \\ t_F(Z,o) &= t_{Fo} \end{aligned} \qquad (9)$$

The aim of optimization is to determine the $x_{Lb}(\tau)$ and $t_{Lb}(\tau)$ functions is such a manner that they should assume their minimum value at function (1), taking the restrictions defined by Equations (3) - (9) into consideration.

The optimization task is the determination of an optimum control and accordingly its first step is the above mathematical

model, i.e. the study of the controllability of the system described by Equations (3) - (9) on the set of controlling parameters:

$$(x_{Lb}, t_{Lb}) \in [x_{Lb\ min}, x_{Lb\ max}] \otimes [t_{Lb\ min}, t_{Lb\ max}] \tag{10}$$

Linearization of the Model

As it was seen, the mathematical model of flowthrough drying can be described by a set of partial differential equations of varying coefficients. The controllability test of such systems is an extremely involved task, frequently it cannot be solved at all. Consequently, the following procedure was carried out in the present studies: the model was linearized in the nodes of the network aligned to a two-dimension range and this linearized model was examined in the following as regards controllability.

Accordingly, the structure of the linear model in a given $t_{Lb} \in [x_{Lb\ min}, t_{Lb\ max}]$ and $x_{Lb} \in [x_{Lb\ min}, x_{Lb\ max}]$ point is considered to be the following:

$$\frac{dx_{Lk}}{d\tau} = a_{11} x_{Lk}(\tau) + a_{12} t_{Lk}(\tau) + b_{11} x_{Lb}(\tau) + b_{12} t_{Lb}(\tau), \tag{11}$$

$$\frac{dt_{Lk}}{d\tau} = a_{21} x_{Lk}(\tau) + a_{22} t_{Lk}(\tau) + b_{21} x_{Lb}(\tau) + b_{22} t_{Lb}(\tau) \tag{12}$$

Coefficients a_{ij} and b_{ij} can be determined on the basis of the assumption that the values pertaining to the derivatives of state variables defined by Equations (11) and (12) further by the model (3) - (9) be minimal at the values of these coefficients, that is to say, integrals

$$I_1 = \int_0^\theta [a_{11}x_L(Z,\tau) + a_{12}t_L(Z,\tau) + b_{11}x_L(0,\tau) +$$

$$+ b_{12}t_L(0,\tau) - \frac{dx_L}{d\tau}(Z,\tau)]^2 \, d\tau \, , \qquad (13)$$

and

$$I_2 = \int_0^\theta [a_{21}x_L(Z,\tau) + a_{22}t_L(Z,\tau) + b_{21}x_L(0,\tau) +$$

$$+ b_{22}t_L(0,\tau) - \frac{dt_L}{d\tau}(Z,\tau)]^2 \, d\tau \qquad (14)$$

assume a minimum value.

The values of $x_L(0,\tau)$, $x_L(Z,\tau)$, $t_L(0,\tau)$, $t_L(Z,\tau)$ and $dx_L/d\tau(Z,\tau)$, $dt_L/d\tau(Z,\tau)$ are known from the numerical solution of the mathematical model (3) - (9) and accordingly the determination of the coefficients can be reduced to the solution of an inhomogeneous set of equations with four unknowns, since e.g. from

$$\frac{\partial I_1}{\partial a_{11}} = 0 \qquad (15)$$

we have

$$a_{11}\int_0^\theta x_L^2(Z,\tau)\, d\tau + a_{12}\int_0^\theta t_L(Z,\tau)x_L(Z,\tau)\, d\tau +$$

$$b_{11}\int_0^\theta x_L(0,\tau)x_L(Z,\tau)d\tau + b_{12}\int_0^\theta t_L(0,\tau)x_L(Z,\tau)d\tau =$$

$$= \int_0^\theta \frac{dx_L}{d\tau}(Z,\tau)x_L(Z,\tau)\, d\tau \qquad (16)$$

where the integrals as constants are the coefficients of the set of equations.

Three similar equations are obtained from the conditions

$$\frac{\partial I_1}{a_{12}} = 0; \qquad \frac{\partial I_1}{b_{11}} = 0; \qquad \frac{\partial I_1}{b_{12}} = 0 \, . \qquad (17)$$

The coefficients of Equation (12) can be determined in a similar manner.

The Examination of Controllability

In general, a system is called controllable if it can be brought from a given state to another within a finite period of time.

The set of Equations (11) and (12) can be written in the following form:

$$\frac{d}{d\tau}\begin{pmatrix} x_{Lk} \\ t_{Lk} \end{pmatrix} = \begin{pmatrix} a_{11} & a_{12} \\ a_{21} & a_{22} \end{pmatrix}\begin{pmatrix} x_{Lk} \\ t_{Lk} \end{pmatrix} + \begin{pmatrix} b_{11} & b_{12} \\ b_{21} & b_{22} \end{pmatrix}\begin{pmatrix} x_{Lb} \\ t_{Lb} \end{pmatrix} \tag{18}$$

This linear system is controllable if, and only if, the order of the controllability matrix [4]

$$\underline{\underline{K}} = [\underline{\underline{B}}, \underline{\underline{A}}\ \underline{\underline{B}}] \tag{19}$$

of the system is 2, i.e.

$$\rho(\underline{\underline{K}}) = 2$$

If the above-mentioned network is chosen to be sufficiently fine, the question of controllability can be solved for the entire range of control parameters.

Numerical Example

The aforesaid is illustrated by numerical examples. The data of the latter are the following:

α_{kv} = 10 kcal/m²hr°C

σ = 40 kg/m². hr

a_p = 1,200 m²/m³

ρ_{szt} = 1,000 kg/m³

c_{mL} = 0.25 kcal/kg°C

c_{pwG} = 0.46 kcal/kg°C

c_{na} = 1 kcal/kg°C

ε = 0.1 m³/m³

L = 6,000 kg/m²hr

X_o = 0.25 kg humid/kg dry material

X_{kr} = 0.15 kg humid/kg dry material

X_e = 0.05 kg humid/kg dry material

t_{Fo} = 20°C

r_o = 577 kcal/kg

The point under examination, where linearization is carried out is

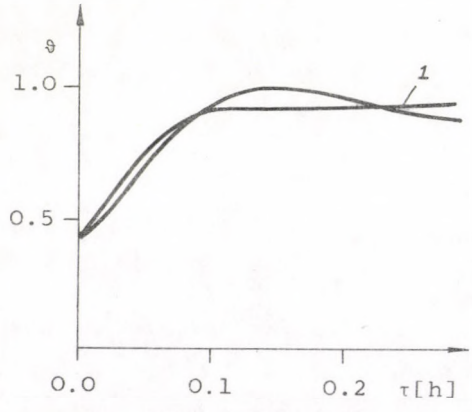

Fig. 2. 1: linearized model

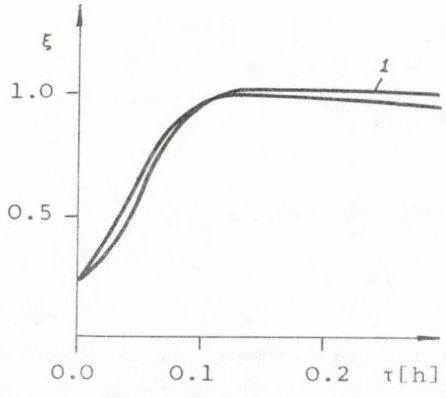

Fig. 3. 1: linearized model

$$t_{Lb} = 50^{\circ}C$$

$$x_{Lb} = 0.06 \text{ kg humid/kg dry air}$$

Figs. 2 and 3 show the curves furnished by the linearized model and the original model, respectively. In the determination of the coefficients, dimensionless variables

$$\vartheta = \frac{t_L}{t_{Lb}}, \quad \xi = \frac{x_L}{x_{Lb}} \tag{20}$$

were used.

The numerical results are summarized in Tables 1 and 2. In the examination of controllability, on the basis of Table 1 we have

$$\underline{\underline{A}} = \begin{pmatrix} 66.126 & -48.821 \\ 124.561 & -85.299 \end{pmatrix} \tag{21}$$

and

$$\underline{\underline{B}} = \begin{pmatrix} 4.050 & -16.000 \\ -61.084 & 32.00 \end{pmatrix}$$

Hereby, the controllability matrix is

$$\underline{\underline{K}} = \begin{pmatrix} 4.050 & -16.000 & 3250 & -2621 \\ -61.084 & 32.00 & 5654 & -4722 \end{pmatrix}$$

Table 1

Coefficients of the linear model			
a_{11}	a_{12}	b_{11}	b_{12}
66.126	-48.821	4.050	-16.000
a_{21}	a_{22}	b_{21}	b_{22}
124.561	-85.299	-61.084	32.000

Table 2

τ	$t_L(Z,\tau)$	$t_{Lk}(\tau)$	$x_L(Z,\tau)$	$x_{Lk}(\tau)$
0.000	0.400	0.400	0.222	0.222
0.020	0.497	0.515	0.308	0.369
0.040	0.624	0.681	0.466	0.531
0.060	0.753	0.809	0.650	0.728
0.080	0.864	0.884	0.825	0.886
0.100	0.946	0.918	0.969	0.973
0.120	0.997	0.930	1.070	1.007
0.140	1.019	0.934	1.127	1.022
0.160	1.018	0.935	1.145	1.023
0.180	1.002	0.935	1.135	1.023
0.200	0.977	0.935	1.106	1.023
0.220	0.950	0.935	1.069	1.023
0.240	0.925	0.935	1.031	1.023
0.260	0.906	0.935	0.999	1.023
0.280	0.893	0.935	0.975	1.023
0.300	0.887	0.935	0.960	1.023

By resolving $\underline{\underline{K}}$ into diades we obtain

$$\underline{\underline{K}} = \begin{pmatrix} -16.000 \\ 32.000 \end{pmatrix} \begin{pmatrix} -0.253 & 1 & -203.01 & 163.9 \end{pmatrix} + \begin{pmatrix} 0.000 \\ -52.994 \end{pmatrix} \begin{pmatrix} 1 & 0 & -228.5 & 188.4 \end{pmatrix}$$

and hence

$$\rho(K) = 2$$

i.e. the system is controllable in the vicinity of the point defined by the data $t_{Lb} = 50^{\circ}C$ and $x_{Lb} = 0.06$ kg humid./kg dry air.

SUMMARY

An approximate method for testing the controllability of a distributive system is presented. The method is based on the linearization of the model at a given point. The coefficients of the linear model were determined numerically on the basis of the original mathematical model.

The concrete model was the mathematical model of a flow-through-type drying process. The procedure was illustrated by a numerical example.

It is self-evident that the technique can be generalized to systems described by other partial differential equations as well.

Finally it is very important to note that in optimization tasks and in their solution, the restrictions pertaining to the controlling parameters play a very important role, and consequently the controllability tests are of basic consequence, since it is self-evident that the set of permissible controls cannot be wider than that set of controlling parameters with reference to which the system is controllable.

SYMBOLS USED

a_p specific surface area, m^2/m^3

b_g exergy of drying air referred to the mass of dry air, kcal/kg dry air

c specific heat, kcal/kg$^{\circ}$C

c_{pwG} specific heat of water vapour at a constant pressure, kcal/kg$^{\circ}$C

ℓ economic value referred to unit exergy, Forints/kcal

r_o latent heat, kcal/kg

t temperature, ^{o}C

X humidity content of drying air, kg humidity/kg dry air

z length co-ordinate, m

B_s exergie of humidity, as referred to dry solid substance, kcal/kg dry substance

C_s economic value of humid material as referred to the mass of dry solid substance, Forints/kg dry material

G amount of solid substance, kg dry material

L amount of drying air, kg dry air/hr

K_p exergy expenses of the process, kcal/kg dry substance

K_p^e expenses of the process as referred to the mass of the dry solid substance, Forints/kg dry substance

N drying rate, kg humidity/m^3hr

X humidity content of solid material, kg humidity/kg dry substance.

Greek characters

α_{kv} heat transfer coefficient, kcal/m^2hr^{o}C

ε porosity, m^3/m^3

ρ_L density of air, kg/m^3

ρ_{szt} volume density of solid material, kg/m^3

τ time, hr

σ evaporation coefficient, kg humidity/m^2hr

Indexes

b input

e equilibrium

k output

kr critical

na humid substance

nb humid air

L air

v final

w water

o initial

REFERENCES

1. SIENIUTYCZ, S., AIChE Journal, 19, 277 (1973)

2. SIENIUTYCZ, S., Computing of the Thermodynamic Functions in the Gas-Solid Systems. Manuscript of the work submitted for publication in Reports of Inst. Chem. Eng. Warsaw Tech. Univ.

3. PALÁNCZ, B., PARTI, M., Acta Technica 3-4, 441 (1973)

4. CHINTAPALLI, P.S.R.K., DOUGLAS, J.M., Chem. Eng. Sci. 29, 403 (1974)

РЕЗЮМЕ

Настоящая работа исследует управляемость дистрибутивной модели, описывающей процесс проточной сушки, с помощью приведения ее к линейному виду. Особое значение проблемы в выборе допустимых управлений при термодинамической оптимализации процесса. Приведенный способ, который может быть использован и в других подобных заданиях, иллюстрируется расчетным примером.

Hungarian Journal
of Industrial Chemistry
Veszprém
Vol.3. pp. 141-156 (1975)

EXAMINATION OF A BAFFLE PLATE-TYPE TUBULAR REACTOR I.

A. LÁSZLÓ, B. BENKŐ*, B. STEFKÓ* and J. KREIDL*

(Department of Chemical Process Engineering, Veszprém University of Chemical Engineering;
Kőbánya Pharmaceutical Works (RICHTER G.)*)

Received: October 15, 1974.

A variant of the possibilities to increase the efficiency of single-phase, laminar-flow tubular reactors is presented. The continuous flow space is destroyed by baffle plates arranged in the reactor, whereby the latter becomes "cascade-like". In the present paper, the flow-dynamic properties of reactor of 1 metre in length, 5 cm. in diameter and containing baffle elements of different size and arrangement are discussed.

A requirement of paramount importance in the design of tubular reactors is to ensure adequate flow conditions, more particularly, to bring about a "plug-like" flow pattern.

This means that the linear mean velocity of the medium flowing in the reactor has to be determined on the basis of the condition $Re > 2500$ (in the case of single-phase flow). If the length of the reactor is for some reason limited, recirculation has to be applied on account of the above mentioned condition in order to ensure a given residence time. If this is impossible, the reactor becomes a laminar-flow system, the disadvantages of which

are generally known. (Due to the uncertain starting up section and the strong axial mixing, the conversion becomes strongly stochastic, its mean value is smaller than in the case of a "plug-like" flow.)

Relatively few papers dealing with mixing processes in laminar-flow tubular reactors or with improving the efficiency of such reactors are found in literature [1-4]; nevertheless, it is known that "segmentation" of the flow space by application of a packing or baffle plates is an effective technique.

If the baffle plates are such as to produce a series of well mixed units by breaking up the flow, i.e. the originally continuous space is resolved into a cascade series (of which it is known that in the case of $n_t > 10$ it fairly approximates the efficiency of the plug-like flow reactor), the solution can be regarded as acceptable from every point of view. In the present work, the baffle-plate type tubular reactor was studied from point of view of operation. The aim was to study a reactor ensuring long residence times and accordingly the experiments were carried out in the $150 \leq Re \leq 750$ range.

Four baffle-plate types were studied. These were different in the free flow cross-section. For the sake of distinction, the different baffle plates were numbered. The baffle plates as well as their arrangement is shown in Figure 1.

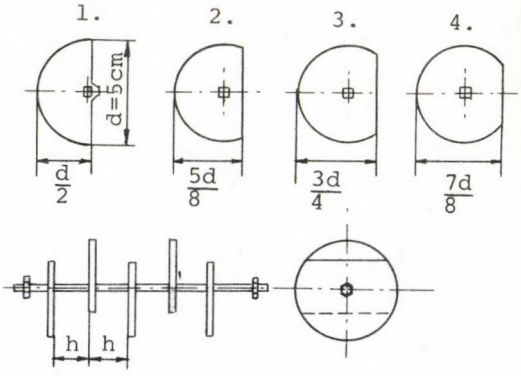

Fig.1. Baffle plate types and their arrangement

The present paper deals with studies on the hydrodynamical characteristics of baffle plate-type tubular reactors. The study was based on results concerning the pressure drop brought about in the reactor and the residence time.

Experimental Apparatus

The reactor was a vertical tube of 1 metre in length, 5 cm. in diameter and equipped with a thermostated jacket. A perforated plate was welded into the bottom of the reactor; the rod holding the baffle plates was supported by this plate. The support rod was of copper and of rectangular cross-section, the baffle plates were arranged on it. Its upper and lower ends were fastened by bolts so that the baffle plates could not move in a vertical direction.

The experimental set up is shown in Figure 2.

The reagents were forwarded from storage tank (1) into overflow tanks (3) by centrifugal pumps (2). The temperature of the reagents was approximately adjusted in the overflow tanks by temperature controller (4). The temperature in the overflow tanks was monitored by thermometers (16). The temperature of the reagents leaving the overflow tanks was adjusted to the required value by ultra-thermostats (5). The amount of the reagents was controlled by valves (6) and rotameters (7). Having passed the rotameters, the reagents enteres flow-dynamical mixing unit (8) where they were mixed. The temperature of the liquid entering the reactor was checked by thermometer (9). Injection was carried out at the nozzle connecting the flow-dynamical mixing unit with reactor (10). The pressure drop brought about in the reactor was measured by differential manometer (12). The upper part, the head of the reactor was made of plastic. A pair of electrodes for conductivity measurement and a bead-type thermistor was built into this plastic head. The conductance signal was measured by conductivity meter (13) and it was recorded by potentiometric recorder (14). The bead thermistor was connected to conductivity meter (15); the latter was calibrated. The bead thermistor ensured the measurement of the temperature at the end of the reactor.

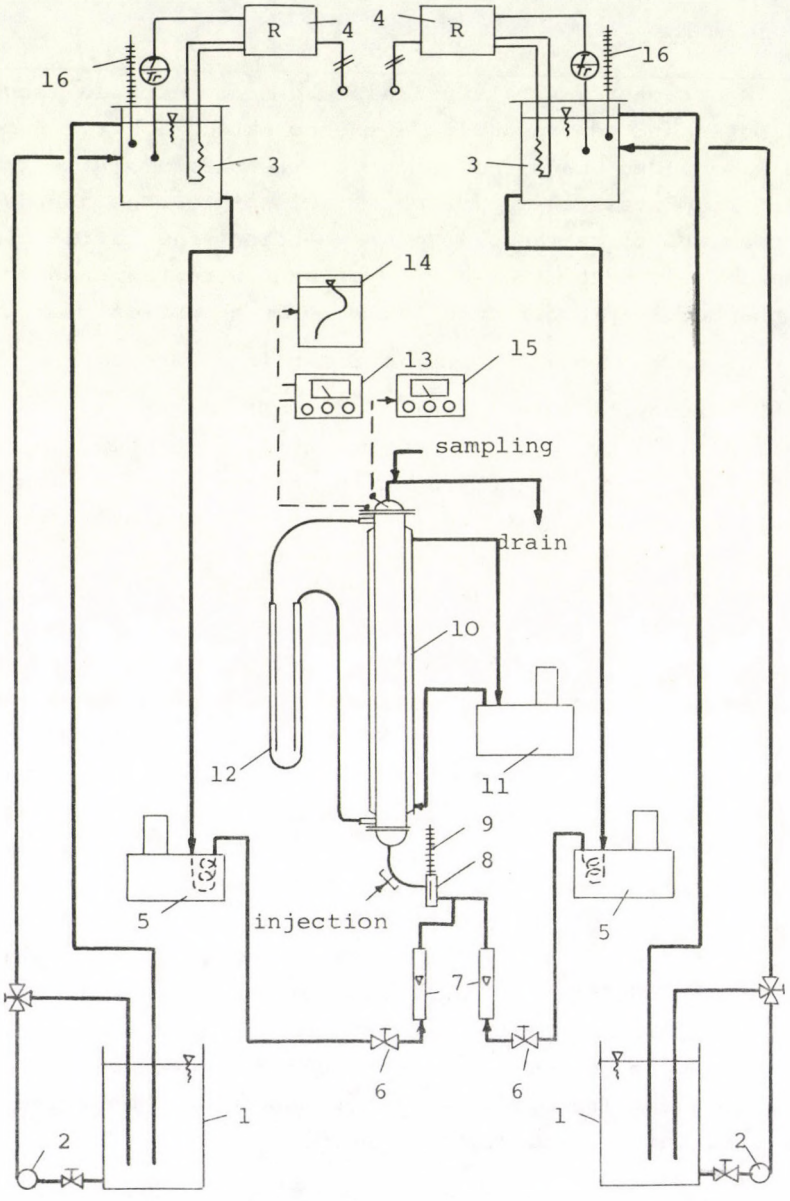

Fig. 2. Schematic diagram of the apparatus

Measurement of Pressure Drop

In order to measure the pressure drop, two measuring nozzles were arranged at a distance of 2.5 cm. as measured from the top and the bottom of the reactor, respectively.The flow being laminar and the expected pressure drop a low value, carbon tetrachloride was used as manometer liquid in the differential manometer. No pressure drop could be observed with the use of baffle plate No.1 and the empty tube.

Studies on Residence Time

The study on residence time was carried out on the basis of the residence time spectrum (density function) of the reactor. When recording the residence time spectrum, the flowing liquid was tap water. In accordance with the details stated in connection with the description of the experimental apparatus, the temperature of the input stream was adjusted to 25°C. A 10 % NaCl solution was applied as tracer. The latter (8 ml.) was introduced through a nozzle set up for this purpose by means of medical syringe. The tracer left in a rapid, turbulent stream at the exit end and it was measured and recorded by a conductometer. The tube cross section at the point of injection and at the place of the conductometric electrode pair was identical.

RESULTS AND DISCUSSION

Studies on Pressure Drop

The value of the pressure drop arising across the reactor was arbitrarily assigned to the distance between the measuring nozzles, since as a consequence of the application of the baffle

plates, the flow of the fluid particles in the reactor was considerably longer than in the empty tube. In the experiments, the Fanning tube friction coefficient was calculated from the pressure drop value on the basis of the force equilibrium:

$$f = \frac{\Delta p \cdot d}{2 L \rho v^2} \qquad (1)$$

The results show that by decreasing the distance between the baffle plates, the rapid change in the friction coefficient, characteristic of laminar flow, gradually disappears. This is illustrated in Figure 3, for the case of baffle plate No.4.

A similar result is observed when the free flow cross section is decreased. The results obtained with a baffle plate distance of 5 cm. are shown, for the case of different baffle plates, in Figure 4.

The pressure drop brought about by the local resistance is composed of the axial flow loss, the tangential flow loss and the turbulence loss [5].

Evaluation of Residence Time Spectra

The residence time spectra were evaluated by a digital computer type ODRA 1204. In the course of the evaluation, the moments of the residence time spectrum, the mean residence time and the variance were calculated and the dimensionless C-curve was constructed.

Depending on the type of the baffle plate and on the distance between the baffle plates, different types of reactors are obtained. The latter were compared on the basis of the dimensionless residence time spectra (C-curves) and the equivalent cascade number - the latter being in close connection with axial mixing.

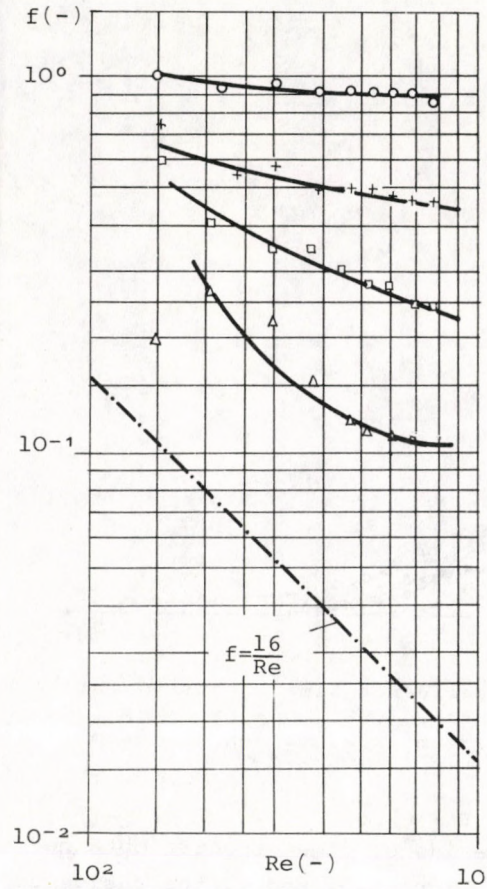

Fig.3. Tube friction coefficient plotted against Re-number
Baffle plate No. 4;
-•- empty tube
o - h = 2.5 cm
+ - h = 5 cm
□ - h = 10 cm
Δ - h = 20 cm

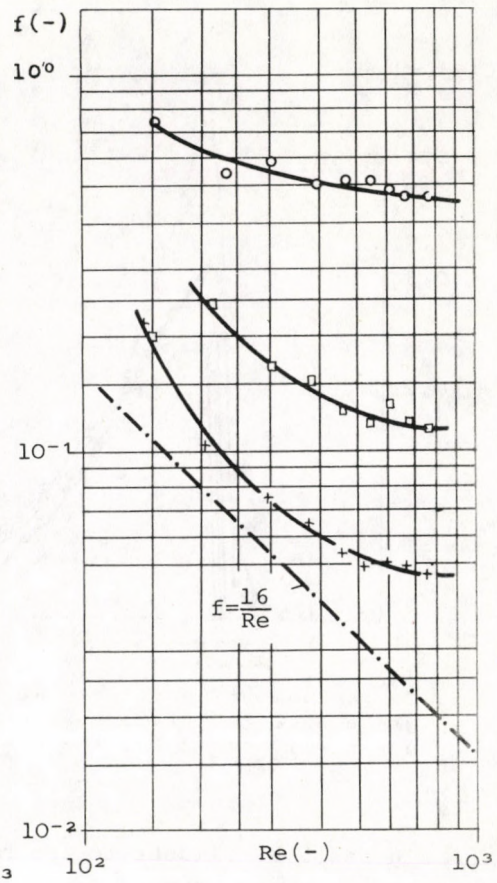

Fig.4. Tube friction coefficient plotted against Re-number
h = 5 cm.
-•- empty tube
+ - baffle plate No. 2
□ - baffle plate No. 3
o - baffle plate No. 4

The equivalent cascade number was determined by the formula proposed by LEVENSPIEL [6]:

$$\sigma^2 = \frac{\sigma t^2}{\bar{t}_B^{\,2}} = \frac{1}{n_{ekv.}} = \frac{2}{(Pe)^2}\,(Pe - 1 + e^{-Pe}) \qquad (2)$$

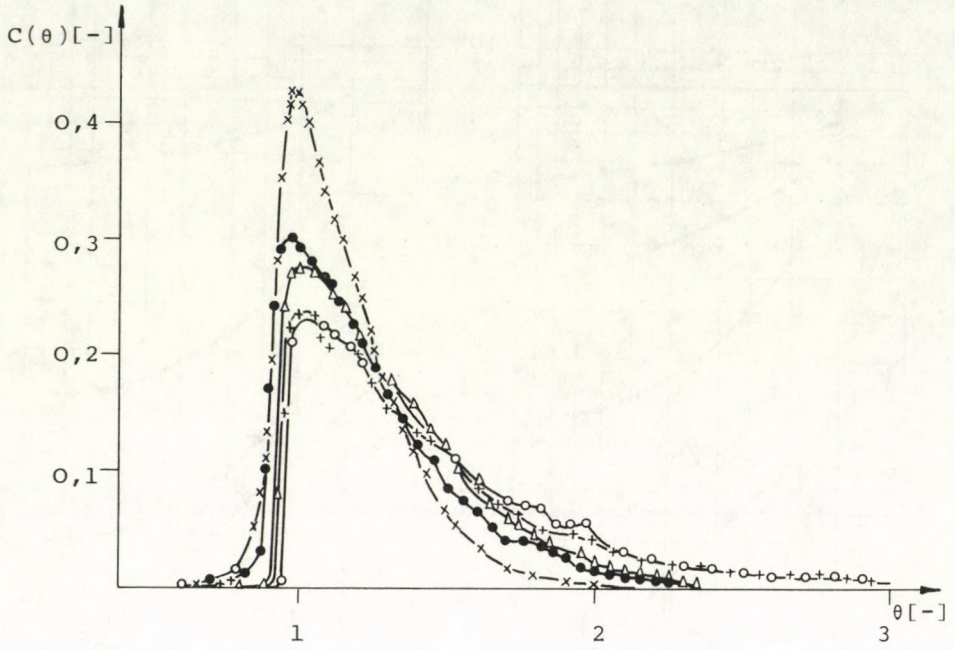

Fig.5. Comparison of experimental residence time spectra. Baffle plate No.2;Re 145; + empty tube (002), o - h= 20 cm (242) Δ - h = 10 cm (232), • - h = 5 cm (222), x - h = 2.5 cm (212)

Figures 5-8 illustrate the residence time spectra obtained for different types of reactors. In Figures 5. and 6. the residence time spectra obtained with reactors shaped by arranging baffle plate No.2 at different distances can be seen in the case of values Re = 145 and Re = 660, respectively. As it is apparent, if the feed rate is low - except for a baffle plate distance of 20 cm - the application of baffle plates had an advantageous effect on the hydrodynamic behavious of the reactor. In the case of higher feed rates, as is apparent from Figure 6, it is only the plate distance of 2.5 cm. that brings about an improvement as compared to the case of the empty tube.

Figures 7 and 8 show the spectra obtained with various types of baffle plates for the case of the 2.5 and 5 cm. plate distance

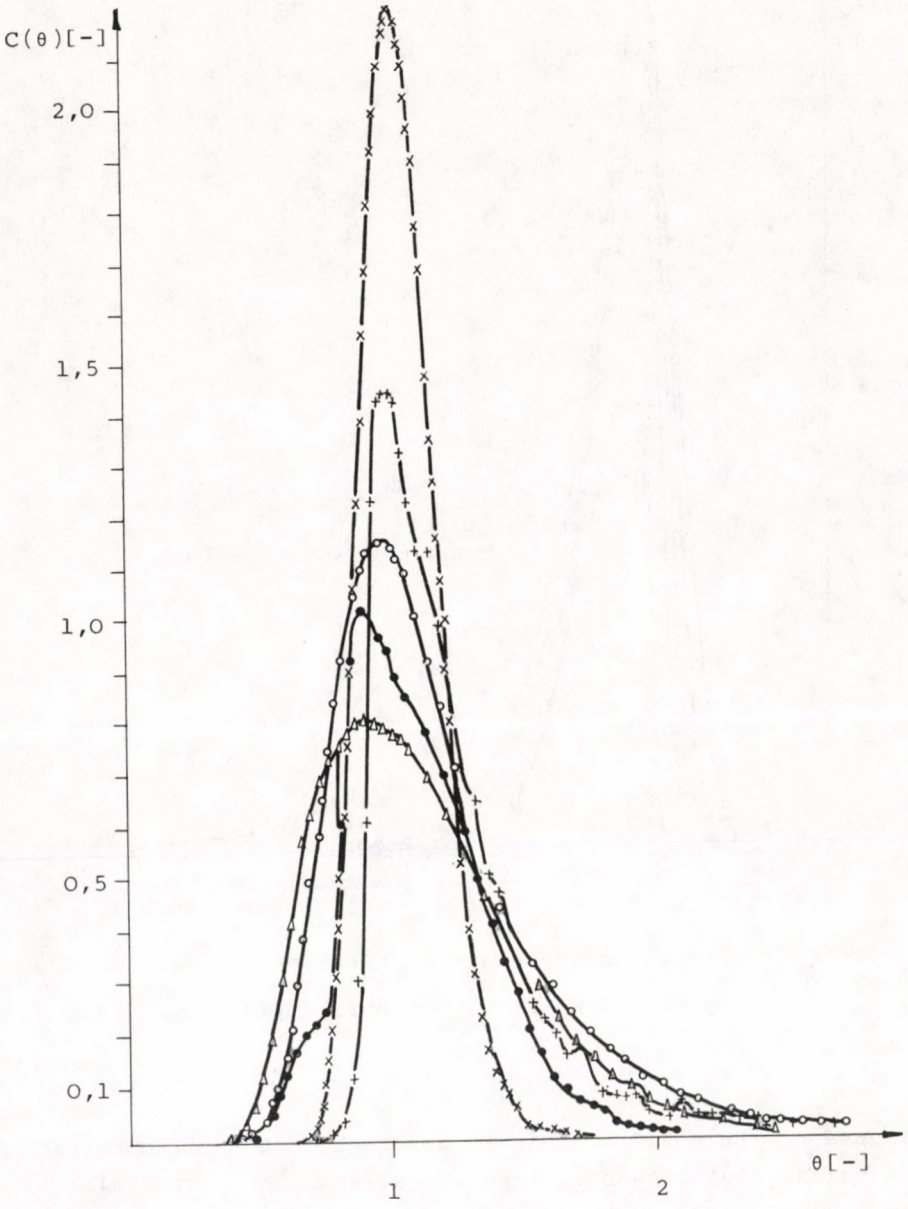

Fig.6. Comparison of experimental residence time spectra. Baffle plate No.2; Re 660; + - empty tube (009), o - h = 20 cm (249), Δ - h = 10 cm (239), • - h = 5 cm (229), x - h = 2.5 cm (219)

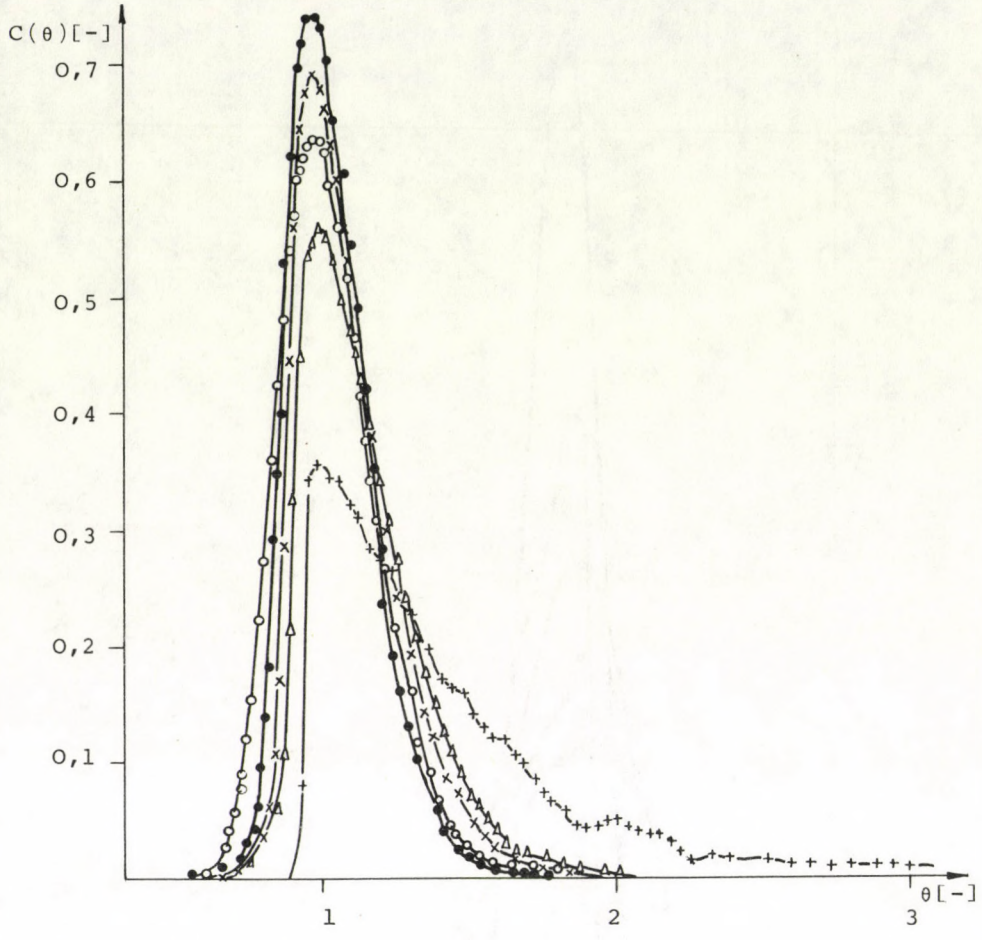

Fig.7. Comparison of experimental residence time spactra. h = 2.5 cm. Re 210, + - empty tube, Δ - baffle plate No.1 (113), x - baffle plate No.2 (213), • - baffle plate No.3 (313), o - baffle plate No.4

in the case of Re = 210. As it is apparent, at a distance of 2.5 cm. the baffle plate ensuring the largest and the one ensuring the smallest flow cross section show the most unfavourable properties, whereas at a distance of 5 cm. plates No. 3 and 4 are the most unfavourable.

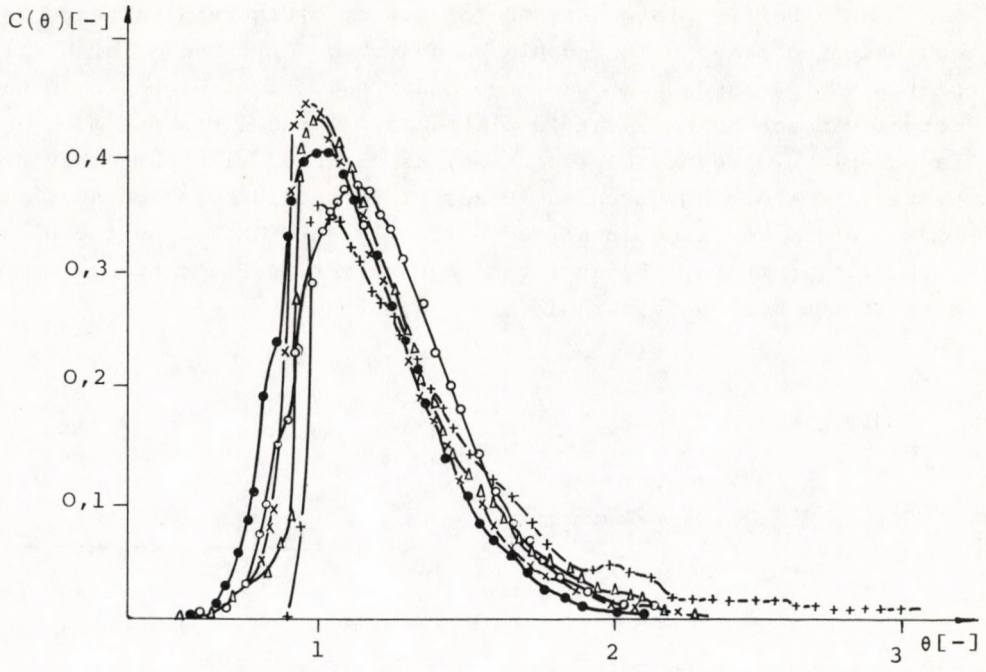

Fig.8. Comparison of experimental residence time spectra. h = 5 cm Re 210; + - empty tube (303); Δ - baffle plate No.1; x - baffle plate No.2 (223); • - baffle plate No.3 (323); o - baffle plate No.4 (423)

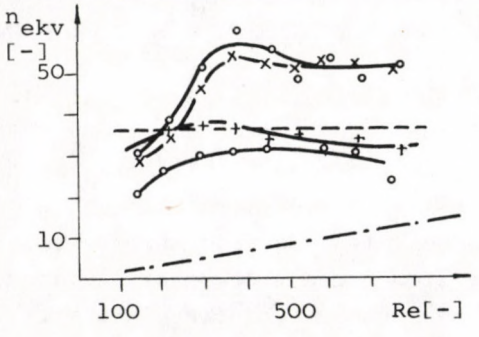

Fig.9. Equivalent cascade number plotted against Re-number. -- n_t = 36, -•- empty tube, o - baffle plate No.1; x - baffle plate No.2; • - baffle plate No.3; + - baffle plate No.4

Figures 9-12 show the equivalent cascade number, plotted against the Reynolds number. The number of space elements obtained by application of the baffle plates (the actual cascade number) is represented by a broken line, whereas the equivalent cascade number obtained by correlation of the parallel determined results obtained with the empty tube are shown by a dotted line.

At a baffle-plate distance of 2.5 cm. (Figure 9) a very high equivalent cascade number could be observed. In the case of baffle plates No. 2 and 3 it was one and a half times higher than the actual cascade number. Baffle plates No. 1 and 4 possess more unfavourable hydrodynamic properties, as compared with the other two plates, in the range studied. However, it should be noted that all four plates resulted in a reactor fairly approximating the plug-like flow pattern, because the equivalent cascade number was, even in the most unfavourable case, about 30.

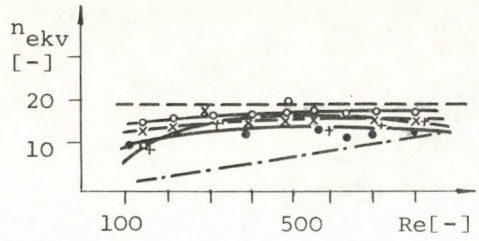

Fig.10. Equivalent cascade number plotted against Re-number. -- n_t = 19, -•- empty tube; o - baffle plate No.1 x - baffle plate No.2 • - baffle plate No.3 + - baffle plate No.4

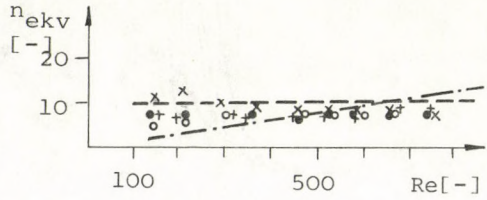

Fig.11. Equivalent cascade number plotted against Re-number. -- n_t = 10, -•- empty tube; o - baffle plate No.1 x - baffle plate No.2 • - baffle plate No.3 + - baffle plate No.4

Results obtained with a baffle plate distance of 5 cm. are summarized in Figure 10. It can be concluded that the hydrodynamic characteristics of the reactor are, up to a certain limit, advantageously influenced by the decrease of the flow cross section (types 1-3), that is to say, the equivalent cascade number is increased. A further decrease in the flow cross section brings about a decrease in the equivalent cascade number (baffle plate No.4). All the baffle plates studied, brought about an equivalent cascade number of ten, or higher than that, in the range studied. This is very favourable, because a cascade system of ten elements realizes in practice the plug-like flow tubular reactor to a good approximation.

It was found at a baffle-plate distance of 10 cm (Figure 11) that up to about Re = 550 the baffle plate improves the hydrodynamics of the reactor as compared to the empty tube, whereas at a plate distance of 20 cm. this is true only up to Re = 300 (Figure 12).

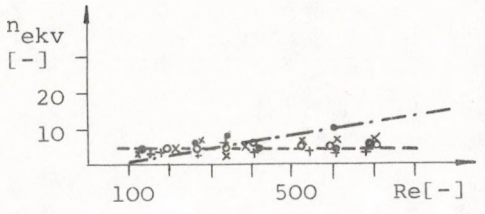

Fig.12. Equivalent cascade number plotted against Re-number. -- $n_t = 5$, -•- empty tube, o - baffle plate No.1 x - baffle plate No.2 • - baffle plate No.3 + - baffle plate No.4 h = 20 cm.

Summarizing the results it can be stated that a tubular reactor equipped with baffle plates is - from the view point of dynamic flow - more similar to cascade systems then to tubular reactors because it can be approximated better by the cascade model than by the tubular model and the characteristic equivalent cascade number remains practically unchanged with changing feed. In the case of higher Reynolds numbers, the application of baffle plates results in both cases in deteriorated dynamic-flow properties as compared to those of the empty tube. The present results indicate that the dynamic-flow properties of the reactor can be improved by the application of baffle plates and with the properly chosen arrangement of the latter it is possible to ensure a practically plug-like flow pattern, even in a laminar flow system.

As to the geometry of the system studied, i.e. the type of baffle plates and the preferable distance between them, the following design principles can be formulated:

1. It is preferable to choose the free flow cross section of the baffle plate (Q),as referred to the cross section of the empty tube, in accordance with the following formula:

$$0.2 \leq Q \leq 0.3$$

2. The following limit for the ratio distance between the baffle plates to the diameter of the empty tube is to be observed:

$$\frac{k}{d} \leq 1$$

Results in connection with the mathematical modelling of the baffle-plate type tubular reactor will be reported on in a subsequent paper.

SYMBOLS USED

$C(\theta) = C$	C-diagram, residence time spectrum (dimensionless)
d	diameter of reactor (m)
f	tube friction coefficient according to Fanning (dimensionless)
h	distance between baffle plates (m)
L	distance between nozzles for the determination of the pressure drop (m)
n_{ekv}	equivalent cascade number (dimensionless)
n_t	actual cascade number (dimensionless)
Δp	pressure drop ($N \cdot m^{-2}$)
Pe	Peclet-number (dimensionless)
Q	free flow area of baffle plate, as referred to the cross sectional area of the empty tube (dimensionless)
Re	Reynolds number (dimensionless)
$\bar{t}_B$	mean residence time, as calculated from the volume of the reactor and the volumetric flow rate (s)
v	linear flow rate ($m \cdot s^{-1}$)
θ	dimensionless time
ρ	density of the fluid ($kg \cdot m^{-3}$)

σ^2 variance (dimensionless)

σ_t^2 variance (s^2)

REFERENCE

1. CLELAND, F.A., WILHELM, R.M., AIChE Journal 2, 489 (1956)

2. VIGNES, J.P., TRANBOUSE, P.J., Chem. Eng. Sci. 17, 73 (1962)

3. JAGADEESH, V., SATYANARAYANA, J., Ind. Eng. Chem. Process Des. Develop. 11, 520 (1972)

4. HOVORKA, R.B., KENDALL, M.B., Chem. Eng. Prog. 56, 58 (1960)

5. SMITHBERG, E., LANDIS, F., J. Heat Transfer 86, 39 (1964)

6. LEVENSPIEL, O., Chemical Reaction Engineering. John Wiley and Sons, Inc. New York-London (1965)

РЕЗЮМЕ

В статье авторы приводят один из вариантов повышения эффективности однофазового ламинарного реактора-трубы. Расположенные в реакторе направляющие пластинки нарушают беспрерывное поле течения, в следствии чего реактор превращается в подобие каскада. Данная работа исследует термодинамические свойства реактора длиной в 1 м, диаметром в 5 см, с направляющими пластинками различного размера и расположения.

Hungarian Journal
of Industrial Chemistry
Veszprém
Vol.3. pp. 157-170 (1975)

EXAMINATION OF A BAFFLE PLATE-TYPE TUBULAR REACTOR II.

(Kőbánya Pharmaceutical Works (RICHTER G.)
and Department of Chemical Process Engineering, Veszprém
University of Chemical Engineering*)

Received: November 5, 1974.

The present paper deals with the mathematical modelling of baffle plate-type tubular reactors. The so-called cascade model employing internal recirculation was applied to a model reaction system of the second order. By studying the adequacy of the experimental data and the data of the model, simplifying conditions were proposed for the model and for the selection of the most efficient baffle plate-type.

In order to improve the efficiency of a laminar-flow tubular reactor, baffle plates were arranged in the latter. Studies on the flow dynamic properties of the baffle plate-type tubular reactor were described in a previous paper [1]. It was concluded that baffle plate-type tubular reactors are from a point of view dynamic flow more similar to cascade reactors than to tubular ones. This is also in agreement with the physical picture, because by the addition of the baffle plates, the reactor is segmented into well-defined space portions.

The present paper deals with the mathematical modelling of baffle plate-type tubular reactors. The cascade model with inter-

nal recirculation has been elaborated for modelling rectifying columns [2, 3 et al.]. LELLI [4] was the first to apply it for the modelling of chemical reactors.

The internal recirculation model is a two-parameter one. The classical cascade model is supplemented, in analogy to axial stirring, with internal recirculation [4-7]. The flow diagram of the model is shown in Figure 1.

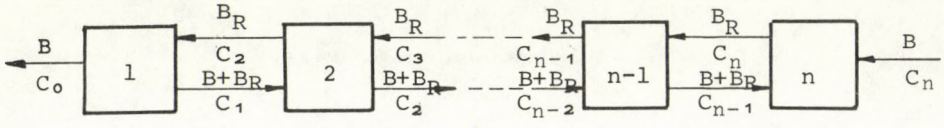

Fig. 1. The diagram of the model

The parameters of the model are the cascade number n and the internal recirculation ratio. The latter is defined by the following expression:

$$\gamma = \frac{B_R}{B} \tag{1}$$

As far as the model is concerned, the introduction of the internal recirculation ratio represents an additional variability. Hereby, mixing phenomena - as well as their effect upon conversion and efficiency of the reactor - can be described by an efficient and flexible model.

The model is formulated for the case of a given operational unit for reaction of the second order. The rate equation of the reaction is the following:

$$\frac{dc}{dt} = - k_2 c^2 \tag{2}$$

The balance equations are for the individual cascade elements as follows:

For the first stage, the balance equation is:

$$Bc_0 - (B + B_R)c_1 + B_R c_2 - V_1 k_2 c_1^2 = - V_1 \frac{dc_1}{dt} \tag{3}$$

for the j^{th} stage:

$$(B+B_R)c_{j-1} - (B + 2\,B_R)c_j + B_R c_{j+1} - V_j k_2 c_j^2 = - V_j \frac{dc_j}{dt} \tag{4}$$

and for the n^{th} stage:

$$(B + B_R)c_{n-1} - (B + B_R)c_n - V_n k_2 c_n = - V_n \frac{dc_n}{dt} \tag{5}$$

In a steady state, first-order non-linear differential equations (3), (4), (5) are simplified to non-linear equations. Let the set of equations be made dimensionless and the following substitutions be introduced:

$$c_j^* = \frac{c_j}{c_0} \tag{6}$$

$$\bar{t}_B = \frac{V}{B} = \frac{nV_j}{B} \tag{7}$$

$$Da = \frac{\bar{t}_B\, k_2\, c_0}{n} \tag{8}$$

The dimensionless set of nonlinear equations is as follows:

$$\begin{aligned} &1 - (1 + \gamma)c_1^* - Da(c_1^*)^2 + \gamma\, c_2^* = 0 \\ &(1 + \gamma)c_{j-1} - (1 + 2\gamma)c_j - Da(c_j) + \gamma c_{j+1} = 0 \\ &\qquad\qquad j = 2, 3, \ldots, n-1 \\ &(1 + \gamma)c_{n-1}^* - (1 + \gamma)c_n^* - Da(c_n^*)^2 = 0 \end{aligned} \tag{9}$$

The set of Equations (9) is linearized in such a way that the nonlinear terms are evolved into a Taylor-series and the terms

of higher order are neglected. The linearized set of equations can be solved by an iterative method. The linearized set of equations, in vector-matrix representation, is the following:

$$\begin{bmatrix} a_1 & \gamma & & & & \\ 1+\gamma & b_2 & \gamma & & & \\ & 1+\gamma & b_3 & \gamma & & \\ & & \ddots & \ddots & \ddots & \\ & & & 1+\gamma & b_{n-1} & \gamma \\ & & & & 1+\gamma & a_n \end{bmatrix} \begin{bmatrix} c^*_{1,i+1} \\ c^*_{2,i+1} \\ c^*_{3,i+1} \\ \vdots \\ c^*_{n-1,i+1} \\ c^*_{n,i+1} \end{bmatrix} = \begin{bmatrix} -Da(c^*_{1,i})^{2-1} \\ -Da(c^*_{2,i})^2 \\ -Da(c^*_{3,i})^2 \\ \vdots \\ -Da(c^*_{n-1,i}) \\ -Da(c^*_{n,i}) \end{bmatrix} \qquad (10)$$

where

$$a_j = -(1 + \gamma + 2\,Da\,c^*_{j,i}) \qquad j = 1, n \qquad (11)$$

$$b_j = -(1 + 2\gamma + 2\,Da\,c_{j,i}) \qquad j = 2,3,\ldots, n-1 \qquad (12)$$

and i is the number of iterative steps.

The first parameter is the cascade number; the latter is, in the case of cascade systems and of tubular reactors divided into physically well-defined portions unequivocally determined by the number of stages. As to the selection of the cascade number, in the case of axially stirred continuous systems, reference is made to literature [5]. The other parameter of the model is the γ internal recirculation ratio whose determination is carried out, according to literature, on the basis of the dynamic-flow-model [8]. The following connection between the variance and the parameters of the model was found to exist [8]:

$$\sigma^2 = \frac{\sigma_t^2}{(\bar{t}_B)^2} = \frac{2}{\Phi^2}\left\{\Phi - \left(1 - \frac{\Phi^2}{4\,n^2}\right)\left[1 - \left(\frac{2\,n - \Phi}{2\,n + \Phi}\right)^n\right]\right\} \qquad (13)$$

where

$$\Phi = \frac{2\,n}{1 + 2\gamma} \qquad (14)$$

While discussing Equation (13), a complete analogy to LEVENSPIEL's dynamic-flow model [9] was found [8]. In the case $\gamma \to \infty$, i.e. at an increase of the internal recirculation over any limit, σ^2 tends to 1 and this case corresponds to a continuous model containing axial mixing. In the case $\gamma \to 0$, i.e. $\Phi \to 2n$, the variance tends to $1/n$ and this corresponds to the model of ideal mixing [9]. (This is the classical cascade model). Finally, if $\Phi \to \infty$, which, in the case of a finite γ value, results in the increase of the cascade number over all limits, the piston flow model is realized.

The classical cascade model does not possess the above-mentioned properties, since that model is based on the dynamic-flow model of ideal mixing.

In order to determine the internal recirculation ratio, Equation (13) has to be solved for γ. The value of the internal recirculation ratio can numerically be determined by a computer.

An approximative solution was proposed in literature [5, 8] based on the fact that the internal recirculation ratio converges to the continuous model containing axial mixing. If $n = 10$, the approximation $Pe = \Phi$ yields a satisfactory accuracy for practical calculations [8].

The value of the internal recirculation ratio was calculated by the Newton-Raphson method; the internal recirculation cascade model was solved by an iteration procedure, using a digital computer type ODRA 1204. In the case of $\gamma = 0$ the model represents the classical cascade model and accordingly the exit concentration was also calculated in every case with the classical cascade model. In the case of the internal recirculation model, the calculations have to be made backwards, starting from the n^{th} cascade element, because the calculation starting from the first cascade element is, on account of the high parameter sensitivity, not convergent. A further disadvantage of the latter technique is that the value of γ may not assume the value $\gamma = 0$, because a division is made by this figure in the programme. In backwards calculation the value of $\gamma = 0$ is also allowed. The iteration can be

started from any optional initial value. In the present calculations, the initial value $c^*_{j,i} = 0.5$ $j = 1,2 \ldots n$ was applied. The calculation is, in accordance with the statements to this effect found in literature, very rapid [5]. The difference between the exit concentrations calculated in the third and fourth iteration, respectively, is lower than 10^{-4}.

In order to determine the adequacy of the model, experiments were made with a model reaction. The saponification of ethyl acetate with sodium hydroxide was chosen as such a model reaction. The reaction is, if the initial concentration of the reactants is equimolar, of the second order. The temperature-dependence of the rate constant of the reaction is known from literature [10].

The rate equation of the saponification of ethyl acetate can be written in the following form:

$$\frac{dc}{dt} = k_2(c_0 - c)^2 \qquad (15)$$

where c_0 is the initial concentration of one of the components, preferably of the sodium hydroxide. By integrating Equation (15) from t = 0 to t and from c = 0 to c, we obtain

$$\frac{c}{c_0} = k_2 \, t \, (c_0 - c) \qquad (16)$$

The experiments were carried out in a system thermostated to 25°C [1]. The initial concentration of the reagents was chosen as 0.1 M. The progress of the reaction was determined from samples taken from the material stream leaving the reactor. A known amount of hydrochloric acid of known concentration was added to the sample, which "froze" the reaction. The alkali content of the sample was determined by back-titration. The samples were taken after establishment of the steady state; the latter was monitored by the conductance of the material stream leaving the reactor being constant.

The arrangement of the baffle plates at different distances results in reactors of different flow-dynamic characteristics and accordingly the adequacy of the model was tested in a reactor equipped with a baffle plate No. 2 [1] (the free flow cross section of the latter was, as compared to the empty tube, 0.343). The dynamic-flow properties of the reactors thus obtained were compared on the basis of the equivalent cascade number, calculated from the second moment of the residence time spectrum. Changes in the equivalent cascade number, plotted against the Reynolds number, are illustrated in Figure 2.

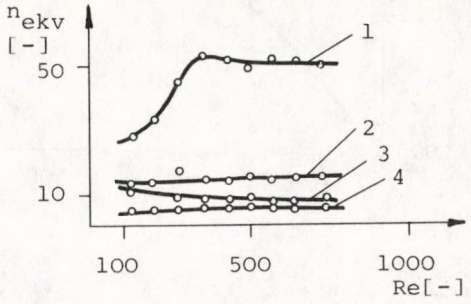

Fig.2. Equivalent cascade number, plotted against the Re--number. Baffle plate No.2. 1 - h=2.5 cm; 2 - h=5 cm 3 - h=10 cm; 4 - h=20 cm

The exit concentrations, measured on the one hand and calculated with the model, on the other, plotted against reactor volume and residence time, as measured from the instant of feeding in, are compared in Figures 3-6. The classical cascade model is marked by KK whereas the internal recirculation cascade model is marked by RK in the Figures. It is apparent from the Figures that there are no large differences - not higher than 5 % - between the measured and calculated values, and consequently both models can be regarded as adequate in the range studied. The small difference between the two models is caused by the fact that a low γ value was obtained ($\gamma < 0.3$), the actual cascade number and the equivalent cascade number calculated from the dynamic-flow model was nearly identical (cf. Table).

As it is apparent from the Table that the internal recirculation ratio may also be a negative value; this may be brought about if $n_t < n_{ekv}$ (at a baffle plate distance of 2.5 cm). It can be concluded that the internal recirculation model possesses very

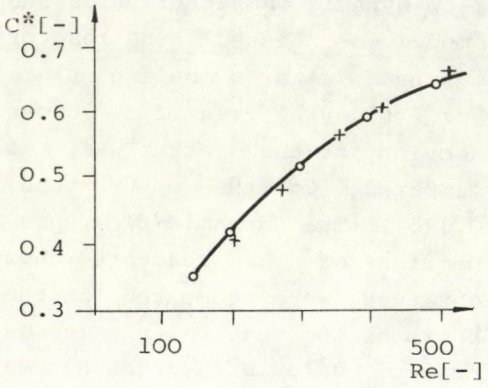

Fig.3. Adequacy test of the models. Baffle plate No.2
h = 2.5 cm, n_t = 36
— RK-model; o KK-model;
+ measured values

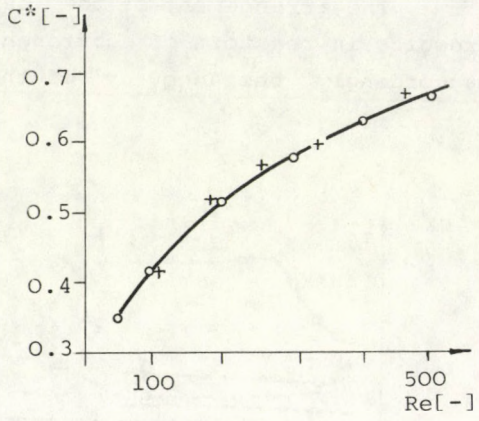

Fig.4. Adequacy test of the model. Baffle plate No.2
h = 5 cm, n_t = 19
— RK-model; o KK-model;
+ measured values

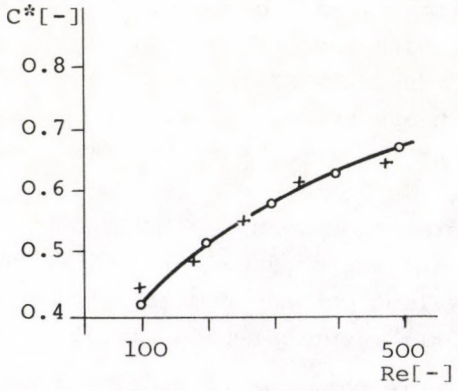

Fig.5. Adequacy test of the models. Baffle plate No.2
h = 10 cm; n_t = 10
— RK-model; o KK-model;
+ measured values

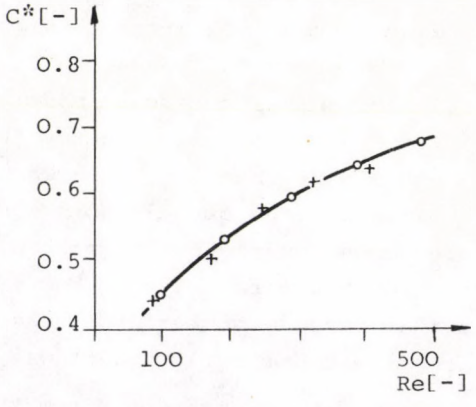

Fig.6. Adequacy test of the models. Baffle plate No.2
h = 20 cm; n_t = 5
— RK-model; o KK-model;
+ measured values

Table 1

h	n	$\bar{t}_B$	Re	γ	c^*_{KK}	c^*_{RK}
cm	-	s	-	-	-	-
		356.8	150	0.1398	0.35345	0.35513
		267.6	200	0.0542	0.42119	0.42178
2.5	36	178.4	300	-0.1140	0.52010	0.51913
		133.8	400	-0.1581	0.58986	0.58878
		107.1	500	-0.1618	0.64319	0.64231
		372.2	150	0.2282	0.35039	0.35514
		279.2	200	0.1994	0.41622	0.42000
5	19	186.1	300	0.1534	0.51418	0.51673
		139.1	400	0.1453	0.58318	0.58505
		111.7	500	0.1361	0.63562	0.63705
		283.6	200	-0.0634	0.42212	0.42007
		189.1	300	0.0492	0.51769	0.51897
10	10	141.8	400	0.1239	0.58576	0.58832
		113.4	500	0.1780	0.63668	0.63964
		286.1	200	0.0094	0.44060	0.44106
		190.8	300	-0.0600	0.53208	0.52966
20	5	143.1	400	-0.0827	0.59725	0.59477
		114.5	500	-0.0976	0.64600	0.64355

attractive properties. By the application of the internal recirculation ratio, the axial mixing can be taken into consideration,

and accordingly the model is a rapid and simple one which also accounts for the dynamic flow characteristics of the reactor. Furthermore, at low values the model practically becomes identical to the classical cascade model; this could be experienced in the course of the experiments.

The previous paper of this series dealt with the dynamic flow properties of the baffle plate-type tubular reactor. An adequate mathematical model, also taking the dynamic flow model into consideration of the baffle plate-type tubular reactor was at our disposal, and consequently a study was made on how the conversion attainable with a plug-like flow pattern can be approximated by the application of baffle-plates in a laminar-flow tubular reactor. The conversion attainable in a perfectly mixed tank reactor and in a plug-like flow system, as well as the conversion values calculated with the internal recirculation cascade model (broken line) plotted against the mean residence time calculated from the reactor vo-

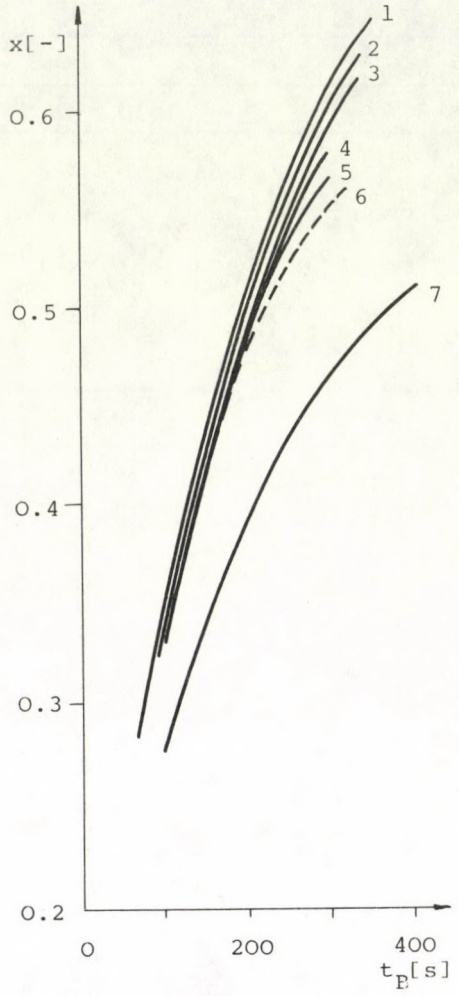

Fig.7. Calculated conversion plotted against the mean residence time. 1 - ideal tubular reactor; 2 - h = 2.5 cm, baffle plate No.2; 3 - h = = 5 cm, baffle plate No.2; 4 - h = 10 cm, baffle plate No.2; 5 - h = 20 cm, baffle plate No.2; 6 - real reactor measured; 7 - perfectly stirred tank reactor

lume and the feed are illustrated in Figure 7. It is apparent from the Figure that at a baffle plate distance of 2.5 or 5 cm the baffle plate-type tubular reactor can practically be regarded as one conforming to the plug-type flow pattern. The efficiency-improving effect of the baffle plates is less pronounced if the residence time is decreased. This follows from the experimental results, since the difference in the conversion values attainable with perfectly stirred tank reactors and with plug-type flow reactors is small.

Despite the aforementioned it can be concluded that the plug-like flow pattern and the conversion corresponding to it can also practically be attained in laminar-flow tubular reactors, provided that the geometrical simplexes [1] postulated by flow dynamic examinations are observed.

SYMBOLS USED

a_j as defined by Equation (11), (dimensionless)

b_j as defined by Equations (12), (dimensionless)

B feed ($\ell \cdot h^{-1}$)

B_R internal recirculation volume stream ($\ell \cdot h^{-1}$)

C concentration (mole$\cdot \ell^{-1}$)

C_o initial concentration of reagent (mole$\cdot \ell^{-1}$)

C_j concentration of reagent in the j^{th} cascade element (mole$\cdot \ell^{-1}$)

C_j^* relative concentration of reagent in the j^{th} cascade element (dimensionless)

C_{KK}^* exit concentration, as calculated by the classical cascade model (dimensionless)

C_{RK}^* exit concentration, as calculated by the internal recirculation cascade model (dimensionless)

Da	Damköhler number, as defined by Equation (8), (dimensionless)
k	distance between baffle plates (cm)
k_2	rate constant ($\ell \cdot mole^{-1} \cdot s^{-1}$)
n	cascade number (dimensionless)
n_{ekv}	equivalent cascade number (dimensionless)
n_t	actual cascade number (dimensionless)
Pe	Peclet-number (dimensionless)
Re	Reynolds-number (dimensionless)
t	time (s)
$\bar{t}_B$	mean residence time calculated from volume and feed (s)
V	volume (ℓ)
V_j	volume of the j^{th} cascade element (ℓ)
x	conversion (dimensionless)
γ	internal recirculation ratio (dimensionless)
σ^2	dimensionless variance
σ_t^2	variance (s^2)
Φ	characteristic number between cascade number and internal recirculation ratio (dimensionless)

Indexes

i	number of iterative steps
j	index of cascades
o	index referring to initial value

REFERENCES

1. LÁSZLÓ, A., BENKŐ, B., STEFKÓ, B., KREIDL, J., Hung. J. Ind. Chem. 3, 141 (1975)
2. NOH, J.C., LEE, E.S., AIChE Journal 17, 886, 1278 (1971)
3. CASAMASSIMA, S.J., ZIEGLER, E.N., AIChE Journal 17, 1250 (1971)
4. LELLI, U., Quad. ing. chimico italiano, 3, 179 (1967)
5. DECKWER, W., POPOVIC, M., Chemie Ing. Techn. 45, 984 (1973)
6. LELLI, U., Quad. ing. chimico italiano, 4, 125 (1968)
7. LELLI, U., MAGELLI, F., SAMA, C., Chem. Eng. Sci. 27, 1109 (1972)
8. ROEMER, M.M., DURBIN, L.D., Ind. Eng. Chem. Fundamentals. 6 120 (1967)
9. LEVENSPIEL, O., Chemical Reaction Engineering. John Wiley and Sons, Inc. New York-London, (1965)
10. HOVORKA, R.B., KENDALL, H.B., Chem. Eng. Progress 56, 58 (1960)

РЕЗЮМЕ

Настоящая работа занимается математическим моделированием реактора-трубы с направляющими пластинками. Авторы используют так называемую модель каскада с внутренней рециркуляцией, применяя ее для системы реакции-модели второго порядка.

Сравнивая опытные данные с данными модели, авторы предлагают упрощающие модель условия и способ более эффективного выбора типа вкладыша.

СОДЕРЖАНИЕ

СМИРНОВ,Н.Н.: Математические модели процесса ионного обмена 1

КИРИЛЛОВ,В.А., КАСАМАНЯН,М.А.: Исследование процессов массообмена между жидкостью и насадкой в трехфазном неподвижном слое 21

ГАРЦМАН,А.Н.,ЕРМАКОВА,А.,БАХВАЛОВА,В.П.,РАССАДНИКОВА,Н.И.: Массоперенос с химической реакцией в трехфазной системе газ-жидкость-твердый катализатор 37

ДЕВАИ,Й.,РАТКОВИЧ,Ф.,СЕЙЛЕР,Б.,ЧАСАР,Э.,ДОМОНКОШ,Л.: Проблемы постоянной работы башни для очистки окиси углерода медно-аммиачным раствором, на заводе синтеза аммиака . . 51

ДЕВАИ,Й.,КОВАЧ,Л.,ХОРКАИ.Ф.,МЕСАРОШ,Л.: Изучение старения полиуретановых лаков на основе явлений диэлектрической релаксации 71

МЕСАРОШ,Л.: Изучение вопросов оптимальной безопасности, надежности и риска в химических системах 79

ВАЙДА,Т.: Расчет распределения времени нахождения в гейзеровом аппарате на основе рециркуляционной модели 91

ФРАТЧЕР,В.,ХЕБЕКЕР,Д.,ХОНША,Д.: Энергетические свойства плазмообразующих газов низкотемпературной плазмотехники 115

ПАЛАНЦ,Б.: Исследование управляемости процесса проточной сушки с помощью приведения дистрибутивной модели к линейному виду 127

ЛАСЛО,А.,БЕНКО,Б.,ШТЕФКО,Б.,КРЕИДЛ,Й.: Изучение реактора-трубы с направляющими пластинками I. 141

БЕНКО,Б.,МАРТОН,Дь.: Изучение реактора-трубы с направляющими пластинками II. 157

A kiadásért felelős: Dr. Nemecz Ernő
Felelős szerkesztő: Dr. Bodor Endre
Példányszám: 950 + 250 különlenyomat cikkenként
Engedélyszám: 48021.
75.228. Áfész Sokszorosítóüzem, Vác.

Ára: 37 Ft

CONTENTS

SMIRNOV, N.N.: The Mathematical models of Ion Exchange Processes (Russian) 1

KIRILLOV, V.A., KASAMANYAN, M. A.: The Investigation of Mass Transfer Taking Place between the Packing and Liquid in a Three Phase Static Bed Reactor (Russian) 21

GARTSMAN, A.N., IERMAKOVA, A., BAKHVALOVA, V.P., RASSADNIKOVA, N.I.: The Mass Transfer Accompanied by Chemical Reaction in a Gas-Liquid-Solid Catalyst Three Phase System (Russian) 37

DÉVAY, J., RATKOVICS, F., SZEILER, B., Mrs. CSÁSZÁR, E. and DOMONKOS, L.: Problems Related to the Long-Term Operation of Copper-Lye Carbon Monoxide Removal Units in Ammonia Plants 51

DÉVAY, J., KOVÁCS, L., HORKAY, F. and MÉSZÁROS, L.: Untersuchungen der Alterung von Lacken auf Polyurethan--Basis auf Grund dielektrischer Relaxationserscheinungen 71

MÉSZÁROS, L.: Prüfung von Fragen der Sicherheits-, Zuverlässigkeits- und Risiko-Optimierung bei Gross-Systemen der chemischen Industrie 79

VAJDA, T.: Berechnung der Verweilzeitverteilung in Fliessbettapparaten auf Grund eines Rezirkulationsmodells 91

FRATZSCHER, W., HEBECKER, D. und HONSCHA, J.: Energetische Eigenschaften plasmabildender Gase der Tieftemperatur--Plasmatechnik 115

PALÁNCZ, B.: Controllability Tests on a Flowthrough Drying Process with Linearization of the Distributive Model . . 127

LÁSZLÓ, A., BENKŐ, B., STEFKÓ, B. and KREIDL, J.: Examination of a Baffle Plate-Type Tubular Reactor I. 141

BENKŐ, B. and MARTON, Gy.: Examination of a Baffle Plate-Type Tubular Reactor II. 157

HUNGARIAN

Journal of

INDUSTRIAL CHEMISTRY

Edited by

the Hungarian Oil & Gas Research Institute (MÁFKI),
the Research Institute for Heavy Chemical Industries (NEVIKI),
the Research Institute for Technical Chemistry of the
Hungarian Academy of Sciences (MÜKKI),
the Veszprém University of Chemical Engineering (VVE).
Veszprém (Hungary)

Volume 3. 1975 Number 3.

CODEN: HJICAI

The "Hungarian Journal of Industrial Chemistry (Veszprém)" is a joint publication of the Veszprém scientific institutions of the chemical industry that deals with the results of applied and fundamental research in the field of chemical processes, unit operations and chemical engineering. The papers are published in three or four numbers at irregular intervals in one annual volume, in the English, Russian, French and German languages.

Editorial Office:
Veszprémi Vegyipari Egyetem,
"Hungarian Journal of Industrial Chemistry" Editorial Board:
H – 8201 Veszprém, Schönherz Z. u. 10. Hungary.

Dr. Márta Ferenc elvtársnak
akadémikus, az MTA főtitkára
1051 Budapest
Roosevelt tér 9.

Tiszteletpéldányként mellékelten megküldöm a Hungarian Journal of Industrial Chemistry 1975. Vol. 3. No. 3. füzetét.

A Szerkesztő Bizottság megbizásából

Veszprém, 1975. dec. 4.

/Dr. Bodor Endre/
főszerkesztő

Hungarian Journal
of Industrial Chemistry
Veszprém
Vol.3. pp. 357-368 (1975)

DEHYDROGENATION OF NORMAL HEXANE ON A MODIFIED PLATINUM CATALYST

Mrs. B. MARKÓ, Cs. CSIKÓS and J. BÁTHORY

(Hungarian Oil and Gas Research Institute, Veszprém)

Received: April 8. 1975.

The dehydrogenation of n-hexane was carried out using a batch microreactor and a four-component catalyst within a temperature range of 400--700 °C. In addition to platinum, the catalyst contains lithium (as a promoter) and arsenic (as a catalyst attenuator) on an alumina carrier. The experimental results show that with the optimal composition of the above catalyst, at a yield of about 25 %, straight chained hexenes form with a selectivity of more than 90 %.

Introduction

The increased demand for long, straight-chained monoolefins is primarily attributed to their use in the manufacture of biologically decomposable detergents. Several possible methods exist for the manufacture of such olefins, among them the most practical and economical seems to be the dehydrogenation of the corresponding normal paraffins.

Dehydrogenation of the longer chained hydrocarbons is extensively hindered by the fact that C-H bonds are stronger than C-C bonds, so that the direct thermal effect primarily causes the breaking up of the latter, in other words cracking results. It is therefore evident that dehydrogenation occurs only if the C-H bonds are preliminarily loosened by means of a catalyst. Such type

of catalysts have been known for decades, mainly for the manufacture of different C_3-C_5 unsaturated hydrocarbons [1]. However, in the case of longer chained hydrocarbons, the use of both the metal oxide or the noble metal catalysts result in deleterious side reactions - primarily dehydrocyclization and cracking - which extensively decreases the yield of the objective reaction. This is the reason behind the failure to find a suitable catalyst composition - until the middle of the 1960s - for the economical dehydrogenation of hydrocarbons containing more than five carbon atoms, although considerable effort was directed towards this. The best noble metal catalysts give a selectivity of less than 80 % at optimal conditions [2] or in the interest of achieving the best selectivity, conversion had to be held at a value below 5--10 % [3].

In recent years, a number of patents have dealt with different composition of dehydrogenation catalysts, the common point being that in addition to the noble metal on a carrier, there is also a catalyst "attenuator", or "modifier" which is actually a catalyst poison such as sulphur, selenium, tellurium [4, 5], arsenic, antimony, or bismuth for the purpose of increasing selectivity [6]. Despite the data concerning the promosing operation of these catalysts, available literature supplies very limited information about the details of research. The aim of the following experiments was to acquire some knowledge in this field.

For the purpose of dehydrogenation experiments, four-component catalysts were prepared in the laboratory. These contained platinum on alumina carrier, lithium as a promoter, and arsenic as a catalyst attenuator. The object of the experiments was to investigate the effect of the catalyst composition and reaction parameters on reaction product composition. It was assumed that for a given temperature, residence time and hydrocarbon raw material, the concentration of each component of the catalyst would show an optimum in respect of the yield of linear olefins.

Dehydrogenation being an equilibrium reaction, it is very sensitive to changes in temperature and pressure. The reaction is endothermic and occurs with an increase in volume, therefore the formation of olefins would favour an increase in temperature and a

decrease in pressure. However, taking into consideration the fact that an intensive increase in temperature leads to destructive reactions, it is evident that the reaction temperature also has an optimum for a given catalyst, residence time and raw material. In connection of each investigated catalyst composition, the effect of temperature on the operation was therefore thoroughly studied in the experiments discussed here.

n-Hexane was used as the starting reagent to simplify the experimental technique, with the aim of conducting experiments later with hydrocarbons of longer chains.

Experimental Technique

The examination of the catalysts was carried out using the method based on the pulse technique [7, 8]. This has some advantages when compared to other continuous tube or circulation reactors, in that it requires a small amount of catalyst and raw material, and the endproducts can be quickly analysed. Its disadvantages include the fact that in the case of kinetic measurements it does not provide reliable information and the equipment cannot be used for experiments requiring longer periods of operational time (e.g. life time tests). Figure 1 shows the diagram of the equipment used in our laboratory.

Hydrogen gas - which partly assured the gaseous atmosphere of the reaction and partly served as a carrier-gas for the chromatographic process - was taken from a gas cylinder through a reductor and a needle valve. The detector prepared in the laboratory was a glass catharometer cell, with two parallel connected, 25 ohm platinum wires. Its outer jacket was filled with water for thermostatic purposes. The cell was supplied from a transistor stabilized mains NB-107 (Gamma, Hungary) the heating current being 160 mA. An EZ-4 (Czechoslovakia) type compensograph was used for recording.

Chromatographic column data: 2.7 m long, 6 mm I.D. glass tube. The stationary phase was 10 % β,β'-oxy-dipropionitrile (ODP) on a diatomaceous earth type support "MH-3" (REANAL, Hungary).

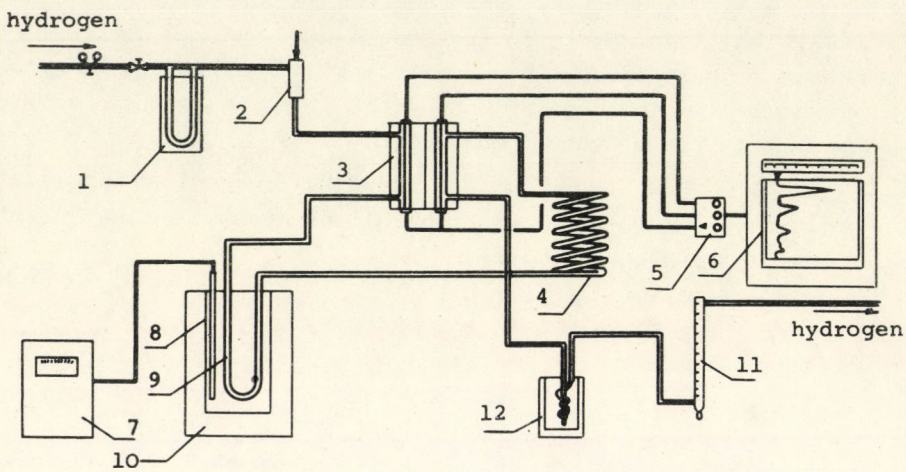

Fig. 1. Diagram of experimental equipment. 1 - Differential manometer; 2 - Injector head; 3 - Catharometer cell; 4 - Column; 5 - Catharometer cell bridge and polarity switch; 6 - Recorder;7 - Temperature controller; 8 - Thermocouple; 9 - Reactor; 10 - Furnace; 11 - Soap-film flowmeter; 12 - Chiller

The reactor which was made of acid-resistant steel, had a total volume of about 3 cc. Its connecting tubes were steel and glass capillaries of 2 mm I.D.The reactor temperature was measured using an iron-constantan thermocouple and its control was provided by a bridle temperature controller.

In addition of obtaining the chromatogram of the products leaving the reactor, the arrangement illustrated on Figure 1 provided the possibility to obtain a peak of the starting hydrocarbon just after injection. A polarity switch enabled all the peaks to be obtained in the same direction.

The raw material used was 3-10 μℓ of "Chemically pure" normal hexane manufactured by "Reachim". The hydrogen gas flow rate was 50 ml/min and the weight of catalyst used was 0.1–0.5 gramme.

The carrier of the catalysts was prepared by dropping aluminium hydroxide gel into paraffin oil and treating the resulting granulate with heat. The resulting carrier was impregnated, using an appropriate mixture of H_2PtCl_6, $(NH_4)_3AsO_4$ and $LiNO_3$ solutions. The impregnated carrier was calcinated for a period of 2 hours at 500 °C and was reduced just before use in a stream of hydrogen gas at 700 °C for 30 minutes.

Experimental Results and Discussion

Figure 2 shows the chromatogram of the reaction product obtained with a four-component catalyst outlined earlier. It can be seen that apart from the unreacted n-hexane, straight-chained hexenes and some cracking products, which can be hardly defined, result as products. With the chromatographic column used it was not possible to obtain a total separation of the resulting hexanes, since the retention data for 1-hexene and trans-3-hexene on one hand and that of cis-3-hexene and trans-2-hexene on the other, coincide on the applied stationary phase [10]. Retention time for aromatic hydrocarbons was several hours, therefore, in certain cases analyses of aromatic hydrocarbons were carried out on another chromatographic column (10 % Apieson L on MH-3 support), from chilled samples.

In testing the quality of the catalysts three data, conversion, yield and selectivity were used. In the evaluation of the results the quantities of n-hexane, or hexene isomers were given relative to the quantity of n-hexane injected. In this way the probable presence of some side products which did not appear on the chromatogram will not induce an error in calculations. The distribution of the side products and hexene isomers was not studied in detail.

To examine the contribution of each active component of the catalyst, three types of catalyst were prepared. The first con-

taining only platinum as the active component, the second platinum and lithium, and the third containing all three components, platinum, lithium and arsenic on an alumina support. Table 1 shows the composition of these catalysts.

Figure 3 shows the result of the dehydrogenation experiments with these catalysts at different temperatures. It can be seen on the diagram that K/1, which contains only platinum, is the most active, and the addition of lithium and arsenic decreases the conversion at equal temperatures. At the same time, it is evident from the yield diagrams that the addition of lithium does not essentially influence the yield. With the addition of arsenic, the yield shows a sharp increase in the interval between 550 °C and 650 °C although the yield of catalysts containing only platinum and lithium decreases to zero within this interval because of side reactions. The diagram is very representative in connection with the contribution of arsenic. At low temperatures, the catalyst attenuator decreases the yield by blocking active centres. However, with an increase in temperature, cracking is relegated to the background and the main reaction is favoured. On the diagrams shown the arsenic containing catalyst appears only relati-

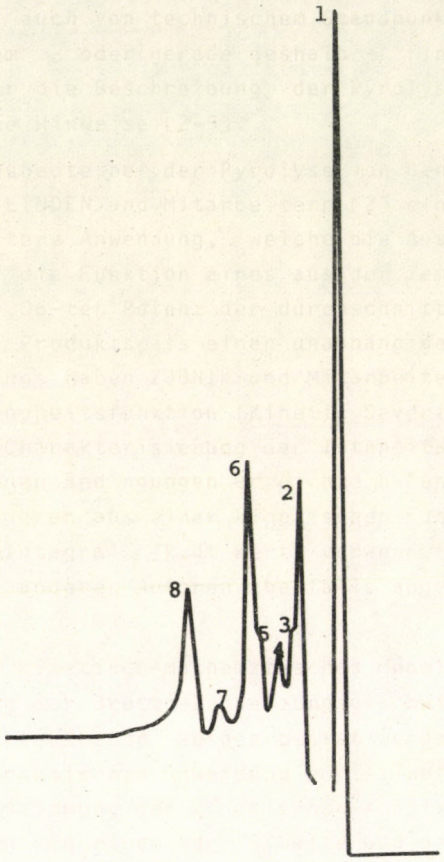

Fig.2. Chromatogram of a product. Catalyst: K/3; $t_{reactor}$: 550 °C; 1 - Injected n-hexane; 2,3,4,5 - Cracking products; 6 - n-hexane; 7 - 1-hexene + trans-3-hexene; 8 - trans-2-hexene + cis-3-hexene

Table 1. Composition of catalysts

Symbol of catalyst	Composition		
	Pt (wt%)	Li (wt%)	As/Pt atomic ratio
K/1	0.75	-	-
K/2	0.75	0.5	-
K/3	0.75	0.5	0.3

tively better than the others, the absolute value of the yield and selectivity are low, as the influence of component concentrations were not yet known in these experiments.

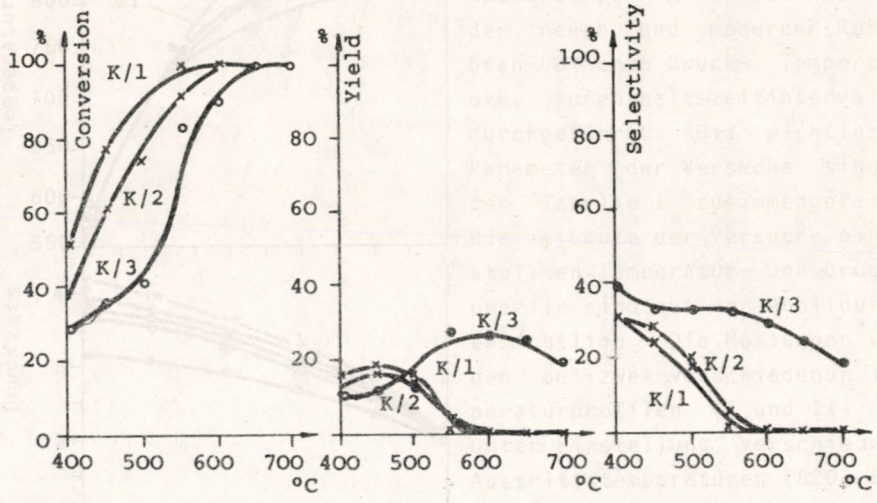

Fig. 3. Influence of catalyst components. Catalyst weight: 0.5 g; Gas flow rate; 50 ml/minute; Quantity of n-hexane: 5 µl

After a clear evaluation had been obtained regarding the qualitative effect of each component of the catalyst, an attempt was made to determine the optimal proportions of the components and the favourable conditions for the dehydrogenation reaction.

The effect of the platinum content was examined using a number of four-component catalysts containing 0.5 per cent by weight of lithium, and a concentration of platinum varying from 0.05—5 wt%. The result of these experiments is shown in Figure 4. It can

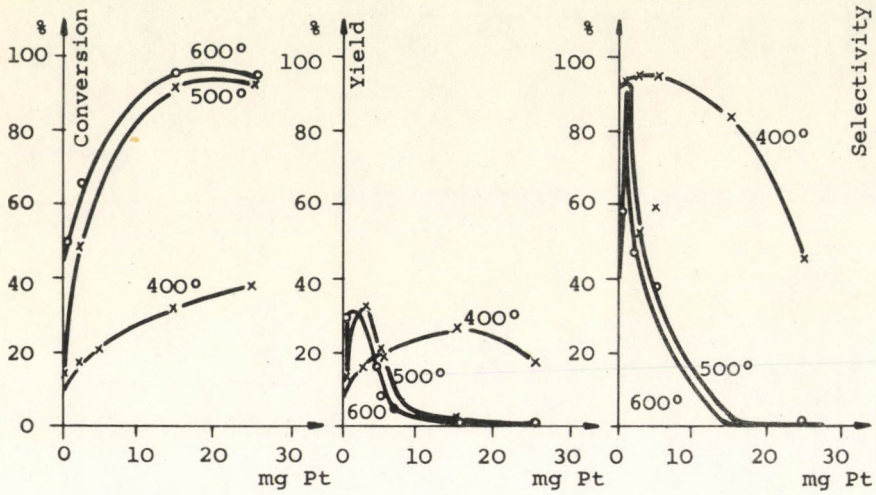

Fig. 4. Effect of quantity of platinum. Gas flow rate: 50 ml/minute; Quantity of n-hexane: 5 µl

be seen from the diagram that conversion increases sharply with the platinum charge in the reactor and there is a strong temperature dependence of activity. The yield curves show maximums, the interval of which determines the suitable platinum concentrations for the applied catalyst charges. The selectivity diagram explicitly shows that with an increase in temperature, the interval for the optimal amount of platinum becomes narrower.

Since the novelty of the catalyst used is its content of a catalyst attenuator particular attention was especially paid to the effect of the As/Pt ratio on the functioning of the active ca-

talyst. In these experiments, catalysts with the As/Pt atomic ratio changing from 0.1–0.75 were tested. In the examination of these catalysts, the composition with 0.3 As/Pt atomic ratio produced conspicuous results at optimal operational conditions, both in connection with olefin yield and selectivity (Figure 5).

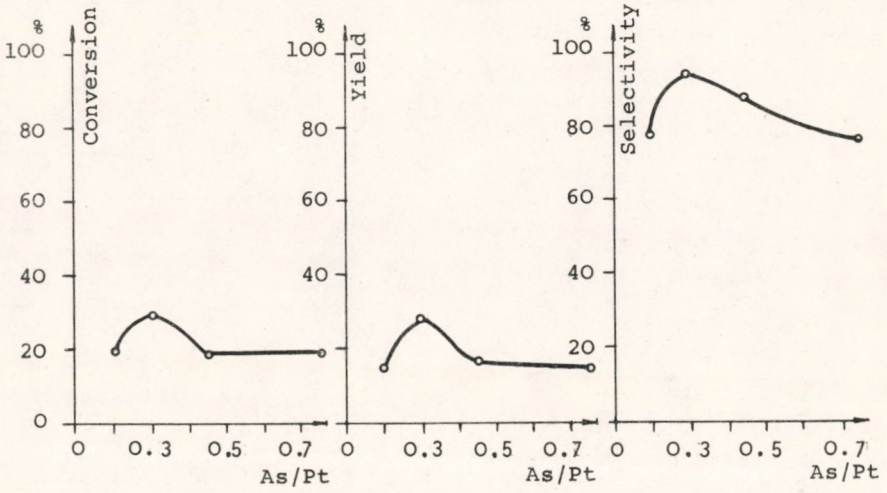

Fig.5. Effect of As/Pt ratio. Temperature: 550°C; Catalyst weight: 0.5 g; Gas flow rate: 50 ml/minute; Quantity of n-hexane: 5 µl

In a few preliminary experiments, it was found that lithium had no decisive effect on the properties of the catalyst. This is why it was not considered important to extend the examination of the composition to the effect of different lithium concentrations. In the same way the influence of the properties of the catalyst carrier was not examined, although this presumably cannot be neglected.

The best catalyst characteristics, namely conversion, yield and selectivity, for the given equipment, given hydrocarbon charges and H_2/hydrocarbon ratio, are shown as a function of temperature in Figure 6.

From the diagram it is clear that conversion increases exponentially with temperature, selectivity is constant up to a given value of temperature and then sharply decreases, while the yield goes through a maximum. The maximum of the yield curve or the break point of the selectivity curve unambiguously determine the optimal operational temperature which in this case is around 550 °C. Here the catalyst functions with a yield of more than 25 % and selectivity exceeding 90 %.

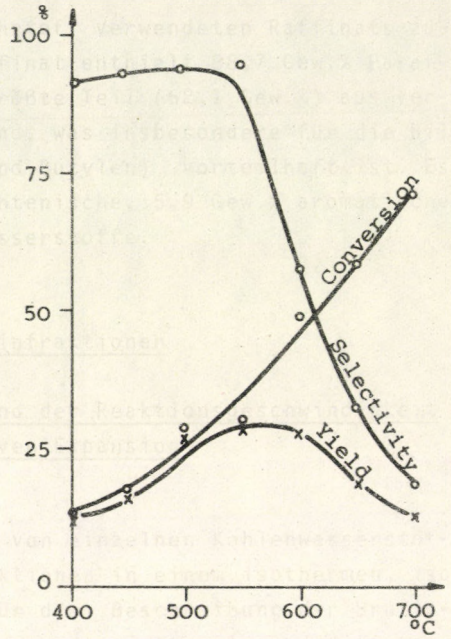

Fig.6. Examination of K5/2 catalyst. Catalyst weight: 0.5 g; Composition: 0.1 % Pt, 0.5 % Li, 0.3 As/Pt; Gas flow rate: 50 ml/minute; Quantity of n-hexane: 5 µl

Working with this catalyst gives a minimum of byproducts which consist of hydrocarbons containing less than six carbon atoms and some benzene formed by dehydrocyclisation of hexane.

From the experiments discussed here, it is possible to conclude that with the catalyst and under the conditions elaborated by systematically changing the catalyst composition and reaction parameters, the conversion and selectivity results given for similar catalyst composition in literature were reproduced in a batch microreactor. Naturally, the numerical results obtained are seriously valid only for the given equipment and method, however, the experienced tendencies can be extended to other systems with complete assurance.

The Assumed Working Mechanism of the Modified Platinum Catalyst

It is known that supported platinum is a very good catalyst for several hydrocarbon reactions. Some of these, such as cracking,

are aided by acidic places on the support. The promotional action of lithium can obviously be explained by its alkaline character, which acts by shielding the acidic centres on the alumina surface.

Active centres in noble metal catalysts fostering dehydrogenation and dehydrocyclization differ from those which promote cracking and isomerization according to literature [11].

One possible explanation for the role of arsenic may be its influence on the concentration of electrons in the d-orbitals of the platinum, any change of which necesserily modifies the strength and character of the olefin-platinum interaction. It is suggested that arsenic exerts its influence by ensuring the rapid desorption of olefins, thus preventing any successive C-H bond splitting which would ultimately lead to aromatization.

The resulting monoolefins have their double bonds in the inferior β, γ or δ positions, since, in addition to the statistical probability, these positions provide the most favourable energetic conditions as a result of inductive effect.

LITERATURE

1. ASINGER, F., Die petrolchemische Industrie I., Akad. Verlag, Berlin, 1971.

2. U.S.P. 3.274.287

3. Fr.P. 1.413.913; CA 64, 7950c (1966)

4. U.S.P. 3.310.599; CA 66, 11768e (1967)

5. U.S.P. 3.439.061; CA 71, 14853 (1969)

6. U.S.P. 3.291.755; CA 66, 30777p (1967)

7. KOKES, R.J., TOBIN, J., EMETT, H., J. Am. Chem. Soc. 77, 5860 (1955)

8. ROZENGART, M.I., MORTIKOV, E.S., KAZANSKI, B.A., Dokl. Akad. Nauk, SSSR, 166, 619 (1966)

9. U.S.P. 2.620.314

10. SMITH, B., OHLSON, R., LARSEN, G., Acta Chem. Scand. 17, 436 (1963)

11. SKARCHENKO, V.V., Usp. Khim., 40, 2145 (1971)

РЕЗЮМЕ

Дегидрогенизация н-гексана была выполнена в микрореакторе периодического действия в присутствии четырехкомпонентного катализатора при температуре 400-700 °С. Платиновый катализатор содержит окись алюминия в качестве носителя, литий в качестве промотора и мышьяк в качестве разбавителя. По экспериментальным данным было установлено, что катализатор оптимального состава обеспечивает выход 25%, а селективность образования гексенов прямой цепи превышает 90%.

Hungarian Journal
of Industrial Chemistry
Veszprém
Vol.3. pp. 369-390 (1975)

KINETISCH-MATHEMATISCHES MODELL DER BENZINPYROLYSE I

ZERSETZUNGSGESCHWINDIGKEITSGLEICHUNG, KINETISCHES MODELL

V. ILLÉS und A. HORVÁTH

(Ungarisches Erdöl- und Erdgasforschungsinstitut, Veszprém)

Eingegangen am 10. Februar 1975

Die Pyrolyse von Raffinatfraktionen mit den Siedegrenzen zwischen 42,5 - 120,0 °C wurde in einem für die Simulierung von industriellen Rohröfen geeigneten, großlaboratoriumsmäßigen Rohrreaktor untersucht. Die Temperatur-, Druck- und Produktenverteilung längs des Reaktorrohrs wurden experimentell gemessen.

Auf Grund der unter nichtisothermen und nichtisobaren Reaktionsbedingungen erhaltenen Pyrolyse-Versuchsergebnissen wurde eine Methode zur Beschreibung der Brutto-Zersetzungsgeschwindigkeit für Raffinate (Benzinfraktionen) unter Voraussetzung einer Reaktionskinetik n-ter Ordnung ausgearbeitet. Unter Verwendung der erhaltenen kinetischen Konstanten wurden ein kinetisches Modell und ein Rechenprogramm zur Berechnung des Zersetzungsgrads sowie der brutto-kinetischen Strengheitsfunktion zusammengestellt.

Einleitung

Ein bedeutender Teil der petrolchemischen Monomeren (z.B. 12-14 Millionen Jahrestonnen Äthylen) wird durch Pyrolyse von Benzinfraktionen hergestellt [1]. Ebenfalls bilden verschiedene Benzinfraktionen den Rohstoff des in Ungarn Anfang 1975 in Betrieb tretenden großen Olefinwerks. Die Ausbeuten und die relativen Mengen der während der Pyrolyse gebildeten Hauptprodukte sind in hohem Maße von den Eigenschaften der eingespeisten Benzinfraktion,

sowie von den Bedingungen der Pyrolyse abhängig. Also ist die eingehende Untersuchung der Pyrolyse auch von technischem Standpunkt von erheblicher Bedeutung. Trotzdem - oder gerade deshalb - findet man in der Fachliteratur über die Beschreibung der Pyrolyse von Benzinfraktionen nur allgemeine Hinweise [2-5].

Zur Berechnung der Äthylenausbeute bei der Pyrolyse von Benzinfraktionen fand früher die von LINDEN und Mitarbeitern [2] eingeführte Strengheitsfunktion breitere Anwendung, welche die Ausbeute des Zielprodukts Äthylen als die Funktion eines aus der Temperatur am Ofenaustritt und der 0,06-ten Potenz der durchschnittlichen Aufenthaltszeit bestehenden Produkts als einen unabhängigen Veränderlichen beschreibt. Neuerdings haben ZDONIK und Mitarbeiter [4] die sogenannte kinetische Strengheitsfunktion (Kinetic Severity Funktion) eingeführt, welche zur Charakterisierung der Intensität der Spaltung, die unter den gegebenen Bedingungen erreichte n-Pentan-Konversion bzw. den auf Grund deren aus einer kinetischen Funktion erster Ordnung berechneten Integral $\int k.dt$-Wert verwendet. Diese Methode wurde von mehreren anderen Autoren ebenfalls angewandt [5].

In unserer Arbeit wird ein kinetisch-mathematisches Modell beschrieben, das zwecks Darstellung der Brutto-Zersetzungsgeschwindigkeit und Berechnung der Produktausbeute ausgearbeitet wurde. Neuartig und vom Standpunkt der praktischen Anwendung vorteilhaft ist bei dieser Methode, daß die Bestimmung der kinetischen Konstanten und der Produktausbeutekurven in einem zur Simulierung der Bedingungen der technischen Pyrolyse geeigneten, nichtisothermen, nichtisobaren Rohreaktor, in großlaboratoriumsmäßig durchgeführten Pyrolyseversuchen erfolgte.

Mit der Bestimmung der Brutto-Zersetzungskinetik von Kohlenwasserstoffen aus nichtisothermen Messdaten befassten sich mehrere Autoren. So untersuchten KERSHENBAUM und MARTIN [6] die Pyrolyse des Propans, KUNZRU und Mitarbeiter [7] die des n-Nonans, LEFTIN und CORTES [8] die Pyrolyse des i-Butens im Laboratoriums-Strömungsreaktor. Die Versuche wurden bei gleichem Temperaturprofil und gleicher Einspeisegeschwindigkeit (gleichem Druckprofil), unter Einstellung verschiedener Kohlenwasserstoffpartialdrucke

durchgeführt. Proben wurden nur am Austrittspunkt des Reaktors genommen. Die Methode der kinetischen Darstellung wurde auf diesen Fall angewandt.

Eine auf dem tatsächlichen Spaltvorgang von Benzinfraktionen beruhende Beschreibungsmethode wurde bis jetzt - unseres Wissens nach - noch nicht veröffentlicht.

Versuchsmethode und Pyrolysebedingungen

Für die Pyrolyse von Benzinfraktionen wurde ein Großlaboratoriumsrohreaktor mit einer Kapazität von 2-4 kg/h verwirklicht [9, 10]. Im Reaktor waren somit die Temperatur, der Druck und die Konzentrationsverteilung messbar.

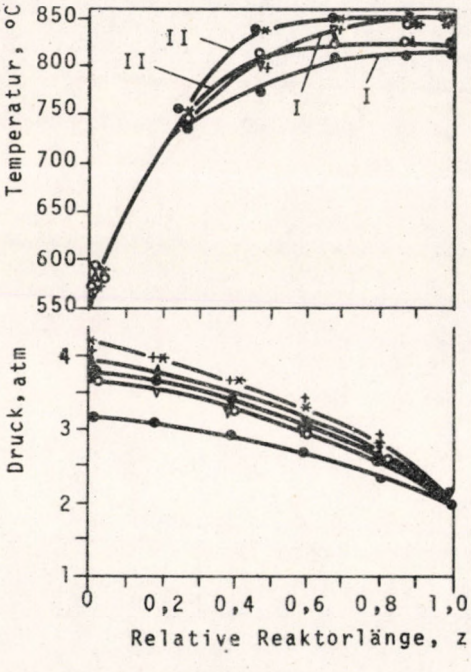

Abb.1. Temperatur- und Druckverteilung als Funktion der relativen Rohrlänge

Die Pyrolysenversuche wurden unter Zuführung von 50 Gew.% Wasserdampf im für den Betrieb der neuen und modernen Rohröfen üblichen Druck-, Temperatur- bzw. Aufenthaltszeitintervallum durchgeführt. Die wichtigsten Parameter der Versuche sind in der Tabelle 1 zusammengefasst. Die im Laufe der Versuche eingestellten Temperatur- und Druckprofile sind aus der Abbildung 1 ersichtlich. Die Messungen wurden bei zwei verschiedenen Temperaturprofilen (I und II) und unter Einstellung verschiedener Austrittstemperaturen (820, 825, 850 °C) durchgeführt.

Die Analyse der im Laufe der Versuche entnommenen gasförmigen und flüssigen Proben erfolgte nach einer von Frau Simon

Tabelle 1. Mit Raffinat durchgeführte Versuche und deren Versuchsbedingungen

Versuch-Nr.	Zeichen	Temperaturprofil	Austrittstemperatur (°C)	Einspeiserate (kg/h)		Austrittsdruck (atm)	Entnahmestellen für Zwischenproben
				Benzin	Wasser		
34	•	I	820	2,39	1,29	1,90	M_2, M_3, M_4, M_5
36	∇	I	850	2,78	1,38	1,90	M_2, M_3, M_4, M_5
37	+	I	850	3,05	1,63	1,90	M_2, M_3, M_4, M_5
38	o	II	825	2,92	1,43	1,90	M_2, M_3, M_4, M_5
39	Δ	II	825	3,30	1,67	1,90	M_2, M_3, M_4, M_5
40	●	II	850	3,00	1,52	1,90	M_2, M_3, M_4, M_5
41	*	II	850	3,32	1,73	1,90	M_2, M_3, M_4, M_5

und vom Herrn Szepesy ausgearbeiteten Methode unter Anwendung eines MÁFKI-Gasanalysators, eines Carlo Erba Fractovap Apparates (Modell PAID) und eines Carlo Erba Apparates (Modell C ATC) [11, 12].

Zur Berechnung der Versuchsdaten und für weiteren Datenverarbeitung wurde ein elektronischer Rechner (Typ Rechenzentrale GIER), sowie ein Mini-Computer Hawlett-Packard 9100 B verwendet.

Tabelle 2. Wichtigere Kennzeichen und Gruppenzusammensetzung des Raffinats

Kennzeichen	Wert
Dichte bei 20 °C, g/ml	0,6745
Durchschnittliches Molekulargewicht	87,00
Fraktionsverteilung, °C	
Siedebeginn	42,5
10 % destillieren bis	57,5
50 % destillieren bis	74,0
90 % destillieren bis	100,0
Siedeende	120,0
Gruppenzusammensetzung, Gew.%	
n-Paraffine	26,6
i-Paraffine	62,1
Naphtene	3,6
Ungesättigte Kohlenwasserstoffe	1,8
Aromaten	5,9
Wasserstoffgehalt, Gew.%	15,65
Schwefelgehalt, Gew.%	0,012

In der Tabelle 2 wurden die wichtigsten Merkmale sowie die durch gaschromatographische Analyse bestimmten Daten der Gruppen-

zusammensetzung des als Pyrolyserohstoff verwendeten Raffinats zusammengefasst. Das untersuchte Raffinat enthielt 88,7 Gew.% Paraffinkohlenwasserstoffe, wovon der größte Teil (62,1 Gew.%) aus verzweigten Kohlenwasserstoffen bestand, was insbesondere für die Bildung höherer Olefine (Propylen und Butylen) vorteilhaft ist. Es enthielt ferner noch 3,6 Gew.% naphtenische, 5,9 Gew.% aromatische und 1,8 Gew.% olefinische Kohlenwasserstoffe.

Brutto-Zersetzungskinetik der Benzinfraktionen

Definition des Zersetzungsgrades und der Reaktionsgeschwindigkeit unter Berücksichtigung der effektiven Expansion

Bei der thermischen Spaltung von einzelnen Kohlenwasserstoffen, Modellgemischen und Benzinfraktionen in einem isothermen, isobaren Rohrreaktor benutzten wir für die Beschreibung der Brutto-Zersetzungsgeschwindigkeit eine sogennante integrale und differentiale Methode [13-20]. Das Wesen der Integralmethode besteht darin, daß wir in den integrierten kinetischen Gleichungen erster Ordnung die Konstante der Zersetzungsgeschwindigkeit durch den Ausdruck $k = k^o - \beta X$ ersetzt haben, wo β einen die Inhibitorwirkung der Reaktionsprodukte (Olefine) berücksichtigenden Faktor bedeutet. Bei der Differentialmethode rechneten wir mit einer temperaturabhängigen, von der Einheit abweichenden Reaktionsordnung. Für die Beschreibung der Brutto-Zersetzungsgeschwindigkeit von Gemischen und Benzinfraktionen verwendeten wir dieselben kinetischen Gleichungen wie für einzelne Kohlenwasserstoffe mit dem Unterschied, daß die Konversion einzelner reiner Stoffe durch einen in folgender Gleichung definierten Zersetzungsgrad ersetzt wurde [16,18-20]:

$$X = \sum_{j}^{k} y_j \cdot x_j \qquad (1)$$

wo y_j die Molbrüche der zersetzbaren Komponenten des Ausgangsbenzins, und

x_j die Konversion der zersetzbaren Komponenten des Ausgangsbenzins bedeuten.

Erfahrungsgemäß zeigen die aromatischen Kohlenwasserstoffe des Ausgangsbenzins in der ersten Phase der Reaktion keine Spaltung (ihre Menge nimmt praktisch nicht ab), also können sie vom Standpunkt der Reaktion als inerte Komponenten betrachtet werden. In der Gleichung (1) haben daher ihre Molbrüche den Wert Null.

Der durch die Gleichung (1) definierte Zersetzungsgrad nimmt bei der Pyrolyse von Benzinfraktionen Werte zwischen 0 - 1 an, ähnlich wie die Konversion bei der Thermospaltung reiner Stoffe. Ob X unter gegebenen Pyrolysebedingungen welchen Wert annehmen wird, das hängt vom Molekulargewicht und von der chemischen Konstitution der Benzinkomponenten, das heißt von ihrer Zersetzungsgeschwindigkeit (Thermostabilität) ab. Bei der Pyrolyse von Benzinfraktionen verschiedener Qualität (verschiedener Siedegrenzen und chemischer Zusammensetzung) wird also - sonst unter gleichen Pyrolysebedingungen - auch die Änderung des Zersetzungsgrades verschieden ausfallen.

Ein wesentlicher neuer Zug unserer vorliegender Arbeit im Vergleich zu den Bisherigen besteht darin, daß die Ausarbeitung eines für die Beschreibung der Brutto-Zersetzungsgeschwindigkeit von Benzinfraktionen geeigneten kinetischen Modells auf Grund von in einem nichtisothermen, nichtisobaren Rohrreaktor bei turbulenter Strömung ausgeführten Pyrolyseversuchen erfolgte. Im Verlauf der Pyrolyseversuche erhöhte sich die Temperatur des Reaktionsgemisches - wie es im vorangehenden Abschnitt ausführlich beschrieben ist - von den am Eingangspunkt des Reaktors eingestellten 580 ^{o}C auf 820-850 ^{o}C bei seinem Durchgang durch den Reaktor. Gleichzeitig verminderte sich der Druck von 3,4 - 4,2 atm auf 1,8 - 2,0 atm. Die effektive Aufenthaltszeit des Reaktionsgemisches im Reaktor schwankte zwischen 0,4 - 0,6 s. Ähnliche Parameterwerte gelten auch bei den modernen technischen Pyrolyseöfen.

Temperatur und Druck änderten sich also auch bei konstantem (stationärem) Betrieb des Reaktors von Punkt zu Punkt entlag des Reaktionrohres. Das bedeutet, daß für die Beschreibung der Brutto--Zersetzungsgeschwindigkeit die Bestimmung der kinetischen Konstanten durch die Differentialgleichung eines Elementarabschnittes des Reaktors (Geschwindigkeitsgleichung) erfolgen kann (Differentialmethode).

Die Definitionsgleichung der Reaktionsgeschwindigkeit in einem Durchströmungsreaktor lautet [21, 22, 14]:

$$r = -\frac{dn}{dV_R} = \frac{B_o \cdot C_o \cdot dX}{dV_R} = C_o \cdot \frac{dX}{d\omega} \qquad (2)$$

wo n mol/s der molare Strom des reagierenden (sich zersetztenden) Stoffes,

B_o ℓ/s Volumengeschwindigkeit beim Eintrittspunkt in den Reaktor,

C_o mol/ℓ Konzentration des Ausgangsstoffes (hier der Benzinfraktion) am Eintrittspunkt des Reaktors,

X Konversion des Ausgangsstoffes (hier der charakteristische Zersetzungsgrad der Benzinfraktion),

V_R ℓ Reaktorvolumen,

$\omega = \frac{V_R}{B_o}$ s fiktive Reaktionszeit.

Andererseits, in Kenntnis der aktuellen Konzentration der zersetzenbaren Komponenten der Ausgangsbenzinfraktion kann für die Geschwindigkeit der thermischen Spaltung, ausgedrückt durch die Brutto-Reaktionsgleichung $A \rightarrow \sum_i v_i \cdot R_i$, allgemein geschrieben werden:

$$r = k \cdot C^n = k \cdot \left[\frac{C_o\,(1-X)}{E_e}\right]^n \qquad (3)$$

wo A Symbol der molaren Menge der Ausgangsbenzinfraktion,

R_i Symbol der molaren Menge des i-ten Reaktionsprodukts,

v_i Brutto-Stöchiometriefaktor des i-ten Reaktionsprodukts,

k $(\text{mol}/\ell)^{1-n}\ s^{-1}$ Zersetzungsgeschwindigkeitskonstante

n Brutto-Reaktionsordnung,

$C = \frac{C_o \cdot (1-X)}{E_e}$ mol/ℓ aktuelle Konzentration der zersetzbaren Komponenten der Ausgangsbenzinfraktion,

$X = \sum y_j \cdot x_j$ Zersetzungsgrad

E_e die zum Zersetzungsgrad X zugehörige effektive Expansion.

Die effektive Expansion (E_e) drückt die gemeinsame Wirkung der von der chemischen Reaktion (Zersetzung) verursachten Molzahländerung (chemische Expansion, E_R) und der von Druck und Temperatur verursachten Änderung (physikalische Expansion, E_f) aus:

$$E_e = E_f \cdot E_R \tag{4}$$

Hier ist

$$E_f = \frac{T(z) \cdot P_o}{T_o \cdot P(z)} \quad \text{und} \quad E_R = \frac{E(X) + s}{1 + s}$$

wo T_o die Temperatur (^oK) beim Eintrittspunkt in den Reaktor,

P_o Druck (atm) beim Eintrittspunkt in den Reaktor,

$T(z)$ Temperaturprofil im Reaktor,

$P(z)$ Druckprofil im Reaktor,

s Wasserdampfmenge bezogen auf die eingespeiste Benzinmenge (mol/mol),

$E(X) = 1 + (\sum v_i - 1) \cdot X$ Kohlenwasserstoffexpansion (eine eindeutige Funktion des Zersetzungsgrads).

Die Kohlenwasserstoffexpansion, definiert durch den Quotienten der Molzahlen der aus dem Reaktor austretenden und der in den Reaktor eingespeisten Kohlenwasserstoffe, drückt die während der Zersetzung eintretende Molzahlerhöhung aus [14]. Ihre Änderung in Abhängigkeit vom Zersetzungsgrad (also die E(X)-Funktion) ist für das Raffinat in Abbildung 2 veranschaulicht. Auf Grund der Abbildung kann festgestellt werden, daß unter den angewandten Spaltungsbedingungen die Kohlenwasserstoffexpansion eine eindeutige Funktion des Zersetzungsgrades ist. Die E(X)-Kurve wurde durch eine empirische Funktion genähert.

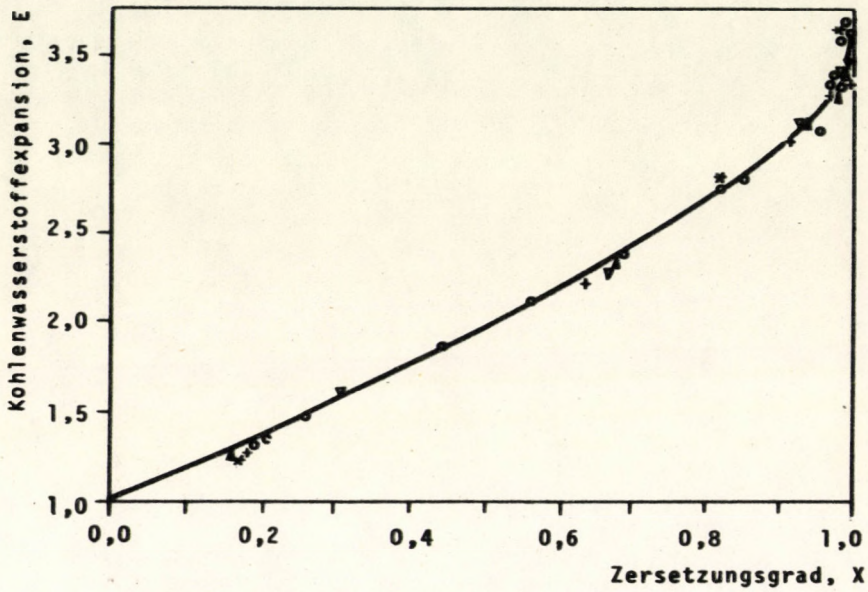

Abb. 2. Kohlenwasserstoffexpansion in Abhängigkeit vom Zersetzungsgrad

Die Kenntnis der effektiven Expansion ist auch bei der Bestimmung der effektiven Reaktionszeit (τ) notwendig, was mit Hilfe der Gleichung:

$$\tau = \int_0^{\omega} \frac{d\omega}{E_e} = \omega_0 \cdot \int_0^{z} \frac{dz}{E_e} \qquad (5)$$

durch numerische Integrierung bestimmt wurde:

wo ω_o s die auf Grund der maßgeblichen Parameter am Eingangspunkt des Reaktors berechnete fiktive Reaktionszeit,

$z = \ell/L$ relative Reaktorlänge bedeuten.

Die Bestimmung der Zersetzungsgeschwindigkeitsleichung sowie der kinetischen Konstanten

Durch Kombination der Gleichung (2) und (3) erhalten wir zur Bestimmung der Brutto-Zersetzungsgeschwindigkeit von Benzinfraktion folgende Geschwindigkeitsgleichung:

$$C_o \frac{dX}{d\omega} = k \left[\frac{C_o \cdot (1 - X)}{E_e}\right]^n \qquad (6)$$

welche durch die Einführung der relativen Reaktorlänge $z = \ell/L$ und nach Substitutirung von $d\omega = \omega_o \cdot dz$ folgende Form annimt:

$$\frac{C_o}{\omega_o} \cdot \frac{dX}{dz} = k \left[\frac{C_o \cdot (1 - X)}{E_e}\right]^n \qquad (7)$$

Zwecks Bestimmung der Konstanten (k und n) wurde die Gleichung (7) linearisiert:

$$\ln\left[\frac{C_o}{\omega_o} \cdot \frac{dX}{dz}\right] = \ln k + n \cdot \ln\left[\frac{C_o\,(1 - X)}{E_e}\right] \qquad (8)$$

Zur Lösung der Gleichung (8) müssen die Differentialquotienten (dX/dz) der als Funktion der relativen Reaktorlänge (z) gemessenen Zersetzungsgradkurven [X(z)] bei gegebenen Temperaturen bestimmt werden. Hierzu ist die Messung wenigstens von zwei solchen X(z)-Kurven nötig, deren Richtungstangenten bei gegebenem T verschieden sind. Dies kann durch Änderung des Temperaturprofils oder der Einspeisegeschwindigkeit erreicht werden. Bei der Pyrolyse des Raffinats wurden 7 solche Kurven gemessen. In der Abbildung 3 wurden als Beispiel die Temperatur- und des Zersetzungsgradverteilungen als Funktion von z in den Versuchsreihen 37 und 40 dargestellt.

Die Richtungstangente der X(z)-Kurve in den zu gegebenen Temperaturen gehörenden Punkten kann durch graphische oder durch numerische Differenzierung bestimmt werden. Da uns eine elektronische

Rechenmaschine zur Verfügung stand, wählten wir die numerische Lösung. Die Versuchspunkte wurden durch eine Funktion vom Typ des Tangens hyperbolicus angenähert. Die in Abbildung 3 kontinuierlich gezeichneten Kurven wurden auf Grund der Näherungsfunktion berechnet. Wie ersichtlich, besteht gute Übereinstimmung zwischen den gemessenen und den gerechneten Werten. Auf die auf Grund des kinetischen Modells berechneten X-Werte kommen wir später zurück.

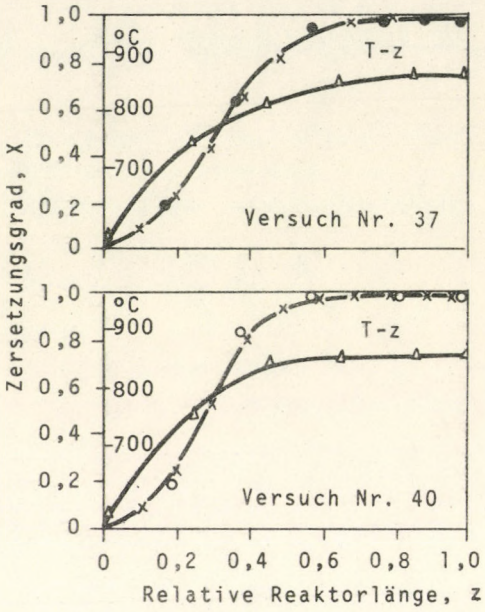

Abb. 3. Änderung der Temperatur und des Zersetzungsgrads in Abhängigkeit von der relativen Reaktorlänge

In der Abbildung 4 ist die nach (8) linearisierte Geschwindigkeitsleichung

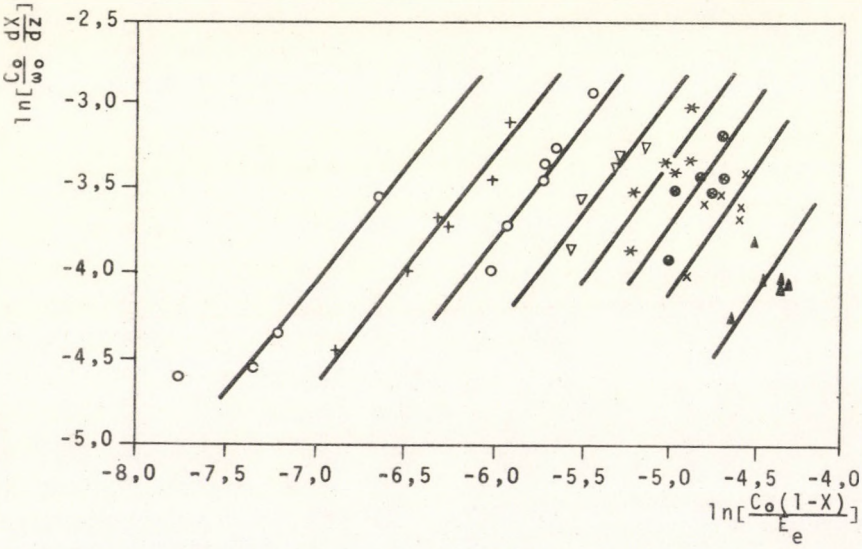

Abb. 4. Darstellung der linearisierten Geschwindigkeitsgleichung für ein Raffinat

des Raffinats wiedergegeben. (Es wurde der Logarithmus der Momentangeschwindigkeit in Abhängigkeit von Logarithmus der aktuellen Konzentration aufgetragen.) Durch die zu gegebenen Temperaturen gehörenden Punkten können mit guter Näherung Geraden gelegt werden, aus deren Richtungstangenten die Brutto-Reaktionsordnung (n) und aus deren Achsenschnitte die Geschwindigkeitskonstante der Zersetzung (ln k) bestimmt werden können. In Abbildung 5 wurde die Änderung der auf diesem Wege bestimmten ln k und n in Abhängigkeit von der reziproken Temperatur dargestellt. Die Temperaturfunktion der Zersetzungsgeschwindigkeitskonstante kann - wie ersichtlich - durch eine Arrhenius-sche Funktion beschrieben werden. Der Wert der Brutto-Reaktionsordnung (n) ändert sich zwischen 1 und 1,5 und nähert sich mit der Erhöhung der Temperatur an die Einheit. Die Änderung der Brutto-Reaktionsordnung als Funktion von 1/T wurde durch die empirische Funktion folgender Form

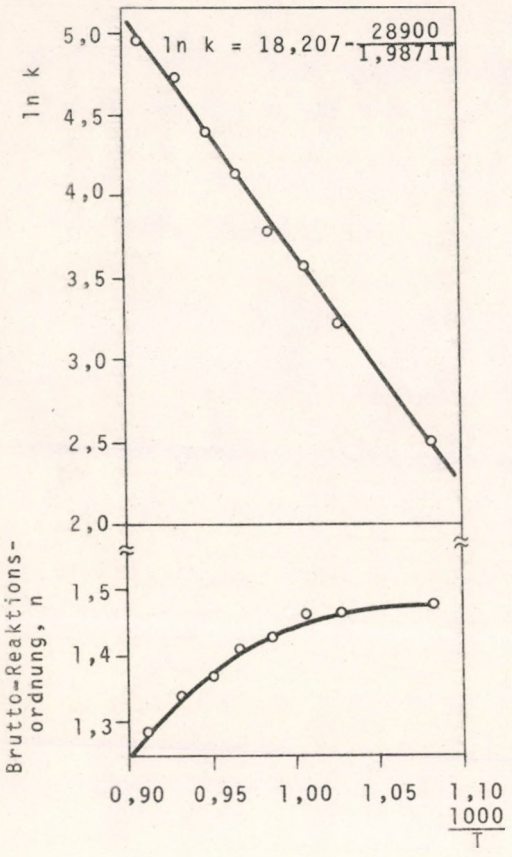

Abb. 5. Darstellung der linearisierten Geschwindigkeitskonstante und der Reaktionsordnung mit der Temperatur

$$n = a + b \cdot \frac{1}{T} + c \cdot \left(\frac{1}{T}\right)^2 \qquad (9)$$

beschrieben. Die Funktion kann innerhalb des für Industrierohröfen wichtigen Temperaturbereichs $0{,}85 < \frac{1000}{T} < 1{,}2$ verwandt werden.

Die beschriebene Methode kann exakt nur auf isotherme Reaktionsbedingungen angewandt werden. (Dann ist nämlich X eine eindeutige Funktion von z.) Da in unserem Falle dieser Umstand nicht gegeben war, können die erhaltenen Werte der Reaktionsordnung und der Aktivierungsenergie als scheinbare Werte angesehen werden, welche aber - wie später gezeigt wird - für praktische Rechnungen (Modellausarbeitung) sehr geeignet sind.

Kinetisches Modell zur Berechnung der Zersetzungsgeschwindigkeit

Zwecks Aufstellung des kinetischen Modells wurde die Geschwindigkeitsgleichung (7) in folgender zweckmäßiger Form geschrieben:

$$dX = \left(\frac{C_o}{E_e}\right)^{n-1} k\,(1 - X)^n \frac{\omega_o}{E_e} \cdot dz \qquad (10)$$

Auf Grund der Gleichung (5) kann hier auch

$$\frac{\omega_o \cdot dz}{E_e} = d\tau$$

eingesetzt, und das Modell statt der Längenkoordinate als Funktion der tatsächlichen Reaktionszeit geschrieben werden. Aus Zweckmäßigkeitsgründen wurde obige Form beibehalten. In der Gleichung (10) sind die Werte C_o und ω_o bei konstanter Einspeisegeschwindigkeit und im stationären Zustand konstant, dagegen ändern sich die effektive Expansion (E_e), die Geschwindigkeitskonstante der Zersetzung (k) sowie die Brutto-Reaktionsordnung (n) kontinuierlich nach der Länge des Reaktionsrohres. Diese Änderung wird durch das Temperatur- und Druckprofil beeinflußt.

Zur Lösung der Gleichung (10) ist also die Kenntnis folgender Größen notwendig:

G_b	kg/h,	Einspeisegeschwindigkeit des Benzins,
G_v	kg/h,	Einspeisegeschwindigkeit des Wassers,
T_o	^oK,	Temperatur an der Stelle z = 0,
P_o	atm,	Druck an der Stelle z = 0,
T(z)		Temperaturprofil,
P(z)		Druckprofil,
k		Temperaturabhängigkeit der Geschwindigkeitskonstante der Zersetzung,
n		Temperaturabhängigkeit der brutto-kinetischen Reaktionsordnung,
E(X)		Kohlenwasserstoff-Expansion.

Zur Näherung der Kohlenwasserstoff-Expansion und des Temperatur- bzw. Druckprofils in Abhängigkeit von z wurden empirische Funktionen angewandt.

Die Lösung der Differentialgleichung (10) kann grundsätzlich über zwei Methoden erfolgen: über eine Umformung zu einer Differenzgleichung und Ausführung der Rechnung auf hintereinandergeschaltete isotherme und isobare Reaktorabschnitte (step-by-step-Methode), oder unter Beibehaltung der Differentialgleichung und Anwendung der in der Richtung der Tangente progressierenden sog. Runge--Kutte-schen Methode.

In der vorliegenden Arbeit wurde aus Zweckmäßigkeitsgründen die sog. step-by-step-Methode angewandt. Hierzu wurde das (insgesamt 22,5 m lange) Reaktionsrohr in 50 gleiche Abschnitte aufgeteilt und die Rechnung auf die so erhaltenen $\Delta z = 0{,}02$ ($\Delta L = 0{,}45$ m) Abschnitte durchgeführt. Als maßgebende Temperatur und Druck eines bestimmten Reaktorabschnitts wurde der arithmetische Mittelwert (T_i', P_i') aus den an den Endpunkten des betreffenden Abschnitts gültigen Temperatur- und Druckwerten angesehen.

Durch Umformung der Differentialgleichung (10) in eine Differenzgleichung und das Aufschreiben für den Reaktorabschnitt i erhält man:

$$\Delta X_i = \left[\frac{C_o}{E_e(z_i)}\right]^{n(T_i')-1} (1 - X_{ij}')^{n(T_i')} \frac{\omega_o k(T_i')}{E_e(z_i')} \Delta z_i \qquad (11)$$

wo Δz_i die relative Länge des i-ten Reaktorabschnitts,

ΔX_i die Erhöhung des Zersetzungsgrades im i-ten Reaktorabschnitts,

$k(T_i')$ den Wert der kinetischen "Konstante" an der Stelle z_i' (in der Mitte des i-ten Reaktorabschnitts),

$n(T_i')$ die Reaktionsordnung an der Stelle z_i'

$X_i' = \sum_1^{i-1} X_i + \frac{\Delta X_i}{2}$ den Wert des Zersetzungsgrads in der Mitte des i-ten Reaktorabschnitts,

$E_f(z_i')$ den Wert der physikalischen Expansion an der Stelle z_i'

$E_R(X_i')$ die zum Zersetzungsgrad X_i' gehörende chemische Expansion,

$E_e(z_i') = E_f(z_i') \cdot E_R(X_i')$ die effektive Expansion an der Stelle z_i' beim Zersetzungsgrad X_i'

C_o die Konzentration des Rohstoffs an der Stelle $z_i = 0$

ω_o die fiktive Reaktionszeit an der Stelle $z_i = 0$ bedeuten.

Das auf der step-by-step Lösung der Änderung des Zersetzungsgrades als eine Funktion der relativen Reaktorlänge beschreibenden Gleichung (11) beruhende kinetische Modell wird als Programm-Blockschema in der Abb. 6 veranschaulicht.

Auf Einzelheiten des Programms kommen wir nicht ausführlich zum Sprechen, sondern beschreiben nur die prinzipiellen Grundzüge der in den einzelnen Programmblocks durchgeführten Berechnungen.

Die Druckverteilung wurde auf Grund der 6 gemessenen Wertpaare durch eine linearisierbare exponentielle Regressionsgleichung mit drei Veränderlichen beschreiben. Die Temperaturprofile der nichtisothermen Abschnitte wurden mit Polynomen genähert.

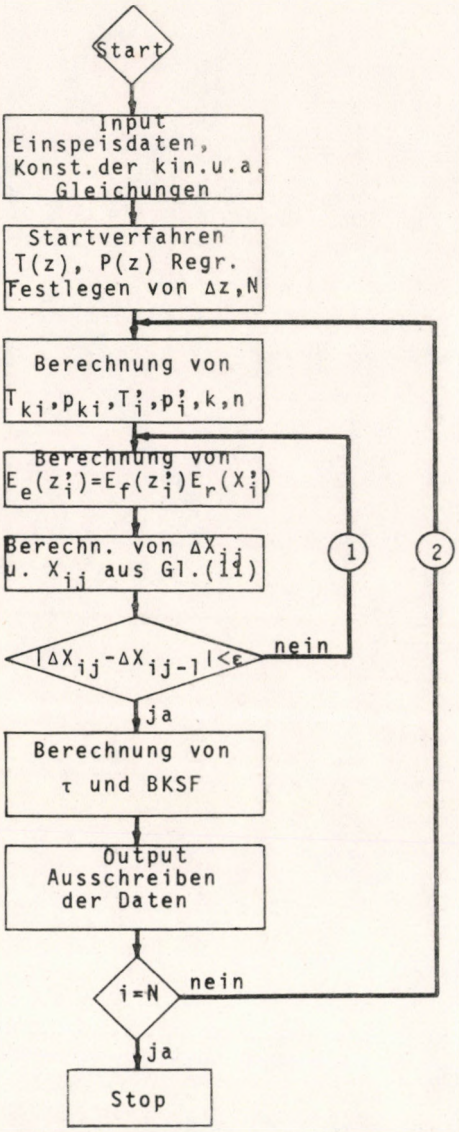

Abb. 6. Programm-Blockschema des kinetischen Modells des Pyrolysereaktors. j = Zahl der Iterationen innerhalb des Reaktorabschnitts; N = Zahl der Reaktorelemente; i = laufender Index der Reaktorelement

Die Berechnung des Zersetzungsgrades erfolgt durch Iteration, während dessen der X'_{ij}-Wert durch wiederholte Korrektion der Expansion und dadurch der tatsächlichen Reaktionszeit immer genauer wird. Die Änderung des gemessenen bzw. berechneten Zersetzungsgrads (X) über die relative Reaktorlänge (z) wurde für ein Raffinat in Abb. 7 dargestellt. Die auf Grund des Programms berechneten Werte sind auch aus der Abbildung 3 ersichtlich.

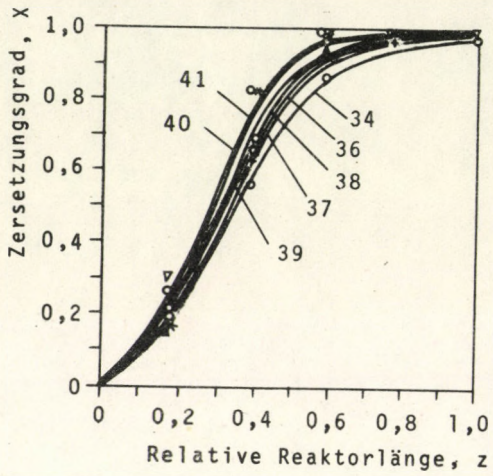

Abb.7. Änderung des Zersetzungsgrads in Abhängigkeit von der relativen Reaktorlänge

Die Berechnung der tatsächlichen Aufenthaltszeit in dem Reaktor erfolgt durch Summierung der durch Iteration bestimmten maßgebenden Teil-Aufenthaltszeiten:

$$\tau = \omega_o \sum_{i=1}^{N} \frac{\Delta z_i}{E_e(z'_i)} \tag{12}$$

Brutto-kinetische Strengheitsfunktion

Die Differentialgleichung (7) bzw. (10) kann nach zweckmäßiger Umformung und Bestimmung der Integrationsgrenzen auf folgende Form gebracht werden:

$$\int_o^X \frac{dX}{(1-X)^n} = \int_o^z \left(\frac{C_o}{E_e}\right)^{n-1} k \frac{\omega_o \, dz}{E_e} \tag{13}$$

Beide Seiten dieser Gleichung sind dimensionslos. Das Integral der rechten Gleichungsseite drückt im Wesentlichen die Streng-

heit der Pyrolyse der durch die Brutto-Geschwindigkeitskonstante k gekennzeichneten Benzinfraktion, im Reaktorabschnitt 0 - z, bei vorgegebenem Temperatur- und Druckprofil und bestimmten Einspeiseparameters (C_o, ω_o) aus. Zu diesem Strengheitsgrad gehört eine Spaltung bestimmter Tiefe, was durch das Integral der linken Seite representiert wird.

Da die durch das Integral der rechten Seite der Gleichung (13) definierte Strengheit die Brutto-Zersetzungsgeschwindigkeitskonstante der Benzinfraktion enthält, wurde dieser Zusammenhang als brutto-kinetische Strengheitsfunktion genannt und weiter mit BKSF bezeichnet:

$$BKSF = \int_o^z \left(\frac{C_o}{E_e}\right)^{n-1} k \frac{\omega_o \, dz}{E_e} \tag{14a}$$

oder, da:

$$\frac{\omega_o \, dz}{E_e} = d\tau,$$

wird

$$BKSF = \int_o^\tau \left(\frac{C_o}{E_e}\right)^{n-1} k \, d\tau \tag{14b}$$

Die auf Grund der Gleichungen (13) und (14) definierte brutto-kinetische Strengheitsfunktion (BKSF) ist sowohl formell wie auch nach ihrem physikalischen Inhalt der von ZDONIK und Mitarbeitern [4] definierten kinetischen Strengheitsfunktion (KSF) analog:

$$KSF = \int_o^Q k_s \cdot dQ \tag{15}$$

wo k_s s^{-1} die Reaktionsgeschwindigkeitskonstante des n-Pentans unter Voraussetzung einer Zersetzungskinetik erster Ordnung, und

Q s die Reaktionszeit bedeuten.

Auf Grund der von Zdonik und Mitarbeitern definierten kinetischen Strengheitsfunktion kann berechnet werden, daß unter gegebenen Bedingungen der thermischen Spaltung (bei gegebenem KSF-Wert),

welche Konversion des n-Pentans eintreten würde, vorausgesetzt, daß die Spaltung durch eine kinetische Funktion erster Ordnung beschrieben werden kann. Sie ist in erster Linie zur zahlenmäßigen Charakterisierung der Strengheit der Pyrolysebedingungen geeignet, steht jedoch nicht in Verbindung mit den tatsächlichen Spaltvorgängen im Rohrreaktor.

Die Einführung der brutto-kinetischen Strengheitsfunktion (BKSF) an Stelle des Zersetzungsgrades (X) bei der Pyrolyse von Benzinfraktionen wird dadurch begründet, daß im Gebiet $X > 0{,}95$ das für die Untersuchung und Beschreibung der technischen Reaktoren wichtig ist - infolge Verlängerung der Skala - eine genauere Bestimmung und Berechnung der Ausbeutekurven ermöglicht wird (s. den zweiten Teil dieser Arbeit).

Den zahlenmäßigen Zusammenhang zwischen dem Zersetzungsgrad (X) und der brutto-kinetischen Strengheitsfunktion (BKSF) veranschaulicht für die Pyrolyse eines Raffinats die Abbildung 8. Auf Grund der Abbildung ist der Zusammenhang zwischen den beiden Veränderlichen eindeutig, und es geht hervor, daß bei hohen Zersetzungsgraden die BKSF sich in viel höherem Maße ändert als X.

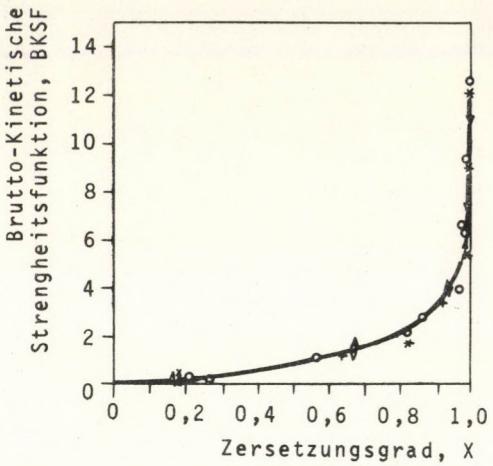

Abb.8. Zusammenhang zwischen der brutto-kinetischen Strengheit und dem Zersetzungsgrad bei der Pyrolyse des Raffinats

Die durch die Gleichungen (13) und (14) definierte brutto-kinetische Strengheitsfunktion (BKSF) ist der in Gleichung (1) definierten Zersetzungsgrad (X) ähnlich dimensionslos, wodurch die unmittelbare Obertragung der Ausbeutekurven bzw. des kinetischen Modells auf größere Reaktoren (Rohröfen) ermöglicht wird.

Das Programm des kinetischen Modells berechnet die Werte der brutto-kinetischen Strengheitsfunktion (BKSF) aus folgender Gleichung:

$$BKSF = \omega_o \sum_{i=1}^{N} \left[\frac{C_o}{E_e(z_i')} \right]^{n(T_i')-1} \frac{k(T_i')}{E_e(z_i')} \Delta z_i \qquad (16)$$

LITERATUR

1. LAMBRIX, J.R., MORRIS, C.S., Chem. Eng. Progr. 68, 24 (1972)
2. LINDEN, H.R., REID, J.M., Chem. Eng. Progr. 55, 71 (1959)
3. KNAUS, J.A., YARZE, J.C., CAMPBELL, W.M., Sixth World Petroleum Congress in Frankfurt/Main, 1963. Section IV - Paper 31.
4. ZDONIK, S.B., GREEN, E.J., HALLE, L.P., The Oil and Gas J., 1967, July 10. pp. 192.
5. de BLIECK, J.L., GOOSSENS, A.G., Hydrocarbon Proc., 1971, No.3. 76.
6. KERSHENBAUM, L.S., MARTIN, J.J., A.I.Ch.E. Journal, 13, 148 (1967)
7. KUNZRU, D., SHAH, Y.T., STUART, E.B., Ind. Eng. Chem., Process Des. Develop., 11, 605 (1972)
8. LEFTIN, H.P., CORTES, A., Ind. Eng. Chem., Process Des. Develop., 11, 613 (1972)
9. ILLÉS, V., RAUSCHENBERGER, J., SZEPESY, L., Magyar Kémikusok Lapja 26, 624 (1971)
10. ILLÉS, V., SZEPESY, L., CSIKÓS, R., RAUSCHENBERGER, J., Erdöl und Kohle 25, 589 (1972)
11. SIMON, J., SZEPESY, L., MÁFKI Közl. (MÁFKI Mitteil.) 9, 47 (1968)
12. SZEPESY, L., ILLÉS, V., WELTHER, K., SIMON, J., Acta Chim. Acad. Sci. Hung. 78, 341 (1973)

13. ILLÉS, V., Szénhidrogéngázok pirolizise laboratóriumi csőreaktorban. (Pyrolyse von Kohlenwasserstoffgasen im Laboratoriumsröhrenreaktor.) (Habilitationsarbeit) Veszprém, 1967.

14. ILLÉS, V., Acta Chim. Acad. Sci. Hung. 59, 35 (1969); ibid 59, 229 (1969); ibid 67, 41 (1971); ibid 67, 339 (1971)

15. ILLÉS, V., Erdöl u. Kohle 25, 464 (1972); ibid 25, 542 (1972)

16. ILLÉS, V., Acta Chim. Acad. Sci. Hung. 72, 117 (1972); ibid 72, 133 (1972)

17. ILLÉS, V., WELTHER, K. PLESZKÁTS, I., Acta Chim. Acad. Sci. Hung. 78, 357 (1973)

18. ILLÉS, V., WELTHER, K., SZEPESY. L., Hung. J. Ind. Chem. 1, 89 (1973)

19. ILLÉS, V., WELTHER, K., SZEPESY, L., The 2nd Conference of Hungarian Chemical Society, Some Applications of Physical Chemistry, Veszprém (Hungary), August 2-5. Vol. 2, 257 (1971)

20. ILLÉS, V., PLESZKÁTS, I., Acta Chim. Acad. Sci. Hung. 80, 247 (1974)

21. FROST, A.A., PEARSON, Kinetics and Mechanism. A Study of Homogeneous Chemical Reactions. New York, London, 1953. p. 183.

22. BENEDEK, P., LÁSZLÓ, A., A vegyészmérnöki tudomány alapjai (Fundamentals of chemical engineering science). Müszaki Könyvkiadó, Budapest, 1964. p. 328.

РЕЗЮМЕ

Авторами был изучен пиролиз рафината с температурой кипения 42,5-120 °С в трубчатом реакторе крупнолабораторного размера, пригодном на симуляцию промышленных трубчатых печей. Экспериментально было установлено распределение в реакторе температуры, давления и продуктов.

Полагая кинетику n-ной степени, авторы выработали метод на описание валовой скорости разложения рафината (дистиллята бензина) по экспериментальным данным, полученным при неизотермических и неизобарияеских условиях. С использованием полученных кинетических констант составили кинетическую модель и вычислительную программу для вычиления степени разложения и валовой кинетической функции требоватеяьности.

Hungarian Journal
of Industrial Chemistry
Veszprém
Vol.3. pp. 391-410 (1975)

KINETISCH-MATHEMATISCHES MODELL DER BENZINPYROLYSE II

PRODUKTVERTEILUNG, AUSBEUTEKURVEN, KINETISCH-MATHEMATISCHES MODELL

V. ILLÉS und A. HORVÁTH

(Ungarisches Erdöl- und Erdgasforschungsinstitut, Veszprém)

Eingegangen am 10. Februar 1975

Im großlaboratoriumsmäßigen Rohrreaktor wurden die Änderung der Ausbeuten der Reaktionsprodukte in Abhängigkeit vom Zersetzungsgrad und von der Strengheit der Pyrolyse eines Raffinats untersucht. Es wurde gefunden, daß mit Ausnahme einiger Produkte (z.B. des Wasserstoffs, des Äthylens) die Ausbeute der Produkte, in Abhängigkeit von den angegebenen Variablen, und unabhängig von der Austrittstemperatur und vom Temperaturprofil, durch je eine einzige Kurve dargestellt werden kann. Die Ausbeutekurven wurden durch mathematische Funktionen vier verschiedener Typen genähert.

Durch Verknüpfung der die Bruttozersetzungsgeschwindigkeit beschreibenden kinetischen Funktionen mit den die Ausbeutekurven beschreibenden mathematischen Gleichungen wurde ein zur Berechnung der Produktverteilung geeignetes kinetisch-mathematisches Modell und Computerprogramm des Rohrreaktors für die Benzinpyrolyse ausgearbeitet.

In unserer früheren Mitteilung [1] wurden zur zahlenmäßigen Kennzeichnung der Spaltung (der Strengheit) zwei grundlegende Variablen definiert.

Dies waren:

a) der Zersetzungsgrad (X) und

b) die brutto-kinetische Strengheitsfunktion (BKSF).

Zwischen diesen beiden Variablen stellt die brutto-kinetische Funktion eine eindeutige Verbindung her, auf Grund deren in Kenntnis einer der Variablen die Werte der anderen berechnet werden können. Vom Standpunkt der Beschreibung des Vorgangs sind also beide Variablen gleichwertig. Anders steht es mit der praktischen Verwendung. Dies wird weiter unten ausführlicher dargestellt.

Produktverteilung

Die Untersuchung und Bedeutung der Produktverteilung in Abhängigkeit vom Zersetzungsgrad

In den Abbildungen 1 - 6 wurden die Ausbeutedaten in Gew.% einiger wichtigerer Produkte der Pyrolyse des Raffinats in Abhän-

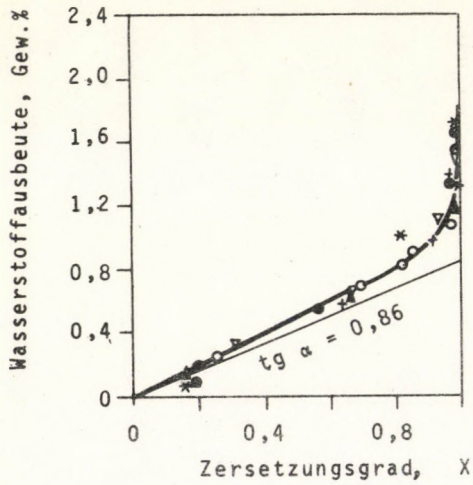

Abb.1. Änderung der Wasserstoffausbeute mit dem Zersetzungsgrad

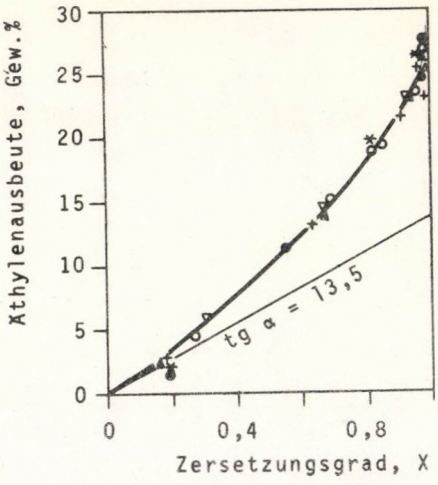

Abb.2. Änderung der Äthylenausbeute mit dem Zersetzungsgrad

gigkeit vom Zersetzungsgrad (X) gezeigt. In die Abbildungen wurde die am Austrittsende und an den Zwischenstellen der Probenahme erhaltenen sämtlichen Werte eingetragen. (Zur Kennzeichnung der ein-

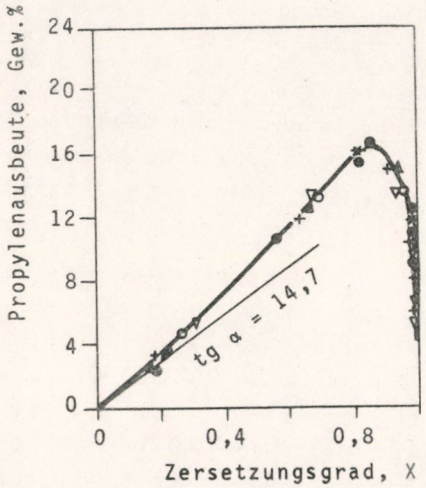

Abb. 3. Änderung der Propylenausbeute mit dem Zersetzungsgrad

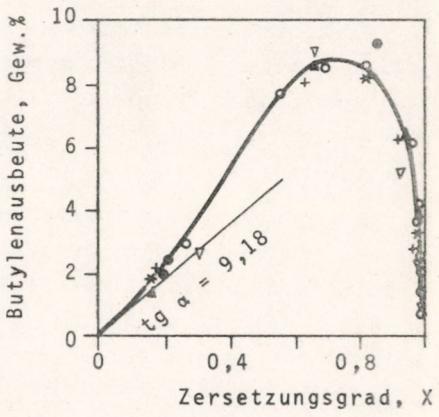

Abb. 4. Änderung der Butylenausbeute mit dem Zersetzungsgrad

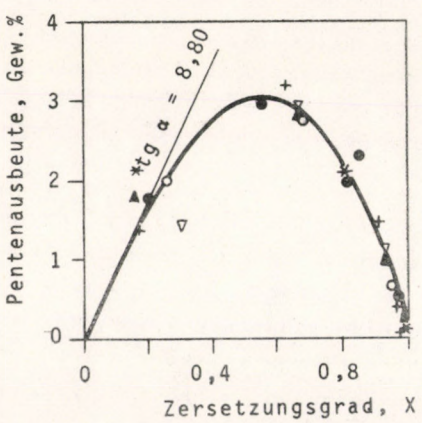

Abb. 5. Änderung der Pentenausbeute mit dem Zersetzungsgrad

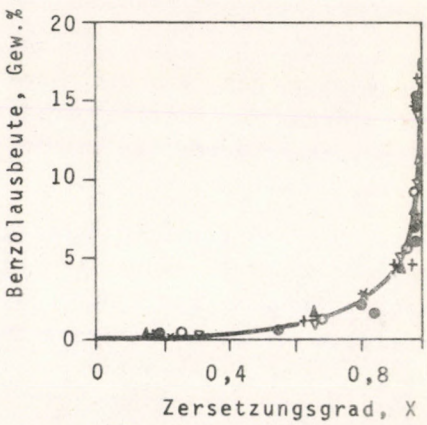

Abb. 6. Änderung der Benzolausbeute mit dem Zersetzungsgrad

zelnen Meßserien wurden auch hier die Bezeichnungen der Tabelle 1 aus unserer Mitteilung I angewandt.) Auf Grund der Abbildungen können mehrere wichtige Feststellungen getroffen werden.

Es konnte unter anderen festgestellt werden, daß parallel zur Erhöhung des Zersetzungsgrades sehr bedeutende Änderungen in der mengenmäßigen Produktverteilung eintreten, welche in der Abweichung der Ausbeutekurven von ihren Tangenten im Anfangsabschnitt zum Vorschein kommen.

Es konnte weiter festgestellt werden, daß unter den von uns eingestellten Bedingungen der thermischen Spaltung fast alle Messpunkte für jedes Produkt nur je eine einzige Ausbeutekurve bestimmen. Das bedeutet praktisch, daß die Ausbeuten dieser Produkte unempfindlich gegenüber der Austrittstemperatur, bezichungsweise der Form des Temperaturprofils, d.h. eine eindeutige Funktion des Zersetzungsgrads bleiben. Die Werte der Ausbeute für Wasserstoff und Äthylen (und in geringerem Maße auch für Äthan) sind von der Austrittstemperatur und vom Temperaturprofil abhängig. Dies geht aus den als Funktion des Zersetzungsgrads aufgezeichneten Abbildungen nicht immer hervor, da die Erscheinung im Allgemeinen bei Werten von $X > 0{,}95$ des Zersetzungsgrads auftritt und in diesem Gebiet die Lage der Ausbeutekurven nicht eindeutig feststellbar ist.

Die später gezeigten und als Funktion der BKSF aufgezeichneten Abbildungen (7 und 8) veranschaulichen, daß bei Einstellung einer höheren Austrittstemperatur und eines steileren Temperaturprofils höhere Werte für die Ausbeute an Wasserstoff und an Äthylen erreicht werden können.

Die Temperaturunabhängigkeit der als Funktion der Konversion aufgezeichneten Ausbeutekurven haben wir zuerst bei der Pyrolyse von Kohlenwasserstoffgasen in einem Laboratoriums-Rohreaktor festgestellt [2-4]. Diese Erscheinung wird dadurch erklärt, daß die an der Bildung der Produkte beteiligten Elementar-(Radikal-)-Reaktionen in Bezug auf ihre Aktivierungsenergien sich nicht wesentlich von einander unterscheiden, also ändern sich ihre relativen Geschwindigkeiten bei einer Temperaturerhöhung nicht oder nur sehr geringfügig. Wesentlich ist jedoch der Unterschied in der Aktivierungsenergie der Zersetzungs- beziehungsweise der Wasserstoff-Ab-

Tabelle 1. Ausbeute der gasförmigen und der wichtigeren flüssigen Produkte bei verschiedener Prozeßführung der Pyrolyse eines Raffinats

Produkte	Produktausbeuten, Gew.%					
	Äthylenmaximum		Olefin-maximum	Propylen-maximum	Butadien-maximum	Butilen maximum
	BKSF=8,0	BKSF=7,0	BKSF=2,7	BKSF=2,5	BKSF=2,2	BKSF=1,7
Gasförmige Produkte:						
Wasserstoff	1,49	1,42	0,90	0,88	0,83	0,70
Methan	25,05	24,50	15,86	15,20	14,10	11,90
Äthylen	27,00	25,70	19,75	19,10	17,90	15,70
Propylen	9,20	10,60	16,20	16,40	16,10	14,82
Äthan	4,10	4,30	4,60	4,60	4,50	4,10
Propan	0,35	0,42	0,69	0,64	0,62	0,56
Azetylen	0,30	0,27	0,07	0,06	0,04	0,02
Butan	0,13	0,14	0,30	0,33	0,35	0,43
Butylen	1,93	2,50	7,50	7,80	8,20	8,50
Butadien	2,20	2,66	4,60	4,75	4,83	4,90
Gasausbeute (C_4 und niedriger)	71,75	72,51	70,47	69,76	67,47	61,62
Wichtigere flüssige Produkte:						
Pentadien	0,70	0,80	1,70	1,77	1,73	1,58
c-Pentadien	1,50	1,55	0,90	0,85	0,77	0,63
Benzol	10,35	9,30	3,60	3,30	2,70	1,90
Toluol	8,00	8,10	7,40	7,40	7,25	7,10
Xylol	0,57	0,54	0,25	0,23	0,21	0,17
Äthylbenzol	0,32	0,39	0,48	0,43	0,41	0,38
Styrol	2,63	2,50	0,70	0,65	0,55	0,38
Inden	0,79	0,70	0,15	0,11	0,07	0,03
C_5-Fraktion	2,54	2,71	8,13	8,86	9,94	12,14
Pyrobenzin (C_5-C_9)	25,95	25,35	29,18	29,96	32,33	38,30
Schweres Kondensat	2,30	2,14	0,35	0,29	0,20	0,08

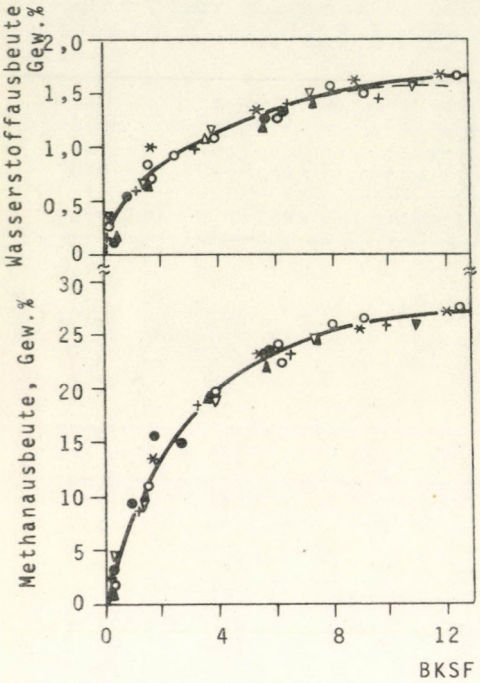

Abb. 7. Änderung der Wasserstoff- und der Methanausbeute in Abhängigkeit von der brutto-kinetischen Strengheit

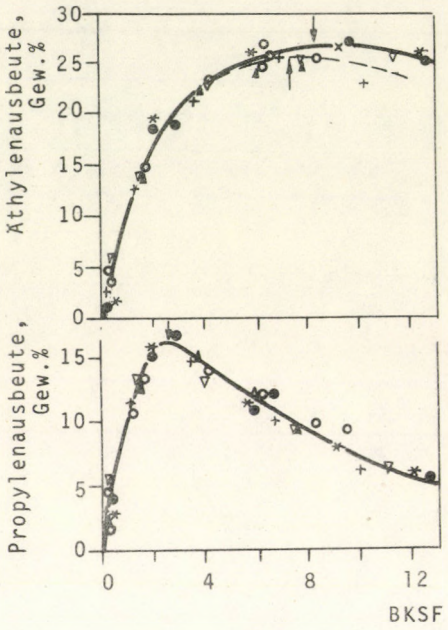

Abb. 8. Änderung der Äthylen- und der Propylenausbeute in Abhängigkeit von der brutto-kinetischen Strengheit

spaltreaktion der Äthylradikale (erstere beträgt 40 kcal/mol, letztere etwa 7 kcal/mol). Deshalb nimmt die Geschwindigkeit der unter Bildung von Äthylen und Wasserstoff verlaufenden Zersetzungsreaktion $C_2H_5 \rightarrow C_2H_4 + H$ des Äthylradikals im Verhältnis zu derjenigen der Wasserstoff-Abspaltreaktion $C_2H_5 + M_p \rightarrow C_2H_6 + R_2$, welche unter Äthanbildung verläuft, bei Erhöhung der Temperatur, zu. Dadurch ergibt sich bei einem gegebenen brutto Zersetzungsgrad eine erhöhte Wasserstoff- und der Äthylenmenge.

Die Ausbeutekurven des Wasserstoffs (Abb. 1) und des Methans verlaufen stets oberhalb der Tangenten zu ihren Anfangsabschnitten, die relative Menge dieser Produkte nimmt also mit der Erhöhung des

Zersetzungsgrads im ganzen Konversionsbereich zu. (Die relative Menge bedeutet hier die bei der Zersetzung der Einheitsmenge des Benzindestillats gebildete Menge des Produkts.)

Es kann festgestellt werden, daß die Ausbeutekurven der Olefin-Kohlenwasserstoffe im Produkt mit Ausnahme des Äthylens Maxima aufweisen. (Aus den in Funktion der BKSF gezeigten Abbildungen wird es später ersichtlich, daß auch die Ausbeutekurve des Äthylens ein Maximum aufweist.) Aus den Abbildungen geht auch hervor, daß mit zunehmendem Molekulargewicht der Olefine die Lage dieser Maxima in den Bereich geringerer Zersetzungsgrade verschoben wird. Die Ausbeutekurven der Diolefine weisen ebenfalls Maxima auf, die Lage diese Maxima ergibt sich im Allgemeinen bei etwas höheren X-Werten als bei den Olefinen mit gleicher Kohlenstoffatomzahl.

Die Ausbeutekurven des Äthylens, Propylens und Butylens liegen oberhalb der Tangenten zu ihren Anfangsabschnitten, die relative Menge dieser Produkte nimmt also mit der Erhöhung der Konversion zu.

Die Ausbeutekurven des Pentens, Hexens und der höheren Olefin-Kohlenwasserstoffe liegen dagegen unterhalb der Richtungstangenten der Anfangsabschnitte (s. z.B. die Abb. 5), und die relative Menge dieser Produkte nimmt also mit Zunahme des Zersetzungsgrades ab.

Wie bereits früher an Hand der Pyrolyse von einzelnen Kohlenwasserstoffen und von Modellgemischen gezeigt wurde [3-6], wird diese Erscheinung in erster Linie durch Vereinigungsreaktionen zwischen den höhermolekularen olefinischen Kohlenwasserstoffen [Hepten, Hexen, Penten, Butylen, symbolische Bezeichnung: $(Olefin)_1$] und den im Reaktionsgemisch vorhandenen kettentragenden Radikalen, in erster Linie den Wasserstoffatomen (Bezeichnung R_1), sowie darauffolgende Zersetzung der Alkylradikale verursacht:

$$(Olefin)_1 + R_1 \rightleftharpoons Alkylradikal \rightarrow (Olefin)_2 + R_1' \qquad (1)$$

Durch diese Reaktionen werden aus den primär gebildeten Olefin-Kohlenwasserstoffen Olefin-Kohlenwasserstoffe mit um eine oder zwei Einheiten geringerer Kohlenstoffatomzahl [Bezeichnung: (Ole-

fin)$_2$] sowie Methyl- oder Äthylradikale (Bezeichnung $R_1^!$) gebildet. Die Geschwindigkeit dieser Reaktionen wird in entscheidender Weise durch die Konzentration der höheren Olefin-Kohlenwasserstoffe bestimmt, welche proportional zur Konversion zunimmt. In der Verschiebung der Reaktion (1) in die Richtung der Bildung der (Olefine)$_2$ spielt auch die Isomerisierung der während der Vereinigungsreaktionen entstandenen Alkylradikale vermutlich eine wichtige Rolle.

Über das angegebene Reaktionsschema entstehen z.B. aus dem 1-Hexen durch Wasserstoffaddition und darauffolgende Zersetzung Propylen, Äthylen und Methylradikale, aus dem 1-Penten Propylen und Äthylradikale und aus dem 1-Butylen Propylen und Methylradikale. Die Isomerisation der in den Vereinigungsreaktionen gebildeten Radikale öffnet neue Reaktionswege bei der Zersetzung der Radikale. Wie wir sahen, liegen die Ausbeutekurven des Pentens und Hexens unterhalb der Tangenten zu dem Anfangsabschnitten der Kurven, bei einer Erhöhung des Zersetzungsgrades vermindert sich daher ihre relative Menge, was mit den vorstehend Gesagten im Einklang steht. Das durch die Zersetzung des Hexens, des Pentens (und Butylens) entstandene Propylen kommt zum in der primären Zersetzungsreaktion entstandenen Propylen hinzu, also nimmt die relative Menge des Propylens bei der Erhöhung der Konversion zu, obwohl gleichzeitig auch die Zersetzung des Propylens stattfindet. Jedoch ist die Zersetzungsgeschwindigkeit des Propylens geringer als diejenige des Butylens [3-5].

Bei höherer Konversion wird die Produktverteilung erheblich beeinflußt auch durch die Reaktionen mit Wasserstoffabspaltung zwischen den Olefin-Kohlenwasserstoffen und den Radikalen der Kettenfortpflanzung. In diesen Reaktionen werden Vinyl-, Allyl- und höhere ungesättigte Radikale gebildet. Die Reaktion dieser Radikale untereinander und mit den Olefin-Kohlenwasserstoffen im Reaktionsgemisch führt zur Bildung von höhermolekularen Dien- und aromatischen Kohlenwasserstoffen. Die Menge der aromatischen Kohlenwasserstoffe nimmt im Gebiet $X > 0{,}6$ mit der Erhöhung der Zersetzungsgrads rasch zu (s. Abb. 6).

Auf Grund der angegebenen Sekundärreaktionen können die Maxima der Ausbeutekurven der Olefin-Kohlenwasserstoffe gedeutet werden.

Auf Grund der angegebenen Abbildungen können die Ausbeutekurven der Reaktionsprodukte folgenden Haupttypen zugeordnet werden:

a) vom Nullpunkt ausgehende, allmählich zunehmende, konkave Kurven (Ausbeutekurven des Wasserstoffs, Methans und Äthylens),

b) vom Nullpunkt ausgehende, allmählich zunehmende, nach dem Maximum rasch abfallende, gegen Null konvergierende Kurven (Ausbeutekurven der Olefine und Diolefine),

c) von einem bestimmten Anfangswert ausgehende, allmählich abnehmende (gegen Null konvergierende) Kurven ("Ausbeutekurven" der Benzinkomponenten im Rohstoff),

d) von einem bestimmten Anfangswert ausgehende, etwa bis $X = 0{,}5$ horizontale, dann rasch zunehmende Kurven (Ausbeutekurven des Benzols, Toluols, der Xylole und anderer Aromaten).

Auf Grund der als Funktion des Zersetzungsgrads aufgezeichneten Ausbeutekurven kann die Änderung der Ausbeuten der Reaktionsprodukte im Bereich zwischen $0 < X < 0{,}95$ des Zersetzungsgrads eindeutig beschrieben werden. Bei der Pyrolyse von Kohlenwasserstoffgasen in industriellen Rohrreaktoren bleibt die Konversion der Ausgangskohlenwasserstoffe in allen Fällen unterhalb 0,95. In diesen Fällen sichert die Darstellung der Änderung der Produktausbeuten in Abhängigkeit von der Konversion eine praktisch anwendbare Möglichkeit zur Ausarbeitung des kinetisch-mathematischen Modells des Rohrofens, da die Änderung der Konversion in Abhängigkeit von den Parametern der Reaktion durch brutto-kinetische Zusammenhänge beschrieben werden kann [7].

Bei der Pyrolyse von Benzinfraktionen - insbesondere unter den strengen Bedingungen der modernen Rohröfen - werden die Komponenten des Ausgangsbenzins vollständig zersetzt (s. z.B. die Abb. 10), und so nimmt also der Ausdruck $(\sum y_j x_j)$ des Zersetzungsgrads einen sehr nahe bei 1 liegenden Wert an. Wie gesehen, kann unter diesen Bedingungen die Lage der Ausbeutekurven in Abhängigkeit vom

Zersetzungsgrad nicht eindeutig festgelegt werden. Daraus entstand die Notwendigkeit der Einführung der brutto-kinetischen Strengheitsfunktion (BKSF) zur Darstellung und Beschreibung der Produktausbeuten.

Produktverteilung in Abhängigkeit der brutto-kinetischen Strengheits-Funktion (BKSF)

Im vorigen Abschnitt wurde dargelegt, daß bei der Pyrolyse von Benzinfraktionen der Zersetzungsgrad im Bereich $X > 0,95$ eine praktisch ungeeignete Variable zur Kennzeichnung der Strengheit der Spaltung und zur Beschreibung der Produktausbeuten darstellt. Deshalb wurden die detaillierte Verarbeitung des Versuchsmaterials sowie die Ausarbeitung eines für die Berechnung des Rohrofens geeigneten kinetisch-mathematischen Modells unter Verwendung der BKSF unternommen.

In den Abbildungen 7 - 11 sind die Ausbeutekurven der bei der Pyrolyse des Raffinats erhaltenen 12 wichtigeren Produkte dargestellt. Die Ausbeutekurven wurden unter Berücksichtigung sämtlicher Messpunkte (einschließlich der Zwischenpunkte) in Abhängigkeit der BKSF konstruiert.

Die erste wichtige Feststellung auf Grund der Abbildungen ist die abweichende Form dieser Kurven von denjenigen der Ausbeutekurven als Funktion des Zersetzungsgrads (X). Diese Darstellungsart zieht den für den Betrieb der industriellen Rohröfen wichtigen Bereich $X > 0,95$ weit auseinander, dadurch kann die Lage der Ausbeutekurven auch in diesem Bereich eindeutig bestimmt werden.

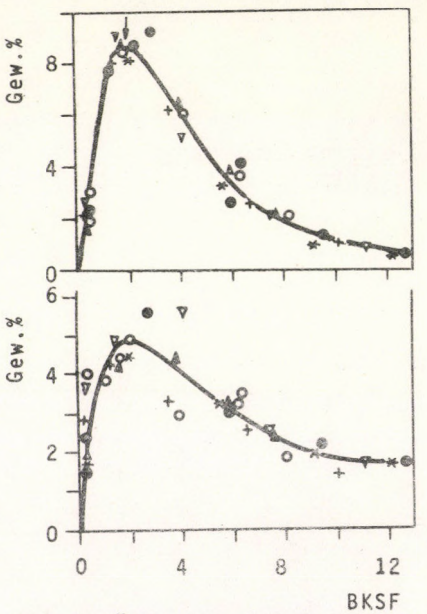

Abb.9. Änderung der Butylen- und der Butadienausbeute in Abhängigkeit von der brutto--kinetischen Strengheit

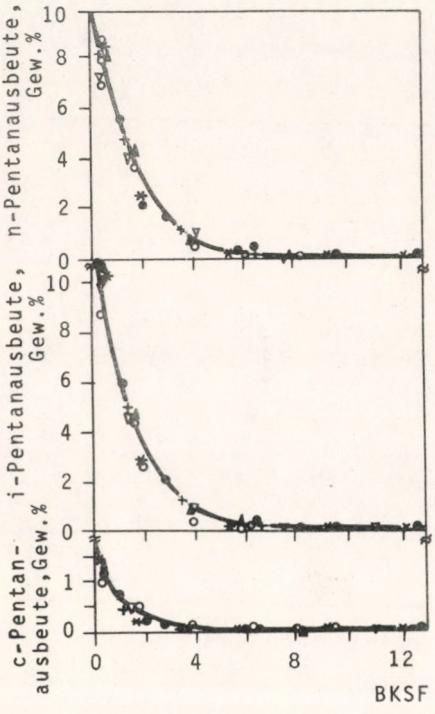

Abb. 10. Änderung der n-Pentan, der i-Pentan- und der Cyklopentanausbeute in Abhängigkeit von der brutto-kinetischen Strengheit

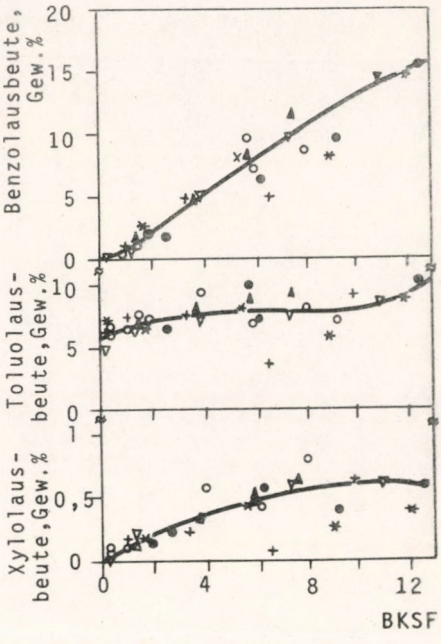

Abb. 11. Änderung der Benzol-, der Toluol- und der Xylolausbeute in Abhängigkeit von der brutto-kinetischen Strengheit

Die andere wichtige Beobachtung besteht darin, daß mit Hilfe dieser Darstellung das Maximum der Äthylenausbeute ebenfalls nachgewiesen werden und die Werte der maximalen Äthylenausbeute bei verschiedener Prozeßführung bestimmt werden konnten.

Ferner kann festgestellt werden, daß mit Ausnahme des Äthylens und des Wasserstoffs die Ausbeutekurven der Reaktionsprodukte auch in dieser Darstellungsweise gegenüber der Austrittstemperatur beziehungsweise dem Temperaturprofil unveränderlich sind. Im Falle des Wasserstoffs und des Äthylens ergibt eine höhere Austrittstemperatur beziehungsweise ein steileres (II.) Temperaturprofil - bei unverändertem Zersetzungsgrad - eine höhere Ausbeute. Dies steht

in vollkommener Übereinstimmung mit den über den Mechanismus der Spaltung im vorigen Abschnitt Gesagten.

Die Ausbeuten der einzelnen Reaktionsprodukte in Abhängigkeit von der BKSF ergeben ebenfalls charakteristische Kurventypen, wodurch die Beschreibung der Ausbeutekurven mit Hilfe mathematischer Funktionen erleichtert wird.

a) Die Expansion sowie die Ausbeute an Wasserstoff und Methan ergeben stetig zunehmende konvexe Kurven,

b) die Ausbeutekurven der Olefine und der Diolefine weisen Maxima auf, die Lage des Maximums verschiebt sich mit zunehmendem Molekulargewicht gegen kleinere BKSF-Werte,

c) die Ausbeutekurven der Komponenten des Ausgangsbenzins beginnen bei bestimmten Anfangswerten, und weisen einen exponentiellen Abfall bis auf Null auf,

d) die Ausbeutekurven der Aromaten beginnen bei bestimmten Anfangswerten, und nehmen stetig zu.

An den Ausbeutekurven des Äthylens, Propylens, Butylens und Butadiens wurden die zur maximalen Ausbeute gehörenden BKSF-Werte angegeben und es wurde die Materialbilanz bei verschiedener Prozeßführung bestimmt. Die Ausbeuteergebnisse der Hauptprodukre für die Pyrolyse des Raffinats sind in der Tabelle I enthalten.

Wie die Tabelle zeigt, können bei der Pyrolyse des Raffinats bei strenger Äthylen-Prozeßführung (T_{aus} = 850 °C, Temperaturprofil II) 27,0 Gew.% Äthylen, 9,2 Gew.% Propylen und 10,35 Gew.% Benzol erhalten werden. Bei einer Äthylenprozeßführung mittlerer Strengheit (T_{aus} = 820-850 °C, Temperaturprofil I) - unseres Erachtens kann eine ähnliche Regime in den modernen Pyrolyseöfen verwirklicht werden - beträgt die Äthylenausbeute 25,7 Gew.%, die Propylenausbeute 10,6 Gew.% und die Benzolausbeute 9,6 Gew.%. Bei Propylen-Prozeßführung betragen die Ausbeuten obiger Produkte der **Reihe** nach: Äthylen 19,1 Gew.%, Propylen 16,4 Gew.%, Benzol 3,3 Gew.%. Dabei erhält man verhältnismäßig hohe (7,8 Gew.%) Butylen- und (4,75 Gew.%) Butadienausbeuten. Die angegebenen Beispiele veranschaulichen deutlich, in welch hohem Maße die Produktausbeuten

durch Änderung der Reaktionsbedingungen beeinflußt werden können. Zur weiteren Illustration soll in der Abb.12 die Änderung der Ausbeuten der gasförmigen Olefine und des Butadiens in Abhängigkeit von der BKSF gezeigt werden. In die Abbildung wurden gleichzeitig auch die Gesamtausbeute der Olefine, die Gesamtausbeute an Olefinen + Butadien sowie das Verhältnis Propylen/Äthylen aufgetragen. Der Maximalwert der Olefinausbeute ergab sich bei BKSF = 2,7, also in der Nähe der maximalen Propylenausbeute (BKSF = 2,45). Das Maximum der Ausbeutekurve des Äthylens liegt bei BKSF = 8. Es geht noch hervor, daß im Gebiet zwischen der maximalen Propylenausbeute und der maximalen Äthylenausbeute (2,45 < BKSF < 8,0) das Verhältnis Propylen/Äthylen von 0,85 auf 0,35 abnimmt, was als ein Beweis der weitgehenden Beeinflußbarkeit der Produktausbeuten durch die Änderung der Reaktionsbedingungen anzusehen ist.

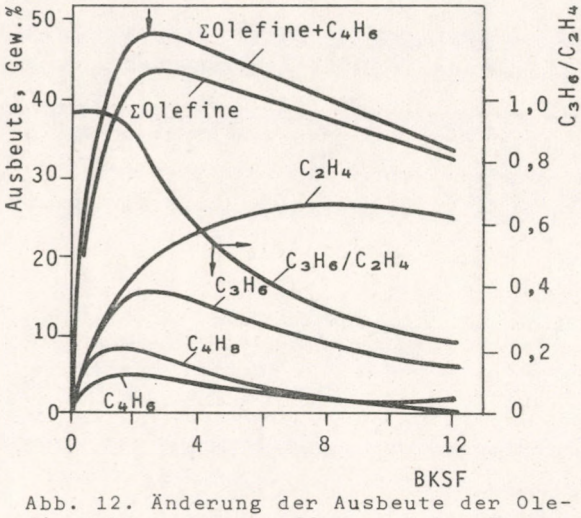

Abb. 12. Änderung der Ausbeute der Olefin-Kohlenwasserstoffen und des Propylen/Äthylen-Verhältnisses in Abhängigkeit von der brutto-kinetischen Strengheit bei der Pyrolyse eines Raffinats

Kinetisch-mathematisches Modell des Rohrreaktors der Benzinpyrolyse

In unserer früheren Mitteilung [1] wurde unser zur Beschreibung der Bruttozersetzungsgeschwindigkeit von Benzinfraktionen ausgearbeitetes kinetisches Modell dargelegt. Daselbst wurde eine neue Strengheitsfunktion (BKSF) definiert, welche die Verfolgung der Produktausbeuten auch in den für den Betrieb von industriellen

Rohröfen wichtigen Bereichen strenger Pyrolysebedingungen zuläßt. Im vorhergehenden Abschnitt wurde gezeigt, daß die Ausbeuten der Mehrzahl der Produkte in Abhängigkeit von der BKSF durch eine einzige Kurve beschrieben werden können. Die Verknüpfung der zur Beschreibung der Bruttozersetzungsgeschwindigkeit dienenden kinetischen und der die Ausbeutekurven beschreibenden mathematischen Zusammenhänge führte zur Ausarbeitung eines für die Berechnung der Produktverteilung geeigneten kinetisch-mathematischen Modells.

Mathematische Beschreibung der Produktausbeutekurven der Pyrolyse

Die mathematische Beschreibung der Ausbeutekurven wurde - unter Berücksichtigung ihres Verlaufs - durch folgende vier Funktionstypen beziehungsweise typischen Funktionsgruppen durchgeführt:

1. $$h_i = a \cdot (1 - \exp b\ BKSF) \qquad (2)$$

wo h_i die Ausbeute des i-ten Produkte in Gew.%,

a, b empirische Konstanten bedeuten.

Mit Hilfe dieses Funktionstyps können die Ausbeutekurven derjenigen Produkte genügend genau beschrieben werden, deren Ausbeute durch Erhöhung der Strengheit der Pyrolyse (BKSF) monoton zunimmt, und sich an einen Grenzwert nähert (z.B. Methan, Wasserstoff).

2. $$h_i = a \cdot (\exp b\ BKSF - \exp c\ BKSF) \qquad (3)$$

$$h_i = (a + b\ BKSF)(\exp c\ BKSF - \exp d\ BKSF) \qquad (4)$$

$$h_i = a \cdot [(1 + b\ BKSF)(\exp c\ BKSF - \exp d\ BKSF)] \qquad (5)$$

wo a, b, c, d empirische Konstanten darstellen.

Mit Hilfe dieser von der Gleichung (3) abgeleiteten Funktionen wurden die Ausbeutekurven derjenigen Komponenten beschrieben, welche sog. Zwischenprodukte darstellen, also deren Ausbeutekurven in Abhängigkeit von der BKSF einen Maximalwert erreicht, und dann abnimmt (z.B. das Äthylen, Propylen, Butylen, Butadien, also die Olefine und die Diolefine).

3. $h_i = a \exp b\ BKSF$ (6)

Durch diese empirische Formel wurden die "Ausbeutekurven" der zersetzbaren Komponenten des Rohstoffs beschrieben (z.B. das n-Pentan, Hexan, usw.).

4. $h_i = a + b\ BKSF$ (7)

Mit Hilfe dieses linearen Zusammenhangs ist nur eine annährende Beschreibung der Ausbeutekurve des Benzols möglich.

Die Konstanten der zur Beschreibung der Ausbeutekurven dienenden angegebenen Funktionen wurden mit Hilfe eines auf die Methode der kleinsten Quadrate gegründeten "Regressions"-Programms, an einem Hewlett Packardschen Mini-Computer bestimmt. Bei der Beschreibung der Ausbeutekurven der Olefine wurde die Regression an den in der Gruppe 2 angegebenen Funktionstypen durchgeführt, und diejenige Funktion ausgewählt, bei welcher das Minimum des Streuungsquadrats am niedrigsten war.

Kinetisch-mathematisches Modell

Auf Grund der in unseren früheren Mitteilung dargelegten brutto-kinetischen Gleichungen sowie der im vorigen Abschnitt angegebenen mathematischen Funktionen wurde ein vereinfachtes kinetisch-mathematisches Modell ausgearbeitet, mit dessen Hilfe, in Kenntnis der Reaktionsbedingungen die Berechnung der Produkt- und Konzentrationsverteilung der Produktkomponenten durchgeführt werden kann. Das vereinfachte Modell besteht also im Wesentlichen aus einer zur Berechnung der für die thermische Spaltung des Rohstoffs charakteristischen BKSF geeigneten kinetischen Funktion und aus mathematischen Beziehungen zur Beschreibung der Ausbeutekurven in Abhängigkeit von der BKSF:

$$BKSF = f\,[T(z),\ P(z),\ G_b,\ G_v] \qquad (8)$$

$$h_i = f(BKSF)$$

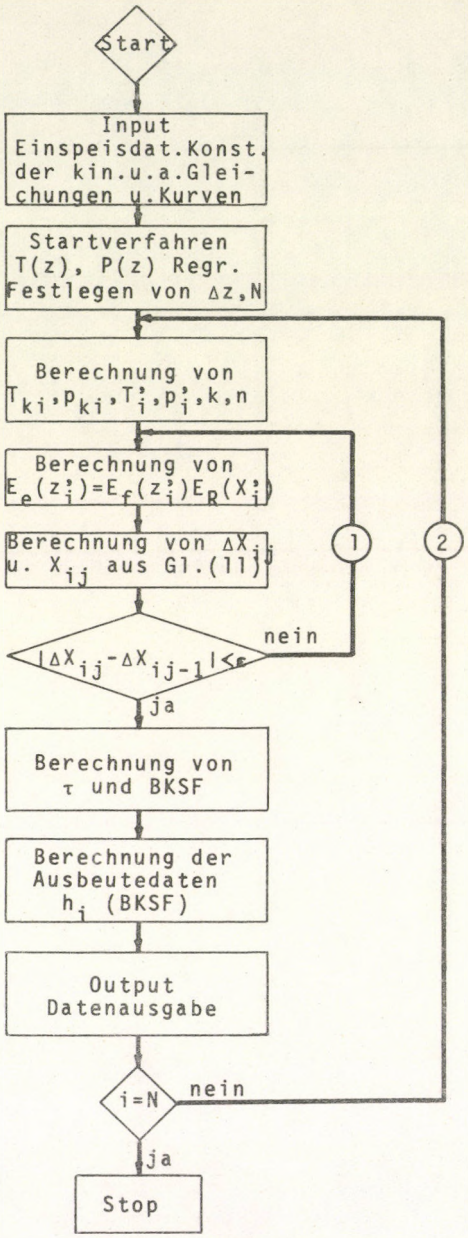

Abb. 13. Programm-Blockschema des kinetisch-mathematischen Modells eines Pyrolysereaktors. j-Zahl der Iterationsschritte innerhalb des Reaktorabschnitts; N-Zahl der Reaktorelemente; i-lauf. Indexzahl der Reaktorelemente

wo BKSF brutto-kinetische Strengheitsfunktion,
T(z) Temperaturprofil
P(z) Druckprofil
G_b Benzineinspeisegeschwindigkeit ($kg \cdot h^{-1}$)
G_v Dampfeinspeisegeschwindigkeit ($kg \cdot h^{-1}$)
h_i Ausbeuten der Produktkomponenten (Gew.%).

Durch Ergänzung des in unserer früheren Mitteilung beschriebenen Rechenprogramms des "kinetischen Modells" durch ein Programmteil betreffend die Berechnung der Komponentausbeuten erhalten wir das Programm der sog. kinetisch-mathematischen Modells, dessen Blockschema in der Abbildung 13 ersichtlich ist.

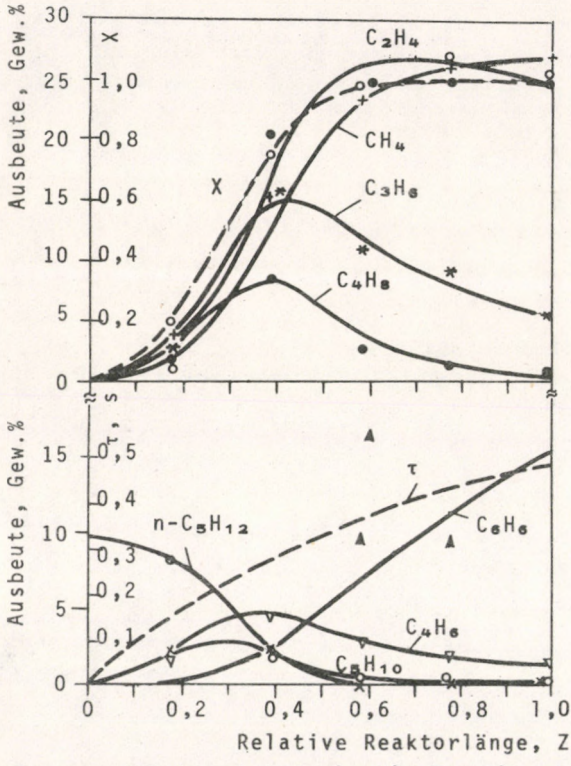

Abb.14. Auf Grund des kinetisch-mathematischen Modells berechnete und gemessene Verteilung der wichtigeren Reaktionsprodukte, Zersetzungsgrad und tatsächliche Aufenthaltszeit bei der Pyrolyse eines Raffinats

In Abbildung 14 wurden die in der Versuchsreihe 37 gemessenen Zersetzungsgrade sowie die Ausbeuten der Hauptkomponenten auf Grund des kinetisch-mathematischen Modells mit den für die gegebenen Bedingungen berechneten Zersetzungsgraden und Produktverteilungen der Pyrolyse des Raffinats verglichen.

Auf Grund der Abbildungen kann festgestellt werden, daß die berechneten Werte sowohl im Bezug auf die Zersetzungsgrade wie auch auf die Ausbeuten der Reaktionsprodukte mit den Gemessenen gut übereinstimmen. Die festgestell-

ten kleineren oder größeren Abweichungen können durch die Streuung der Ergebnisse erklärt werden.

In die Abbildung wurden auch die Kurven der Änderung der tatsächlichen Reaktionszeit (Aufenthaltszeit, τ) eingezeichnet. Es kann festgestellt werden, daß bis zur Erreichung der maximalen Äthylenausbeute (bei welcher der Vorgang zweckmäßigerweise unterbrochen wird), und in Abhängigkeit von der Strengheit der Pyrolysebedingungen (der Austrittstemperatur, dem Temperaturprofil), das Reaktionsgemisch 0,46-0,51 Sekunden im Radiationsabschnitt des Rohrofens verbringen muß.

Das beschriebene kinetisch-mathematische Modell kann auch zur Bestimmung der Produktverteilung bei gegebenem Benzinrohstoff und Pyrolysebedingungen beziehungsweise der zur Sicherung der erwünschten Ausbeuten an Zielprodukten notwendigen Bedingungen verwandt werden. Da die Anwendung des Modells durch die Kenntnis der Kinetik und der Ausbeutekurven des gegebenen Benzins bedingt ist, müssen zu deren Bestimmung Messungen im Großlaboratorium-Rohrreaktor durchgeführt werden. Diese Messungen sowie die Ausarbeitung des kinetisch-mathematischen Modells kann - auf Grund unserer bisherigen Erfahrungen - in kurzer Zeit erfolgen.

In unseren weiteren Arbeiten wurde die Weiterentwicklung des kinetisch-mathematischen Modells in zwei Richtungen vorgesehen:

a) Ergänzung des Modells und des Programms durch entsprechende hydrodinamische und Wärmeübertragungsgleichungen zur Berechnung des Druckabfalls sowie des Wärmestroms. Letztere wird die Anwendung des Programms auf Grund der Verteilung der Wandtemperatur des Pyrolyserohres gestatten;

b) Anpassung des Modells und des Programms zur Berücksichtigung der Eigenart des Ausgangsbenzins. Dies scheint eine sehr schwierige Aufgabe zu sein, es besteht jedoch Hoffnung auf ihre Lösung durch Meßreihen an weiteren Benzinfraktionen.

Wir sprechen unseren Dank gegenüber Frau J. Simon für die Leitung der analytischen Arbeiten sowie Z. Csermely für die Ausarbeitung der in unserer Arbeit verwandten Regressionsmethoden aus.

LITERATUR

1. ILLÉS, V., HORVÁTH, A., Hung. J. Ind. Chem. 3, 369 (1975)

2. ILLÉS, V., Szénhidrogéngázok pirolizise laboratóriumi csőreaktorban. (Pyrolyse von Kohlenwasserstoffgasen im Laboratoriums--Röhrenreaktor.) Kandidátusi értekezés. (Habilitationsarbeit). Veszprém, 1967.

3. ILLÉS, V., Acta Chim. Acad. Sci. Hung. 59, 35 (1969); ibid 59, 229 (1969); ibid 67, 41 (1971); ibid 67, 339 (1971)

4. ILLÉS, V., Erdöl u. Kohle 25, 464 (1972); ibid 25, 542 (1972)

5. ILLÉS, V., PLESZKÁTS, I., SZEPESY, L., Acta Chim. Acad. Sci. Hung. 79, 259 (1973); ibid 80, 1 (1974)

6. ILLÉS, V., PLESZKÁTS, I., SZEPESY, L., Acta Chim. Acad. Sci. Hung. 80, 267 (1974)

7. ILLÉS, V., MÁFKI Közlemßnyei (MÁFKI Mitteil.) 10, 52 (1969)

РЕЗЮМЕ

Авторами было изучено изменение выхода продуктов реакции в реакторе крупнолабораторного размера в зависимости от степени разложения и кинетической требовательности при пиролизе рафината. Было установлено, что выход продуктов (исключая некоторые, напр., водород и этилен) в зависимости от переменных требовательности можно изображать одной кривой - независимо от выходной температуры и профиля температуры.

С использованием валовой кинетической функции требовательности и математических выражений, описывающих кривые выхода, составили кинетическую математическую модель и вычислительную программу для вычисления распределения продуктов.

Hungarian Journal
of Industrial Chemistry
Veszprém
Vol.3. pp. 411-428 (1975)

KINETICS OF VAPOUR PHASE SYNTHESIS OF VINYLACETATE[+]

B. SINGH[*], R.N. KUMAR[**], G.N. BHAT[***]

(Department of Chemical Engineering, Indian Institute of Science, Bangalore - 12, India)

Received: November 6, 1974.

This paper presents the results of the systematic study of the vapour phase vinylation of acetic acid using zinc acetate impregnated on charcoal as a catalyst. The determinations of the effective diffusivities of acetylene and hydrogen in the catalyst showed that the diffusion phenomenon is of the Knudsen type. The activation energy for chemisorption of acetylene on the catalyst was found to be 13.5 K cals. per g. mole. A rate equation was derived, and the energy of the activation was computed for the vinylation of acetic acid in a fixed bed of the catalyst, and the data seem to suggest the possibility of a surface reaction as the rate controlling step.

I. INTRODUCTION

Most of the vinylacetate is prepared by the addition of acetylene to acetic acid, the overall reaction being represented by:

$$CH \equiv CH + CH_3COOH = CH_3COO \cdot CH = CH_2.$$

[+]Paper presented at the 39th International Congress of Industrial Chemistry, held in Bucharest, September 1970.

Present Addresses:

*Central Research Laboratories, Shortland, N.S.W., Australia.

**Indian Polywood Industries Research Institute, Bangalore-22.

***Professor and Head of the Department of Chemical/Petrochemical Engineering, College of Science & Technology, Port Harcourt, Nigeria.

The addition may be carried out in the liquid phase [1], but such a process is obsolete. It is however more convenient to carry out the reaction in the vapour phase by passing a preheated mixture of acetylene and acetic acid vapours over a catalyst. Thermodynamic calculations [2] indicated that the reaction is highly feasible in the temperature range 175° - 245 °C.

Zinc acetate impregnated on charcoal was found to be a suitable catalyst [3], activity of the catalyst being a function of the ratio [4] of charcoal to zinc acetate. The catalyst was prepared [5] by allowing a known weight of charcoal to attain equilibrium in a solution of zinc acetate of suitable concentration, so that the immersed charcoal adsorbed the desired amount of zinc acetate. Relevant adsorption isotherms and kinetic data for the zinc acetate charcoal-water system were obtained, so that for all the catalysts prepared, their conditions of preparation were exactly defined, since the method of the preparation of the catalysts highly influence the reactions in which the catalysts are subsequently used. The results of these studies were reported earlier [6].

II. THE KINETICS OF CHEMISORPTION OF ACETYLENE ON THE CATALYST

Procedure for an Experimental Run

The main features of the apparatus used in the studies are shown in Figure 1. Runs were carried out by degasification of the catalyst for 4 hours at 270°C and at a pressure of less than 1 mm Hg. The degasification was considered to be complete when the monometer reading remained for at least one hour. The temperature of the sand bed was lowered and maintained at the operating temperature. The adsorption tube was then connected to the burette filled with acetylene and the volume by the acetylene introduced was found out. After the introduction of the gas, the adsorption unit was disconnected from the burette and changes in the reading of the manometer connected to the absorption unit were noted as a function of time from the instant of disconnecting the adsorption

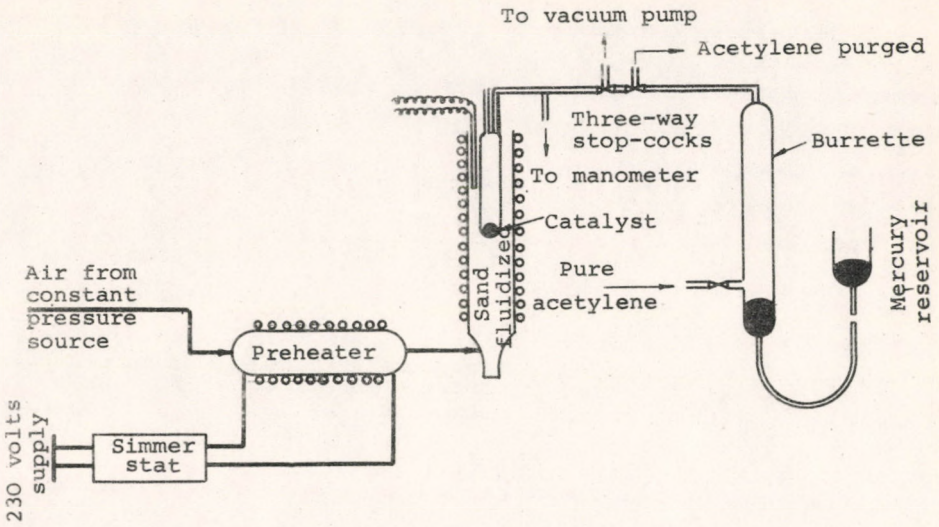

Fig. 1. Apparatus for chemisorption studies

unit from the burette. Gas uptake was followed by changes in the manometer reading, the volume of the unit being kept constant.

Results and Discussion

Runs were carried out at four different temperatures (175°C, 202°, 225° and 245°C) and at two catalyst compositions (zinc acetate/charcoal) 0.25:1 and 0.1:1. The initial pressure in all cases was approximately the same, i.e. between 25 to 27 mm Hg. Typical data showing the relationship between time and the pressure of the acetylene at a temperature of 202°C for a zinc acetate/charcoal ratio of 0.25:1 are shown in Figure 2. Similar trends were observed at other temperatures and other ratios of zinc acetate to charcoal.

Chemisorption data were found to be not amenable for correlation by the treatment of ASHMORE [7]. The alternative was to consider the procedure suggested by ELOVICH [8, 9].

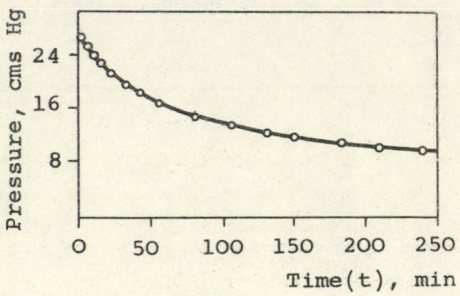

Fig.2. Kinetics of chemisorption of acetylene by catalyst of composition 0.25:1 (zinc acetate charcoal) at 202 °C. W: 0.27 gms

The Elovich equation in its differential form is:

$$\frac{dq}{dt} = a\, e^{-\alpha q} \qquad (1)$$

or in its integrated form:

$$q = \frac{2.3}{\alpha} \log (t + t_o) - \frac{2.3}{\alpha} \log t_o \qquad (2)$$

where:

$$t_o = \frac{1}{a\ \alpha} \qquad (3)$$

Equation (2) can be written in the form:

$$q = \frac{2.3}{\alpha} \log \frac{t_o + t}{t_o} \qquad (4)$$

and for any two values of q_1 and q_2:

$$\frac{q_1}{q_2} = \frac{\log \dfrac{t_1 + t_o}{t_o}}{\log \dfrac{t_2 + t_o}{t_o}} \qquad (5)$$

The validity of Equation (5) can be checked at random from mathematical computations by assigning different values to t_o and the value of t_o which satisfies the largest number of sets of data points can be tested for its suitability through graphical representation of the data by Equation (2). The present results were treated by this procedure and it was found that Equation (2) was

valid over the entire range as shown in Figure 3 and 4. The satisfactory value of t_o and corresponding values of "a" and "α" for various cases are given in Table 1.

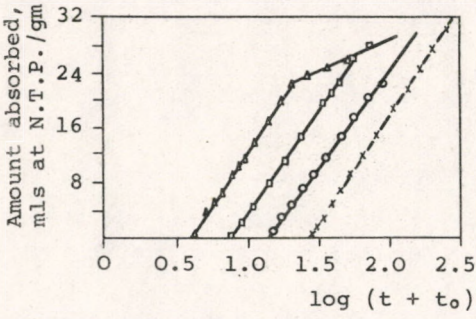

Fig.3. Elovich plots for catalyst of composition 0.25:1 (zinc acetate/charcoal) at various temperature: x - 175°C, o - 202°C, □ - 225°C, Δ - 245°C

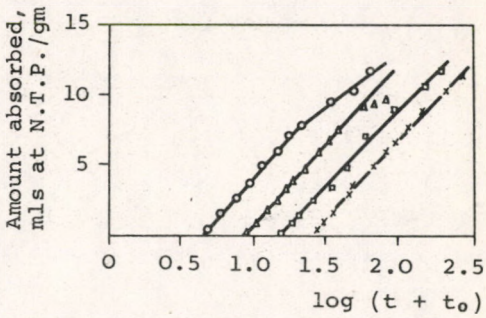

Fig.4. Elovich plots for catalyst composition of 0.1:1 (zinc acetate/charcoal) at various temperatures: x - 177°C, □ - 200°C, Δ - 225°C, o - 245°C

Table 1. Constants of Elovich Equation

Composition of Catalyst							
0.25:1 (Zinc acetate/Charcoal)				0.1:1 (Zinc acetate/Charcoal)			
Temp. °C	t_o	α	a	Temp. °C	t_o	α	a
175	27.5	0.074	0.49	177	26.0	0.196	0.196
202	14.0	0.080	0.89	200	15.0	0.211	0.316
225	7.5	0.079	1.686	225	8.5	0.201	0.584
245	4.0	0.082	3.05	245	4.5	0.202	1.09

From this table it is obvious that "α" remains practically constant for a given composition of the catalyst, while the value of "a" continuously increases with temperature. In general, both

"a" and "α" are temperature functions. However, TAYLOR and THON [10] while treating the data of EMMET and BRUNAUER [11] on chemisorption of nitrogen on iron found that "o" remains practically constant.

However, one isothermal anomaly is found at a temperature of 245°C. There is an abrupt change in the value of "α" from 0.082 to 0.25 after a lapse of 15 minutes which then remains constant as shown in Figures 3 and 4. Such tendencies are not uncommon and are generally interpreted as a consequence of the change in the type of chemisorption under conditions at which the discontinuity appears in the plot. In the present case such behaviour is possible, since in addition to chemisorption at zinc-acetate-charcoal sites [12], further chemisorption at charcoal sites alone occurs above 240°C.

The energy of activation of the process can be determined by making use of the equation:

$$\ln \frac{r_{T_1}}{r_{T_2}} = \left[\frac{E}{R} \frac{1}{T_1} - \frac{1}{T_2}\right] \tag{6}$$

Combining Equation (1) and (6), we get:

$$\frac{E}{R}\left[\frac{1}{T_1} - \frac{1}{T_2}\right] = \ln \frac{a_2}{a_1} - q\,(\alpha_1 - \alpha_2) \tag{7}$$

Since for the present case "o" is independent of temperature, Equation (7) becomes:

$$\frac{E}{R}\left[\frac{1}{T_1} - \frac{1}{T_2}\right] = \ln \frac{a_2}{a_1} \tag{8}$$

Thus a plot of ln a vs. 1/T should yield a straight line and is found to be so as shown in Figure 5. The two lines for different compositions are approximately parallel, thus indicating that the

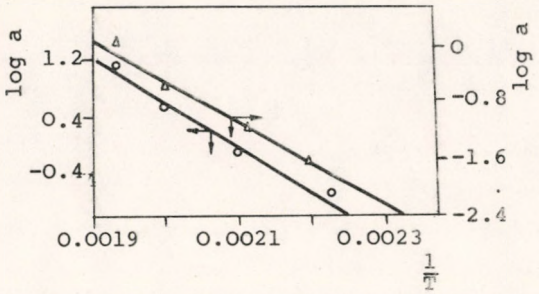

Fig.5. Calculation of activation energy of chemisorption by catalyst of different composition. Zinc acetate/charcoal o - 0.25:1, Δ - 0.10:1

activation energy is not a function of composition. This observation is in agreement with observations of previous workers [12]. The value of the activation energy computed from the slope of the lines is 13.5 Kcal per g. mole.

III. MEASUREMENT OF EFFECTIVE DIFFUSIVITIES

Experimental

Effective diffusivities inside catalyst pores were determined by making use of the pressure gradient of a single gas across the pellet with the assumption of quasi-stationary state.

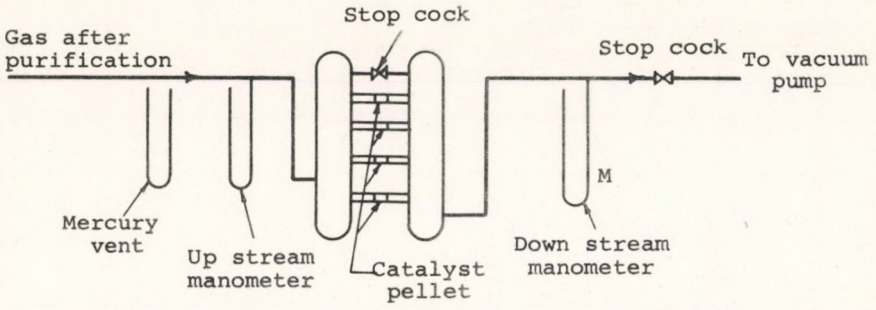

Fig.6. Apparatus for measurement of diffusivity

The apparatus used was similar to that used by VILLET and WILHELM [13] and is shown in Figure 6. The volume of tubes joining

either side of the catalyst pellet was 100 ml. The pressure was kept constant only 1.2 cm Hg above the atmospheric pressure by providing a vent through the mercury trap.The pellets were tightly secured in undersize plastic tubes which were fixed to the capillaries, and the joints were made leak proof by applying Araldite adhesive. The gases were technical grade electrolytic hydrogen and purified acetylene.

Procedure

The equipment was thoroughly purged with the gas under test before each run. A vacuum was created downstream and incremental changes in the manometer M were read to 0.5 mm with the help of a travelling microscope. The net change in the pressure difference across the pellet was 1.5 cm. The pellet diameter and length were measured with the aid of a travelling microscope.

Since the changes in volume in the downstream section, because of the change in the mercury level of the manometer, were negligible compared with the total volume, the downstream volume was considered to be constant. Under these conditions, the diffusion process can be represented by:

$$\frac{dp}{dt} = \frac{AD_k}{LV}(P_o - P) \tag{9}$$

Integration of this equation leads to:

$$2.303 \log \frac{P_o - P_i}{P_o - P} = (A\, D_k/LV)t \tag{10}$$

Thus a plot of $\log (P_o - P_i)/(P_o - P)$ vs. "t" should give a straight line of a slope equal to $(AD_k/LV)t$ and the diffusivity is calculated from:

$$D_k = \frac{2.3\ (\text{slope})\ LV}{A} \tag{11}$$

Results and Discussion

(i) Effect of Pressure

Figure 7 shows that the calculated points lie on the same line irrespective of the downstream pressure. It is therefore obvious that the pressure has no effect on the diffusivity. Hence, the observed diffusivity appears to be of the Knudsen type.

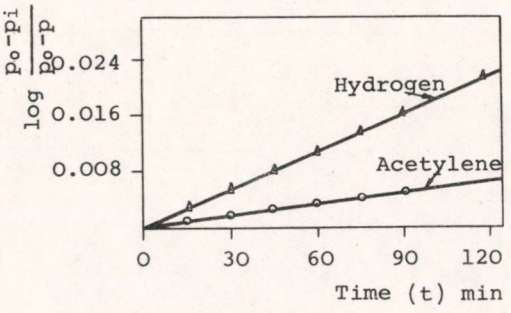

Fig. 7. log pressure function vs. time for pure charcoal

(ii) Effect of the Nature of Gas

The average values of diffusivities for acetylene and hydrogen and the ratio of these values obtained are shown in Table 2. From these results it is obvious that

Table 2. Average Values of Diffusivities

Composition Zinc Acetate/ /Charcoal	Acetylene	Hydrogen	Ratio
0:1	0.0028	0.0098	3.50
0.1:1	0.0025	0.0082	3.28
0.25:1	0.0015	0.0052	3.47

the ratio of diffusivities of the two gases studied are less than 3.64 which is theoretically expected on the basis of the molecular weights of hydrogen and acetylene. This implies the possibility of acetylene travelling faster than required by the laws of diffusion. Thus the phenomena of surface diffusion in addition to the Knudsen flow may also to a certain extent determine the overall diffusio-

nal characteristics of gases such as acetylene, which are known to be adsorbed on charcoal.

(iii) Effect of Composition

Diffusivities of acetylene and hydrogen continuously decrease with an increase in the zinc acetate content and the average of these values obtained are plotted in Figure 8.

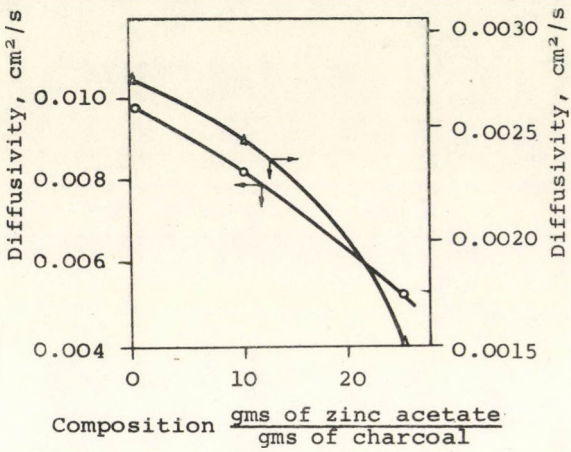

Fig. 8. Gas: Δ - acetylene, o - Hydrogen

With increasing zinc acetate content on charcoal, the effective pore size may decrease linearly, if the deposition is uniform. This behaviour would result in a linear decrease diffusivity since Knudsen diffusivity is directly proportional to the pore size. However, the present observations are not in complete agreement with this condition the deviation noticed may be due to the binding of the pores.

IV. KINETICS OF VAPOUR PHASE SYNTHESIS OF VINYLACETATE

Materials and Apparatus

Acetic acid used in all the experiments was of Analar quality and was more than 99.9 % pure. Zinc acetate impregnated on charcoal (-14 + 20 Tyler mesh), prepared by the method described earlier, was used as the catalyst. A flow diagram of the experimental set up is given in Figure 9.

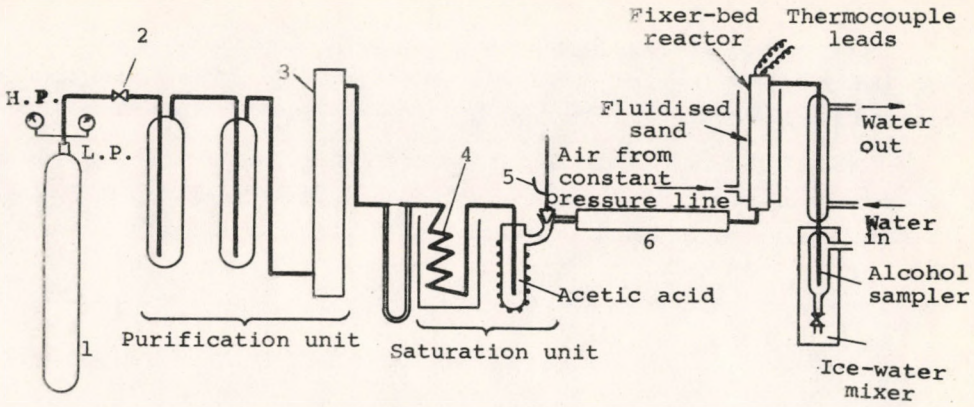

Fig. 9. Flow diagram of the process of vinylation of acetic acid

1. Acetylene cylinder
2. Needle valve
3. Acetylene drier
4. Water bath preheater
5. Thermometer
6. Preheater

Experimental Procedure

Air from the constant pressure line was turned on, and the heating of the reactor and the preheater started with a continuous flow of acetylene set at the desired rate, the composition being controlled from the saturation temperature. A steady state was reached within half an hour, after the saturation temperature was established. The sampling was carried out by bubbling through the sampling unit for a definite time.

Analytical Methods

Free Acetic acid: This was determined by 0.1 N caustic soda using phenolphtalein as an indicator. The titration was carried out in the presence of crushed ice to prevent the hydrolysis of esters.

Total ester: Total ester was determined by saponification with excess alkali and back-titrating the residual alkali against 0.1 N H_2SO_4. The difference between the saponification value and free acid value corresponds to the total ester.

Unsaturation: This was determined by bromination. The procedure adopted was that of LUCAS and PRESSMAN [14]. Under these conditions both acetylene and vinyl acetate are completely brominated.

ROBEY [15] reported that in an acetate buffer, only one mole of bromine per mole of acetylene is added, while olefinic linkage is completely brominated. From the difference of Robey's bromine value and Lucas et al. bromine, the amount of bromine for vinyl-acetate was calculated. The difference between the bromine values in almost all cases agreed with the total ester value, thereby indicating the formation of saturated ester to be negligible.

Results and Discussion

The variables studied were:

(i) Time factor W/F 20 to 120 (g. catalyst)(hour)/g. mole fed.

(ii) Molar ratio, M, 1:1 to 1:3.7 mole of acetylene/mole of acetic acid.

(iii) Temperature: 175 to 215°C.

The results are plotted in Figures 10 to 13.

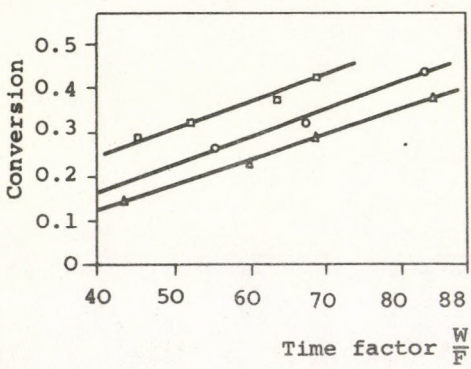

Fig. 10. Effect of time factor on conversion of acetic acid at 175 °C. C_2H_2/CH_3COOH
Δ - 1.8:1, o - 2.42:1
□ - 3.7:1

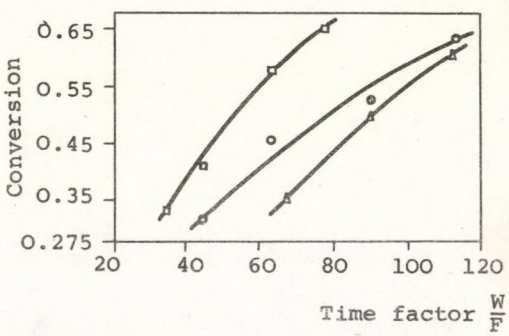

Fig. 11. Effect of time factor on conversion of acetic acid at 186 °C. C_2H_2/CH_3COOH
Δ - 1.51:1, o - 2.42:1
□ - 3.50:1

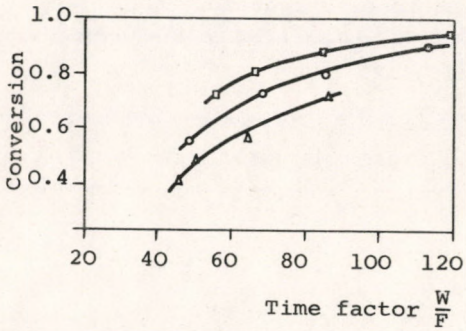

Fig. 12. Effect of time factor on conversion of acetic acid at 202°C. C_2H_2/CH_3COOH
Δ - 1.20:1, o - 2.10:1
□ - 3.12:1

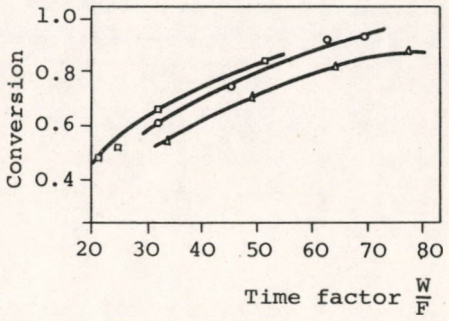

Fig. 13. Effect of time factor on conversion of acetic acid at 215°C. C_2H_2/CH_3COOH
Δ - 1.70:1, o - 2.60:1
□ - 3.15:1

Kinetic Analysis

The basic kinetic equation for a reaction in a flow system is given by:

$$\frac{W}{F} = \int_o^x \frac{dx}{r} \tag{12}$$

Assuming ideal gas behaviour, the concentration of various components in the stream at any conversion level of acetic acid "x" are:

$$\text{Concentration of acetic acid} = \frac{F_{Ao}(1 - x)}{V} \tag{13}$$

$$\text{Concentration of acetylene} = \frac{F_{Bo} - F_{Ao}\, x}{V} \tag{14}$$

$$\text{Concentration of vinylacetate} = \frac{F_{Ao}\, x}{V} \tag{15}$$

where

$$V = \frac{RT}{p} F_{Bo} + F_{Ao}(1 - x) \tag{16}$$

From thermodynamic calculations, the reverse reaction is negligible, and hence the concentration of vinylacetate has no effect on the rate of reaction.

From a survey of literature, there is no agreement about the order of the reaction. Since, in the present studies, the partial pressure of both reactants are comparable, the rate equation is assumed to be given by:

$$r = k\, C_A\, C_B \tag{17}$$

Substitution of Equations (13), (14), (15) and (17) in Equation (12) leads to the expression:

$$\frac{W}{F_{Ao}} = \frac{R^2\, T^2}{p^2\, k} \int_o^x \frac{(M + 1 - x)^2}{(1 - x)(M - x)}\, dx \tag{18}$$

where:

$$M = \frac{F_{Bo}}{F_{Ao}}$$

Integration of Equation (18) and defining the time factor on the basis of the total molal flow rate leads to the expression:

$$\frac{W}{F} = \frac{R^2\, T^2}{p^2\, k} \left[Y_{Ao}\, x - (M^2/M - 1) \ln (1 - x) + (1/M - 1) \ln \frac{M - x}{M} \right] \tag{19}$$

where Y_{Ao} is the mole fraction of acetic acid in the feed.

Equation (19) can be tested for its validity either by the constancy of "k" or by linear plots of the expression within the brackets against (W/F). The expression was found to hold good at all temperatures. The value of the reaction rate constant (k) was obtained from the slopes of the lines at various temperatures. The energy of the reaction and the frequency factor were found to be as follows:

Frequency factor = A = 1.68×10^9

Energy of activation (E) = 16.4 K. cals./g.mole

Hence the final design equation for the synthesis of vinylacetate is:

$$\frac{W}{F} = \frac{R^2 T^2}{p^2} \frac{Y_{Ao}}{1.68 \times 10^9 \, e^{-16400/RT}} \left[x - \frac{M^2}{M-1} \ln (1-x) + \frac{1}{M-1} \ln \frac{M-x}{M} \right]$$

This work is based on the thesis of Mr. Baldev Singh accepted by the Indian Institute of Science, Bangalore, for the award of the degree of M.Sc. The authors are indebted to the late Professor N.R. Kuloor who was the Professor and Head of the Department of Chemical Engineering, Indian Institute of Science, Bangalore and the co-guide during this investigation.

SYMBOLS USED

A Area of cross section (cm^2)

a Elovich Equation constant

C_A Concentration of acetic acid (mole/litre)

C_B Concentration of acetylene (mole/litre)

D_k Effective diffusivity in gases (cm^2/sec)

E Energy of activation (Cal./mole)

F Total feed rate (mole/hr.)

F_{Ao} Feed rate of acetic acid at the inlet of the reactor, (mole/hr.)

F_{Bo}	Reaction rate constant	$\frac{\text{mole product (litre)}^2}{\text{(catalyst)(hr)(moles of acetic acid)(moles of acetylene)}}$
M	Molar ratio of acetylene to acetic acid	
P_o	Upstream pressure (cm.Hg.)	
P	Instantaneous down stream pressure (cm.Hg.)	
P_i	Initial down stream pressure (cm.Hg.)	
p	Atmospheric pressure	
q	Amount of acetylene adsorbed (ml. N.T.P./g)	
t	Time (minutes)	
t_o	Constant in integrated form of Elovich equation	
T	Temperature (K)	
R	Gas constant [1.987 cal./(mole)(K)]	
r	Rate of reaction [mole product/(catalyst)(hour)]	
r_T	Rate of adsorption of acetylene at temperature T (K)	
V	Volume of the down stream container (ml.)	
W	Weight of catalyst (g)	
x	Conversion (mole converted/mole of reactant)	
Y_{Ao}	Mole fraction of acetic acid at the inlet of the reactor	
α	Elovich equation constant	

REFERENCES

1. ANONYM, Chem. and Met. Eng., 42, 596 (1935)

2. FRANKLIN, J.L., Ind. Eng. Chem., 41, 1070 (1949)

3. AKIO MITSUTANI and TSUGIO KOMINAMI, Nippon Kagaku Zasshi, 80, 886 (1959)

4. NOBRU YAMADA, Kogyo Kagaku Zasshi, 62, 1458 (1959); Chem. Abstr., 57, 10563f (1962)

5. MAATMAN, R.W., PRATER, G.D., Ind. Eng. Chem., 49, 253 (1957)

6. SINGH, B., BHAT, G.N., KULOOR, N.R., Indian J. of Technology, 3, 119 (1965)

7. ASHMORE, P.G., "Catalysis and Inhibition of Chemical Reaction", Butterworth Publication 1963.

8. ZELDOVICH, Ya., Acta Physicochim (USSR), 1 No. 3/4, 449 (1934)

9. LOW, M.J.D., Chem. Reviews, 60, 267 (1960)

10. THON, N., TAYLOR, H.A., J. Am. Chem. Soc. 74, 4169 (1952)

11. EMMET, P.H., BRUNAUER, S., J. Am. Chem. Soc., 56, 35 (1934)

12. AKIO MITSUTANI, MASAKAZU MUTSOMOTO, Nippon Kagaku Zasshi, 79 948 (1958)

13. WILLET, R.H., WILHELM, R.H., Ind. Eng. Chem., 53, 837 (1961)

14. LUCAS, H.J., PRESSMAN, P., Ind. Eng. Chem., Anal. Ed., 10, 140 (1938)

15. ROBEY, R.F., Analytical Chemistry, 24, 1080 (1952)

РЕЗЮМЕ

В статье сообщаются результаты испытаний, относящиеся к реакции винилирования уксусной кислоты на активном углероде, промоченном уксуснокислым цинком. По определению эффективного коэффициента диффузии можно сделать вывод, что перед нами диффузия Кнудсенового типа. Энергия активации хемосорбции ацетилена на катализаторе равняется 13,5 ккал/гмоль. Выводится уравнение для описания скорости реакции. Была вычислена энергия активации винилирования уксусной кислоты на неподвижном слое катализатора. По данным было установлено, что вероятно реакция, происходящая на поверхности, является ограничителем скорости.

Hungarian Journal
of Industrial Chemistry
Veszprém
Vol.3. pp. 429-448 (1975)

DATA CONCERNING THE CALCULATION OF KINETIC CONSTANTS CHARACTERISTIC OF REACTION RATES IN HETEROGENEOUS CATALYTIC HYDROGENATION DEHALOGENATION

Z. KISS, T. BLICKLE and A. UJHIDY

(Research Institute for Technical Chemistry of the Hungarian Academy of Sciences, Veszprém)

Received: December 19, 1973.

The hydrogenization process of a methanolic solution of 2-ethyl-6-chloro isonicotinamide - the compound chosen as the model of catalytic hydrogenation at atmospheric pressure - at a granular activated charcoal catalyst containing 0.5 per cent metallic palladium was compared in four experimental set-ups applied in parallel. The experiments were carried out in a shaking apparatus, a tank-type reactor equipped with a stirrer, a bubble- and a sieve plate column.

The theoretical connection was deduced for the determination of the constants characteristic of the reaction of hydrogenation. This enabled a comparison of the rates of the reactions occurring in the various types of reactors.

In the course of the evaluation of the experiments it was concluded that in the case of the model reaction and apparatus types chosen, hydrogenation can be carried out under the most favourable circumstances in the sieve plate (or "foam") column.

In catalytic chemical reactions, one of the main purposes of the application of a catalyst is to increase the reaction rate. Accordingly, an important characteristic of contact catalytic processes is the numerical value of the reaction rate or a mathemati-

cal function describing the dependence of the reaction rate upon the individual parameters.

In heterogeneous reactions - such as e.g. in catalytic hydrogenation - the components may be present in a phase in which the reaction in question does not occur. In such cases, the reacting components have to be transferred from the various phases to that particular one where the reaction in question occurs. Furthermore, the products have to leave this phase; accordingly material transport of the components has to occur between the various phases simultaneously with the elementary chemical reaction.

From among the partial processes, it is possible to make conclusions concerning the rate of the sorption-type partial processes. At the same time, on account of the involved and complicated nature of such reactions, it is not possible even to estimate the rate of the surface reactions occurring at the surface of the catalyst. At present, elucidation of the partial surface reaction necessitates separate research for each individual reaction; today it can be stated in connection with very few reactions that the partial processes occurring at the catalyst surface are known. Accordingly, in the calculation of the reaction rate of contact catalytic reactions it is necessary to apply simplifications and neglections even in the simpler cases; in more complicated cases, the calculation cannot be carried out at all.

The aim of the present work was to calculate the reaction rate and the constants characteristic of the latter for the case of heterogeneous catalytic hydrogenation at an atmospheric pressure. This was necessary in order to be able to compare the reaction rates of hydrogenation carried out in different types of apparatus and to decide the most preferable procedure for carrying out a given operation.

The model substance for these experiments was 2-ethyl-6--chloro iso-nicotinamide; 2-ethyl iso-nicotinamide was prepared from this compound by removing a chlorine atom and substituting it with a hydrogen atom.

A catalyst containing 0.5 per cent metallic palladium on a granular activated charcoal support was applied to direct the reaction in the desired reaction. This catalyst reduces neither aromatic carbon ring nor acid-amide groups; on the other hand, it hydrogenates the carbon-chlorine bond in the above mentioned molecule at a suitable rate.

The experiments were carried out in four types of apparatus: a tank-type reactor equipped with a stirrer, a shaking apparatus, a bubble-column and a foam-reactor.

A schematic drawing of the bubble-column apparatus is presented in Figure 1.

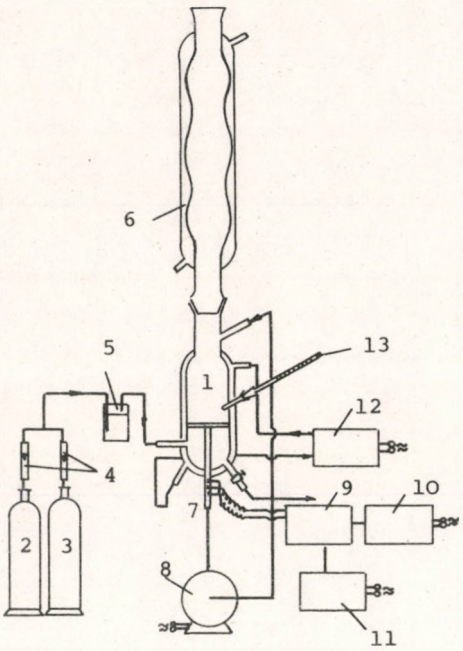

Figure 1

The central part of the apparatus is a bubble-column (1) of 30 mm internal diameter, equipped with a jacket, a gas distributor plate and adequate ground joints. Hydrogen and ammonia were conducted to the column from a hydrogen cylinder (2) and an ammonia cylinder (3) through pressure reducer valves, rotameters (4) and a saturator vessel (5) filled with methyl alcohol. The gases, having passed the reaction mixture, reached the outlet through a bulb-type condenser (6). Application of the condenser was necessary in order to condense methyl alcohol vapours carried away from the reaction mixture. Otherwise changes in the concentration of the reaction mixture on

account of vapour carryaway would have interfered both with the hydrogenation process and the accuracy of the analysis based on conductivity measurement. Part of the reaction mixture was kept in forced circulation through the glass tube containing the electrodes (7) by means of peristaltic pump (8). In this manner it was ensured that an electrolyte of a conductivity corresponding to the instantaneous state of the conversion was at all times in contact with the electrodes. In the interior of the reaction zone, conductivity determination was rendered impossible by gas bubbles and catalyst granules present. The electrodes were connected to a conductivity meter (9), operated from a stabilizer (10) and the signal monitored by the conductivity meter was measured by a potentiometric recorder. Constant reactor temperature was maintained by warm water provided by a thermostat (12) and circulated in the heating jacket. The temperature of the reaction mixture was monitored by a thermometer placed into the reaction zone.

In order to construct the foam-column type hydrogenation apparatus, the column of the former apparatus had to be exchanged. With regard to dimensions and general layout, the new column was totally identical to the former one, with the difference that the gas distributor glass frit was replaced by a plate perforated with holes 1 mm in diameter, of a total free surface of 30 % and of considerably lower resistance.

The central unit of the shaking and stirring hydrogenation apparatus was a glass reactor of 100 ml capacity, equipped with a thermostating jacket, connected to the necessary ancillary units.

In order to determine the optimum reaction parameters for the case of the given model substance and catalyst, the temperature of the reaction mixture, the concentration of the starting material (as referred to the solvent), the amount of the catalyst, the grain size of the catalyst and - in the case of two of the apparatuses - the gas flow rate were varied, whereas the other parameters were kept at a constant value. Furthermore, crumbling of the catalyst was studied in each apparatus and poisoning experiments were carried out in the stirred tank reactor and in the

stirred tank reactor and in the foam column by the addition of ethyl mercaptan and hydrogen sulphide at different concentration levels.

A conductometric determination procedure, applicable with all four types of reactors, was developed to enable the hydrogenation reaction to be followed and to evaluate the experiments.

The apparatus types described in the foregoing and the procedures realized in them were compared on the basis of the maximum reaction rate attainable. The evaluation was carried out on the basis of the following considerations:

The change in the composition of the reaction mixture during the reaction period can be expressed by the following Equation:

$$a_1(x' - a_2x) = V \frac{dx}{dt} + kcx \qquad (1)$$

whereas with regard to the decrease of the amount of the substrate we can write:

$$-\frac{dc}{dt} = kcx \qquad (2)$$

where

- x' is the gas concentration in the gaseous phase (g/l)
- x is the gas concentration in the liquid phase (g/l)
- c is the concentration of the material in the liquid (g/l)
- V is the volume of the liquid (l)
- a_1 is the hydrogen absorption transfer coefficient (1/s)
- a_2 is the Henry-constant
- k is the apparent rate constant
- t is time (s)

The expression $V \frac{dx}{dt}$ (the change in the amount of hydrogen in the liquid) in Equation (1) can be neglected and consequently we can write:

$$x = \frac{a_1x'}{a_1a_2 + kc} \qquad (1.1)$$

by substituting x into Equation (2) and rearranging, we have:

$$\frac{a_1 \cdot a_2 + kc}{c} dc = - ka_1x'dt \tag{2.1}$$

The definite integral of the latter between limits O and t, moreover c_o and c is,

$$a_1a_2 \ln \frac{c}{c_o} + k(c - c_o) = - ka_1x't \tag{2.2}$$

$$\frac{1}{a_1x'} (c_o - c) - \frac{a_2}{kx'} \ln \frac{c}{c_o} = t \tag{2.3}$$

Let us introduce:

$$\frac{1}{a_1x'} = A[s/g] \quad \text{and} \quad \frac{a_2}{kx'} = A_2 \, [l^2s/g^2]$$

By introduction of the above designation, and by contracting unknowns a_1, x', a_2 and k into two constants, the equation thus obtained is the following:

$$A_1(c_o - c) - A_2 \ln \frac{c}{c_o} = t \tag{2.4}$$

by derivating Equation (2.4) according to c, we obtain:

$$-A_1 - \frac{A_2}{c} = \frac{dt}{dc} \tag{2.5}$$

after rearrangement:

$$\frac{dc}{dt} = \frac{1}{-A_1 - (\frac{A_2}{c})} \tag{2.6}$$

where

$$- \frac{dc}{dt} = w \quad \text{is the reaction rate.}$$

Accordingly:

$$w = \frac{1}{A_1 + \frac{A_2}{c}} \tag{2.7}$$

A_1 and A or $\frac{1}{A_1}$ and $\frac{1}{A_2}$ are the two constants, characteristic of the reaction rate, by whose determination the whole course of the hydrogenation reaction can be described.

In order to determine A_1 and A_2, A_2 is expressed from Equation (2.7):

$$A_2 = -\frac{c}{w} - A_1 c \tag{2.8}$$

Considering that in our case the obtained signal is proportional to the amount of the product produced (the ionic concentration of chlorine splitted is determined in the reaction mixture by conductometry), further that it is not concentration, but percentage conversion values that can be read from the curve recorded from the potentiometric recorder, we can write:

$$c_o - c = by \tag{3}$$

$$c_o = by_v \tag{4}$$

where

c_o is the starting concentration of the substrate (g/l)

c is the actual concentration of the substrate (g/l)

y is the recorder deflection pertaining to the actual conversion (%)

y_v is the recorder deflection corresponding to 100 % degree of conversion (%)

$y_o = \frac{y}{yv}$

furthermore:

$$\frac{dc}{dy} = -\frac{c_o}{y_v} \tag{4.1}$$

$$\frac{dc}{dt} = \frac{dc}{dy}\frac{dy}{dt} \tag{4.2}$$

$$w = -\frac{c_o}{y_v}\frac{dy}{dt}$$

by substituting w into Equation (2.8):

$$A_2 = - \frac{c_o - \frac{c_o}{y_v} y}{- \frac{c_o}{y_v} \frac{dy}{dt}} - A_1 \left(c_o - \frac{c_o}{y_v}\right) y \qquad (2.9)$$

$$A_2 = \frac{\frac{1 - y}{y_v}}{\frac{1}{y_v} \frac{dy}{dt}} - A_1 c_o \left(1 - \frac{y}{y_v}\right) \qquad (2.10)$$

$$A_2 = \frac{1 - y_o}{\frac{dy_o}{dt}} - A_1 c_o (1 - y_o) \qquad (2.11)$$

introducing designation $\frac{dy_o}{dt} = V'$ and rearranging we obtain:

$$\frac{A_2}{1-y_o} = \frac{1}{V'} - A_1 c_o \qquad (2.12)$$

$$\frac{1}{V'} = \frac{A_2}{1-y_o} + A_1 c_o \qquad (2.13)$$

further, let us introduce

$$\frac{1}{V'} = z \qquad \frac{1}{1-y_o} = u$$

and by introduction of the new designation we obtain:

$$z = A_2 u + A_1 c_o \qquad (2.14)$$

The values z, u and c_o in Equation (2.14) can be calculated in any instant of the measurement. The z values, calculated from the curve of the measurement at adequate time intervals, t, when plotted in a cartesian co-ordinate system as a function of the pertaining n values, results in a straight line (Figure 2). The intersection of the straight line thus obtained with the ordinate gives the value of the product A_1, c_o, whereas its slope gives the value

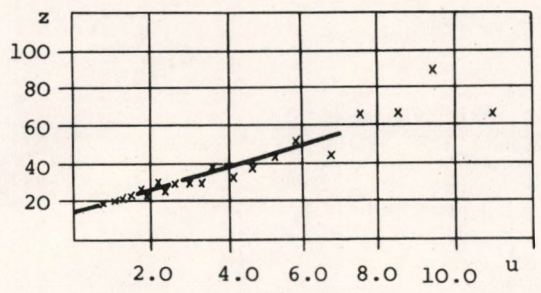

Fig. 2

of A_2. Accordingly, the values $1/A_1$ and $1/A_2$, characteristic of the rate of the catalytic reaction, can be determined.

All data obtained in the course of the experiments, as well as the constants characteristic of them and determined as described in the foregoing, are summarized in Tables I-VII. A diagrammatic representation of the $1/A_1$ and $1/A_2$ values is given in the present paper only as an example, as a function of the most important parameters.

The temperature dependence of the values mentioned above is presented in Figures 3 and 4.

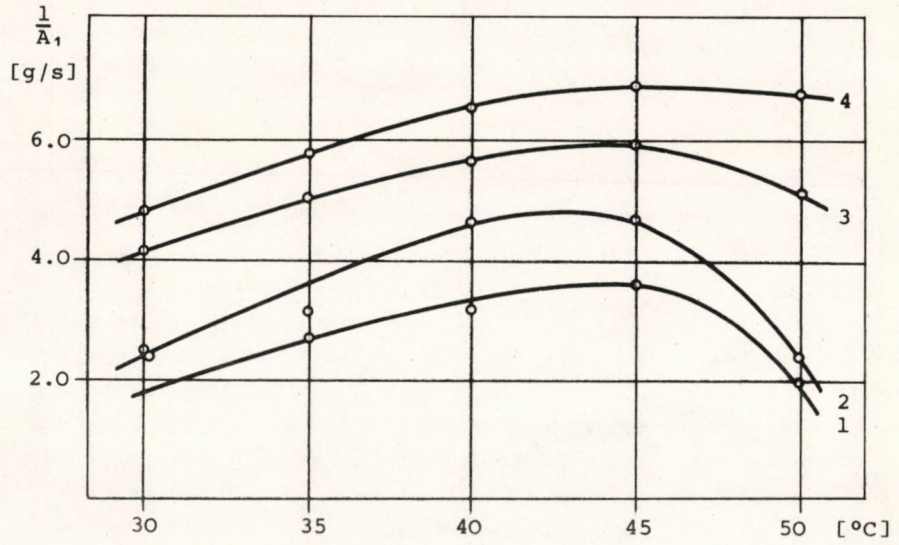

Fig. 3. 1 - Stirred tank reactor; 2 - Shaker; 3 - Bubble column; 4 - Foam column

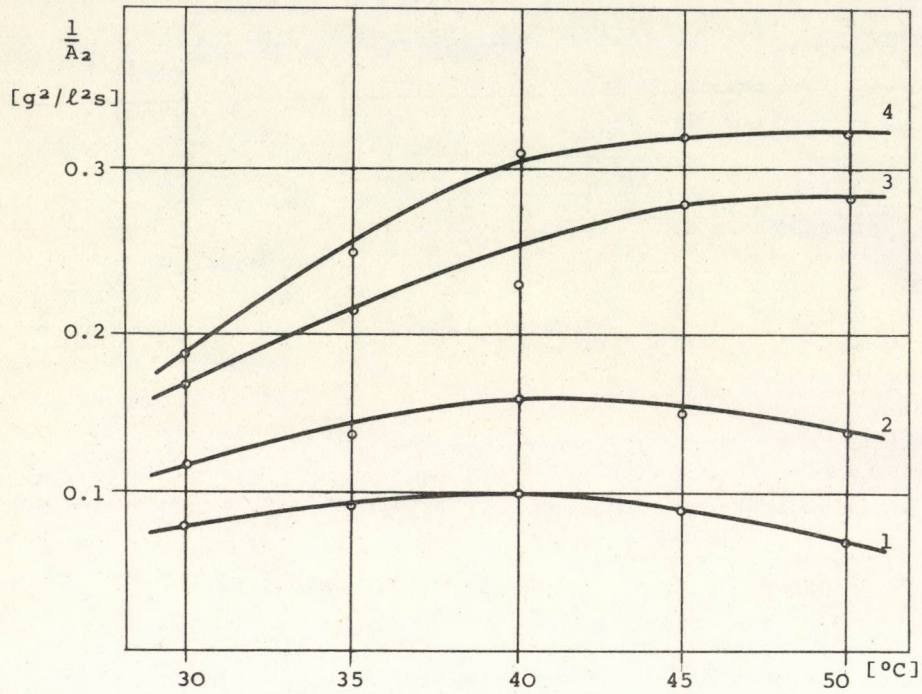

Fig. 4. 1 - Stirred tank reactor; 2 - Shaker; 3 - Bubble column; 4 - Foam column

It can be concluded that the value of $1/A_1$ shows a maximum at 40-50 °C in the temperature range of 30-50 °C studied in the case of all types of apparatus. Having passed the maximum, the value of $1/A_1$ shows in the case of the stirrer- and the shaker--type reactors an abrupt decrease, in the case of the bubble column a moderate and in the case of the foam column a barely perceptible decrease. The value of $1/A_1$ depends on the hydrogen absorption transfer coefficient and consequently it can be assumed that the phenomenon mentioned in the foregoing is brought about by the decreasing solubility of hydrogen with increasing temperature. Furthermore, it is also probable that especially in the foam column, but to a certain extent also in the bubble column, the decreased solubility is partially compensated by the better transfer circumstances.

Table 1

Apparatus	Temperature (°C)														
	30			35			40			45			50		
	Reaction time	$1/A_1$	$1/A_2$	Reaction time	$1/A_1$	$1/A_2$	Reaction time	$1/A_1$	$1/A_2$	Reaction time	$1/A_1$	$1/A_2$	Reaction time	$1/A_1$	$1/A_2$
Stirred reactor	60	2.5	0.08	58	2.63	0.09	50	3.15	0.1	58	3.57	0.09	74	1.92	0.07
Shaker	55	2.5	0.12	50	3.13	0.14	41	3.57	0.6	46	3.57	0.15	57	2.33	0.14
Bubble column	40	4.17	0.17	35	5.0	0.21	32	5.56	0.23	30	5.88	0.32	30	5.0	0.28
Foam column	39	4.53	0.19	30	5.63	0.25	28	6.40	0.31	28	6.65	0.26	28	6.6	0.32

Reaction time: (min)

$1/A_1$: (g/min)

$1/A_2$: (g^2/ℓ^1 min)

Table 2

Apparatus	Amount of catalyst, as referred to 1 g material (mg)														
	5			10			20			30			40		
	Reaction time	$1/A_1$	$1/A_2$	Reaction time	$1/A_1$	$1/A_2$	Reaction time	$1/A_1$	$1/A_2$	Reaction time	$1/A_1$	$1/A_2$	Reaction time	$1/A_1$	$1/A_2$
Stirred reactor	220	0.75	0.02	145	1.85	0.035	30	3.13	0.10	42	3.85	0.12	40	4.47	0.12
Shaker	240	0.86	0.02	102	1.66	0.075	41	3.33	0.16	38	4.00	0.30	37	1.72	0.42
Bubble column	70	2.50	0.06	49	3.85	0.14	32	6.67	0.23	25	9.09	0.39	22	9.50	0.46
Foam column	65	3.34	0.09	45	5.57	0.19	28	8.33	0.31	25	10.0	0.43	20	10.6	0.56

Reaction time: (min)

$1/A_1$: (g/min)

$1/A_2$: ($g^2/\ell^2 min$)

Table 3

Apparatus	Concentration (g/l)								
	30			50			100		
	Reaction time	$1/A_1$	$1/A_2$	Reaction time	$1/A_1$	$1/A_2$	Reaction time	$1/A_1$	$1/A_2$
Stirred reactor	45	4.0	0.13	50	3.1	0.10	81	2.5	0.05
Shaker	35	4.2	0.22	41	3.5	0.17	73	2.5	0.14
Bubble column	31	6.2	0.28	32	5.5	0.23	41	2.0	0.19
Foam column	27	7.6	0.33	28	6.4	0.31	40	4.5	0.23

Reaction time: (min)

$1/A_1$: (g/min)

$1/A_2$: ($g^2/\ell^2 min$)

Table 4

Apparatus	Grain size (mm)								
	0.5 - 2			0.5 - 6 (mean)			4 - 6		
	Reaction time	$1/A_1$	$1/A_2$	Reaction time	$1/A_1$	$1/A_2$	Reaction time	$1/A_1$	$1/A_2$
Stirred reactor	31	3.64	0.13	41	3.13	0.1	58	2.78	0.075
Shaker	39	4.44	0.22	50	3.56	0.17	90	3.23	0.14
Bubble column	25	6.25	0.36	32	5.56	0.23	51	4.80	0.14
Foam column	20	7.30	0.54	28	6.30	0.31	48	5.80	0.17

Reaction time: (min)

$1/A_1$: (g/min)

$1/A_2$: ($g^2/\ell^2 min$)

Table 5

Volumetric flow rate of A_2 at 40°C (l/h)	Linear gas flow rate, as referred to the empty apparatus (cm/sec)	Foam height (cm)	Gas volume fraction	Linear gas flow rate, as referred to the filled apparatus (cm/sec)	Time of hydrogenation (min)	$1/A_1$	$1/A_2$
41	1.51	13.3	0.095	14	61	3.7	0.05
61	2.24	13.5	0.12	19	46	4.6	0.17
81	3.00	13.5	0.12	25	37	5.56	0.23
122	4.49	14.0	0.15	30	32	5.5	0.22
163	6.01	14.0	0.15	40	30	6.2	0.22
244	9.00	14.5	0.18	50	29	6.7	0.27
326	12.00	15.00	0.20	60	28	6.4	0.31
406	14.95	15.5	0.23	65	27	6.7	0.28
488	17.97	16.0	0.25	72	26	6.3	0.27
570	20.99	19.0	0.28	75	26	6.2	0.29

Table 6

Apparatus	Reaction time without poisoning (min)	Ethyl mercaptan weighed in (mg)					
		6		9		12	
		Reaction time (min)	Residual ethyl mercaptan	Reaction time (min)	Residual ethyl mercaptan	Reaction time (min)	Residual ethyl mercaptan
Tank reactor with stirrer	12	135	5.65	280	8.4	-	11.31
Foam column	9	65	3.61	105	4.9	220	8.5

Table 7

Apparatus	Reaction time without poisoning (min)	Hydrogen sulfide (mg)					
		6		9		12	
		Reaction time (min)	Residual hydrogen sulfide	Reaction time (min)	Residual hydrogen sulfide	Reaction time (min)	Residual hydrogen sulfide
Tank reactor with stirrer	12	45	8.02	80	12.61	151	16.44
Foam column	9	15	1.80	32	2.78	73	4.21

While studying the changes in the value of $1/A_2$ it can be concluded that whereas a maximum is incountered at 40 °C in the shaking and stirring-type reactors, a moderate increase is observed above 40 °C in the other two types of reactors. This effect can be ascribed to the maximum activity of the palladium catalyst, attained at the optimum temperature, in the present case at 40 °C. The prolongation of the maximum in the case of the bubble and foam--columns can be explained in the following manner: the reaction proceeds at the surface and within the pores of the catalyst. As a consequence of the exothermic reaction, the temperature of the interior of the catalyst is higher than the measured temperature of the solvent surrounding it and this causes a decrease in its activity. In the bubble and foam columns, where the heat transfer is better, heating of the catalyst is of a lower degree and consequently the maximum activity of the catalyst attains a constant level within a certain temperature range.

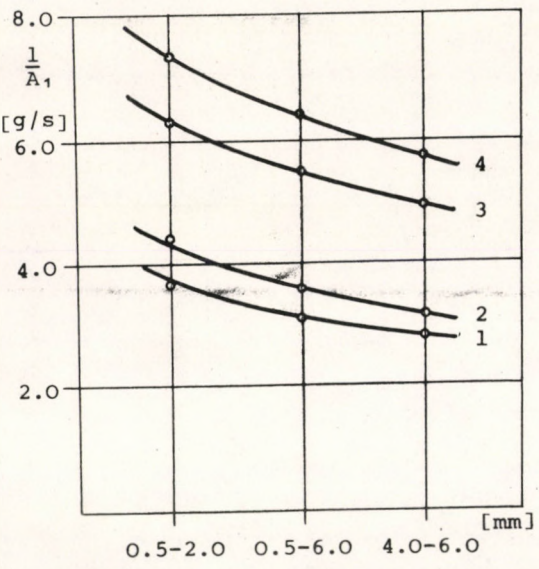

Fig.5. 1-Stirred tank reactor; 2-Shaker; 3-Bubble column; 4-Foam column

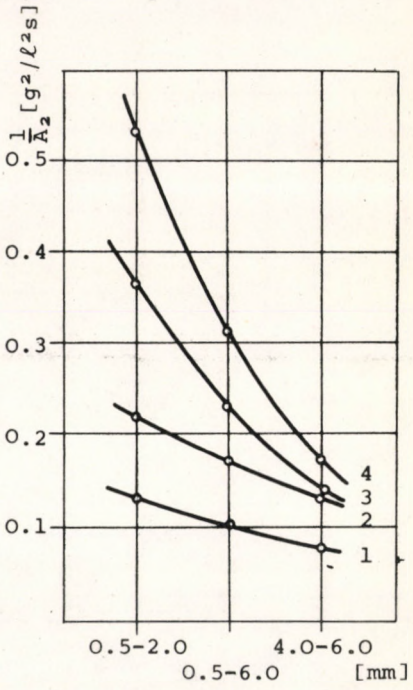

Fig.6. 1-Stirred tank reactor; 2-Shaker; 3-Bubble column; 4-Foam column

The dependence of the values characteristic of the reaction rate on the grain size of the catalyst are presented in Figures 5 and 6.

In this case, it can be concluded that the values of $1/A_1$ and $1/A_2$ increase with decreasing grain size in the case of all of the four apparatus types. Decreasing the grain size brings about essentially the same effect as increasing the amount of the catalyst. In both cases, the active catalyst surface is increased, which brings about in all four apparatus types an increase in the reaction rate dependent on the transfer circumstances. The results obtained with various grain sizes were in agreement with results obtained and conclusions drawn in connection with experiments carried out with various amounts of catalyst.

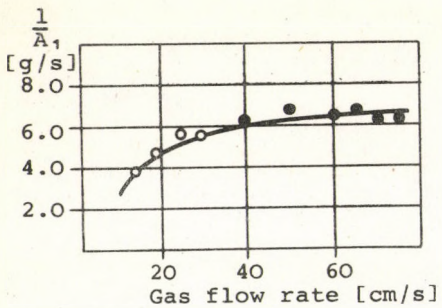

Fig. 7. o-Bubble column; •-Foam column

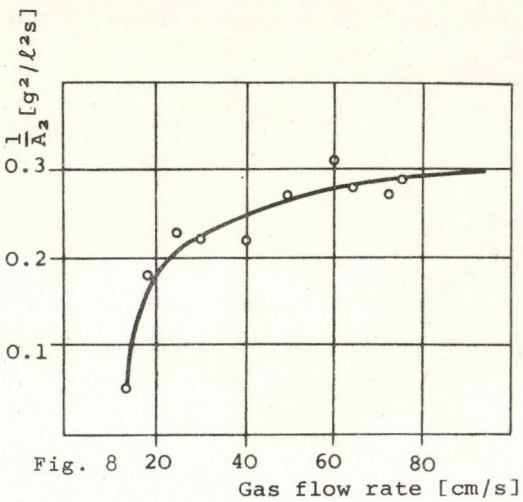

Fig. 8

It is apparent from Figures 7 and 8 that by increasing the linear gas flow rate up to a value of 14-75 cm/s, the value of $1/A_1$ and, together with it, that of $1/A_2$ increases. Both in the bubble and the foam columns, increasing gas flow rate brings about a considerable increase in the rate of the absorption process, and since in the present case the rate of the overall hydrogenation process increases with absorption, in accordance with the previous chapter it can be concluded that in the hydrogenation of the sub-

strate used as a model substance, the rate-determining partial process is the absorption of hydrogen in the solvent.

Considering the results of experiments mentioned in the foregoing - but not evaluated here in detail - (cf. Tables I-VII) it can also be stated as a conclusion that the theoretical connection developed for the determination of the constants characteristic of the reaction rate can also be applied in practice; the results of experiments evaluated by its aid can be summarized as follows:

1. In the case of the model reaction in question, the rate determining partial process of hydrogenation is the absorption of hydrogen in methyl alcohol, used as the solvent of the compound to be hydrogenated.

2. With the reaction in question, from among the four experimental set-ups it is the foam column which enables the highest reaction rate to be reached. Accordingly, in the above model reaction as well as with other hydrogenation reactions where the rate-determining step is absorption, the reaction rate can be increased by carrying out the reaction in a foam-column.

3. Crumbling of the catalyst is, according to microscopic measurements and sieve analyses carried out, of the smallest degree in the bubble column. Also in the foam column, catalyst crumbling does not reach the degree encountered in the stirred tank or shaker-type hydrogenation reactors.

4. Despite the addition of ethyl mercaptan and hydrogen sulphide catalyst poisons to the reaction mixture, the hydrogenation reaction processes to conclusion - at a considerably slower rate - in the foam column, as opposed to the shaker and the tank reactor.

REFERENCES

1. KISS, Z., Néhány eljárás összehasonlitó vizsgálata atmoszferikus nyomásu heterogén katalitikus hidrogénezés esetén (Comparative examination of a few processes in the case of atmospheric heterogeneous catalytic hydrogenation). Dissertation for a Doctor's Degree, University of Chemical Engineering, Veszprém, 1972.

2. UJHIDY, A., KISS, Z., Proceedings of the 2nd Conference on Applied Physical Chemistry, Vol. 2. 311. Akadémiai Kiadó, Budapest, 1971.

РЕЗЮМЕ

Авторы изучали каталитическую гидрогенизацию при атмосферном давлении. Моделью служил метаноловый раствор 2-этил-6-хлор-амида изоникотинной кислоты. Процесс, происходящий на гранулированном катализаторе с 0,5% металлическим палладием и активным углеродом, в качестве носителя был изучен на четырех экспериментальных установках: в встряхивателе, в реакторе бакового типа, в пузырьковой колонне и в пенной колонне.

Была выработана теоретическая формула для определения констант, характерных для скорости реакции гидрогенизации. Эта формула позволила сопоставление скоростей реакции гидрогенизации, происходящей в разных установках.

По данным было установлено, что из выбранных установок пенная колонна обеспечивает наилучшие результаты гидрогенизации для данной модельной реакции.

Hungarian Journal
of Industrial Chemistry
Veszprém
Vol.3. pp. 449-458 (1975)

KINETICS AND MECHANISM OF THE DIMERIZATION OF ETHYLENE USING $[Co(C_2H_4)(PPh_3)_3]_2$ AS CATALYST

G. SPEIER

(Department of Organic Chemistry, Veszprém University of Chemical Engineering)

Received: March 31, 1975.

$[Co(C_2H_4)(PPh_3)_3]_2$ catalyses the dimerization of ethylene at ambient conditions. The following rate equation fits the experimental data:

$$\text{Rate} = \frac{k_4K_2K_3[Co][C_2H_4]}{[PPh_3] + K_2 + K_2K_3[C_2H_4]}$$

where $[Co]$, $[C_2H_4]$ and $[PPh_3]$ are the concentrations of catalyst, ethylene and free phosphine.

INTRODUCTION

Homogeneous catalysts for the dimerization of ethylene and other mono-olefins [1] have aroused considerable interest in recent years. Several authors used first-row transition-metal compounds combined with aluminium organyls to catalyse dimerization reactions [2, 3-9].Only in a few cases were single metal compounds reported to be active catalysts for ethylene dimerization [4] and practically no kinetic studies of ethylene dimerization were carried out using such transition metal complexes.

RESULTS

Initial rates were used to determine the rate law. This procedure avoids influences due to codimerization of ethylene with butenes, formed during the reaction, which was monitored by glc. Typical product composition can be seen in Table 1.

Table 1. Dimerization products (weight %) of ethylene catalysed by $[Co(C_2H_4)(PPh_3)_3]_2$ 2.42×10^{-2} mol·ℓ^{-1} in benzene at 20°; reaction time 30 minutes

trans-2-butene	63.0
cis-2-butene	24.5
1-butene	1.5
hexenes	10

Ethylene uptake was followed by volume (Fig. 1.). The reaction rate was found to be fairly constant during the first few minutes, but hexenes appeared in the reaction mixture already rather early. Assuming ethylene and butene codimerization to have a lower reaction rate, this explains the diminishing rate of ethylene consumption.

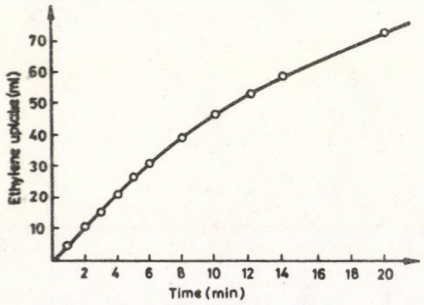

Fig. 1. Typical dimerization of ethylene using $[Co(C_2H_4)(PPh_3)_3]_2$ Solvent benzene; catalyst concn. 2.42×10^{-2} mol.ℓ^{-1}; temp. 20 °C; ethylene pressure 1 atm.

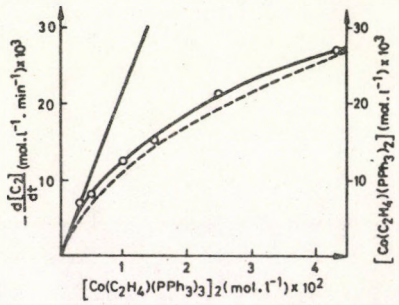

Fig. 2. Rate of dimerization of ethylene as a function of cobalt concentration. Solvent benzene; temp. 20 °C; ethylene pressure 1 atm. (The dotted line shows the concentration of $Co(C_2H_4)(PPh_3)_2$ calculated from Equation (13) as a function of cobalt concentration)

The experiments were reproducible to within ± 5 %, and the initial rates were obtained from the tangents of plots of the type shown in Figure 1.

The influence of catalyst concentration is shown in Figure 2. The parabolic curve obtained by plotting the reaction rates against the catalyst concentration indicates a lower order than one with respect to cobalt catalyst. If the reaction rate is plotted against the square root of the catalyst concentration, a straight line results which does not go through the origin and has a negative intercept on the y-axis (Figure 3). This means, that no half order dependence on the catalyst exists, which could be expected by assuming a pre-equilibrium of the dissociation of the dinuclear catalyst to the mononuclear form largely shifted to the side of dimeric species.

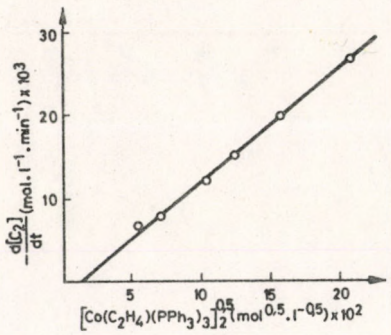

Fig.3. Rate of dimerization of ethylene as a function of the cobalt concentration. Solvent benzene; temp. 20°C; ethylene pressure 1 atm.

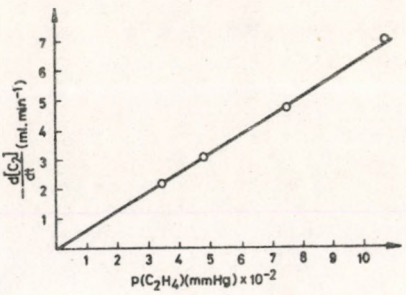

Fig.4. Rate of dimerization of ethylene as a function of ethylene pressure. Solvent benzene; cobalt concn. 2.86x10^{-2} mol.ℓ^{-1}; temp. 20°C

Experiments at various ethylene pressures resulted in a linear plot of the rate against the pressure with zero intercept as shown in Figure 4. This demonstrates a linear dependence of the reaction rate on the ethylene concentration in the solution.

An excess of triphenyl phosphine reduces the rate of dimerization. In Figure 5, the reciprocal of the rate is plotted against added phosphine at constant catalyst concentration. The linear trend with an intercept suggests a reciprocal first order in free triphenyl phosphine.

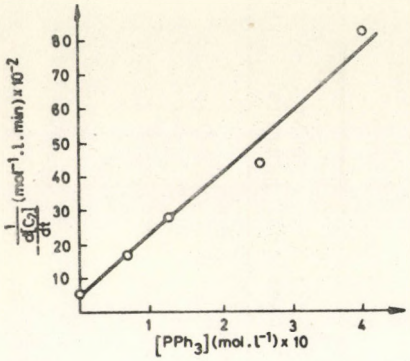

Fig. 5. The reciprocal rate of ethylene dimerization as a function of excess phosphine concentrations. Solvent benzene; catalyst concn. 2.01×10^{-2} mol.ℓ^{-1}; ethylene pressure 1 atm; temp. 20°C.

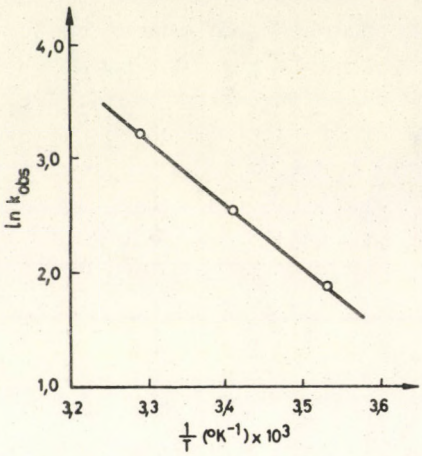

Fig. 6. Arrhenius plot of ln k_{obs} against $\frac{1}{T} \times 10^3$

The effect of the temperature on the reaction rate is shown in Table 2. The k_{obs} values were calculated using the empirical rate expression showing first order dependence with respect to the catalyst and ethylene concentrations. The constants give a linear Arrhenius plot, as shown in Figure 6. The activation parameters were calculated as ΔE_a = 12.4 kcal.mol^{-1}; $\Delta H^{\neq}$ = 11.8 kcal.mol^{-1} and $\Delta S^{\neq}$ = 16 cal.mol^{-1}.K^{-1}.

Table 2. The reaction rate constants k_{obs} at different temperatures, equilibrium constant K_2 and degree of dissociation at 20°C

Temperature (°C)	k_{obs} ($mol^{-1}.\ell.min^{-1}$)	$K_2 \times 10^2$ ($mol.\ell^{-1}$)	Degree of dissociation (%)
10	6.59		
20	12.9	1.17	41*
30	24.9		

*at 2.01×10^{-2} $mol.\ell^{-1}$ catalyst concentration

DISCUSSION

According to YAMAMOTO and co-workers [10] the ethylene complex $[Co(C_2H_4)(PPh_3)_3]_2$ is diamagnetic and does not show any signals in the high field area of the NMR spectrum indicating the absence of a cobalt-hydrogen bond. No absorption in the IR spectrum attributable to ν(Co-H) could be found either. These observations support the dimeric structure accepted for this complex in the solid state.

The kinetic data reported in this paper may be interpreted in terms of scheme 1. Based on this scheme the reaction rate is described by the following equation:

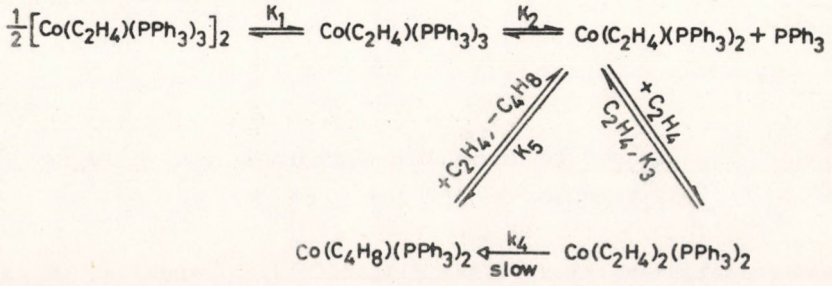

Scheme 1

$$\text{Rate} = -\frac{d[C_2H_4]}{dt} = 2\frac{d[C_4H_8]}{dt} = k_4[Co(C_2H_4)_2(PPh_3)_2] \qquad (1)$$

Supposing K_1 to be large the catalyst is present mainly in the mononuclear form and we can write:

$$[Co] = [Co(C_2H_4)(PPh_3)_3] + [Co(C_2H_4)(PPh_3)_2] + [Co(C_2H_4)_2(PPh_3)_2] + \\ + [Co(C_4H_8)(PPh_3)_2] \qquad (2)$$

where [Co] is the total catalyst concentration. If the initial rates are measured, the concentration of butenes can be regarded to be zero and the last term of Equation (2) can be omitted. The relative concentrations of the other mononuclear species are determined by the following equations:

$$K_2 = \frac{[Co(C_2H_4)(PPh_3)_2][PPh_3]}{[Co(C_2H_4)(PPh_3)_3]} \qquad (3)$$

$$K_3 = \frac{[Co(C_2H_4)_2(PPh_3)_2]}{[Co(C_2H_4)(PPh_3)_2][C_2H_4]} \qquad (4)$$

Incorporating equilibria (3) and (4) into Equation (2) we obtain (5)

$$[Co] = [Co(C_2H_4)_2(PPh_3)_2]\left\{\frac{[PPh_3]}{K_2K_3[C_2H_4]} + \frac{1}{K_3[C_2H_4]} + 1\right\} \qquad (5)$$

Substituting (5) into (1) the following rate equation is obtained:

$$\text{Rate} = \frac{k_4K_2K_3[Co][C_2H_4]}{[PPh_3] + K_2 + K_2K_3[C_2H_4]} \qquad (6)$$

This rate equation is in agreement with the kinetic results if K_2 and K_3 are assumed to be small, which seems to be reasonable. The rate order with respect to ethylene is zero if:

$$[PPh_3] + K_2 \ll K_2K_3[C_2H_4] \qquad (7)$$

and becomes of first order if:

$$[PPh_3] + K_2 >> K_2K_3[C_2H_4] \tag{8}$$

Assuming K_3 to be small (K_2 can be determined) the first order dependence on ethylene is expected at small ethylene concentrations, which was actually found.

According to Equation (6) there is a first order dependence on cobalt, however, the experimental data (Figures 2 and 3), show a more complicated picture. This apparent contradiction is resolved by considering the effect of phosphine ligands dissociated from the catalyst. The concentration of free phosphine is determined by Equation (9):

$$[PPh_3] = [Co(C_2H_4)(PPh_3)_2] + [Co(C_2H_4)_2(PPh_3)_2] \tag{9}$$

If K_3 is small (as assumed earlier) Equation (9) simplified to (10):

$$[PPh_3] \simeq [Co(C_2H_4)(PPh_3)_2] \tag{10}$$

and the total cobalt concentration can be expressed by Equation (11):

$$[Co] = [Co(C_2H_4)(PPh_3)_3] + (PPh_3) \tag{11}$$

Substituting (10) and (11) into (3), Equations (12) and (13) are obtained:

$$K = \frac{[PPh_3]^2}{[Co] - [PPh_3]} \tag{12}$$

$$[PPh_3] = (K_2\{[Co] - [PPh_3]\})^{\frac{1}{2}} \tag{13}$$

If $[PPh_3]$ is not large the concentration of free phosphine, according to (12), is approximately proportional to the square root of the total cobalt concentration and thus $[PPh_3]$ in Equation (6) reduces the first order of dependence on the catalyst concentration, if no extra phosphine is added.

Adding extra phosphine ($[PPh_3]_{add}$) to the reaction mixture, Equation (12) modifies to (14), where $[PPh_3']$ is the concentration of the phosphine, in this case originating from the catalyst by dissociation.

$$K_2 = \frac{[PPh_3'](PPh_3'] + [PPh_3]_{add}\}}{[Co] - [PPh_3']} \qquad (14)$$

The ratio of the rates of the uninhibited (r) and inhibited (r_i) reactions is proportional to the ratio of the corresponding $[Co(C_2H_4)(PPh_3)_2]$ concentrations which are equal to $[PPh_3]$ and $[PPh_3']$:

$$\frac{r}{r_i} = \frac{[PPh_3]}{[PPh_3']} \qquad (15)$$

From Equations (12), (14) and (15), $[PPh_3]$, $[PPh_3']$ and the pre--equilibrium constant K_2 could be calculated (Table 2).

The concentrations of $[Co(C_2H_4)(PPh_3)_2]$ calculated from Equations (10) and (13) were plotted against the catalyst concentration (Figure 2,dotted line). It can be seen that in both curves, the reaction rate vs. the catalyst concentration, and the active species concentrations vs. the catalyst concentration are almost identical, which means that the dependence on the actual catalyst is of the first order and the bend off from a straight line, with respect to the overall cobalt concentration, is caused by the phosphine dissociation from the complex applied as the catalyst.

The scheme proposed above on the basis of kinetic data does not provide any details about the nature of the rate-determining step. PARSHALL [11] showed that the C-H bond in the ortho position of the phosphine phenyl groups undergoes oxidative addition on the cobalt atom in $CoH(N_2)(PPh_3)_3$. This type of reaction was also observed with other compounds having different metals and phosphines [12]. It was assumed that in the investigated ethylene dimerization, a cobalt hydride formed through such an oxidative addition

may play an essential role in the catalytic cycle. This possibility is outlined in detail in Scheme 2.

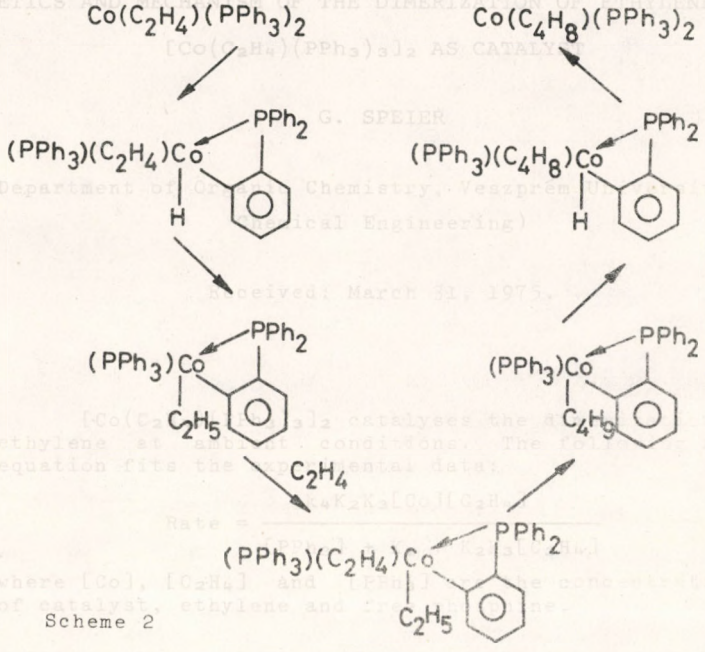

Scheme 2

EXPERIMENTAL

$[Co(C_2H_4)(PPh_3)_3]_2$ was prepared according to literature [10]. The benzene used as a solvent was distilled over sodium-potassium alloy under dinitrogen. Commercial ethylene was purified by bubbling through diethyl aluminium ethoxide after drying with silica gel and P_2O_5. Experiments were performed in a water thermostated 100 ml reaction vessel connected to a thermostated gas burette.

ACKNOWLEDGEMENT

The author is indebted to Professor L. Markó for his useful discussions.

REFERENCES

1. FEL'DBLYUM, V.Sh., OBESHALOVA, N.N., Russ. Chem. Rev., 37, 789 (1968)

2. U.S. Pat. 3.364.378

3. U.S. Pat. 3.424.816

4. TSUTSUI, M., KOYANO, T., J. Polymer Sci., Part A-I, 5, 861 (1967)

5. KUSUNOKI, Y., KATSUNO, R., HASEGAWA, N., KUREMATSU, S., NAGAO,Y., ISHII, K., TSUTSUMI, S., Bull. Chem. Soc. Japan, 39, 2021 (1966)

6. PU, L.S., YAMAMOTO, A., IKEDA, S., J. Am. Chem. Soc., 90, 7170 (1968)

7. CRAMER, R., Accounts Chem. Res., 1, 186 (1968)

8. KETLEY, A.D., FISCHER, L.P., BERLIN, A.J., MORGAN, C.R., GORMAN, E.H., STEADMAN, T.R., Inorg. Chem., 6, 657 (1967)

9. VAN GEMERT, J.T., WILKINSON, P.R., J. Phys. Chem., 68, 645 (1964)

10. YAMAMOTO, A., KITAZUME, S., PU, L.S., IKEDA, S., J. Am. Chem. Soc., 93, 371 (1971)

11. PARSHALL, G.W., J. Am. Chem. Soc., 90, 1669 (1968)

12. PARSHALL, G.W., Accounts Chem. Res., 3, 139 (1970)

РЕЗЮМЕ

Разложение этилена при разных условиях катализируется соединением $[Co(C_2H_4)(PPh_3)_3]_2$. Экспериментальные данные подтверждают следующее уравнение скорости реакции:

$$\text{Скорость} = \frac{k_4 . K_2 . K_3 [Co][C_2H_4]}{[PPh_3]+K_2+K_2K_3[C_2H_4]}$$

где [Co], $[C_2H_4]$ и $[PPh_3]$ концентрации катализатора, этилена и свободного фосфина.

Hungarian Journal
of Industrial Chemistry
Veszprém
Vol.3. pp. 459-466 (1975)

A RAPID METHOD FOR CHECKING THE VALIDITY AND FOR DETERMINING THE PARAMETERS OF A PISTON-FLOW DISPERSED TUBULAR MODEL

R. MOHILLA

(Department of Chemical Process Engineering,
Veszprém University of Chemical Engineering)

Received: April 18, 1975.

The turbulent axial-dispersed plug-flow tubular model is often applied for the description of the dynamic behaviour of tubular operational units. If the residence time spectrum has been determined experimentally, the points of the frequency response of the operational unit can be determined - for the purpose of process control - with the known numerical procedure. The preparation of a standard set of curves is proposed, with the aid of which both the adequacy of the selected model and two parameters of the model: the Bodenstein Number and the mean residence time can be determined in a simple manner. The same set of curves enables - in design work - the construction of the Bode-diagram of an operational unit having known parameters.

The turbulent axial-diffusion (dispersed) plug-flow tubular model is very often applied for the description of the dynamic behaviour of tubular operational units.

When applying the model to a stream of components, the following differential equation is obtained:

$$- D_{ax} \frac{\partial^2 c(z,t)}{\partial z^2} + v \frac{\partial c(z,t)}{\partial z} = - \frac{\partial c(z,t)}{\partial t} \qquad (1)$$

where

c is the concentration of the component $[\frac{kg(component)}{kg(mixture)}]$

z is the space co-ordinate, taken in axial direction (m)

t is time (s)

v is the convective flow rate ($m\ s^{-1}$)

D_{ax} is the coefficient of turbulent axial diffusion ($m^2 s^{-1}$)

Let the following initial condition be chosen:

$$c(z,t) \equiv c(z,o) \equiv 0 \quad \text{when} \quad t \leq 0 \qquad (2)$$

Furthermore, let us consider an operational unit that is finite in both directions and let the feed occur in the strating point of the co-ordinate system. Under such conditions, the boundary conditions used by DANCKWERTS [1] and PEARSON [2] can be applied to the disturbance in feed:

$$v\ c_o(t) = v\ c(t)\Big|_{z=+0} - D_{ax} \left(\frac{\partial c(z,t)}{\partial z} \right)_{z=+0} \qquad (3)$$

$$\left(\frac{\partial c(z,t)}{\partial z} \right)_{z=H} = 0 \qquad (4)$$

where

c_o is the disturbance in feed (dimensionless)

H is the length of the operational unit (m)

The analytical solution of the differential equation in question, at the initial and boundary conditions described, is so far unknown. Naturally, this can be solved by numerical procedures between given margins of error. However, when used for process control, the solution is not generally needed. In these cases it is generally sufficient to produce the transfer function or frequency response or the logarithmic amplitude-angular frequency and phase-angular frequency functions (Bode-diagram).

With reference to the takeoff point (z = H) of the tube, the frequency response is the following [3, 4]:

$$F(\omega) \equiv \frac{c(H,\omega)}{c_o(o,\omega)} = \frac{4\gamma}{(1+\gamma)^2 e^{-\frac{Bo}{2}(1-\gamma)} - (1-\gamma)^2 e^{-\frac{Bo}{2}(1+\gamma)}} \qquad (5)$$

where

$$\gamma \equiv (1 + j\frac{4\omega\bar{t}}{Bo})^{1/2} \qquad (6)$$

$Bo = \frac{vH}{D_{ax}}$ is the Bodenstein number (dimensionless)

$\bar{t} = \frac{H}{v}$ is the mean residence time (s)

ω is the angular frequency ($rad.s^{-1}$)

In the dynamic characterization, Equation (5) was regarded as the descriptive equation calculated from the mathematical model. It is apparent that this function has two parameters: the "Bo" Bodenstein number and the $\bar{t}$ mean residence time. Knowing these, the points of the frequency response can be calculated numerically and this is thoroughly sufficient for application in process control.

The reverse of the statement is also true: the operational unit is perfectly characterized from a dynamical point of view by presenting the numerical value of the two parameters. However, this statement needs to be supplemented: it has to be seen whether the chosen model is adequate for the description of the operational unit in question.

It is known that it is possible to determine the above mentioned two parameters experimentally. The method is generally applied. Its essence is that a tracer material is injected into the feed and the concentration-transient is studied at the takeoff point. The two parameters can be calculated from the first and second momentum according to time of this transient. However, this procedure involves a number of problems. It is known from experimental experience that the calculation of the second moment is

rather uncertain and the result considerably depends on how large a section of the asymptotically decreasing transient is taken into consideration. Furthermore, it is difficult to verify whether the model was adequate or not. For this purpose, the transient calculated from the model has to be produced after substitution of the calculated parameters with a numerical technique (i.e. the differential equation has to be solved) and the result thus obtained has to be compared with the measured figure. However, another method leading to a faster result and furnishing more information can also be chosen.

As mentioned earlier, the numerical presentation of the points of the frequency response is necessary in many cases and is also adequate for our purposes. For this purpose, an algorithm is applied in the evaluation of the transient obtained which presents the numerical values of the frequency response (i.e. the points of the Bode-diagram) in a single step [5, 6].

Using the technique proposed in the present paper, both the adequacy of the model and the numerical value of the parameters can be determined with a minimum of computing work from the curve thus obtained, whose production is necessary anyway.

This is true within a limit of error that occurs in the application of the numerical method and in making neglections while establishing the model.

It can be shown with the application of Shannon's sampling rule that the calculated values are reliable only up to a value

$$\omega_{max} = \frac{\pi}{\Delta t}$$

where Δt is the time interval between sampling operations. This, however, is only a theoretical upper limit. According to LEES and DOUGHERTY [7], the practical upper limit is lower by one order of magnitude.

Let us substitute various numerical values into Equation (5) in place of the Bo number. Further let us select to each of these

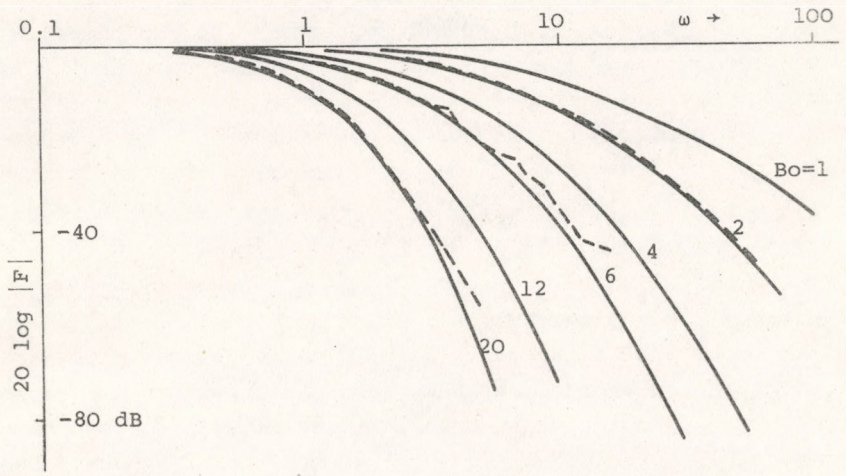
0.1
1
10
ω →
100
Bo=1
2
4
6
12
20
-40
20 log |F|
-80 dB

Fig. 1

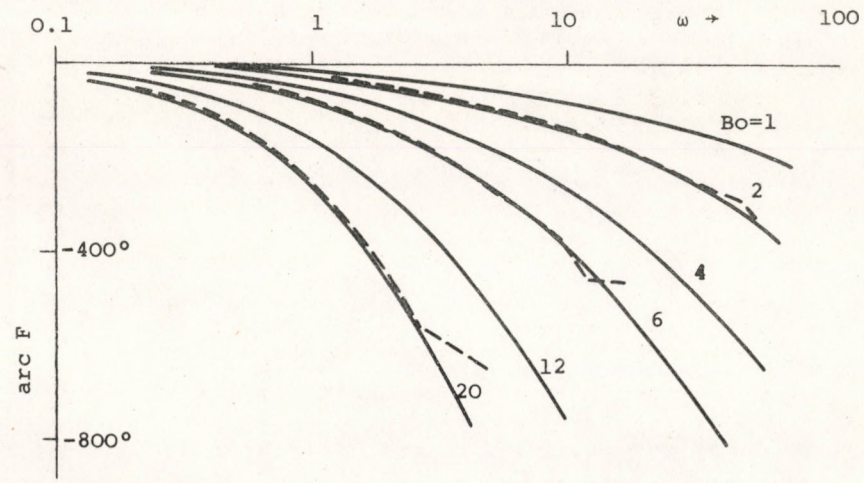
0.1
1
10
ω →
100
Bo=1
2
4
6
12
20
-400°
arc F
-800°

Fig. 2

a $\bar{t}$ mean residence time in such a manner that the condition Bo = = 4 $\omega\bar{t}$ is fulfilled. Hereupon, the values of ω are run preferably from 0.1 to 100, for the case of all Bo numbers and the numerical values of the frequency function are calculated. The result is presented in the usual form in a Bode-diagram in such a manner that log ω is measured on the abscisse, whereas on the ordinate twentyfold of the logarithm of the absolute value of the complex function respectively the areas thereof. A set of curves of normalized angular frequency, whose parameter is the Bo number, is obtained in this manner (Figures 1 and 2).

The same - but single - pair of curves is also obtained in the evaluation of the measured transient. If the set of calculated curves is drawn on a transparent paper and the drawing placed upon the curve obtained in the measurement, it can immediately be decided whether the chosen model was applicable. In this case, the curve calculated from one Bo number coincides with that obtained in the measurement.

Accordingly, the Bo number pertaining to the operational unit under test has also been determined.

Having aligned the curves it is determined which abscisse value of the diagram representing the result of the measurements is found under the point corresponding to the abscisse value $\omega = 1$ of the set of curves. Let this angular frequency be of the numerical value of ω_o. The mean residence time of the operational unit under test can be calculated hereform with the formula

$$\bar{t} = \frac{Bo}{4\ \omega_o} \tag{7}$$

No further explanation is necessary if the second term on the right side of Equation (6) is considered.

Accordingly, a single computer algorithm is to be applied with the proposed technique. This directly presents the evaluation of the measurement in a form adequate for process control applications.

Accordingly, a single computer algorithm is to be applied with the proposed technique. This directly presents the evaluation of the measurement in a form adequate for process control applications.

By means of the previously prepared curve-set template, the application of the chosen model as well as the two characteristic parameters can be examined with a minimum of expenditure. It is be noted that by the inversion of Equation (7), i.e. by adequate shifting of the origo of the abscisse, the previously prepared set of curves also naturally enables the Bode diagram of an operational unit characterized by a given Bo-number and mean residence time to be constructed immediately.

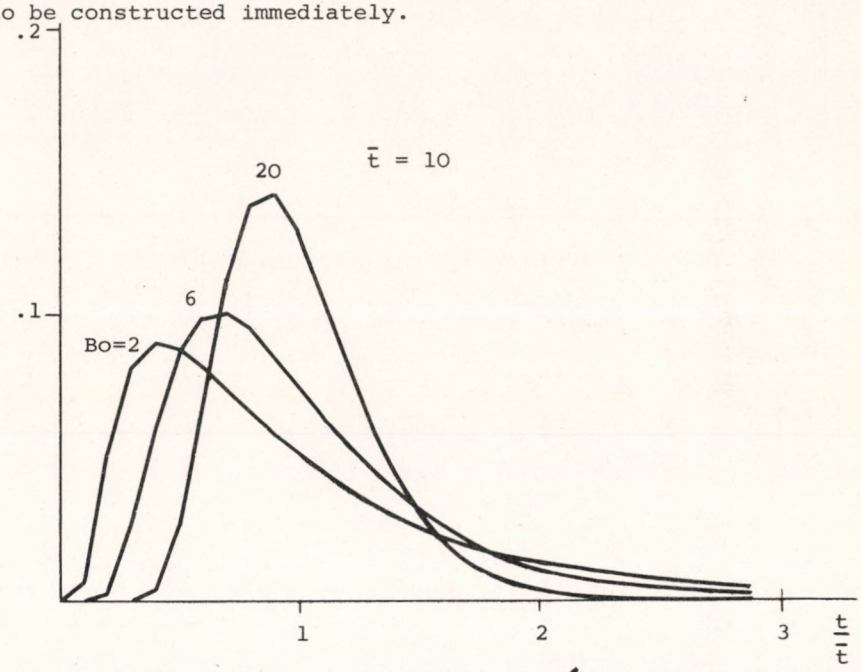

Fig. 3

As an example, three residence time spectra (weight functions) are presented in Figure 3. In this case, the parameters (also determined with a different method) were the following: $\bar{t}$ = 10 sec. Bo = 2, 6 and 20. The points of the Bode diagram were prepared from the 30 points shown by a numerical technique [6]. After shifting according to (7), the curves corresponding to the numeri-

cal values obtained were drawn into Figures 1 and 2 with a dotted line. The theoretical confidence limits, as calculated with the technique mentioned in connection with the estimation of the errors, were found to be ω_{max} = 63; 21 and 6.3 (rad.s^{-1}). This presents an approximative picture of the applicability and expectable accuracy of the approximative technique.

The author is indebted to Professor Dr.A. László for his valuable comments upon reading the manuscript and to Dr. B. Ferencz for checking the calculations.

REFERENCES

1. DANCKWERTS, P.V., Chem. Engng. Sci. 1, 1 (1953)
2. PEARSON, I.R.A., Chem. Engng. Sci. 10, 281 (1959)
3. FAN, L.T., AHN, Y.K., Chem. Engng. Progr. Symp. Ser. 59, 46, 91 (1963)
4. MOHILLA, R., FERENCZ, B., Vegyipari folyamatok dinamikája (Dynamics of Chemical Industrial Processes) Budapest, Müszaki Könyvkiadó, 1972.
5. HUSS, C.R., DONEGAN, J.J., NACA Technical Note 3598, Jan. 1956.
6. DREIFKE, G.E., HOUGEN, J.O., Joint Aut. Contr. Conf. 1963. 608-633 p.
7. LEES, S., DOUGHERTY, R.C., Journal of Basic Engineering. 1967. June, 445-449.

РЕЗЮМЕ

Для описания динамического поведения трубчатых процессовых единиц часто используется модель, полагающая турбулентную осевую диффузию и идеальное вытеснение. После экспериментального определения спектра времени пребывания известным числовым способом можно определить точки кривой по частоте в целях техники регулирования. Автором предлагается приготовление семейства шаблонных кривых, с помощью которого можно проверить адекватность выбранной модели и просто определить два параметра модели: число Боденштейна и среднее значение времени пребывания. Те же кривые используются для планирования при начертании диаграммы Бодэ процессовой единицы с известными параметрами.

Hungarian Journal
of Industrial Chemistry
Veszprém
Vol.3. pp. 467-488 (1975)

AN EXPERIMENT FOR THE DETERMINATION OF THE DEGREE OF MIXING OF A SUSPENSION

G. HORVÁTH

(Department of Chemical Process Engineering,
Veszprém University of Chemical Engineering)

Received: April 18, 1975.

In connection with all stirred systems, the determination of the degree of mixing is a problem of basic importance. The aim of the present paper is the presentation of a mathematical procedure that utilizes the probability calculus and enables the efficiency of mixing to be judged. The mathematical model proper is sufficiently general, involving the customary advantages and drawbacks of this fact. The practical example presented shows that even with very simple suppositions - in a given case - adequate results are furnished by the model.

The stirring of suspensions is classified as a separate group of two-phase flow [1]. This classification is supported by the generally large difference in specific gravity and the fact that the solid particles cannot be united and cannot - in the majority of cases - be designated. This practically means that these particles can be regarded as discrete ones in the continuous medium. In order to sustain the suspended state, mechanical energy has to be continuously introduced into the system. In order to be able to discuss the phenomenon, it is inevitably necessary to know the degree of stirring; the next step is to establish a connection between the introduced energy and the degree of stirring.

The problem can be approached from more than one angle; ample examples are found in literature.

The logical discussion starts from the examination of the space of flow of liquids. Of course, in such cases, the motion nature of the momentum balances [2] is of primary importance. The difficulties which manifest themselves in connection with the mathematical discussion of the space of flow of a stirred system are generally known. Accordingly, papers containing only experimental results are abundant [3, 4, 5, 6, 7, 8, 9].

Groups of the research workers do not deal separately with the motion of the supporting phase, but directly study the behaviour of the particles [10, 11]. Such theory is correct, but its field of validity becomes limited due to the many simplifications when calculations are carried out.

A different category of work, utilizing the similarity theory, calculates on the basis of experiments with a number of practically important data. These Equations contain generally 5-8 empirical constants [12, 13, 14, 15, 16]. Lacking an adequate theory, these are of major significance despite the fact that the Equations are valid only in a narrow range.

The empirical measures and mixing models used for the characterisation of stirred systems also constitute a new group with regard to content. Their common feature is that they disregard the micro structure.

In establishing the models, formulas used for the description of totally different physical phenomena are frequently utilized in order to obtain a result similar to those encountered in practical systems. These include the well-known diffusion, cascade and recirculation models, as well as their combinations.

There are also experiments in which the authors do not deal with the mechanism of stirring, even to the extent usual in modelling. Usually the systems are ordered with regard to mixing on the basis of some arbitrarily selected criterion [16, 17].

A new way to judge the degree of mixing of practical systems is the application of the entropy of mixing [18]. The application

of the concept of entropy in this respect is based upon its connection with information theory. The concentration distribution has to be known for the calculation.

The Probability Model of Mixing

Let us consider first what processes can be discussed within the framework of probability calculus and whether a stirred system fulfills these requirements in our case.

A number of occurrences can be described by the following scheme [19]. A certain totality of the prevailing circumstances is the experiment, as a result of which, one of the possible events occurs. Our instantaneous knowledge does not permit - theoretically or practically - the determination of this event. In such cases it can be stated that the occurrence of the event is "random". In the examination of events of this class, it is absolutely essential that the events, together with their results, can be repeated many times, since the relative frequency of the occurrence of the events has to be known in order to be able to draw conclusions on the probability of the occurrence of the event. All processes complying with the above conditions can be discussed on the basis of the probability calculus.

Our system is limited by walls and it comprises a fluid medium into which discrete particles having identical properties were introduced.

A possible approach is that all prevailing conditions are regarded as an experiment and the system is examined at certain given times and the probability of a given particle emerging from a given part of space is examined. Accordingly, the elementary event is that a given particle is in one of the space elements. What is now the condition to be able to state that the system in question is perfectly mixed. The condition is that the probability of finding the particle in question in any of the limited space elements is equal. If these probability values are not equal and some of the individual space elements are of exceptional importance compared to the others, a very large number of variations - identical with

regard to the degree of mixing - can be produced, evidently depending on the fineness of division. For example, if the particle contents of two space elements are exchanged, the two systems can be considered identical with regard to mixing, despite the fact that a new spatial distribution has been produced. Considering spatial distribution in this manner does not promise any results. The problem of the complicated space of streaming emerges here again.

There is another possible approach and this is the examination of the following question: from what particle density environment the given particle originates. In this case, the fact where the environment of the particle is found in the stirred system is disregarded and only one characteristic of the environment, important for our reasoning, is taken into consideration. In the system under test, the elementary event is the concentration of the environment of the given particle, i.e. the particle concentration is regarded as probability variable.

If the total volume of the space elements of the concentration c_1 is $V(c_1)$, the probability that the optionally selected particle has come from an environment of the concentration c_1 is

$$\frac{c_1 \rho_s V(c_1)}{M}$$

where ρ_s is the density of the solid and

M is the mass of the total solids weighed in.

Now, assuming that the concentration in the stirred system varies continuously between the minimum and maximum value found in the system, the probability density function

$$\varphi'(c) = \frac{c \rho_s V(c)}{M}$$

can be introduced. The corresponding distribution function is the following:

$$\Phi'(c) = \int_{c_{min}}^{c} \varphi'(c)\, dc$$

According to the experience, the value of maximum concentration can unequivocally be determined in such a system, and accordingly the distribution and density functions are calculated starting from the maximum concentration values with the following Equation:

$$\varphi'(c) = \varphi(c_{max} - c) = \frac{c\ \rho_s\ V(c)}{M}$$

In this way, all that was done was to assign the probability, pertaining to a given a concentration, to the value $(c_{max} - c)$.

Let us now consider that our stirred system is influenced by an independent interaction. All of the actions produce a random particle distribution and their totality represents the prevailing circumstances, the system having been exposed to the latter for a considerable period of time. In this manner, the resulting deviation from the maximum concentracion is obtained as the sum of the individual actions:

$$t = c_{max} - c = \xi_1 + \xi_2 + \ldots + \xi_i + \ldots + \xi_n$$

On the basis of the aforesaid, the resultant concentration difference is brought about by action n. Since

$$t = \sum_{i=1}^{n-1} \xi_i + \xi_n$$

as a consequence of the independence, the resultant density function can be calculated successively from the convolution of the individual distribution:

$$\varphi_n = \varphi_{n-1} * \varphi_1$$

From now on, a theoretical model is at our disposal. Different assumptions can be introduced in connection with the individual actions and accordingly different distribution types can be obtained, ranging from the simple to the most complicated. Accordingly,the model incorporates both the good and the bad properties of the general one.

It is - at least theoretically - advantageous that a wide variety can be theoretically characterized by it, whereas it is a drawback that it cannot be applied directly in this form. An example will be presented in the following which demonstrates that even in the case of very simple assumptions, a satisfactory result is obtained for the concentration distribution in a given case.

The aim of the present experiments was to study the concentration distribution in a stirred tank-type reactor. The measured data are evaluated with the mathematical procedure described in the foregoing. The characteristics of the suspension applied, the experimental setup and the measured data will be described first.

The Model Suspension and its Preparation

An anion exchange resin type VARION-AD—water system was used in the experiments. The data of the commercial VARION-AD resin are the following:

capacity:	3.5 mval/g	1.2 mval/ml
density:	1.23 g/cm^3	
grain size:	0.25 - 1.0 mm in dia.	

The concentration of the model suspension was measured by AC conductivity. It is necessary in order to obtain reproducible results that the conductivity of the resin and the water do not change in time, consequently the system was brought to equilibrium and any water or resin brought into the apparatus subsequently was of the prepared materials. In this manner it was ensured that the conductivity was a function only of the amount or resin brought between the electrodes.

Description of the Experimental Setup

The experimental setup comprises a SIMAX (Czechoslovakia) self-supporting glass tank reactor of the dimensions usual in the pharmaceutical industry. The volume of the reactor is 20 litres; 5 litres of resin were placed into it and it was filled up with liquid so as to have a final total volume of 15 litres.

The stirrer motor - a VKM product - was placed above the reactor. The former was connected to the stirrer through a multi--step gear. The adjustable speeds were the following: 50, 150, 250, 350, 450, 550, 650, 750 and 850 r.p.m.

The measurements were carried out with two stirrer types, one being a closed turbine whereas the other was a disc-type stirrer (60 mm in dia.) (Figure 1).

Concentration of the Suspension

Prior to the description of the measurements, what should be understood by the concentration of the suspension, has to be stressed. It seems self-evident to express the concentration of the suspension as some sort of density. However, from the point of view of the measurements it is much simpler to use concentrations expressed in volume per cent. In the following, the concentration will be calculated with an intrinsic measure. A suspension is regarded as 100 % by vol. if when left alone to stand it does not become more compact upon the action of gravitational force. Naturally, in addition to the previous concentration values, the mean density of the suspension of 100 % by vol. as well as the density of the solid and of the liquid have to be given. The mean density of the suspension of 100 % by vol. can be expressed by

$$\rho_{sz} = \rho + \varepsilon (\rho_s - \rho)$$

where

ρ_{sz} is the mean density of the suspension
ρ is the density of the liquid
ρ_s is the density of the solid
ε is the voidage.

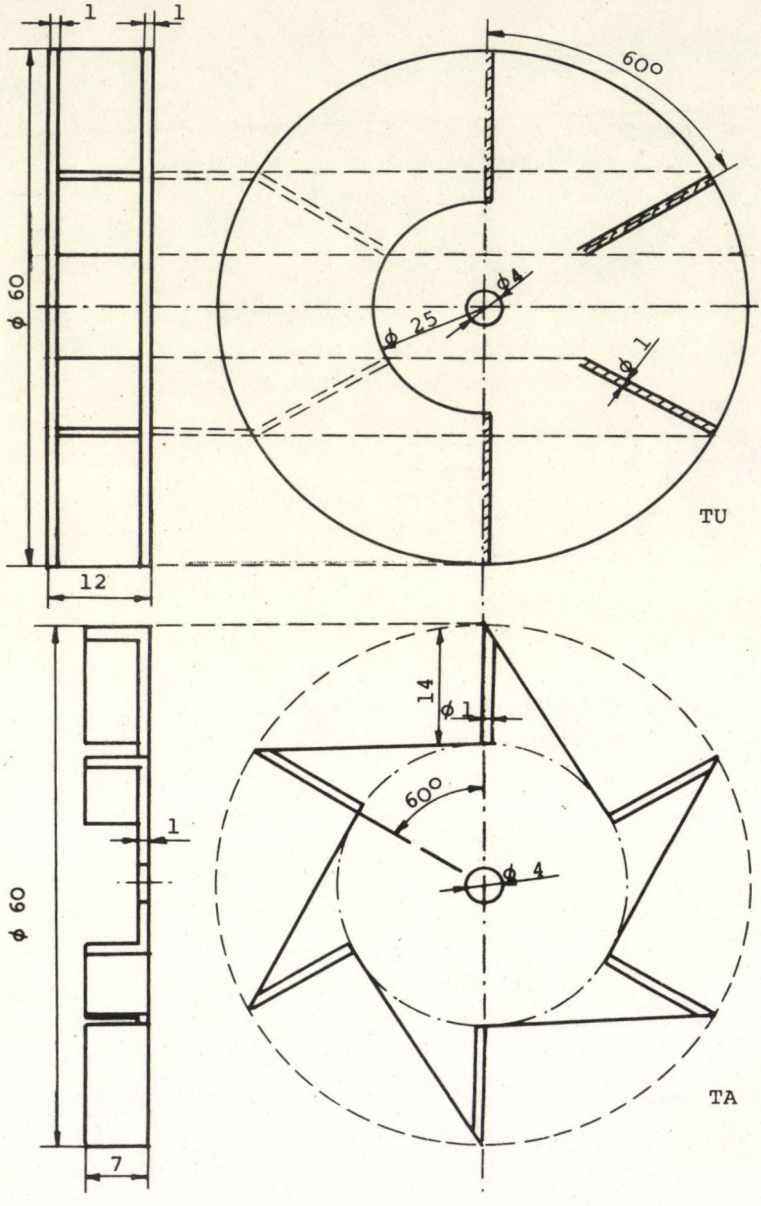

Fig. 1. Turbine-type (TU) and disc-type (TA) stirres

In the present case, with substitution of numerical values and on the basis of [20, 21]

$$\rho_{sz} = 1.128 \text{ g/cm}^3$$

Measurements

Concentration charts were determined with the speeds adjustable with the two stirrer types mentioned above (disc and turbine). Compared to the dimensions of the electrode used, the measuring points were located at the highest density in horizontal and in vertical direction at a distance of 30 mm. The concentration, when plotted against time, did not show appreciable variations in a given measuring point and accordingly reading a mean value presented no difficulty. This empirical finding supports the view that the concentration charts are stable despite the swirling streaming.

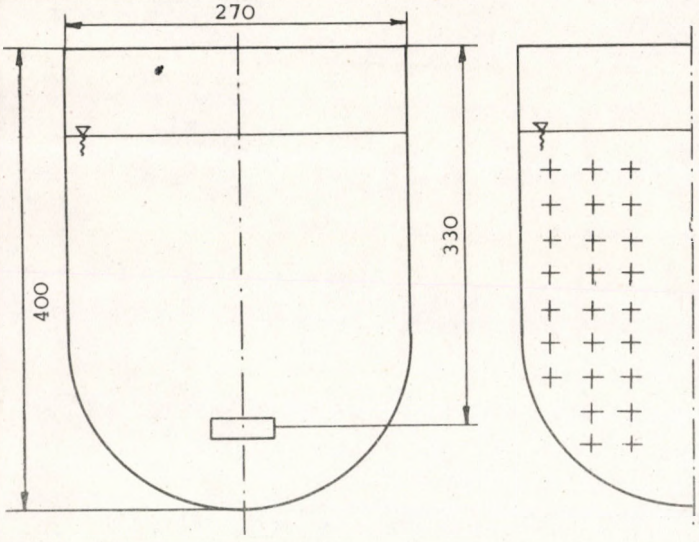

Fig. 2

Only half a plane was measured in all cases in vertical section. The location of the measuring points and of the stirrers is shown in figure 2.

The concentration charts are presented in Figure 3. They were arranged in such a manner that those pertaining to the same stirrer speed are beside one another. There is a heading on each chart. The disc-type stirrer is marked TA and the turbine-type one TU in the heading. The figure before the letters is the serial number of

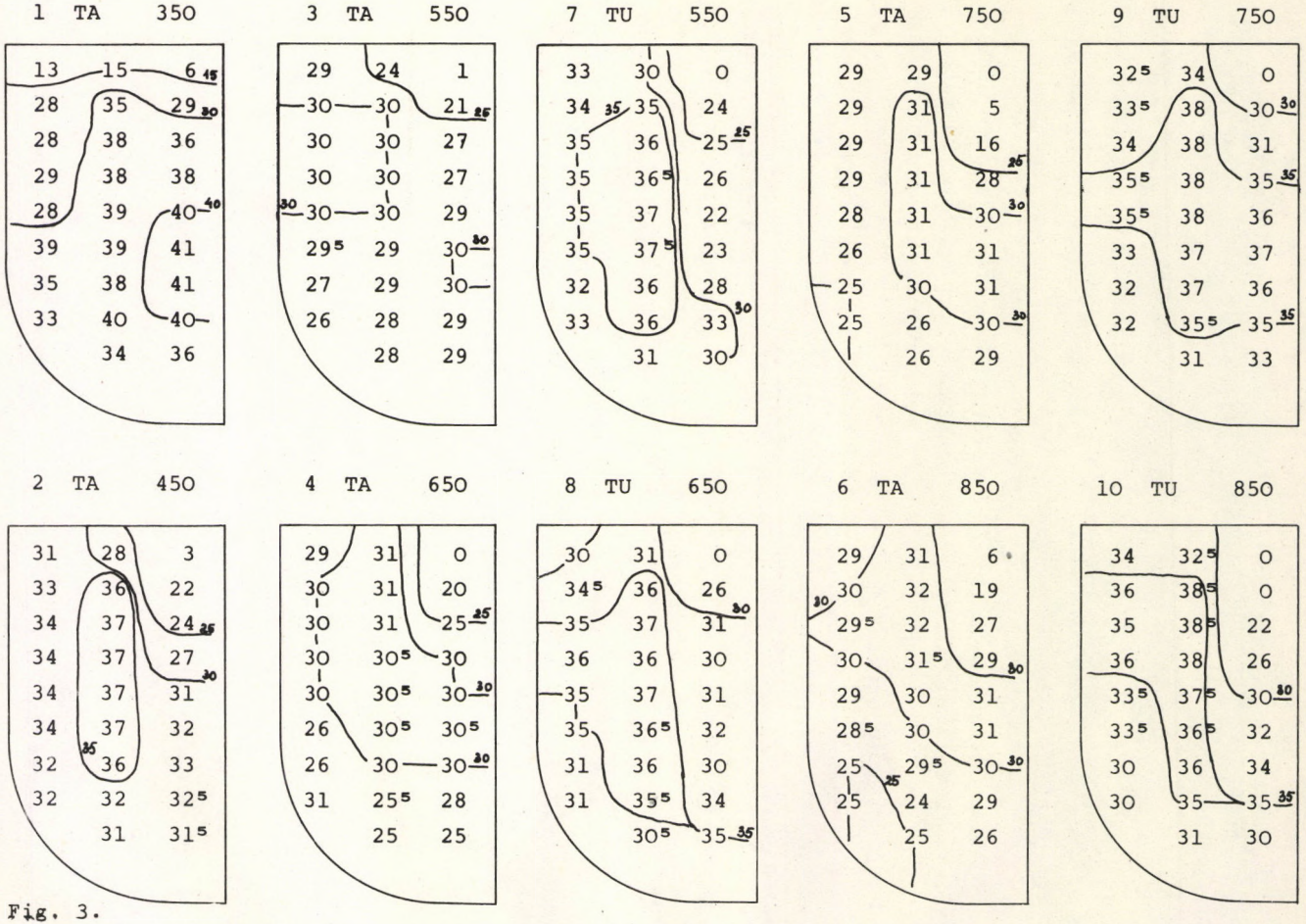
1 TA 350
13 15 6 15
28 35 29 30
28 38 36
29 38 38
28 39 40 40
39 39 41
35 38 41
33 40 40
34 36
3 TA 550
29 24 1
30 30 21 25
30 30 27
30 30 27
30 30 30 29
29⁵ 29 30 30
27 29 30
26 28 29
28 29
7 TU 550
33 30 0
34 35 35 24
35 36 25 25
35 36⁵ 26
35 37 22
35 37⁵ 23
32 36 28
33 36 33 30
31 30
5 TA 750
29 29 0
29 31 5
29 31 16
29 31 28 25
28 31 30 30
26 31 31
25 30 31
25 26 30 30
26 29
9 TU 750
32⁵ 34 0
33⁵ 38 30 30
34 38 31
35⁵ 38 35 35
35⁵ 38 36
33 37 37
32 37 36
32 35⁵ 35 35
31 33
2 TA 450
31 28 3
33 36 22
34 37 24 25
34 37 27
34 37 31 30
34 37 32
35 32 36 33
32 32 32⁵
31 31⁵
4 TA 650
29 31 0
30 31 20
30 31 25 25
30 30⁵ 30
30 30⁵ 30 30
26 30⁵ 30⁵
26 30 30 30
31 25⁵ 28
25 25
8 TU 650
30 31 0
34⁵ 36 26
35 37 31 30
36 36 30
35 37 31
35 36⁵ 32
31 36 30
31 35⁵ 34
30⁵ 35 35
6 TA 850
29 31 6
30 30 32 19
29⁵ 32 27
30 31⁵ 29 30
29 30 31
28⁵ 30 31
25 29⁵ 30 30
25 24 29
25 26
10 TU 850
34 32⁵ 0
36 38⁵ 0
35 38⁵ 22
36 38 26
33⁵ 37⁵ 30 30
33⁵ 36⁵ 32
30 36 34
30 35 35 35
31 30

Fig. 3.

the measurement, and that after the letters is the speed in r.p.m. There was no appreciable churning up under 350 r.p.m. with the disc and under 550 r.p.m. with the turbine stirrer.

For the purpose of qualitative examination, the iso-concentration lines were drawn into the charts. In a qualitative manner it can be stated that the chart becomes more uniform with increasing stirrer speed up to a speed of 650 r.p.m. in the case of the disc-type stirrer and above this value the concentration differences between the individual points start to rise again. The same can also be stated in connection with the turbine-type stirrer with the difference that in this case the "maximum of uniformity" is even more pronounced.

Evaluation of the Measured Data

The essence of the mathematical model described is that the following Equation holds for the probability variable t:

$$t = c_{max} - c = \xi_1 + \xi_2 + \ldots + \xi_i + \ldots + \xi_n$$

If the supposed density function of $\xi_i (i = 1, 2 \ldots n)$ is

$$f(t) = \lambda e^{-\lambda t}; \quad t > 0$$

it can be shown by total induction that a density function of the form

$$\varphi_n(t) = \frac{\lambda^n \, t^{(n-1)} \, e^{-\lambda t}}{(n-1)!}$$

is obtained as the resultant. The variable t follows the Γ distribution. The corresponding distribution function is obtained from the integral

$$\Phi_n(t) = \int_0^t \varphi_n(\nu) \, d\nu$$

At the same time, the Equation

$$\varphi_n(t) = \frac{c \, \rho_s \, V(c)}{M}$$

holds. On the basis of this, discrete distribution functions can

be calculated from the measured data because the half section of the reactor was - in accordance with the measuring points - subdivided to cells. A ring corresponds to each cell in the reactor and on account of the symmetry, the concentration at any point in this ring is equal to the measured mean value (experimental finding).

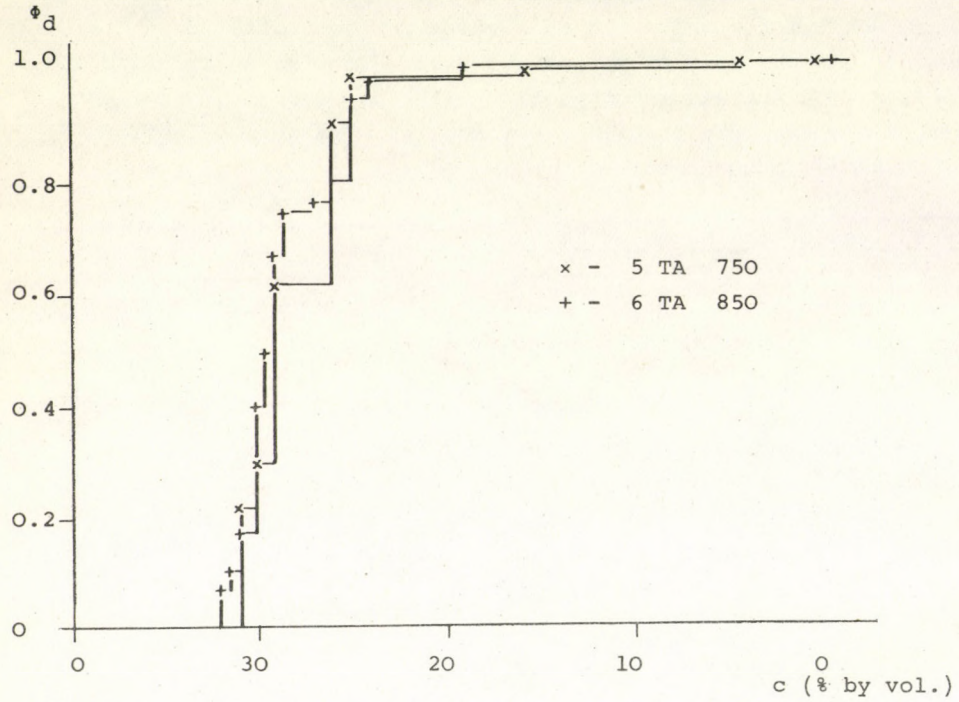

Fig. 4. Discrete distributions

A digital computer was used for processing the numerical data. As an example, a discrete distribution function is shown in Figure 4.Hence only one more step and the continuous distributions are reached. The concentration was considered to change continuously between the maximum and minimum values measured in the system, in such a manner that the middle points of the steps of the discrete distributions correspond to the points of the continuous

distribution. A continuous distribution function is shown in Figure 5.

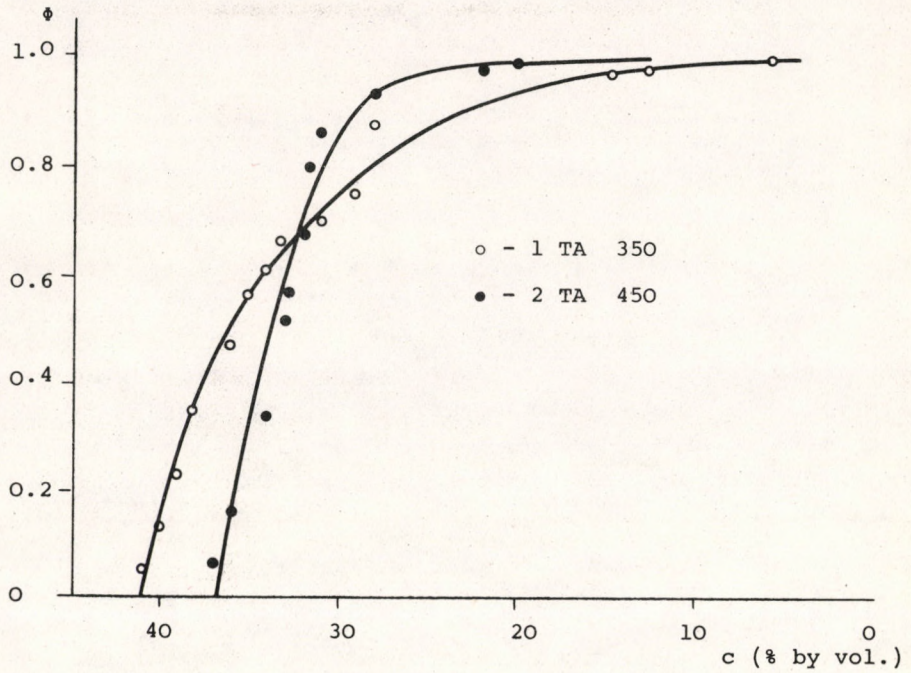

Fig. 5. Continuous distributions

Accordingly, the numerically calculated distribution functions are at our disposal from the experimental data. The value of c_{max} is obtained from their intersection with the abscissa. The theoretical distribution itself is of the two parameter type (n,λ). The parameter are determined in the following manner. The expected value of the Γ distribution is n/λ. Any positive integral number was chosen for n, the ordinate value pertaining to the expected value could be calculated from this. The expected value was determined by the help of the ordinate values of continuous distribution functions.

The ordinate values pertaining to the expected values can be determined from the corresponding density functions. E.g. in the case of n = 3, the integral — substituting $x = -\lambda t$ — is the following:

$$\int_0^{3/\lambda} \lambda^3 \frac{t^2}{2!} e^{-\lambda t}\, dt = \left[\frac{e^x}{2}(x^2 - 2x + 2)\right]_{-3}^{0} = 0.575$$

With a similar procedure

$$\int_0^{2/\lambda} \lambda^2 t\, e^{-\lambda t}\, dt = 0.594 \quad \text{or} \quad \int_0^{1/\lambda} e^{-\lambda t}\, dt = 0.632$$

The parameters of the calculated continuous distributions are contained in the Table. A few diagrams are shown, as examples, in Figure 6 where the measured data and the calculated curves are presented. These prove that the general model describes the distributions even in the case of very simple suppositions to a fairly good approximation.

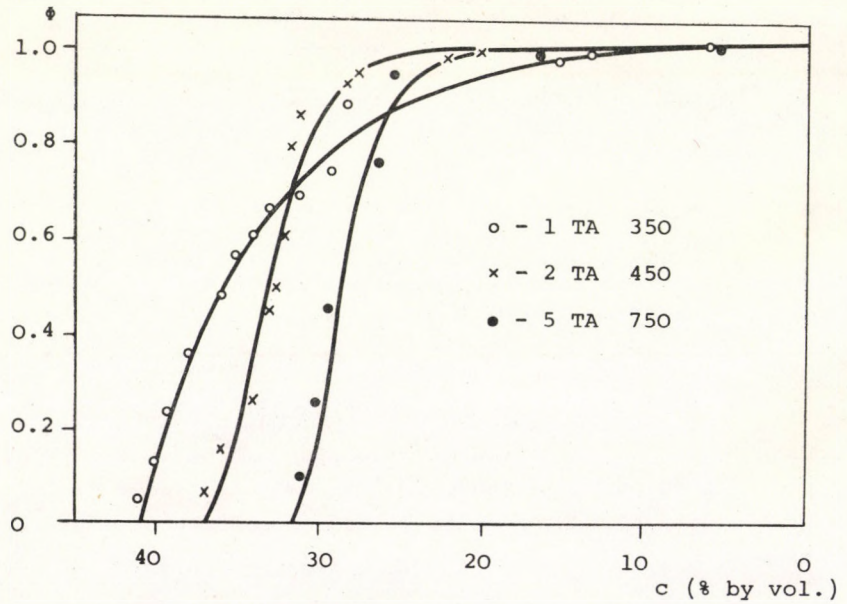

Fig. 6 a. Calculated distribution

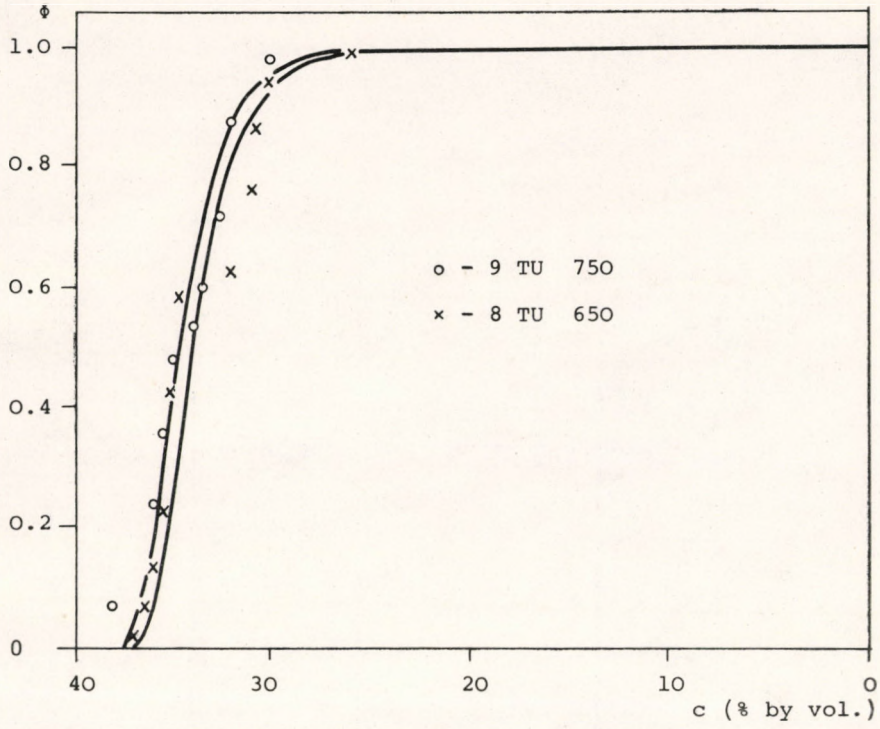

Fig. 6 b. Calculated distribution

The expected value and the variance, plotted against stirrer speed, are shown in Figure 7. Both the expected value and the variance pass a pronounced minimum in the vicinity of 650 r.p.m.This suggests the conclusion that stirrer speed has an optimum value with respect to the mixing of the given system inasmuch as the distribution produced is the most uniform. On the basis of the variance it can be stated that the extreme value is not very "sharp", partically a range covering 150 r.p.m. and is such that further improvement of mixing is not possible.

These experiments prove that the disc-type stirrer is considerbly more flexible, it can be operated satisfactorily within a

Table 1. Parameters of continuous distributions

Stirrer type	Serial No.	Speed r.p.m.	n	λ	c_{max} (measured % by vol.)	c_{max} (calculated % by vol.)	Accuracy of material balance %
TA	1	350	1	13.3	39.0	41.0	96.5
	2	450	3	62.5	37.0	37.5	96.0
	3	550	3	136.4	30.0	31.0	83.9
	4	650	3	176.5	31.0	31.0	84.3
	5	750	3	83.3	31.0	31.5	80.0
	6	850	3	75.0	32.0	32.0	83.6
TU	7	550	3	68.2	37.5	38.0	96.1
	8	650	3	88.2	37.0	37.5	98.2
	9	750	3	83.2	38.0	38.0	100.7
	10	850	3	51.7	38.5	39.0	95.8

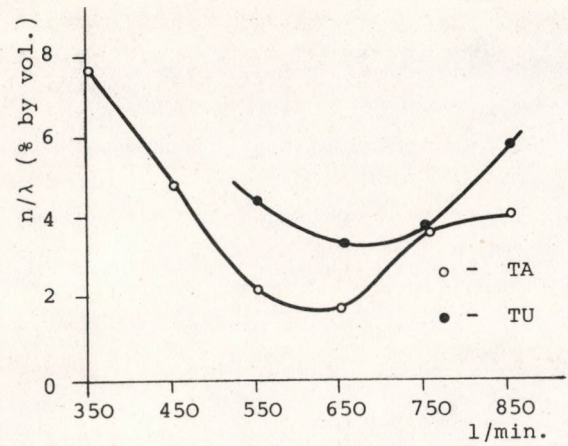

Expected value vs. speed diagram

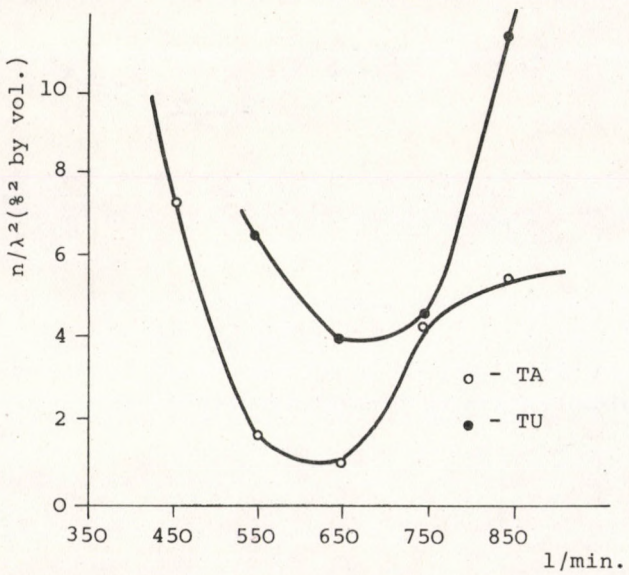

Fig. 7. Variance vs. speed diagram

wide range. With the turbine-type stirrer it was found that above a "threshold" speed value the system assumed a state of mixing and afterwards there were practically no changes.

The curves of the disc-type stirrer were always under those of the turbine stirrer. This means that at a given speed, the disc stirrer stirs more uniformly and the same state of mixing can be reached by the disc-type stirrer at a considerably lower speed.

Another interesting and practically utilizable fact should be mentioned here. The c_{max} values were plotted against speed in Figure 8. These concentration values also show a pronounced minimum as a function of speed. This minimum is within the practically acceptable speed range, mentioned above. Consequently, when examining a given similar system, it is unnecessary to calculate the distributions, and it is sufficient to find the minimum of the maximum concentration value in the vertical half-section of the reactor as a function of stirrer speed; the stirrer is to be operated at that speed.

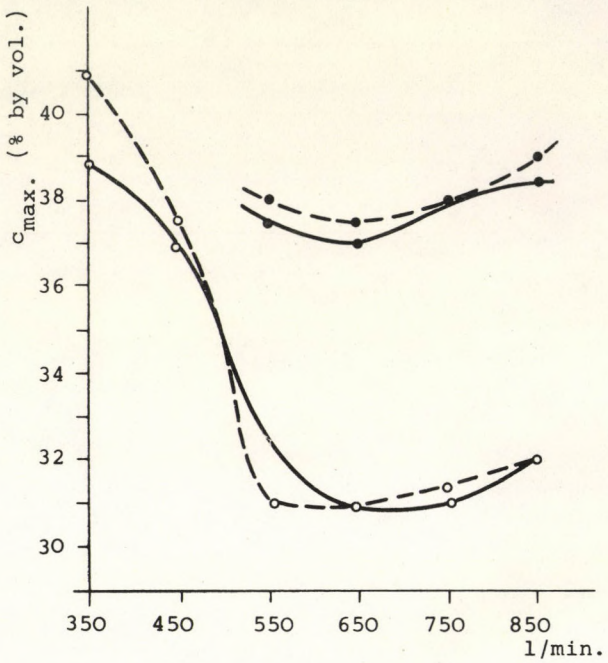

Fig. 8. — measured curves; -- calculated curves; o - TA; • - TU

SYMBOLS USED

ε	voidage (dimensionless)
$\varphi'(c)$; $\varphi_n(c)$	probability density function (dimensionless)
ξ_i	probability variable (dimensionless)
ρ	density of the liquid (ML^{-3})
ρ_s	density of the solid (ML^{-3})
ρ_{sz}	mean density of the suspension (ML^{-3})
λ	parameter (dimensionless)
$\varphi_n(t)$	probability density function (dimensionless)
$\Phi_n(t)$	distribution function (dimensionless)
c	concentration (% by vol.)
c_{max}	value of maximum concentration (% by vol.)
$f(t)$	probability density function (dimensionless)
i	current index (dimensionless)
M	mass of total solid material weighed in (M)
n	parameter (dimensionless)
t	probability variable (dimensionless)
$V(c)$	total volume of space elements of the concentration c (L^3)

REFERENCES

1. SZOLCSÁNYI, P., Transzportfolyamatok (Transport Process) Tankönyvkiadó, Budapest, 1972.

2. BENEDEK, P., LÁSZLÓ, A., A vegyészmérnöki tudomány alapjai (Fundamentals of Chemical Engineering Science) Müszaki Kiadó, Budapest, 1964.

3. BLASINSKI, H., TYCZKOWSKI, A., Int. Chem. Engng., 8, 43 (1968)

4. COOPER, R.G., WOLF, D., The Canad. J. Chem. Engng. 47, 268 (1969)

5. PETERS, D.G., SMITH, J.M., Trans. Inst. Chem. Engrs. 45, 360 (1967)

6. NAGATA, S., YAMAMOTO, K., HAHIMOTO, K., NARUSE, Y., Mem. of the Fac. Engng. Kyoto Univ. 22, 68 (1960)

7. NAGATA, S., JAMAMOTO, K., UJIHARA, M., Mem. of the Fac. Engng. Kyoto Univ. 20, 336 (1958)

8. THOMAE, H., Chemie Ing. Techn. 42, 317 (1970)

9. BOWERS, R.H., A.J.Ch.E. - I.Ch.E. Symposium Ser. 1965. No. 10.

10. LAWRENCE, H., WEISS, J., FICK, L., HOUSTON, R.H., VERMEULEN,I., UC-4 Chemistry, TID-4500, 1962. 17.

11. ZWIETERING, T.N., Chem. Eng. Sci. 8, 244 (1958)

12. OYAMA, Y., ENDOH, U., Chem. Eng. (Japan) 20, 666 (1956)

13. WEISMAN, I., EFFERDING, L.E., A.I.Ch.E.J. 6, 419 (1960)

14. FEJES, G., Ipari keverőberendezések (Industrial Stirrers). Müszaki Kiadó, Budapest, 1970.

15. UHL-GRAY, Mixing Theory and Practice, Academic Press, New York, London, 1967. 5. 251-254, II. 76-84.

16. OLDSHUE, Y.Y., Ind. Engng. Chem. 61, 79 (1969)

17. HIXSON, A.W., TENNEY, A.A., Trans. Am. Inst. Chem. Eng. 31, 113 (1935)

18. TŐRÖS, R., A keveredési entrópia általánositása (Generalization of the Entropy of Mixing. Dissertation for a Candidate's Degree.) Kandidátusi értekezés, Budapest, 1971.

19. RÉNYA, A., Valószinüségszámitás (Probability Calculus) Tankönyvkiadó, Budapest, 1971.

20. Varion NIKE termékismertető (Varion NIKE products catalogue) 1970.

21. NYERS, Á., Szilárd és folyadékfázisok közötti anyagátadás tanulmányozása. Diplomadolgozat (Studies on Material Transfer between Solid and Liquid Phases. Dissertation for a Chemical Engineer's Diploma) Veszprém, 1970.

РАЗЮМЕ

Правильное определение смешанности является основной задачей для смешанных систем. Целью этой работы является представление математического способа. Этот способ использует математическую статистику и позволяет судить об эффективности смешения. Математическая модель является довольно общей, и имеет обычные преимущества и недостатки. По представленному примеру видно, что в данном случае модель приводит к удовлетворительным результатам при очень простых допущениях.

Hungarian Journal
of Industrial Chemistry
Veszprém
Vol.3. pp. 489-496 (1975)

POWER REQUIREMENT OF THE INTENSIFICATION OF STIRRING

P. SZOLCSÁNYI and G. HORVÁTH

(Department of Chemical Process Engineering,
Veszprém University of Chemical Engineering)

Received: April 18, 1975.

The intensity of stirring is a parameter of high importance with certain chemical industrial apparatus types. This intensity can, in certain respects, be visualized as an entropy representation of relative energy. Based on experimental data gained in examinations on model suspensions, a procedure is presented for the illustration of the calculation of the intensity. The calculated intensity values are compared with the theoretical limiting intensity and the invested power.

The intensification of stirring can be understood in a number of different manners. It can be regarded as a constructional assignment where the object is to design a stirrer which enables the production of a mixture of the highest degree of homogeneity. In this case, the power requirement is a question of secondary importance. However, from another point of view, the power requirement that enables a certain degree of mixing to be attained with the application of a given stirring device is the primary question. As a first approximation, it seems self-evident that more thorough stirring can be attained by investing a higher power. However, this is only true most generally speaking. A more thorough inves-

tigation has revealed that the connection between the degree of homogenization and invested power is not unequivocal.

The problem is made more complex by the fact that a distinction must be made between mixtures that are formed spontaneously and those formed only upon the action of some kind of force. Part of the latter group separates when the force ceases. Separation can be brought about as the results of a number of forces.

The present investigations were carried out on a system with forced mixing. Such systems are suspensions which tend to separate as a result of the normally always present difference in specific gravity upon the action of gravitational or centrifugal force. Intensification of the mixing of a suspension is understood to be homogenization carried out against the separating influences. The aim is, evidently, to produce a suspension as uniform as possible. In most cases attempts are made to reach this homogeneity by the application of rotary stirres.

The model tested during the present work is identical to that described in paper [1]. In this case, the solid particles were of a higher density and consequently they were sedimented upon the action of the forces or were transported in a radial direction by the action of the rotary stirrer. It is self-evident that there exists an optimum method of stirring in which the arrangement of the particles in the liquid is of the highest uniformity.

The aim of the present work was to determine how the homogeneity of the suspension varies as the function of invested energy. From this point of view, two things have to be distinguished: one is the preparation of the suspension within a period of time that can technically be realized, the other is sustaining the suspension already prepared.

The two actions in question were not studied separately and quantitatively from the point of view of the forces, instead a phenomenological description of mixing was aimed at.

The entropy was applied for the energetical characterization of mixing.

TŐRÖS [3] established a connection between the classical mixing models through the entropy. The applicability of the concept of entropy in this respect was theoretically supported.

It is a known fact that when increasing the volume of a given heap of particles from v_o to v, an amount of entropy

$$S_i = R \cdot M_i \ln \frac{V_i}{V_{oi}} \tag{1}$$

is produced. In this case, the system executes, in an isothermal and reversible manner, a work

$$L = TS \tag{2}$$

This is regarded as the formal energetical degree of mixing. Its relative value refers to the "thermal" energy and the connection thus obtained is a function only of the volume ratio:

$$L_{r_i} = \frac{L_i}{RTM_i} = \ln \frac{V_i}{V_{oi}} \tag{3}$$

The total mass of the particles is

$$M = \sum_i M_i \tag{4}$$

In our case, the following connection is valid:

$$\frac{V_i}{V_{oi}} = \frac{c_o}{c_i} \tag{5}$$

since the concentration c_o in the case of the sedimented granular material, is regarded <u>per definitionem</u> 100 %. V_{oi} is, on the other hand, the volume of the i-th fraction in this state.

By introducing continuous functions, the relative mixing work made on the system can be given by the following formula:

$$L_r = \frac{L}{RT} = \int_o^{c_{max}} M \cdot \varphi(c_{max} - c) \ln \frac{c_o}{c} \, dc \tag{6}$$

where $\varphi(c_{max} - c)$ is the probability density function as defined in [1]:

$$\varphi(c_{max} - c) = \frac{\lambda^n (c_{max} - c)^{(n-1)} \, e^{-\lambda(c_{max}-c)}}{(n-1)!} \tag{7}$$

The product $M \cdot \varphi(c_{max} - c)$ gives exactly the mass of the heap of particles of the concentration c. According to the definition mentioned above, $c_o = 1$. Now we express the specific value of the relative mixing work, with the substitution of the function $\varphi(c_{max} - c)$:

$$\frac{L_r}{M} = \int_o^{c_{max}} \frac{\lambda^n (c_{max} - c)^{(n-1)} \, e^{-\lambda(c_{max}-c)}}{(n-1)!} \ln \frac{1}{c} \, dc \tag{8}$$

The equation can be interpreted in the following manner: there are entropy-increasing and entropy-decreasing effects active in the system. The irregular motion brought about by the stirrer is entropy-increasing, whereas the effects of the gravitational and centrifugal forces are entropy-decreasing. A stationary concentration distribution is brought about in the system as a dynamical equilibrium of these actions which can be described by the entropy of the system.

The equilibrium of the dynamic actions is determined by the amount of energy introduced into the system. Consequently, the specific value of the relative mixing work is studied as a function of the power requirement of the liquid mixing.

The power requirement of the mixing of the liquids can be calculated from the known formula [2]:

$$Eu_k = k \cdot Re_k^{\,a} Fr^{\,b}$$

The stirrer power N is expressed, considering that in the turbulent range, $a \approx 0$ and $b \approx 0$.

Hence we can write:

$$Eu_k = k$$

and

$$N = k \quad u^3 \, d^5 \, \bar{\rho}$$

$\bar{\rho}$ represents the mean density of the suspension.

$$\bar{\rho} = 1.13 \times 10^3 \text{ kg/m}^3$$

$$d = 6 \times 10^{-2} \text{ m}$$

The value of k depends on the type of the stirrer.

The power values at the usual stirrer speeds were the following:

u (1/min)	350	450	550	650	750	850
N (W)	0.168	0.357	0.665	1.08	1.74	2.62

If the specific value of the stirring work, chosen as the characteristic of the intensity of stirring is numerically calculated with the application of the data at our disposal in [1] on the basis of Equation (8), the following result is obtained.

TA in the Table represents a disk-type, whereas TU a turbine type stirrer. n and λ are the two parameters of the probability density function and L_r/M is the value, with reference to the unit mass of the solid substance, of the relative mixing work.

Considering that:

$$3 \, V_o = V$$

the L_r/M value pertaining to perfect mixing is:

$$\ln \frac{V}{V_o} = 1.098$$

The Equation expresses that the 33 % solid granular material present in the system uniformly fills the entire volume of the reactor.

Stirrer type	Serial (No.)	Speed (r.p.m.)	n (-)	λ (-)	L_r/M (l/kg)
TA	1	350	1	13.3	1.049
	2	450	3	62.5	1.070
	3	550	3	136.4	1.076
	4	650	3	176.5	1.076
	5	750	3	83.3	1.074
	6	850	3	75.0	1.073
TU	7	550	3	68.2	1.071
	8	650	3	88.2	1.075
	9	750	3	83.2	1.074
	10	850	3	51.7	1.070

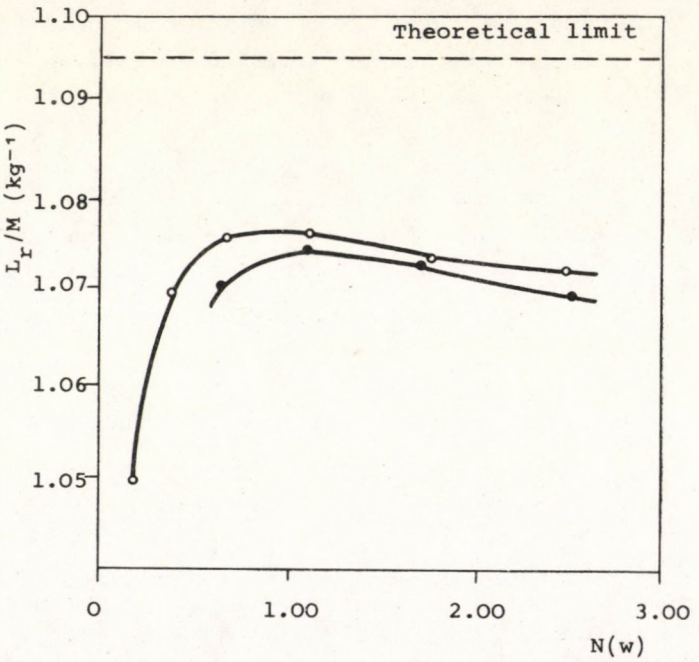

Fig. 1. o - TA, • - TU

By correlating the L_r/M values with the N invested power values it is found that the function is not monotonic, but it passes a maximum. In the latter point, the suspension is of the most uniform composition, the higher L_r/M values meaning a more uniform concentration distribution. This phenomenon can be explained only in the following manner: at lower input power values the action of the gravitational force causing the solid particles to sediment is not totally compensated, whereas at higher input powers the action of centrifugal force predominates causing the particles to be forced outwards and thereby bringing about separation.

The resultant of the entropy-increasing and entropy-decreasing actions, as a stationary state, characterized by the entropy as a state parameter, can be correlated with the single parameter of the system under the given circumstances, i.e. with the input power.

REFERENCES

1. HORVÁTH, G., Hung. J. Ind. Chem. 3, 467 (1975)

2. FEJES, G., Ipari keverőberendezések (Industrial mixers) Müszaki Könyvkiadó, Budapest, 1970.

3. TŐRÖS, R., Generalization of the entropy of mixing. Dissertation for a Candidate's Dgree, Budapest, 1971.

SYMBOLS USED

λ parameter (dimensionless)

$\bar{\rho}$ mean density of the suspension (ML^{-3})

$\varphi(c_{max.}-c)$ probability density function (dimensionless)

a constant (dimensionless)

b constant (dimensionless)

c	concentration (dimensionless)
c_{max}	maximum concentration in the system (dimensionless)
d	diameter of stirrer (L)
Eu_k	Euler-number of mixing (dimensionless)
Fr	Froude Number
k	constant (dimensionless)
L	work (ML^2T^{-2})
L_r	relative work (dimensionless)
M	mass (M)
N	power (ML^2T^{-3})
n	parameter (dimensionless)
R	gas constant ($L^2T^{-2}\ \theta^{-1}$)
Re	Reynolds Number (dimensionless)
S	entropy ($ML^2T^{-2}\theta^{-1}$)
u	speed of rotation (T^{-1})
V	volume (L^3)

РЕЗЮМЕ

Степень интенсивности смешения является очень важным данным оборудований химической промышленности. В некотором смысле интенсивность можно сопоставить с относительной репрезентацией энтропии. По экспериментальным данным испытания модельной суспенсии представляется способ для вычисления интенсивности. Сравниваются вычисленные значения интенсивности, теоретическое предельное значение интенсивности и внесенная мощность.

Hungarian Journal
of Industrial Chemistry
Veszprém
Vol.3. pp. 497-518 (1975)

THE REACTION BETWEEN SODIUM AMALGAM AND ETHYL ALCOHOL

J. de JONGE

(Department of Chemical Technology,
Veszprém University of Chemical Engineering)

Received: May 29, 1975.

In the reaction taking place between sodium amalgam and ethyl alcohol, the sodium concentration of the amalgam and the water concentration and conductance of the ethylate solution have a definite influence on the reaction rate. The experimental technique used for the determination of the reaction rate is described. An empirical kinetic equation is given, based on the determined data.

INTRODUCTION

Among the alkali alcoholates sodium ethylate is one of the most important compounds. It is widely used as the raw material or as catalyst for the preparation of pharmaceutics, cosmetics, paints and different products of the organic chemical industry [1].

For the production of sodium ethylate today, the use of the reaction between ethyl alcohol and sodium amalgam is stated to be an up-to-date method [2].

$$[Hg]Na + C_2H_5OH = C_2H_5ONa + 1/2\ H_2 + [Hg] \qquad (1)$$

Water free ethyl alcohol must be used for the reaction otherwise the formed sodium ethylate reacts with the water and an undesired product, sodium hydroxide is produced as the following equilibrium reaction shows:

$$H_2O + C_2H_5ONa \rightleftharpoons C_2H_5OH + NaOH \qquad (2)$$

During the Second World War, the Mathieson Chemical Corporation applied sodium amalgam and methyl alcohol for the production of solid sodium methylate [3] and elaborated the details of the technology. The same technology can be used for the production of sodium ethylate.

The reaction between aliphatic alcohols and sodium amalgam is very similar to that of amalgam and water. In both reactions the products are hydrogen and alkaline solutions. A striking difference occurs in the reaction rate, this is fairly high if amalgam reacts with water, but it lessens if the amalgam is in contact with alcohol. Moreover, the reaction rate decreases with the increasing number of carbon atoms consisting of the alcohol molecule.

The sluggish reaction can be made vigorous, as CUNNINGHAM discovered [4], in the presence of an electrically conducting, but non-amalgamating electrode being in contact with the amalgam and alcohol. For this electrode - or catalyst - CUNNINGHAM recommended carbon and particularly graphite or alloys of iron, chromium and nickel.

The idea of CUNNINGHAM's discovery is well known to caustic soda producers. In the amalgam denuders or decomposition towers graphite blocks or lumps are placed to enhance the reaction between amalgam and water.

The different type of reactors proposed for the production of alcoholate solution [5, 6, 7, 8] are equally suitable for the preparation of caustic soda, but in the latter case, as a matter of course, water must be reacted with amalgam.

Although the close relation between the amalgam—water and amalgam—alcohol reaction is evident, relatively little research work and observations were published in literature dealing with the latter reaction.

The aim of the present work was to investigate the decomposition of sodium amalgam in the presence of ethyl alcohol and based on the experimental data to derive an empirical rate equation.

EXPERIMENTAL TECHNIQUE

It is easy to demonstrate that no reaction occurs if alcohol is poured over the layer of pure amalgam. The reaction i.e. the evolution of hydrogen starts at once if a metal sheet e.g. molybdenum - which completely fulfils the earlier mentioned requirements of CUNNINGHAM's patent - is immersed into both the phases. Similarly, it was found in connection with the thoroughly investigated amalgam—water reaction [9] that a short circuited galvanic cell comes into existence. In this cell the amalgam is the anode, the molybdenum sheet is the cathode and the alcohol plays the role of the electrolyte. The evolution of hydrogen is due to an electrochemical reaction.

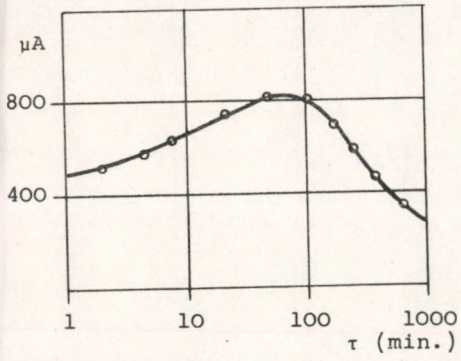

Fig. 1. The current intensity vs. time function of the amalgam | ethyl alcohol | molybdenum galvanic cell

A small amalgam—molybdenum galvanic cell was elaborated, and pure ethyl alcohol was used as the electrolyte. The electrodes were short circuited through a galvanometer and the current vs. time curve was registered.

It can be seen in Figure 1 that the result was a curve having a definite maximum. As it is known the electromotive force, the external and internal resistances determine the current intensity of a cell. In the discussed case among these factors only the internal resistance changed — decreased — sharply. This was due to the newly formed ions produced in the electrode reactions and this caused the temporary growth of the current intensity. Later, as the driving force of the cell decreased, the current intensity i.e. the decomposition rate of the amalgam dropped. As a result of this experiment it is evident that the conductance of the electrolyte plays

an important role in the amalgam decomposition. It controls the reaction rate if the amalgam is in contact with pure alcohol or with very diluted alcoholate solution.

If the alcohol was diluted with traces of water, the current intensity increased. To examine this phenomenon a purpose-made galvanic cell was elaborated, this is illustrated in Figure 2.

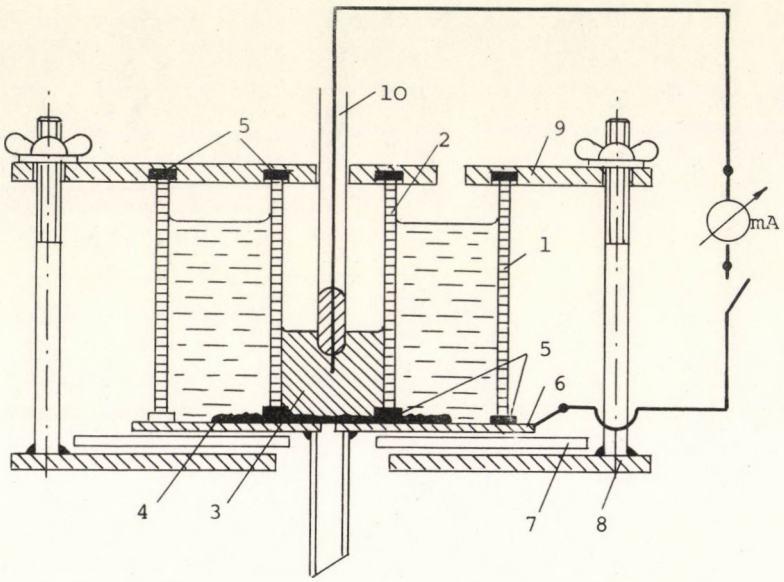

Fig. 2. Galvanic cell for the investigation of the role of water 1,2-glass tubes, 3-amalgam, 4-filter paper, 5-rubber rings, 6-molybdenum sheet, 7-rubber sheet, 8,9-support plates, 10-electric contact

As it can be seen in Figure 2 the amalgam and molybdenum electrodes are separated by a filter paper and the electrolyte which was poured between the glass tubes, trickled through the filter paper and left the cell. If the electrodes were whort circuited, the formed ions continuously left the system.

Using ethyl alcohols with different water concentration, the current intensity of the galvanic cell (measured at the moment the electrodes were connected together) is characteristic of the effect of the electrolyte water concentration on the amalgam decomposition grade. The result of this experiment is summarized in Table 1.

Table 1. The water concentration of alcohol and the current intensity of the short circuited galvanic cell

Water concentration of ethyl alcohol* (wt. per cent)	0.027	0.07	0.14	0.20	0.28
Current intensity (mA)	0.83	1.10	2.70	4.49	4.65

*The commercial grade alcohol used contained 0.42 wt. per cent water. It was dehydrated by the method described by ADICKES [10]. The water concentration was determined by Karl Fischer's method.

Regarding the data collected in Table 1 it is obvious from the viewpoint of sodium ethylate production that in contrast to literature, the processing of absolutely water free ethyl alcohol is certainly uneconomic due to the low reaction rate. (The commercially available pure ethyl alcohol usually contains about a tenth per cent of water.)

For the determination of the rate of the investigated reaction the method based on the measurement of the evolved hydrogen gas was selected. A glass reactor was constructed, the reaction was catalyzed by molybdenum sheets (Figure 3).

The reactor was operated as follows: Through the funnel (8) of the charging tube (7) 50 millilitres of alcohol were poured into the reactor. Then operating the amalgam charger (9) 42 grammes of amalgam was fed. As the required temperature of the alcohol was

reached - thermostated water was circulated through the heating jacket - the molybdenum sheet comb mounted at the end of a glass rod was pushed downwards so that it was immersed into the amalgam pool. At the moment the sheet comb touched the amalgam surface, the reaction started and bubbles of hydrogen appeared. The hydrogen gas left the reactor through a condenser cooled with tap water. At the end of the reaction, when the hydrogen evolution stopped, the molybdenum comb was lifted and the depleted amalgam was discharged. (The depleted amalgam contained 0.003 to 0.006 weight per cent sodium.) From the alcoholic solution a sample was taken and its sodium content was analyzed. (The sample was diluted with water and titrated with 0.1 N sulphuric acid.) The reactor was filled again with a known amount of amalgam and the procedure was repeated until the sodium concentration of the alcoholic solution reached three—five weight per cent.

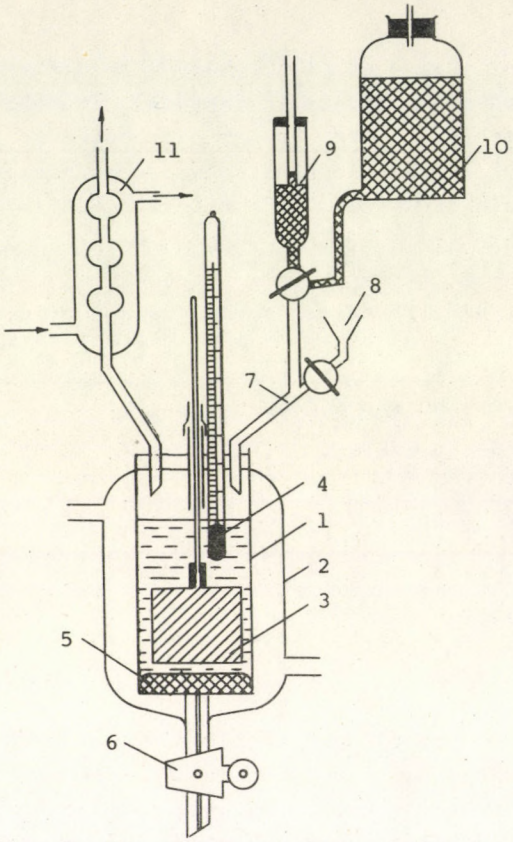

Fig. 3. The glass reactor. 1-inner glass tube, 2-heating jacket, 3-molybdenum sheet, 4-thermometer, 5-amalgam, 6-cook, 7-charging tube, 8-funnel, 9-amalgam charger, 10-amalgam reservoir, 11-condenser.

The volume of the evolved hydrogen was determined at constant pressure and temperature. To measure and record the hydrogen volume vs. time function, an automatic instrument was constructed based on SCHMIDT's article [11]. The hydrogen volume meter and recorder is depicted in Figure 4.

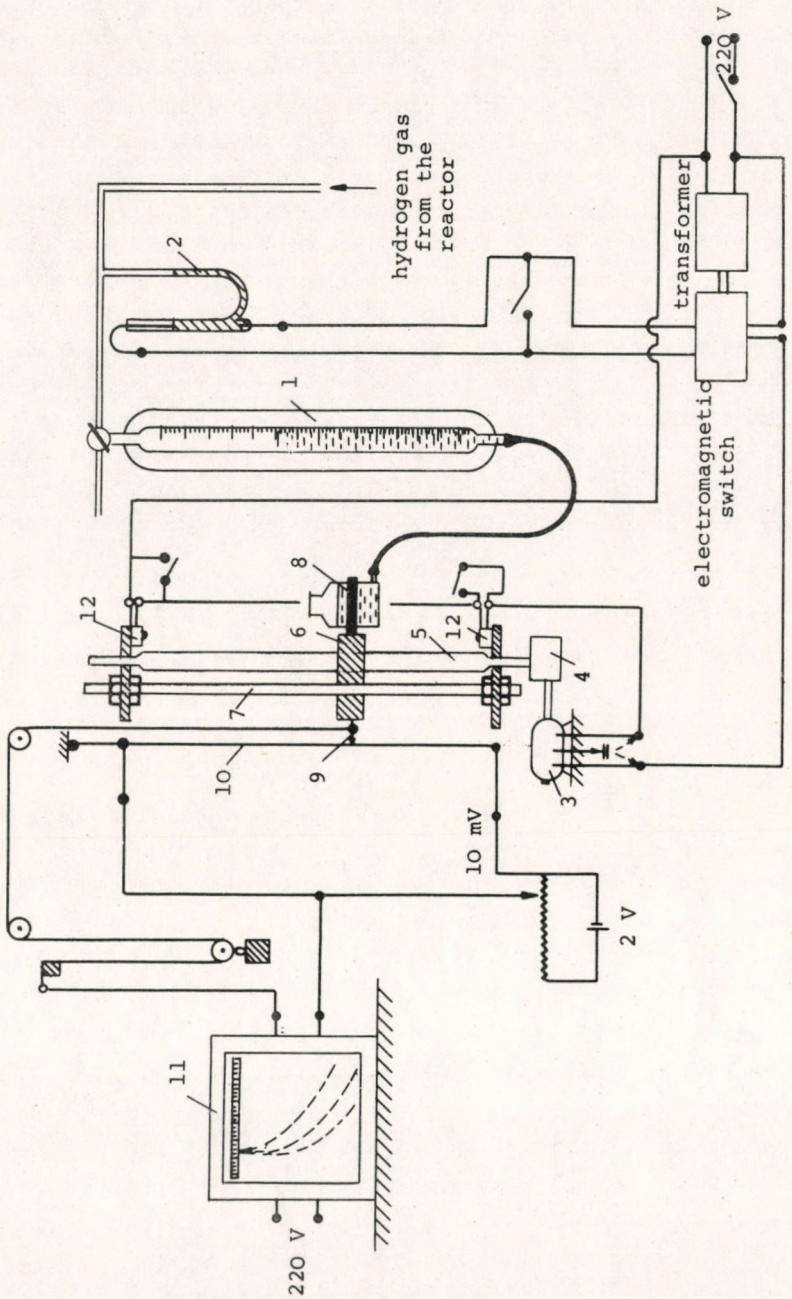

Fig. 4. The hydrogen volume meter and recorder. 1-burette, 2-U-tube, 3-electric motor, 4-speed reducer, 5-spindle, 6-support, 7-guide stem, 8-vessel, 9-slide contact, 10-manganin wire, 11-recorder, 12-limit switch

The basic idea of the operation is as follows: the hydrogen gas arriving from the reactor passes into the thermostated gas burette (1) and according to this the liquid level in the burette sinks. The increasing pressure causes a level difference in the U--manometer (2) which is filled with diluted sodium hydroxide solution. The liquid level increases in the left leg of the U-tube and short circuits the platinum wire electrodes mounted in the manometer. Due to the mentioned short circuit, an electric impulse is given to the electromagnetic switch which starts the electric motor (3). This rotates the shaft of the speed reducer (4) and the spindle (5) and due to this, the vessel (8) sinks. The motor runs until the liquid levels equalize in the vessel (8) and the burette. At the same time, this means the equality of the levels in the U--tube and the break of the electric contact between the platinum wires, which at last stops the running of the motor (3). The axial position of the vessel (8) is transferred to a recorder (11).

The curve drawn by the recorder is in linear relation with the evolved hydrogen volume vs. time function.

EXPERIMENTS and RESULTS

Experiments were carried out for the determination of the amalgam decomposition rate at 30, 40, 50, 60 and 70 ^{o}C. Pure ethyl alcohol was used in the experiments. The water concentration of the ethyl alcohol was 0.19 weight per cent. (The experiments carried out with alcohols of different initial water concentration are not discussed here.)

The sodium concentration of the amalgam was 0.338 weight per cent. The wetted perimeter of the molybdenum sheet comb was 207 millimetres.

During the experiments the volume of the evolved hydrogen and the conductance of the ethylate solution was determined. At the end of each run a sample was taken from the alcoholate solution and its sodium concentration was titrated.

It is easy to show that during the reaction the volume of the evolved hydrogen is inversely proportional to the amount of sodium being present in the amalgam. Knowing the amount and the initial and final sodium concentration of the amalgam, moreover the hydrogen volume vs. time function, the sodium content of the amalgam vs. time function could be calculated.

The sodium content and concentration of the amalgam were expressed in moles and molar fractions, respectively. If c_A is the sodium concentration of the amalgam in weight per cent and m_A is the same one in molar fractions, then

$$m_A = \frac{200\ c_A}{2{,}300 + 177\ c_A} \tag{3}$$

The sodium concentration of the different alcoholate solutions was also expressed in molar fractions. If c_E is the sodium concentration of the alcoholate solution in weight per cent and c_W (wt.%) is the water concentration of the ethyl alcohol the molar fraction of sodium in the alcoholate solution is

$$m_E = \frac{9}{450 + 7\ c_W} \cdot \frac{c_E}{1 - \frac{0.22}{23} c_E} \tag{4}$$

Equation (4) is valid if during the amalgam—alcohol reaction the losses of alcohol can be neglected. The latter can be assumed although the hydrogen gas leaving the reactor is saturated with alcohol vapours.

From among the others, the experiment carried out at 70 °C was selected. In Figure 5 the sodium content of the amalgam vs. time functions of the different runs are shown. In Table 2 the sodium concentrations of the alcohol solution measured at the beginning and end of each run are summarized.

The dotted lines in Figure 5 show the selected sodium concentrations of the amalgam. Knowing the slope of the full lines at the given amalgam concentrations, the reaction rate, i.e. the moles of sodium leaving the amalgam during the unit time period

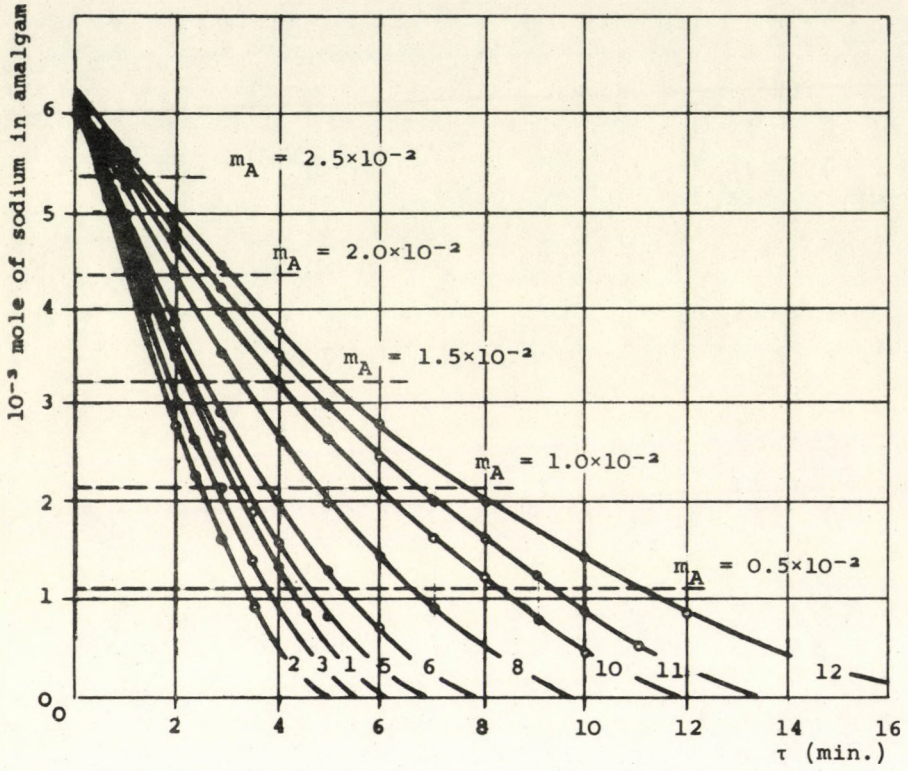

Fig. 5. The sodium content of the amalgam vs. time function. Temperature = 70 °C

Table 2. The sodium concentration of the alcoholic solution at the beginning and at the end of the runs

Number of the run	1	2	3	5	6	8	10	11	12
m_{Eo}	0	.0090	.0178	.0361	.0460	.0652	.0849	.0955	.1085
m_{Ef}	.0090	.0178	.0269	.0460	.0562	.0743	.0955	.1085	.1221

can be calculated. The reaction rate data of the different runs, but at the same amalgam concentration, differ from each other due to the different sodium concentration of the alcoholate solution being in contact with the amalgam. Fortunately this sodium concentration of the ethylate solution can be calculated because the concentrations at the beginning and at the end of the runs are known and it is assumed that during the runs the increase of the sodium concentration of the solution and the volume of the evolved hydrogen are in linear relationship.

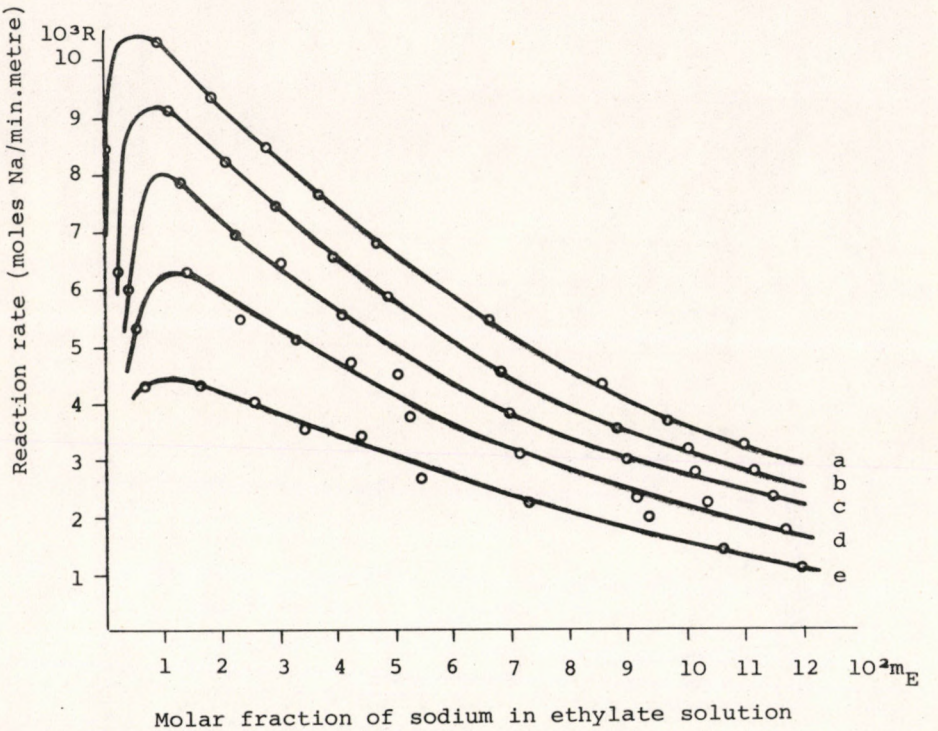

Fig.6. The dependence of the reaction rate from the sodium concentration of the amalgam and ethylate solution. The molar fraction of sodium in the amalgam: a - 2.5×10^{-2}, b - 2.0×10^{-2}, c - 1.5×10^{-2}, d - 1.0×10^{-2}, e - 0.5×10^{-2}

Earlier, it was found that a linear relation exists between the reaction rate and the wetted perimeter of the molybdenum catalyst sheet. The reaction rate data presented in Figure 6 were calculated for one metre wetted perimeter of the catalyst. The curves in Figure 6 have maximum values similarly as seen in Figure 1. The explanation of the existance of maximum values is the same as described earlier. Investigating the effect of the temperatur on the reaction rate, similar experiments were carried out as discussed above.

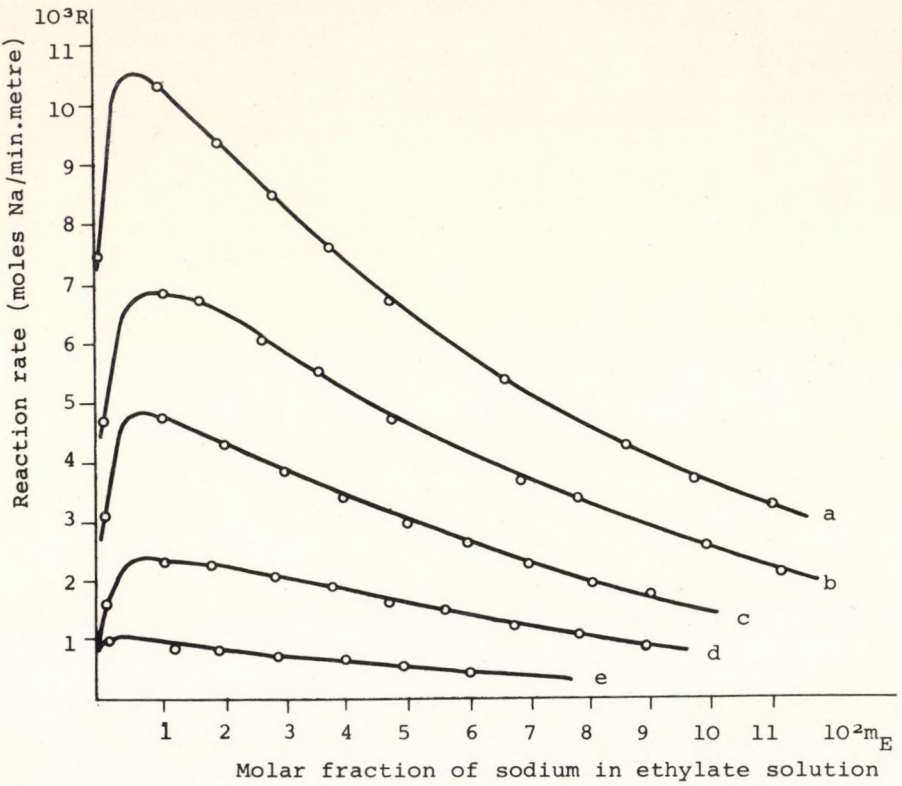

Fig. 7. The alteration of the reaction rate with the temperature. a - 70 °C, b - 60 °C, c - 50 °C, d - 40 °C, e - 30 °C

From among the reaction rate data these were selected and presented in Figure 7 which were determined with amalgams having 2.5×10^{-2} (molar fraction) sodium concentration and ethylate solutions of different concentrations.

As mentioned earlier, during the experiments the conductance of the sodium ethylate solution was determined. To this platinized platinum electrodes and a conductivity meter (RADELKIS type OK 102/1) was used. The results are shown in Figure 8. The curves in Figure 8 are similar to the known conductance vs. concentration functions of several electrolytes presented in literature [14].

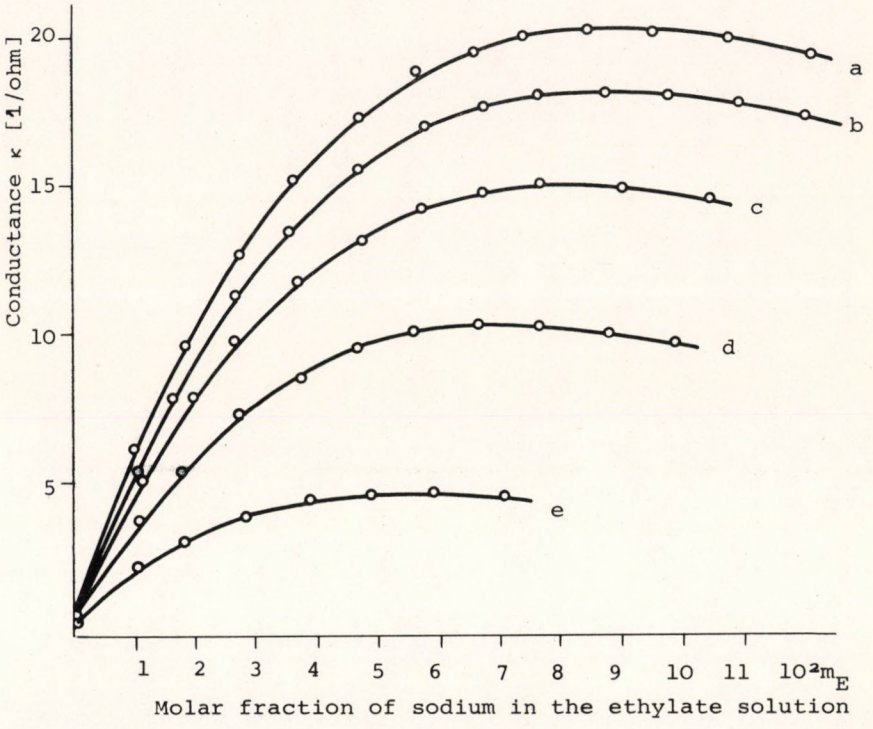

Fig. 8. The conductance of sodium ethylate solution at different temperatures. a - 70 °C, b - 60 °C, c - 50 °C, d - 40 °C, e - 30 °C

DISCUSSION

Regarding the sodium concentration of the amalgam, it was assumed that the reaction rate can be described as a power function

$$R = k' \, m_A^{\,n} \qquad (5)$$

Eq. (5) implies that both the temperature and the concentration of the alcoholate solution are constant.

Taking the contour plot in Figure 6 and drawing parallel lines with the ordinate at given concentrations of the ethylate solution, the appropriate reaction rate data can be obtained. These are collected in Table 3.

Table 3. The relation between the sodium concentration of the amalgam and the reaction rate (10^3 R, moles of sodium/ /min.metre)

m_A \ m_E	0.02	0.04	0.06	0.08	0.10
0.025	9.26	7.42	5.83	4.57	3.60
0.020	8.36	6.60	5.08	3.93	3.15
0.015	7.27	5.66	4.30	3.40	2.72
0.010	5.90	4.68	3.61	2.78	2.15
0.005	4.22	3.47	2.77	2.11	1.53
n	0.489	0.472	0.454	0.470	0.529

Eq. (5) can be easily linearised by taking the logarithms of both sides, and the exponent n determined by the method of least squares. The values of n are presented in the last row of Table 3. Taking the arithmetic mean of n:

$$\bar{n} = 0.483 \approx 1/2$$

The same result was found by BRÖNSTED and KANE [12] who examined the decomposition of sodium amalgam in aqueous and non-aqueous media.

It was also assumed that instead of the concentration of the alcohol molecules being in the solution, the conductance and the existing water concentration can be used for the mathematical description of the reaction rate. But to do this and to be in accordance with the determined rate data, both the conductance and the water concentration must be expressed with the sodium concentration of the ethylate solution. The above assumption is based either on the electrochemical character of the reaction or on the fact that the reaction rate can be increased by diluting the ethylate solution - or ethyl alcohol - with water.

Between the investigated limits the conductance of the ethylate solution can be described by the following empirical equation:

$$\varkappa - \varkappa_0 = A\, m_E\, e^{-Bm_E} \tag{6}$$

where

$\varkappa$ is the conductance of ethylate solution $(\text{Ohm})^{-1}$

$\varkappa_0$ is the conductance of ethyl alcohol $(\text{Ohm})^{-1}$

m_E is the sodium molar fraction in ethylate solution

A and B are constants.

From the determined conductance data and from the slopes and ordinate intersections of the lines in Figure 9 the constants of Eq. (6) and their dependence on temperature could be calculated. These are as follows:

$$\varkappa_0 = 10^{-3}\,(0.008\ t + 0.335) \tag{7}$$

$$A = -2.187\times10^{-4}\cdot t^2 + 3.16\times10^{-2}\cdot t + 4.101 \tag{8}$$

$$B = 14{,}441\times t^{-2} - 290.8 \times t^{-1} + 12.579 \tag{9}$$

The concentration of the water being present in the ethylate solution can be calculated with the help of the equilibrium reac-

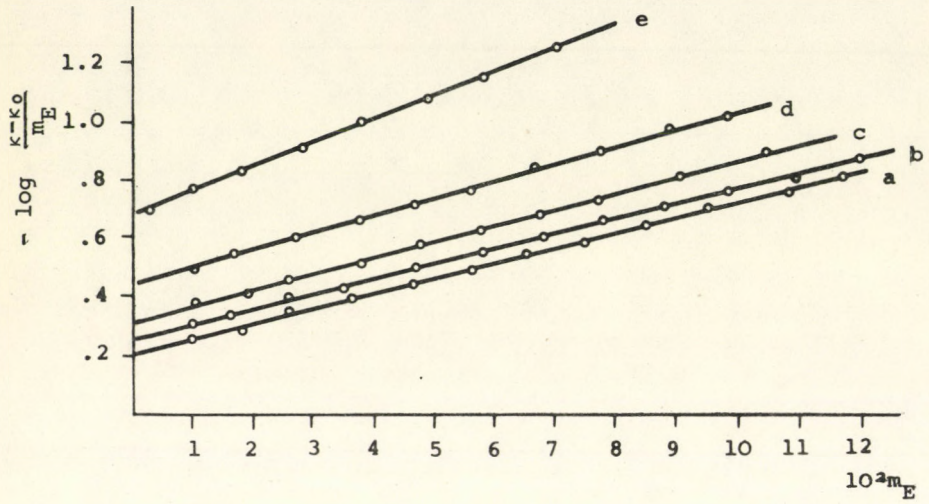

Fig.9. The $-\log \frac{\varkappa - \varkappa_0}{m_E} = f(m_E)$ function at different temperatures
a - 70 °C, b - 60 °C, c - 50 °C, d - 40 °C, e - 30 °C

tion (Eq. 2) of sodium hydroxide and ethyl alcohol.

$$NaOH + C_2H_5OH \rightleftharpoons C_2H_5ONa + H_2O \qquad (2)$$

This reaction is very fast and instantaneously reaches its equilibrium. Although attempts were made [13] the reaction - perhaps due to hard analytical problems - was not studied in detail and so the correct value of the equilibrium constant and its temperature dependence are unknown.

Assuming an ideal solution, the equilibrium constant of Eq. (2) is:

$$K = \frac{[m_e] \cdot [m_W]}{[m_C] \cdot [m_a]} \qquad (10)$$

where the symbols represent the molar fractions of the components:

$[m_e]$ = sodium ethylate

$[m_W]$ = water

$[m_C]$ = sodium hydroxide

$[m_a]$ = ethyl alcohol

being in the solution.

During the reaction the number of moles in the solution was constant, it equalled the number of moles being present in the alcohol used for the reaction:

$$m_{ao} + m_{Wo} = 1 \tag{11}$$

and

$$m_e + m_W + m_C + m_a = 1 \tag{12}$$

Moreover

$$m_{ao} = m_a + m_e \tag{13}$$

$$m_{Wo} = m_W + m_C \tag{14}$$

$$m_E = m_e + m_C \tag{15}$$

where m_{ao} and m_{Wo} are the molar fractions of C_2H_5OH and H_2O of alcohol at the beginning of the reaction.

Using Eq. (12), (13), (14) and (15):

$$m_a = 1 - m_E - m_W \tag{16}$$

$$m_C = m_{Wo} - m_W \tag{17}$$

$$m_e = m_E - m_{Wo} + m_W \tag{18}$$

The equilibrium constant of Eq. (10) can be expresses as:

$$K = \frac{(m_E - m_{Wo} + m_W) \cdot m_W}{(1 - m_E - m_W)(m_{Wo} - m_W)} \tag{19}$$

With regard to m_W, Eq. (19) is of second order. Although it can be solved, its handling is still cumbersome. If the water concentration of the alcohol used for the reaction is small and if the sodium concentration of the alcoholic solution is relatively

high, the $-m_{Wo} + m_W$ components in the brackets of the numerator and $-m_W$ in the first bracket of the denominator can be neglected. So

$$K \approx \frac{m_E \, m_W}{(1 - m_E)(m_{Wo} - m_W)} \tag{20}$$

and from Eq. (20) the water concentration is:

$$m_W \approx m_{Wo} \frac{K (1 - m_E)}{K(1 - m_E) + m_E} \tag{21}$$

It was assumed that the reaction rate is proportional to the product of the water concentration and the conductance of the ethylate solution. If Eq. (5) is also taken into account, the reaction rate is:

$$R = k \, m_A^{1/2} \, m_{Wo} \frac{K (1 - m_E)}{K(1 - m_E) + m_E} \cdot \varkappa \tag{22}$$

Rearranging Eq. (22):

$$\frac{\varkappa}{R} = \frac{1}{k \, m_A^{1/2} \, m_{Wo}} + \frac{1}{k \, m_A^{1/2} \, m_{Wo} \, K} \cdot \frac{m_E}{1 - m_E} =$$

$$= \frac{1}{\alpha} + \frac{1}{K \alpha} \cdot \frac{m_E}{1 - m_E} \tag{23}$$

where $\alpha = k \, m_A^{1/2} \, m_{Wo}$

Using the appropriate reaction rate and conductance data presented in Figure 6 and 7, $\varkappa/R$ was plotted against $m_E/(1-m_E)$. This is shown in Figure 10.

The straight lines obtained in Figure 9 seem to prove the validity of the assumptions made previously. The slope and ordinate intersection data of the lines in Figure 9 give the values of the

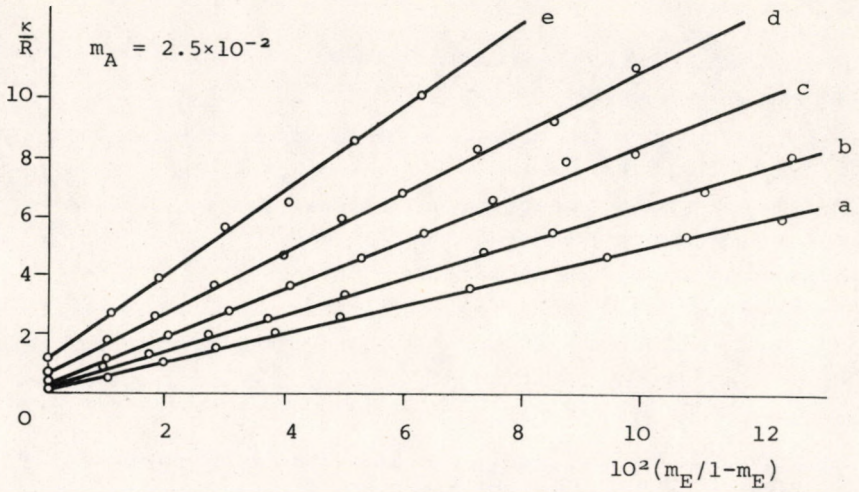

Fig.10. The κ/R vs. $m_E/(1-m_E)$ plot. a - 70 °C, b - 60 °C, c - 50 °C, d - 40 °C, e - 30 °C

Table 4. The temperature dependence of the reaction rate constant and equilibrium constant

Temperature °C	1/α	1/α K	10^{-3} k	10^3 K
30	1.20	142.35	1.099	8.43
40	0.62	106.76	2.128	5.81
50	0.26	81.91	5.263	3.17
60	0.16	63.20	8.333	2.53
70	0.09	50.15	14.658	1.79

reaction rate constant and equilibrium constant of reaction given in Eq. (2). These data are collected in Table 4.

CONCLUSION

It was found that in addition to the sodium concentration of the amalgam also the water molecules being present in the alcohol play an important role in the amalgam—ethyl alcohol reaction. Based on the determined reaction rate data and the derived rate equation it is tempting to draw interference on the mechanism of the discussed reaction, but this cannot be done. The derivation of the rate equation [Eq. (22)] was far from the rigorous theoretical treatment of the problem, so e.g. the determined kinetic constant (k) and the equilibrium constant (K) are not the true, but apparent values.

Eq. (22) is an empirical equation and it is useful for the determination of the reaction rate or the rate constant being valid for the investigated reactor.

Although the log k vs. 1/T plot is - more or less - a straight line and this is very useful from the viewpoint of the calculations, to determine the activation energy of the reaction is theoretically meaningless.

SYMBOLS USED

A	constant (1/ohm)
B	constant (dimensionless)
c_A	sodium concentration of amalgam (weight per cent)
c_E	sodium concentration of ethylate solution (weight per cent)
c_W	water concentration (weight per cent)
k	apparent reaction rate constant (mole.ohm/min.metre)
K	apparent equilibrium constant (dimensionless)
m_A	sodium molar fraction of amalgam (dimensionless)
m_a	molar fraction of sodium ethylate (dimensionless)

m_C molar fraction of sodium hydroxide (dimensionless)

m_E sodium molar fraction of ethylate solution (dimensionless)

m_e molar fraction of sodium ethylate (dimensionless)

m_W molar fraction of water (dimensionless)

R reaction rate (Na moles/min. metre)

$\varkappa$ conductance of ethylate solution (1/ohm)

Suffixes

o initial condition

f final condition

REFERENCES

1. RODD, E.H., Chemistry of Carbon Compounds. 2nd Edit. Vol. I/B. Elsevier Publ. Co. Amsterdam-London-New York. 1965. pp. 33--34.

2. HOUBEN, J., WEYL, Th., Methoden der organischen Chemie. 4th Edit. Vol. VI/2. G. Thieme Verlag. Stuttgart. 1963. pp. 5-14.

3. MacMULLIN, R.S., Chem. Eng. Progr. 46, 440 (1950)

4. U.S. Pat. 2,069,403

5. D.R. Pat. 752,283

6. U.S. Pat. 2,761,880

7. U.S. Pat. 2,336,045

8. U.S. Pat. 2,483,963

9. JAKSIC, M.M., CSONKA, I.M., Electrochem. Technol. 4, 49 (1960)

10. ADICKES, F., Ber. 2753 (1930)

11. SCHMIDT, K., RUMMEL, S., TAMME, G., KRUMBIEGEL, E., HÜBNER, M., Chem. Technik 20, 357 (1968)

12. BRÖNSTED, J.N., KANE, R.N.L., J. Amer. Chem. Soc. 53, 3624 (1931)

13. CALDIN, E.F., LONG, G., J. Chem. Soc. (London) 3737 (1954)

14. MILAZZO, G., Electrochemistry. Elsevier Publ. Co. Amsterdam--London-New York, 1963. p. 53.

РАЗЬЮМЕ

Скорость реакции амальгамы натрия и этилового спирта зависит от концентрации натрия в амальгаме, от концентрации воды и от электропроводности раствора. В статье излагается метод определения скорости реакции. Пользуясь экспериментальными данными, автор составил эмпирическое кинетическое уравнение.

Hungarian Journal
of Industrial Chemistry
Veszprém
Vol.3. pp. 519-526 (1975)

EVALUATION OF TEMPERATURE PROFILE IN A GAS-SOLIDS REACTING FIXED BED AT CONSTANT WALL TEMPERATURE

W.O. OLBRICH* and G.N. BHAT**

(*Monash University, Clayton, Victoria, Australia,
**College of Science & Technology, Port Harcourt, Nigeria)

Received: April 29, 1975.

A method is presented for the determination of the temperature profile existing in a gas-solid reacting fixed bed having constant wall temperature.

THE SYSTEM:

A gas flows through a tube of circular cross-section packed with granules of a solid containing a component that reacts exothermically with the gas. The heat generated in this way is transported by various processes to the wall of the tube where it is removed by a coolant maintained at a constant temperature.

THE PROBLEM:

An expression for the radial temperature profile set up in the system described above is derived on the basis of the following assumptions:

ASSUMPTIONS:

1. The system may be treated as pseudo-homogeneous.
2. No changes in packing geometry occur due to reaction.
3. Due to operating conditions, the reaction is essentially first order with respect to solids concentration.
4. The reaction rate is independent of temperature, over the radial temperature variations existing in the bed.
5. Axial temperature gradients are negligible so that axial transport may be neglected.
6. Radial heat transport is effected by an "effective radial conductivity" assumed to be constant.
7. Heat transfer at the wall of the tube occurs via constant heat transfer coefficient to a coolant at constant temperature.

SYMBOLS USED

a_1, a_2 = arbitary constants obtained in the solution of Equation (10)

Bi = Biot Number = $h\ R/k_{er}$

C = concentration of reactive solid per unit volume of packed bed

C_o = initial value of C

Cp_m = mean heat capacity of bed

$(-\Delta H)$ = heat liberated by the conversion of one mole of reactant

i = $\sqrt{-1}$

J_o = Bessel function of the first kind of order zero

J_1 = Bessel function of the first kind of order one

k = reaction rate constant

k_{er} = effective radial thermal conductivity

K = $k\ C_o\ (-\Delta H)\ R/(\nu \rho_m\ Cp_m)$

Pe = Peclét number = $\nu\ R\ \rho_m\ Cp_m/k_{er}$

q = heat generation rate per unit volume of bed

r = radial co-ordinate

R = radius of tube

r^* = r/R

s = Laplace transform operator

t = time

t^* = $\nu t/R$

T = temperature of bed

T_c = coolant temperature

T^* = $(T - T_c)/K$

U = $\theta - 1/(s^2 + \beta s)$

ν = mean gas velocity based on empty cross-sectional area of the tube

Y_o = Bessel function of the second kind order zero

y = $i\sqrt{Pes}\, r^*$

α = $\sqrt{Pe\ \beta}$

β = $k R/\nu$

θ = Laplace transform of T^*, with respect to t^*.

λ_n = nth eigenvalue obtained as the nth positive root of Equation (25)

ρ_m = mean density of packed bed

$\phi(\alpha)$ = $\alpha \cdot J_1(\alpha) - Bi \cdot J_o(\alpha)$

DERIVATION:

Since reaction occurs in the solid which are stationary and since reaction does not depend on gas phase composition, the solids concentration at any point in the bed is given by:

$$\frac{dc}{dt} = -k \cdot C \tag{1}$$

The solution to this D.E. with appropriate initial condition may be written:

$$C = C_o \exp [- \beta t^*] \tag{2}$$

and hence the heat generation rate may be found:

$$q = k\, C_o\, (-\Delta H) \exp [-\beta t^*] \tag{3}$$

Turning now to the heat balance in the packed bed, and neglecting terms dealing with axial transport, we may derive the P.D.E.:

$$\frac{\partial T}{\partial t^*} = K \exp [-\beta t^*] + \frac{1}{Pe \cdot r^*} \frac{\partial}{\partial r^*} \left(r^* \frac{\partial T}{\partial r^*}\right) \tag{4}$$

Let $\theta(s)$ be the Laplace transform of the dimensionless temperature difference, T^*, where T^* is given by:

$$T^* = (T - T_c)/K \tag{5}$$

then

$$\theta(s) = L\{T^*(t^*)\} \tag{6}$$

$$= \int_o^\infty e^{-st^*} T^*(t^*)\, dt^* \tag{7}$$

Hence, as $T^* = 0$ for all r^* at $t^* = 0$, we have:

$$s \cdot \theta = \frac{1}{s + \beta} + \frac{1}{Pe \cdot r^*} \frac{d}{dr^*} \left(r^* \frac{d\theta}{dr^*}\right) \tag{8}$$

Let

$$U = \theta - \frac{1}{s(s + \beta)} \tag{9}$$

then:

$$U = \frac{1}{Pe \cdot s \cdot r^*} \frac{d}{dr^*} \left(r^* \frac{dU}{dr^*}\right) \tag{10}$$

This ordinary D.E. may be solved in terms of Bessel functions of the first and second kind of order zero (1), if we rewrite Eq. (10) in terms of y, a redefined form of the independent variable.

Thus if

$$y = i\sqrt{Pe \cdot s}\ r^* \tag{11}$$

where

$$i = \sqrt{-1} \tag{12}$$

we have:

$$U = a_1 J_o(y) + a_2 Y_o(y) \tag{13}$$

The arbitrary constants a_1 and a_2 in Eq. (13) must now be determined by means of boundary conditions before the inverse Laplace transform of this equation can be found to give the time--dependent solution for T*.

B.C.1. At the centre of the tube the radial temperature gradient is zero.

$$\text{i.e.} \quad \left.\frac{\partial T^*}{\partial r^*}\right|_{r^*=0} = 0 \tag{14}$$

$$\therefore \quad \left.\frac{d\theta}{dy}\right|_{y=0} = 0 \tag{15}$$

Hence

$$a_2 = 0 \tag{16}$$

B.C.2. At the tube wall the heat flux due to thermal conduction within the bed equals the heat flux due to transport across the thermal resistance to the coolant.

$$\text{i.e.} \quad -ke_r \frac{\partial T}{\partial r} = h\,(T - T_c) \tag{17}$$

$$\therefore \quad \left.\frac{\partial T^*}{\partial r^*}\right|_{r^*=1} = \left. -Bi \cdot T^* \right|_{r^*=1} \tag{18}$$

$$\therefore \quad \left.\frac{d\theta}{dy}\right|_{y=1\sqrt{Pes}} = \left.\frac{-Bi}{i\ Pes}\right|_{y=i\sqrt{Pes}} \tag{19}$$

$$\therefore\ -a_1 J_1(i\sqrt{Pes}) = \frac{-Bi}{i\sqrt{Pes}}\left[\frac{1}{s(s+\beta)} + a_1 J_0(i\sqrt{Pes})\right] \tag{20}$$

$$\therefore\ a_1[BiJ_0(i\sqrt{Pes}) - i\sqrt{Pes}\ J_1(i\sqrt{Pes})] = \frac{-Bi}{s(s+\beta)} \tag{21}$$

Having found a_1 and a_2 one finds the expression for θ:

$$\theta = \frac{1}{s(s+\beta)} - \frac{Bi\ J_0(i\sqrt{Pes}\ r^*)}{s(s+\beta)[Bi\ J_0(i\sqrt{Pes}) - i\sqrt{Pes}\ J_1(i\sqrt{Pes})]} \tag{22}$$

To invert this Laplace transform, we note that this may be done by use of the residue theorem [2]. The poles of the first fraction of Eq.(22) are:

$$s = 0,\ -\beta \tag{23}$$

While for the second fraction they are

$$s = 0,\ -\beta,\ -\frac{\lambda_n^2}{Pe}\ ;\quad n = 1,\ 2,\ \ldots\ \infty \tag{24}$$

Where the values of λ_n are found from the successive positive roots of

$$Bi\ J_0(\lambda_n) - \lambda_n\ J_1(\lambda_n) = 0 \tag{25}$$

Proceeding by the method of residues, the following inverse Laplace transform is obtained for θ:

$$T^* = \sum_{n=1}^{\infty} \frac{2\ J_1(\lambda_n)\ J_0(\lambda_n r^*)\ e^{-\lambda_n^2 t^*/Pe}}{\lambda_n(\beta-\lambda_n^2/Pe)[J_0^2(\lambda_n) + J_1^2(\lambda_n)]} - \frac{e^{-\beta t^*}}{\beta}\left\{1 + \frac{Bi \cdot J_0(\alpha r^*)}{\phi(\alpha)}\right\} \tag{26}$$

Where the newly introduced variables α and $\phi(\alpha)$, signify the following:

$$\alpha = \sqrt{\beta Pe} \tag{27}$$

$$\phi(\alpha) = \alpha J_1(\alpha) - Bi\, J_0(\alpha) \qquad (28)$$

Equation (26) is the desired solution.

Numerical evaluation of the infinite series must be preceded by solution of Equation (25) for as many eigenvalues λ_n, as are required to give a desired numerical accuracy to the initial conditions. Some of these eigenvalues are listed in CARSLAW and JAEGER [3] for a selection of Biot numbers.

Values of the Peclet number Pe tend to be independent of Reynolds number, for $Re > 50$. In the present derivation Pe is based on the tube radius R, but if instead it is based on the particle diameter its value lies in the range of 8.0 → 10.0 for velocities giving a sufficiently high Re.

Hence k_{er} is evaluated and is then used to give Bi.

The Reynolds number is also based on the particle diameter.

REFERENCES

1. HILDEBRAND, F.B., Advanced Calculus for Applications, Prentice Hall, 1962, p. 142, et seq.

2. SPIEGEL, M.R., Theory and Problems of Laplace Transforms, Schaum Publishing Co., 1965.

3. CARSLAW, H.S., JAEGER, J.C., Conduction of Heat in Solids, Oxford University Press, 1959, p. 493.

РАЗЮМЕ

Авторами излагается метод расчета, используемый для определения распределения температуры в реакторе с неподвижным слоем и с постоянной температурой стены.

Hungarian Journal
of Industrial Chemistry
Veszprém
Vol.3. pp. 527-536 (1975)

THEORETISCHE UNTERSUCHUNG DES AUSWASCHUNGSMECHANISMUS VON SALZHALTIGEN FILTERSCHLAMMSCHICHTEN

J. FÖLÖP, E. MONOSTORI, G. NÉMETH und T. VAJDA

(Forschungsinstitut für Technische Chemie der Ungarischen Akademie der Wissenschaften, Budapest)

Eingegangen am 20. Mai 1975.

In unserer Arbeit beschreiben wir auf Grund eines physiko-mathematischen Modells den Prozeß der Gas- und Flüssigkeitsdiffusion bzw. der konvektiven Strömungsverhältnisse in einem salzhaltigen Filterkuchen, der von einer Seite mit Waschflüssigkeit berieselt, auf der anderen Seite einem Vakuum ausgesetzt wird. Die erzielten Resultate ermöglichen die Bestimmung der notwendigen Waschdauer bzw. der Waschflüssigkeitsmenge mit größerer Genauigkeit als es bisher möglich war.

I. Einleitung. Das physiko-mathematische Modell

In der Praxis geschieht das Auswaschen eines, irgendeine leichtlösliche Verunreinigung enthaltenden Filterkuchens, bzw. die Rückgewinnung eines im Filterkuchen zurückgebliebenen wertvollen Stoffes mit obiger Eigenschaft zweckmäßigerweise durch Kontaktierung des Filterkuchens auf der einen Seite mit einer entsprechenden Waschflüssigkeit, während er auf der anderen Seite angesaugt wird. Falls die Flüssigkeit auf die einfachste Weise durch Berieselung auf der Oberfläche aufgebracht wird, so beginnt infolge der Vakuumwirkung auf der anderen Seite im porösen Filterkuchen eine

gemischte Gas- und Flüssigkeitsströmung, und der Filterkuchen wird durch die Flüssigkeitskomponente ausgewaschen [1].

Bei dem beschriebenen Prozeß muß zur Bestimmung der Waschdauer bzw. der Menge der Waschflüssigkeit die Konzentration des gesuchten Stoffes in der austretenden Waschflüssigkeit als Funktion der Zeit bekannt sein. Um die zeitabhängige austretende Konzentration aufschreiben zu können, muß man aber den sich abspielenden transienten Prozeß modellieren. Die Hauptmerkmale des aufzustellenden physikalischen Modells werden daher die folgenden sein:

a) Die Dicke des Filterkuchens ist auf der x-Koordinate aufgetragen. Die Waschflüssigkeit tritt bei $x = 0$ an die Oberfläche und wird an der Stelle $x = L$ abgesaugt.

b) Es wird nur der Transportprozeß der Waschflüssigkeit bzw. des in dieser gelösten Stoffes untersucht. Alle übrigen Prozesse werden als die Art dieses Transportes beeinflussenden Effekte betrachtet.

c) Wir nehmen an, daß in einem Filterkuchen von der Dicke L - infolge des Ansaugens - eine Flüssigkeitsströmung entscheidend von konvektivem Charakter auftritt. Auf diese Weise kann, ausgehend von der Volumengeschwindigkeit der aus der Oberflächeneinheit austretenden Waschflüssigkeit, die konvektive Stoffgeschwindigkeit v im Filterkuchen abgeleitet werden.

d) Die Wirkung des parallel mit der Flüssigkeit strömenden Gases, sowie der - infolge der unvollkommenen Struktur des Filterkuchens - vorhandenen Risse und des in den Poren des Filterkuchens angehäuften, auszuwaschenden Stoffes auf die Konzentration c des in der Waschflüssigkeit schon gelösten Stoffes, wird im Modell durch eine mit einem Koeffizienten Δ multiplizierte Derivierte zweiten Grades (Diffusionsglied) berücksichtigt. Dieses Glied berücksichtigt die dispergierende Wirkung des parallel strömenden Gases, die kurzschließende Wirkung der Risse sowie die Tatsache, daß das Auswaschen als Ergebnis eines in der Zeit verzögerten Prozesses stattfindet.

Auf Grund obiger Ausführungen wird der Transport des gelösten Stoffes im Filterkuchen von folgender Gleichung beschrieben:

$$\frac{\partial c}{\partial t} + v \frac{\partial c}{\partial x} = \Delta \frac{\partial^2 c}{\partial x^2} \tag{1}$$

welche in den Intervallen der unabhängigen Veränderlichen $0 \leq x \leq L$ und $0 < t < +\infty$ gültig ist; t ist offenbar die Zeitkoordinate. Die zu Gleichung (1) gehörenden Rand- und Anfangsbedingungen sind, wie folgt:

$$c(x,0) = c_o \tag{2a}$$

$$vc(0,t) - \Delta \left(\frac{\partial c}{\partial x}\right)_{x=o} = 0 \tag{2b}$$

Gemäß (2a) wurde also der Einfachheit halber angenommen, daß der Filterkuchen im Zeitpunkt t = 0 bereits auf entsprechende Weise mit Flüssigkeit, welche die Gesamtmenge des auszuwaschenden Stoffes in der Lösung mit Konzentration c_o enthält, gesättigt ist. Die Gleichung (2b) könnte aus jener physikalischen Bedingung abgeleitet werden, daß an der Stelle x = 0, also an der Stelle, wo die Waschflüssigkeit an die Oberfläche gelangt, kein gelöster Stoff den Filterkuchen verläßt, so daß dort die gesamte Strömungsdichte des gelösten Stoffes (die Summe der konvektiven und diffusiven Ströme) gleich Null ist.

Wir führen nun die neuen, dimensionlosen Veränderlichen $\xi = \frac{x}{L}$ und $\vartheta = \frac{vt}{L}$ ein, und erhalten aus den Zusammenhängen (1), (2a) und (2b) folgendes mathematische Problem:

$$\frac{\partial c}{\partial \vartheta} + \frac{\partial c}{\partial \xi} = a^2 \frac{\partial^2 c}{\partial \xi^2} \tag{3a}$$

$$c(\xi,o) = c_o \tag{3b}$$

$$c(o,\vartheta) = a^2 \left(\frac{\partial c}{\partial \xi}\right)_{\xi=o} \tag{3c}$$

$$|c(\xi,\vartheta)| < +\infty \tag{3d}$$

wobei $a^2 = \Delta/vL$ ein neuer Parameter ist. Wir bemerken, daß - nachdem an der Stelle $x = L$ von physikalischer Überlegung ausgehend, keinerlei Annahme hinsichtlich der Natur der Lösungsfunktion c abgeleitet werden konnte - die Begrenzheit von c wegen mathematischer Überlegungen gemäß (3d) als physikalisch plausibel angenommen werden muß.

II. Lösung des mathematischen Modells

Wir führen die Laplace-Transformierte von c in folgender Weise ein [4]:

$$Z(\xi) = \mathcal{L}[c(\xi,\vartheta)] = \int_0^\infty c(\xi,\vartheta)\, e^{-p\vartheta}\, d\vartheta \tag{4}$$

Wenn man nun (3a) nach Laplace transformiert, so erhält man durch Anwendung von (3b) und (4) folgende Gleichung:

$$a \frac{d^2Z}{d\xi^2} - \frac{dZ}{d\xi} - pZ = - c_o \tag{5}$$

deren Lösung ist wie üblich [2]:

$$Z(\xi) = \frac{c_o}{p} + A \exp\left[\frac{1 - \sqrt{1 + 4\, a^2 p}}{2\, a^2}\, \xi\right] \tag{6}$$

wobei A eine Konstante ist. Bei der Aufstellung von (6) wurde die Bedingung (3d) berücksichtigt, welche voraussetzt, daß jene von den Lösungen (5) ausgewählt wird, die begrenzt ist.

Die Konstante A kann durch Einsetzen von (6) in die Bedingung (3c) bestimmt werden. Ihr Wert beträgt:

$$A = - \frac{2\, c_o}{p(1 + \sqrt{1 + 4\, a^2 p})} \tag{7}$$

Wenn nun (7) in (6) rücksubstituiert wird, so erhalten wir:

$$Z(\xi) = \frac{c_o}{p}\left(1 - e^{\frac{\xi}{2a^2}} \frac{e^{-\frac{\xi}{a}\sqrt{p+\frac{1}{4a^2}}}}{a\sqrt{p+\frac{1}{4a^2}} + \frac{1}{2}}\right) \tag{8}$$

Es wird dann (8) in die Form gebracht, welche die Durchführung der inversen Laplace-Transformation erleichtert:

$$Z(\xi) = \frac{c_o}{p} - \frac{c_o}{a} e^{\frac{\xi}{2a^2}} \frac{p+\frac{1}{4a^2}}{p} \frac{e^{-\frac{\xi}{a}\sqrt{p+\frac{1}{4a^2}}}}{(p+\frac{1}{4a^2})(\sqrt{p-\frac{1}{4a^2}} + \frac{1}{2a})} \tag{9}$$

Unsere Aufgabe besteht nun darin, (9) einer inversen Laplace--Transformation zu unterziehen. Das Wiedereinsetzen des ersten Gliedes von $Z(\xi)$ ist trivial, für das zweite Glied werden folgende Zusammenhänge verwendet:

$$\mathcal{L}^{-1}\left[\frac{p+\frac{1}{4a^2}}{p}\right] = \delta(\vartheta) + \frac{1}{4a^2} \tag{10}$$

wobei $\delta(\vartheta)$ die Dirac-sche Deltafunktion darstellt,

$$\mathcal{L}^{-1}\left[\frac{e^{-\frac{\xi}{a}\sqrt{p+\frac{1}{4a^2}}}}{(p+\frac{1}{4a^2})(\sqrt{p+\frac{1}{4a^2}}+\frac{1}{2a})}\right] = e^{-\frac{\vartheta}{4a^2}} \mathcal{L}^{-1}\left[\frac{e^{-\frac{\xi}{a}\sqrt{p}}}{p(\sqrt{p}-\frac{1}{2a}}\right] = \tag{11}$$

$$= 2a\left[e^{-\frac{\vartheta}{4a^2}} \operatorname{erfc}\left(\frac{\xi}{2a\sqrt{\vartheta}}\right) - e^{\frac{\xi}{2a^2}} \operatorname{erfc}\left(\frac{\sqrt{\vartheta}}{2a} + \frac{\xi}{2a\sqrt{\vartheta}}\right)\right] \equiv M(\xi,\vartheta)$$

Hier wurde zuerst der Translationssatz angewandt, sodann die Fehlerfunktion eingeführt [3]:

$$\operatorname{erfc} z = \frac{2}{\sqrt{\pi}} \int_z^\infty e^{-\lambda^2}\, d\lambda$$

Mit Hilfe von (10) und (11) kann - unter Anwendung des Konvolutionssatzes - die inverse Transformierte von (9) wie folgt aufgeschrieben werden:

$$c(\xi,\vartheta) = c_o - \frac{c_o}{a} e^{\frac{\xi}{2\,a^2}} \left[\delta(\vartheta) * M(\xi,\vartheta) + \frac{1}{4\,a^2} * M(\xi,\vartheta)\right] \qquad (12)$$

wobei * den Konvolutionsprozeß bedeutet. In Anbetracht dessen, daß

$$\delta(\vartheta) * M(\xi,\vartheta) = M(\xi,\vartheta)$$

erhalten wir die gesuchte Konzentration schließlich in folgender Form:

$$c(\xi,\vartheta) = c_o - \frac{c_o}{a} e^{\frac{\xi}{2\,a^2}} \left[M(\xi,\vartheta) - \frac{1}{4\,a^2} \int_o^{\vartheta} M(\xi,\tau)\, d\tau\right]$$

oder wenn M aus (11) substitutiert wird:

$$c(\xi,\vartheta) = c_o\Big[1 - 2^{\frac{\xi}{2\,a^2} - \frac{\vartheta}{4\,a^2}} \operatorname{erfc}\left(\frac{\xi}{2\,a\sqrt{\vartheta}}\right) + 2\, e^{\frac{\xi}{a^2}} \operatorname{erfc}\left(\frac{\sqrt{\vartheta}}{2\,a} + \frac{\xi}{2\,a\sqrt{\vartheta}}\right) -$$

$$- \frac{1}{a^2} e^{\frac{\xi}{2\,a^2}} \int_o^{\vartheta} e^{\frac{\tau}{4\,a^2}} \operatorname{erfc}\left(\frac{\xi}{2\,a\sqrt{\tau}}\right) d\tau + \frac{1}{a^2} e^{\frac{\xi}{a^2}} \int_o^{\vartheta} \operatorname{erfc}\left(\frac{\sqrt{\tau}}{2\,a} + \frac{\xi}{2\,a\sqrt{\tau}}\right) d\tau\Big] \qquad (13)$$

III. Diskussion der Resultate. Konklusionen

Für die Feststellung des Auswaschungsgrades des untersuchten Filterkuchens ist offenbar die Kenntnis der Konzentration (13) an der Stelle $\xi = 1$, also an der Absaugstelle, notwendig. Es ist leicht einzusehen, daß unserem Modell gemäß im untersuchten Inter-

vall $0 \leq \xi \leq 1$ der Wert der Konzentration an der Stelle $\xi = 1$ ein Maximum hat. Wenn also die Konzentration hier genügend niedrig ist, so können wir mit Sicherheit annehmen, daß sie überall im untersuchten Intervall nur mehr einen geringeren Wert als diesen erreichen kann. Die Konzentration $c^*(\vartheta)$ des gesuchten Stoffes in der austretenden Waschflüssigkeit kann als Funktion der Zeit wie folgt aufgeschrieben werden:

$$c^*(\vartheta) = c(1,\vartheta) = c_o[1 - 2\, e^{\frac{2-\vartheta}{4a^2}} \operatorname{erfc}\left(\frac{1}{2a\sqrt{\vartheta}}\right) + 2\, e^{\frac{1}{a^2}} \operatorname{erfc}\left(\frac{\sqrt{\vartheta}}{2a} + \frac{1}{2a\sqrt{\vartheta}}\right) - \tag{14}$$

$$- \frac{1}{a^2}\, e^{\frac{1}{2a^2}} \int_o^{\vartheta} e^{-\frac{\tau}{4a^2}} \operatorname{erfc}\left(\frac{1}{2a\sqrt{\tau}}\right) d\tau + \frac{1}{a^2}\, e^{\frac{1}{a^2}} \int_o^{\vartheta} \operatorname{erfc}\left(\frac{\sqrt{\tau}}{2a} + \frac{1}{2a\sqrt{\tau}}\right) d\tau]$$

In Abbildung 1 sehen wir die auf Grund des Zusammenhanges (14), unter Annahme verschiedener Parameterwerte a bzw. c_o-Einheitswerte beobachteten Resultate. Es kann festgestellt werden, daß die Kurvenschar eine monoton abnehmende Tendenz zeigt, und ein Teil derselben um die Zeitkoordinate $\vartheta = 1$ einen Inflexionspunkt hat (das sind die Kurven, die den relativ geringeren a-Parameterwerten entsprechen). All dies folgt logisch aus der Tatsache, daß der Wert $\vartheta = 1$ gerade dem Zeitpunkt $t = L/v$ entspricht, und das ist die Zeitdauer, während welcher, unserer Annahme nach, ein Volumenelement der Waschflüssigkeit bei korkartiger Strömung ($a = 0$) den Filterkuchen durchläuft.

Mit Hilfe obiger Überlegungen kann eine Methode zur Bestimmung der Parameter a bzw. Δ angegeben werden. In Kenntnis der konvektiven Strömungsgeschwindigkeit, der Anfangskonzentration und der Schichtdicke kann nähmlich zu einem gegebenen Zeitpunkt $t^* \ll L/v$ durch die Bestimmung der austretenden Konzentration mit Hilfe der als Nomogramm benutzten Abbildung 1 eindeutig festgestellt werden, welche Kurve laut unseres Modells den untersuchten Auswaschungsprozeß beschreibt. Daraus ergibt sich dann der Wert der fraglichen Parameter.

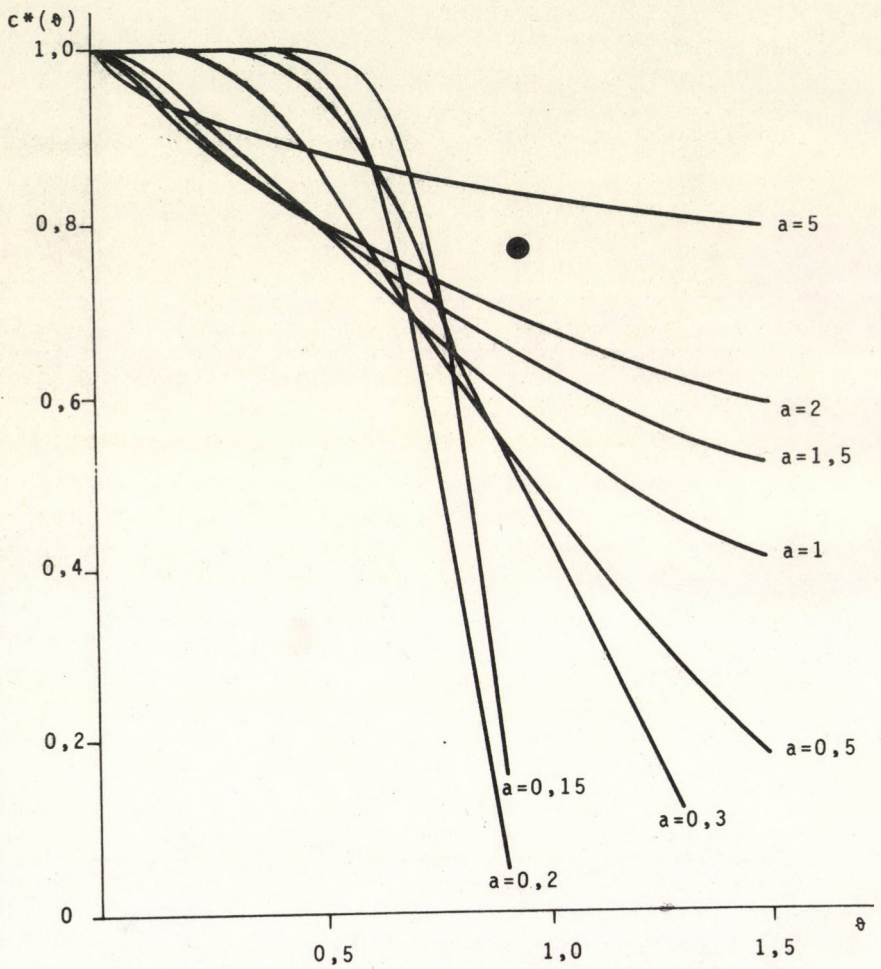

Abb. 1

Unter Verwendung der gewonnenen Resultate kann die erwünschte Waschdauer (bzw. die damit linear proportionelle, benötigte Waschflüssigkeitsmenge) auf theoretischem Wege wie folgt geschätzt werden. Der Filterkuchen kann den gegebenen Ansprüchen gemäß offenbar in dem Fall als ausgewaschen angesehen werden, wenn sich die Konzentration des auszuwaschenden Stoffes in der austretenden Waschflüssigkeit auf einen bestimmten Teil des Anfangskonzentrationswertes vermindert (aus unseren vorausgehenden Überlegungen her ist es bekannt, daß dann überall im Filterkuchen die Konzentrationen einen geringeren Wert erreichen). Jetzt wollen wir also Abbildung 1 wieder als Nomogramm betrachten - da uns bereits bekannt ist, zu welchem Parameterwert a gehörende Kurve den untersuchten Auswaschungsprozeß beschreibt - dann kann die für die Erzielung der gewählten endgültigen Konzentration notwendige Waschdauer aus der Abbildung abgelesen werden.

Schließlich ist zu bemerken, daß es beim Vergleich mit der Praxis zweifellos als Mangel des theoretischen Modells erscheinen könnte, daß sämtliche den Transport des auszuwaschenden Stoffes beeinflußenden Effekte bloß durch ein Diffusionsglied berücksichtigt werden, umsomehr als dieses Glied,mathematisch gesehen, einen Stoffstrom des Types generiert, der in der Wirklichkeit nicht auftreten kann. Die Modellierung des untersuchten Prozesses auf diese Weise kann man aber auf ähnliche Weise akzeptieren, wie es im allgemeinen bei den Diffusionsmodellen üblich ist.

ZEICHENERKLÄRUNG

A Integrationskonstante

a^2 dimensionsloser Koeffizient des Derivationsgliedes zweiten Grades (1)

c Konzentration des auszuwaschenden Stoffes im Filterkuchen (kg/m³ Flüssigkeit)

c_o Anfangskonzentration (kg/m³ Flüssigkeit)

c^* Konzentration des auswaschenden Stoffes in der austretenden Waschflüssigkeit (kg/m³ Flüssigkeit)

L Dicke des Filterkuchens (m)

M Funktionskomplex
p Parameter der Laplace-Transformation
t Zeitkoordinate (Stunde)
t* Zeitpunkt der Bestimmung der Derivierten (Stunde)
v Konvektive Geschwindigkeit der Waschflüssigkeit (m/h)
x Ortskoordinate (m)
Z Laplace-Transformierte der Konzentration
Δ Koeffizient des Derivationsgliedes zweiten Grades (m^2/h)
ϑ dimensionslose Zeitkoordinate (1)
ξ dimensionslose Ortskoordinate (1)

SCHRIFTTUM

1. PERRY, J.H., Chemical Engineers Handbook, McGraw-Hill, New York--London, 1967
2. GRÖBNER, W., HOFREITER, N., Integraltafeln, Springer Verlag, Wien, 1961
3. LÖSCH, F. et al., Tafeln höherer Funktionen, Teubner Verlagsgesellschaft, Stuttgart, 1966.
4. SPIEGEL, M.R., Laplace Transforms, McGraw-Hill, New York-Toronto, 1965.

РЕЗЮМЕ

В статье описывается отжатый осадок, содержащий соль. С одной стороны отжатый осадок обрызгивается промывной жидкостью, а с другой стороны подвергается влиянию вакуума. На основе физико-математической модели описали процессы газовой и жидкостной диффузии и конвективного потока. Полученные результаты позволяют определение - с точностью большей обычной - требуемого периода промывания и количества промывной жидкости.

СОДЕРЖАНИЕ

МАРКО-МОНОШТОРИ, Б., ЧИКОШ, Ч. и БАТОРИ, Й.: Дегидрогенизация н-гексана с применением модифицированного платинового катализатора 357

ИЛЛЕШ, В. и ХОРВАТ, А.: Кинетическая математическая модель пиролиза бензина I. Уравнение скорости разложения, кинетическая модель 369

ИЛЛЕШ, В. и ХОРВАТ, А.: Кинетическая математическая модель пиролиза бензина II. Распределение продуктов, кривые выхода, кинетическая математическая модель 391

СИНГ, Б., КУМАР, Р.Н. и БАТ, Г.Н.: Кинетика синтеза винилацетата в паровой фазе 411

КИШШ, З., БЛИКЛЕ, Т. и УЙХИДИ, А.: Данные к вычилению кинетических констант, характерных для скорости реакции при гетерогенной каталитической дегидрогенизации с дегалогенизацией 429

ШПЕЙЕР, Г.: Кинетика и механизм димеризации этилена с применением $[Co(C_2H_4)(PPh_3)_3]_2$ в качестве катализатора 449

МОХИЛЛА, Р.: Быстрый метод для проверки правильности дисперсионной трубчатой модели идеального вытеснения и для определения ее параметров 459

ХОРВАТ, Г.: Испытание на определение смешанности суспензии . . . 467

СОЛЧАНИ, П. и ХОРВАТ, Г.: Потребляемая мощность интенсификации перемешивания 489

ДЭ ЙОНГЕ, Я.: Реакция между амальгамой натрия и этиловым спиртом 497

ОЛБРИХ, В.О. и БАТ, Г.Н.: Определение распределения температуры в реакторе с неподвижным слоем псевдоожиженного материала и с потоянной температурой стены 519

ФЮЛЕП, Я., МОНОШТОРИ, Э., НЕМЕТ, Г. и ВАЙДА, Т.: Теоретическое испытание механизма промывания слоя фильтрующегося отжатого осадка, содержащего соль 527

Ára: 39 Ft

CONTENTS

Mrs. MARKÓ-MONOSTORY, B., CSIKÓS, Cs. and BÁTHORY, J.: Dehydrogenation of Normal Hexane on a Modified Platinum Catalyst 357

ILLÉS, V. und HORVÁTH, A.: Kinetisch-mathematisches Modell der Benzinpyrolyse I. Zersetzungsgeschwindigkeitsgleichung kinetisches Modell. (The Kinetic Model of Naphtha Steam Cracking I. The Rate Equation of Decomposition, the Kinetic Model) 369

ILLÉS, V. und HORVÁTH, A.: Kinetisch-mathematisches Modell der Benzinpyrolyse II. Produktverteilung, Ausbeutekurven, kinetisch-mathematisches Modell. (The Kinetic Model of Naphtha Steam Cracking II. Production Distribution, Yield Curves, the Mathematics of the Kinetic Model) 391

SINGH, B., KUMAR, R.N. and BHAT, G.N.: Kinetics of Vapour Phase Synthesis of Vinylacetate 411

KISS, Z., BLICKLE, T. and UJHIDY, A.: Data Concerning the Calculation of Kinetic Constants Characteristic of Reaction Rates in Heterogeneous Catalytic Hydrogenation Dehalogenation 429

SPEIER, G.: Kinetics and Mechanism of the Dimerization of Ethylene Using $[Co(C_2H_4)(PPh_3)_3]_2$ as Catalyst 449

MOHILLA, R.: A Rapid Method for Checking the Validity and for Determining the Parameters of a Piston-Flow Dispersed Tubular Model 459

HORVÁTH, G.: An Experiment for the Determination of the Degree of Mixing of a Suspension 467

SZOLCSÁNYI, P. and HORVÁTH, G.: Power Requirement of the Intensification of Stirring 489

de JONGE, J.: The Reaction between Sodium Amalgam and Ethyl Alcohol 497

OLBRICH, W.O. and BHAT, G.N.: Evaluation of Temperatur Profile in a Gas-Solid Reacting Fixed Bed at Constant Wall Temperature 519

FÜLÖP, J., MONOSTORI, E., HORVÁTH, G. und VAJDA, T.: Theoretische Untersuchung des Auswaschungsmechanismus von salzhaltigen Filterschlammschichten. (Theoretical Examination of the Washing Mechanism of Filter Cakes) 527

A kiadásért felelős: Dr. Nemecz Ernő
Felelős szerkesztő: Dr. Bodor Endre
Példányszám: 950 + 250 különlenyomat cikkenként
Engedélyszám: 53248.

HUNGARIAN

Journal of

INDUSTRIAL CHEMISTRY

Edited by

the Hungarian Oil & Gas Research Institute (MÁFKI),
the Research Institute for Heavy Chemical Industries (NEVIKI),
the Research Institute for Technical Chemistry of the
Hungarian Academy of Sciences (MÜKKI),
the Veszprém University of Chemical Engineering (VVE).
Veszprém (Hungary)

Volume 3. 1975 Number 4.

CODEN: HJICAI

The "Hungarian Journal of Industrial Chemistry (Veszprém)" is a joint publication of the Veszprém scientific institutions of the chemical industry that deals with the results of applied and fundamental research in the field of chemical processes, unit operations and chemical engineering. The papers are published in three or four numbers at irregular intervals in one annual volume, in the English, Russian, French and German languages.

Editorial Office:
Veszprémi Vegyipari Egyetem,
"Hungarian Journal of Industrial Chemistry" Editorial Board:
H – 8201 Veszprém, Schönherz Z. u. 10. Hungary.

Hungarian Journal
of Industrial Chemistry
Veszprém
Vol.3. pp. 537-548 (1975)

UNTERSUCHUNGEN ÜBER DIE ZUSAMMENHÄNGE DES DURCHSCHNITTSWERTES VON DEN DIE CHEMISCHEN TRANSPORTPROZESSE BESCHREIBENDEN POTENTIALFUNKTIONEN

P. BOSCHÁN, J. FÜLÖP, K. SEITZ und T. VAJDA

(Forschungsinstitut für Technische Chemie der Ungarischen Akademie der Wissenschaften, Budapest)

Eingegangen am 23. Juni 1975

In der Arbeit wird untersucht, welchen Typ einer Integralgleichung der räumliche Durchschnittswert der Potentialfunktion einer eindimensionellen Diffusionsgleichung befriedigt, bzw. mit Hilfe welcher ad hoc Reihenentwicklung er erzeugt werden kann, ohne die ursprüngliche Gleichung lösen zu müssen. Die erzielten Resultate ermöglichen einen tieferen Einblick in die mathematische Struktur der Transportgleichung.

I. Einleitung

In der chemischen Verfahrenstechnik sind die durch geleiteten Wärme- und Stofftransport charakterisierten Prozesse von großer Bedeutung. In diesen Fällen kann die entsprechende Potentialverteilung - also die Temperatur- bzw. Konzentrationsverteilung - mit Hilfe der Fourier- bzw. Fick-schen Gleichungen, sowie der zu diesen gehörenden entsprechenden Anfangs- und Randbedingungen in üblicher Annäherung beschrieben werden. Obiger Problemenkreis ist zwar bereits von vielen Seiten untersucht worden, doch ist jedes Ergebnis, welches das Verhalten der genannten Potentialfunkti-

onen von einer neuen Seite her beleuchtet, von Bedeutung. In dieser Tatsache liegt auch der Sinn unserer Arbeit.

Wie bekannt, sind bei der mathematischen Behandlung der chemischen Prozesse die Resultate, die aus einzelnen Modellkonstruktionen auf analytische Weise, also ohne Komputer gewonnen werden können, von großer Bedeutung. Analytische Formeln können aber häufig nur für den räumlichen oder zeitlichen Durchschnittswert der in den Gleichungen figurierenden Potentialfunktionen aufgestellt werden. Aus diesem Grunde ist es wichtig, die Zusammenhänge bezüglich der Durchschnittswerte auch von rein mathematischem Gesichtspunkt aus zu untersuchen. Diejenigen der räumlichen Durchschnittswerte spielen hierbei eine viel größere Rolle.

Ziel gegenwärtiger Arbeit ist es, die mathematischen Eigenschaften des räumlichen Durchschnittswertes der Potentialfunktion im Laufe der Ausgleichungsprozesse eines, mit seiner Umgebung durch die Newton-sche Randbedingung beschreibbar verbundenen, eindimensionellen Systems zu untersuchen, in welchem die Potentialverteilung u zum Zeitpunkt $t = 0$ als u_0 bekannt ist, und wo ausschließlich Diffusionsströme auftreten. Als Ausgangspunkt ist also folgendes mathematisches Problem zu betrachten:

$$a^2 \frac{\partial^2 u}{\partial x^2} = \frac{\partial u}{\partial t} \tag{1a}$$

$$u(x,o) = u_o(x) \tag{1b}$$

$$\left(\frac{\partial u}{\partial x}\right)_{x=-L} = -h[u^* - u(-L,t)] \tag{1c}$$

$$\left(\frac{\partial u}{\partial x}\right)_{x=L} = h[u^* - u(L,t)] \tag{1d}$$

Aus den Gleichungen (1a) ... (1d) geht hervor, daß auch eine inhomogene Anfangsverteilung im untersuchten System gestattet, sowie daß das System auf den Origo symmetrisch ist (Ausbreitung von 2 L), und daß sich die Umgebung des Systems hinsichtlich des betrachteten Potentials als Reservoir verhält (u^* = konstant).

Wir möchten zwei Fragen behandeln: zuerst untersuchen wir, zu welchem Typ eines Integralzusammenhanges bezüglich des räumlichen Durchschnitts $\bar{u}$ der Potentialfunktion die Aufgabe (1a)...(1d) umgeformt werden kann, aus welchem der Durchschnitt prinzipiell - ohne Lösung der ursprünglichen partiellen Differentialgleichung - bestimmbar ist. Ein wesentliches Moment der Umformung besteht darin, daß der Durchschnitt an einer solchen Form der Potentialfunktion gebildet wird, aus welcher die Zeitveränderliche mit Hilfe der Laplace-Transformation beseitigt worden ist.

Als zweites Problem untersuchen wir, mit Hilfe welcher ad hoc Reihenentwicklung obiger Durchschnitt, ausgehend von den Gleichungen (1a) ... (1d) - ebenfalls ohne Lösung der ursprünglichen partiellen Differentialgleichung - erzeugt werden kann. Die Reihenentwicklung wird durch einen mathematischen Griff, die Fourier-sche Entwicklung der Einheit, sowie durch Festsetzung des Verhaltens der Fourier-Komponenten mit Hilfe der Gleichungen (1a)...(1d) erhalten.

Die Bedeutung der erzielten Resultate besteht vor allem darin, daß es in den beiweitem nicht trivialen Problemkreis einen Einblick gewährt, wie sich die abhängige Variable der vom Gesichtspunkt der Praxis her sehr wichtigen, untersuchten partiellen Differentialgleichung verhält, wenn eine der unabhängigen Variablen aus dieser beseitigt wird. Die gewonnenen Zusammenhänge können als Ausgangspunkt für praktisch gut anwendbare Näherungsberechnungen dienen.

II. Angabe des Durchschnitts mittels einer Integralgleichung

Betrachten wir der Einfachheit halber in dem Problem (1a)... ...(1d) vor allem die den Anfangswert angebende Funktion $u_0(x)$ als konstant, also $u_0(x) \equiv u_0$. Wir erhalten durch Einführung der Laplace-Transformierten $V(x)$ der Potentialfunktion $U(x,t)$:

$$V(x) = \int_0^\infty u(x,t)\, e^{-pt}\, dt \qquad (2)$$

für die Transformierte unter Benützung der Zusammenhänge (1a)-(1b) und (2) folgende Gleichung:

$$a^2 \frac{d^2V}{dx^2} = pV - u_o \tag{3}$$

Die Lösung der Gleichung (3) kann auf übliche Weise unter Berücksichtigung der Randbedingungen (1c)-(1d) gewonnen werden:

$$V(x) = \frac{u_o}{p} + \frac{(u^* - u_o)h\frac{1}{p}}{\frac{\sqrt{p}}{a} \operatorname{sh} \frac{\sqrt{p}}{a} L + h \operatorname{ch} \frac{\sqrt{p}}{a} L} \operatorname{ch} \frac{\sqrt{p}}{a} x \tag{4}$$

Es kann leicht eingesehen werden, daß die Laplace-Transformierte F(p) des zu untersuchenden räumlichen Durchschnitts

$$\bar{u}(t) = \frac{1}{2L} \int_{-L}^{L} u(x,t)\, dx \tag{5}$$

jetzt mit Hilfe der Transformierten (2) bzw. (5) laut folgendem Zusammenhang

$$F(p) = \int_o^\infty \bar{u}(t)\, e^{-pt}\, dt = \frac{1}{2L} \int_{-L}^{L} V(x)\, dx \tag{6}$$

gewonnen werden kann. Aus dem Vergleich von (4) und (6) ergibt sich die Funktionsform der Transformierten des Durchschnitts wie folgt:

$$F(p) = \frac{u_o}{p} + \frac{h}{p}(u^* - u_o) \frac{\frac{\operatorname{sh} \frac{\sqrt{p}}{a} L}{\frac{\sqrt{p}}{a} L}}{\frac{\sqrt{p}}{a} \operatorname{sh} \frac{\sqrt{p}}{a} L + h \operatorname{ch} \frac{\sqrt{p}}{a} L} \tag{7}$$

Nun wird der Zusammenhang (7) in eine Form gebracht, welche die Durchführung der inversen Laplace-Transformation erleichtert:

$$(pF(p) - u_o)\left(\frac{L}{a^2} + \frac{hL}{a\sqrt{p}} \frac{\operatorname{ch} \frac{\sqrt{p}}{a} L}{\operatorname{sh} \frac{\sqrt{p}}{a} L}\right) = \frac{h}{p}(u^* - u_o) \tag{8}$$

Das Wiedereinsetzen der rechten Seite von (8) ist trivial, während die erste Klammer der linken Seite gerade die Transformierte der zeitlichen Ableitung des Durchschnitts darstellt. Das zweite Gleid der zweiten Klammer ist hingegen die Laplace-Transformierte der mit der Konstanten h multiplizierten, elliptischen Theta(3)-Funktion, wo die erste Variable an der Nullstelle genommen wurde, und deren übliche Aufschreibung nach [5] wie folgt ist:

$$\mathcal{L}^{-1}\left[\frac{L}{a\sqrt{p}}\,\frac{\operatorname{ch}\frac{\sqrt{p}}{a}L}{\operatorname{sh}\frac{\sqrt{p}}{a}L}\right] = \vartheta_3\left(0,\frac{a^2}{L^2}t\right) \equiv \sum_{n=-\infty}^{\infty} e^{-\frac{a^2}{L^2}\pi n^2 t} \tag{9}$$

Die inverse Transformierte des Zusammenhanges (8) ergibt unter Verwendung des Konvolutionssatzes, sowie unter Berücksichtigung von (9) und obiger Ausführungen, bzw. durch Umgestaltung des erhaltenen Resultates:

$$\frac{d\bar{u}}{dt} + \frac{a^2h}{L}\int_0^t \vartheta_3\left(0,\frac{a^2}{L^2}s\right)\cdot\left.\frac{d\bar{u}}{dt}\right|_{t-s}\cdot ds = \frac{a^2h}{L}\left(u^* - u_0\right) \tag{10}$$

wobei wir das Argument der hinter dem Integral stehenden Derivierten des Durchschnitts besonders bezeichnen.

Wir bemerken, daß (10) bereits als einer der gesuchten Integralzusammenhänge betrachtet werden kann. (10) ist nämlich eine lineare, inhomogene, Volterra-sche Integralfunktion des Faltungstyps für die zeitliche Ableitung des Durchschnitts mit einer Kernfunktion

$$\vartheta_3\left(0,\frac{a^2}{L^2}t\right)$$

Einen wichtigeren Zusammenhang erhalten wir jedoch aus einer anderen Form von (8):

$$(F(p) - \frac{u_0}{p})(\frac{L}{a^2} + \frac{h\,L}{a\sqrt{p}} \frac{ch\,\frac{\sqrt{p}}{a}\,L}{sh\,\frac{\sqrt{p}}{a}\,L}) = \frac{h}{p^2}\,(u^* - u_0) \tag{11}$$

Führen wir nun folgenden Simplex des Durchschnitts ein:

$$R(t) = \frac{\bar{u}(t) - u_0}{u^* - u_0} \tag{12}$$

so erhalten wir durch die inverse Transformierung von (11) folgende, auf die unter (12) definierte Menge bezogene Integralgleichung:

$$R(t) + \frac{a^2h}{L} \int_0^t \vartheta_3(0, \frac{a^2}{L^2}\,s) R(t-s)ds = \frac{a^2h}{L}\,t \tag{13}$$

Die Charakteristika der Gleichung (13) sind identisch mit jenem der Gleichung (10). Sie unterscheiden sich nur darin, daß das inhomogene Glied hier zeitabhängig ist. Mit dem Resultat von (13) haben wir unser gesetztes Ziel, nämlich die Formulierung einer Integralzusammenhanges erreicht, aus dem der Durchschnitt ohne Benützung der ursprünglichen Gleichung bestimmt werden kann.

III. Bestimmung des Durchschnitts mittels ad hoc Reihenentwicklung

Ändern wir bei unserem zweiten zu untersuchenden Problem die Gleichung (1a)...(1d) insofern, als wir einesteils die den Anfangswert angebende Funktion $u_0(x)$ als symmetrisch betrachten: $u_0(-x) = u_0(x)$, andernteils die Transformierung des Potentials $u \to u^* - u$ durchführen, wodurch - wie leicht einzusehen ist - nur die Form der Randbedingungen (1c) - (1d) verändert wird:

$$(\frac{\partial u}{\partial x})_{x=-L} = - hu(-L,t) \tag{14a}$$

$$(\frac{\partial u}{\partial x})_{x=L} = hu(L,t) \tag{14b}$$

Nun wird die Fourier-Transformierte der Potentialfunktion U(t) auf folgende Weise eingeführt:

$$U(t) = \int_{-L}^{L} u(x,t) \cos qx \, dx \tag{15}$$

Unser Ziel ist es nun, mit Hilfe der Gleichungen (1a)...(1d) die Zeitabhängigkeit obiger Transformierten festzustellen.

Mit Hilfe partieller Integrationen kann gezeigt werden, daß die Fourier-Transformierte der Derivierten zweiten Grades auf der linken Seite der Gleichung (1a) (unter Verwendung von (15)) folgende Form annimt:

$$\int_{-L}^{L} \frac{\partial^2 u}{\partial x^2} \cos qx \, dx = \left(\frac{\partial u}{\partial x}\right)_{x=L} \cos qL - \left(\frac{\partial u}{\partial x}\right)_{x=-L} \cos qL + \tag{16}$$

$$+ q[u(L,t) \sin qL + u(-L,t) \sin qL] - q^2 U(t)$$

Sodann setzen wir (14a)-(14b) in (16) ein:

$$\int_{-L}^{L} \frac{\partial^2 u}{\partial x^2} \cos qx \, dx = [h \cos qL + q \sin qL] \, u(L,t) + \tag{17}$$

$$+ [h \cos qL + q \sin qL] \, u(-L,t) - q^2 U(t)$$

Im Laufe unserer Untersuchungen wollen wir nur die aus der transzendenten Gleichung (18) bestimmbaren q Werte (Eigenwerte) berücksichtigen: $q = q_1, q_2, \ldots, q_n, \ldots$

$$h \cos qL + q \sin qL = 0 \tag{18}$$

dann nimmt (17) die endgültige Form an:

$$\int_{-L}^{L} \frac{\partial^2 u}{\partial x^2} \cos qx \, dx = - q^2 U(t) \tag{19}$$

Die Transformierte der rechten Seite von (1a) ist einfach die zeitliche Ableitung von U(t). Unter Berücksichtigung obiger Ausführung ist die aus (1a) abgeleitete Gleichung bezüglich der

unter (15) definierten Menge folgende:

$$\frac{dU}{dt} = - a^2q^2U \tag{20}$$

Die zu dieser gehörende Anfangsbedingung ergibt sich durch Transformierung von (1b):

$$u(t=0) = \int_{-L}^{L} u_0(x) \cos qx \, dx = U_0 \tag{21}$$

Schließlich ist die Lösung von (20) unter Berücksichtigung von (21) wie bekannt:

$$U(t) = U_0 \, e^{-a^2q^2t} \tag{22}$$

Die Fourier-Transformierte des Potentials ist bei speziellen, von (18) bestimmten Parameterwerten - laut (22) - von der Zeit exponentiell abhängig. Aus (15), (22), sowie aus obigen Überlegungen gilt daher folgendes:

$$\int_{-L}^{L} u(x,t) \cos q_n x \, dx = U_0(q_n) \, e^{-a^2q_n^2t} \tag{23}$$

$n=1, 2, \ldots$

Schreiben wir nun den Durchschnitt in Form einer Reihe auf. Nützen wir dabei die Tatsache aus, daß das Potential den Anfangsbedingungen entsprechend eine x-symmetrische Funktion ist,und daß die mit den durch (18) bestimmten q_n Werten gebildeten Cosinus-Funktionen unter obigen symmetrischen Funktionen ein vollständiges, ortogonales Funktionssystem bilden [1]. Demnach gilt zum Beispiel nachstehende Reihenentwicklung der Einheit:

$$1 = \sum_{n=1}^{\infty} c_n \cos q_n x \tag{24}$$

wobei die Fourier-Koeffizienten folgende sind:

$$c_n = \frac{2 \sin q_n L}{q_n L + \sin q_n L \cos q_n L} \tag{25}$$

An dem in (5) definierten räumlichen Durchschnitt der Potentialfunktion kann mit Hilfe von (24) eine ähnliche Umformung vorgenommen werden, nämlich:

$$\bar{u}(t) = \frac{1}{2L} \int_{-L}^{L} u(x,t)\, dx = \frac{1}{2L} \int_{-L}^{L} 1 \cdot u(x,t)\, dx = \tag{26}$$

$$= \frac{1}{2L} \int_{-L}^{L} \sum_{n=1}^{\infty} c_n \cos q_n x \cdot u(x,t)\, dx$$

oder, wenn man in (26) die Reihenfolge des Integrals und der Summierung austauscht:

$$\bar{u}(t) = \frac{1}{2L} \sum_{n=1}^{\infty} c_n \int_{-L}^{L} u(x,t) \cos q_n x\, dx \tag{27}$$

Wir merken nun, daß die explizite Form der in (27) figurierenden Integrale gerade durch (23) angegeben wurde, so ergibt sich also als endgültige Form für den Durchschnitt:

$$\bar{u}(t) = \frac{1}{2L} \sum_{n=1}^{\infty} c_n U_0(q_n)\, e^{-a^2 q_n^2 t} \tag{28}$$

In der exponentiellen Reihe (28) können die hinter dem Summierungszeichen stehenden einzelnen Größen mit Hilfe von (25), (21) und (18) der Reihe nach sofort bestimmt werden. Mit dem Resultat unter (28) wurde auch unser zweites Ziel verwirklicht: der Ausdruck des Durchschnitts konnte ohne Lösung der ursprünglichen Gleichung, mit Hilfe einer ad hoc Reihenentwicklung aufgeschrieben werden.

IV. Zusammenfassung, Konklusionen

Wir befassten uns in unserer Arbeit mit zwei Problemen:

a) Für den räumlichen Durchschnitt der Potentialfunktion des eindimensionellen Diffusionssystems, welches sich durch die Newton-schen Randbedingung an ihre Umgebung anschließt, wurde im Laufe des Ausgleichsprozesses eine Integralgleichung bekannten Typs aufgestellt, die relativ leicht anwendbar ist, und deren Kernfunktion eine elliptische Funktion darstellt. Aus anderen Untersuchungen [6] und im allgemeinen aus der Theorie der partiellen Differentialgleichungen her ist es bekannt, daß das Vorhandensein eines solchen Zusammenhanges, der sich auf obige Größe - auf das für eine Variable genommene Durchschnittspotential - bezieht, und aus welchem Zusammenhang die betreffende Größe "sich selbst bestimmt", nicht trivial ist. Es kann zum Beispiel bewiesen werden, daß es eine derartige Differentialgleichung überhaupt nicht gibt;

b) Dieselbe Größe wurde mit Hilfe der Fourier-schen Reihenentwicklung auch auf indirekte Weise erzeugt, wobei die ursprüngliche partielle Differentialgleichung nur zur Feststellung der Zeitabhängigkeit der Fourier-Komponenten verwendet wurde. Die Vollständigkeit der Entwicklungsmethode war darauf begründet, daß wir als Anfangswert des ursprünglichen Potentials eine symmetrische Funktion wählten, so daß die bei der Entwicklung der Einheit eintretenden Funktionskomponenten tatsächlich eine komplette Beschreibung des Problems lieferten.

Beide Annäherungen des untersuchten Problemenkreises können als neuartig bezeichnet werden, und sie bedeuten bei der Lösung von für die Praxis wichtigen Annäherungs- bzw. numerischen Aufgaben Ausgangspunkte, die bisher nicht verwendet worden sind.

ZEICHENLISTE

a^2 Leitungskoeffizient

c_n Fourier-Koeffizienten

F Laplace-Transformierte des Durchschnitts der Potentialfunktion

h Übertragungsfaktor

L Ausbreitung des Systems

n laufender Index

p Parameter der Laplace-Transformation

q Parameter der Fourier-Transformation

R Simplex des Durchschnitts

s Integrationsparameter

t Zeitkoordinate

u Potentialfunktion

$\bar{u}$ räumlicher Durchschnitt der Potentialfunktion

u_o Anfangspotentialverteilung

u* Potentialwert in der Umgebung

U Fourier-Transformierte der Potentialfunktion

U_o Anfangswert der Fourier-Transformierten

V Laplace-Transformierte der Potentialfunktion

x Längskoordinate

ϑ die elliptische Theta-Funktion

SCHRIFTTUM

1. CARSLAW, H.S., JAEGER, J.C., Conduction of Heat in Solids, Oxford, Clarendon Press, 1959.

2. ECKERT, E.R.G., DRAKE, R.M., Heat and Mass Transfer, New York - - Toronto, McGraw-Hill, 1959.

3. CRANK, J., The Mathematics of Diffusion, Oxford, Clarendon Press, 1957.

4. BIRD, R.B., STEWART, W.E., LIGHTFOOT, E.N., Transport Phenomena, New York - London, J. Wiley & Sons, 1966.

5. LÖSCH, F. et al., Tafeln höherer Funktionen, Stuttgart, Teubner Verlagsgesellschaft, 1966.

6. POLINSZKY, K. et al., Acta Chimica, 85, 161 (1975)

РЕЗЮМЕ

Данная статья изучает какому типу интегральных уравнений удовлетворяет объемное среднее значение потенциальной функции одномерного диффузионного уравнения и каким случайным методом разложения в ряд оно получается без решения соответствующего уравнения. Полученные результаты позволяют более тщательное познание математической структуры транспортного уравнения.

Hungarian Journal
of Industrial Chemistry
Veszprém
Vol.3. pp. 549-556 (1975)

THE ROLE OF NATURAL INHIBITORS IN THERMAL DEGRADATION OF POLYMETHACRYLATE ADDITIVES

I. MÉSZÁROS

(Danubean Refinery, Százhalombatta)

Received: June 16, 1975.

The paper presents a study on the thermal stability of polyalkyl methacrylate viscosity index improvers. It is demonstrated that the thermal stability of the polymer is considerably influenced by the chemical nature of the base oil. In ester oils and white oils, the thermal degradation of the polymer molecule is significant, however, in mineral lubricating oils, the breakdown is markedly reduced by the natural inhibitors of the mineral oil.

INTRODUCTION

One way to fulfil the more and more stringent requirements imposed on motor oils is based on the application of "partially--synthetic" oils, produced by blending synthetic and mineral lubricating oils. Ester oils are the most promising candidates for the synthetic components of such blends, not only because they offer an excellent balance of the essential lubricating properties (outstanding viscosity-temperature characteristics, low volatility, and low pour point, etc.), but also because they are widely employed in the lubrication systems of aircraft gas turbine engines and are thus commercially available in large quantities [1].

When formulating such a partially-synthetic lubricating oil, careful attention should be focused on how the esters interfere - if at all - with the additives commonly used in motor oils.

The Thermal Stability of Ester Oils

The present paper reviews the thermal stability of polymeric viscosity index improvers in synthetic ester oils and partially--synthetic base stocks. Curiously enough, this problem has been rather neglected in literature, although the thermal stability of pure esters has been dealt with in a large number of papers, moreover, the classification of the ester oils used in the lubrication systems of jet engines is based on their thermal stability.

The group of the Type I ester oils includes esters of aliphatic dicarboxylic acids. Their thermal decomposition occurs by means of a cyclic intermediate. Type II oils are sterically hindered esters, each hydrogen atom on the β-carbon atom of their alcohol moiety is replaced by alkyl groups. The decomposition of Type II esters proceeds by a free radical mechanism, and since free radicals require more energy of formation than the cyclic intermediate, Type II esters possess considerably greater thermal stability than Type I oils.

In both cases, the thermal decomposition of ester oils results in an olefinic hydrocarbon and a carboxylic acid [2].

Experimental

The thermal stability of synthetic and partially synthetic oils containing polymeric viscosity index improver was investigated. Typical representatives of both types of ester oils: di-(2--ethylhexyl) sebacate (DOS) and trimethylolpropane tripelargonate (TMPP) were chosen as synthetic components, while as the mineral base stock, a heavy oil raffinate - produced from Algyő crude oil by solvent extraction, dewaxing, and hydrofinishing - was used. A

commercial polymethacrylate (Reonit M) was added to the base oils as the viscosity index improver. The compositions of the experimental oils are listed in Table 1.

Table 1. The compositions of the experimental oils

Sample	Mineral oil raffinate wt.%	DOS wt.%	TMPP wt.%	Reonit M (1) wt.%	Viscosity at 98.9°C cs(mm²/s)
1	100	-	-	-	9.46
2	88	-	-	12	25.31
3	-	100	-	-	3.31
4	-	88	-	12	13.06
5	-	-	100	-	4.78
6	-	-	88	12	17.72
7	60	40	-	-	5.66
8	48	40	-	12	19.14
9	60	-	40	-	6.74
10	48	-	40	12	21.91
11(2)	-	99.5	-	-	3.32
12(2)	-	87.5	-	12	13.10

(1): commercial product containing approximately 50 wt.% light white mineral oil as diluent

(2): containing 0.5 wt.% 2,6-di-tert-butyl-4-methylphenol

The thermal stability was tested according to the following procedure:

40 ml of the test fluid was placed in a glass test tube. The test tube was submerged in a constant temperature bath to a point slightly above the level of the oil sample, and was held in the bath at 200 °C for 12 hours. At the end of the ageing period, the test tube was removed and allowed to cool to ambient temperature. The tests were carried out both in air and under a carbon dioxide

atmosphere. In the first case, the test tube was stoppered with a cork with a 2 mm diameter bore in it. In the second case, the test tube was connected through a ground glass joint to a glass vessel in which a slight carbon dioxide pressure was maintained. (Carbon dioxide was continuously introduced into the vessel and bubbled out of it through a glass tube immersed into water to a depth of approximately 5 mm.) At the beginning of the test, the air was removed from the test tube by blowing carbon dioxide through it, and after the 12 hour period, the sample was allowed to cool under a carbon dioxide atmosphere.

The thermal stability of the compositions was evaluated on the basis of the changes in viscosity and acid number. The reproducibility of the test is fairly good. The difference in the acid number increase of two determinations never exceeded the error limit of the standardized acid number determination. The viscosities of two parallelly aged samples differed by not more than 1 per cent of the mean in the tests under carbon dioxide, and by not more than 4 per cent of the mean in the experiments carried out in air.

The thermal stability of the polymer was characterized by the thermal stability index which is defined by the following equation:

$$TSI = \frac{V_1 - V_2}{V_1 - V_0} \cdot 100 \quad (\%)$$

where TSI is the thermal stability index of the polymer

V_1 and V_2 are the kinematic viscosities of the polymer-containing compositions, before and after ageing, respectively

V_0 is the kinematic viscosity of the base oils (without polymer) after ageing.

(Kinematic viscosities were measured at 98.9 °C, in cs.)

Since the change of the base oil viscosity during the ageing is negligible, the thermal stability index gives a good approximation of the thermal stability of the polymer.

The results of ageing are summarized in Table 2.

Table 2. Characteristics of aged samples

Sample	Ageing in air			Ageing in carbon dioxide		
	Viscosity at 98.9°C cs(mm²/s)	Acid number increase mg KOH/g	TSI (%)	Viscosity at 98.9°C cs(mm²/s)	Acid number increase mg KOH/g	TSI (%)
1	9.51	0.13	-	9.44	0.00	-
2	24.36	0.07	6.01	24.69	0.01	3.91
3	3.38	1.26	-	3.29	0.02	-
4	6.82	0.67	64.46	10.46	0.04	26.61
5	4.91	0.64	-	4.85	0.06	-
6	10.78	0.44	54.18	14.17	0.07	27.58
7	5.68	0.49	-	5.67	0.01	-
8	17.12	0.30	15.01	18.50	0.01	4.75
9	6.72	0.36	-	6.74	0.02	-
10	19.86	0.21	13.50	21.18	0.00	4.81
11	3.36	0.08	-	3.32	0.02	-
12	13.06	0.06	0.41	12.80	0.02	3.07

CONCLUSIONS

It is apparent from the results obtained that the Reonit M additive exhibits a fairly good thermal stability when heated in mineral oil. The viscosity of the additive-containing mineral oil does not significantly decrease during the ageing. The same polymer, however, decomposes to a remarkable extent when dissolved in ester.

The acid number increase of the esters aged under carbon dioxide atmosphere exceeded the error limit of the acid number determination. This fact suggests that in addition to the polymer degradation, the esters also decompose to a slight extent. In the tests carried out in the presence of air, the simultaneous oxidative and thermal reactions result in an appreaciable deterioration

of the ester which is apparent from the acid number increase of the samples aged in air.

According to our present knowledge it is known that the thermal and oxidative breakdown of polymers proceeds by a free radical chain mechanism [3]. It is evident that during the ageing, reactive radicals are formed which are capable of initiating the chain reaction of the polymer decomposition. As it might be expected, the formation of free radicals is expressed more in the presence of oxygen than under merely a thermal effect. This is confirmed by comparing the viscosity and acid number changes of the samples aged in air and carbon dioxide.

The free radical chain mechanism is in agreement with the observation that 2,6-di-tert-butyl-4-methylphenol - a typical chain-breaking inhibitor [4] - appreciably improved the thermal stability of the polymer dissolved in pure ester oil: the viscosity of the inhibitor-containing composition remained practically unchanged during the ageing (Sample 12).

The fact that the thermal stability of polymer solutions in partially-synthetic oils is considerably enhanced, compared to that of the solutions in pure esters, suggests that the thermal breakdown is inhibited in the partially-synthetic compositions.

It is a matter of common knowledge that mineral oils contain numerous substances - mainly sulphur compounds, and aromatic hydrocarbons - which function as natural chain-breaking inhibitors in oxidative reactions [5, 6].

It can be assumed that the fairly good thermal stability exhibited by the Reonit M additive in mineral and partially-synthetic base stocks is the result of the inhibiting effect of the natural anti-oxidants rather than the inherent property of the additive. From the above assumption it can be concluded that the determination of the polymer in ester oils is mainly due to the absence of natural inhibitors. This conclusion is obviously confirmed by the data of Table 3. In Table 3, data concerning the thermal stability of a light white mineral oil containing 12 wt.% Reonit M additive are given.

Table 3. Thermal stability of a light white mineral oil containing 12 wt.% additive

	Viscosity at 98.9°C cs(mm^2/s)	Acid number mg KOH/g	TSI (%)
Fresh sample	10.85	0.00	-
Sample aged in air	6.39	0.22	60.43
Sample aged in CO_2	9.31	0.00	20.73

White oils contain no natural inhibitors. The thermal degradation of the polymeric additive in white oil is noticeable, for the value of the thermal stability index is nearly the same as those obtained in pure esters. This experience substantiates the above assumption concerning the effect of natural inhibitors on the thermal stability.

SUMMARY

In the thermal decomposition of polymeric additives, the free radical chain reaction is initiated by reactive radicals. These radicals are formed mainly from the polymer itself. The thermal breakdown of the polymer is considerably influenced by the chemical composition of the base oil. The natural anti-oxidants of the mineral oils, acting as chain-breaking inhibitors, considerably reduce the polymer degradation.

***

The experiments were carried out at the Department of Hydrocarbon and Coal Processing, Veszprém University of Chemical Engineering.

REFERENCES

1. FAIRBANKS, D.R., KNAPP, M.H., LAZARUS, A.K.: Machine Design, 16, 140 (1969)

2. ROBSON, R.: Ind. Lubr. Trib. No. 1, pp. 7-11 (1971)

3. GORDON, G.J.: Stabilizatija sinteticheskih polimerov. Gos. Nauch. -Technich. Izd., Moscow, 1963.

4. VESELY, V.: Ropa a Uhlie 11, 297 (1969)

5. BURN, A.J., GREIG, G.: Journal IP 58, 346 (1972)

6. STUDT. P.: Erdöl u. Kohle 27, 195 (1974)

РЕЗЮМЕ

В статье излагается изучение термической устойчивости добавок полиметакрилатного типа, повышающих индекс вязкости. Было показано, что термическая устойчивость полимера очевидно зависит от природы основного масла. В эфирных и белых маслах термическая деградация полимерной молекулы является значительной, а в минеральных смазочных маслах пластикация прямо уменьшается природными ингибиторами минеральных масел.

Hungarian Journal
of Industrial Chemistry
Veszprém
Vol.3. pp. 557-564 (1975)

EINE VEREINFACHTE METHODE ZUR ERMITTLUNG DES STOFFÜBERGANGES IN BLASENSÄULEN

F. TUREK* und M. MAGYAR

(*Technische Hochschule "Carl Schorlemmer", Leuna-Merseburg,
Ungarisches Erdöl- und Erdgasforschungsinstitut, Veszprém)

Eingegangen am 15. Juli 1975

Die Blasensäulenreaktoren finden in der chemischen Industrie immer verbreitende Anwendung, weil die Verfolgung der Stoffübergangsverhältnisse in diesen Apparaten sehr vorteilhaft ist. Trotz der breiten Anwendung der obigen Apparaten sind die Einzelheiten der Stoffübergangsprozesse nur teilweise erforscht. In dieser Arbeit beschreiben die Verfasser eine schnelle und den technischen Anforderungen entsprechende Experimentalmethode, wodurch die Bestimmung der Stoffübergangsparameter bei halbkontinuierlichen und kontinuierlichen Reaktortypen leicht durchzuführen ist.

In vielen Verfahren der chemischen Industrie spielt der Stoffübergang Gas-Flüssigkeit in Blasensäulen eine wesentliche Rolle. Zur Dimensionierung und Optimierung von Blasensäulen ist die Kenntnis der Phasengrenzfläche und des Stoffübergangskoeffizienten für das betrachtete technische Problem erforderlich. Dazu sind in den letzten Jahren eine Vielzahl von Untersuchungen durchgeführt und entsprechende Korrelationen erarbeitet worden [1, 2, 5, 6, 7].

Es zeigt sich jedoch, daß sehr abweichende Ergebnisse bei der Berechnung von Stoffübergangsparametern nach Korrelationsbeziehungen Verschiedener Autoren erhalten werden. Aus diesem Grunde ist es in vielen Fällen, besonders auch bei Blasensäulen als Reaktionsapparate erforderlich, zum konkreten technischen Problem zu-

sätzliche experimentelle Untersuchungen zum Stoffübergang Gas-Flüssigkeit durchzuführen. Im folgenden wird eine Methode zur experimentellen Ermittlung von Stoffübergangsparametern vorgeschlagen, die relativ schnell und ohne größeren technischen Aufwand für eine Reihe von technischen Problemen hinreichend genaue Ergebnisse liefert.

Hierbei werden die Experimente in einer halbkontinuierlichen Versuchsanlage durchgeführt und anschließend die Ergebnisse auf die kontinuierliche Blasensäule übertragen.

Versuchsanordnung

Die Versuchsanordnung zur Untersuchung des Stoffübergangs ist auf Bild 1 schematisch dargestellt. In die Blasensäule, die aus

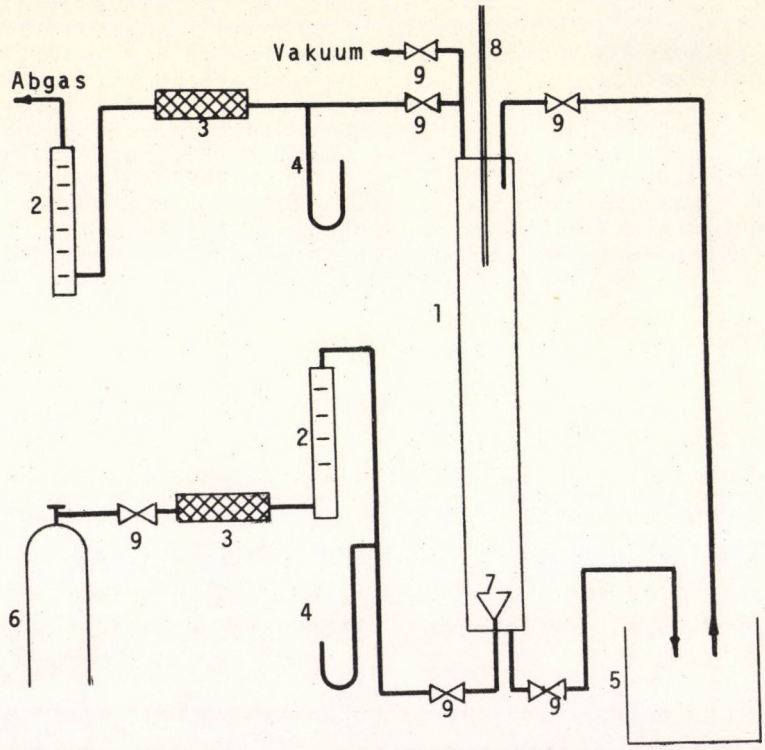

Bild 1. Versuchsanordnung. 1-Blasensäule, 2-Präzisionsseifenblasenzähler, 3-Gastrockner, 4-U-Manometer, 5-Flüssigkeitsbehälter, 6-Druckgasflasche, 7-Glasfritte, 8-Thermometer, 9-Absperr- bzw. Regelventil

einem Glasrohr von 2 m Länge und 7 cm Durchmesser bestand, wurde die Flüssigphase mittels Vakuum aus dem Vorratsbehälter (5) eingesaugt. Dadurch konnte gleichzeitig das in der Flüssigkeit gelöste Gas weitesgehend desorbiert werden. Das Gas wurde einer Druckgasflasche (6) entnommen und durch eine Glasfritte (7) in die Blasensäule geleitet und der Durchsatz vor und nach der Blasensäule mit Präzisionsseifenblasenzählern (2) gemessen. Die Differenz zwischen dem Eingangs- und Austrittsgasstrom ergab die in der Flüssigkeit absorbierte Gasmenge. Die Durchsatzmessungen mußten gleichzeitig und in möglichst geringen zeitlichen Abständen durchgeführt werden.

Meßergebnisse und Auswertung

Man erhält auf diese Weise den Molenstrom des absorbierten Gases in Abhängigkeit von der Zeit (s. Bild 2). Die Fläche unter dem n(t)-Verlauf ergibt die Gesamtmolenzahl des in der Flüssigkeit absorbierten Gases.

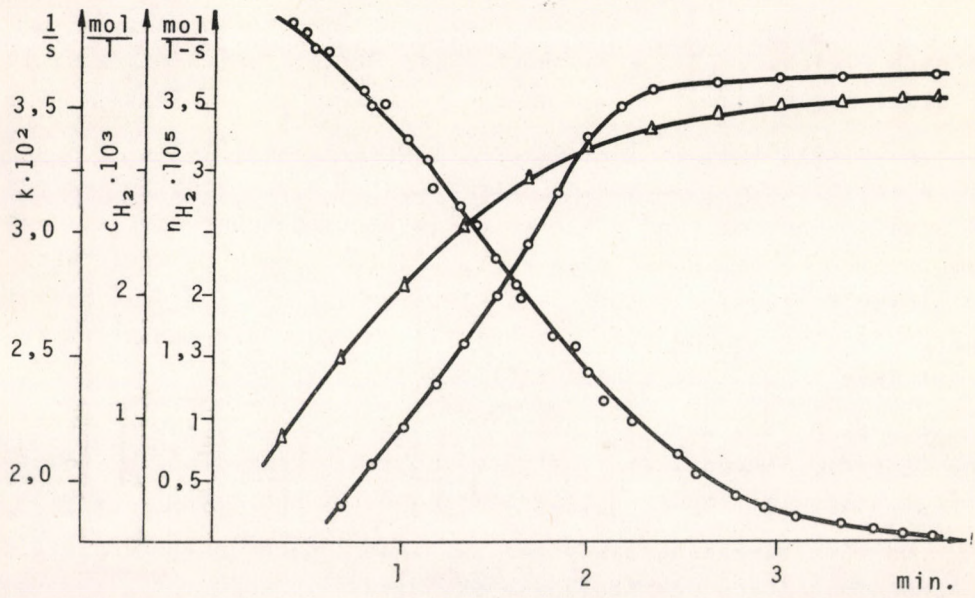

Bild 2. Zeitverläufe der absorbierten Molzahl, der Gaskonzentration und des Stoffüberganges für Alkohol-H_2. V_g= 11,2 ℓ/m²s;

Bei der Auswertung wird unter der vereinfachenden Annahme einer homogenen Gasblasenverteilung, von der Stoffübergangsgleichung

$$n_j = k_g \cdot F(c_j^* - c_j)\, V_\ell \qquad (1)$$

ausgegangen. Wegen der Instationärität des Prozesses sind n_j und c_j Funktionen der Zeit.

$c_j(t)$ wird nach folgender Beziehung aus der Meßreihe $n_j(t)$ ermittelt:

$$c_j = \frac{1}{V_\ell} \cdot \int_0^t n_j(t)\, dt \qquad (2)$$

Damit kann das Produkt $(k_g F) = k$ als Funktion der Zeit bestimmt werden (s. Bild 2).

$$k = \frac{\dot{n}_j(t)}{c_j^* - c_j(t)} \quad \text{bzw.} \quad k = -\frac{d\dot{n}_j}{dc_j} \qquad (3)$$

Die nach Gleichung (2) erhaltenen k(t)-Werte stellen Mittelwerte für Blasensäule dar.

Der zeitliche Verlauf des Stoffübergangskoeffizienten k auf Bild 2 zeigt, wie zu erwarten ist, zunächst einen nahezu linearen und steilen Anstieg und nähert sich im Bereich hoher Gassättigung asymptotisch einem konstanten Wert. Dieser konstante Wert wurde für einige Kohlenwasserstoffe als Flüssigphase und die Gase Wasserstoff, Stickstoff und Luft bei Variation des Gasdurchsatzes bestimmt. Die Ergebnisse sind auf Bild 3 dargestellt.

Es ist nahezu über den gesamten untersuchten Parameterbereich eine lineare Abhängigkeit vom Gasdurchsatz festzustellen. Diese Aussage stimmt mit anderen Literaturangaben überein [1, 2, 3, 4].

Der Stoffübergangsparameter k ändert sich erwartungsgemäß in Abhängigkeit von der Säulehöhe (s. Bild 4).

Bei der Übertragung der in der halbkontinuierlichen Blasensäule erhaltenen Stoffübergangsparameter auf den kontinuierlichen Pro-

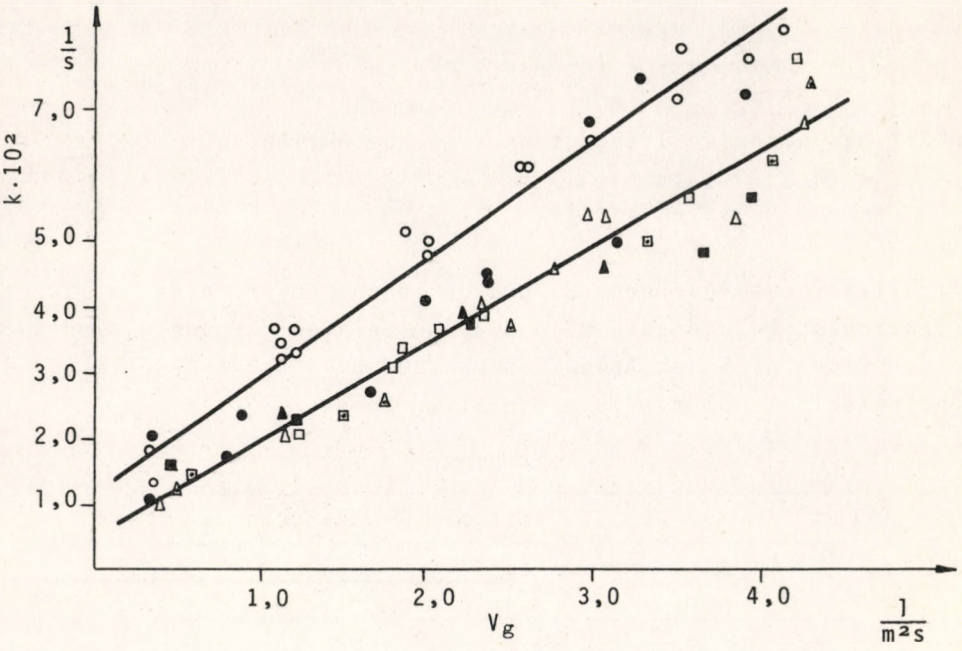

Bild 3. Stoffübergangsparameter k in Abhängigkeit vom Gasdurchsatz V_g · H = 1,5 m, D_S = 7,5 cm, T = 25 °C
● Alkohol - H_2, ○ Cyclohexan - H_2, ● Benzol - H_2
▲ Alkohol - N_2, △ Cyclohexan - N_2, ◬ Benzol - N_2
■ Alkohol-Luft, □ Cyclohexan - Luft ⊡ Benzol-Luft

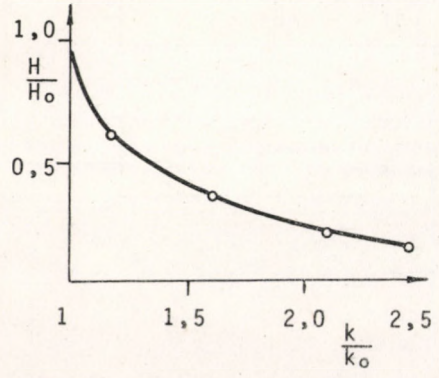

Bild 4. Stoffübergangsparameter k in Abhängigkeit von der Blasensäulenhöhe

zeß wird davon ausgegangen, daß sowohl der Stoffübergangskoeffizient als auch die Phasengrenzfläche relativ unabhängig vom Flüssigkeitsdurchsatz sind [1, 2, 3, 5, 6]. Unter dieser Voraussetzung kann man unabhängig von der Flüssigkeitsströmung jedem k-Wert eine Gaskonzentration c_j entsprechend Gleichung (3) zuordnen.

Aus der Bilanzgleichung der Gasabsorption in der Blasensäule mit strömender Flüssigphase

$$\dot{dn}_j = - k \, (c_j^* - c_j) \, dV_\ell \tag{4}$$

erhält man nach der Integration folgende Beziehung

$$c_j = c_j^* - (c_j^* - c_{jo}) \, e^{-k\bar{t}} \tag{5}$$

Mit Hilfe von Gleichung (5) und der nach Meßwerten der halbkontinuierlichen Anlage auf Bild 2 dargestellten k- und c_j-Verläufen lassen sich nach dem Ablaufschema auf Bild 5 die k-Werte für die kontinuierliche Blasensäule iterativ finden.

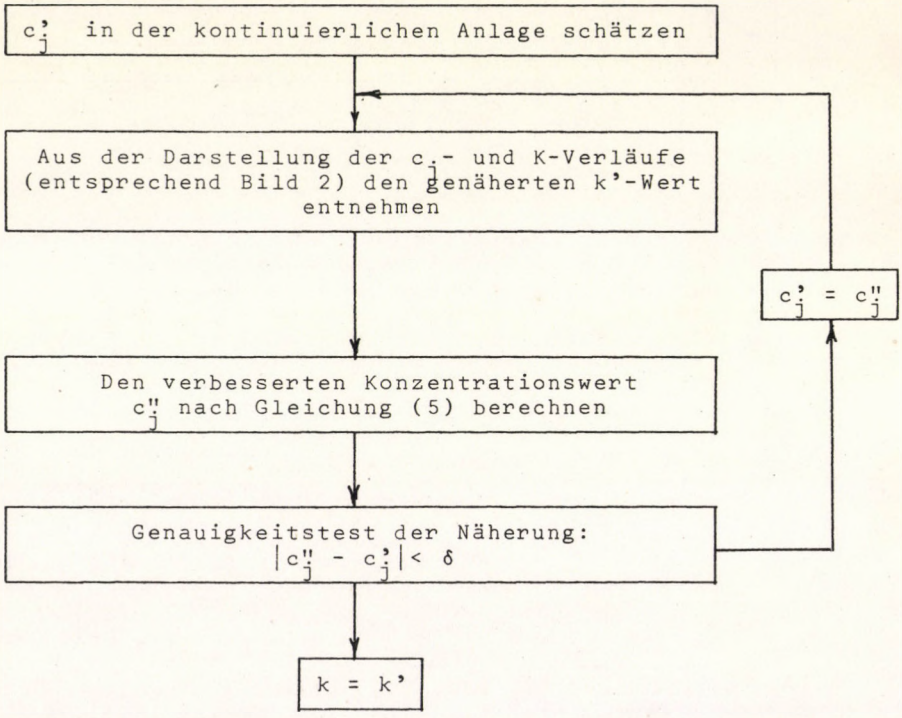

Bild 5. Ablaufschema zur Ermittlung des Stoffübergangsparameter k

Der auf diese Weise ermittelte Stoffübergangsparameter k weist wegen der gemachten einschränkenden Voraussetzungen, die im konkreten Fall nicht voll zutreffen dürften, keine sehr große Genauigkeit auf. Man kann jedoch nach der beschriebenen Methode relativ schnell und unter Berücksichtigung konkreter Bedingungen des betrachteten Prozesses und des Stoffsystems die Stoffübergangsparameter bestimmen.

Symbolverzeichnis:

c_j Konzentration der Komponente j (mol/ℓ)

c_{jo} Eintrittskonzentration (mol/ℓ)

c_j^* Gleichgewichtskonzentration (mol/ℓ)

D_S Säulendurchmesser (cm)

F Austauschfläche (ℓ/m)

H Säulenhöhe (m)

k_g Stoffübergangskoeffizient (m/s)

$k = k_g \cdot F$ (ℓ/s)

$\dot{n}_j$ absorbierte Molzahl der Komponente j (mol/s)

t Zeit (min)

$\bar{t}$ mittlere Verweilzeit (min)

$\dot{V}_g$ Gasdurchsatz (ℓ/m²·s)

V_ℓ Flüssigkeitsvolumen (ℓ)

LITERATUR

1. AKITA, K., YOSHIDA, F., Ind. Eng. Chem. Process Des. Develop. 12, 76 (1973)

2. CALDERBANK, P., MOO-JOUNG, M., Chem. Engng. Sci. 16, 39 (1961)

3. KÖLBEL, H., MATSUURA, T., HAMMER, H., Chemie-Ing. Techn. 42, 1149 (1970)

4. WÖHLER, F., STEINER, R., Chemie-Ing. Techn. 42, 481 (1970)

5. HAMMER, H., RÄHSE, W., Chemie-Ing. Techn. 45, 968 (1973)

6. NAGEL, O., KÖRTEN, H., HEGNER, B., Chemie-Ing. Techn. 45, 913 (1973)

7. CALDERBANK, P., Trans. Inst. Chem. Engr. (London) 37, 173 (1959)

РЕЗЮМЕ

Реакторы продувного типа приобретают широкое применение в химической промышленности, так как испытание условий массопередачи в этих аппаратах является очень выгодным. При широком применении этих аппаратов единицы процесса массопередачи до сих пор изучены только частично. В данной работе авторами описывается быстрый экспериментальный метод, отвечающий техническим требованиям. Применением этого метода можно легко определить параметры массопередачи в случае полунепрерывных и непрерывных реакторов.

Hungarian Journal
of Industrial Chemistry
Veszprém
Vol.3. pp. 565-576 (1975)

BESTIMMUNG DER VERFÜGBARKEIT EINER KAPAZITÄTSGETEILTEN PARALLELSCHALTUNG MIT INTERNER KAPAZITÄTSRESERVE

J. VONDRAN und J. KARDOS

(Ingenieurhochschule Köthen, Abteilung Mathematik und Sektion Verfahrenstechnik, Wissenschaftsbereich Systemverfahrenstechnik)

Eingegangen am 14. September 1975

Die bei der Berechnung der Zuverlässigkeit und Verfügbarkeit von Systemen bisher verwendete Duallogik - es funktioniert oder es funktioniert nicht - konnte für Systeme mit kapazitätsgeteilter Parallelschaltung und interner Kapazitätsreserve keine befriedigenden Ergebnisse liefern. Durch Einbeziehung des Teillastverhaltens derartiger ausfallgestörter Systeme wurde eine Möglichkeit zur Erfassung objektiverer Verfügbarkeitsverhältnisse geschaffen. In diesem Beitrag wird eine Gleichung zur Berechnung der Durchsatzverfügbarkeit für eine kapazitätsgeteilte Parallelschaltung mit interner Kapazitätsreserve und statistischer Unabhängigkeit entwickelt.

Die ökonomische Bewertung des Langzeitverhaltens von Chemieanlagen besitzt besondere Bedeutung in den einzelnen Etappen der Verfahrens- und Anlagenentwicklung, insbesondere bei der Auswahl technologischer Schaltungen in der Projektierungs- sowie in der Betriebsphase.

Während bei der Verbesserung und Sicherung der Zuverlässigkeit von Bauteilen, Baugruppen, Funktionsgruppen und Grundausrüstungen qualitative Zuverlässigkeitsverfahren dominieren, erfordert die Gestaltung und Bewertung zuverlässiger Anlagenkomplexe einen zunehmenden Anteil an quantitativen Verfahren. In diesem Beitrag

wird eine Berechnungsgrundlage zur analytischen Bestimmung der Verfügbarkeit von kapazitätsgeteilten Parallelschaltungen mit interner Kapazitätsreserve mitgeteilt.

Charakteristik der kapazitätsgeteilten Parallelschaltung mit interner Kapazitätsreserve

Die Anwendung von redundanten Schaltungen stellt eine von vielen Möglichkeiten dar, die Zuverlässigkeit und Verfügbarkeit von Chemieanlagen unter bestimmten Voraussetzungen zu erhöhen und damit Produktionsausfällen entgegen zu wirken.

Bisher ist die Zuverlässigkeit und Verfügbarkeit von Parallelschaltungen nur für die "heiße" (parallel) und "kalte" (standby) Redundanz nach den BOLLE-schen und MARKOW-schen Modellen untersucht worden [1-3].

Es sind in der chemischen Technologie jedoch häufig solche Parallelschaltungen anzutreffen, bei denen keine Reserveelemente im klassischen Sinne vorhanden sind. In solchen Fällen werden die einzelnen Elemente nicht selten überdimensioniert, damit sie nach Bedarf größerer Durchsätze mächtig sind. Eine derartige Überdimensionierung entspricht einer internen Kapazitätsreserve und stellt gleichfalls eine "heiße" Redundanz dar.

Für den Fall, daß ein oder mehrere Elemente zur gleichen Zeit ausfallen (nicht intakt sind) oder planmäßig wegen Instandhaltungsmaßnahmen stillgelegt werden, sollen die übrigen intakten Elemente durch Erhöhung ihrer Kapazität bzw. ihres Durchsatzes die Funktion der ausgefallenen Elemente übernehmen.

Dieser Sachverhalt wird nach Bild 1 näher beschrieben.

Diese Parallelschaltung ist durch folgende Merkmale und Voraussetzungen gekennzeichnet:

- Es sind insgesamt n Elemente parallelgeschaltet $n \geq 2$
- Die Gesamtkapazität darf in einem vorgegebenen Intervall schwanken

$$\dot{C}_{min} \leq \dot{C} \leq \dot{C}_{max} \qquad (1)$$

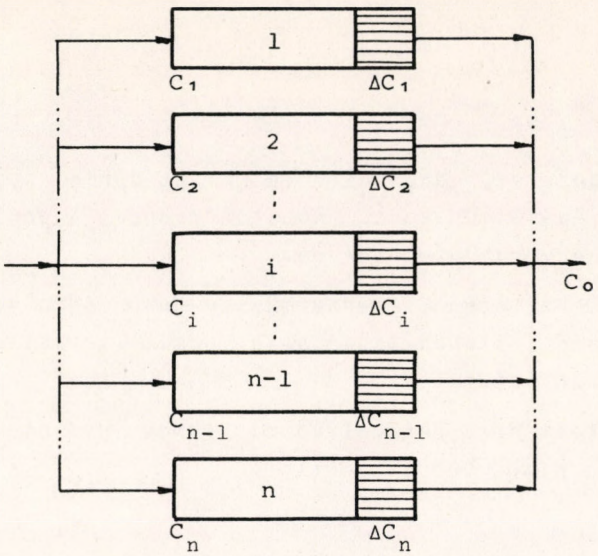

Bild 1. Schematische Darstellung einer kapazitätsgeteilten Parallelschaltung mit zusätzlicher interner Kapazitätsreserve

- Jedes einzelne Element i = 1,2,3,...,n besitzt die gleiche Nennkapazität (Sollwert $\dot{C}_o$) von

$$\dot{C}_{o_i} = \frac{\dot{C}_o}{n} \tag{2}$$

- Alle Elemente besitzen die gleiche interne Kapazitätsreserve (Überdimensionierung)

$$\Delta\dot{C}_{o_i} = \varphi_i \cdot \dot{C}_{o_i} = n \cdot \varphi \cdot \dot{C}_{o_i} = \varphi \cdot \dot{C}_o \tag{3}$$

- Bei gleichzeitigem Ausfall von k Elementen ist folgende Teillast zu erwarten

$$\dot{C}_k = (n-k)\,\frac{\dot{C}_o}{n}\,(1 + \varphi_i) = (n-k)\,\dot{C}_o\,(\frac{1}{n} + \varphi) \tag{4}$$

- Jedes Element ist durch die gleiche Intaktwahrscheinlichkeit bzw. Zeitverfügbarkeit gekennzeichnet

$$p_{O_1} = p_{O_2} = p_{O_3} = \ldots = p_O$$
$$V_{O_1} = V_{O_2} = V_{O_3} = \ldots = V_O \qquad (6)$$

- Es wird vorausgesetzt, daß Ausfälle nicht durch systemfremde bzw. gemeinsame Ausfallursachen (Rohstoffmangel, Energieausfall, Unwetter usw.) hervorgerufen werden.
- Alle parallelgeschalteten Elemente müssen unabhängig voneinander funktionieren und instandsetzbar sein, damit statistische Unabhängigkeit gegeben ist.
- Die Zuverlässigkeit der Umschaltvorrichtungen und die Umschaltzeitdauer werden nicht berücksichtigt.

Wechselbeziehungen zwischen Zeit- und Durchsatzverfügbarkeit

Die stationäre Zeitverfügbarkeit eines Systems/Elementes ist wie folgt definiert:

$$V(T) = \frac{T_O}{T_O + T_S + T_{PVI}} = \frac{T_O}{T_A} \leq 1 \qquad (7)$$

Darin sind:

T kumulative Erwartungswerte der Zeit;

T_S bezogen auf die Stillstandszeit wegen unplanmäßiger bzw. Störreparatur (eingeschlossen sind Abfahr- bzw. Anfahrzeiten, Wartezeiten sowie Reparaturzeiten)

T_{PVI} bezogen auf die Stillstandszeit wegen planmäßig vorbeugender Instandhaltung

T_O bezogen auf die Gesamtsumme der störungsfreien Betriebszeiten (alle Elemente intakt)

T_A bezogen auf die gesamte Kalenderzeit (Betrachtungszeitraum)

Durch die Erweiterung der Gleichung (7) unter Berücksichtigung der Nennkapazität $\dot{C}_o$ und der Einbeziehung der Teilkapazitäten $\dot{C}_k$ beim gleichzeitigen Ausfall von $k = 1,2,3,\ldots,n$ Elementen läßt sich die Durchsatzverfügbarkeit V(D) wie folgt formulieren

$$V(D) = \frac{T_o \cdot \dot{C}_o + (T_1 \cdot \dot{C}_1 + \ldots + T_k \cdot \dot{C}_k + \ldots T_n \dot{C}_n)}{T_A \cdot \dot{C}_o} \qquad (8)$$

Daraus wird deutlich, daß der in Klammern gesetzte Ausdruck die durch die Struktur der Schaltung hervorgerufene Verfügbarkeitserhöhung quantitativ erfaßt und damit den realen Sachverhalt gegenüber der Zeitverfügbarkeit objektiver wiedergibt. Die bei der Berechnung der Zuverlässigkeit und Verfügbarkeit von Systemen bisher verwendete Duallogik - es funktioniert oder es funktioniert nicht - konnte für Systeme mit kapazitätsgeteilter Parallelschaltung und interner Kapazitätsreserve keine befriedigenden Ergebnisse liefern.

Zur Veranschaulichung des Teillastzeitverhaltens einer kapazitätsgeteilten Parallelschaltung mit interner Kapazitätsreserve soll noch Bild 2 dienen.

In diesem Bild sind die Laufzeiten (dick ausgezogene Linien) entsprechend dem Ausfall- und Instandsetzungsverhalten der Elemente dargestellt.

Darin haben die Indices folgende Bedeutung:

erster Index = Anzahl der zur gleichen Zeit ausgefallenen Elemente,

zweiter Index = Kennzeichnung der Wiederholung der zur gleichen Zeit ausgefallenen Anzahl von Elementen,

so bedeuten z.B.:

T_{13} = Laufzeitperiode, in der zum dritten Mal ein Element ausgefallen ist,

T_{04} = Laufzeitperiode, in der zum vierten Mal kein Element ausgefallen ist. usw..

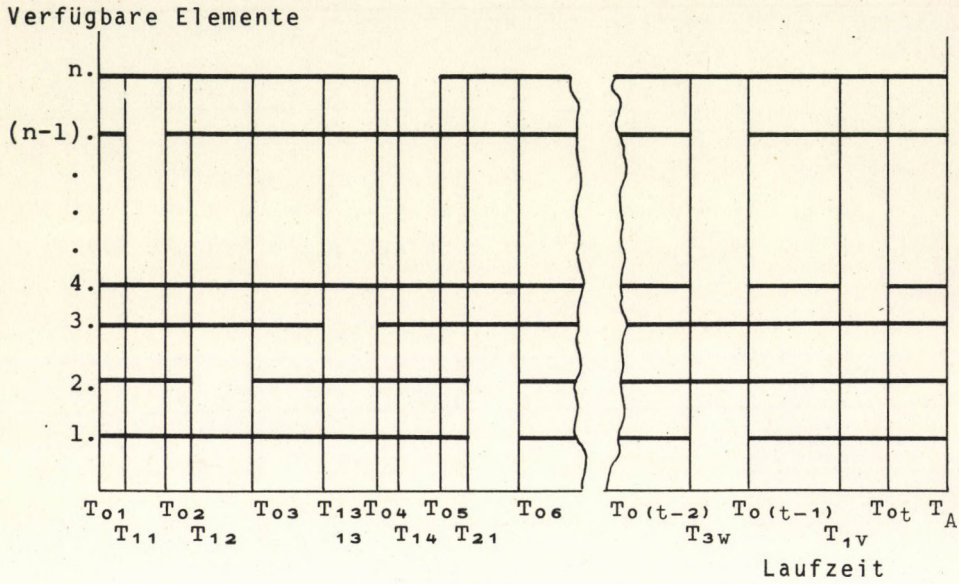

Bild 2 Symbolische Darstellung der Laufzeiten und Stillstandszeiten von n parallelgeschalteten Elementen

Eine qualitäts- und quantitätsgerechte Produktion ist nur möglich in der Zeit

$$T_o = \sum_{s=1}^{t} T_{os} \tag{9a}$$

In den Zeitintervallen, in denen ein oder mehrere Elemente der Parallelschaltung gleichzeitig ausfallen, ist nur eine Teilproduktion nach Gleichung (4) möglich. Die dazugehörigen Zeiten ergeben sich ebenfalls durch Summation analog zur Gleichung (9a).

$$T_1 = \sum_{u=1}^{v} T_{1u} \tag{9b}$$

Für die Durchsatzverfügbarkeit ergibt sich unter Einbeziehung

$$V(D) = \sum_{k=o}^{n} \frac{n-k}{n} (1 + \varphi_k) \frac{T_k}{T_A} \qquad (10)$$

Zum Erreichen der geplanten Durchsatzmenge C_o besteht die Möglichkeit in den Zeitabschnitten, in denen Ausfälle - eines oder mehrerer Elemente gleichzeitig - auftreten, durch Nutzung der vorgesehenen internen Kapazitätsreserve die eintretenden Verluste einzuschränken bzw. auszugleichen.

Setzt man Gleichung (3) voraus, dann muß folgende Beziehung gelten [4]

$$0 \leq \varphi_k \leq \frac{k}{n - k} \qquad (11)$$

Hierbei stellt k die Anzahl der gleichzeitig ausgefallenen Elemente dar, deren Kapazität von der Überdimensionierung der übrigen Elemente "mit übernommen" werden muß.

Das in Gleichung (10) vertretene Verhältnis T_k/T_A kann nach Wahrscheinlichkeitsgesichtspunkten bestimmt werden.

Wahrscheinlichkeitstheoretische Aufteilung der Gesamtzeit T_A in Teilausfallzeiten

Das gleichzeitige Versagen eines oder mehrerer Elemente ist ein zufälliges Ereignis.

Unter Voraussetzung der Unabhängigkeit der Einzelelemente hinsichtlich ihres Ausfall- und Instandhaltungsverhaltens kann der Multiplikationssatz für Wahrscheinlichkeiten angewendet werden.

Für die Wahrscheinlichkeit des g l e i c h z e i t i g e n A u s f a l l s von n Elementen, d.h. sowohl das Ereignis E_1 (Ausfall eines zweiten Elementes) tritt ein usw., gilt somit

$$P(E_1 \cap E_2 \quad \ldots \quad E_n) = (1 - V_n)^n = P(n) \qquad (12)$$

bzw. für das komplementäre Ereignis, daß n i c h t g l e i c h z e i t i g n Elemente ausfallen

$$P(\overline{E_1 \quad E_2 \quad \ldots \quad E_n}) = 1 - (1 - V_o)^n = P(\bar{n}) \qquad (13)$$

Entsprechend dieser Ausfallwahrscheinlichkeiten nach Gleichung (12) und (13) erfolgt die Aufteilung der Gesamtzeit T_A rekursiv:

$$
\begin{aligned}
T_n &= T_A (1 - V_o)^n \\
T_{n-1} &= T_A (1 - V_o)^{n-1} \quad [1 - (1 - V_o)^n] \\
&\vdots \\
T_k &= T_A (1 - V_o)^k \ldots [1 - (1 - V_o)^{n-1}][1 - (1 - V_o)^n] \\
&\vdots \\
T_2 &= T_A (1 - V_o)^2 \ldots [1 - (1 - V_o)^{n-1}][1 - (1 - V_o)^n] \\
T_1 &= T_A (1 - V_o)^1 \ldots [1 - (1 - V_o)^{n-1}][1 - (1 - V_o)^n] \\
T_o &= T_A (1 - V_o)^o \ldots [1 - (1 - V_o)^{n-1}][1 - (1 - V_o)^n]
\end{aligned}
\tag{14}
$$

Hieraus folgt das gesuchte Verhältnis

$$\frac{T_k}{T_A} = (1 - V_o)^k \prod_{j=k+1}^{n} [1 - (1 - V_o)^j] \tag{15}$$

An Hand einer tabellarischen Übersicht kann der Einfluß der diskreten Zufallsvariablen k aufgezeigt werden. In Tabelle 1 ist die Wahrscheinlichkeitsverteilung der diskreten Zufallsgröße k (gleichzeitige Ausfälle) dargestellt.

Tabelle 1 Wahrscheinlichkeitsverteilung der Zufallsgröße k bei n = 4 und V_o = 0,9

k	P(k)
0	0,8900199
1	0,0988911
2	0,0099891
3	0,0009999
4	0,0001000
	1,0000000

Wie diese Verteilung zeigt, ist die Wahrscheinlichkeit des gleichzeitigen Auftretens von zwei oder mehreren Ausfällen sehr gering, so daß bei überschlägigen Berechnungen dieser Anteil durchaus vernachlässigbar ist. Unter dieser Voraussetzung kann für die Überdimensionierung nach Gleichung (10) näherungsweise folgender Zusammenhang gelten

$$0 \leq \varphi_k \leqq \frac{1}{n - 1} \tag{16}$$

Schließlich soll noch eine Kontrolle des Gleichungssystems (14) mit $T_A = \sum_{k=o}^{n} T_k$ durchgeführt werden.

Die Summation der Teillastzeiten nach Gleichung (14) liefert

$$\sum_{k=o}^{n} T_k = T_A \left\{ (1 - V_o)^n + \sum_{k=o}^{n-1} \left[(1 - V_o)^k \prod_{j=k+1}^{n} [1 - (1 - V_o)^j] \right] \right\} \tag{17}$$

Demnach muß der gesamte Klammerausdruck "eins" ergeben:

$$(1 - V_o)^n + \sum_{k=o}^{n-1} \{ (1 - V_o)^k \sum_{j=k+1}^{n} [1 - (1 - V_o)^j] \} = 1 \tag{18}$$

Der Beweis kann wie folgt geführt werden:

Mit $x = (1 - V_o)$ wird die Induktionsvoraussetzung formuliert

$$x^n + \sum_{k=o}^{n-1} x^k \prod_{j=k+1}^{n} (1 - x^j) = 1 \tag{19}$$

Der Schluß von n auf n+1 liefert die Induktionsbehauptung

$$x^{n+1} + \sum_{k=o}^{n} x^k \prod_{j=k+1}^{n+1} (1 - x^j) = 1 \tag{20}$$

Durch Multiplikation mit $1 - x^{n+1}$ wird Gleichung (19) in

$$x^n (1 - x^{n+1}) + \sum_{k=o}^{n+1} x^k \prod_{j=k+1}^{n+1} (1 - x^j) = 1 - x^{n+1} \tag{21}$$

überführt und durch Zusammenfassung ergibt sich

$$\sum_{k=o}^{n} x^k \prod_{j=k+1}^{n+1} (1 - x^j) = 1 - x^{n+1} \tag{22}$$

woraus nach Umstellung Gleichung (20) entsteht.

Analytische Beziehung der Durchsatzverfügbarkeit von kapazitätsgeteilten Parallelschaltungen mit interner Kapazitätsreserve

Mit der Einführung der Gleichung (15) folgt schließlich für die Durchsatzverfügbarkeit nach Gleichung (10)

$$V(D) = \sum_{k=0}^{n-1} \left\{ \frac{n-k}{n} (1 + \varphi_k)(1 - V_o)^k \prod_{j=k+1}^{n} [1 - (1 - V_o)^j] \right\} \quad (23)$$

Mit dem in Gleichung (23) entwickelten Modell ist eine Möglichkeit zur Berechnung der Durchsatzverfügbarkeit für solche Fälle dargestellt, in denen die Verbesserung der Verfügbarkeit durch Teilung der Kapazität und Einführung einer technisch realisierbaren Überdimensionierung (Flexibilität) erreicht werden kann.

Setzt man voraus, daß die Überdimensionierung nur im Falle des Versagens eines oder mehrerer Elemente genutzt wird, dann läßt sich Gleichung (23) wie folgt spezifizieren:

$$V(D) = \prod_{i=1}^{n} [1 - (1 - V_o)^i] + \sum_{k=1}^{n-1} \left\{ \frac{n-k}{n} (1 + \varphi_k) \times \right.$$

$$\left. \times (1 - V_o)^k \prod_{j=k+1}^{n} [1 - (1 - V_o)^j] \right\} \quad (24)$$

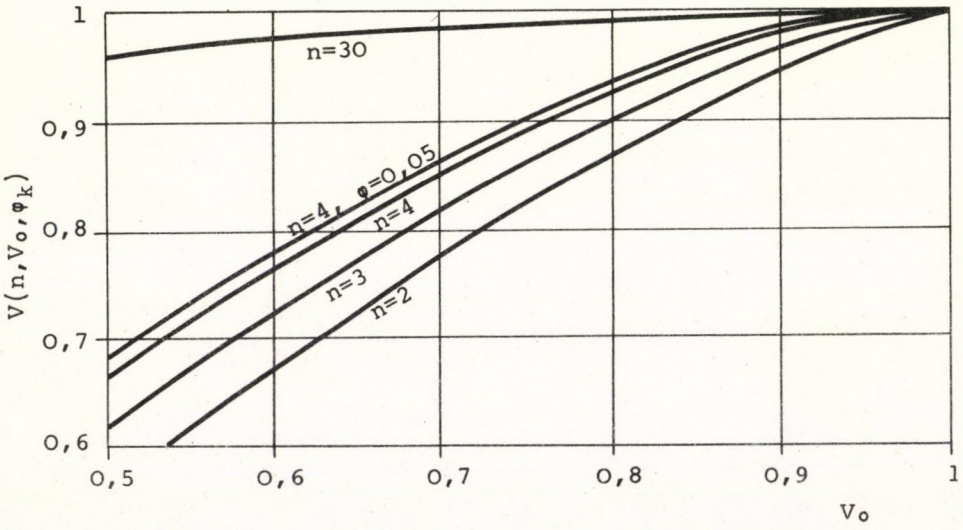

Bild 3 Einfluß der Parameter (n, φ_k) auf die Durchsatz- bzw. Kapazitätsverfügbarkeit

Im Bild 3 ist die numerische Auswertung der Gleichung (24) für einige spezielle Fälle grafisch dargestellt.

Die Anwendung der Gleichung (24) erfolgt im Rahmen einer kalkulativen zuverlässigkeitsökonomischen Bewertung und Optimierung von chemisch-technologischen Schaltungen [5, 6].

SYMBOLE

C Kapazität, zeitbezogen

C_0 Nennkapazität

E Ereignis (Ausfall eines Elements)

k Anzahl der gleichzeitig ausgefallenen Elemente

n Anzahl der Elemente der kapazitätsgeteilten Parallelschaltung

P Wahrscheinlichkeit

p_0 Intaktwahrscheinlichkeit des Einzelelements

T kumulativer Erwartungswert der Zeit

V_0 Zeitverfügbarkeit des Einzelelements

$V(D)$ Durchsatzverfügbarkeit

φ interne Kapazitätsreserve (Überdimensionierung)

LITERATURANGABE

1. GNEDENKO, B.W., BELJAJEW, J.K. und SOLOWJEW, A.P., Mathematische Methoden der Zuverlässigkeitstheorie I/II Akademie Verlag, Berlin 1968

2. STRÖMER, H., Mathematische Theorie der Zuverlässigkeit. R. Oldenburg-Verlag München/Wien 1970.

3. REINSCHKE, K., Zuverlässigkeitstheorie von Systemen. VEB Verlag Technik, Berlin 1973.

4. KARDOS, J. und VONDRAN, J., "Ausgewählte Probleme der Verfügbarkeits-, Flexibilitäts- und Kostenbewertung von parallelgeschalteten Betrachtungseinheiten mit Kapazitätsteilung und interen Störreserven bei kontinuierlicher Betriebsweise", veröffentlicht in: Zuverlässigkeit von Chemieanlagen, Sammlung der Vorträge der 2. Fachtagung "Zuverlässigkeit von Chemieanlagen" am 10.10.74, herausgegeben vom Ministerrat der DDR, ASMW, Berlin 1975.

5. KARDOS, J. und VONDRAN, J., Chem. Technik 25, 268 (1973)

6. KARDOS, J. und VONDRAN, J., CHISA-Vortrag 1975 L 2.4

РЕЗЮМЕ

Дуальная логика, применяемая до сих пор при расчете надежности и применяемости системы, - действует или не действует, - в случае параллельного соединения с деленной емкостью и внутренним запасом емкости не дает удовлетворительных результатов. С учетом доли нагрузки системы с выходным воздействием, возникали более объективные методы для определения условий применяемости. В данной статье составили уравнение для вычисления пропускной способности параллельного соединения с деленной емкостью, внутренним запасом емкости и статистической независимостью.

Hungarian Journal
of Industrial Chemistry
Veszprém
Vol.3. pp. 577-588 (1975)

INVESTIGATIONS ON THE DECARBONYLATION OF FURFURAL OVER METAL-OXIDE CATALYSTS IN THE PRESENCE OF STEAM

Gy. GÁRDOS, L. PÉCHY, Á. RÉDEY, and Mrs. E. CSÁSZÁR*

(Department of Hydrocarbon and Coal Processing,
Veszprém University of Chemical Engineering and
*Pétfürdő, Nitrogen Works)

Received: September 28, 1975

Investigations were carried out in the production of furan from furfural over chromite catalysts. The temperature, furfural/water molar ratio, and space velocity were the experimental parameters. From the investigated catalysts, the promoted version of the zinc-iron-chromite catalyst appeared to be the most advantageous and a furan yield of more than 90 % was obtained with it. However, an endurance test showed that the metal oxide catalysts lose their activities and hence they are unsuitable for industrial use.

In recent, years the importance of furan and its derivatives have considerably increased. They play an important role in the manufacture of many intermediates (polyamides, synthetic rubbers, drugs and many other organic compounds).

Reactions take place either in the side chains or in the heterocyclic ring, and many heterocyclic compounds can be produced: furan, tetrahydrofuran, methylfuran, furfural alcohol, thiophene, and pyrrol, etc.

The production of furan from furfural could be of growing importance, since large quantities of the raw material are available.

In this paper, decarbonylation over metal-oxide catalysts in the presence of steam is discussed. The results of experiments on the reductive decarbonylation in the presence of hydrogen over noble metal catalysts will be dealt with in following papers.

Furan Production Methods

In former papers [1, 2] processes - carried out under laboratory circumstances that resulted in small amounts of furan - were discussed. The decarbonylation of pyromucic acid [3], the reaction of acetylene with steam [4] and the production of furan from furfural over a nickel catalyst can be mentioned. WILSON [5] succeeded in converting the furfural to furan in vapour phase over a nickel catalyst in the presence of hydrogen (the conversion was about 50-60 %), in addition to the formation of carbon monoxide.

A number of patents and papers [5, 6, 7, 8, 9, 10, 11] have appeared since 1940 that give accounts of the decarbonylation of furfural in the presence of steam over the oxides of iron, zinc, manganese, chrome and their mixtures. The reaction was considered to be an oxidative decarbonylation:

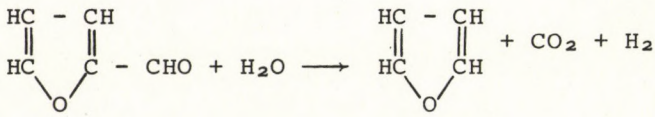

The optimum temperature of the reaction is between 300 and 500 °C depending upon the composition of the catalyst, while the yields are considerably affected - in addition to the temperature - by the furfural/water molar ratio.

Among the works on the mechanism of the oxidative decarbonylation that of VÁNDOR is of importance [12]. According to it the reaction is a second-order one and the reaction takes place in the following three steps, like a Canizarro reaction:

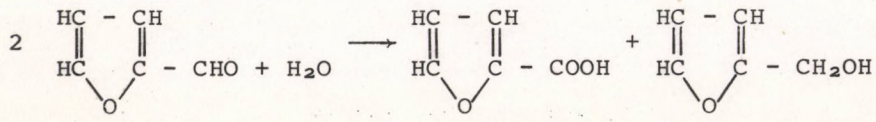

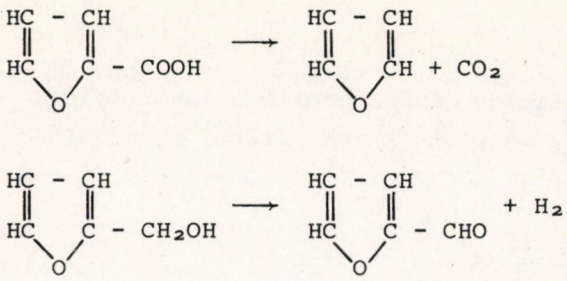

Soviet researchers dealt with the efficiency of chromite type catalysts pelletized without any supporter [13, 14, 15]. They studied the influence of the reactive agent (steam, hydrogen,and nitrogen), the temperature, the furfural/water molar ratio, and the efficacy of the promotion of metal oxide catalysts. The effects of chrome - manganese - zinc on alumina were studied by KARMILCHIK [16, 17]. At 450°C he observed a furan yield of more than 90 %. The furfural formed a complex with the catalyst, which yielded a metal-carbonyl-complex and furan. The metal-carbonyl-complex results in formic acid, which decomposes to carbon dioxide and hydrogen.

Hungarian researchers have also dealt with the vapour phase decarbonylation of furfural [18, 19]. Tungsten pentoxide on alumina, lead oxide, lead melt and mercuric oxide were used as catalysts.

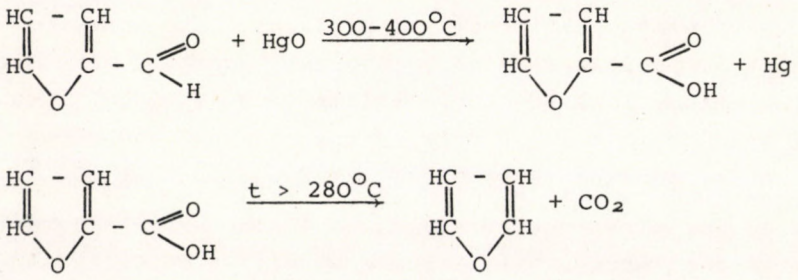

From the reported processes, only the oxidative decarbonylation has so far gained industrial application.

Experimental

The decarbonylation of furfural was investigated to find a metal oxide catalyst that satisfies all the demands of industrial utilization.

The Experimental Apparatus

The decarbonylation experiments were carried out in a small (20 cc) tubular "integral" reactor. It had a cylindric form, on its external brim there were two borings for the preheating of the furfural and water. These were connected by a horizontal boring to the reactor tube made of stainless steel, placed in the axis of the cylinder, that had an internal diameter of 10 mm. The reactor was electrically heated, and the temperature was controlled by a Pt-PtRh thermocouple. Furfural and water were fed into the reactor by a micropump. The product was led to a water-cooled condenser, where the excess of water and the unconverted furfural were condensed. The condensed products were separated in an funnel and the phases were analyzed by a chromatograph. The uncondensed product (furan) was absorbed in toluene.

A tube packed with active carbon was used to seize the furan traces.

Samples taken from both the condensed and the gaseous products were analyzed. The condensed products were analyzed with a Becker-Delft (Type 2040 C-2) chromatograph, equipped with a flame-ionization detector using a 4 m column (I.D. 4 mm) of 10 % Apieson L on Chromosorb W. The rate of the carrier gas stream was 3 litres an hour, and the temperature was maintained at 100 ^{o}C.

Several chromite type catalysts were made and evaluated: zinc-chromite without promotion and promoted with K_2CO_3, zinc-manganese-chromite and zinc-iron-chromite, where the zinc/manganese and zinc/iron molar ratios were varied.

These metal oxides are difficult to granulate, therefore magnesium stearate binder was applied for the granulation. Its effects were also examined.

The catalysts were made as follows: the measured substances ($ZnCl_2$, $FeSO_4 \cdot 7\ H_2O$, $(NH_4)_2Cr_2O_7$; $ZnSO_4 \cdot 7\ H_2O$, $MnSO_4 \cdot 4\ H_2O$, $(NH_4)_2Cr_2O_7$) were dissolved in water. From the aqueous solution a precipitate was formed by reacting with ammonium hydroxide. It was washed and dried at 110 °C. The dried precipitate was soaked in a 1 w.% potassium carbonate solution for the sake of promotion. After that the suspension was dried and incandesced at 400 °C for 4 hours. The powder like product obtained was pressed into tablets of 3 mm.

With X-ray diffraction it was found that there was only a small amount of crystalline substance in the catalysts, the bulk of the catalysts was amorphous. In the case of the two catalyst types spinel structure was observed. In the spinel structure the iron was in magnetite Fe_3O_4 form, while the manganese was in Mn_3O_4.

DISCUSSION

For the first experiments, catalysts were produced free of iron and manganese respectively, both without promotion and promoted with K_2CO_3. In the following tables the average values of the results of parallel experiments are given. The temperature was varied between 330 and 400 °C, the furfural/water molar ratio was 1:10, while the space velocity was maintained at the same value (1500 h^{-1}). The furfural conversion and the furan yield are shown in Table 1. Better results were obtained with the promoted catalyst, although the furan yields did not attain 30 %. On the basis of the results, it can be concluded that none of the different catalysts is suitable for the oxidative decarbonylation of the furfural.

Further experiments were carried out with zinc-chromite type catalysts, where manganese oxide and iron oxide were incorporated in the structure of the catalysts.

The zinc/iron and manganese/iron molar ratios were 90:10. It was studied whether the addition of manganese oxide and iron oxide

improves the efficiency of the zinc-chromite catalyst and the furan yield.

Table 1. Decarbonylation of furfural over zinc-chromite catalysts

Type of the catalyst	Temperature [°C]	Furfural water molar ratio	Space velocity [h^{-1}]	Conversion [%]	Furan yield [%]
Zinc-chromite without promotion	330	1:10	1580	23.0	1.8
	350	1:10	1600	23.9	2.8
	375	1:10	1500	51.7	12.6
	400	1:10	1510	60.0	17.1
Promoted zinc-chromite	330	1:10	1540	43.6	8.9
	350	1:10	1500	49.8	17.2
	375	1:10	1480	53.9	24.9
	400	1:10	1600	63.0	25.3

Table 2 shows the results of the experiments carried out over zinc-manganese-chromite and zinc-iron-chromite in the temperature range of 300-400°C at three different (1:6, 1:10, 1:15) furfural/ /water molar ratios.

Further conclusions can also be drawn from the results:

- the temperature has the bigger role in the furfural conversion to furan;
- 350°C, 1:10 furfural:water molar ratio and 1000-1200 h^{-1} space velocity were considered to be the optimum parameters.

The favourable effect of the promotion on the conversion and yield data is verified unambiguosly.

The incorporation of manganese oxide and iron oxide in the structure of the catalyst considerably improved the decarbonylating property of the catalyst.

Table 2. Decarbonylation of furfural over zinc-manganese-chromite and zinc-iron chromite catalysts respectively

			Type of the catalyst					
			zinc-manganese-chromite zinc/manganese molar ratio = 1:10			zinc-iron-chromite zinc/iron molar ratio = 1:10		
	Temperature [°C]	Furfural / water molar ratio	Space velocity [h^{-1}]	Conversion [%]	Furan yield [%]	Space velocity [h^{-1}]	Conversion [%]	Furan yield [%]
Promoted	330	1:6	722	66.0	33.3	748	79.9	51.9
	330	1:10	1240	70.1	48.6	1240	88.8	62.4
	330	1:15	1480	68.7	44.8	1500	70.0	44.1
	350	1:6	748	80.4	43.5	725	86.5	67.9
	350	1:10	1193	84.6	64.3	1180	73.0	67.2
	350	1:15	1476	79.7	57.4	1390	77.6	58.8
	375	1:6	747	71.2	50.3	790	84.9	50.9
	375	1:10	1100	77.8	63.6	1260	71.0	55.5
	375	1:15	1490	70.0	52.7	1480	73.0	52.0
	400	1:6	810	73.8	51.3	698	86.8	48.6
	400	1:10	1180	74.0	52.6	1230	84.0	52.9
	400	1:15	1420	76.0	51.1	1510	80.1	52.1
Without promotion	330	1:10	1260	62.0	40.5	1210	64.0	44.2
	350	1:10	1200	71.7	50.5	1130	61.3	48.5
	375	1:10	1250	71.1	51.2	1200	77.1	49.3
	400	1:10	1180	79.9	59.2	1150	77.6	46.6

The effect of manganese oxide and iron oxide was also investigated. The results obtained with different manganese oxide and iron oxide contents (90:10, 80:20, 70:30) at constant furfural/water molar ratio (1:10) in the 300-400 °C temperature range and the 1200-1500 h^{-1} space velocity range are given in Table 3.

Table 3. Decarbonylation of Furfural in the function of the manganese oxide and iron oxide content respectively

Type of the catalyst			Temperature [°C]	Furfural water molar ratio	Space velocity [h^{-1}]	Conversion [%]	Furan yield [%]
Promoted zinc-manganese-chromite catalyst	zinc/manganese molar ratio 90:10	without magnesium stearate	300	1:10	1190	28.5	13.8
			350	1:10	1535	57.2	30.2
			375	1:10	1396	84.0	61.7
			400	1:10	1442	97.0	75.4
		with magnesium stearate	300	1:10	1400	8.4	5.0
			350	1:10	1545	53.2	22.4
			375	1:10	1515	78.6	48.5
			400	1:10	1480	97.0	65.0
	80:20	without magnesium stearate	300	1:10	1460	52.8	31.6
			350	1:10	1420	81.3	44.0
			375	1:10	1580	82.4	57.5
			400	1:10	1386	100.0	64.0
	70:30	with magnesium stearate	300	1:10	1390	85.0	60.6
			350	1:10	1415	73.5	40.4
			375	1:10	1490	65.2	40.4
			400	1:10	1345	87.0	50.3
Promoted zinc-iron-chromite catalyst	zinc/iron molar ratio 90:10	without magnesium stearate	300	1:10	1195	52.0	27.0
			350	1:10	1465	84.0	62.5
			375	1:10	1460	99.0	74.5
			400	1:10	1480	100.0	81.0
	80:20	without magnesium stearate	300	1:10	1480	38.0	11.0
			350	1:10	1400	75.4	55.5
			375	1:10	1400	93.5	75.6
			400	1:10	1438	100.0	91.0

The effect of catalysts granulated with magnesium stearate was also examined. From the data shown in Table 3 it is clear that although the magnesium stearate makes the granulation of the catalyst easier, its effect is disadvantageous on the conversion and yield data.The incorporation of the manganese oxide and iron oxide in the structure of the catalyst helps to decrease the temperature of the decarbonylation. By increasing the manganese content 2 or 3 times, the same conversion and yield data can be reached at lower temperatures. In addition, it is the temperature that is the worst point in the oxidative decarbonylation of furfural over chromite type catalysts.

While in the case of manganese oxide the optimum temperature is 300-350°C, in the case of iron oxide it is 375-400°C. In a comparison of manganese and iron oxides, the latter is more efficient, although the required temperature is higher, it gives a furan yield of 80-90 %.

An additional aim was to establish the activity and active period of the zinc-iron-chromite catalyst, and its effeciency after regeneration. A catalyst with a 90:10=zinc:iron molar ratio was used for the endurance test. A solution of furfural and water, with a molar ratio of 1:10 was fed in the reactor packed with the catalyst. The space velocity was about 1500 h^{-1}, the temperature of the reactor was 375°C.

The quantity of the formed furan was continually measured. The obtained data are shown in Figure 1. The activity of the catalyst decreased after a few hours, thus after 4 hours the furan yield was about 50 %; after 10 hours it was about 10 %.

The deposit on the catalyst was blazed off in an air stream. The catalyst was activated in hydrogen stream, and the furfural and water feed was started again. The catalyst almost entirely recovered its original activity, but after repeated regenerations it was lost.

On the basis of the result of the endurance test it can be concluded that the metal oxide catalysts that were investigated are unsuitable for the industrial application of oxidative decar-

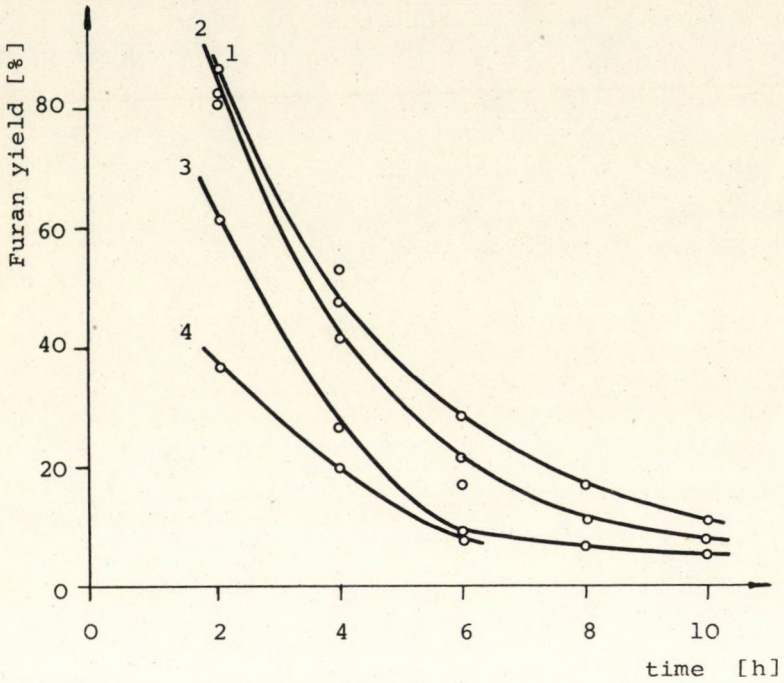

Fig. 1. The change of the activity of the zinc-iron-chromite catalyst in the function of the time. 1 - the original promoted catalyst; 2 - after the first regeneration; 3 - after the second regeneration; 4 - after the third regeneration

bonylation, because of their short active period and the need for frequent regenerations.

REFERENCES

1. BOURGIGNON, C., Bull. Soc. Chem. Belg. 22, 89 (1908)

2. PRINGSHEIM, H., NOTH, H., Berichte der Deutschen Chem. Gesell. 53, 114 (1920)

3. GILMAN-JOUSTIAN, Rec. Trav. Chim. 52, 152 (1933)
4. CSICSIBABIN, A.E., Zs.R.F.H.O. 47, 710 (1915)
5. WILSON, L., J. Am. Chem. Soc. 67, 61 (1945)
6. U.K. Patent 553.175 (1943)
7. U.K. Patent 575.362 (1944)
8. U.S. Patent 2 374 149 (1945)
9. U.S. Patent 2 572 300 (1951)
10. U.S. Patent 2 634 276 (1953)
11. U.S. Patent 2 776 981 (1954)
12. VÁNDOR, I., Acta Chim. Acad. Sci. Hung. 3, 169 (1953)
13. KARMIL'CHIK, A.Ya., GILLER, S.A., Latvijas PSR Zinotnu Akademijas Vestis No.8. 105 (1956)
14. KARMIL'CHIK, A.Ya., GILLER, S.A., Trudi Inst. Lesokhoz. Problem. Akad. Nauk. Latv. S.S.R. Voprosi Lesokhim. i. Khim. Drevesinii 12. 251 (1957)
15. KARMIL'CHIK, A.Ya., GILLER, S.A., U.S.S.R. Pat. 110 962
16. KARMIL'CHIK, A.Ya., GILLER, S.A., Nauchnie Osnovi podbora i proizvodstva katalizatorov. Akad. Nauk. S.S.S.R. Novosibirsk 1964. p. 255.
17. KARMIL'CHIK, A.Ya., GILLER, S.A., Geterogenii kataliz v reakciyakh polucheniya i prevrasheniya geterocsiklicheskikh soedinenii Riga, 1971. p. 35.
18. MÉSZÁROS, L., Melt-Bed Catalysts. Lecture at a conference of the Society of Hungarian Chemists. Szeged, Oct. 15. 1959.
19. MÉSZÁROS, L., SCHÖBEL, Gy., Acta Physica et Chemica 14, 61 (1968)

РЕЗЮМЕ

С целью получения фурана из фурфурола были проведены опыты на разработанном нами катализаторе хромитового типа. Параметрами опытов были температура, молярное отношение фурфурола и воды и объемная скорость. Из испытанных катализаторов оказалась самой выгодной промотированная модификация цинко-железного хромита, с применением которой достигалась выход фурана, превышающий 90%. Но испытания на усталость показали, что катализаторы типа окисла металла быстро теряют свою активность и таким образом, применение их в промышленных целях не рекомендуется.

Hungarian Journal
of Industrial Chemistry
Veszprém
Vol.3. pp. 589-602 (1975)

INVESTIGATION OF FURAN PRODUCTION FROM FURFURAL OVER NOBLE METAL CATALYSTS

Gy. GÁRDOS, L. PÉCHY, Mrs. E. CSÁSZÁR* and Mrs. B. SZIGETI*

(Department of Hydrocarbon and Coal Processing,
Veszprém University of Chemical Engineering and
*Pétfürdő, Nitrogen Works)

Received: October 9, 1975.

A catalyst with different metal contents was investigated in the heterogeneous decarbonylation of furfural. It was found that for furan production, catalysts containing palladium are most suitable. Endurance test were carried out with catalysts containing 1.6 and 2.5 % metal palladium. Both catalysts are suitable for industrial utilization, but more reliable operation can be guaranteed with a catalyst containing 2.5 % Pd.

In the previous paper [1] the furan production from furfural over metal oxide in the presence of steam was dealt with. The reductive decarbonylation of furfural is also of industrial importance. It is carried out over noble metal catalysts in the presence of hydrogen and the furan yields are good.

In this paper the reductive furfural decarbonylating experiments and the selection of an appropriate catalyst are reviewed.

The Catalytic Effect of Metals on the Decarbonylation of Furfural

Several attempts [2, 3, 4] were made regarding the decarbonylation of furfural over metal catalysts, but only small furan yields were obtained. The yields were affected by the reduction of the side chain and by the breaking of the furan ring. The active life of the applied catalysts was short.

Table 1. Catalytic effects of different metals and alloys

Catalyst	Furfural conversion [%]	Furan yield [%]	Methylfuran yield [%]
Metal nickel cloth	66	53	8
Nickel on holystone	75	42	16
Nickel chromite	30	33	10
Raney-alloy (Ni, Al)	77	33	8.5
Monel-metal (Ni, Cu)	69	65	2
Ferry-metal (Ni, Cu)	66	63	6
Copper-nickel alloy (80:20)	40	48	2
Cobalt on holystone	42	21	18
Iron on holystone	21	0	18

The effect of some metals and alloys on the decarbonylation of furfural are summarized in Table 1 [4]. Methyl-furan formation was observed especially in the case of catalysts containing nickel, cobalt or iron. The metal copper is inactive, the copper-chromite results in methyl-furan. Nickel applied as a metal cloth appeared to be the most effective catalyst. The optimum temperature for the metal catalysts is 250-350°C. The yields are affected by the pressure and by the furfural/hydrogen molar ratio, in addition to the temperature.

Noble Metal Catalysts

ESCHINAZI was the first to use metal palladium for the decarbonylation of furfural. The experiments were carried out in liquid phase, the palladium was on a sodium carbonate supporter treated with barium sulphate [5].

American patents have reported results with metal palladium on alumina since 1953 [6, 7, 8]. The optimum temperature range is 250-400°C. Yields are affected by the ratio of the liquid feed rate and the amount of the catalyst (cc furfural/cc catalyst·hour) in addition to the temperature. In the case of large liquid-loads the unconverted furfural disactivates the catalyst. The hydrogen considerably influences the yields despite the findings of KARMIL'CHIK [9].

From the noble metals, palladium has the lowest density and melting point, but has the highest magnetic susceptibility. Because of its favourable physical properties and high selectivity its application as a catalyst is increasingly important in several reactions: in dehydrogenation, dehydro-halogenation, aromatization, disproportionation, and decarbonylation, etc. It is resistant against chemical reagents, it can be regenerated many times, and the metal content can easily be obtained from the exhausted catalyst.

A palladium-hydrogen system is formed in the presence of hydrogen. In this the electric resistance increases and the magnetic susceptibility decreases. According to many researchers the hydrogen behaves as a composition metal in the lattice structure of the palladium [10]. The palladium content of the applied catalysts is lower than 10 w.%. Salts of alkali and earth-alkali metals can be used as supporters, although the strong alkali metals step into reaction with the furfural, and increase its tendency for resin formation. Silica gel and alumina are preferred as supporters which are washed with an alkaline solution before treatment.

The decarbonylation in the presence of hydrogen was also investigated by WILSON [11] and LUKES [12]. According to WILSON the

hydrogen molecule decomposes to active atoms on the surface of the catalyst, which reacting with the furfural results in furyl radical. However, this uniting with another hydrogen atom gives furan.

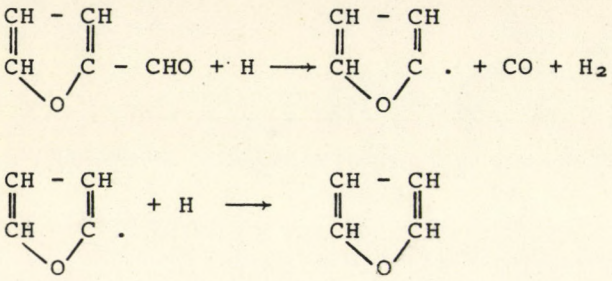

According to LUKES, the aldehyde absorbs on the surface of the catalyst at a higher temperature. At first furfuroyle radical is formed from the furfural, that yields furyl radical by the splitting off of carbon monoxide. The reaction of the furyl radical with hydrogen results in furan.

1.

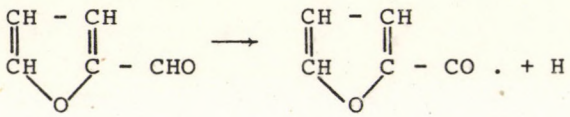

2.

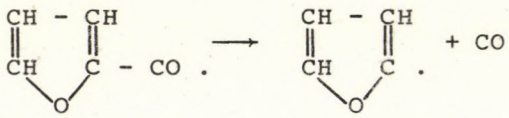

3.

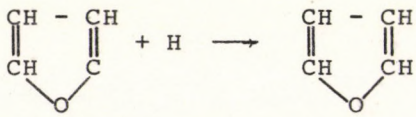

Japanese researchers [13, 14, 15] also dealt with the decarbonylation of aldehydes. Their experiments were carried out in a liquid phase, and olefin and saturated hydrocarbons were formed at higher temperatures than 180°C over palladium catalyst.

$$R\text{-}CH_2\text{-}CH_2\text{-}CHO \xrightarrow[200^{\circ}C]{Pd} R\text{-}CH = CH_2 + R\text{-}CH_2\text{-}CH_3 + CO + H_2$$

It was suggested that the aldehyde and metal palladium form an acyl-palladium complex from which the alkyl-palladium complex derives with carbon monoxide emerging. Metal palladium, hydrogen and the corresponding ligandum derive from the palladium hydride.

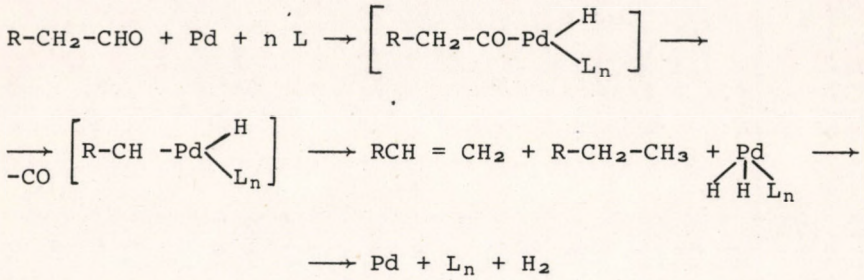

Experimental

The experiments were carried out in the experimental apparatus described in the previous paper [1]. Furfural and hydrogen were separately fed into the reactor and arrived at the reactor preheated and well mixed.

The analysis was carried out as described earlier [1]. During the endurance test of the catalyst, the gases leaving the reactor were led directly to the gas chromatograph and the composition of the gas was determined injecting in instantaneous samples in every hour.

Several noble metal catalysts on an alumina supporter were studied to see which can justify an industrial application. Before the experiments the catalysts were pretreated and were activated at least for 24 hours in a hydrogen stream at 300°C.

Discussion

The decarbonylating experiments - taking into consideration the specific properties of the catalysts - were carried out in the 240-400°C temperature range. The furfural/hydrogen molar ratio was about 1:1 and the liquid-load was about 0.5 cc furfural/cc catalyst·hour. Small amounts of methyl-furan and tetrahydrofuran

Table 2. The investigation of the decarbonylation of furfural over different metal catalysts

Type of the catalyst	Temperature [°C]	Furfural / hydrogen molar ratio	Liquid-load cc furfural / cc catal.hr	Furfural conversion [%]	Furan yield [%]	Methylfuran+tetrahydrofuran yield [%]
Leuna 8197	300	1:1	0.50	51.1	9.8	11.8
Ni+Mo/Al_2O_3	340	1:1	0.50	67.9	16.3	15.4
	375	1:1	0.50	81.1	25.2	16.4
Leuna 8199/K						
(3 % Ni + 12 % MoO/Al_2O_3)	375	1:1	0.50	78.5	40.7	27.8
Leuna 8199/S						
(3 % Ni + 12 % MoO/Al_2O_3)	375	1:1	0.50	63.4	37.3	20.9
Leuna 6524						
(46 % Ni/Al_2O_3)	300	1:1	0.50	70.8	6.8	-
	350	1:1	0.50	97.4	1.8	-
	400	1:1	0.50	100.0	0.5	-
0.65 % Pd/Al_2O_3	240	1:1	0.40	11.0	8.0	2.1
	280	1:1	0.40	20.0	17.5	1.5
	320	1:1	0.40	18.0	16.2	1.2
	360	1:1	0.40	5.5	4.1	0.4
1.6 % Pd/Al_2O_3	240	1:1	0.50	29.0	28.0	1.0
	280	1:1	0.50	45.0	44.0	1.0
	320	1:1	0.50	39.5	37.5	1.6
	360	1:1	0.50	18.5	16.2	2.3

2.5 % Pd/Al_2O_3	270	1:1	0.50	88.0	87.0	1.0
	300	1:1	0.50	100.0	99.0	1.0
	340	1:1	0.50	99.0	98.1	0.9
5 % Pd/Al_2O_3	240	1:1	0.50	89.0	87.5	1.5
	270	1:1	0.50	99.5	98.2	1.3
	300	1:1	0.50	100.0	99.0	1.0
	340	1:1	0.50	100.0	99.0	1.0
1.6 % Pt/Al_2O_3	240	1:1	0.60	43.7	33.6	10.1
	260	1:1	0.50	67.0	65.8	1.2
	300	1:1	0.60	85.1	84.3	0.8
	350	1:1	0.60	97.4	96.4	1.0
5 % Pt/Al_2O_3	260	1:1	0.50	50.3	49.0	1.3
	300	1:1	0.50	94.2	93.0	1.2
	300	1:5	0.30	83.5	61.8	21.7
5 % Ru/Al_2O_3	200	1:1	0.50	31.2	9.6	8.5
	250	1:1	0.50	47.7	20.8	8.1
	300	1:1	0.50	26.7	10.1	1.4
5 % Rh/Al_2O_3	300	1:1	0.50	51.8	47.6	4.2

were formed beside the furan. The gas consisted of a small amount of carbon dioxide and course hydrogen and carbon monoxide.

The evaluation of the experiments was carried out on the basis of furfural conversion and furan yield. The experimental results are summarized in Table 2.

It was found that the Leuna catalysts containing nickel are less suitable for the furan production from furfural. In the case of a Leuna 6524 type catalyst the conversion was over 90 %, but the reaction did not go into the direction of furan formation. Other kinds of nickel catalysts are unsuitable for the decarbonylation of furfural, because of the low furan yield.

A conversion of about 18 % was obtained with a palladium catalyst on a alumina supporter at 280°C and 320°C. A comparison with metal nickel showed that the relative difference (side reactions) between the conversion and yield values is smaller in the case of a palladium catalyst containing 0.65 % Pd, than in the case mentioned before. The 280-320°C temperature range was found to be the optimum.

Other palladium catalysts of higher palladium content (1.6, 2.5 and 5.0 %) were also studied. The conversion was 45.6 and the furan yield 44.6 % in the case of a palladium catalyst containing 1.6 % Pd, and a conversion of nearly 100 % and a furan yield of 99 % were observed in the case of palladium catalysts containing 2.5 % and 5 % Pd respectively.

Other types of metal catalysts were also investigated: catalysts containing 5 % ruthenium or 5 % rhodium on active alumina. These catalysts yield low conversion and yield data.

These investigations showed that the palladium catalysts of higher palladium content (1.6, 2.5 and 5.0 %) are suitable for furan production from furfural.

Hence these catalysts were studied from the point of view of industrial application.

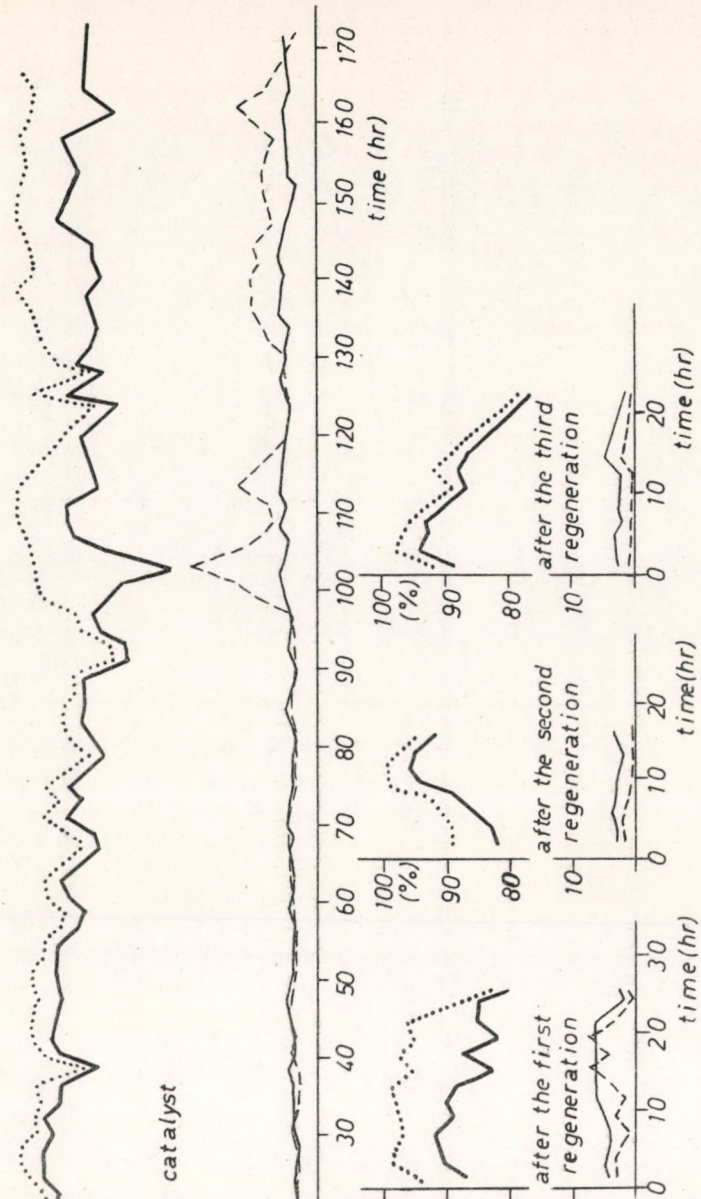

Fig.1. The change of the activity of a catalyst containing 1.6 % Pd on alumina
... furfural conversion; ——— furan yield; --- methylfuran yield; —— tetrahydrofuran yield

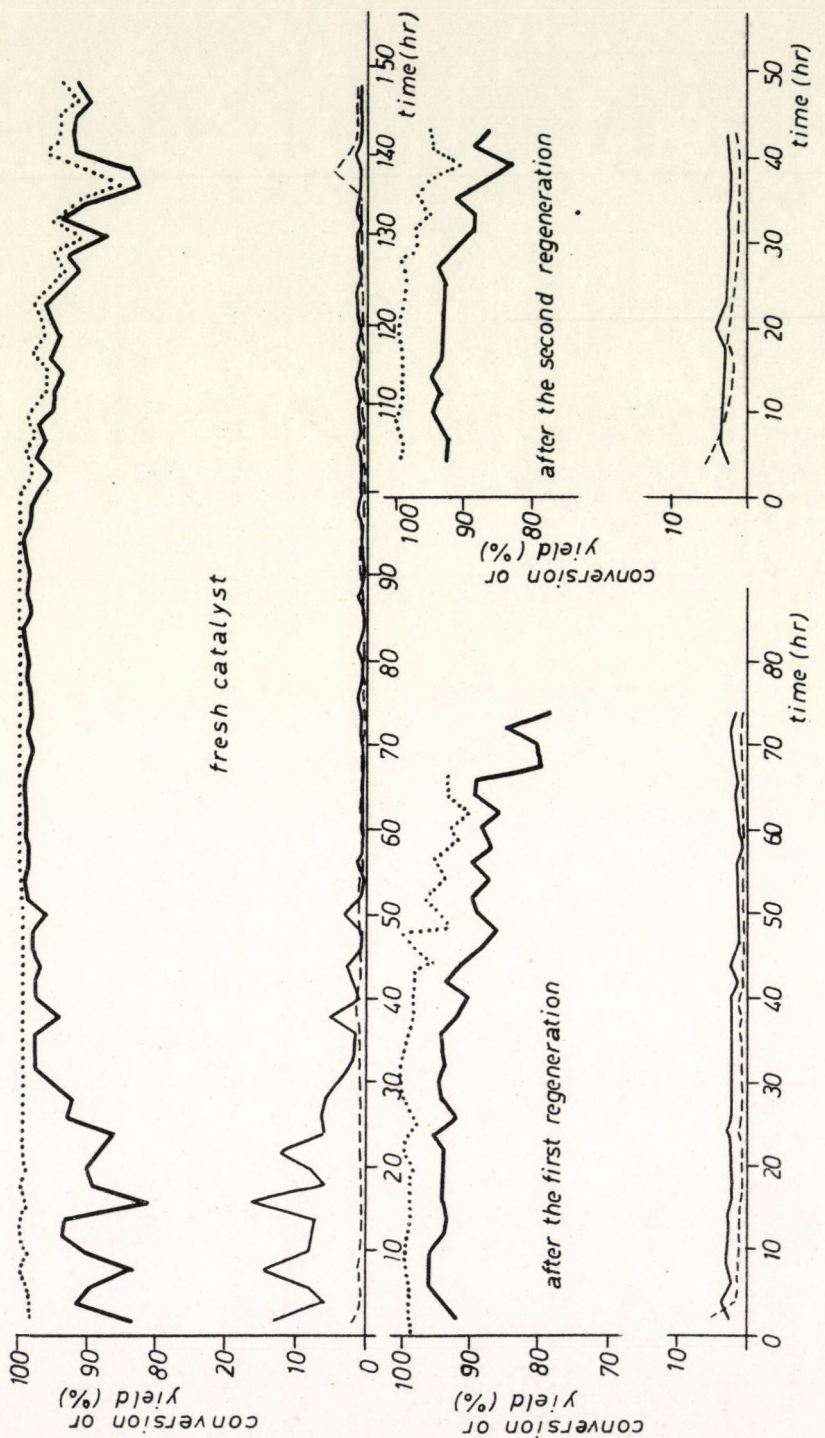

Fig.2. The change of the activity of a catalyst containing 2.5 % Pd on alumina
... furfural conversion; ——— furan yield; --- methylfuran yield
—— tetrahydrofuran yield

Table 3. Investigation of the activity of catalysts containing 1.6 % Pd and 2.5 % Pd respectively on alumina supporter at 300°C, beside 1:1 = furfural/hydrogen molar ratio and at 0.5 cc furfural/cc catalyst·hour of liquid-load

Type of the catalyst		Time of the endurance test (hour)	Loadability (g furfural/g Pd)	Productivity (g furan/g Pd)
1.6 % Pd/Al_2O_3	Fresh catalyst	171	10400	6500
	After the 1st regeneration	25	1500	908
	After the 2nd regeneration	16	1155	696
	After the 3rd regeneration	23	1070	610
	Total	235	14125	8714
2.5 % Pd/Al_2O_3	Fresh catalyst	148	2937	1962
	After the 1st regeneration	74	1775	1128
	After the 2nd regeneration	43	1100	1040
	Total	265	5812	4130

Catalysts containing 1.6 % and 2.5 % Pd were chosen and endurance tests were carried out with them. The reactor worked in continuous operation, samples were taken and analyzed hourly, and material balances were also calculated. The experimental results (furfural conversion, furan, methylfuran, and tetrahydrofuran yields) are illustrated in Figures 1 and 2. When a large decrease of the catalyst activity (conversion and yields respectively) was noticed, the experiments were stopped and the catalysts were regenerated in a nitrogen stream containing 5 vol.% oxygen.The deposit that settled on the surface of the catalyst was burnt off, and the catalyst was activated in a hydrogen stream for 24 hours. After this the hydrogen and furfural feed was started and continued until an important decrease of the catalyst activity was observed again.

The results of the endurance test are summarized in Table 3.

The loadability of the catalyst was calculated as g furfural/ /g Pd, the productivity as g furan/g Pd. It was found that both catalysts are excellent in loadability and productivity under the given conditions. The catalysts were used for more than 100 hours without regeneration and for more than 200 hours with several regenerations.

There are relatively major differences in loadibilities and productivities for the two palladium catalysts. The palladium catalyst containing 1.6 % Pd seemed to be of higher loadability and productivity, especially in the first period. However, it needs daily regenerations because of the rapid decrease of the conversion and yield after the first regeneration.

In the case of the palladium catalyst containing 2.5 w.% Pd the results seemed to be worse because of the palladium reference, although its use is more advantageous since it has a longer active period after regeneration.

The decrease of activity is a consequence of the decrease in the number of active sites.

The results obtained are better than those so far published.

REFERENCES

1. GÁRDOS, Gy., PÉCHY, L., RÉDEY, Á., Mrs. CSÁSZÁR, E., Hung. J. Ind. Chem. 3, 577 (1975)
2. PADOA, M., PONTI, H., Gazette Chimica Italiana 37, 105 (1907)
3. HURD, C.D., GOLDSBY, A.R., OSBORN, E.W., J. Am. Chem. Soc. 54 2532 (1932)
4. WILSON, L., Chem. Educ. 13, 273 (1935)
5. ESCHINAZI, H.E., Bull. Soc. Chim. France 19, 967 (1952)
6. U.S. Patent, 3 007.941 (1953)
7. U.S. Patent, 3.223.714 (1965)
8. U.S. Patent, 3.692.859 (1972)
9. KARMIL'CHIK, A.Ya., Het. Katal. Reakts. Pd. 35, (1971)
10. WISE, E.M., Palladium Academic Press (1968)
11. WILSON, C.L., J. Am. Chem. Soc. 67, 61 (1945)
12. LUKES, R.M., WILSON, C.L., J. Am. Chem. Soc. 73, 4790 (1951)
13. TSUJI, J., OHNO, K., Organic Syntheses 70, 55 (1968)
14. TSUJI, J., OHNO, K., J. Am. Chem. Soc. 90, 94 (1968)
15. TSUJI, J., Accounts of Chem. Research 2, 144 (1969)

РЕЗЮМЕ

В целях гетерогенного каталитического декарбонилирования фурфурола были изучены различные катализаторы, содержащие благородный металл. Было установлено, что для производства фурана - при условиях опытов - оказались самыми выгодными катализаторы, содержащие палладий. Также проведены испытания на усталость с катализаторами, содержащими 1,6 и 2,5% металличесвого палладия. В результате этих испытаний было установлено, что оба катализатора являются применимыми в промышленных целях, но с применением катализатора, содержащего 2,5% палладия, можно обеспечить более надежный режим работы.

Hungarian Journal
of Industrial Chemistry
Veszprém
Vol.3. pp. 603-616 (1975)

THE POSSIBILITY OF APPLYING ALUMINIUM ALLOYS AS SACRIFICIAL ANODES IN CATHODIC PROTECTION

T. GARAI, D. RÓNAY* and J. DÉVAY

(Research Group of Electrochemistry of the Hungarian Academy of Sciences, Department of Physical Chemistry, Veszprém University of Chemical Engineering and *Research Institute of High Pressures, Budapest)

Received: August 1, 1974

The polarization of various aluminium alloys (containing zinc, magnesium, iron and copper) were studied with reference to their use as sacrificial anodes in cathodic protection. An aluminium alloy containing 5 per cent zinc and one containing 2.5 per cent zinc and 3.5 per cent magnesium were found to be suitable materials for the use as galvanic anodes under appropriate conditions.

Cathodic protection - without an external power source - of underground structures is generally performed by sacrificial anodes made of magnesium or magnesium alloys. However, the current efficiency of these anodes is about 50 per cent of the theoretical one calculated according to Faraday's law, because of the high rate of corrosion of magnesium and its alloys [1]. There is an abundance of literature on the types of magnesium alloys that are suitable for use as galvanic anodes and on their utilization (cf. e.g. [1, 2]).

The substitution of magnesium alloys by other metals and/or alloys in cathodic protection has also been investigated. Literature data are at variance concerning the use of aluminium and aluminium alloys as sacrificial anodes. In fact, it has been pointed out that a passive film is formed on the surface of

aluminium and aluminium alloys in the pH range from pH = 4 to 9 which hinders the anodic dissolution of the metal and thus the current density generated by the anode is insufficient for efficient cathodic protection [3].

Some decades ago an aluminium alloy containing 5 per cent zinc was proposed as a material for galvanic anodes, because it was found to be the best choice among many aluminium alloys investigated [4]. This alloy ensured efficient cathodic protection when immersed in a backfill of suitable composition, containing salts such as calcium chloride, sodium chloride, calomel or magnesium oxychloride cement [4]. Other authors did not find convincing proof of the advantages of aluminium sacrificial anodes in their experiments carried out in sea-water with various aluminium based alloys and zinc [5].

Aluminium alloys containing mercury were recently found to yield good results when used as sacrificial anodes in sea-water [5]. The effect of some constituents (such as tin, cadmium, indium and zinc) on the aluminium-mercury alloys was also investigated and an aluminium alloy containing 0.1 per cent zinc, 0.2 per cent lead and 0.05 per cent mercury was found to exhibit the most uniform corrosion and the least tendency to pitting corrosion [6].

Since literature data are scanty and rather contradictory concerning the behaviour of aluminium alloys in the cathodic protection of underground structures, it was deemed worth while to further investigate the possibility of the use of aluminium alloys as galvanic anodes.

Efficient sacrifical anodes can be made of aluminium alloy having a corrosion potential which is sufficiently negative compared to that of the iron alloy to be protected. Thus the anode will generate an adequate amount of current for the underground structure to reach its protective potential at a suitable value of ground resistance.

Aluminium alloys are rather corrosion resistant on account of an uniform thin, oxide layer formed on their surface and thus

they are generally ill-suited for use as sacrificial anodes. Accordingly some alloys which are more easily corroded had to be choosen for polarization studies in various media in order to select for further investigation the alloy suitable for the use as a galvanic anode in cathodic protection.

It is well known that the presence of some alloying metals considerably hinders the corrosion resistance of aluminium alloys. In addition to the quality of the alloying components, the metallurgical structure of the alloys also affects the corrosion resistance of the latter [7]. Among the commonly used alloying metals of aluminium copper promotes the corrosion of aluminium alloys to the greatest extent. This effect is manifested even at 0.005 per cent concentration of copper. The rate of penetration in pitting corrosion decreases when the copper content is below 0.5 per cent although the number of pits is increased [7]. Similarly to copper, but to a lesser extent, zinc also decreases the corrosion resistance of the alloy especially in acidic media. The occurrence of pitting corrosion is increased by the iron content of the alloy. The corrosion of aluminium alloys is also promoted by the following rarely used alloying metals: boron, calcium, molybdenum, mercury, nickel, phosphorous, sulphur and tungsten.

It is interesting to note that graphite in contact with an aluminium surface also accelerates the corrosion of the metal in the presence of humidity.

EXPERIMENTAL PART

Taking into account the above data, preliminary experiments were performed on the commercially available copper, zinc, iron and magnesium containing alloys listed in Table 1. The anodic polarization of these alloys was investigated by a potentiostatic method.

Previous experiments [8] proved that the pretreatment of the alloy had an important influence on the corrosion of the metal.

Thus the casting used for the preparation of the electrodes was subjected to the following heat treatment [8]. First the casting was heated at 350 °C for two hours in a nitrogen atmosphere, then it was slowly cooled (for 4 to 5 hours) to room-temperature in a nitrogen atmosphere. The electrodes were etched at 90°C in ethylene glycol containing 1 per cent nitric acid.

Table 1. Composition of the aluminium alloys used in the present investigation

Sign.	Number	Type	Mn	Mg	Cu	Zn	Fe	Ti
			per cent					
I.	941	AlMgCu	0.4	0.6	4.3	-		
II.	942	AlMgZn		2.5		3.5		0.15
III.	943	AlMgZnCu	0.4	2.2	1.5	6.0		
IV.	944	$AlFe_2$		-	-		2.0	-
V.		AlZn	-	-	-	5.0	-	-

Before the experiments, the surface of the electrode (0.1 to 0.2 sq.cm) was abraded with an F 20 emery paper wetted with ethylene glycol containing 1 per cent nitric acid. Then the electrode was rinsed in distilled water to remove all traces of the abrasive material.

The anodic polarization curves of the electrodes were recorded by a linearly programmed potentiostat, whose potential and current outputs respectively were connected to an X-Y recorder. The potentials referred to a 1 N standard calomel electrode.

RESULTS

The results of the experiments in 0.01 M calcium chloride are represented in Figure 1. It is apparent on Figure 1 that the alloys containing copper and iron respectively (curves I, III, IV) are

unsuitable for the use as sacrificial anodes because their respective corrosion potentials are not sufficiently negative compared to that of iron alloys and thus these aluminium alloys cannot be expected to polarise the latter to an extent required in cathodic protection. However, the corrosion potentials of Al-Mg-Zn and Al-Zn alloys are -1.0 V approximately (with reference to a 1 N standard calomel electrode) and the anodic polarization curves of these alloys (Figure 1 curves V and II respectively) are nearly

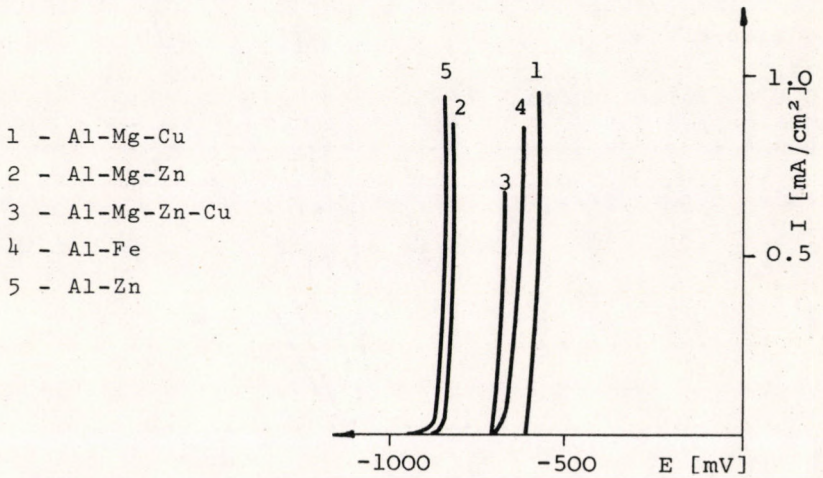

Figure 1. Anodic polarization curves of various aluminium alloys

identical. Thus it was deemed worth while to study in detail the polarization of these alloys in various media. These studies provided useful information regarding the soil parameters (resistance, and pH, etc.) and the appropriate backfill composition by which the use of Al-Zn or Al-Mg-Zn alloys as sacrificial anodes would be advantageous. The solutions selected for the polarization studies contained the cations (e.g. sodium, magnesium) and anions (e.g. sulphate, chloride) which are most frequently present in soil and soil water.

The effect of oxygen dissolved in soil water was also studied and the interaction of various parameters was taken into consideration.

Chloride ions caused the largest corrosion effect among the anions which could be anticipated. The results of the measurements in chloride containing solutions were practically identical in the case of both Al-Zn and Al-Mg-Zn alloys. The steepness of the anodic polarization curves is increased with increasing chloride concentration.

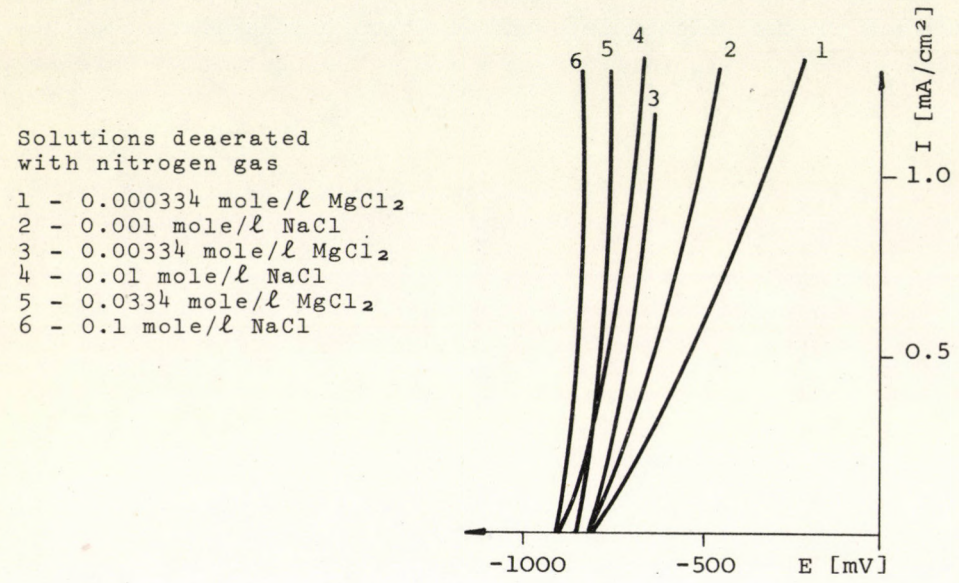

Figure 2. Anodic polarization curves of Al-Zn alloy in deaerated solutions of various chloride concentrations

It is apparent in Figure 2 that the effect of the cation on the polarizability of the alloys is negligible compared to that of the anions in solutions deaerated with nitrogen gas. However, in solutions containing oxygen, the cation also affects the electrochemical behaviour of the alloy. The polarization curves shown in Figure 3 indicate that the corrosion potential of the alloy in magnesium containing solutions is more positive in the presence of oxygen than in the absence of the latter (cf. Figure 2). This phenomenon was not observed in solutions containing sodium chloride, although the anodic polarization curves of the alloys were steeper

in the presence of oxygen in both magnesium chloride or sodium chloride containing solutions. This fact points to the conclusion that the corrosion of the alloys is enhanced under the effect of oxygen in these solutions.

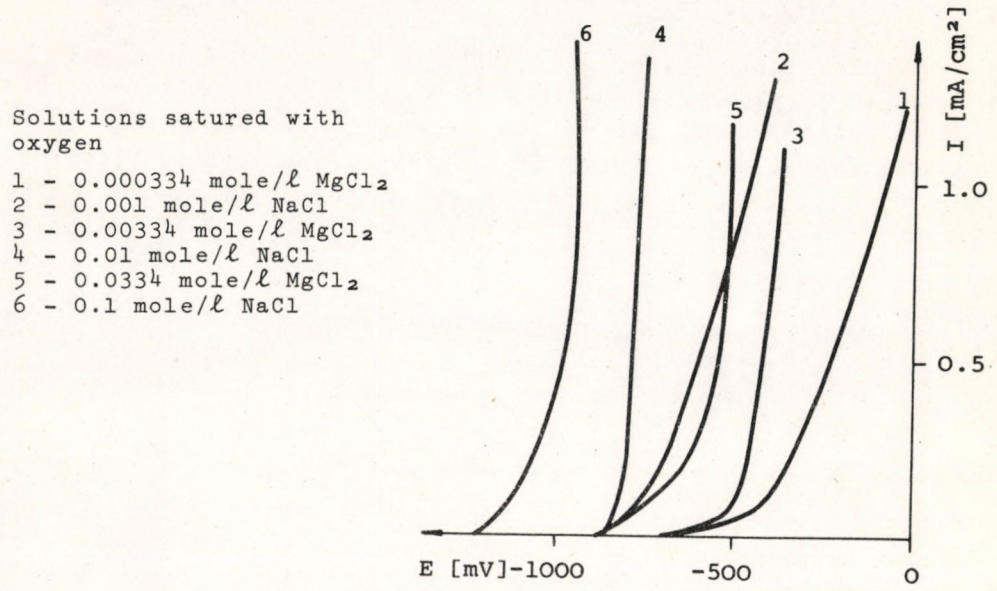

Figure 3. Anodic polarization curves of Al-Zn alloy in oxygen containing solutions of various chloride concentrations

The Al-Zn and Al-Mg-Zn alloys under investigation exhibited different polarization characteristics in sulphate containing solutions than in chloride containing media. The polarizability is increased by increasing the sulphate concentration and it is larger in oxygen containing solutions than in deaerated ones at a constant sulphate content (Figure 4). These results support the view that an increase in sulphate concentration and the presence of oxygen promotes the formation of a passive layer on the surface of the alloys.

The pH dependence of the polarization of the Al-Zn and Al-Mg-Zn alloys under investigation is practically identical. The

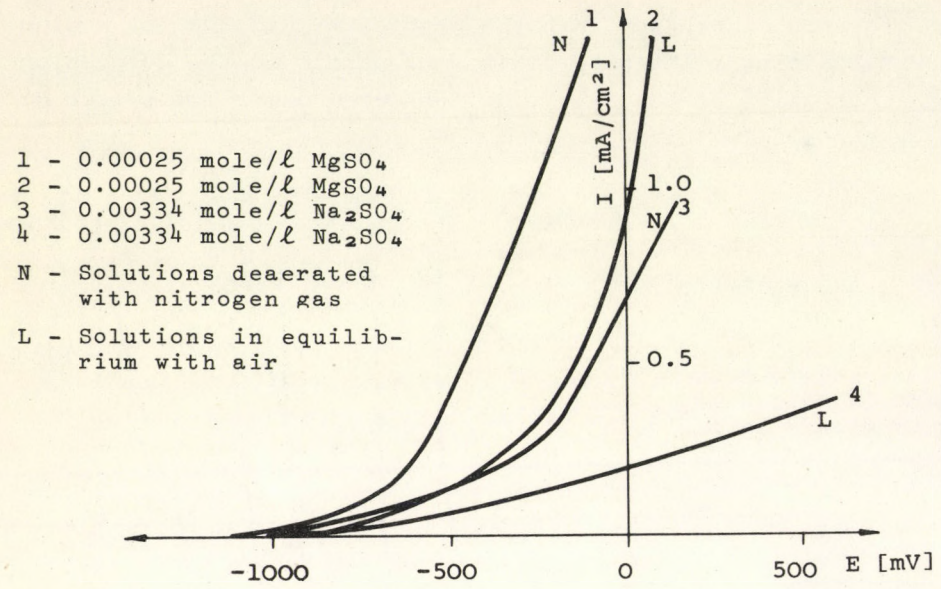

Figure 4. Anodic polarization curves of Al-Zn alloy in solutions of various sulphate concentrations

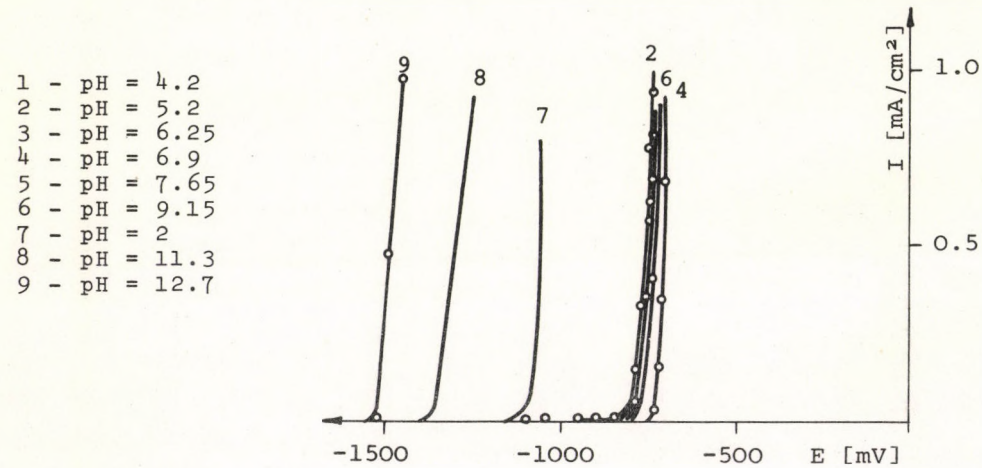

Figure 5. Anodic polarization curves of Al-Mg-Zn alloy in solutions at various pH

polarization curves of the latter in solutions having various pH are shown in Figure 5 as an example. Since in addition to the hydrogen ion activity of the buffer solutions, other components also affect the polarization of the alloys, the measurements were performed in hydrochloric acid – calcium chloride and calcium hydroxide - calcium chloride mixtures respectively at various pH. It is apparent in Figure 5 that the anodic polarization of the alloy was slightly affected by the hydrogen ion activity in the pH = 4 to 9 range. However, the corrosion potential of the alloy was considerably shifted in the cathodic direction in strong acidic (pH < 3) and strong alkaline (pH > 10) solutions. Above pH ≥ 11 the corrosion potential of aluminium alloys approached that of the magnesium alloys.

DISCUSSION

The polarization studies of Al-Zn and Al-Mg-Zn alloys led to the conclusion that the latter is also suitable for use as a sacrifical anode in addition to the former alloy investigated previously [1, 4]. These alloys can ensure the negative potential shift required for effective cathodic protection of underground structures, provided that a suitable backfill containing chloride and having an alkaline pH (pH = 10) is used.

Various heavy metal salts (e.g. calomel) were suggested in literature [4, 6] as additives to the backfill material in order to improve the performance of galvanic anodes made of Al-Zn alloy Our experiments did not furnish evidence to confirm these statements, since neither the zero-current potential nor the polarization of Al-Zn or Al-Mg-Zn alloys could be measured reproducibly in lead hydroxide and calomel suspensions respectively, because the heavy metal was spontaneously reduced on the electrode. These data indicate that heavy metal salts do not improve, but instead tend to make the performance of galvanic anodes unstable.

The polarization studied permitted some conclusions to be drawn concerning the suitable conditions that are required to

obtain effective cathodic protection when sacrificial anodes made of Al-Zn and Al-Mg-Zn are used.

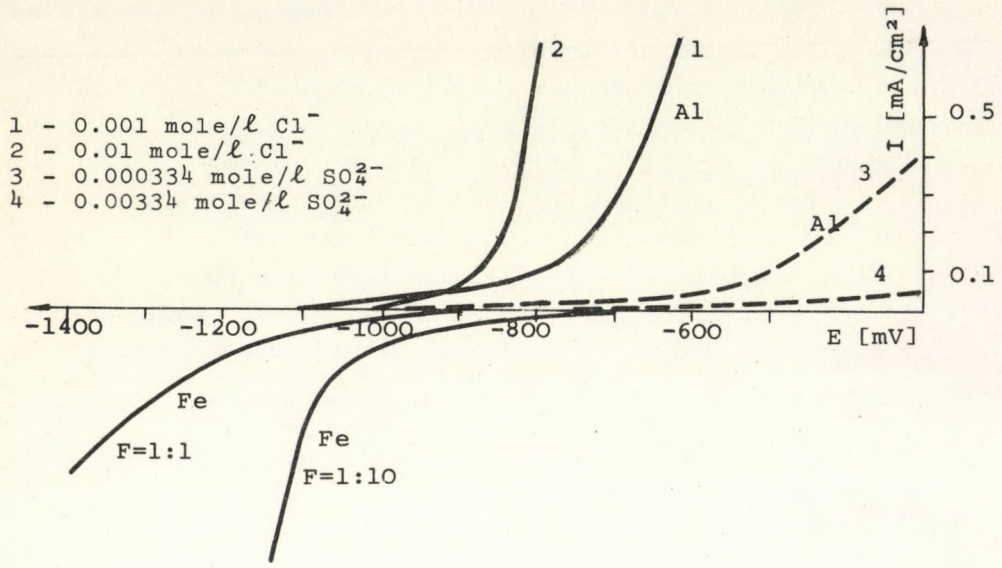

Figure 6. Cathodic and anodic polarization curves of C-20 type iron and Al-Zn respectively in various solutions

The anodic polarization curve of the Al-Zn alloy and the cathodic polarization curve of C-20 type iron in sulphate and chloride containing solutions respectively are shown in Figure 6 as an example, assuming F = 1:1 and F = 1:10 as the ratio of the surface areas of the anode and cathode respectively. As pointed out earlier, aluminium alloys are to a large extent polarizable in sulphate containing solutions. Consequently the potential of iron in an iron-aluminium alloy galvanic cell is only slightly shifted to cathodic potentials, even when the electrodes are short circuited which is apparent on the Figure. Thus aluminium alloys cannot provide effective cathodic protection in such media. However, in chloride containing systems, especially with a large chloride concentration, the aluminium alloys investigated are much less polarizable than in sulphate containing solutions, and the potential of iron can attain the value required for effective cathodic pro-

tection if the ratio of the surface of the aluminium alloy anode to the cathode and the soil resistance have suitable values. This fact is shown in Figure 7. The figure shows the cell current of a galvanic cell consisting of iron and Al-Zn alloy as plotted vs. the cell voltage for a F = 1:1 and F = 1:10 anode:cathode surface area ratio respectively.

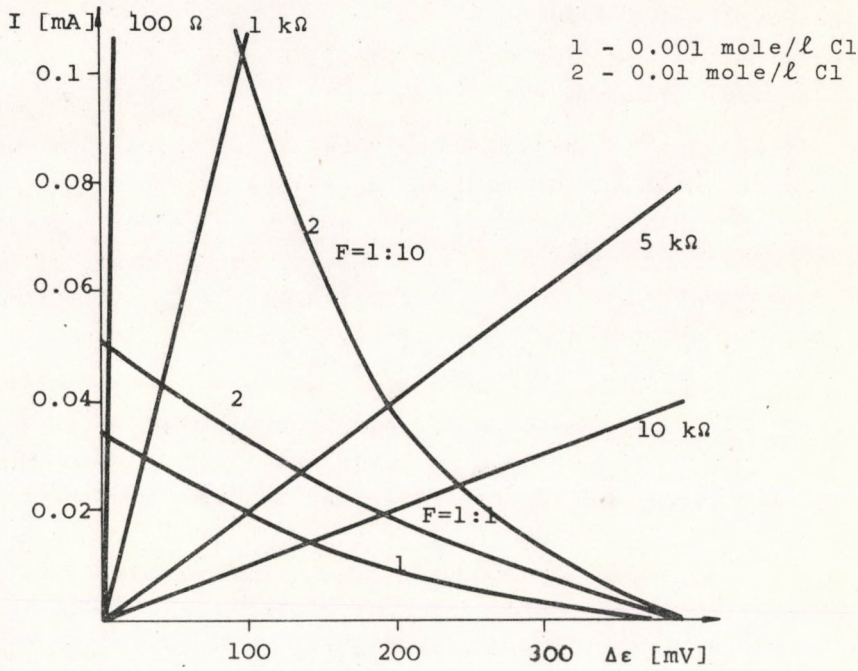

Figure 7. Cell current vs. cell voltage curves of C-20 type iron and Al-Zn cell at various ratios of the surface areas of the anode and the cathode

The straight lines on the Figure represent the current vs. cell voltage relation at the various inner resistance of the cell. The inner resistance of the cell, i.e. the soil resistance should be sufficiently small to permit a shift of the iron potential to a more cathodic value by at least 200 mV. Hence, the cell voltage must be approximately 200 mV less than the value observed at zero--current (400 mV approx.) in order to fulfil this requirement. It is apparent on the figure that the soil resistance should be below

10 KOhm at a suitable anode:cathode area ratio. At lower resistances than this, the cell current is increased and the potential of iron is increasingly shifted to negative potentials and effective cathodic protection can be attained, while at larger soil resistance, the iron cannot be sufficiently polarized by the aluminium alloy. It is noteworthy that the potential of iron is not shifted to a cathodic direction to such an extent as to produce hydrogen evolution, even in the case of zero soil resistance when aluminium alloys are used as sacrificial anodes, while in the case of anodes made of magnesium alloys such effects were also reported.

It is worth while comparing some of the results of the studies of the use of Al-Zn and Mg-Al-Zn alloys as sacrificial anodes [2]. The Mg-Al-Zn alloy can provide effective cathodic protection at lower ratios of surface areas. The economical use of the anode can be ensured by reducing the corrosion of the alloy by employing a backfill of appropriate composition. However, the dissolution of the anode is considerable in any case.

Sacrificial anodes made of aluminium alloys can provide efficient cathodic protection at a larger ratio of the anode:cathode surface area only and the backfill must contain components which hinder the oxide formation on the surface of the alloy. The use of aluminium alloys can be economic even in such circumstances, if the difference in the price of the two alloys is taken into consideration. These considerations justify the necessity of further investigations into the possibility of using aluminium alloys as galvanic anodes. These investigations will be especially directed to the selection of suitable backfill materials and the control of the results in the field.

REFERENCES

1. BAECKMANN, W., SCHWENK, W., Handbuch des katodischen Korrosionsschutzes, Verlag Chemie GmbH., Weinheim, BRD, 1971.

2. RÓNAY, D., LENGYEL, B., MÉSZÁROS, L., DÉVAY, J., Symposium on Soil Corrosion, Siófok, 1972.

3. GIRARD, R., POIRIER, G., La corrosion des conduits d'eau et de gaz (Ed.: M. Neveux) Eyrolles Paris, 1968.

4. HOXENG, R.B., VERINK, N.D., BROWN, R.M., Corrosion NACE, 3, 263 (1947)

5. LENNOX, T.J., PETERSON, M.H., GROOVER, R.E., Materials Protection, 7, 33 (1968)

6. YANAGIDA, K., HATANO, I., KAWAI, M., Light Metals (Japan) 17, 16 (1967)

7. GODARD, H.P., JEPSON, W.B., BOTHWELL, M.R., KANE, R.L., The corrosion of light metals, J. Wiley and Sons Inc. New York, 1967.

8. RÓNAY, D., Developments of galvanic anodes for cathodic protection and of insulation techniques. NAKI, Budapest, 1970.

РЕЗЮМЕ

Авторами были изучены поляризационные свойства различных алюминиевых сплавов, содержащих цинк, магний, железо и медь с точки зрения их применяемости в качестве автономного гальванического анода. Было установлено, что с применением алюминиевых сплавов, содержащих 5% цинка, а также 2,5% цинка и 3,5% магния, при определенных условиях можно обеспечить защитный потенциал, удовлетворяющий требованиям катодной защиты от коррозии.

Hungarian Journal
of Industrial Chemistry
Veszprém
Vol.3. pp. 617-630 (1975)

STUDIES ON THE FLOW DYNAMIC CHARACTERISTICS OF THE FLOTATION TECHNIQUE

J. FILKA, Z. ORMÓS and B. CSUKÁS

(Research Institute for Technical Chemistry of the Hungarian Academy of Sciences, Veszprém)

Received: July 2, 1975.

One possible means to bring about contact between granules and a gas in counter-current is the flotation technique. A number of operations (e.g. drying, and grading) can satisfactorily be carried out in this manner. After a brief summary of the literature on the question, an experimental technique and apparatus - developed in the last few years in order to study the flow dynamic characteristics of the technique - are described. Changes in the most important flow dynamic characteristics (grain volume fraction, residence time, and the fraction ratio of granules falling downwards) are presented in Figures, plotted against various parameters applied in the technique (gas flow rate, mass flow rate of solid materials, and grain size, etc.). The experimental results are evaluated and formulae - enabling the calculation of the average residence time, the fraction ratio of granules falling downwards and the grain volume fraction - are presented.

The technique according to which a granular solid is added into a fluid streaming upwards (hereinafter, a gas) whereby the dynamic lifting force acting upon the granules is smaller than or equal to the weight of the granules and the latter are allowed to escape the system, is termed a flotation technique.

Phenomena occurring in systems consisting of granules and gas were studied by ZENZ [1], who summarized the various forms c streaming in a consistent state diagram. The latter enables one t follow the limiting cases of fluidized state from a stationary be through fluidization and flotation to pneumatic material transpor in the function of the flow rate, as related to the whole cros section. If the flow rate of the gas is gradually increased, moving (fluidized) layer is formed. Over a given gas flow rate, "slugging" form of motion is characteristic, and the system is un stable. At an adequately high gas flow rate, the system become stabilized again, and at the same time the concentration of th solid material shows an abrupt change. This is the region of th dilute phase. Upon a further increase in the gas flow rate, th concentration of the solid in the layer is rapidly decreased. Th void fraction value approaches unity. The granules present in th system are in a floating state, if the flow rate of the fluid i equal to the "falling" rate of the granules. Upon a further in crease in the gas flow rate, the granule travels in an upward di rection, i.e. pneumatic material transport is brought about [2].

In the practical realization of the flotation technique, par of the solid granular material added to the upwards-flowing gas i generally carried away by the latter. In spite of this fact, th counter-current contact between the gas and the granules fallin downwards upon the action of gravitation is characteristic of thi technique. In the case of materials of approximately homodisperse particle size distribution it is possible to find a gas flow rate at which all of the solid material added is in the zone of counter -current contact. It follows from the aforesaid that flotation can be realized only in a given gas flow rate range. If the flow rate is higher than the falling rate of the granules, the latter will be carried away by the gas, that is to say, pneumatic transporta- tion will be brought about. Accordingly, the most important cha- racteristic of the flotation technique is the falling (flotation) rate of the granules.

As far as the point of view of the flotation technique is concerned, the concept of the falling rate does not mean the

avelling velocity of the solid granules, but that particular li-
ar gas flow rate at which the pulse flux transferred by the gas
the granule exactly counteracts the gravitational force acting
on the same; theoretically, in this case the granule is in a
ationary state, it is floating. The equilibrium of forces is es-
ntially identical to the equilibrium state of a granule sedi-
nting in a stationary medium when, after the establishment of
e equilibrium of the gravitational forces and those of the re-
stance of the medium, the granule moves at the sedimentation li-
ting rate. In this case, the falling rate actually means the
uilibrium propagation rate of the granule. However, with regard
pulse transfer, it is essentially irrelevant, whether the force
resistance of the medium, acting upon a granule falling in a
ationary medium is considered, or the dynamic lifting force of
e flowing gas acting upon the granule in a gravitational (or
her) force field.

It follows from the aforesaid that the techniques applicable
r the calculation of the flotation rate are essentially identi-
l to the determination techniques of the sedimentation limiting
te: in both cases, the essence of the problem is the formulation
the pulse transfer coefficient pertaining to the body surrounded
the streaming medium. The pulse flux (force of resistance of
e medium, dynamic lifting force) acting upon the body surrounded
the streaming medium can be described in terms of the following
ll-known Equation:

$$P = c \frac{d^2\pi}{4} \cdot \frac{\gamma u_e^2}{2g} \qquad (1)$$

equilibrium state is established, if the pulse flux (force of
sistance of the medium) is equal to the gravitational force act-
g upon the granule:

$$P = c \frac{d^2\pi}{4} \cdot \frac{\gamma u_e^2}{2g} = \frac{d^3\pi}{6}(\gamma_{sz} - \gamma) \qquad (2)$$

e following Equation can be deduced for the calculation of the
lling rate (u_e) from the equilibrium of forces:

$$u_e = \sqrt{\frac{4(\gamma_{sz} - \gamma)g \cdot d}{3\,\gamma c}} \qquad (3)$$

The dimensionless quantity c in the Equation is the pulse transfer (resistance of the medium) coefficient, depending on the parameters of streaming and the shape characteristics of the granule. In different Re-number ranges, the coefficient of the resistance of the medium can be described by different formulae, whereby different Equations are obtained for the calculation of u_e [1, 3, 4, 5].

Experiments were carried out to determine the falling rate by measurement. In this studies carried out in connection with the flotation technique, HITES [6] applied water as the fluid. In his experiments, the flow rate of water was chosen in the case of the individual fractions in such a manner that the carryaway should not be larger than 20 per cent of the granules added even at the highest fluid flow rate. Consequently, the fluid flow rate applied in the case of the individual granule fractions practically included the flotation rate interval characteristic of the fraction. Accordingly, the arithmetic mean of the flow rate interval applied was accepted as the flotation rate.

ORMÓS [7] determined the falling rate as the upper limiting rate of fluidization. The experiments were carried out in the following manner: the dependence of the grain volume fraction on the flow rate of the fluid was determined and the fluid flow rate was graphically extrapolated to a void fraction value $E' = 1$ in a lg-lg co-ordinate system.

Recently OSTROVSKIJ and ISAKOV [8] published date for the determination of the falling rate. In many cases, nomographs [9] are applied for the determination of the falling rate.

Over the past few years, an experimental setup was designed and constructed by the authors, and experimental and calculation methods were elaborated in order to determine the dependence of the flow dynamic characteristics on various parameters.

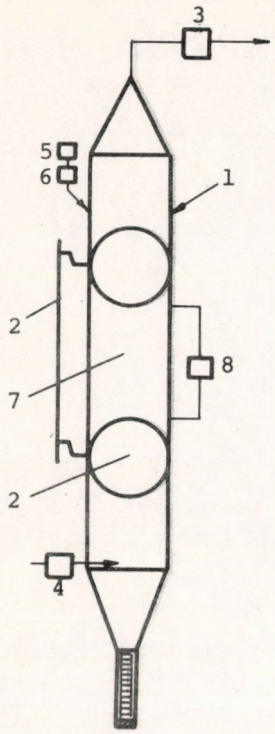

Figure 1

The experimental setup (cf. Figure 1) is a glass apparatus of 2 m length and 38, 52 or 92 mm in internal diameter. The length of the measuring section, enclosed by two butterfly valves (2), is 1 m. Air enters the apparatus via the rotameter (4) and leaves through the cyclone (3). The granular material is introduced by a worm-type feeder (6). The feeding rate of the granular material was adjusted to the desired value by controlling the speed of the driving motor. The pressure drop of the streaming air across the experimental section was determined by oblique-tube type pressure gauges (8) connected above and under the butterfly valves.

The mass flux of the solid material leaving the apparatus and the amount of solid material present in a chosen 1-m section of the apparatus were determined during the experiments.

The experiments were carried out with two model substances: sand and an ion-exchange resin. The following grain fractions were used in the experiments made with quartz sand:

0.1 to 0.2 mm;
0.2 to 0.315 mm;
0.315 to 0.4 mm;
0.4 to 0.5 mm.

The following 3 fractions of the ion-exchange resin model substance were applied in the experiments:

0.4 to 0.5 mm;
0.315 to 0.4 mm;
0.2 to 0.315 mm.

In the flow dynamic studies of the flotation technique, the following independent and dependent variables were studied:

Independent variables:

- u flow rate of air, m/s
- w feeding rate of solid material, kg/m²s
- ρ density of solid granules, kg/m³

Dependent variables:

- ε granule volume fraction, %
- L fraction of granules falling downwards, %
- τ residence time, s

In the determination of the granule volume fraction, first the air flow and thereupon the feeding rate of the granules was adjusted. As soon as the pressure drop of the gas became stationary, the measuring section of 1 m length was closed by the two butterfly valves, and simultaneously the air flow and granule feeding were stopped. Knowing the mass of the solid material present in the measuring section, the granule volume fraction was calculated by the following Equation:

$$\varepsilon_{\%} = \frac{G}{F \cdot Y \cdot \rho} \cdot 100 \qquad (4)$$

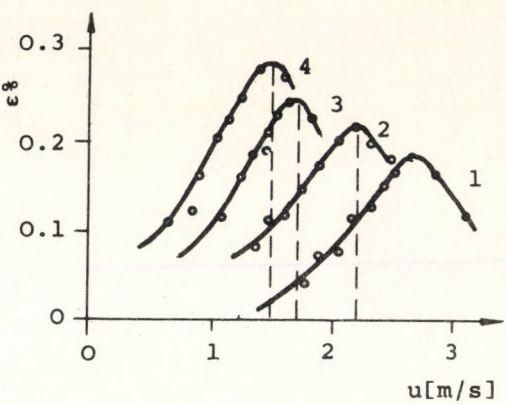

Fig.2. 1 - d = 0.4-0.5 mm
2 - d = 0.315-0.4 mm
3 - d = 0.2-0.315 mm
4 - d = 0.1-0.2 mm
D = 52 mm
W = 1 kg/m²s

The curve of the granule volume fraction determined in the above manner, when plotted against flow rate, passes a maximum (Figure 2).

The average residence time was determined on the basis of the amount of solid material present in the system and the feeding rate. Of course, when determining the residence times, it had to be taken into consideration that only a certain fraction (L %) of

the solid material fed in gets into the zone of counter-current contact, and accordingly we can write:

$$\tau = \frac{G}{W \cdot L \cdot Y} \tag{5}$$

It was concluded that the mean residence time increases with increasing gas flow rate in the range studied (Figure 3), it is dependent on the feeding rate of the granules only to a moderate degree and it decreases with increasing granule size.

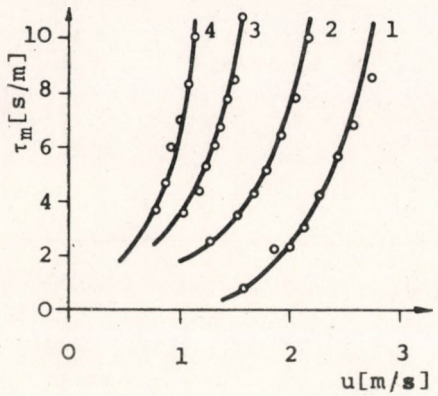

Fig.3. D = 52 mm; W = 1 kg/m²s
1 - d = 0.4-0.5 mm
2 - d = 0.315-0.4 mm
3 - d = 0.2-0.315 mm
4 - d = 0.1-0.2 mm

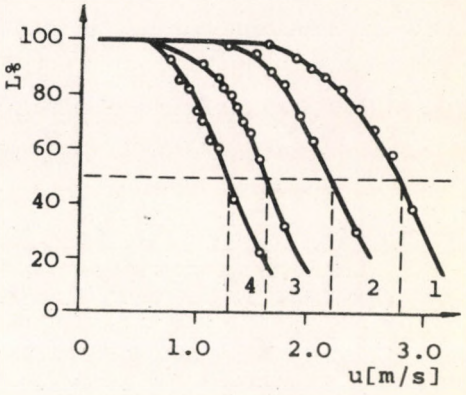

Fig.4. D = 52 mm; W = 1 kg/m²s
1 - d = 0.4-0.5 mm
2 - d = 0.315-0.4 mm
3 - d = 0.2-0.315 mm
4 - d = 0.1-0.2 mm

Part of the granules introduced into the system (L %) falls downwards where it comes into counter-current contact with the gas (in the present case, air) streaming upwards, whereas another part is carried away pneumatically. In addition to the physical characteristics of the heap of grains the ratio of grains falling downwards naturally depends on the flow rate of the gas streaming upwards. Changes in L plotted against the flow rate for a solid material feeding rate of w = 1 kg/m²s are presented in Figure 4 (the model substance in these experiments was quartz sand). It clearly appears from the Figure that at a certain gas flow rate, 50 per cent of the solid material fed in falls down and 50 per cent of it

comes into the domain of pneumatic conveyance. This gas flow rate value is characteristic of the given granule fraction and consequently the mean flotation rate of the fraction can be characterized by the linear gas flow rate pertaining to the value L = 50 %.

In the evaluation of the experimental results it was concluded that the frain volume fraction, when plotted against the gas flow rate, passes a maximum in all cases (cf. Figure 2), that is to say, there exists a certain gas flow rate at which the amount of the granules travelling downwards in the system is the highest. The maximum of this function may be interpreted as the flotation rate. In the case of narrow fractions, there is a negligible difference between the flotation rates as determined on the basis of conditions L = 50 % and ε: = max!, respectively. A few examples are presented in Table 1.

Table 1. Flotation rate

on the basis of L = 50 %	on the basis of ε_{max}	Difference, %
2.85	2.75	-3.54
2.25	2.20	-2.23
1.70	1.60	-5.90
1.28	1.25	-2.35

The starting point of the explanation for the deviation is the grain size distribution within the fraction. No matter how narrow a grain fraction may be, there is a characteristic grain size distribution and generally a relative abundance of smaller granules is characteristic. Accordingly, the distribution function is asymmetric, the modus being smaller than the median. Flotation rates determined on the basis of L = 50 % is characteristic of the grain size of the median, whereas that derived from the condition ε: max! of that of the maximum. Of course, the deviation is negligible only in the case of narrow fractions; in cases where the interval of the particle size distribution is large, the deviation may be considerable. In such cases the question as to which is the falling rate characteristic of the average may arise. This problem can be solved knowing the definition of the flotation process ac-

cording to which the latter is characterized by counter-current contact between the falling granules and the gas. The quantity of material present in the zone of counter-current contact is maximum and consequently the falling rate value determined on the basis of the condition $\varepsilon := \max!$ (i.e. of the modus) is more characteristic of the heterodisperse system. Accordingly, the flotation rate thus defined is characteristic of the technique and the flotation rate determined according to the aforesaid can be applied as the reducing factor of the linear gas flow rate.

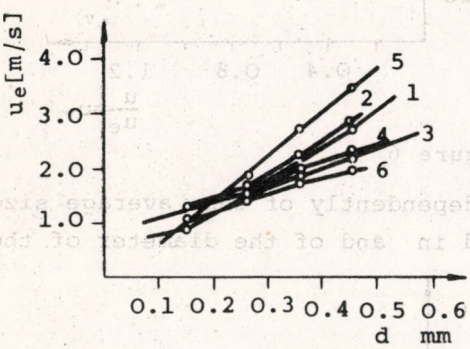

Figure 5. 1 - ε_{max}; 2 - L; 3 - ORMÓS [5] 4 - SZOLCSÁNYI [3] 5 - ALLEN [4]; 6 - FRÖSSLING [1]

Experimentally determined values of the flotation rate were compared to those calculated on the basis of correlations found in literature. In the calculation formulae, the arithmetic mean of the fraction size limits was applied as granule size. The values obtained for flow rate, as plotted against grain size, are presented in Figure 5. It is apparent that the calculation formulae pertaining to the individual granules can be applied to calculate the flotation rate only with reservations.

In the course of the evaluation of the experimental results, empirical correlations for calculation of the fraction of the granules falling downwards, the average residence time and the grain volume fraction were sought. In order to calculate the fraction of the granules falling downwards, the flotation rate value, as determined on the basis of considerations described in the foregoing, was applied as the reducing factor of the linear gas flow rate. When plotting the experimentally determined value of the fraction of the granules falling downwards against the reduced gas flow rate, the values obtained fall, independently of the mean dimensions of the heap of grains and of the shape of the granules, with a good approximation into a characteristic band (cf. Figure 6). By

determination of the function approximately defining this band, the following Equation was obtained for the calculation of the fraction of the granules falling downwards:

$$L = 100 - 50 \left(\frac{u}{u_e}\right)^4 \qquad (6)$$

In calculating the average residence time, a procedure similar to the determination of L % was adopted: the average residence time was plotted against the gas flow rate reduced by the falling rate, as determined on the basis of the condition ε: = max! and dimensions of the granules apparatus, it was found that the average residence time values fall within a narrow band (cf. Figure 7). The relationship:

$$\tau = 10 \left(\frac{u}{u_e}\right)^3 \qquad (7)$$

was found, on the basis of correlation calculus, to present an average approximation of the above mentioned band.

Due to the large difference between the measured residence time values, on the one hand, and those calculated by Equation (7), on the other, the dependence of the average residence time on two parameters was taken into

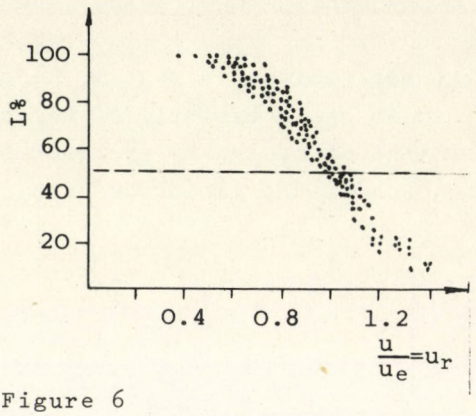

Figure 6

Independently of the average size fed in and of the diameter of the

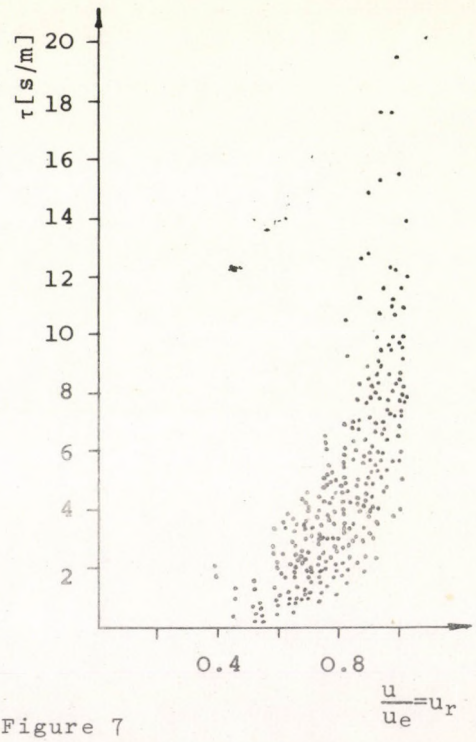

Figure 7

consideration with a correction term. It was found that the dependence on granule size, as an additive term, can be accounted for by the formula:

$$K_1 = 4.5 - 12.5\ \bar{d} \tag{8}$$

whereas changes in feeding rate by multiplication factor:

$$K_2 = 1.2 - 0.2\ w \tag{9}$$

and, accordingly, Equation (7) can be written as:

$$\tau_{sz} = [10(\frac{u}{u_e})^3 + (4.5 - 12.5\ \bar{d})](1.2 - 0.2\ w) \tag{10}$$

From among the flow dynamic characteristics, the knowledge of the ratio of the two phases is of high importance; the latter can be described by the grain volume fraction. In order to calculate the latter, the starting point was:

$$\tau = \frac{G}{Y \cdot w_1 \cdot F} = \frac{\varepsilon\rho}{wL} \tag{11}$$

where:

$$w_1 = w\ \frac{L_{sz}}{100} \tag{12}$$

Considering this, on the basis of the grain volume fraction and the volume of the floating layer, the mass (G) of the floating layer is expressed by

$$G = F \cdot Y \cdot \frac{\varepsilon}{100} \cdot \rho \tag{13}$$

Considering Equations (12) and (13), Equation (11) can also be written in the following form:

$$\tau_{sz} = \frac{F \cdot Y \cdot \frac{\varepsilon_{sz}}{100} \cdot \rho}{w\ \frac{L_{sz}}{00}\ F \cdot Y} = \frac{\varepsilon_{sz}\ \rho}{w\ L_{sz}} \tag{14}$$

Expressing the grain volume fraction from Equation (14) we obtain:

$$\varepsilon_{sz} = \frac{w}{\rho} L_{sz} \cdot \tau_{sz} \qquad (15)$$

and by substituting the empirical Equations determined for the calculation of the average residence time and the fraction of the granules falling downwards, the following Equation is obtained:

$$\varepsilon_{sz} = \frac{w}{\rho} [100 - 50 (\frac{u}{u_e})^4][10(\frac{u}{u_e})^3 + (4.5 - 12.5 \bar{d})] \cdot (1.2 - 0.2 w) \qquad (16)$$

For the case of sand as a model substance (at an apparatus diameter of D = 52 mm), the differences of the measured and calculated grain colume fraction values, plotted against the measured grain volume fraction, is presented in Figure 8. The agreement is satisfactory, the relative deviation is lower than ± 30 %.

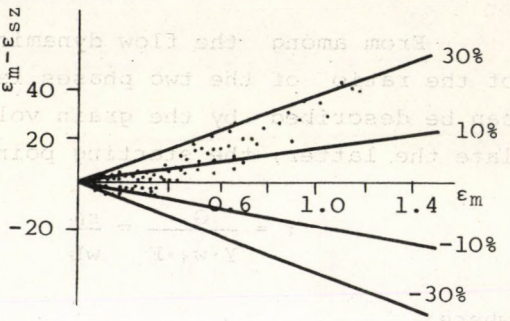

Figure 8. D = 52 mm

On the basis of the experimental results, one of the technique can be grading of granules according to dimensions or weight, as well as the realization of operations carried out with solid-gas counter-current containing, e.g. drying.

SYMBOLS USED

d granule diameter, mm

D diameter of apparatus, mm

F Cross section of apparatus, m^2

G mass of floating granules, kg

L	fraction of granules falling downwards, %
u	linear gas flow rate, m/s
u_e	floating rate of the granules, m/s
w	feeding rate of the solid, kg/m²s
Y	length of the measuring section of the apparatus, m
ε	grain volume fraction, %
τ	average residence time, s/m
ρ	density of the granules, kg/m³
γ	specific gravity of the fluid, kp/m³
γ_{sz}	specific gravity of the granules, kp/m²

REFERENCES

1. LEVA, M., Fluidizáció (Fluidization) Müszaki Könyvkiadó, Budapest (1964)

2. KUNII, D. and LEWENSPIEL, O., Fluidization Engineering, John Wiley and Sons, Inc. New York, London, Sydney, Toronto (1969)

3. SZOLCSÁNYI, P., Magyar Kémikusok Lapja 2, 84 (1961)

4. SZOLCSÁNYI, P., Veszprémi Vegyipari Egyetem Közleményei 2, 49 (1958)

5. KONCZ, I., Portalanitás és porleválasztás (Dust Removal, Dust Separation). Müszaki Könyvkiadó, Budapest (1970)

6. HITES, F., Dissertation for a Doctor's Degree, Veszprém (1966)

7. ORMÓS, Z., Dissertation for a Doctor's Degree, Veszprém (1968)

8. OSTROVSKI, G.M. and ISAKOV, V.P., Zhurn. Prikl. Khim 1, 100 (1973)

9. SZŐNYI, J., Fluidizációs anyagszállitási vizsgálatok (Studies on Material Transport by Fluidization) (Dissertation for a Candidate's Degree) Veszprém (1969)

РЕЗЮМЕ

Одним из методов противоточного соприкосновения гранулы и газа является способ взвешивания, с применением которого можно выгодно совершать ряд процессов (напр. сушка, сортировка).После короткого обзора касающейся литературы авторами излагается метод и аппарат опытов, выработанный ими в последные годы для изучения аэродинамических условий способа взвешивания. На рисунках показано изменение важнейших аэродинамических параметров (объемная доля гранулы, время пребывания, доля падающих вниз гранул) в зависимости от разных параметров способа (скорость газа, массовый поток твердого вещества, размер гранулы и.т.д.). Опытные результаты анализируются и предлагаются уравнения для вычисления среднего значения времени пребывания, доли падающих вниз гранул и объемной доли гранул.

Hungarian Journal
of Industrial Chemistry
Veszprém
Vol.3. pp. 631-646 (1975)

STUDIES ON GRANULATION IN FLUIDIZED BED VI.

GRANULATION IN MECHANICALLY AGITATED FLUIDIZED BED

Z. ORMÓS, B. CSUKÁS and K. PATAKI

(Research Institute for Technical Chemistry of the
Hungarian Academy of Sciences, Veszprém)

Received: September 24, 1975.

The study of the granulation in mechanically agitated fluidized bed is justified by two practical requirements: the extension of the field of application of the process on one hand, and the need for the control of the physical properties of the produced granulates within wider ranges, on the other. The numerical agitation of the fluidized bed prevents the development of anomalies in the fluidized bed, thus it renders the granulation of raw materials of bad fluidization characteristics possible, and the granulation can be carried out with increased bed moisture content. Due to the mechanical energy input, the conditions of the particle formation change, so the physical characteristics of the granulates can be efficiently influenced, varying the parameters of the auxiliary processes.

In the previous papers [1, 2, 3, 4] the main relationship found during the study of the fluidized bed granulation process in batch form were presented. In this paper experiences connected to the application of mechanical agitation - a very useful auxiliary process to the fluidized bed granulation - are summarized.

The application of auxiliary processes in the development of intensive processes is of ever increasing importance [5]. The

auxiliary processes used most often in solid-gas operations (e.g. fluidization) are mechanical agitation, vibration and special ways to introduce the gas phase (e.g. tangentially or through a nozzle).

Research on the auxiliary processes for fluidization began throughout the world with works aimed eliminating the anomalies of the fluidization process [6]. Two of these anomalies, the variation of the void fraction along the height of the bed and the formation of bubbles, are unavoidable with gas fluidization, and these two anomalies cannot be omitted even by auxiliary processes. However, three further anomalies (formation of stagnant layers, chennelling and formation of gas plugs) can be eliminated by suitable auxiliary processes.

Formation of a stagnant layer takes place in fluidized beds of heterodisperse granulates or in beds that are too high relative to their diameters. Because of this anomaly, a stagnant layer develops above the underplate, consisting of the granulates of larger size and higher densities.

Channelling is characteristic of the fluidization of sticky materials (e.g. materials of small particle size or wet materials). When channelling occurs, the gas flows through vertical channels of high void fraction, while the major part of the bed remains stagnant.

Formation of gas plugs takes place in the fluidized beds of sticky materials at an increased bed height to bed diameter ratios. In such cases a part of the solid material in the bed is lifted up like a plug by the gasflow.

In fluidized bed granulation the preconditions for all of these anomalies are often present. In many cases, the raw material to be granulated is a heterogeneous, heterodisperse mixture, the particle size is small, and the particles are of irregular shape and their surface is uneven. Adhesion is also fostered because a certain moisture content is maintained within the bed. The larger particles formed during the agglomeration phase often establish a stagnant layer at the bottom of the bed. Thus fluidization anomalies can prevent the realization of the process or deteriorate the qualities of the granulates produced.

THE CHARACTERISTICS OF MECHANICALLY AGITATED FLUIDIZED BEDS

It was generally found [7, 8] that mechanical agitation decreases the minimum fluidization velocity and the pressure drop on the bed, and it makes the expansion of the fluidized bed more even. In mechanically agitated beds the probability of the development of fluidization anomalies diminishes, so the process can be used for materials that otherwise cannot be fluidized. Because of the change in the flow conditions, the mixing is better and there is an increase in the rates of the mass and heat transfer [9]. Agitation is most efficient at the bottom of the bed and the optimum speed of rotation is relatively low.

By increasing the speed of rotation up to a given limit the minimum fluidization velocity and the pressure drop decrease, and the uniformity of the fluidization improves. A further increase in the speed of rotation impairs the fluidization properties and eddies are formed in the bed. Optimum speed of rotation values found by various authors are summarized in Table 1 and the diameters of the apparatus used are also shown.

Table 1

Material studied	Diameter of the apparatus (m)	R.p.m., (1/min)	Reference
Fine powders (ZnO, PbO, $BaSO_4$)	0.03-0.3	20-60	[7]
Glass beads	0.225	100	[8]
Silica gel	0.1	60	[10]
Catalyst	0.05	57	[11]
Fluor	0.15	25	[12]

It was universally found that agitation is most efficient if the stirrer is mounted just above the underplate. This suggests that agitation is needed, not so much to keep the fluidized bed in motion, but rather to ensure the uniformity of the gas distribution.

There are numerous references on the types of stirrers, some of them are contradictory. It was found [8] that rod stirrers have some advantages over blade stirrers, since in the case of a rod stirrer particles more easily get behind the stirrer. According to other authors [11] blade stirrers are also suitable, provided the wings of the stirrer are bent forward into the direction of the rotation, thus avoiding the compacting effect of the centrifugal force along the periphery. Several authors describe cage stirrers, underlining the advantages of the agitation along the full height of the fluidized bed [9].

After the development of the fluidized state, the power requirement of the mechanical agitation of the loosened bed is independent of the gas velocity. The power demand is given by the following expression [7]:

$$Eu_k = c_1 \, Re_k^{-c_2} \tag{1}$$

and since $c_2 \approx 1$, in the case of a given material system:

$$N = c_3 \, n^2 \, D^3 \tag{2}$$

To describe the relationship between the linear gas velocity and the average void fraction of mechanically agitated fluidized beds, the following expression was suggested [10]:

$$u'' = c_4 \, \bar{\varepsilon}^{c_5} \tag{3}$$

where c_4 and c_5 depend on the parameters of the agitation.

Fluidization in mechanically agitated fluidized beds was used to realize several processes (e.g. mixing [7], drying [14], heterogeneous chemical reaction [13], heterogeneous catalytic chemical reaction [11]). However, no reference was found to granulation processes carried out in mechanically agitated fluidized beds.

EXPERIMENTAL APPARATUS AND METHOD [16]

The laboratory granulation experiments were carried out in the apparatus shown in Figure 1. In the 1-fluidization apparatus (diameter: 0.1 m, height: 0.4 m) the 3-fluidized bed is above the 2-underplate. Air is introduced into the space below the air-distributing underplate via the 4-flowmeter and 5-electric preheater. The air having passed through the bed, leaves through the 6-sieve cylinder located at the top of the apparatus. The temperature of the air is measured at the inlet and outlet by the 7-thermometers.

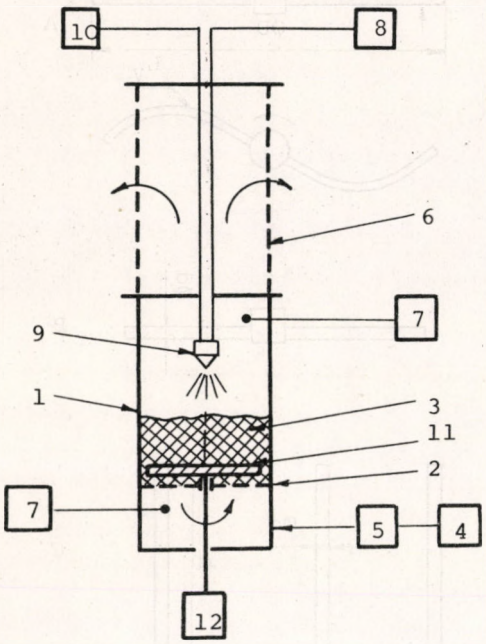

Figure 1

The granulating liquid containing the binder is fed into the 9-atomizer by the 8-pump. The amount of atomizing air needed for the operation of the two-fluid atomizer is measured by the 10-rotameter. The 11-stirrer above the underplate is driven by the 12--variable speed electromotor.

Three different types of stirrers were used throughout the experiments (Figure 2):

A: blade stirrer bent in the direction of the rotation (this gives a centripetal impulse to the particles offsetting the compacting effect of the centrifugal force along the periphery);

B: rod stirrer;

C: anchor stirrer with vertical rods efficient in the full height of the dense layer.

- a 2:1 mixture of lactose and starch (this is a model substance of bad fluidization properties, it is marked further on as M1);
- and a quartz sand fraction of 0.1-0.2 mm (that is a model substance with good fluidization characteristics, it will be marked further on as M2).

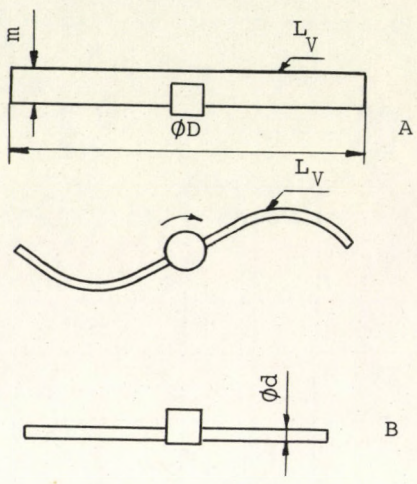

Fig.2. L_V = 2, Ø D = 100, Ø d = 5, m^V = 15, h = 60

The granulating liquid was an aqueous gelatine solution (concentration: 60 g/l).

Having preheated the raw material to be granulated, the solution containing the binder was fed in at a given rate. During the atomization, the minimum height of the fluidized bed was measured at certain intervals, and the velocity of the fluidizing air was adjusted so that the bed extension (that is the ratio of the bed height to the minimum bed height) should always be 1.6. Having finished the introduction of the liquid, the granulates produced were dried, maintaining the fluidized state for a while. Finally, the particle size distribution, porosity, bulk density, rollingness and the wear-strength of the granulates were determined. The physical properties of the granulates were determined according to the methods described in the previous papers [1, 15].

Throughout the experiments presented here, the inlet air temperature was 70 °C, the minimum bed height of the raw material was

0.007 m, the distance between the underplate and the atomizer was 0.19 m. The volumetric flow rate of the atomizing air was adjusted to an optimum value corresponding to the liquid feed rate.

EXPERIMENTAL RESULTS [16]

The most important operational parameter of fluidized bed granulation is the relative quantity of the granulating liquid, which can be characterized by the volume of the liquid used for a unit volume of the particles to be granulated. At a given liquid feed rate, the relative amount of the binder-containing solution determines the time of the granulation process and the amount of the solid binder ensuring the agglomeration, i.e. the binder content of the granulates. On the other hand, the amount of the solvent in the granulating liquid determines the heat demand of both the granulation and the drying process.

An experimental series will be presented in the following section as an example. It was carried out using the "A" blade stirrer (100 r.p.m.) and the effect of the relative amount of the liquid on the granulation process was studied. The feed rate of the granulating liquid was constant ($w' = 6.8 \times 10^{-5}$ kg/s).

It is clear from Figure 3 that because of the disintegrating effect of the agitation, the slope of the approximately linear average particle size vs. relative amount of liquid curves decreases errespective of the quality of the model substance studied. This means that to obtain a given average particle size, more binder has to be introduced into the fluidized bed. At the same time, it was found that with mechanical agitation the relative amount of the liquid could be increased (without agitation, a relative wetting value as high as 50 per cent cannot be realized).

In Figure 4 the size deviation of the particle size distribution is shown as the function of the relative amount of the liquid. The deviation was calculated by the following expression

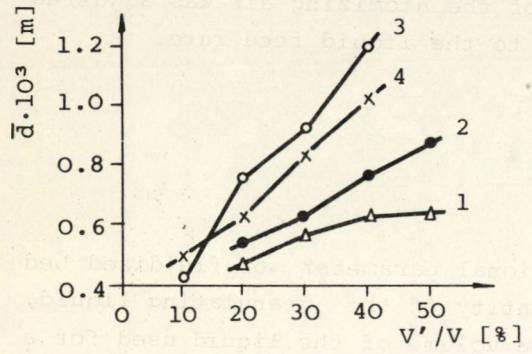

Fig.3. 1-M1} with 3-M1} without
2-M2} stirrer 4-M2} stirrer

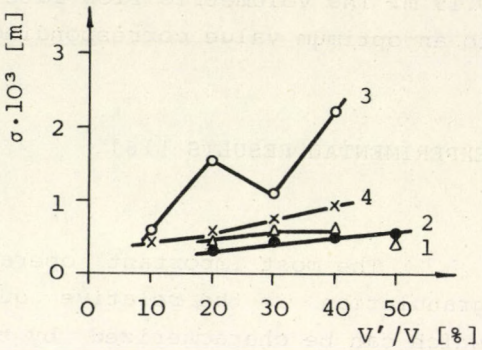

Fig.4. 1-M1} with 3-M1} without
2-M2} stirrer 4-M2} stirrer

$$\sigma = ae^{\frac{7}{2}b^2}\sqrt{e^{b^2} - 1} \qquad (4)$$

substituting the parameters of the lognormal distribution function

$$W'(x) = \frac{x^2}{a^3\, be^{\frac{9}{2}b^2}\sqrt{2\pi}} \exp\left[-\frac{(\ln x - \ln a)^2}{2\, b^2}\right] \qquad (5)$$

approximating rather correctly the particle size distribution of the granulates.

It can be seen from Figure 4 that without mixing (especially with the model substance M1) the deviation increases with increasing V'/V, while with mechanical agitation the deviation is invariant with regard to changes in the relative amount of the liquid.

The cause of the invariance of the deviation becomes clear if one inspects the changes of the amount of the ungranulated particles smaller than 0.2 mm, and that of the "overgranulated" particles of more than 2.0 mm. It is shown in Figure 5 that the amount of the ungranulated particles as a function of the duration of the atomization approaches a minimum and this change is not influenced by the mechanical agitation. However, in Figure 6 it can be seen

that the amount of the particles larger than 2 mm is considerably decreased by the agitation. Without agitation the amount of the overgranulated fraction increases in function of V'/V, but in a mechanically agitated fluidized bed there is no significant change. The stirrer rotating at the bottom of the bed disintegrates the larger particles, and restricts the upper limit of the particle size distribution, thereby decreasing the size deviation.

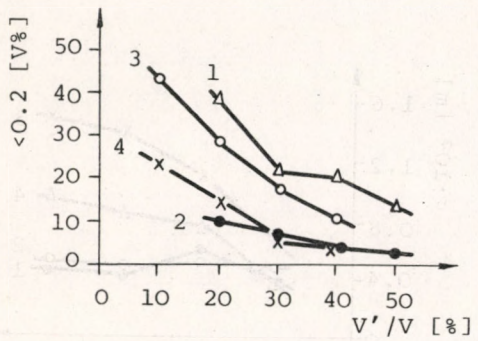

Fig.5. 1-M1, 2-M2 with stirrer; 3-M1, 4-M2 without stirrer

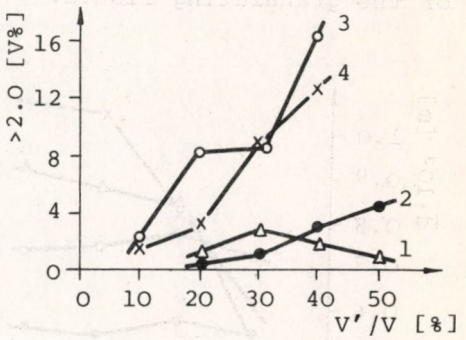

Fig.6. 1-M1, 2-M2 with stirrer; 3-M1, 4-M2 without stirrer

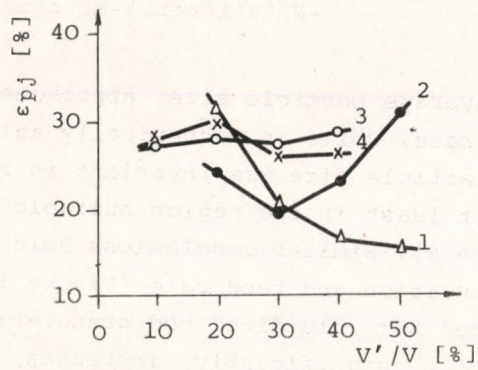

Fig.7. 1-M1, 2-M2 with stirrer; 3-M1, 4-M2 without stirrer

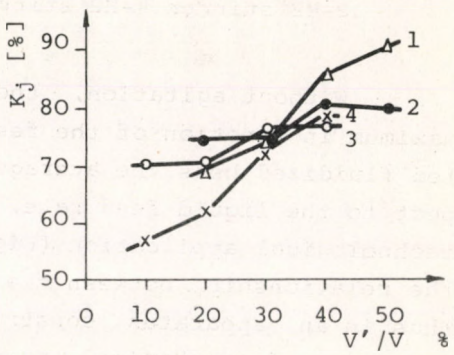

Fig.8. 1-M1, 2-M2 with stirrer; 3-M1, 4-M2 without stirrer

It can be seen in Figure 7 that the mechanical agitation decreases the porosity of the characteristic product fraction (the particle size range of the latter is 0.63-1.0 mm), while it some-

what improves its wear-strength (Figure 8). Agitation breaks up the weaker bonds, decreases the average particle size and the porosity of the particles, and increases the wear-strength of the granulates.

In another experimental series the effects of mechanical agitation (stirrer: "A"; 100 r.p.m.) were studied at a constant relative liquid amount of $V'/V = 40$ per cent, changing the feed rate of the granulating liquid.

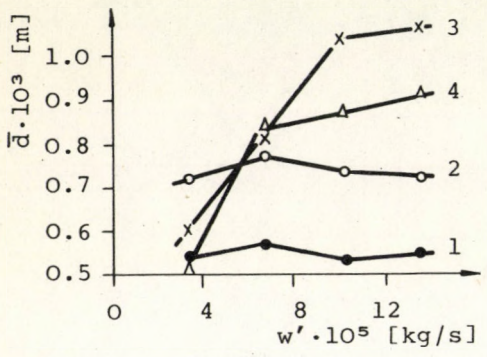

Fig.9. 1-M1 } with 2-M2 } stirrer 3-M1 } without 4-M2 } stirrer

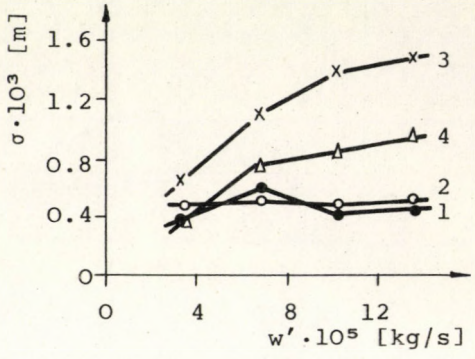

Fig.10. 1-M1 } with 2-M2 } stirrer 3-M1 } without 4-M2 } stirrer

Without agitation, the average particle size approaches a maximum in function of the feed rate, while in mechanically agitated fluidized beds the average particle size was invariant in respect to the liquid feed rate, at least in the region suitable for technological application (Figure 9). Similar conclusions hold for the relationship between the deviation and feed rate (Figure 10) Thus in an apparatus constructed for fluidized bed granulation the use of mechanical agitation significantly increases the achievable rate of atomization, this means that the duration of the operation can be reduced. This very advantageous effect of the agitation is achieved because the mechanical energy input permits the fluidized state to be maintained at a higher bed moisture content, and at the same time the mixing element disintegrates the larger loose particles almost at the very instant of their formation.

The effects of this type of stirrer and its speed of rotation upon the physical properties of the granulates produced were also studied, granulating the model substance M1 at a V'/V = 50 per cent relative liquid amount and $w' = 10.2 \times 10^{-5}$ kg/s feed rate (under conditions where the granulation of the model substance M1, which is difficult to fluidize, would be impossible without agitation).

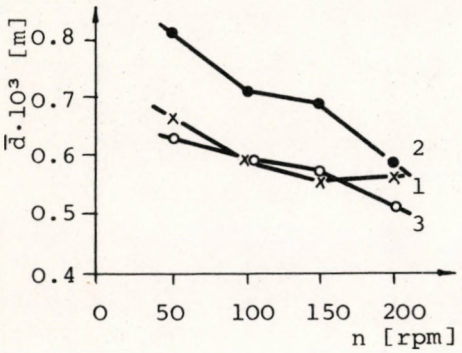

Fig.11. Stirrer type 1-II, 2-III, 3-IV

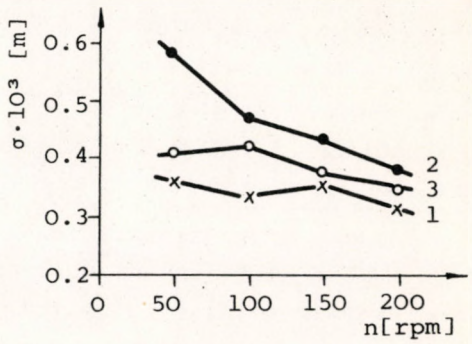

Fig.12. Stirrer type 1-A, 2-B, 3-C

It can be seen in Figures 11 and 12 that by increasing the speed of rotation, both the average particle size and the size deviation decrease. The rod stirrer marked "B" is less efficient; the use of the bent blade stirrer marked "A" seems to be best, because a bigger decrease of the deviation is achieved.

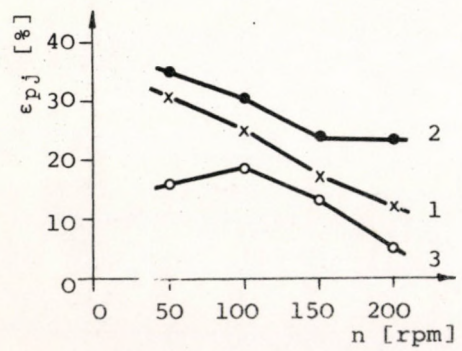

Fig.13. Stirrer type 1-A, 2-B, 3-C

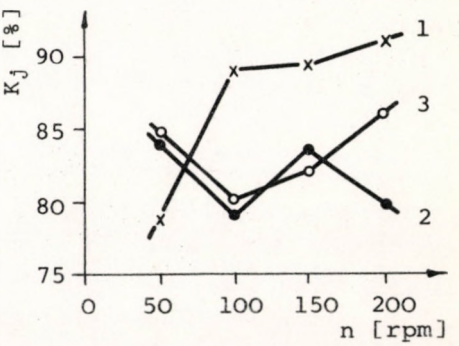

Fig.14. Stirrer type 1-A, 2-B, 3-C

The porosity of the product fraction decreases when the speed of rotation of the stirrer is increased (Figure 13); in this respect the influence of the anchor stirrer marked "C", which is efficient through the full height of the dense layer, is the most significant. A considerable improvement in the strength could be observed only with the bent blade stirrer marked A.(cf. Figure 14) upon increasing the rotation speed.

On the basis of the experimental results presented (and others not given here) it was concluded that the most suitable stirrer from the types studied here is the blade stirrer bent in the direction of the rotation, and the optimum rotation speed in a fluidized bed of a diameter of 0.1 m is 50 ∿ 100 r.p.m.

In view of these experimental results, attention can be turned to a more detailed discussion of the effect of the agitation on the particle size distribution and how the amount of the product fraction of given size limits (δ_1, δ_2) is effected by the mechanical agitation. Using the distribution function (1), the

$$\int_{\delta_2}^{\delta_1} \frac{x^2}{a^3 b e^{\frac{9}{2} b^2} \sqrt{2\pi}} \exp\left[-\frac{(\ln x - \ln a)^2}{2 b^2}\right] dx: = \max! \qquad (6)$$

extreme value of Equation (6) is sought to determine the most abundant product fraction.

In a previous paper [4] the conditional equations of the extreme value of Equation (6) were described:

$$a e^{3b^2} = \sqrt{\delta_1 \delta_2} \qquad (7)$$

and

$$\frac{1}{b} \ln \left(\frac{\delta_2}{\delta_1}\right): = \max! \qquad (8)$$

On the basis of the example given in Figure 15 it can be seen that mechanical agitation decreases the values of both the distribution parameters "a" and "b", if the speed of rotation is increased. According to a

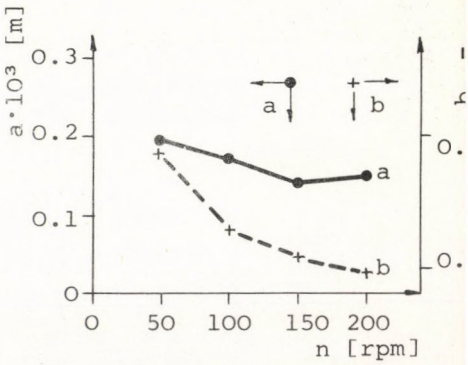

Fig. 15

trivial interpretation of Equation 8 , the amount of a fraction of any size limits (δ_1, δ_2) can be increased by the application of mechanical agitation.

CONCLUSIONS

The main conclusions drawn from the experimental results are as follows:

1. In fluidized beds of model substances suitable for developing fluidization anomalies, channelling can be stopped by mechanical agitation.
2. Particles of larger size, formed in the fluidized bed and gathered in the bottom, are kept in motion by the mechanical stirrer.
3. Because of the agitation, the relative amount and feed rate of the granulating liquid can be increased, for the fluidized state can be maintained even at higher bed moisture contents.
4. The stirrer disintegrates the larger particles gathered at the bottom of the fluidized bed, and cuts back the upper limit of the particle size distribution.
5. The deviation of the particle size distribution is decreased by the mechanical agitation and the amount of the "product fraction" of given size limits is increased.
6. The weaker bonds are broken up by the agitation, therefore the wear-strength of the granulates produced improves.
7. The porosity of the granulates is decreased by mechanical agitation.
8. The relative deviation of the size distribution of the granulates is decreased by the agitation, therefore the value of the rollingness-coefficient increases.
9. Among the stirrer types studied, the blade stirrer bent into the direction of the rotation is more efficient than either the rod stirrer or the anchor stirrer.

10. The optimum speed of rotation in an apparatus of 0.1 m diameter was found to be 70 ∿ 100 r.p.m.

SYMBOLS USED

a	parameter of the lognormal distribution (mm)
b	parameter of the lognormal distribution (dimensionless)
c_1-c_5	constants (dimensionless)
d	diameter of the stirrer rod (mm)
$\bar{d}$	average particle size (mm)
D	diameter of the stirrer (mm)
Eu_k	mixing Euler's Number (dimensionless)
h	height of the stirrer rod (mm)
K_j	wear-strength of the granulates (per cent)
L_v	width of the stirrer blade (mm)
m	height of the stirrer blade (mm)
N	power demand of the agitation (watt)
Re_k	mixing Reynolds' Number (dimensionless)
u"	gas velocity (m/s)
V	volume of the particles of the solid material to be granulated (cm^3)
V'	volume of the granulating liquid (cm^3)
w'	feed rate of the granulating liquid (kg/s)
W'(x)	density function of the lognormal distribution based on the particle volume (dimensionless)
x	particle size (mm)
δ_1, δ_2	size limits (mm)
$\bar{\varepsilon}$	average void fraction (dimensionless)

ε_{pj} porosity of the characteristic fraction (per cent)

σ deviation of the W'(x) distribution (mm)

REFERENCES

1. ORMÓS, Z., PATAKI, K., CSUKÁS, B., Hung. J. Ind. Chem. 1, 307 (1973)

2. ORMÓS, Z., PATAKI, K., CSUKÁS, B., Hung. J. Ind. Chem. 1, 463 (1973)

3. ORMÓS, Z., PATAKI, K., CSUKÁS, B., Hung. J. Ind. Chem. 1, 475 (1973)

4. ORMÓS, Z., CSUKÁS, B., PATAKI, K., Hung. J. Ind. Chem. 3, 193 (1975)

5. BLICKLE, T., ORMÓS, Z., Energiagazdálkodás, 13, 2 (1972)

6. BLICKLE, T., A fluidizációs eljárás készülékei, alkalmazása és számitásai. (The apparatus, applications and calculations of the fluidization process.) Akadémiai Kiadó, Budapest 1963.

7. KOZULIN, N.A., KULYAMIN, A.F., Intern. Chem. Eng. 5, 157 (1965)

8. BORLAI, O., ANGELINO, H., Lecture presented at the Chemists' Conference Miskolc, 1968.

9. COUDREC, J.P., ANGELINO, H., ENJALBERT, M., Chem. Eng. Sci. 21, 533 (1966)

10. GODARD, K., RICHARDSON, J.F., Chem. Eng. Sci. 24, 194 (1969)

11. BEBER, O.L. et al., US. Pat. 2,856,273 (1958)

12. BREKHON, R.A. et al., Chem. Eng. Progr. Symp. Ser. 66, 277 (1970)

13. BRATER, D.C. et al., Chem. Eng. Progr. Symp. Ser. Nuclear Eng. 65, 1 (1966)

14. KHUNSTOV, I.P., SHCHICHETKIN, V.I., SAZHIN, B.S., Khim. neft. mashinostr. 10, 42 (1968)

15. ORMÓS, Z., Hung. J. Ind. Chem. 1, 207 (1973)

16. CSUKÁS, B., Granulation in Mechanically Agitated Fluidized Bed. D. Techn. Thesis. University of Chemical Engineering, Veszprém, 1972.

РЕЗЮМЕ

Изучение грануляции в механически смешанном псевдоожиженном слое является важным по двум практическим требованиям: с одной стороны по расширению применения способа, а с другой стороны по требованию регулирования в расширенных пределах физических свойств полученных гранул. Механическое перемешивание псевдоожиженного слоя исключает возможность сложения ненормальностей флуидизации. Таким образом станет возможной грануляция исходных материалов с невыгодными свойствами с точки зрения флуидизации, а также грануляция сможет осуществляться и при повышенном содержании влаги слоя. Вследствие механической подводки энергии изменяются условия образования гранул и таким образом, изменением параметров подсобного процесса можно эффективно влиять на физические свойства гранул.

Hungarian Journal
of Industrial Chemistry
Veszprém
Vol.3. pp. 647-662 (1975)

GENERALIZATION AND CLASSIFICATION OF THE COEFFICIENTS OF TRANSPORT PROCESSES

A. LÁSZLÓ

(Department of Chemical Process Engineering,
Veszprém University of Chemical Engineering)

Received: September 30, 1975.

It is demonstrated that the three transport terms supplementing the continuity equation can be written in two forms: with reference to the potential and density. It is shown that the coefficients on the terms written with reference to the density can be arranged into a consistent system: their dimension according to length is L^2T^{-1}, that according to surface area is LT^{-1} and that according to the volume is L^0T^{-1}. The advantages of classification and generalization are presented for the case of dimensionless numbers, which are extremely important in engineering practice. Finally, an example is given for the application.

1. Introduction

It is generally known that the fundamental Equation of all flow systems is the continuity law:

$$\operatorname{div} [\bar{j}] = \operatorname{div} [\Gamma \bar{v}] = - \frac{\partial \Gamma}{\partial t} \qquad (1)$$

In a three-dimensional space, this Equation can have three supplementary terms, according to whether the possible process occur along the l e n g t h, the s u r f a c e or in s p a c e.

Generally these processes are termed:

1. along the length: transport
2. on the surface: transfer
3. in space: transformation

processes. An example for the first point is diffusion, for the second one, a transfer process occurs at the boundary of two phases (e.g. heat transfer), for the third one a chemical reaction taking place in space.

The first step of generalization is the following: an e x t e n s i v e quality characteristic of the streaming fluid can always be found and generally the symbol Ψ is used for it. The intensive quantity pertaining to Ψ is the well-known potential Φ. The connection between these two quantities is, at a first approximation, a linear one:

$$\Psi = C\,\Phi \tag{2}$$

The proportionality factor is the capacity for which the symbol C is used (at the same time, the above Equation is the definition of capacity). Similarly, at a first approximation, there is a linear connection between current (or current intensity) and potential:

$$J = K\,\Phi \tag{3}$$

It is important from the point of view of the order that a further characteristic intensive quantity exists: the generalized density, which can be derived from Equation (2) in such a manner that both sides of the Equation refer to unit volume:

$$\frac{\Psi}{V} = \Gamma \tag{4}$$

where Γ is the generalized density and

$$\frac{C}{V} = c \tag{5}$$

where c is the specific capacity which maintains a connection between the two intensive quantities:

$$\Gamma = c\,\Phi \tag{6}$$

On the basis of Equation (6) there are two possible ways of discussion of the currents, the two being equivalent to each other. The currents can be deducted as the results of the $\Delta\Phi$ potential differences arising in the potential space $\Phi\,(x \cdot y \cdot z \cdot t)$, or as the results of the $\Delta\Gamma$ density differences in the $\Gamma(x,y,z,t)$ density space.

In the case of the longitudinal transport laws - mentioned in the introduction - this generalization has been performed in the course of historic evolution and as a result of practice. It has gained a broad field, although in many cases it is not used consciously. Consequently it was included in summarizing Table 1 for the sake of comparison as well as that of completeness.

The physical base and the justification of the generalization is that the densities are in every case unequivocal functions of the potentials. The reason for the generalization and the basis of the systematization is the recognition that if this is required in practice in the case of the diffusion-type, i.e. longitudinal currents, the same necessarily has to be carried out in the case of transfer processes occurring on a surface and for transformation processes occurring in space. It will be seen that in addition to the systematization, this leads to new recognitions.

2. Transfer Current-Densities or Fluxes

According to Equation (6), the transfer current densities can be written in two manners into Equation (1):

$$\text{current-density} = (\text{transfer coefficient})\ \text{potential}$$

$$\text{current-density} = \frac{\text{transfer coefficient}}{\text{specific capacity}}\ \text{density}$$

Accordingly, the following Equations can be written:

for a component:	$\bar{j} = \beta \Delta c_i$	$\bar{j} = \beta' \Delta c_i$	(7)
for heat:	$\bar{j} = \alpha \Delta T$	$\bar{j} = \alpha' \Delta(\rho c_p T)$	(8)
for momentum:	$\bar{j} = \gamma \Delta \bar{v}$	$\bar{j} = \gamma' \Delta(\rho \bar{v})$	(9)
generally:	$\bar{j} = \varepsilon \Delta \Phi$	$\bar{j} = \varepsilon' \Delta \Gamma$	(10)

Table 1

	Extensive quantity	Density	Potential	Specific capacity	Currents	Convection	TRANSFORMATION with density	TRANSFORMATION with potential	Volumetric flow rate
Mass	m	$\rho = \frac{m}{V}$	ρ	1	$\frac{dm}{dt}$	$\bar{j} = \rho\bar{v}$	$k^{*\prime}\rho$	$k^{*}\rho$	$k^{*\prime} = k$
Component	$N_i = \frac{m_i}{M_i}$	$c_i = \frac{N_i}{V}$	c_i	1	$\frac{dN_i}{dt}$	$\bar{j} = c_i\bar{v}$	$k'c_i$	kc_i	$k' = k$
Heat	$Q = mc_pT$	$\frac{Q}{V} = \rho c_pT$	T	ρc_p	$\frac{dQ}{dt}$	$\bar{j} = \rho c_pT\bar{v}$	$\ell'\rho c_pT$	ℓT	$\ell' = \frac{\ell}{\rho c_p}$
Momentum	$m\bar{v}$	$\rho\bar{v} = \frac{m\bar{v}}{V}$	$\bar{v}$	ρ	$\frac{d(m\bar{v})}{dt}$	$\bar{j} = (\rho\bar{v})o\bar{v}$	$n'\rho\bar{v}$	$n\bar{v}$	$n' = \frac{n}{\rho}$
Generalized quantity	Ψ	$\Gamma = \frac{\Psi}{V}$	Φ	$c = \frac{\Gamma}{\Phi}$	$J = \frac{d\Psi}{dt}$	$\bar{j} = \Gamma\bar{v}$	$\frac{J}{V} = \frac{K}{cV}\Gamma$	$\frac{K}{V}\Phi$	$k' = \frac{k}{c}$

	TRANSPORT with density	TRANSPORT with potential	Diffusivity	TRANSFER with density	TRANSFER with potential	Generalized rate
Mass	$\bar{j} = -\mathfrak{D}'\text{grad}\ \rho$	$\bar{j} = -\mathfrak{D}\text{grad}\ \rho$	$\mathfrak{D} = \mathfrak{D}'$	$\bar{j} = \beta^{*\prime}\Delta\rho$	$\bar{j} = \beta^{*}\Delta\rho$	$\beta^{*\prime} = \beta^{*}$
Component	$\bar{j} = -D'\text{grad}\ c_i$	$\bar{j} = -D\text{grad}\ c_i$	$D = D'$	$\bar{j} = \beta'\Delta c_i$	$\bar{j} = \beta\Delta c_i$	$\beta' = \beta$
Heat	$\bar{j} = -a\ \text{grad}(\rho c_pT)$	$\bar{j} = -\lambda\ \text{grad}\ T$	$a = \frac{\lambda}{\rho c_p}$	$\bar{j} = \alpha'\Delta(\rho c_pT)$	$\bar{j} = \alpha\Delta T$	$\alpha' = \frac{\alpha}{\rho c_p}$
Momentum	$\bar{j} = -\nu\ \text{Grad}(\rho\cdot\bar{v})$	$\bar{j} = -\eta\ \text{Grad}\ \bar{v}$	$\nu = \frac{\eta}{\rho}$	$\bar{j} = \gamma'\Delta(\rho\bar{v})$	$\bar{j} = \gamma\Delta\bar{v}$	$\gamma' = \frac{\gamma}{\rho}$
Generalized quantity	$\bar{j} = -\varkappa'\text{grad}\ \Gamma$	$\bar{j} = -\varkappa\ \text{grad}\ \Phi$	$\varkappa' = \frac{\varkappa}{c}$	$\bar{j} = \varepsilon'\Delta\Gamma$	$\bar{j} = \varepsilon\Phi$	$\varepsilon' = \frac{\varepsilon}{c}$

The first result is that the coefficients of the transfer current-densities: β', α' and γ' are of the same dimension: LT^{-1} and consequently they are termed generalized rates. The connection between the transfer coefficients used in practice and the generalized rates defined by Equations (7), (8), (9) and (10) can be expressed by the following Equations:

$$\beta' = \beta \tag{11}$$

$$\alpha' = \frac{\alpha}{\rho c_p} \tag{12}$$

$$\gamma' = \frac{\gamma}{\rho} \tag{13}$$

$$\varepsilon' = \frac{\varepsilon}{c} \tag{14}$$

Accordingly, in analogy to thermal diffusivity, $a = \frac{\lambda}{\rho c_p}$ and kinematic viscosity $\nu = \frac{\eta}{\rho}$, a heat transfer rate and a momentum transfer rate can be defined on the basis of Equations (12) and (13). It should be remarked that Equations (7), (8), (9) and (10) are in close relation to the generalized Ohm's law, as has been pointed out in a number of papers [1].

3. Transformations in Space

Generalization is more difficult in this case as in the two previous ones. The fact is that along a length or a surface it is a p r i o r i current densities ($\bar{j}$) that are defined and accordingly, these quantities can be written into Equation (1) without any difficulty.

In the case of volume fluxes, the following transformations are carried out, starting from the definition:

$$\frac{J}{V} = \frac{K}{V}\Phi = k\,\Phi = \frac{K}{c\,V}\Gamma = k' \tag{15}$$

where the following connections prevail between the coefficients:

$$\frac{K}{V} = k \quad \text{and} \quad \frac{K}{c\,V} = \frac{k}{c} = k' \tag{16}$$

Any form presented in Equation (15) can now be written into Equation (1) since their dimension is identical to that of the terms of the Equation.

However, the generalization of the coefficients is a more difficult assignment. There is no problem in the case of a component stream and if the chemical transformation is of the first order, since

$$k' = k \tag{17}$$

and their dimension is T^{-1}. If the order of the transformation studied is other order than one, either of two ways can be followed. First, the concentrations in the rate equation are expressed in the form of mole fractions (mathematically speaking, they are normalized to one) whereby Equation (17) is rendered valid to chemical transformations of any order. The second possibility is that according to classical reaction kinetics, concentrations are raised to some power and in this case the logarithm of the volume currents is applied. Equation (17) is also valid in this case, only both sides of it are taken into consideration with the same multiplication factor.

In the case of heat, when convective or conductive heat currents are studied, the heat source or heat absorber is in all cases proportional to the temperature [2]. The generalization is successful even in this case, since - in a manner similar to Equation (12) - we can write:

$$\ell' = \frac{\ell}{\rho c_p} \quad [T^{-1}] \tag{18}$$

Radiant heat was disregarded in this case. In the case of heat radiation, the heat quantity liberated (or absorbed) is proportional to some power of the temperature T. For example, in the case of the well-known Stefan-Boltzmann law it is the fourth power of temperature: T^4.

In the case of momentum the connection corresponding to Equation (1) is the Navier-Stokes law, known for the longest time. However, in this case the volumetric current i.e. the momentum source or absorber was so far written as the gradient of the pressure p by the authors, and the other terms as the function of the rate. This problem is also solved by the uniform description and point of view.

It can be written for the momentum source or absorber in the direction x:

$$\frac{d\ m\ v_x}{dt\ d\ V} = \frac{d}{dt}\ \frac{dm}{d\ V}\ \frac{d\ v_x}{d\ V} \tag{19}$$

differentiation with respect to time can be written as an operator $\frac{d}{dt} = n'$ and, accordingly, considering all the three directions of space, we obtain:

$$n'\Delta(\rho\bar{v}) = n\Delta\bar{v} \quad \text{grad } p \tag{20}$$

and, in analogy to Equation (13) we can write:

$$n' = \frac{n}{\rho} \tag{21}$$

where the dimension of n' is also T^{-1} and n $[ML^{-3}T^{1}]$ is the momentum liberated or absorbed in unit volume during unit time.

4. Applications

As the results of generalization and classification, the coefficients are summarized in Tables 2 and 3 first in generalized form, and thereupon for the case of the component, heat and momentum. The coefficients expressed with potentials and already known were included in Table 2 in order to enable comparison with the generalized coefficients presented in Table 3.

It is apparent from Table 2 that the dimensions of the coefficients are different in all three cases (line 2) and so are their units (lines 3, 4 and 5).

Table 2. Expression of the coefficients with potentials

Definition	$\frac{K}{L} = \kappa$ $(\frac{\text{conductivity}}{\text{length}})$	$\frac{K}{S} = \varepsilon$ $(\frac{\text{conductivity}}{\text{length}})$	$\frac{K}{V} = k$ $(\frac{\text{conductivity}}{\text{length}})$
General	$\kappa(\Psi L^{-1}T^{-1}\Phi^{-1})$	$\varepsilon(\Psi L^{-2}T^{-1}\Phi^{-1})$	$k = (\Psi L^{-3}T^{-1}\Phi^{-1})$
Component	D m^2s^{-1}	β m s^{-1}	k s^{-1}
Heat	λ(kcal $m^{-1}s^{-1}$degree^{-1})	α(kcal $m^{-2}s^{-1}$degree^{-1})	ℓ(kcal $m^{-3}s^{-1}$degree^{-1})
Momentum	η kg $m^{-1}s^{-1}$	γ kg $m^{-2}s^{-1}$	n kg $m^{-3}s^{-1}$

Table 3. Expression of the coefficients with densities

	1. Transport	2. Transfer	3. Transformation
Definition	$\kappa' = \frac{K}{cL} = \frac{\kappa}{c}$	$\varepsilon' = \frac{K}{cS} = \frac{\varepsilon}{c}$	$k' = \frac{K}{cV} = \frac{k}{c}$
Generalized	$L^z\ T^{-1}$	$L\ T^{-1}$	$L^0\ T^{-1}$
Component	$D' \equiv D\ (m^2 s^{-1})$	$\beta' \equiv \beta\ (m\ s^{-1})$	$k' \equiv k\ (s^{-1})$
Heat	$a = \frac{\lambda}{\rho c_p}\ (m^2 s^{-1})$	$\alpha' = \frac{\alpha}{\rho c_p}\ (m\ s^{-1})$	$\ell' = \frac{\ell}{\rho c_p}\ (s^{-1})$
Momentum	$\nu = \frac{\eta}{\rho}\ (m^2 s^{-1})$	$\gamma' = \frac{\gamma}{\rho}\ (m\ s^{-1})$	$n' = \frac{n}{\rho}\ (s^{-1})$

It is readily apparent from Table 3 that the dimension of the longitudinal coefficients is always $[L^2T^{-1}]$, that of the coefficients pertaining to the surface is $[L \cdot T^{-1}]$, that is to say, the generalized rate; in the case of the volume it is $[L^0T^{-1}]$ which can be called the volumetric rate, or, with a well-established industrial term, volumetric flow rate.

An important field of application is the generalization classification and reduction to a simpler form of dimensionless numbers. If the right side of Equation (1) is regarded as zero, i.e. a stationary state is considered, the Equation contains four terms: the original convective term and the three fluxes discussed in the foregoing for all quantities, i.e. separately for component, heat and momentum. These possibilities are presented in Table 4. It can be seen that when reflected across the diagonal, the reciprocal values of the numbers appear on the other side. Due to historical reasons, from among the numbers under the diagonal it is only $(\frac{\text{convection}}{\text{conduction}})$ that became generally used. It is to be noted that the dimensionless quantities presented in Table 4 are not all independent of one another; however, this problem is outside of the scope of the present paper.

It is shown in Table 5 to what extent the generalized coefficients simplify the dimensionless numbers. (For the sake of comparison, the old expressions were also included.) The classification also has a theoretical significance in addition to generalization. Actually, if the dimensionless numbers thus expressed are compared by pairs, in the cases $(\frac{\text{momentum}}{\text{heat}})$, $(\frac{\text{momentum}}{\text{component}})$ and $(\frac{\text{heat}}{\text{component}})$ dimensionless numbers of the character of efficiency are obtained, very much like the Prandtl, Schmidt and Lewis numbers in the case of diffusion. Accordingly, we obtain:

$$\frac{\gamma'}{\alpha'} \quad \text{corresponds to the Pr number} \tag{22}$$

$$\frac{\gamma'}{\beta'} \quad \text{corresponds to the Sc number} \tag{23}$$

and

$$\frac{\alpha'}{\beta'} \quad \text{corresponds to the Lewis number} \tag{24}$$

Table 4. System of dimensionless numbers of stationary current

	$\frac{\text{convection}}{\text{convection}}$	$(\frac{\text{transport}}{\text{convection}})$	st'		Da I
			st	$\frac{\text{transfer}}{\text{convection}}$	Da III $\frac{\text{transformation}}{\text{convection}}$
			f/2		We^{-1}
Pe'			Nu'		Da II
Pe	$\frac{\text{convection}}{\text{transport}}$	$\frac{\text{transport}}{\text{transport}}$	Nu	$\frac{\text{transfer}}{\text{transport}}$	Da IV $\frac{\text{transformation}}{\text{transport}}$
Re			Nu*		B*
					C*
	$(\frac{\text{convection}}{\text{transfer}})$	$(\frac{\text{transport}}{\text{transfer}})$		$\frac{\text{transfer}}{\text{transfer}}$	D* $\frac{\text{transformation}}{\text{transfer}}$
					E*
	$(\frac{\text{convection}}{\text{transformation}})$	$(\frac{\text{transport}}{\text{transformation}})$		$(\frac{\text{transfer}}{\text{transformation}})$	$\frac{\text{transformation}}{\text{transformation}}$

Table 5. Generalized and usual forms of dimensionless numbers

Component	$(\frac{\text{convection}}{\text{transport}})$	$(\frac{\text{transfer}}{\text{convection}})$	$(\frac{\text{transformation}}{\text{convection}})$	$(\frac{\text{transformation}}{\text{transport}})$
	$Pe' = \frac{vd}{D}$	$st' = \frac{\beta}{\bar{v}}$	$Da\ I = \frac{k'd}{\bar{v}} = \frac{i\ d}{c_i\ \bar{v}}$	$Da\ II = \frac{k'd^2}{D} = \frac{\nu_i d^2}{c_i D}$
Heat	$Pe = \frac{vd}{a}$	$st = \frac{\alpha'}{\bar{v}} = \frac{\alpha}{\rho c_p \bar{v}}$	$Da\ II = \frac{\ell' d}{\bar{v}} = \frac{\nu_i \Gamma \Delta H d}{\rho c_p T \bar{v}}$	$Da\ IV = \frac{\ell' d^2}{a} = \frac{\nu_i \Gamma \Delta H d^2}{\lambda T}$
Momentum	$Re = \frac{vd}{\nu}$	$\frac{f}{2} = \frac{\gamma'}{\bar{v}} = \frac{\gamma}{\rho\ \bar{v}}$	$\frac{1}{We} = \frac{n'd}{\bar{v}} = \frac{F}{\rho \bar{v}^2 d^2}$ Note: F = generalized power	$B^* = \frac{n'd}{\nu} = \frac{F}{\eta \bar{v} d}$

These numbers are very important and very useful if the efficiency of component, heat or pulse transfer between two phases in contact with each other is to be calculated.

In a manner similar to Equations (22), (23) and (24), the following dimensionless numbers of the character of efficiency are obtained for the rates in a volume:

$$\frac{We}{Da_{III}} = \frac{n'}{\ell'} \tag{25}$$

$$\frac{We}{Da_{I}} = \frac{n'}{k'} \tag{26}$$

$$\frac{Da_{III}}{Da_{I}} = \frac{\ell'}{k'} \tag{27}$$

For example, the practical significance and application of the last Equation (27) can easily be demonstrated. For the sake of simplicity let us consider a chemical reaction of the first order whose rate is expressed by the well-known equation:

$$\nu_i r = k' c_i \tag{28}$$

As it is known, according to the aforesaid, the heat source corresponding to this is:

$$\nu_i r \Delta H = \ell' \rho c_p T \tag{29}$$

From Equations (28) and (29) we obtain:

$$k' c_i \Delta H = \ell' \rho c_p T \tag{30}$$

which can be also written in the following form:

$$\frac{\ell'}{k'} = \frac{c_i \Delta H}{\rho c_p T} \tag{31}$$

This latter is an explicit form of Equation (27) and represents a direct connection between theory and the quantity $(\frac{c_i \Delta H}{\rho c_p T})$, well known in reactor techniques.

SYMBOLS USED

a	thermal diffusivity ($m^2 s^{-1}$)
C	capacity (Farad)
c_i	concentration of the i^{th} component ($mole \cdot m^{-3}$)
c_p	specific heat at a constant pressure ($kcal\ kg^{-1} degree^{-1}$)
c	specific capacity ($Farad \cdot mole^{-3}$)
D_i	diffusion coefficient of the i^{th} component ($m^2 s^{-1}$)
$\bar{j}$	current-density or flux ($density \cdot m^1 s^{-1}$)
J	current intensity ($extensive\ quantity \cdot s^{-1}$)
ΔH	reaction heat ($kcal \cdot mole^{-1}$)
k	rate constant of first-order reaction (s^{-1})
k'	$\frac{K}{V}$ = ($conductivity \cdot m^{-3}$)
K	conductivity (ohm^{-1})
ℓ	coefficient of heat source ($kcal\ m^{-3} s^{-1} degree^{-1}$)
ℓ'	$\frac{\ell}{\rho c_p}$ = coefficient of heat source, as expressed with density (s^{-1})
m	mass kg
M_i	molecular weight of the i^{th} component ($kg \cdot mole^{-1}$)
N_i	mass of the i^{th} component (mole)
n	coefficient of momentum source ($kg\ m^3 s^{-1}$)
n'	coefficient of momentum source, as expressed with density (s^{-1})
Q	heat quantity (kcal) = 4.186×10^3 Joule
T	temperature (degree)
t	time (s)
$\bar{v}$	flow rate ($m\ s^{-1}$)
V	volume (m^3)

α heat transfer coefficient (kcal $m^{-2}s^{-1}degree^{-1}$)

α' heat transfer coefficient, as expressed with density (m s^{-1})

β^* mass transfer coefficient (kg s^{-1})

β component transfer coefficient (mole s^{-1})

γ momentum transfer coefficient (kg $m^{-2}s^{-1}$)

γ' momentum transfer coefficient (m s^{-1})

ε generalized transfer coefficient ($\Psi m^{-1}s^{-1}\Phi^{-1}$)

ε' generalized transfer coefficient, as expressed with density (m s^{-1})

η dynamic viscosity (kg $m^{-1}s^{-1}$)

κ generalized diffusion coefficient (Ψ $m^{-1}s^{-1}\Phi^{-1}$)

κ' generalized diffusion coefficient, as expressed with density (m^2s^{-1})

λ heat conductivity coefficient (kcal $m^{-1}s^{-1}degree^{-1}$)

ν kinematic viscosity (m^2s^{-1})

ν_i stoichiometric coefficient of the i^{th} component (-)

ρ density (kg m^{-3})

Γ generalized density

Ψ generalized extensive quantity

Φ generalized potential

REFERENCES

1. BENEDEK, P., LÁSZLÓ, A., A vegyészmérnöki tudomány alapjai (Fundamentals of Chemical Engineering Science) Müszaki Könyvkiadó, Budapest, 1964.

2. BENJAMIN, T.F. et al., Can. J. Chem. Eng. 51, 756 (1973)

РЕЗЮМЕ

Автором показывается, что три транспортных члена, дополняющих уравнение неразрывности можно представить двояким образом: при помощи потенциала и при помощи плотности. Автором выявляется, что коэффициенты членов, представленных при помощи плотности, можно включить в единую систему: размерность их по длине L^2T^{-1}, по поверхности LT^{-1}, по объему L^0T^{-1}. Преимущества систематизации и обобщения показываются в случае безразмерных чисел, важных в инженерной практике. Также излагается пример применения метода.

Hungarian Journal
of Industrial Chemistry
Veszprém
Vol.3. pp. 663-676 (1975)

STUDIES ON THE OPTIMUM OPERATION MODE OF A TWO-PHASE, EXTRACTION-COUPLED REACTOR CASCADE

Gy. MARTON

(Department of Chemical Process Engineering,
Veszprém University of Chemical Engineering)

Received: October 4, 1975.

One of the several possibilities to intensify a process unit is to carry out the selective completion of complex processes in the very same unit. Extraction is widely used in the organic synthesis industry to separate some products from other products or byproducts. If the valuable reaction product is to be extracted immediately, before its decomposition starts, the appropriate sequence of a consecutive process series has to be planned. A selective solvent has to be chosen and the solvent flow scheme has to be matched with the given conditions of the technical reaction kinetics. For a continuously operated reactor cascade the problem occurs of establishing an optimum transfer flow allocation. As an example, the algorithm of an optimum allocation is shown in the case of a continuous, extraction-coupled reactor cascade, operated in a crossed-streams mode.

INTRODUCTION

A number of technologies are known in the practice of organic synthesis industry, more specifically in pharmaceutical industry, where the valuable product of a liquid (or solid-liquid) phase reaction is separated from the reaction mixture by a diffusion separation process (stripping out, rectification, and extraction etc.). Practically all those technological steps belong to

that group which employs the extraction of a product, e.g. a hydrolysis product, from the aquaeous phase into the organic phase. This process series can be represented by the following scheme:

$$\bar{F}^{\alpha} \xrightarrow{k_{r1}} \bar{R}^{\alpha} \xrightarrow{k_D} \bar{E}^{\beta} \qquad (1)$$

where:

$\bar{F}$ is the phase state of the original (liquid) phase

$\bar{R}$ is the phase state of the raffinate state representing the product of a reaction characterized by the k_{r1} rate constant

$\bar{E}$ is the phase state of the extract phase obtained in the extraction step, characterized by the k_D effective rate constant

α, β are the phase characteristics.

However, in the given particular form the problem is not sufficiently typical, for the reaction is generally much faster than the separation, therefore the problem is reduced to a simple extractor design without any particular consequence.

However, a totally new situation arises of the R_j valuable product in the phase $\bar{R}$ decomposes in a consecutive reaction (generally speaking, a penalty function is introduced):

$$\begin{array}{ccccc} \bar{F}^{\alpha} & \xrightarrow{k_{r1}} & \bar{R}^{\alpha} & \xrightarrow{k_D} & \bar{E}^{\beta} \\ & & \downarrow {\scriptstyle M^{\alpha} k_{r2}} & & \end{array} \qquad (2)$$

Thus, in the diffusion process, the extraction can be - or rather as the aim of the optimation - should be made a competitor of the decomposition reaction. Obviously, the extraction solvent and the reaction mixture must be immiscible, the solvent must be nonreactive towards all the components involved and the yield must be sufficiently high.

The complex process outlined above is only an optimum control problem if the operation is discontinuous or an optimum allocation problem, if the process is carried out in a continuous, crossed--stream cascade system.

1. FORMULATION OF THE OPTIMUM ALLOCATION PROBLEM IN THE CASE OF AN OBJECT CONSISTING OF DISCRETE ELEMENTS

The state of an object is generally characterized by k phase co-ordinates at each discrete t, i.e. it is characterized by an $\underline{x}(x^1, \ldots, x^k)$ point of an Euclidian space [1]. Thus any $\underline{x}(t)$ phase state can be described as:

$$\underline{x}(t) = [x^1(t), \ldots, x^k(t)] \tag{3}$$

If the number of the control parameters is r, the $\underline{u}(t)$ control vector at any t discrete point is given as:

$$\underline{u}(t) = [u^1(t), \ldots, u^r(t)] \tag{4}$$

Control is therefore considered as a series of the u(1), u(2), ..., u(N) points defined within the range of the $u^1, \ldots, u^r$ variables, while the object passes through the x(0), x(1),...,x(N) phase states, thereby producing the motion trajectory of the object the t = 0, 1,..., N point [1-4].

The behaviour of the object is thereby given by the:

$$\underline{x}(t) = f_t[\underline{x}(t-1), u(t)] \tag{5}$$

formula. The t index in the f_t symbol implies that it is not necessary that the very same f(x,u) function should be considered at each of the t = 1,... N points. However, in practice this generalization is not employed to a full extent and the reduced:

$$\underline{x}(t) = f[\underline{x}(t-1), \underline{u}(t)] \tag{6}$$

formula is applied.

Let us apply the above equation to the cascade reactor and the phase states described in Equation (2). The system should consist of perfectly mixed tanks of the same volume and the system should be isotherm. It is conceivable that according to Figure 1 the u(t) control modifies the state of the extract in the successive stages or the allocation of it, respectively.

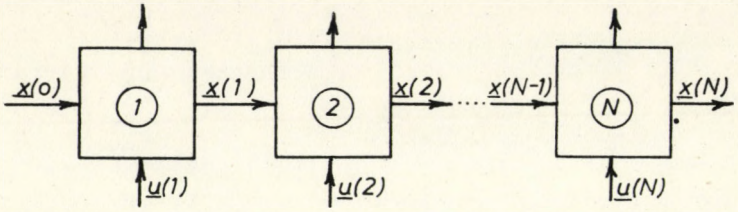

Figure 1. Schematics of the optimum control of the cascade

The optimation problem outlined above can only be applied to the crossed-stream phase contact, within the conditions given [5].

2. OPTIMATION BASED ON THE PRINCIPLE OF THE DISCRETE MAXIMUM

In most cases, the PONTRJAGIN maximum principle and dynamic programming readily lend themselves performing optimised control on such continuous processes that can be described by simple differential equations [3, 6]. A version of the former principle allowing for the handling of discrete systems, can be very efficiently algorithmised to optimise discrete objects, even within the most diverse limitations.

Let Equation (6) be the motion equation of the object, and let V be the real control area belonging to the former, the result of the optimation should be given by the following objective-function functional:

$$J = \sum_{t=o}^{N} f^{o} [\underline{x}(t-1), \underline{u}(t)] \tag{7}$$

Let us select the basic problem of optimation, when the problem can be described by the $\underline{x}(o) = \underline{y}_o$ initial condition formula and the optimity is observed at the maximum point of the functional (7).

To solve the problem the $\Psi_o, \Psi_1, \ldots, \Psi_N$ aid variables are introduced and the optimation aid function (the HAMILTONIAN) is constructed [3]:

$$H(\underline{\Psi}, \underline{x}, \underline{u}) = \sum_{i=o}^{k} \Psi_i f^{i}(\underline{x}, \underline{u}) \tag{8}$$

where f^o is the function found in the definition of functional (7), $f^1,\ldots,f^k$ are the components of the vactor function on the right hand side of Equation (6) (independent variables). Then Equation (9) is applied to the aid variables:

$$\Psi_j(t-1) = \frac{\partial H\,[\underline{\Psi}(t),\ \underline{x}(t-1),\ \underline{u}(t)]}{\partial\, x_j} \tag{9}$$

where: $j = 1,\ldots,k$

$t = 1,\ 2,\ldots,N$

Boundaries:

$$\Psi_o \equiv 1$$

$$\Psi_1(N) \equiv \Psi_2(N) \equiv \ldots \equiv \Psi_k(N) \equiv 0$$

If the $\underline{u}(t)$ control is optimised then the following equation:

$$H[\Psi(t),\underline{x}(t-1),\underline{u}(t)] = \max_{\underline{u} \in V} H[\Psi(t),\underline{x}(t-1),\underline{u}(t)] \tag{10}$$

holds at each of the $t = 1,\ 2,\ldots,\ N$ points, and consequently:

$$J = J_{opt} = J_{max} \tag{11}$$

If the same optimum is sought as a minimum value, the form of functional (7) remains unchanged but there is a boundary $\Psi_o \equiv -1$ to be recognized!

3. THE MODEL OF THE CROSSED STREAM UNIT AND THE SPECIFIC OPTIMATION PROBLEM

Based on Equation (2) assuming an unidimensional case, the balance equations of the i^{th} element of the cascade read as follows. In the α phase:

$$F_{i-1} - F_i = k_1 F_i t_i \tag{12}$$

$$R_{i-1} - R_i = -k_1 F_i t_i + k_2 R_i t_i + k_{Di}(KR_i - E_i)t_i \tag{13}$$

$$M_{i-1} - M_i = -k_2 R_i t_i \tag{14}$$

In the β phase:

$$E_{oi} - E_i = \frac{-q_i^{\alpha}}{q_i^{\beta}} K_{Di}(KR_i - E_i)t_i \tag{15}$$

where

$$k_{Di} = f(q_i^{\alpha}; q_i^{\beta}) \tag{16}$$

q is the volumetric flow rate.

Let us introduce a new variable, as follows:

$$u_i \hat{=} k_{Di} (K - \frac{E_i}{R_i}) \tag{17}$$

which is the product of the dimensionless driving force defined according to the two-film theory and of the effective component--transfer rate. In other words, this quantity is the transfer flow rate per mass unit. For k_{Di} is always a positive quantity, u_i can assume any real value (i.e. positive, negative and zero values alike).

If the objective-function relating to a certain objective is given in the following form:

$$J = \sum_{i=1}^{N} u_i t_i = \min! \tag{18}$$

then, due to the absence of limitations, the real value of u_i makes the construction of the optimizing algorithm fairly easy.

This, in fact, gives the optimum distribution of the transfer flow in each of the elements of the cascade.

3.1 The Optimizing Algorithm

Rearranging Equations (12), (13), (14) and (15), the following expressions are obtained:

$$F_i = \frac{F_{i-1}}{1 + k_1 t_i} \tag{12a}$$

$$R_i = \frac{R_{i-1} + k_1 F_i t_i}{1 + k_2 t_i + u_i t_i} \tag{13a}$$

$$M_i = M_{i-1} + k_2 R_i t_i = M_{i-1} + \frac{(R_{i-1} + k_1 F_i t_i) k_2 t_i}{1 + k_2 t_i + u_i t_i} \tag{14a}$$

$$E_i = E_{oi} + \frac{q^\alpha}{q^\beta} k_i R_i t_i \tag{15a}$$

The end state of the system should be determined by the unwanted product, M (i.e. the minimum value of $u_i t_i$ corresponding to a given M_N value is sought or conversely: the minimum value of M_N corresponding to a given $u_i t_i$ value is sought). This indeed can be done for the M_i, for it can be described by the following expression:

$$M_i = M_{i-1} + f(u_i) \tag{19}$$

Let us introduce the Z aid variable as follows:

$$Z_i \hat{=} Z_{i-1} + u_i \qquad i = 1,\ldots,N \tag{20}$$

For a cascade consisting of elements of the same volume, $t_i = t_{i+1} = t_N = t$, thereby substituting Equation (20) into the functional (18), the later becomes:

$$J = CZ_N = \max! \tag{21}$$

where $C = -1$ t (for minimalization is carried out!).

Therefore the components of the $\underline{x}$ state vector, considered as independent variables, are M_i and Z_i. In the following M; and Z; read as:

$$M_i \hat{=} x_{1i}$$

and

$$Z_i \hat{=} x_{2i}$$

Thus, the general form of the model corresponding to Equation (6) reads as:

$$x_{1i} = f_{1i}\,[x_{1(i-1)},\ \underline{u}_i] \tag{22}$$

and

$$x_{2i} = f_{2i}\,[x_{2(i-1)},\ \underline{u}_i] \tag{23}$$

In the case of n = 2, based on Equation (8), the H function reads as:

$$H_i = \sum_{k=1}^{2} \Psi_{ki}\, f_{ki}\ \underline{x}_{i-1},\ \underline{u}_i \tag{24}$$

According to Equation (9):

$$\Psi_{2O} \equiv \Psi_{2i} \equiv \Psi_{2N} \equiv -1 \tag{25}$$

According to Equation (10):

$$\frac{\partial H_i}{\partial \underline{u}_i} = O = \Psi_{1i}\,\frac{\partial f_{1i}[\underline{x}_{i-1},\ \underline{u}_i]}{\partial\ \underline{u}_i} - 1 \tag{26}$$

and

$$\frac{\partial H_{i+1}}{\partial \underline{u}_{i+1}} = O = \Psi_{1(i+1)}\,\frac{\partial f_{1(i+1)}[\underline{x}_i,\ \underline{u}_{i+1}]}{\partial \underline{u}_{i+1}} - 1 \tag{27}$$

respectively.

For, according to Equation (9):

$$\Psi_{1i} = \frac{\partial H_{i+1}}{\partial x_{1i}} = \Psi_{1(i+1)}\,\frac{\partial f_{1(i+1)}[\underline{x}_i, \underline{u}_{i+1}]}{\partial x_{1i}} \tag{28}$$

it follows from Equations (26), (27) and (28) that:

$$\frac{\partial f_{1(i+1)}(\underline{x}_i, \underline{u}_{i+1})/\partial \underline{u}_{i+1}}{\partial f_{1(i+1)}(\underline{x}_i, \underline{u}_{i+1})/\partial x_{1i}} = \frac{\partial f_{1i}(\underline{x}_{i-1}, \underline{u}_i)}{\partial\ \underline{u}_i} \tag{29}$$

In our case, considering Equation (14a), the above expression becomes more simple:

$$\frac{\partial f_{1(i+1)}(\underline{x}_i, \underline{u}_{i+1})}{\partial\ x_{1i}} = \frac{\partial M_i}{\partial M_i} \equiv 1 \tag{30}$$

Be Π_i' the sensitivity of the control and be:

$$\Pi_i' = \frac{\partial f_{1i}(\underline{x}_{i-1}, \underline{u}_i)}{\partial \underline{u}_i} \tag{31}$$

then the criterium of the optimation according to Equations (29), (30) and (31), respectively, reads as:

$$\Pi_i' = \Pi_{i+1}' = (\text{constant})'$$

$$i = 1, \ldots, N-1$$

Let the value of the optimizing parameter be:

$$\frac{\Pi_i'}{t} = \Pi = \text{constant} \tag{32}$$

Based on Equations (13a), (14a), (31) and (32):

$$\Pi = \frac{k_2 R_i t}{1 + k_2 t + u_i t} \tag{33}$$

and

$$u_{i+1} t = \sqrt{\frac{k_2 t (R_i + k_1 F_{i+1} t)}{\Pi}} - (1 + k_2 t) \tag{34}$$

respectively.

It follows from Equation (33), the criterium of the optimation is that a linear relationship should exist between u_i and R_i.

3.2 A Numerical Example to Demonstrate the Optimum Allocation

In the previous part it was shown that for a given Π value the optimizing algorithm deduces the value of the $\underline{u}_{i+1}$ control, based on the $\underline{x}_i$ state (cf. Equation (34)) then it proceeds to compute the $\underline{x}_{i+1}$ state, etc. This means that in this case the series of values of F, R and Z are found by a simple calculation, while based on these computed values, according to Fquation (14a), the

value of M_i, according to Equations (15), (16) and (17) the values of K_{Di}, E_i and q_i can be calculated, respectively.

Table 1. The effect of the Π control parameter on the $u_i t$ controls of a cascade consisting of N = 5 elements with $k_1 t = k_2 t = 1.0$; $F_o = 1.0$ and $R_o = M_o = 0.0$

	i	$u_i t$ [-]	F_i [-]	R_i [-]	M_i [-]
	1	-1.0000	0.5000	0.5000	0.5000
	2	-0.7753	0.2500	0.6124	1.1124
0.5000	3	-0.7856	0.1250	0.6072	1.7196
	4	-0.8427	0.0625	0.5786	2.2982
	5	-0.8956	0.0313	0.5522	2.8504
	1	0.0000	0.5000	0.2500	0.2500
	2	0.0000	0.2500	0.2500	0.5000
0.1250	3	-0.2679	0.1250	0.2165	0.7165
	4	-0.5060	0.0625	0.1868	0.9033
	5	-0.6794	0.0313	0.1651	1.0683
	1	1.0000	0.5000	0.1666	0.1666
	2	0.7386	0.2500	0.1521	0.3188
0.0555	3	0.2335	0.1250	0.1241	0.4429
	4	-0.1674	0.0625	0.1018	0.5447
	5	-0.4524	0.0313	0.0860	0.6307
	1	2.0000	0.5000	0.1250	0.1250
	2	1.4641	0.2500	0.1083	0.2333
0.0312	3	0.7321	0.1250	0.0854	0.3186
	4	0.1753	0.0625	0.0680	0.3866
	5	-0.2181	0.0313	0.0557	0.4423
	1	3.0000	0.5000	0.1000	0.1000
	2	2.1833	0.2500	0.0837	0.1837
0.0200	3	1.2301	0.1250	0.0646	0.2483
	4	0.5209	0.0625	0.0504	0.2987
	5	0.0207	0.0313	0.0404	0.3391

As an example, be $k_1 t = k_2 t = 1.000$ [-], $F_o = 1.000$ [-], and $R_o = M_o = 0.000$.

The Π optimising parameter is given by assigning the $u_1 t$ initial value for a cascade consisting of N = 5 elements.A limited number of the possible solutions are summarized in Table 1.

The $u_i t$ vs. i series of points are plotted on Figure 2. It can be seen that an increase in the value of i results in a levelling off of all the coupled series of points.

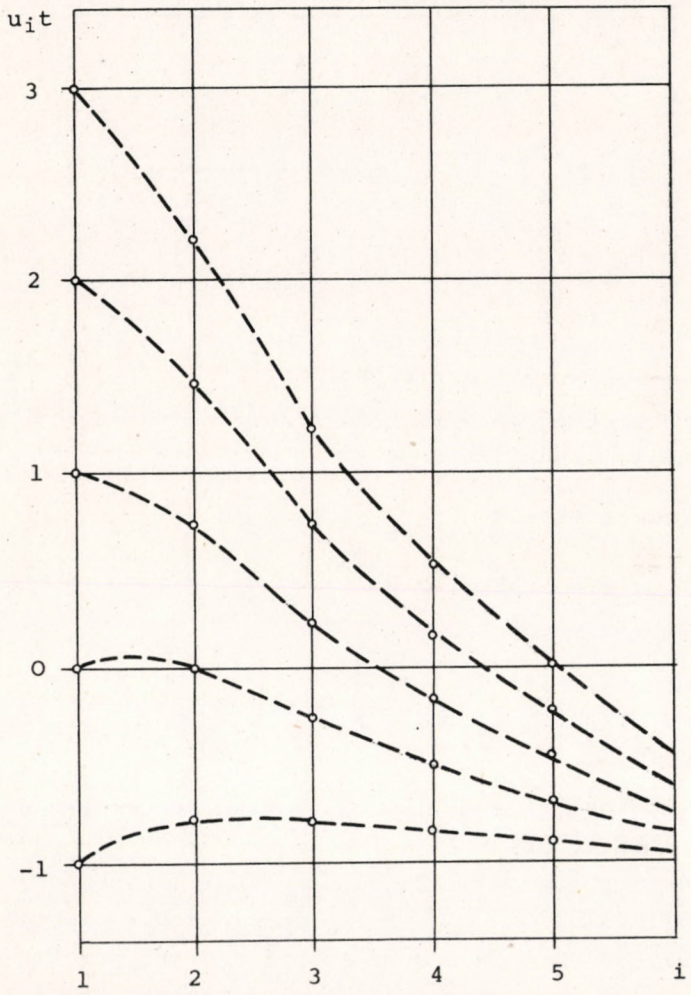

Fig.2. Changes of the $u_i t$ controls throughout the elements of the cascade with different initial values

It follows from Equations (33) and (34) that:

$$u_{i+1}t = \sqrt{\frac{(R_i + k_1 F_{i+1} t)(1 + k_2 t + u_i t)}{R_i}} - (1 + k_2 t) \quad (35)$$

For, if $i \to \infty$ then $F_i \to F_{i+1} \to 0$

$$\lim_{F_{i+1} \to 0} (u_{i+1}t) = \sqrt{1 + k_2 t + u_i t} - (1 + k_2 t) \quad (36)$$

and

$$\lim_{F_{i+1} \to 0} (1 + k_2 t + u_{i+1} t) = \sqrt{1 + k_2 t + u_i t} \quad (37)$$

respectively.

As this is certainly a limiting value, $u_i t \to u_{i+1} t$ and it holds only if both the left and the right hand sides of Equation (37) approach unity. Thus:

$$\lim_{F_{i+1} \to 0} (u_i t) = \lim_{F_{i+1} \to 0} (u_{i+1} t) = -k_2 t \quad (38)$$

and

$$\lim_{F_{i+1} \to 0} R_i = \lim_{F_{i+1} \to 0} R_{i+1} = \frac{\Pi}{k_2 t} \quad (39)$$

Due to technical reasons, the negative set of the u_i values is irrelevant, therefore, in a realistic case, in addition to fixing the number of the elements of the cascade, it is adviseable to set the actual value of $u_N = 0$. In this example, assuming that $u_N t = u_5 t = 0.02$, only the $\Pi \leq 0.02$ solution bears practical significance. The value of Π considered as the maximum value thereby determines the technically acceptable minimum sum of $u_i t$ i.e. this makes the problem unambiguous.

SYMBOLS USED

$\bar{E}$ phase state of the extract

E concentration of the aim product in the extract phase

$\bar{F}$ phase state of the initial phase

F concentration of the initial component in the raffinate phase

H Hamiltonian defined by Equation (8)

J symbole of the objective-function defined by Equation (7)

k_{r1}, k_{r2} reaction rate constants

k_1, k_2 reaction rate constants, first order kinetics (h^{-1})

k_D compounded component transfer coefficient (h^{-1})

K equilibrium distribution coefficient (-)

M concentration of the byproduct (-)

N number of the elements to the cascade (-)

$\bar{R}$ phase state of the raffinate phase

R concentration of the valuable product in the raffinate phase

$\underline{x}$ state vector (its components are $x^1,\ldots,x^k$)

$\underline{u}$ control vector (its components are $u^1,\ldots,u^r$)

t discrete time (h)

α raffinate phase

β extract phase

Ψ aid variable, defined in Equation (8)

Π optimizing parameter, defined in Equation (33)

Indexes

$i,\ldots,N$ serial number of the elements of the cascade

REFERENCES

1. FAN, L.Ts., VAN, Ch.S., Discretny princip maximuma. Izd. "Mir", 1967.

2. OSTROVSKY, G.M., VOLIN, U.M., Methody optimizacii chim. reaktorov. Izd. "Chimia", 1967.

3. BOJARINOV, A.J., KAFAROV, V.V., Optimatizálás a vegyiparban. Müszaki Könyvkiadó, Budapest, 1973.

4. JORDAN, B.W., POLAK, E., Theory of a class of Discrete Optimal Control Syst. I. Electr. and Control 17, 6 (1964)

5. ARIS, R., The Opt. Design of Chem. Reactors. New York-London, Acad. Press, 1961.

6. BELLMAN, R., Dynamic Programming. Princeton Univ. Press. 1957.

РЕЗЮМЕ

Одной из возможностей интенсификации процессовой единицы является избирательное осуществление сложных процессов в одной установке. В органической химической промышленности в ряде случаев продукты реакции разделяются от других реагентов и от продуктов побочных реакций при помощи экстракции. Вытягивая тотчас целевой продукт - после его образования и до разложения - мы должны планировать целесообразное осуществление ряда консекутивных процессов. Кроме выбора избирательного растворителя надо согласовать трафик растворителя с данными цловиями технической реакционной кинетики. В случае реактора-каскада непрерывного действия речь идет об оптимальном разделении потоков передачи. В качестве примера представляется альгорифм оптимального разделения в случае режима поперечного потока для реактора-каскада непрерывного действия, комбинированного с экстракцией.

Hungarian Journal
of Industrial Chemistry
Veszprém
Vol.3. pp. 677-688 (1975)

DETERMINATION OF THE QUASI-OPTIMUM OPERATION MODE OF A TWO PHASE, EXTRACTION-COUPLED REACTOR

Gy. MARTON

(Department of Chemical Process Engineering,
Veszprém University of Chemical Engineering)

Received: October 4, 1975.

The extracting phase of a continuously operated cascade consisting of N elements can at maximum be divided into (allocated to) N partial feed and discharge streams, according to a given objective-function. Thus an optimized, crossed stream system is generated. Because the implementation of optimized control (stream allocation) generally involves significant additional capital cost, the technically more simple (therefore cheaper) co-current, counter-current or mixed stream system are implemented, respectively.

This paper presents the results of a study comparing the mentioned operation modes to the optimized one and based on those results a rational means is presented to select one of the above mentioned modes as a quasi-optimum mode. For the numerical calculation the elements of the cascade are assumed to be perfectly mixed tanks of equal volume.

INTRODUCTION

In an earlier paper [1], the basic problem of optimum solvent (or transfer flow) flow rate allocation of an extraction-compled reactor cascade was introduced, the optimizing algorithm of a scheme consisting of consecutive reactions and a competetive dif-

fusion process was given. The schematics of the optimized crossed stream system is shown on Fig. 1.

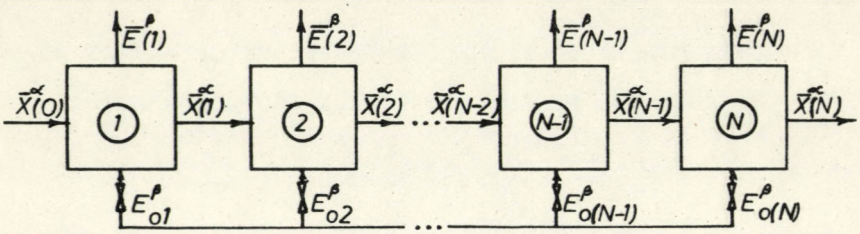

Fig.1. Schematics of the control of a crossed stream cascade system, carried out through the extract phase

The following expressions hold for the α and β phase, respectively.

For the α phase:

$$F_i = \frac{F_{i-1}}{1 + k_1 t} \tag{1}$$

$$R_i = \frac{R_{i-1} + k_1 F_i t}{1 + k_2 t + u_i t} \tag{2}$$

$$u_i = k_D (K - \frac{E_i}{R_i}) \tag{3}$$

$$M_i = M_{i-1} + k_2 R_i t \tag{4}$$

For the β phase:

a) in case of crossed streams

$$E_i = E_{oi} + \frac{q^{\alpha}}{q^{\beta}_i} u_i R_i t \tag{5a}$$

Let us now consider those cases, where the extract and raffinate phases flow co-currently or counter-currently instead of

being allocated to N partial substreams and the volumetric flow rates are the same.

It is conceivable that for counter-current or co-current flow the only formal change occurs in the balance equation of the β phase, while only the numerical parameter values of the α phase are or can be modified e.g. the value of q^{β} is by all means modified, thereby driving forces are modified through E_i as well; k_D the value is also changed).

Thus for the β phase in case of

b) co-current flow:

$$E_i = E_{i-1} + \frac{q^{\alpha}}{q^{\beta}} u_i R_i t \qquad (5b)$$

c) counter-current flow:

$$E_i = E_{i+1} + \frac{q^{\alpha}}{q^{\beta}} u_i R_i t \qquad (5c)$$

1. CALCULATION OF THE COMPOUNDED MASS TRANSFER COEFFICIENT

To aid further (numerical) calculations, the compounded mass transfer rate, k_D has to be discussed. k_D is the product of the mass transfer coefficient and the specific transfer area. Both of these values are strongly dependent on the given geometrical, hydrodynamical and phase conditions. Nevertheless, the

$$\mathrm{HTU} \approx \text{constant} = \frac{v_d}{k_D} \ (\mathrm{m})$$

relationship is widely accepted to hold for extractions carried out in aqueous solutions in rather different apparatuses, assuming that the dispersed phase appears as discrete, separate drops. (The numerical value of the constant considerably varies according to the conditions of the measurements, the types of the systems studied and the authors, i.e. $0.2 < \mathrm{HTU} < 2.5$ [2].) In the following,

for there is nothing better available, the expression

$$k_D = a\, q_i^{\beta} \tag{6}$$

is used. This expression indicates that the resistance against the mass transfer is realized in the extract phase, i.e. there is a much greater concentration gradient in the film of the organic phase than there is of the aqueous phase. Accordingly, the chemical reaction can exersize no effect at all. This assumption is fulfilled if the volumetric flowrate of the organic phase is sufficiently large, for a considerable difference can occur between the E_i actual concentration and the E_i saturation concentration of the extract phase. Considering the same thing from another point of view, assuming that the rate controlling factor is the state of the dispersed organic phase, the transfer rate in a certain drop size range can be considered constant [3] while the drop size, and consequently the specific surface area is proportional to the $0.75\text{-}1.25^{th}$ power of the phase flowrate (or in a mixed space of the speed of the relation). The 1.00 value can certainly be considered as a good average value.

To ensure a uniform calculation mechanism, let us introduce the variable E', that is equal to the E_{oi} value for crossed streams, to the E_{i-1} value for co-current streams and to the E_{i+1} value for counter-current streams, respectively. Based on Equations (2) to (6), R_i reads:

$$R_i = \frac{(R_{i-1} + k_1 F_i t)(1 + aq^{\alpha} t) + aq_i^{\beta} E'}{(1+ aq^{\alpha} t)(1+ k_2 t + aq_i^{\beta} K) - a^2 q^{\alpha} q_i^{\beta} K t} \tag{7}$$

Based on given process parameters and initial conditions, any of the operation states can be calculated from Equations (1), (5) and (7).

2. DETERMINATION OF THE QUASI-OPTIMUM OPERATION STATE

Let us once more consider the numerical example discussed in the previous paper [1]. The optimum allocation problem was solved there for a cascade consisting of N = 5 elements when $k_1 t = k_2 t =$

= 1 [-], F_0 = 1 [-] and $R_0 = M_0 = 0$. Be $u_1 t = 3$ and $E_{01} = E_{12} = \ldots$ $\ldots = E_{05} = 0$. It follows from Equations (3), (5a) and (6) that

$$u_i = a q_i \frac{K}{1 + a q^{\alpha} t} \tag{8}$$

If the following values are chosen: $a = 1$ [m^{-3}]; $q = 1$ [$m^3 h^{-1}$]; $t = 1$ [h] and $K = 2$ [-] then the

$$u_i \equiv q_i$$

$$R_i \equiv E_i$$

equivalences are obtained, therefore the numerical values of u_i become equal to the feed values allocated to q_i.

Table 1. The optimized characteristics of the system ($k_1 t = k_2 t = 1$)

i	q_i^{β} [$m^3 h^{-1}$]	R_i [-]	M_i [-]
0	-	0.0000	0.0000
1	3.0000	0.1000	0.1000
2	2.1833	0.0837	0.1837
3	1.2301	0.0646	0.2483
4	0.5209	0.0504	0.2987
5	0.0207	0.0404	0.3391

From the data summarized in Table 1, it is evident that in that case the amount of solvent utilized is:

$$\sum_{i=1}^{5} u_i = \sum_{i=1}^{5} q_i^{\beta} = 6.955 \text{ m}^3/\text{h}$$

Assuming a uniform allocation pattern (i.e. an average feed rate of 6.955/5 = 1.391 m^3/h) it can easily be calculated that the value of M_5 becomes 0.3965 (which is 17 % greater than the value in the optimum case). For the allocation of the extract phase is uniform in the case of co-current and counter-current systems, it is obvious that the optimity has to be ensured by the appropriately selected driving-force values. (In this example, for crossed streams $E_i/R_i \equiv 1$ and $K = 2$, therefore the dimensionless driving-

-force in each of the subsequent units is 2 - 1 = 1!) In this case the decreasing trend of the u_i values is indicated by the continuously decreasing driving-force values. It is known that such diffusion processes can be implemented either as co-current or as counter-current systems [4]. Assuming that the solvent consumption is expectedly lower, let us first choose the co-current version.

Table 2. Characteristics of the co-current system ($k_1t = k_2t = 1$)

i	u_i [h^{-1}]	R_i [-]	M_i [-]	E_i [-]
0	-	0.0000	0.0000	0.0000
1	4.3500	0.0787	0.0787	0.0787
2	2.1750	0.0787	0.1575	0.1181
3	0.8087	0.0725	0.2300	0.1316
4	0.0355	0.0663	0.2964	0.1321
5	-0.3904	0.0606	0.3570	0.1267

The figures of Table 2 were obtained with the simplex searching method for a pure solvent feedrate value of 4.350 m^3/h. The value of M_5 is hardly 5 % higher than the optimum value although the corresponding R_i values differ as much as 25-30 %.

Similarly - by on essentialy random or regular search - the counter-current version of the problem outlined can also be found. Furthermore, applying some combinatorial methods the problem of mixed stream systems can also be tackled.

However, the search processes can be considerably simplified applying Equations (3) and (6), if the optimum values of u_i and R_i are known. Having set the value of the solvent flowrate available ($q^\beta = 6.955$, in the above case), the E_i^h values can be calculated irrespective of the operation mode:

$$E_i^h = R_i \left(K - \frac{u_i}{a q^\beta}\right) \qquad (9)$$

These E_i^h values are hypothetic values which are independent from the operation mode, but constructing usual E_i^h vs. R_i diagram, the

series of points clearly indicate that operation mode which is the best approximation of the optimum state. Furthermore, in this way the limiting values of the concentrations are also set, so the calculation process is actually only a more exact determination of the already known values.

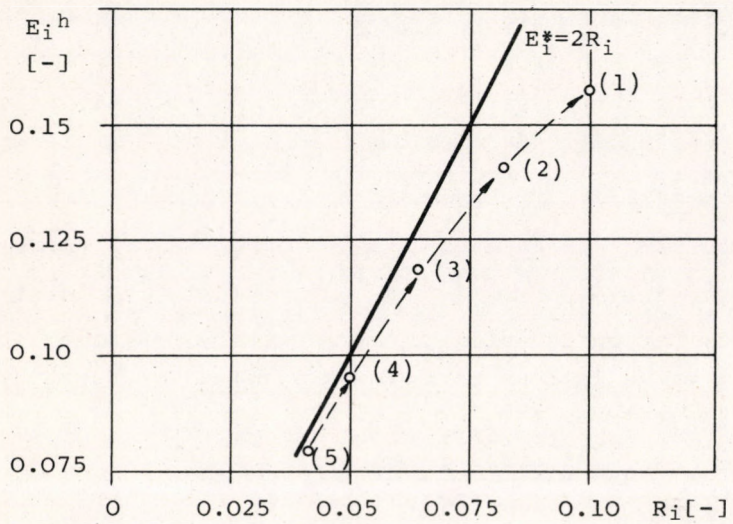

Fig.2. The operation diagram of a counter-current, quasi-optimum operation mode

It is clear from Figure 2 that for this problem the counter-current operation mode combined with some reflux of the extract phase is the best solution, for the input concentration of the β phase is required to be equal to 0.0800.

The best approximation is shown in Table 3. The sixth column of Table 3 (δ_i) presents the relative deviation of R_i from the optimum value.

Table 3. Characteristics of the counter-current operation mode ($k_1t = k_2t = 1$)

i	E_i^h [-]	E_i [-]	R_i^{opt} [-]	R_i [-]	δ_i [%]	M_i [-]	u_i [t^{-1}]
0	-	-	0.0000	0.0000		0.0000	-
1	0.1570	0.1740	0.1000	0.1075	+7.5	0.1075	2.655
2	0.1420	0.1330	0.0831	0.0806	-4	0.1881	2.435
3	0.1190	0.1048	0.0646	0.0587	-11	0.2468	1.500
4	0.0960	0.0921	0.0504	0.0497	-1.5	0.2947	0.532
5	0.080	0.0885	0.0404	0.0447	+11	0.3394	0.165
6	-	0.0899	-	-	-	-	

$$\sum_{i=1}^{5} u_i = 6.957$$

That approximation is evidently good for the deviation of M_5 from the optimum value is less than 0.1 per cent. The quantity of the fresh solvent utilized is:

$$q_o^\beta = 6.957 \frac{0.174 - 0.0899}{0.174} = 3.374 \text{ m}^3/\text{h}$$

while the ratio of the reflux is:

$$\frac{q^\beta}{q_o^\beta} = \frac{6.957}{3.374} = 2.1$$

Thus this operation mode is considered as the quasi-optimum operation mode.

If the k_2t and u_1t values in this example are modified and $k_2t = 0.1$ and $u_1t = 0.01$, the results of the optimation problem applied for $N_{max} = 4$ are shown in Table 4.

The corresponding figures of E_i^h and R_i^{opt} in Table 4 are plotted on Figure 3, the input order of the extract phase to be planned is shown by arrows. According to that the mixed stream flow-schematic shown on Figure 4 was obtained. The quasi-optimum figures of Table 4 and the less than 1 % deviation of the M_i values indicate that the system is inteed rather good.

Table 4. Characteristics of the optimized mixed stream system ($k_1 t = 1$; $k_2 t = 0.1$)

i	u_i^{opt}	u_i^{kv}	R_i^{opt}	R_i^{kv}	E_i^h	E_i	M_i^{opt}	M_i^{kv}
0	-	-	0	0	-	0.400	-	-
1	0.010	0.009	0.450	0.476	0.892	0.943	0.045	0.048
2	0.214	0.301	0.533	0.518	0.835	0.718	0.098	0.099
3	0.174	0.140	0.516	0.515	0.851	0.874	0.150	0.151
4	0.095	0.049	0.485	0.498	0.876	0.934	0.199	0.201

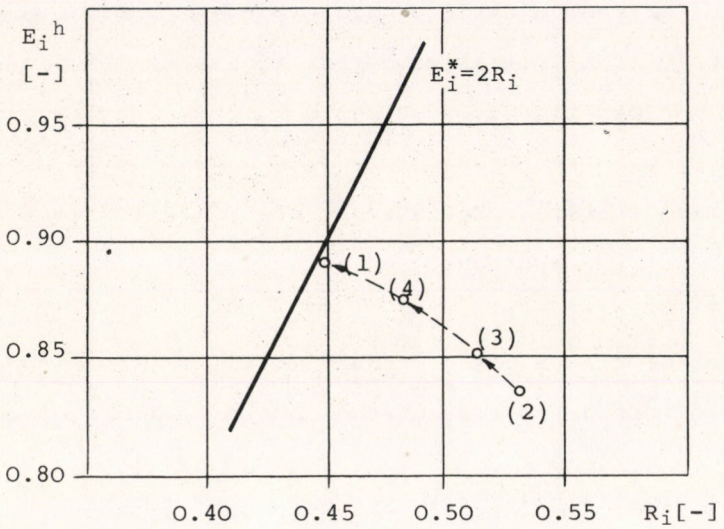

Fig. 3. The operation diagram of a mixed stream quasi-optimum operation mode

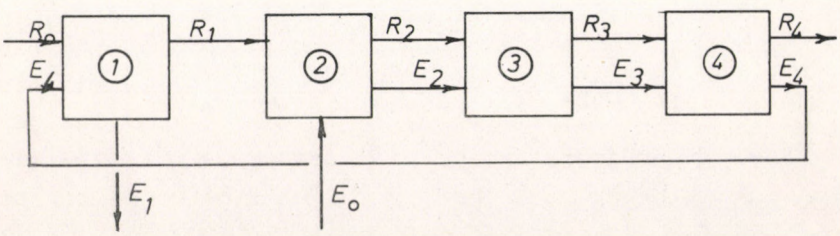

Fig. 4. The schematics of the quasi-optimum mixed stream system

In summary, it was shown that the optimum transfer conditions of the extraction-coupled reactor cascades can be calculated by a fairly simple procedure [1]. This paper presents the method used to select that operation mode. Although the discussion presented is related to an actual cascade system, the principles outlined seem to be general enough for the tubular systems can be fairly well described by the cascade model.

SYMBOLS USED

a constant proportional to HTU, cf. Equation (6), m^3

E concentration of the valuable product in the extract phase, -

F concentration of the initial component in the raffinate phase, -

K equilibrium distribution coefficient, -

k_1, k_2 reaction rate constants, h^{-1}

k_D compounded mass transfer coefficient, h^{-1}

M concentration of the byproduct, -

q volumetric flow rate, m^3h^{-1}

R concentration of the valuable product in the raffinate phase, -

t discrete time (residence time of the raffinate phase in one tank), h

u control variable (transfer flow per unit component), h^{-1}

α raffinate phase

β extract phase

Indexes

$i,\ldots,N-1,N$ serial number of the cascade element

h hypothetic value

kv quasi-optimum value

opt optimum value

REFERENCES

1. MARTON, Gy., Hung. J. Ind. Chem. 3, 663 (1975)

2. PERRY, J.H., Chemical Engineers' Handbook. McGraw-Hill, New York - Toronto - London, 1964.

3. GRIFFITH, R.M., Chem. Eng. Sci. 12, 198 (1960)

4. BENEDEK, P., LÁSZLÓ, A., A vegyészmérnöki tudomány alapjai. (The foundaments of chemical engineering science.) Müszaki Könyvkiadó, Budapest (1964)

РЕЗЮМЕ

Экстракционную фазу ряда каскадов непрерывного действия, состоящего из элементов числа N, можно разделить максимально на N частичных подач и отбираний по отношениям, соответствующим данной целевой функции. Таким образом получается оптимизированная система поперечного потока. Имея в виду, что осуществление оптимального управления (разделения) требует значительных инвестиционных расходов, вместо него строим одну из технически более простых (т.е. дешевых) систем: прямоточную, противоточную или смешанную систему.

В статье обсуждается применяемость отдельных режимов для осуществления оптимального состояния, а также планирование квазиоптимального режима в некоторых случаях. При числовых расчетах было предположено, что элементы каскада имеют одинаковый объем и считают их полностью смешанными.

Hungarian Journal
of Industrial Chemistry
Veszprém
Vol.3. pp. 689-704 (1975)

AGITATORS BUILT UP OF NEW ELEMENTS AND THE APPLICATION THEREOF

L. MÉSZÁROS*, M. SZABÓ*, J. GREGA** and L. TASI**

(*Institute for Applied Chemistry, József Attila University of Sciences, Szeged

**Northern Hungarian Chemical Works, Sajóbábony)

Received: May 2, 1975.

The new agitators are built up of elements which are different from the conventional ones and can be regarded as point-like, zero dimensional, or line-like, one-dimensional ones. Their important characteristic is that their geometric dimensions approach the dimension range of disperse systems.

The elements of which the agitators consist are made of a solid (metallic or non-metallic) material of construction, which is resilient and indifferent towards the fluid. Their most important parameters are the following: the mean diameter q (10-5000 μm), the length of the element l ($l > 50.q$) and the number, sz of the elements representing the agitator.

The application of these new-type agitators for the purpose of dispersion is demonstrated by emulsification experiments with the system oil/water. A comparison of the turbine stirrer with the rotation-type line agitator revealed that with the application of the new elements the time necessary for effective stirring is decreased to half its original value and at the same time, the time necessary for the complete separation of the emulsion is increased to a tenfold value.

The rotation-type line agitators can advantageously be applied for dispersing liquid-liquid, solid-liquid and gas-liquid heterogeneous systems.

In their application, the improved efficiency can be explained on the basis of the surface area of the elements, as referred to unit volume (F/Q) or the shearing edge length, as referred to unit volume ($\sum I/V_{sum.}$); these values are considerably higher than those encountered with conventional stirrer types.

INTRODUCTION

The intensification of chemical reactions carried out in a heterogeneous phase in a batchwise manner and, in connection with it, going over to continuous operation is an assignment whose solution has been in the centre of research work on unit operations for a number of years now. Even theoretically, there exist a large number of possible solutions and although innumerable embodiments were designed, the multifariousness and specific nature of these tasks is an innexhaustable source of new solutions.

It is a common characteristic of reactions occurring in a homogeneous liquid or vapour phase that the distribution of the components is practically uniform along any direction of space and in any small unit of it. This might also be defined in the following manner; the components are present in the reaction space in a molecularly dispersed state and this ensures the short operation time (which can be regarded as practically identical to the reaction time) and continuous execution of the operation.

As opposed to the aforasaid, neither uniform spatial distribution of the components, nor identity of the time of operation and that of the reaction can be considered in the case of heterogeneous reactions. Consequently, such reactions cannot be realized as a continuous operation without active external interaction or intensification.

At the same time, an up-to-date heavy chemical industry is impossible without continuous processes, because these offer - as opposed to batchwise processes - advantages such as

- high productivity and, connected with it, decreased operating costs and manpower requirements
- decreasing specific investment costs,
- uniform, high-quality product.

The solution of the problem of the continuous process, of the continuous operational unit can be approached from two directions:

1. one of the possibilities could be described in the following manner: the heterogeneous system of two or more components is brought into a "quasi-molecular" state, i.e. it is to approximate the homogeneous systems;

2. the second possibility is that the rate of the transport processes occurring in the heterogeneous phase (pulse, component and heat transport) is increased by their intensification [1].

Basically, from whichever angle the problem is approached, the aim to be reached is the same and the methods of approach are analogous to each other. Both in order to increase the degree of dispersion (i.e. to approach the granule size and dispersion to the molecular size range, i.e. to reach "quasi-molecular dispersion") and to increase the rate of the transport processes, to intensify them, the energy brought into the system from the outside has to be increased. This energy introduced into the system has to be spent as irreversible energy, as power becoming valueless in the operational unit [1].

In order to have the largest possible portion of the energy introduced from the outside spent in an irreversible manner, to have the largest possible portion of the power introduced become valueless, it is necessary that

- as much introduced energy as possible be transferred, to
- as little a unit volume as possible, within
- as short a time as possible.

The common characteristics of the operational units so far developed at the Institute are exactly those mentioned above, because

- in pneumatic pulverization, the gases streaming out along the narrow edge of the slit-type pulverizer at a small cross section with a high velocity, transfer a high momentum to a small volume of the liquid, within a very short period of time [2, 3, 4, 5, 6];
- in the electromagnetic metal pulverization technique, in the course of spark discharge, a high electrical energy pulse

(which is transformed to heat) appears in a very short time in a very small, point-like volume (μm^3) [7].

Of course, these techniques using a high energy density with respect to time and space for intensification can be utilized only in certain, and not in all cases of heterogeneous-phase chemical reactions, since these differ from one another in a number of their parameters, i.e. they are specific. Accordingly, it is necessary to seek for and continually develop new solutions; however, the theoretical principles of the possibilities of the solution are the same as described in the foregoing.

The development of new methods for the intensification by high energy density with respect to space and time was the subject of cooperation between the Institute and the Nothern Hungarian Chemical Works on the development of unit operations. The result of this cooperation was the development of the agitators built up of new-type elements; these are the subject of the present paper [8, 9].

DESCRIPTION OF THE NEW-TYPE AGITATOR ELEMENTS

What is characteristic of these agitators built up of new elements? First of all their difference, the fact that they are built up of elements which are basically different from those of the known, conventional ones. It is a common characteristic of known agitator and stirrer elements (blade, turbine blade, propeller, disc or the combination thereof) that they possess a size of three (or at least two) dimensions which is comparable to those of the stirred volume, whereas the elements developed in the course of the present work are, as compared to the stirred volume:

- practically dimensionless, point-like and consequently they can be regarded as zero-dimensional bodies;
- or they possess practically a single dimension (length), they are linear and consequently they can be regarded as one-dimensional bodies.

These elements are illustrated symbolically (drawing to scale being necessarily impossible) in Figures 1a and 1b, respectively.

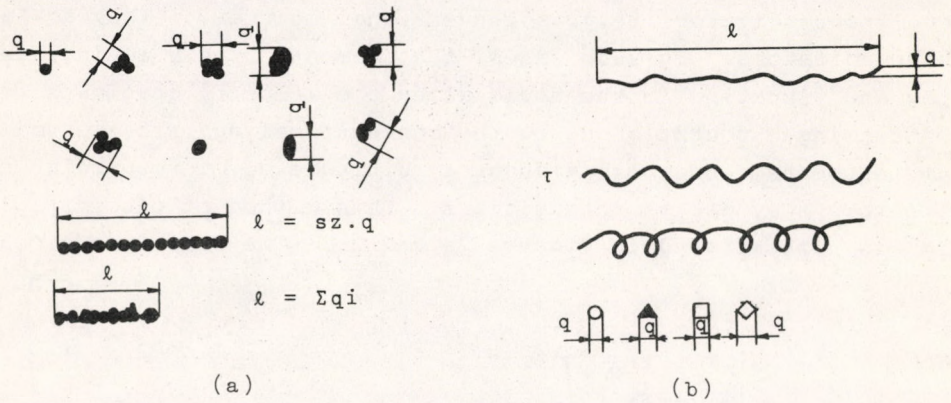

Fig.1. Point-like (a) and linear (b) elements

Accordingly, the geometric dimensions of these elements are considerably different from those of the conventional elements and the difference is in decreasing direction, in the direction of microscopic dimensions. The dimensions essentially approximate the dimension range of dispersions, of course to such an extent as is enabled by the material properties (deformability, strength, and elasticity, etc.) of the structural materials that can be used to produce the elements.

The geometric characteristics of the zero and one-dimensional elements are the following: thickness or mean diameter "q" and the length of the element "l". q may be of the order of 10-5000 μm, whereas l is generally (in the case of one-dimensional elements) 50-5,000 times the value of q: l = 50 q - 5,000 q. Another important characteristic is the number of the elements "sz", present in the dispersing space.

There are two possibilities to bring about dispersion with the point-like and linear elements: they can be applied either as passive or active agitators. The essential difference between these two dispersion techniques is that in the one case the elements take part in the introduction of the energy necessary for dispersion, whereas in the other case they do not.

In those cases where they do not take part in the introduction of the external energy and the latter is supplied by some other known agitator (e.g. a conventional stirrer), they act as passive agitators. In such cases, the elements freely moving, rotating and vibrating in the fluid alter the velocity gradients of the streaming brought about by the conventional agitator in small volume elements, they bring about a multitude of microturbulences and thereby they act as intensifiers. This method of passive agitation is illustrated in Figures 2a and 2b. The zero-dimensional

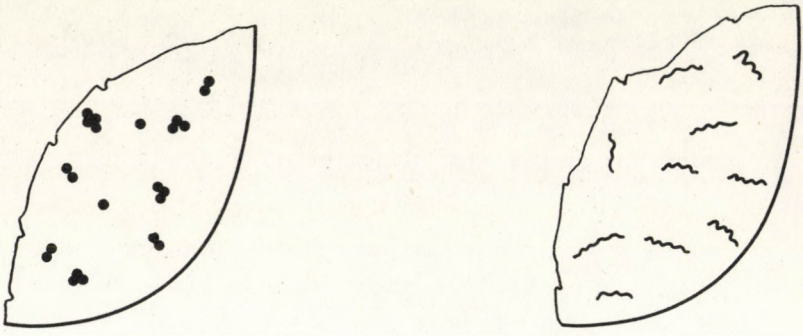

Fig.2. Passive agitation with point-like (a) and linear (b) elements

or one-dimensional elements used for passive agitation are made of a structural material that is solid, resilient and indifferent in relation to the fluid; their geometric dimensions are nearer to the lower limit of the already defined dimension range. In such cases, the number of the elements is preferably expressed as the fraction of the volume of the fluid and it is at least 0.1 %. The upper limit is variable and it is determined mainly by the viscosity of the fluid; the number of the elements can be increased as long as the system behaves as a fluid (generally max.40 % by vol.). In the case of both types of elements it is advantageous if their shape is anisodimensional ($q_1 \neq q_2 \neq q_3 \ldots \neq q_i$) and if their size distribution is heterogeneous ($l_1 \neq l_2 \neq l_3 \ldots \neq l_i$).

If the introduction of external energy necessary for dispersion is carried out by these new elements, i.e. they take part in the introduction of energy, they function as active agitators. In

this case, the geometric dimensions of the elements correspond to the upper limit of the already defined dimension range (e.g. q = 10 - 5,000 m, l = min. 50 q) and the upper limit of the number (sz) of elements to be applied is defined by their length (l), the elasticity of the structural material applied (ρ) and the viscosity of the liquid (η). The active agitators comprising linear-shaped elements differ in a further important characteristic from conventional agitators. In the case of the latter, the suspension of the elements (e.g. turbine blades) is rigid and while rotating they behave as rigid bodies, whereas the linear elements are rigidly suspended only at one (or, at least, at a few) of their points, e.g. at the shaft end of the agitator and their other parts resiliently deflect or vibrate (cf. Figure 3).

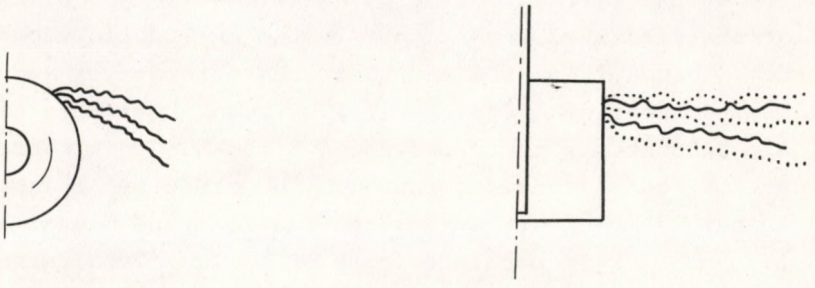

Fig. 3. One active element (in two projections)

The shape of these linear elements may be varied: straight, wave-like, and spiral, etc. Their lengths may be identical or different. Their material of construction is generally a solid, resilient - metallic or non-metallic - material indifferent towards the fluid. In certain cases, active linear elements can be made of a gas or liquid (possibly, $l_1 = l_2 = l_3 \ldots = l_i$, but, it is also possible that $l_1 \neq l_2 \neq l_3 \ldots \neq l_i$; in general, $q_1 = q_2 = q_3 \ldots = q_i$).

It is apparent from the aforesaid that the new agitator elements produced as the result of the present research offer a wide field of various possibilities, the parameters can be varied within wide limits and accordingly they enable the solution of a multitude of tasks in a new manner and at a higher technical level.

In the following, the limit of the variation of the parameters as well as the explanation of the efficiency of dispersion operations carried out with the new elements will be demonstrated by means of a concrete agitator system, the rotation-type linear agitator. The study of these experiments and of their results enables generalizations concerning the operation of the new elements to be arrived at.

The rotation-type linear agitator as a new rotary stirrer type

The rotary stirrer built up of linear elements, i.e. the active rotation-type linear agitator is the most evident form of realization of the agitators made of new elements, which are the subjects of the described invention. In the examinations carried out with them, comparisons between their characteristics and those of the known, conventional agitators, i.e. rotary stirrers can easily be made. Undoubtedly the experience gained in this manner covers only part of the advantages that can be gained by the application of these new elements (just as the rotation-type linear agitators are only one of their possible forms of realization); nevertheless, they are applicable for their demonstration and to draw conclusions. The rotation-type linear agitator is a rotary stirrer whose dispersing elements are linear elements and they are coupled at one point (or a few points) to the rotary axis and the element of q thickness can freely be deflected along its length l. The degree of this deflexion depends on the ρ elasticity of the structural material of the element, the η viscosity of the fluid and the n number of revolutions per minute. An agitator is built up of linear elements whose number is sz and the latter is also of decisive importance with regard to the efficiency of the agitator.

Accordingly, the parameters effecting the number of the possible variations in the case of rotation-type linear agitators are the dollowing: q, l, sz, ρ and n.

A simple inspection of the above proves that by the appropriate choice of these parameters there is a wide possibility for the solution of intensification tasks of the most varied nature.

However, the differences between conventional stirrers and rotation-type linear agitators are not only those described in the foregoing, but there also exist further differences which considerably influence their mode of application.

Conventional stirrer elements, as a consequence of their three-dimensional structure possess a considerable mass (especially if it is calculated as a specific value, with reference to the unit surface area of the stirrer) whereas in the case of linear agitators the mass with reference to the unit surface area of the elements is as little as one third to one fifth as that of those. This fact and the non-rigid suspension of the elements, i.e. the "free deflection" of the elements results in the fact that increasing the peripheral speed (and, together with it the Re number) is by far not limited as much by the ω_{crit} critical angular speed, influencing the design, as in the case of conventional stirrers.

It was found in the course of the experiments that in the case of linear agitators, no imbalance of the rotating mass is encountered. This can be explained by the fact that the resiliently deflecting elements "adjust themselves" to the shape corresponding to the resistance of the medium.

The differences and the advantages can realistically be estimated if a conventional stirrer and a rotation-type linear agitator is examined under identical experimental conditions; for this purpose, experiments were carried out for the production of oil-in-water type emulsion with both stirrer types, under totally identical experimental conditions.

The volume of the oil and water applied (V_{oil} = 100 ml, V_{water} = 1,000 ml, V_{total} = 1,100 ml) was identical in the case of the two stirrer types: turbine stirrer and rotation-type linear agitator, and similarly the diameter of the vessel used for emulsification was also the same (D = 130 mm) as well as the diameter of the two agitators (d = 43 mm), the driving motor was the same and consequently so was its idling speed (n = 4,200 r.p.m.). The number of the turbine blades was varied in the experiments (sz_t = = 2, 3, 4) and so was the number of linear elements (sz_v = 8, 16, 24, 40).

The evaluation of the emulsification tests (the comparison of the degree of dispersion) was carried out by the measurement of the time necessary for efficient mixing and of the stability of the emulsion (the time necessary for total separation). The time necessary for efficient mixing was measured on the basis of light transmitted (this was recorded by means of a photo-electric cell). The period, measured from starting of the mixing, until there was no longer a change in the intensity of transmitted light was regarded as the time necessary for efficient mixing. It was measured in seconds and the symbol τ was used for it. The other parameter of evaluation was the stability of the emulsion; it was examined in such a manner that the emulsion was poured into a graduated cylinder and the time t necessary for total separation of the phases was measured (minutes). The results of these experiments are summarized in the following Table.

The measurement results (n_k, τ and t) are presented in the Table and they are supplemented with the calculated values with reference to the surface area of the agitator elements (F mm²), their volume (Q mm³) the total length of the elements (or the total length of the shearing edges: $\sum$ l, mm) and their length with reference to the unit of the stirred volume ($\sum l/V_{total}$, mm/ml).

What can be seen from the results, and what connections are revealed by the Table?

It is apparent at a first glance that in the case of emulsification with linear elements, the time necessary for efficient mixing is as low as half of that required in the case of the turbine-type stirrer.

Similarly it is readly apparent that at the same time, the stability of the emulsion (more particularly, the efficiency of dispersion) is practically of fenfold value when carrying out the emulsification with the linear agitator, as when whit the turbine stirrer, since the time necessary for the separation of the phases was increased to tenfold value.

The results of these experiments convincingly prove that the dispersion operation can be carried out by means of the linear

No.	Type of stirrer element	d	D/d	Speed (loaded) n_k	sz	F	Q	F/Q	$\sum l$	$\frac{\sum l}{V_{total}}$	τ	t
		mm		l/min	pieces	mm^2	mm^3	mm^{-1}	mm		s	min
1.	turbine blade	43	3.02	3300	2	252.0	176.4	1.428	28	0.0254	145	14
2.	turbine blade	43	3.02	3200	3	378.0	264.6	1.428	42	0.0508	141	14
3.	turbine blade	43	3.02	3100	4	504.0	352.8	1.428	56	0.0762	135	12
4.	linear element	43	3.02	3700	8	87.4	22.1	3.950	112	0.1010	80	97
5.	linear element	43	3.02	3700	16	174.8	44.2	3.950	224	0.2036	78	100
6.	linear element	43	3.02	3600	24	262.2	66.3	3.950	336	0.3054	74	105
7.	linear element	43	3.02	3600	40	437.0	110.5	3.950	560	0.5090	70	130
8.	linear element	80	1.62	2950	24	616.2	153.0	4.000	780	0.7090	65	210
9.	linear element	80	1.62	2950	40	1020.4	255.0	4.000	1300	1.1818	60	232

agitators at a multiple efficiency as compared to turbine stirrers. What is the cause and the explanation of this increase in efficiency? By studying the calculated data present in the Table and the diagrams, prepared on the basis of the latter, shown in Figure 4, the following most essential conclusions can de drawn:

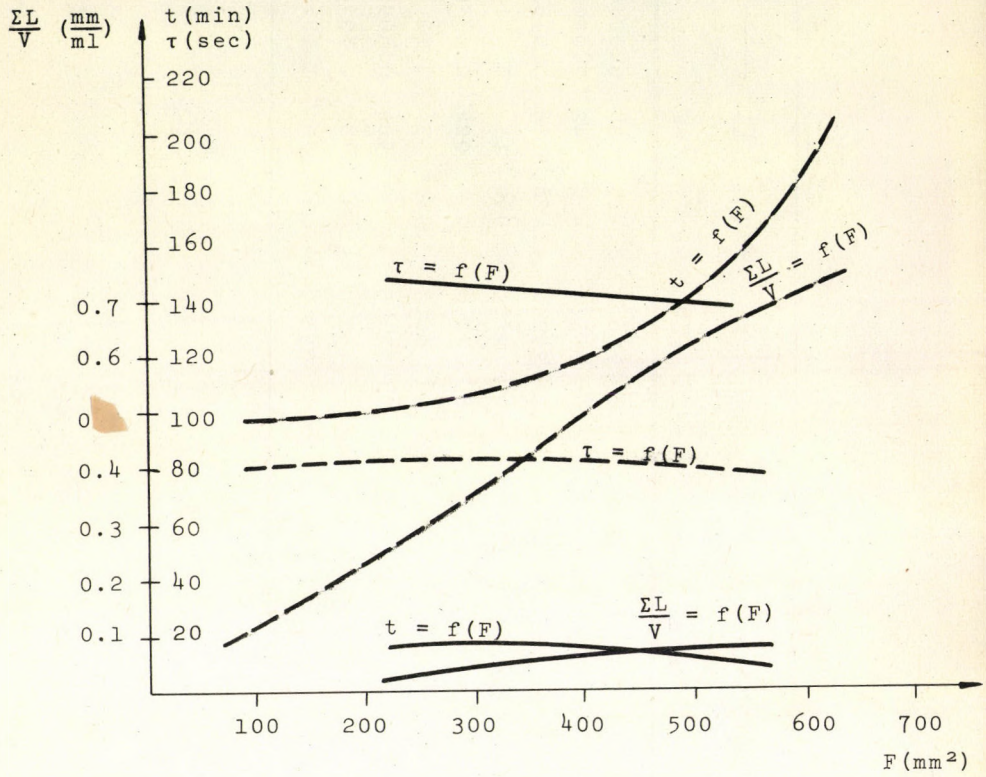

Fig.4. Turbine stirrer —— ; linear agitator ---

1. The stirring surface, with reference to the unit volume of the stirrer elements (F/Q) is larger in the case of the linear agitators by a factor of three to five.
2. The total element length (streaming edge length: $\Sigma l/V_{total}$), with reference to unit volume, is in the case of the linear agitators larger by a factor of fifty to a hundred.
3. The difference and its nature is even more apparent in the graphical representation, where the "longitudinal density" is shown plotted against changes in the surface area of the stirrer elements.

On the basis of these considerations it becomes understandable and explainable why the rotation-type linear agitator is more efficient in dispersing; a considerable contribution to this efficiency is represented by the vibration of the linear elements during their motion, which, however, could not be included numerically into the Table.

In the course of the experiments, the ratio D:d was not only studied at custorary design values (D/d = 3), but also in experiments No. 8 and 9 at the more unaccustomed value of 1.62. Surprisingly it was found that τ showed a further decrease and, at the same time, the time t necessary for separation showed a further increase.

In these experiments, the stirrers were placed at a height corresponding to the stationary phase boundary (boundary water--oil). In the following, experiments were carried out in which

- $V_{oil} = V_{water}$ = 500 ml was maintained and
- the stirrers were located at a height corresponding to the middle of the upper stationary oil phase.

It was experienced that - whereas in the case of the turbine-stirrer there was no emulsification at all - the linear agitator enabled the preparation of an emulsion stable for nearly the same time.

The significance of the experimental results showing the advantages of the linear agitators is further enhanged when it is considered that in the experiments:

- no use was made of the possibilities of the "rotatability" of the linear agitators (a relatively low speed was applied)
- variation of the number of the elements was restricted to a narrow range.

Summarizing the aforesaid it can be concluded that the efficiency of the rotation-type linear agitator (as an embodiment of the new agitator elements developed) can, at a first approximation, be explained by the following:

- on account of the decreased geometric dimension of the elements, considerable velocity fradients arise in small volumes of the fluid (consider, for example, the difference in the flow rate of two fluid layers moved by two elements of q = = 0.5 mm and the "non-moved" layer between them);
- velocity vectors considerably different with regard to magnitude and direction are formed along the l length of the elements "adjusting themselves" in the direction of the resistance of the medium;
- the vibration of the end portions of the resilient linear elements is, in addition to the aforementioned, the source of further microturbulences.

An additional feature is that less restrictions are valid in connection with increasing the speed of stirring and the diameter of the stirrer, as opposed to conventional stirrers, and accordingly higher Re number ranges can be reached.

Accordingly, it can unequivocally be stated that the increase in efficiency is connected with changes in the longitudinal density, i.e. in $\frac{\sum l/F}{V_{total}}$ which is, of course, also influenced by the values of q, l, sz and ρ.

On account of space restrictions, only one type of the new agitator elements was described in the foregoing, moreover, only part of the experiments could be reported.

The results of further experiments together with a few chemical applications will be described in a further paper.

REFERENCES

1. SZOLCSÁNYI, P., Vegyipari müveletek energetikai analizise (Energy Analysis of Chemical Operations) Müszaki Könyvkiadó, Budapest, 1972.

2. Brit. Pat. 1 115 041 (1969)

3. Hung. Pat. 161 140 (1970), Oe. P. 310 713 (1973), Fr. P. 2 162 270 (1974), Brit. P. 1 379 977 (1974), DAP. 93 992 (1972)

4. Hung. P. 161 699 (1970)

5. Hung. P. 163 586 (1970) DWP. 100 158 (1973), Ital P. 971 196 (1974), SWP. 361 603 (1973), Schw. P. 545 119 (1973), DOS

6. Hung. P. 164 286 (1970)

7. Hung. P. 155 475 (1968), Brit. P. 1 229 867 (1971), US. P. 3 529 867 (1971), Jap. P. 675 775 (1973)

8. Hung.-pat. appl. No. EA-116 (166.693 sz); British pat.appl. No. 45 553; Austrian pat. appl. A-4188, Bulgarian pat.appl. No. 26 913; Chechoslovak pat. appl. No. PV-3691; Danish pat. appl. No. 2817; French pat. appl. No. 74 22 496; Japanese pat. appl. No. 49-124665; Yugoslav pat. appl. No. P-1680; Polish pat. appl. No. P 173 895; West German pat. appl. No. P 24 29 255,5; Norwegian pat. appl. No. 74 3713; Romanian pat. appl. No. 79 082; Swedish pat. appl. No. 74 06754-7; Soviet pat. appl. No. 2038 429; and GDR, Canadian, Italian, Swiss and USA patent applications are pending.

9. MÉSZÁROS, L., GREGA, J., LAKÓ, L., MARKÓ, L., SALAMON, Z., SZATMÁRY, I., TASI, L., Stirrers Built up of New Elements Address presented at the Chemists' Congress, Miskolc, 1974).

РЕЗЮМЕ

Мешалки нового типа построены из новых, отличающихся от обычных, элементов, считающихся нульмерными, точечными или одномерными, линейными. Характерное для них свойство, что их геометрические размеры приближаются к размерам дисперсных систем. Составные части мешалки изготовлены из твердого (металлического или неметаллического), упругого, инертного для флюида материала. Важнейшие характерные свойства: средний диаметр $\underline{q}$ (10-5000 μм), длина элемента $\underline{l}$ ($\underline{l} \geq 50.q$) и число составных частей мешалки.

Применяемость мешалки нового типа для диспергирования была доказана на опытах с целью эмульгации водно-масляной системы. Сопоставление смесителей с турбинной мешалкой и ротационной линейной мешалкой доказало, что с применением новых элементов время, требуемое для эффективного перемешивания, уменьшается наполовину, а время, нужное для полного разделения эмульсии, увеличивается в десять раз.

Ротационные линейные мешалки полезно применимы при диспергировании гетерогенных систем: жидкость-жидкость, твердое тело-жидкость и газ-жидкость.

Повышение эффективности при их применении характеризуется величиной F/Q, (поверхность элемента/объем элемента), также величиной $\Sigma I/V_{общ}$ (длина сдвигающей кромки/смешанный объем). Эти величины значительно превышают соответствующие величины мешалок классического типа.

СОДЕРЖАНИЕ

БОШАН, П., ФЮЛЭП, Я., СЕЙЦ, К. и ВАЙДА, Т.: Испытания соотношений, связанных со средним значением потенциальной функции, описывающей транспортные процессы химической промышленности 537

МЕСАРОШ, И.: Роль природных ингибиторов в термической деградации добавок полиметакрилатного типа 549

ТУРЕК, Ф. и МАДЯР, М.: Упрощенный метод оценки массопередачи в реакторе продувного типа 557

ВОНДРАН, Й. и КАРДОШ, И.: Определение применяемости параллельного соединения с деленной емкостью и внутренним запасом емкости 565

ГАРДОШ, Дь., ПЕЧИ, Л., РЕДЕИ, А. и ЧАСАР, Э.: Изучение декарбонилирования фурфурола в присутствии водяного пара на окисле металла, применимом в качестве катализатора . . 577

ГАРДОШ, Дь., ПЕЧИ, Л., ЧАСАР, Э. и СИГЕТИ, Б.: Изучение получения фурана из фурфурола на катализаторе из благородного металла 589

ГАРАИ, Т., РОНАИ, Д. и ДЕВАИ, Й.: Возможности применения алюминиевых сплавов в протекторной защите от коррозии . . 603

ФИЛКА, Ю., ОРМОШ, З. и ЧУКАШ, Б.: Изучение аэродинамических условий способа взвешивания 617

ОРМОШ, З., ЧУКАШ, Б. и ПАТАКИ, К.: Изучение грануляции в псевдоожиженном слое VI. Грануляция в механически смешанном псевдоожиженном слое 631

ЛАСЛО, А.: Обобщение и систематизация коэффициентов транспортных процессов 647

МАРТОН, Дь.: Изучение оптимального режима двухфазного реактора-каскада, комбинированного с экстракцией 663

МАРТОН, Дь.: Изучение квазиоптимального режима двухфазного реактора-каскада, комбинированного с экстракцией . . . 677

МЕСАРОШ, Л., САБО, М., ГРЕГА, Й. и ТАШИ, Л.: Мешалки, построенные из новых элементов, и их применение 689

A kiadásért felelős: Dr. Nemecz Ernő
Felelős szerkesztő: Dr. Bodor Endre
Példányszám: 950 + 250 különlenyomat cikkenként
VÁCI ÁFESZ Nyomda, 1976

Ára: 39 Ft

CONTENT

BOSCHÁN, P., FÜLÖP, J., SEITZ, K. und VAJDA, T.: Untersuchungen über die Zusammenhänge des Durchschnittswertes von den die chemischen Transportprozesse beschreibenden Potentialfunktionen. (The Examination of the Relations Existing Among the Mean Values of Potential Functions which Describe the Chemical Transport Processes) 537

MÉSZÁROS, I.: The Role of Natural Inhibitors in Thermal Degradation of Polymethacrylate Additives 549

TUREK, F. und MAGYAR, M.: Eine vereinfachte Methode zur Ermittlung des Stoffüberganges in Blasensäulen. (A Simple Method to Ascertain the Mass Transfer in Bubble Cap Plate Columns) 557

VONDRAN, J. und KARDOS, J.: Bestimmung der Verfügbarkeit einer Kapazitätsgeteilten Parallelschaltung mit interner Kapazitätsreserve. (Determination of Applicability of a Parallel Connection Consisting of More Capacity Units and Having Inner Capacity Reserves) 565

GÁRDOS, Gy., PÉCHY, L., RÉDEY, Á. and Mrs. CSÁSZÁR, E.: Investigations on the Decarbonylation of Furfural over Metal-Oxide Catalysts in the Presence of Steam 577

GÁRDOS, Gy., PÉCHY, L., Mrs. CSÁSZÁR, E. and Mrs. SZIGETI, B.: Investigation of Furan Production from Furfural over Noble Metal Catalysts 589

GARAI, T., RÓNAY, D. and DÉVAY, J.: The Possibility of Applying Aluminium Alloys as Sacrificial Anodes in Cathodic Protection 603

FILKA, J., ORMÓS, Z. and CSUKÁS, B.: Studied on the Flow Dynamic Characteristics of the Flotation Technique 617

ORMÓS, Z., CSUKÁS, B. and PATAKI, K.: Studies on Granulation in Fluidized Bed VI. Granulation in Mechanically Agitated Fluidized Bed 631

LÁSZLÓ, A.: Generalization and Classification of the Coefficients of Transport Processes 647

MARTON, Gy.: Studies on the Optimum Operation Mode of a Two-Physe, Extraction-Coupled Reactor Cascade 663

MARTON, Gy.: Determination of the Quasi-Optimum Operation Mode of a Two Phase, Extraction-Coupled Reactor 677

MÉSZÁROS, L., SZABÓ, M., GREGA, J. and TASI, L.: Agitators Built Up of New Elements and the Application Thereof .. 689